AD-A112 310 ADVISORY GROUP FOR AEROSPACE RESEARCH AND DEVELOPMENT--ETC F/G 1/2
COMBAT AIRCRAFT MANOEUVRABILITY.(U)
DEC 81
UNCLASSIFIED AGARD-CP-319 NL

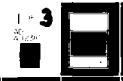

AGARD-CP-319





# AGARD

ADVISORY GROUP FOR AEROSPACE RESEARCH & DEVELOPMENT

7 RUE ANCELLE 92200 NEUILLY SUR SEINE FRANCE

AGARD CONFERENCE PROCEEDINGS No. 319

# Combat Aircraft Manoeuvrability



NORTH ATLANTIC TREATY ORGANIZATION

DISTRIBUTION AND AVAILABILITY
ON BACK COVER

AGARD-CP-319

NORTH ATLANTIC TREATY ORGANIZATION

ADVISORY GROUP FOR AEROSPACE RESEARCH AND DEVELOPMENT

(ORGANISATION DU TRAITE DE L'ATLANTIQUE NORD)

AGARD Conference Proceedings No.319

# COMBAT AIRCRAFT MANOEUVRABILITY

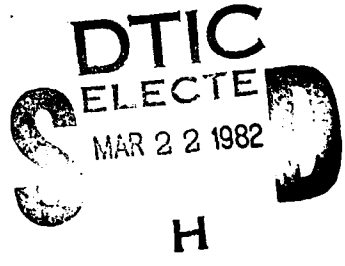


Papers presented at the Flight Mechanics Panel Symposium on Combat Aircraft Manoeuvrability held in Florence, Italy, 5–8 October 1981.

## THE MISSION OF AGARD

The mission of AGARD is to bring together the leading personalities of the NATO nations in the fields of science and technology relating to aerospace for the following purposes:

- Exchanging of scientific and technical information;
- Continuously stimulating advances in the aerospace sciences relevant to strengthening the common defence posture;
- Improving the co-operation among member nations in aerospace research and development;
- Providing scientific and technical advice and assistance to the North Atlantic Military Committee in the field of aerospace research and development;
- Rendering scientific and technical assistance, as requested, to other NATO bodies and to member nations in connection with research and development problems in the aerospace field;
- Providing assistance to member nations for the purpose of increasing their scientific and technical potential;
- Recommending effective ways for the member nations to use their research and development capabilities for the common benefit of the NATO community.

The highest authority within AGARD is the National Delegates Board consisting of officially appointed senior representatives from each member nation. The mission of AGARD is carried out through the Panels which are composed of experts appointed by the National Delegates, the Consultant and Exchange Programme and the Aerospace Applications Studies Programme. The results of AGARD work are reported to the member nations and the NATO Authorities through the AGARD series of publications of which this is one.

Participation in AGARD activities is by invitation only and is normally limited to citizens of the NATO nations.



Published December 1981



ISBN 92-835-0304-X

*Printed by Technical Editing and Reproduction Ltd*
*Harford House, 7–9 Charlotte St, London, W1P 1HD*

## PREFACE

Current and recent technology developments have opened up a range of possibilities for major improvements in the manoeuvrability of combat aircraft in the air-air and air-ground modes. There are now real prospects of exploiting a whole new regime of controlled flight, at angles of attack well beyond the normal stall limit, given the availability of automatic departure/spin prevention systems. There is, in addition, a range of new and not-so-new concepts capable of changing the traditional modes of control, of which thrust vectoring and direct lift and side-force generation are examples.

The Flight Mechanics Panel of AGARD held a symposium in Florence, Italy, from 5- 8 October 1981, in order to review these recent developments and the relationship between technical possibilities and operational requirements. 25 papers were presented in four sessions covering:

- Operational Requirements
- Prospects for Improvements in Manoeuvrability
- Prediction Methods for Aircraft Performance and Manoeuvrability
- Assessment Methods and their Value

However, the papers showed a wide variety of style and technical coverage which allowed a freer exploration of the topic than indicated by the session titles above.

Certain papers, for example those of R.H.Hoh et al (9) and P. Guicheteau (17) developed an abstract, highly mathematical approach. Others considered the global aspects of aircraft behaviour in combat. During the first session, for instance, Lt Col de Brouwer (2) laid emphasis on the importance of persistence and internal fuel capacity for a combat aircraft; tactical considerations were developed also in paper 21 of J. Pedotti and Y. Hignard. The "end product" was examined in the notable paper of Col F. Zamparelli and A. Armando (26) on the Decimomannu tactical evaluation range.

A third class of authors chose to isolate particular detailed points and to develop them in depth. Examples are the papers of R. C. A'Harrah and R. J. Woodcock (7) and of W. E. Fellers et al (20) which stimulated a lively discussion amongst participants on the hypotheses determining the choice of tail configuration, with far from unanimous opinions being expressed. Thanks are due to the Fluid Dynamics Panel of AGARD for their contributions to the success of the symposium, namely the presentations on the development of cryogenic wind tunnels (E. C. Polhamus and R. P. Boyden, 15) and on simplified methods of calculation for aerodynamic prediction (T. D. Beatty and W. B. Brooks, 18). Of note also was the presentation of M. Falco and G. Carpenter (22), whose methods would apply equally to helicopter combat. In contrast, the absence of any paper discussing the utility of thrust vectoring in air combat was much regretted.

Finally, the closing Round Table Discussion proved to be one of the most interesting of recent years. The discussion chairman, W. T. Hamilton (formerly FMP member and chairman of an AGARD Working Group on Manoeuvre Limitations of Combat Aircraft - see AGARD AR 155A and AR 155B), encouraged the constructive participation of the audience in the analyses of the Round Table. Amongst the topics raised were the key issues of cost-effectiveness of combat aircraft - what price can one afford to pay for technological progress and should emphasis be laid on maximum force size or on maximum performance capability - and of the interrelationship of human factors with technical advances.

An overall review of the papers given, the accompanying discussions and the Round Table session will be included in the forthcoming Technical Evaluation Report (AGARD Advisory Report AR-179).

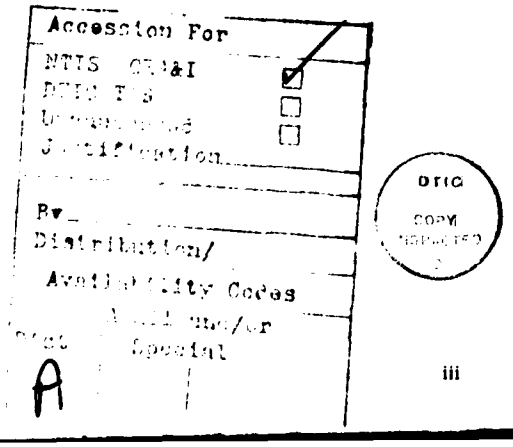


W. C. DIETZ
J-M. DUC
Members, Flight Mechanics Panel

CONTENTS



* Published in CP-319 (Supplement) Classified NATO Confidential.

* Published in CP-319 (Supplement) Classified NATO Confidential

# RETROSPECTIVE DE RECENTS SYMPOSIUMS AGARD SOUS L'ANGLE DE LA MANOEUVRABILITE DES AVIONS DE COMBAT

par

L'Ingénieur en Chef de l'Armement Jean-Michel Duc
Direction des Recherches, Etudes et Techniques
Service des Recherches/Groupe 6
26 Bld Victor
75996 Paris Armées
France

et

L'Ingénieur de l'Armement Michel Vergne
Direction Technique des Constructions Aéronautiques
Service Technique des Programmes Aéronautiques/
Section Etudes Générales
4 Ave de la Porte d'Issy
75015 Paris
France

## 0. - Notations :

| | |
|---|---|
| Cz | : Coefficient de portance ($C_L$ sur les figures en Anglais). |
| Cz max | : Coefficient de portance maximal ($C_L$ max. sur les figures en Anglais) |
| $C_\mu$ | : Coefficient de soufflage |
| $\varphi$ | : Angle de gite |
| $\theta$ | : Assiette de tangage (ou longitudinale) |
| $\psi$ | : Cap |
| $\alpha$ | : Incidence |
| $\beta$ | : Dérapage |
| p | : Vitesse angulaire de roulis |
| q | : Vitesse angulaire de tangage |
| r | : Vitesse angulaire de lacet |
| v, u, w | : Composantes du vecteur vitesse |
| $n_x$, $n_y$, $n_z$ | : Composantes du facteur de charge |
| M | : Nombre de Mach |
| Re | : Nombre de Reynolds |
| LCDP | : Critère de perte de contrôle latéral |
| $Cn_\beta$ dyn | : Stabilité de route apparente (sous-entendu : lorsqu'on tente de contrôler l'assiette latérale) |

## 1. - Introduction :

De nombreux symposiums AGARD tenus ces dernières années, en particulier ceux du FDP et du FMP, ont été l'occasion de communications ayant trait d'une manière ou d'une autre à la manoeuvrabilité des avions. Le sujet est si important qu'il a paru utile d'organiser le présent symposium, entièrement consacré à ce problème (en particulier pour en aborder certains aspects confidentiels).

En préalable, il nous est agréable de rappeler le remarquable ouvrage qui a été réalisé par un groupe de travail présidé par W. HAMILTON et qui a été édité sous forme de l'Advisory Report n° 155A "Manoeuvre Limitations of Combat Aircraft" (Réf. 13). Ce document reprend lui-même certains éléments donnés dans l'Advisory Report n° 82 "The Effect of buffeting and other transonic phenomena on Maneuvering Combat Aircraft" rédigé sous la direction de W.E. LAMAR (Réf. 12).

## 2. - Définitions - Etendue du sujet :

Nous serions tentés de définir la manoeuvrabilité d'un avion comme cette qualité qui lui permet à la fois d'effectuer des évolutions serrées (par opposition au vol rectiligne à vitesse constante) soit pour un court instant (maniabilité), soit pendant une durée relativement longue et de changer rapidement de type d'évolutions (sens de virage par exemple) ou de conditions de vol (vitesse, altitude).

En termes mathématiques cela peut s'exprimer de la manière suivante : la position et le mouvement d'un avion peuvent être représentés par un vecteur d'état très général comprenant des "positions" (assiettes $\varphi$, $\theta$, $\psi$, angles d'incidence $\alpha$ ou de dérapage $\beta$, etc....) "des vitesses" (linéaires u, v, w, V, ou angulaires p, q, r, $\dot{\alpha}$, $\dot{\beta}$, etc...) et des "accélérations" (linéaires $n_x$, $n_y$, $n_z$, ou angulaires $\dot{p}$, $\dot{q}$, $\dot{r}$, $\ddot{\alpha}$, $\ddot{\beta}$, etc...)

Pour une manoeuvre donnée, certaines de ces variables prennent pendant plus ou moins longtemps des valeurs de très grande amplitude (ou au contraire tendant vers 0, pour la vitesse par exemple) très différentes de celles qu'elles ont en vol "de croisière" ($n_z$ = 1, V = Cte , $\alpha$ petit, $\beta$ = p = q = r = $\dot{\alpha}$ = $\dot{\beta}$ = 0).

Des illustrations de ces combinaisons extrêmes ont été souvent données, par exemple par B.R.A. BURNS (Réf. 1) (Fig. 1), par W.E. LAMAR (Réf. 2) (Fig. 2), par J. STALONY-DOBRZANSKI et N. SHAH (Réf. 8) (Fig. 3), par K.W. LOTTER et J. MALEFAKIS (Réf. 7), et mieux encore par A.M. SKOW, W.A. MOORE et D.J. LORINCZ (Réf. 9)(Fig. 4).

Le sujet à traiter est à la fois très particulier et très vaste.

Très particulier parce qu'il ne recouvre qu'un aspect parmi tous ceux qui préoccupent la construction aéronautique. En matière de performances on pourrait citer comme autres objectifs la vitesse et l'altitude maximales, le rayon d'action, l'endurance, les distances de décollage et d'atterrissage, etc... En matière de qualités de vol, la stabilité s'oppose souvent à la maniabilité. De même la rapidité et la précision de réponse aux ordres du pilote, le risque ou non de dépasser les limites du domaine de vol, constituent des sujets d'étude qui ne sont pas strictement inclus sous le vocable manoeuvrabilité mais qui lui sont si étroitement liés qu'on devra en parler.

Très vaste aussi, parce que les spécifications de performances et de qualités de vol en combat aérien sont souvent celles qui déterminent les principaux choix des bureaux d'études (formule aérodynamique et charge alaire, empennages stabilisateurs, commandes de vol, cycle thermodynamique du moteur, taux de motorisation, entrées d'air, tuyères, dimensionnement des structures et donc finalement devis de masse et coût de l'avion). Les exigences peuvent varier d'une mission à une autre, et donc la formule de l'avion s'en ressentir. Une mission contraignante est certainement la protection aérienne à moyenne altitude du champ de bataille qui impose un rôle d'interception et d'engagement en combat des agresseurs éventuels.

Néanmoins, tous les avions d'armes ont besoin d'une grande capacité de manoeuvre, même si leur mission principale (pénétration basse altitude par exemple) ne le requiert pas, car même si on choisit de refuser le combat, l'évasive nécessite virages serrés et fortes accélérations sur trajectoire. Ainsi donc, l'évolution des caractéristiques d'avions comme représentées par R.S. HOOPER (Réf. 5) (Fig. 5 et 6) et P. BOHN (Réf. 6) (Fig. 7) est liée à l'évolution des besoins opérationnels et illustre par ailleurs les progrès technologiques réalisés par les constructeurs (les deux allant souvent de pair).

Notons que certains auteurs ont cru pouvoir établir des paramètres globaux d'efficacité en combat, groupant plusieurs termes. Citons par exemple, une formule donnée par A. VINT (Réf. 11) (Fig. 8).

Le sujet est donc très important. Il met en jeu de nombreuses disciplines. L'AGARD, le Flight Mechanics Panel et le FDP surtout, s'est toujours largement préoccupé de manière plus ou moins explicite des questions gravitant autour du thème de la manoeuvrabilité. Il suffit pour s'en convaincre de relire la liste des titres des symposiums de ces dix dernières années. La plupart ont abordé, parfois dans une ou deux communications seulement, parfois dans la majorité des exposés, les divers aspects qu'il faudrait évoquer pour traiter la question dans son ensemble.

Quels sont ces aspects ? On peut citer :

- l'expérience acquise au cours de combats réels ou simulés,
- l'expression des besoins opérationnels qui en découle,
- les critères et normes de performances et qualités de vol associés,
- les méthodes pour la conception d'avions plus manoeuvrants. Cette rubrique à son tour se divise en plusieurs chapitres :
  - les méthodes de calcul en aérodynamique, propulsion, résistance des structures, etc...
  - les méthodes d'essais en soufflerie, sur bancs au sol, sur simulateurs.

A un niveau de synthèse plus élevé on pourra alors se référer au Contrôle Automatique Généralisé qui permet en intégrant les derniers progrès venus de l'aérodynamique, de la propulsion, des structures, mais aussi de l'électronique, de l'informatique et des commandes de vol de tirer un meilleur parti de l'ensemble, en se libérant par exemple de certaines contraintes de stabilité classiques et en réduisant la charge de travail du pilote.

- les principales réalisations actuelles ou futures, expérimentales ou en vue d'une production en série,
- les méthodes d'essai et d'évaluation, avec tout ce que cela comporte de techniques de mesure, de modélisation, d'identification, de simulation, d'utilisation de maquettes télépilotées, etc.....
- enfin, dernier point mais non le moindre, l'"acceptabilité" des gains de manoeuvrabilité par les équipages, non seulement sous l'aspect ergonomique (conception des cabines de pilotage : présentation des informations, dispositions des commandes, confort du pilote, etc..) mais aussi sous l'angle médical (jusqu'où l'organisme humain pourra-t-il supporter la brutalité des mouvements permis par les futurs avions?)

3. - Objet du présent symposium et de la conférence d'introduction :

Traiter l'ensemble du sujet en un seul symposium est apparu une tâche sinon impossible en tout cas difficile. C'est pourquoi, la présente réunion organisée par le F.M.P. a dû voir son champ de réflexion limité, pour l'essentiel, aux aspects de mécanique du vol et de synthèse qui sont de son ressort (utilisation opérationnelle, critères et normes, architecture des avions, essais en vol) avec quelques apports des spécialistes d'aérodynamique, structures et systèmes.

De la même manière, relire tous les compte-rendus de conférences AGARD des dix dernières années, en faire le résumé et la synthèse aurait été une ambition déraisonnable et nous avons choisi, très arbitrairement, de nous limiter à une sélection des conférences du F.D.P. et du F.M.P. Nous prions les auteurs des autres commissions qui ont apporté une contribution au sujet ici traité de nous excuser de ne pas les citer. La liste des documents auxquels il sera fait allusion, constitue les références (1) à (11) incluses pour les Symposiums et Spécialists Meetings. Nous avons cru bon d'y ajouter quelques AGARDograph's, références (12) à (14).

Le plan de l'exposé consistera à reprendre la notion de manoeuvrabilité, essentiellement en termes de mécanique du vol. Chaque point sera illustré par des planches extraites des compte-rendus AGARD précités. Le temps et la place disponibles ne nous ont pas permis de développer largement les aspects opérationnels, ni le chapitre particulier de la simulation du vol à grande incidence.

4. - La manoeuvrabilité :

4.1. - Facteur de charge maximal instantané :

La première demande des pilotes en combat air-air est de pouvoir effectuer des virages plus serrés que l'adversaire et pointer les canons dans la direction voulue le plus rapidement possible.

Dans l'immédiat, ceci se rattache à la notion de limite de manoeuvre (facteur de charge maximal instantané) et il faut avant tout pouvoir obtenir une très grande portance * et, ce qui n'est pas toujours équivalent, pouvoir voler à très grande incidence. Au début du combat, l'avion sera en général en régime de vol supersonique ou transsonique, à la fin il sera le plus souvent en subsonique. Les principales limitations de la portance maximale instantanément disponible ont été indiquées par W.E. LAMAR (Réf. 2) (Fig. 9) et également citées dans l'Advisory Report, Réf. 12.

La portance maximale peut être d'origine purement aérodynamique et dans ce cas dépend exclusivement de la configuration retenue (flèche, allongement, épaisseur de la voilure, becs, volets hypersustentateurs, etc...) et de la possibilité de voler à grande incidence.

Un très bel exemple de mesure de l'incidence en vol jusqu'à plus de 50 degrés a été fourni par K.W. ILIFF (Réf. 4) (Fig. 10) à comparer à celui de J.M. ABERCROMBIE (Réf. 6) (Fig. 11) relatif au F15 Eagle. Malheureusement le nombre de Mach n'est pas indiqué sur ces figures. (Cette absence de valeurs numériques est très fréquente chez de nombreux auteurs, pour d'évidentes raisons de discrétion. Nous ne pouvons que le déplorer).

W. STAUDACHER, B. LASCHKA, PH. POISSON-QUINTON et J.P. LEDY (Réf. 7) (Fig. 12 et 13) ont montré comment soufflage ou installation de nageoires peuvent améliorer ce $C_z$ max, comme l'ont fait B. SCHULZE et M. CANU (Réf. 4) (Fig. 14), avec, ce qui est appréciable dans ce dernier cas, des graduations précises de nombre de Mach et d'incidence. De même A.H.SKOW, A. TITIRIGA Jr. et W.A. MOORE (Réf. 7) (Fig. 15) ont signalé l'effet de cloisons de voilure et celui du braquage des élevons. Dans le même esprit les performances relatives de différentes configurations delta ont été présentées par C.W. SMITH et C.A. ANDERSON (Réf. 7) (Fig. 16).

* Notons plus précisément que cette portance est à considérer autant de façon relative par rapport au poids de l'avion (et à la poussée des moteurs dans le cas d'un avion à poussée orientable) qu'en absolu aérodynamique ($C_{z\ max} = f(\alpha, M, Re, C_\mu, etc...)$) et que le lien entre ces deux approches passe par la notion de charge alaire (cf. Réf. 5, Fig. 5).

Du point de vue de l'aérodynamicien, il est essentiel de maîtriser le problème du décrochage (décollement local ou généralisé de l'écoulement) et comme sur les ailes à forte flèche une grande partie de la portance est d'origine tourbillonnaire (cf. D. HUMMEL, Réf. 7, Fig. 17) il faut chercher à retarder l'éclatement des tourbillons d'apex et ne pas se laisser pénaliser par ceux qui prennent naissance au nez de l'avion, d'où l'importance de l'élancement de celui-ci (cf. A.M. SKOW et A. TITIRIGA Jr. Réf. 4, Fig. 18). L'influence du nombre de Reynolds sur ces écoulements a été rappelée par J. MIRANDE, V. SCHMITT et H. WERLÉ (cf. Réf. 7, Fig. 19).

Une limitation aérodynamique fréquemment rencontrée est le "buffeting" (tremblement). Il s'agit de vibrations déclenchées par des phénomènes aérodynamiques instationnaires très dépendants de la configuration de l'avion. Un exemple précis de variation de niveau vibratoire avec le braquage des volets a été donné par L.E. ERICSSON (Réf. 8) (Fig. 20) concernant le YF 16 CCV. De même l'effet des "onglets de voilure" a été signalé par G. MOSS (Réf. 7) (Fig. 21) sur un projet dérivé du Harrier.

Ce dernier avion nous amène à rappeler que le facteur de charge obtenu peut résulter d'une intégration propulsion/portance (soufflage de voilure, poussée orientable). Il faut bien dire que l'article de S.F. STAPLETON et B.V. PEGRAM (Réf. 2) (Fig. 22), s'il montre quelques configurations d'emport d'armes insiste sur l'aérodynamique de la voilure plutôt que sur la déflexion de la poussée. En revanche, L.D. WOLFE et A.E. FANNING (Réf. 5) (Fig. 23 et 24) ont donné quelques concepts de tuyères orientables et exemples de gains de limite de manoeuvre théoriquement possibles.

Pour clore ce chapitre sur la portance maximale utilisable nous dirons enfin que les effets d'aéroélasticité statique sont souvent oubliés dans les articles précités. Par exemple, T.M. WEEKS, G.C. UHUAD et R. LARGE (Réf. 11) (Fig. 25) n'en parlent pas explicitement dans le cas de la voilure à flèche inverse pour laquelle on manque en général de données.

## 4.2. - Les Qualités de Vol à grande incidence :

Il ne suffit pas qu'en théorie à une certaine incidence la voilure produise une certaine portance. Encore faut-il qu'en pratique le pilote puisse en disposer. D'abord il y a à respecter les limites structurales ce qui implique la détermination des charges aérodynamiques locales tant statiques qu'instationnaires ("buffeting", risque de flottement). Ensuite il faut que l'avion soit pilotable.

### 4.2.1. Stabilité statique longitudinale - Efficacité de gouvernes - Maniabilité.

Un compromis entre stabilité et maniabilité s'impose et il a des implications directes sur la configuration d'ensemble de l'avion : non seulement la voilure principale mais également les empennages (classiques ou canards) et les gouvernes doivent être dimensionnés et mis en place astucieusement. Un remarquable échantillon de caractéristiques de moments de tangage en fonction de la portance (ou de l'incidence) pour différentes configurations a été donné par A.J. ROSS et H.H.B.M. THOMAS (Réf. 9) (Fig. 27). Dans le cas d'une configuration delta sans empennage, W.T. KEHRER (Réf. 9) (Fig. 28) a bien résumé les principales limitations résultant à la fois des exigences de stabilité, de l'efficacité des gouvernes et en particulier du fait que les élevons peuvent être saturés à la fois en tangage et en roulis. Une autre comparaison des effets fastes et néfastes de la stabilité longitudinale statique a été présentée par P. BOHN (Réf. 5) (Fig. 29) en ce qui concerne les Mirage III, F 1, G 8A et 2000. Il est certain qu'autrefois on exigeait une stabilité longitudinale statique positive jusqu'à l'incidence de décrochage (centre de gravité placé en avant du foyer aérodynamique) ce qui s'accompagnait d'hyperstabilité, soit à grande incidence, soit en transsonique, du fait du recul important du foyer (cf. les figures précédentes 27, 28 et 29). En plus on n'était pas à l'abri d'accidents de stabilité (du genre autocabrage ou autre) survenant parfois même à des incidences modérées. Dans l'article de T.S. WEBB, D.R. KENT et J.B. WEBB (Réf. 6) sur le F 16, la comparaison de la figure 30 qui montre des $C_z$ non équilibrés allant jusqu'à 1,75 et de la figure 31 où ils sont limités vers 0,9 laisse présager la difficulté des problèmes d'équilibrage que l'on peut rencontrer. Les effets particuliers de l'aéroélasticité sur la stabilité ont été évoqués par W.T. KEHRER (Réf. 9) (Fig. 26).

Il faut noter que l'apport du Contrôle Automatique généralisé dans ce domaine est décisif. Nous y reviendrons dans un chapitre spécial.

Le manque de contrôle longitudinal à grande incidence peut provenir d'une diminution d'efficacité des gouvernes classiques et certains auteurs ont proposé un soufflage des gouvernes ou l'utilisation de gouvernes nouvelles, par exemple onglet mobile comme G. MOSS (Réf. 7) (Fig. 32).

A faible vitesse la pression dynamique est de toute façon insuffisante et certains comme W.T. KEHRER (Réf. 9) (Fig. 33) ont proposé l'orientation du vecteur-poussée comme moyen de contrôle. A grande vitesse c'est au contraire la saturation des servo-commandes qui peut être cause de la réduction de maniabilité.

Une dernière mention doit être faite. Elle concerne les limitations de manoeuvrabilité qui résultent d'une perte d'un circuit hydraulique ou d'un endommagement des gouvernes, dus à une panne ou à l'impact de projectiles. Une maniabilité minimale doit être assurée dans ce cas. Ce problème a été évoqué par Lt Cl REMERS (Réf. 3).

4.2.2. Stabilité statique transversale - Couplage longitudinal/latéral

Ce qui précède concernait surtout le mouvement longitudinal de l'avion. Mais la stabilité statique transversale est également source de gros problèmes à résoudre. L'idéal serait évidemment que, jusqu'aux plus grandes incidences utiles sur le plan opérationnel, l'avion ne présente pas d'instabilité de route. Pour cette raison par exemple la taille relative des dérives des avions s'est régulièrement accrue comme l'a rappelé D.J. WALKER (Réf. 9) (Fig. 34) ce qui devait malheureusement se payer par une augmentation corrélative de masse et de trainée. La comparaison entre l'efficacité d'une ou de deux dérives, l'utilisation de quilles, et l'effet en général néfaste des charges emportées sous fuselage ou voilure a déjà été signalé par H. WUNNENBERG et W.J. KUBBAT (Réf. 5) (Fig. 35) et par B.R.A. BURNS (Réf. 1) (Fig. 36). Cependant encore une fois le problème aérodynamique à grande incidence, est sans doute lié aux éclatements de tourbillons. L'évolution typique des coefficients aérodynamiques, telle que représentée par J.R. CHAMBERS, W.P. GILBERT et L.T. NGUYEN (Réf. 4) (Fig. 37), dépend donc surtout de la forme du nez (cf. A.M. SKOW, A. TITIRIGA Jr.et W.A. MOORE, Réf. 7, Fig. 38), de la présence ou non de virures, de moustaches ou d'onglets (cf. A.M. SKOW et A. TITIRIGA Jr. Réf. 4, Fig. 39 et 40), de canards (cf. W.T. KEHRER, Réf. 9, Fig. 41). De très belles visualisations des écoulements tourbillonnaires éclatés ont été réalisées dans l'eau et signalées par A.M. SKOW, A. TITIRIGA Jr.et W.A. MOORE (Réf. 7) (Fig. 42), même s'il n'est pas sûr qu'au nombre de Reynolds du vol on retrouve bien la même structure d'écoulement. Par ailleurs, des phénomènes d'instabilité des tourbillons et d'hystérésis en fonction de l'incidence ont été souvent rapportés (cf. K.J. ORLICK-RUCKEMANN, Réf. 7, Fig. 43).

La mécanique du vol traditionnellement enseignée découple de façon excessive les mouvements longitudinaux et transversaux. Néanmoins des phénomènes importants de couplage, même en statique, ont été indiqués par D.E. JOHNSTON (Réf. 4) (Fig. 44) à propos du F.4 Phantom ou par A.M. SKOW, A. TITIRIGA Jr. et W.A. MOORE (Réf. 7) (Fig. 45) pour différentes formes de nez d'avions.

4.2.3. Stabilités dynamiques - Réponses transitoires aux commandes

Au-delà des équilibres et des stabilités statiques, le comportement dynamique de l'avion est évidemment un sujet important. En longitudinal on souhaiterait avoir suffisamment d'amortissement pour que la réponse à la profondeur, souhaitée rapide soit cependant assez pure et que le risque de dépasser l'incidence ou le facteur de charge maximal soit aussi faible qu possible, ainsi que le risque de pompage piloté. En transversal de même, il ne faut pas que les ordres du pilote déclenchent des oscillations divergentes de type linéaire (roulis hollandais) ou cycle-limite ("wing rock") ou des échappées non contrôlées en roulis ("wing drop") ou en lacet ("nose slice"). Du point de vue du mécanicien du vol, c'est en fait la combinaison des stabilités statiques et dynamiques, longitudinales et transversales, des efficacités et effets secondaires des gouvernes (y compris et surtout les non-linéarités, hystérésis, etc....) qui conditionne le comportement global de l'avion. Des exemples de "wing rock" ont été donnés par J.R. CHAMBERS, W.P. GILBERT et L.T. NGUYEN (Réf. 4) et par D.E. JOHNSTON (Réf. 4) (Fig. 46) qui montrent bien également l'évolution des modes propres de l'avion avec l'incidence et le dérapage. La modélisation mathématique de ce cas de vol reste problématique. Les aérodynamiciens ont introduit de nouveaux coefficients, ou cherché à étudier l'influence d'une rotation permanente sur l'aérodynamique de l'avion. Les principaux montages tournants en service ont été rappelés par L.E. ERICSSON (Réf. 8) (Fig. 47) et des comparaisons de coefficients en oscillation et en rotation ont été présentées par K.J. ORLICK-RUCKEMANN (Réf. 7) (Fig. 48).

4.2.4. Résistance à la vrille

Il n'est cependant pas facile de dessiner des configurations résistant à la vrille. De nombreux critères ont été proposés : LCDP, $Cn_\beta$ dynamique, Kalviste, Weissman, etc... L'article de A.M. SKOW et A. TITIRIGA Jr. déjà cité (Réf. 4) fait remarquablement le point sur le sujet. On ne saurait conseiller mieux que de le relire attentivement. Les figures 49, 50, 51, 52 en sont extraites à titre d'exemples. Notons enfin que, dans ce domaine, le Contrôle Automatique Généralisé apportera certainement une fois encore des gains fantastiques.

4.2.5. Maniabilité latérale :

Les problèmes de stabilité dynamique transversale nous amènent tout naturellement à parler de maniabilité en roulis, le renversement du sens de virage, rapide et sans danger de perte de contrôle, étant une nécessité en combat aérien.

Différents auteurs comme W.T. KEHRER (Réf. 9) (Fig. 53) et O. SENSBURG et H. ZIMMERMANN (Réf. 5) (Fig. 54) ont montré les avantages respectifs d'ailerons, d'élevons, de spoïlers, de la poussée orientable et de l'interconnexion roulis-lacet, pour satisfaire les besoins de maniabilité en roulis présentés sur les Fig. 1, 3 et 4.

Nous reviendrons à propos du Contrôle Automatique Généralisé sur les limitations qu'on est encore obligé d'imposer à la maniabilité en roulis.

4.3. - Fonctionnement et rendement des entrées d'air et moteurs :

Si les qualités de vol de l'avion lui confèrent des capacités d'évolution accrues, il faut s'assurer aussi que les équipements et surtout le moteur supportent ces conditions de vol extrêmes. Le fonctionnement des entrées d'air à grande incidence et leur rendement fait l'objet de nombreuses études. P. BOHN (Réf. 5) (Fig. 55) a montré les progrès réalisés sur Mirage 2000 par rapport au Mirage F1, J. DUNHAM (Réf. 5) (Fig. 56) a donné des exemples relatifs aux F15 et F16, tandis que K.W. LOTTER et L. MALEFAKIS (Réf. 7) (Fig. 57, 58, 59 et 60) ont présenté des solutions envisageables pour le futur et les avantages relatifs qu'il y a à placer des entrées d'air sous fuselage, sous onglet, ou sous canard, avec ou sans dispositifs mobiles.

4.4. - Les performances en évolution (Taux d'accélération - Facteur de charge maximal soutenu).

Les aspects précédemment évoqués concernaient surtout les qualités de vol. Le chapitre des performances est le deuxième qu'il est essentiel d'associer à la notion de manoeuvrabilité. Il faut d'abord parler de la possibilité d'accélérer rapidement sur trajectoire ou de freiner brutalement ce qui présente un grand avantage tactique. On voit donc se poser la question de la rapidité de réponse du moteur et d'allumage de la réchauffe à partir d'un régime d'attente intermédiaire. Ceci a été traité dans certains symposiums du Propulsion and Energetics Panel. Il faut également prendre en considération le bilan poussée-trainée à incidence et facteur de charge faibles. Un bon exemple des objectifs visés par rapport à ce que font les chasseurs actuels est donné par R.D. CHILD, G. PANAGEAS et P. GINGRICH (Réf. 10) (Fig. 61) à propos du véhicule télépiloté Hi Mat. On doit immédiatement y associer le bilan poussée-trainée à incidence et facteur de charge moyens ou grands qui gouverne la notion de marge de manoeuvre (facteur de charge maximal soutenu). Des auteurs comme P. BOHN (Réf. 5) (Fig. 62) en ce qui concerne l'effet des becs du Mirage 2000, où RF. SIEWART et R.E. WHITEHEAD (Réf. 5) (Fig. 63) pour la programmation des becs et volets du F18 Hornet ont montré les gains de finesse qu'il est possible de réaliser aujourd'hui. L'avenir pourrait être dans les profils continuement déformables présentés par R.F. SIEWART et R.E. WHITEHEAD (Réf. 5) (Fig. 64) et D.S. WOODWARD, R.F.A. HEATING et C.S. BARNES (Réf. 9) (Fig. 65). L'objectif de meilleure finesse explique aussi pourquoi on revient parfois à des ailes avec moins de flèche et davantage d'allongement. Par ailleurs, les contraintes de stabilité longitudinale et transversale classiques ont des implications néfastes (trainée d'équilibrage, trainée de frottement et masse de grands empennages), c'est pourquoi la stabilité artificielle, premier pas dans le Contrôle Automatique Généralisé, permet des gains spectaculaires. En parallèle, l'amélioration du rapport poussée/poids (voir Fig. 5) qui tend à devenir supérieur à 1 à basse altitude augmente aussi les performances. On voit arriver le moment où la manoeuvrabilité serait telle qu'à la limite de résistance des structures (8 ou 9 g) l'avion pourrait encore accélérer. On ressent alors le besoin de pouvoir freiner et l'utilisation d'aérofreins ou de la reverse en vol peut s'imposer (cf. Réf. 5) (Fig. 23).

4.5. - Le Contrôle Automatique Généralisé :

Quelles sont les nouvelles possibilités offertes par le Contrôle Automatique Généralisé ?

4.5.1. La stabilité artificielle

Tout d'abord nous avons déjà évoqué le vol à stabilité longitudinale statique réduite, voire même négative (avec stabilisation artificielle) qui apporte des avantages immédiats :

- diminution de trainée d'équilibrage, donc meilleure finesse, meilleures marges de manoeuvre comme rappelé par R.A. WHITMOYER (Réf. 4) (Fig. 66) et J. STALONY-DOBRZANSKI et N. SHAH (Réf. 8) (Fig. 67),

- diminution de la taille des empennages, et même de l'avion complet, d'où gain de masse et de manoeuvrabilité comme l'a rappelé P.R. KURZHALS (Réf. 8) (Fig. 68),

- diminution de la déportance d'équilibrage, ou ce qui revient au même, augmentation de la portance maximale de l'avion complet, donc meilleure limite de manoeuvre.

Remarquons cependant que la combinaison d'un cas de vol à grande incidence avec une marge statique négative introduit un risque supplémentaire de perte de contrôle si l'on approche du moment où les gouvernes de profondeur arrivent en butée (à piquer dans ce cas). Ceci est très bien illustré par W.T. KEHRER (Réf. 9) (Fig. 69). Une circonstance aggravante est un ordre en roulis au même moment (couplage par inertie faisant cabrer et déraper l'avion). C'est pourquoi la plupart des constructeurs s'orientent vers une solution du genre limiteur automatique de domaine (incidence, taux de roulis) comme signalé par A.M. SKOW, W.A. MOORE et D.J. LORINCZ (Réf. 9) (Fig. 70) par exemple.

La possibilité de créer une stabilité transversale artificielle permet aussi de réduire la taille des dérives ou d'accroître le domaine en incidence. Mais sur ce dernier point les avis sont partagés, car les accidents aérodynamiques engendrés par des éclatements de tourbillons de nez ou d'apex peuvent avoir des effets d'un ordre de grandeur supérieur à l'efficacité des gouvernes de direction (cf. Fig. 38, 39, 42 43).

Remarquons en outre que sur un avion à Contrôle Automatique Généralisé la notion de stabilité dynamique proprement dite perd de son intérêt. En revanche, la réponse initiale de l'avion aux ordres du pilote peut être améliorée (cf. J. STALONY-DOBRZANSKI et N. SHAH (Réf. 8) (Fig. 71), mais elle peut aussi déconcerter l'utilisateur par son caractère artificiel (soit qu'elle corresponde à un système d'équations différentielles d'ordre plus élevé que sur l'avion naturel, soit que la digitalisation des commandes de vol électriques introduise des retards purs ou des sauts, eux-mêmes sources potentielles de pompage piloté), et aussi parce qu'on manque de critères efficaces (insuccès relatif de la notion de $C^*$ par exemple) pour la conception des lois de pilotage.

Ces points ont été abondamment développés dans l'AGARDograph n° 234 (Réf. 14), en particulier dans l'article de K.J. SZALAI, S.R. BROWN et K.L. PETERSEN de la NASA Dryden.

4.5.2. L'anti-flottement et l'anti-turbulence

Parmi les autres avantages apportés de façon indirecte par le CAG, nous pourrions encore citer le contrôle du flottement des structures, surtout avec charges externes, qui devrait permettre d'alléger l'avion donc d'améliorer la charge alaire donc la manoeuvrabilité, mais n'est sans doute pas près d'être utilisé en série, et les dispositifs anti-turbulence. Ceux-ci ont un effet indirect sur la manoeuvrabilité, en particulier pour un avion qui serait polyvalent : pénétration à basse altitude ou appui tactique et combat tournoyant. En effet, la manoeuvrabilité requiert une assez faible charge alaire ce qui donne une très forte réponse à la rafale et c'est pourquoi on limite parfois la surface de voilure. La levée de cette contrainte par un dispositif anti-turbulence permettrait des gains de manoeuvrabilité importants.

4.5.3. Le Contrôle Direct de Forces

Un dernier avantage qu'apporte le Contrôle Automatique Généralisé est la possibilité de découpler les forces et les moments, ou autrement dit le contrôle direct de forces. Cela permet de dépointer le fuselage (effet de tourelle) à trajectoire constante ou de moduler la trajectoire à cap et assiettes constants. (Voir F.R. SWORTZEL et Dr. J.D. Mc. ALLISTER (Réf. 8) et R.A. WHITMOYER (Réf. 4) (Fig. 72)). Certains auteurs ont montré, à partir de l'expérience en vol sur YF 16 que cela apporterait un avantage opérationnel certain (Notons d'ailleurs que ces nouveaux modes de pilotage sont sans doute essentiels pour la fonction anti-turbulence). Dans le même esprit une meilleure régulation du moteur, entrées d'air et tuyère (y compris la reverse en vol) améliorerait la rapidité de contrôle de la vitesse. On peut citer l'article de F.R. SWORTZEL et Dr. J.D. McALLISTER (Réf. 8) (Fig. 73) qui indique des autorités-objectifs pour ces nouveaux degrés de liberté, et (Fig. 74) qui donne les résultats atteints sur YF 16. Remarquable est le papier de R.A. WHITMOYER (Réf. 4) (Fig. 75) qui montre en contrepartie ce qu'on risque de perdre en performances lorsqu'on effectue de telles manoeuvres de dépointage.

4.6. - Problèmes médicaux - Aspects ergonomiques :

Après cette revue technique nous souhaiterions rappeler le Specialists Meeting organisé par l'Aerospace Medical Panel (Réf. 15) où fut montrée entre autres l'importance de la dérivée par rapport au temps du facteur de charge (nombre de Jolt). La brutalité accrue des manoeuvres que pourront réaliser les avions futurs ne sera supportable par l'équipage que moyennant une meilleure disposition des cabines et des organes de commande, en particulier en jouant sur l'inclinaison du siège comme signalé par H.E. VON GIERKE (Réf. 3) (Fig. 76 et 77) et A.G. BARNES (Réf. 5) (Fig. 78). La question de la présentation des informations au pilote (en particulier pour le pilotage des modes nouveaux) constitue également un chapitre de l'ergonomie très vaste et qui sort du cadre que nous nous sommes ici fixé.

5. - Conclusion :

Une bonne manoeuvrabilité est pour les avions d'armes un facteur décisif de supériorité en combat aérien.

L'AGARD (en particulier le FMP et le FDP) a abordé ce sujet d'une manière ou d'une autre dans la plupart des réunions de ces dernières années, comme nous avons essayé de le montrer. Notre exposé n'aura été qu'un survol rapide, une série très limitée d'exemples choisis, il faut bien le dire, avec un certain arbitraire, devant l'abondance de la matière disponible. Puissent les auteurs non cités ou mal cités nous comprendre et nous pardonner !

Une remarque doit être faite : ce thème de la manoeuvrabilité est un sujet assez confidentiel et beaucoup d'articles publiés dans le passé ont vu leur intérêt sérieusement réduit parce que les auteurs ont dû masquer les valeurs numériques relatives à tel ou tel avion par souci de discrétion.

Ceci explique pourquoi le Comité de Programme Technique chargé d'organiser le présent Symposium qui vise à couvrir en une seule fois les principaux aspects de la question (Besoins Opérationnels, Espoirs d'amélioration, Méthodes de Prédiction, Méthodes d'Evaluation) a choisi de tenir ces conférences dans un cadre Confidentiel-OTAN. Cette protection devrait permettre, nous l'espérons, davantage de liberté d'expression, pour le plus grand profit de toute la communauté AGARD.

Références :


1/ CP 119 : Stability and Control
FMP Meeting held in Braunschveig, Germany, on 10-13 April 1972

2/ CP 187 : Flight/Ground testing facilities correlation
FMP Meeting held at Valloire, France, on 9-13 June 1975

3/ CP 212 : Aircraft operational experience and its impact on safety and survivability
FMP Symposium held at Sandefjord, Norway, 31 May-3 June 1976

4/ CP 235 : Dynamic Stability Parameters
FDP Symposium held in Athens, Greece, 22-24 May 1978

5/ CP 241 : Fighter Aircraft Design
Multi-Panel Symposium on Fighter Aircraft held at the Scuola di Guerra Aerea, Florence, Italy, 3-6 October 1977

6/ CP 242 : Performance Prediction Methods
FMP Specialists Meeting held in Paris, France, 11-13 October 1977

7/ CP 247 : High Angle of Attack Aerodynamics
FDP Symposium held at Sandefjord, Norway, on 4-6 October 1978

8/ CP 260 : Stability and Control
FMP Symposium held in Ottawa, Canada on 25-28 September 1978

9/ CP 262 : Aerodynamic Characteristics of Control
FDP Symposium held in Pozzuoli, Italy, on 14-17 May 1979

10/ CP 280 : The Use of Computers as a Design Tool
FMP Symposium held in Neubiberg, Germany, 3-6 September 1979

11/ CP 285 : Subsonic/Transonic Configuration Aerodynamics
FDP Symposium held in Munich/Neubiberg, Germany, 5-7 May 1980

12/ AR 82 : The Effects of Buffeting and other Transonic Phenomena on Maneuvering Combat Aircraft
FMP report prepared by a working group sponsored by the Flight Mechanics Panel (July 1975)

13/ AR 155 : Manoeuvre Limitations of Combat Aircraft
FMP report prepared by a working group sponsored by the Flight Mechanics Panel (August 1979)

14/ AG 234 : Active Controls in Aircraft Design
AGARDograph prepared at the request of the Guidance and Control Panel (November 1978)

15/ CP 266 : Operational Roles, Aircrew Systems and Human Factors in Future High Performance Aircraft
Aerospace Medical Panel's Specialists Meeting held in Lisbon, Portugal, 22-26 October 1975.

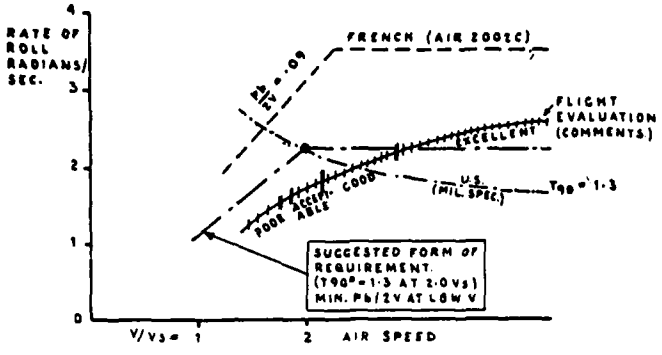


RATE OF ROLL REQUIREMENTS COMPARED WITH PILOT COMMENT FROM FLIGHT EVALUATION

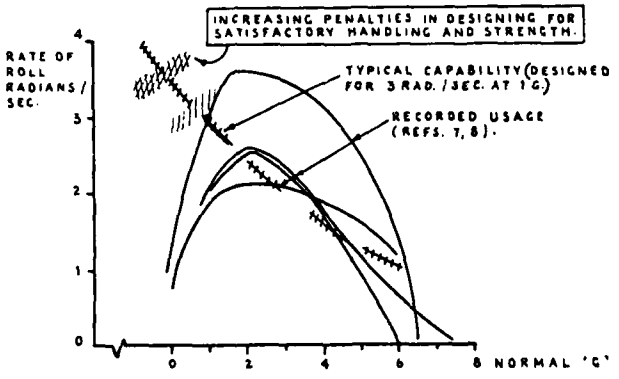


RATE OF ROLL VARIATION WITH NORMAL ACCELERATION.

Fig. 1 (Extrait de CP 119 papier n° 7)

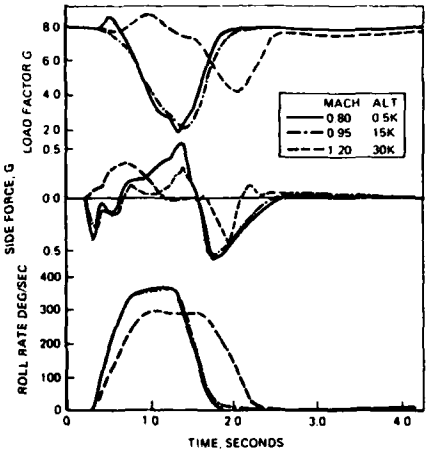


MAXIMUM ROLL RATE MANEUVER AT 8G TRIM

Fig. 3 (Extrait de CP 260 papier n° 7)

**VARIATION OF BATTLE ARENA IN SIMULATED AIR COMBAT**

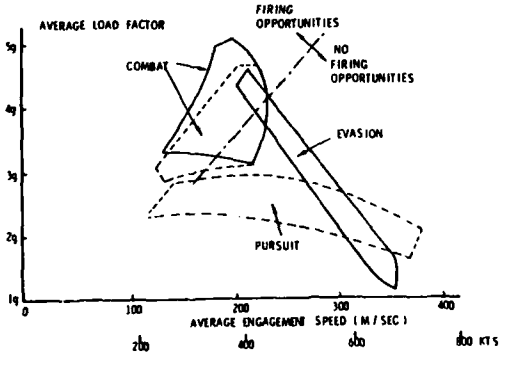


Fig. 2 (Extrait de CP 187 papier n° 20 B)

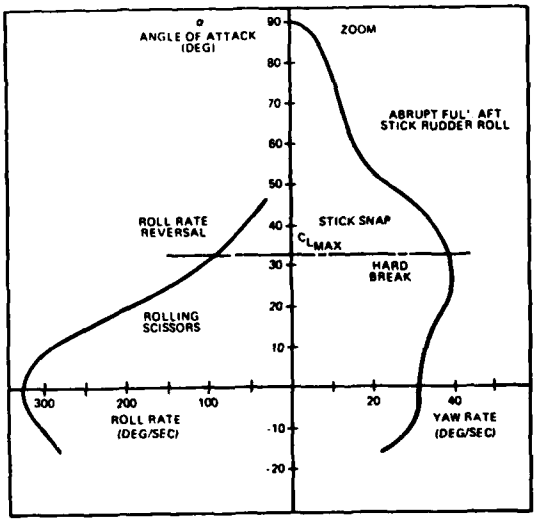


TYPICAL HIGH PERFORMANCE FIGHTER ACM GROSS MANEUVER ENVELOPE

Fig. 4 (Extrait de CP 262 papier n° 24)

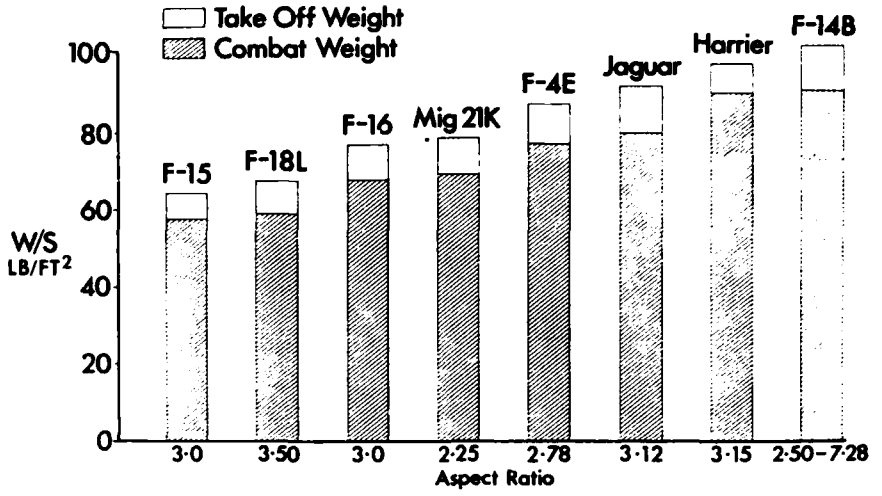


Wing loading comparison

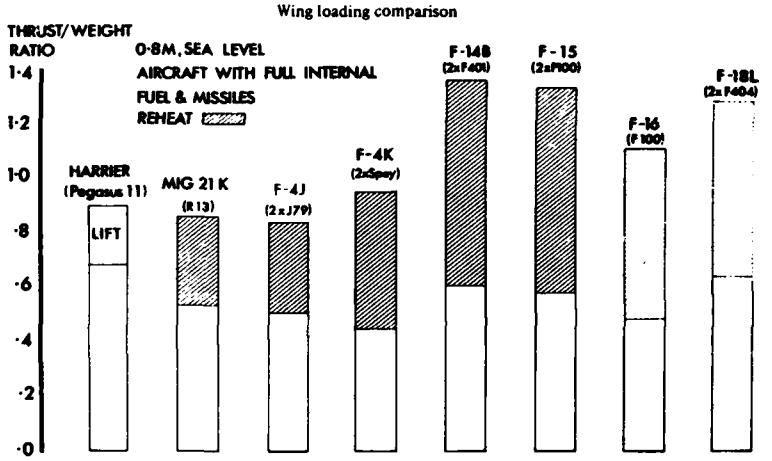


Thrust/weight ratio comparison

Fig. 5 (Extrait de CP 241 papier n° 2)

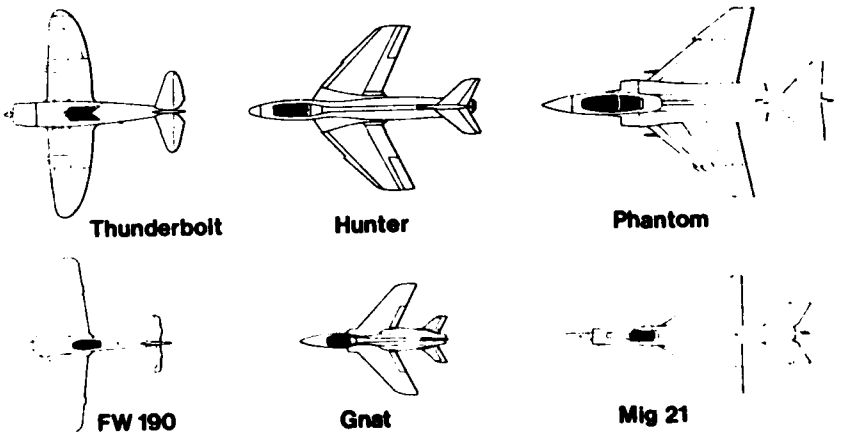


Fighter comparison

Fig. 6 (Extrait de CP 241 papier n° 2)

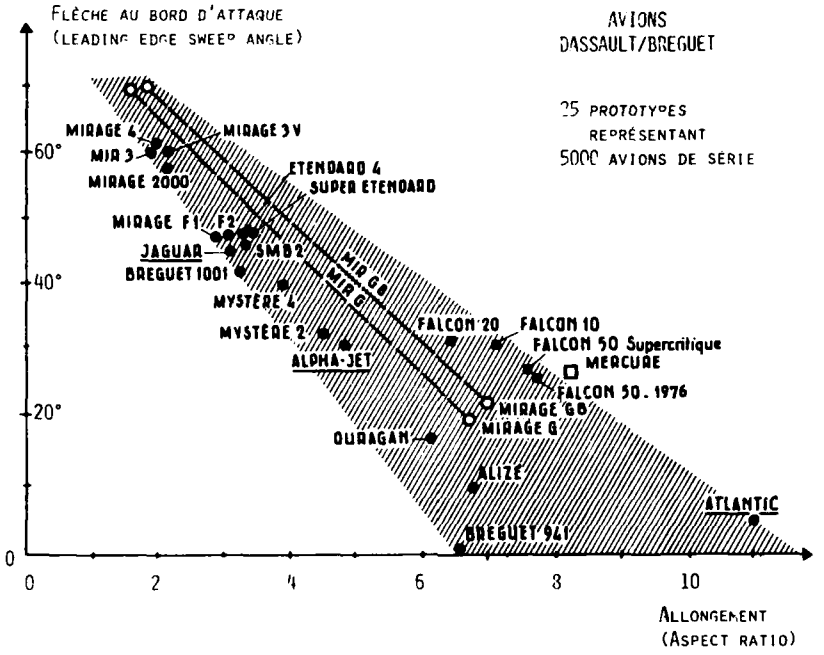


Fig. 7 (Extrait de CP 242 papier n° 12)

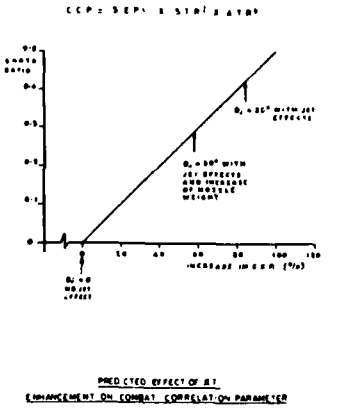

Fig. 8 (Extrait de CP 285 papier n° 17)

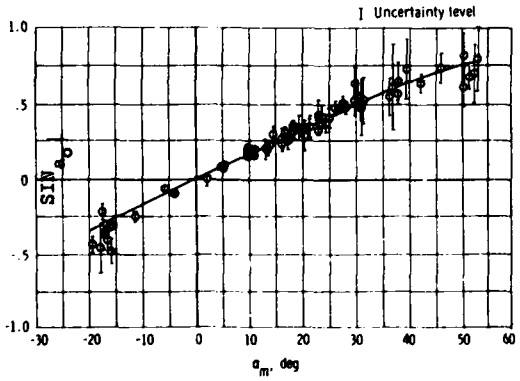


*Comparison of angle of attack estimated from flight data and measured angle of attack.*

Fig. 10 (Extrait de CP 235 papier n° 15)

**INFLUENCE OF HANDLING QUALITIES ON USEABLE LIFT CAPABILITY**

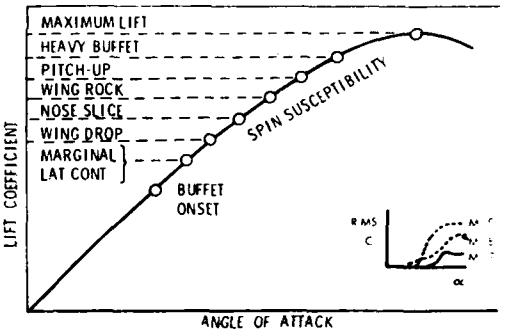


**COMBAT MANEUVERING BOUNDARIES LIMITED BY AERODYNAMIC STABILITY & CONTROL DEGRADATION**

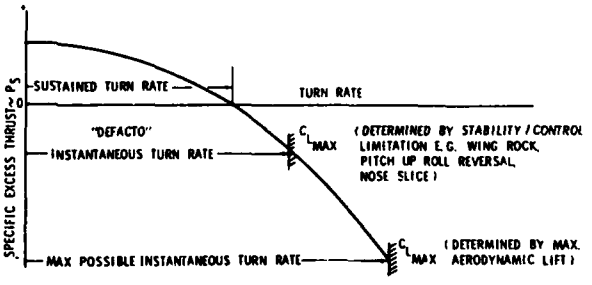


Fig. 9 (Extrait de CP 187 papier n° 20 B)

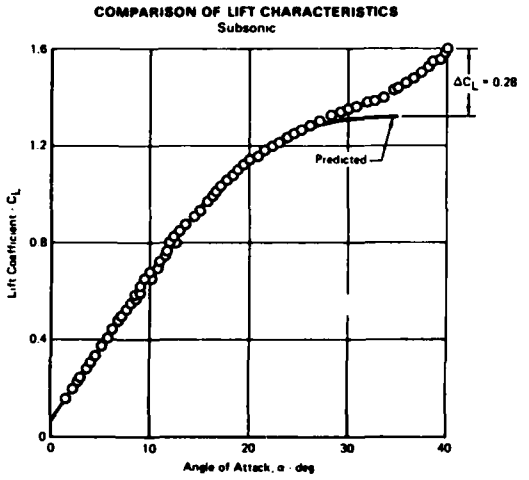


Fig. 11 (Extrait de CP 242 papier n° 17)

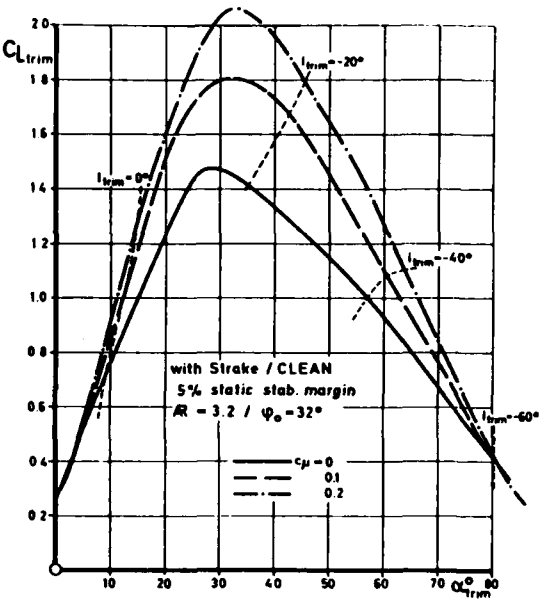


TRIMMED LIFT POLARS FOR DIFFERENT BLOWING INTENSITIES $c_\mu$

Fig. 12 (Extrait de CP 247 papier n° 8)

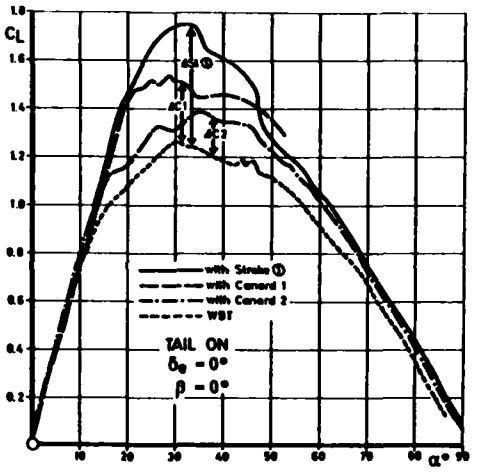


EFFECT OF STRAKE OR CANARDS ON LIFT

Fig. 13 (Extrait de CP 247 papier n° 8)

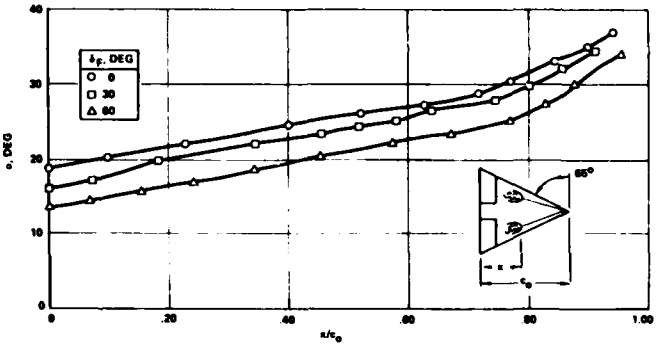


EFFECT OF DEFLECTED TRAILING-EDGE FLAP ON VORTEX BREAKDOWN

Fig. 15 (Extrait de CP 247 papier n° 6)

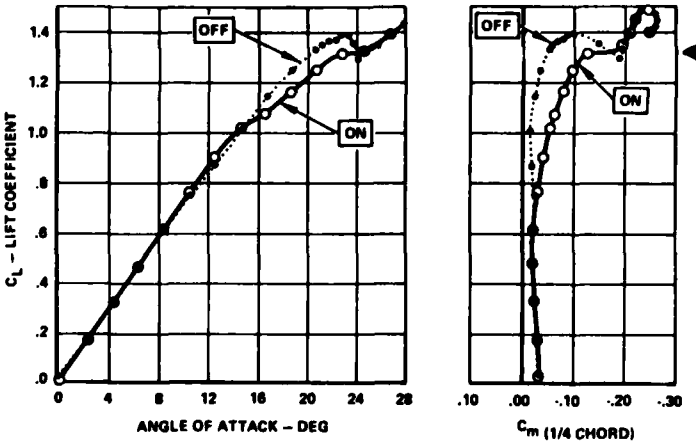


EFFECT OF WING FENCES IN PITCH

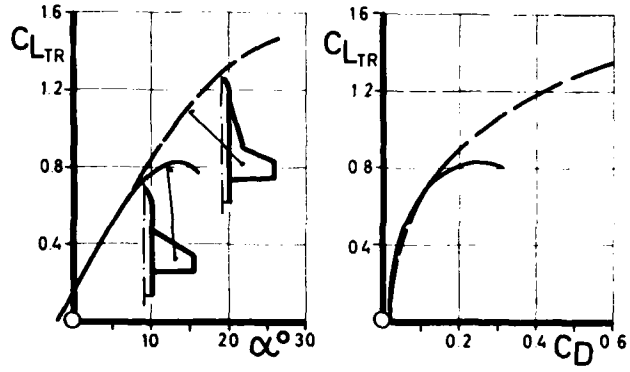


EFFECT OF STRAKES ON TRIMMED LIFT AND DRAG CHARACTERISTICS
(M = 0.8, 5% STABILITY MARGIN)

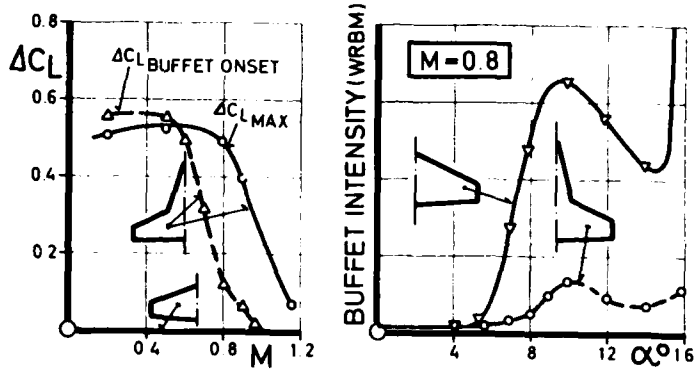


IMPROVEMENT OF MANOEUVRE BOUNDARIES DUE TO STRAKE
(WING-BODY, CLEAN)

Fig. 14 (Extrait de CP 235 papier n° 11)

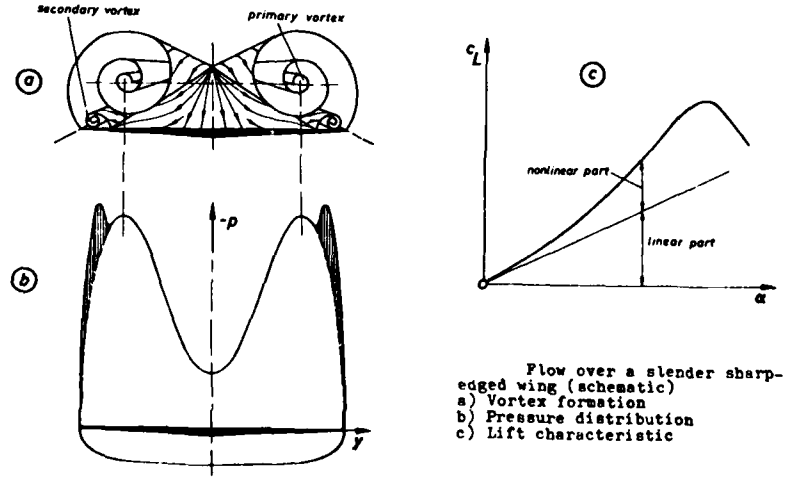


Flow over a slender sharp-edged wing (schematic)
a) Vortex formation
b) Pressure distribution
c) Lift characteristic

Fig. 17 (Extrait de CP 247 papier n° 15)

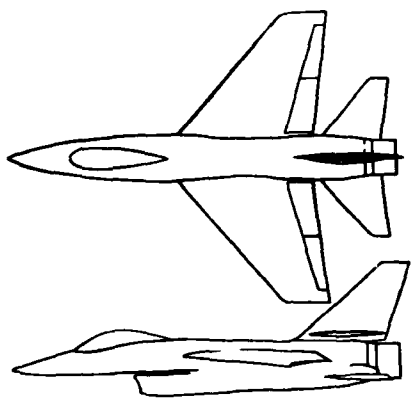

Sketch of Configuration 785

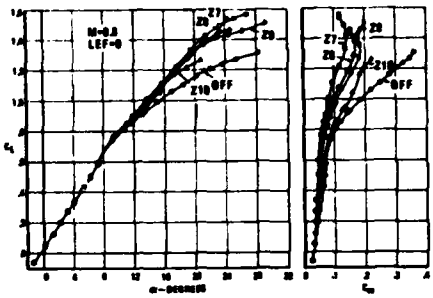


Lift Effects of a Family of Delta Planform Forebody Strakes on Configuration 785

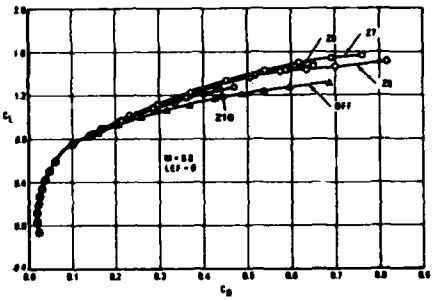


Drag Effects of a Family of Delta Planform Forebody Strakes on Configuration 785

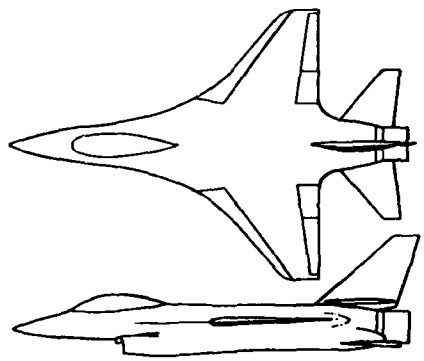

Sketch of Configuration 401F-5

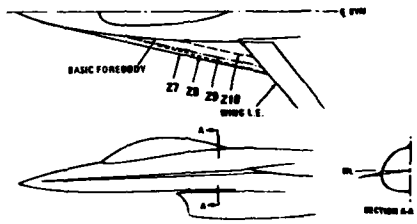


Delta Planform Strakes on Configuration 785

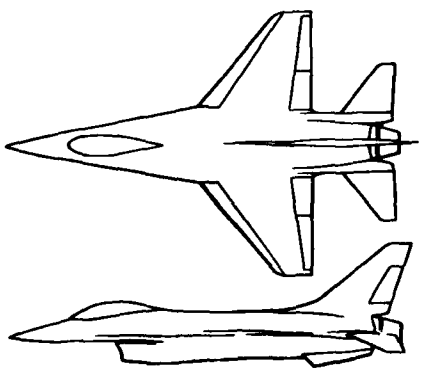

Sketch of Configuration 401F-18A

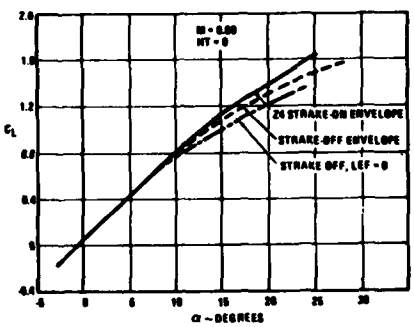


Effect of Forebody Strake on the Envelope Lift Curve

Fig. 16 (Extrait de CP 247 papier n° 5)

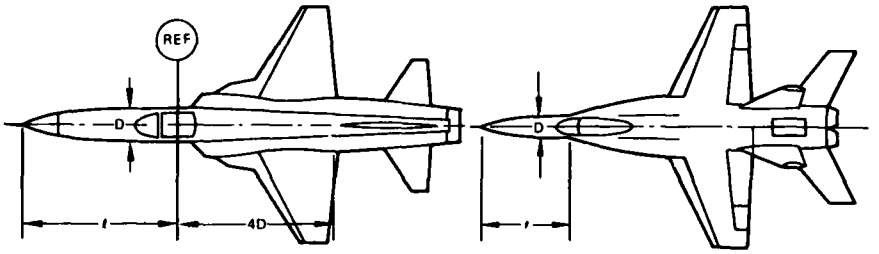


DEFINITION OF FINENESS RATIO

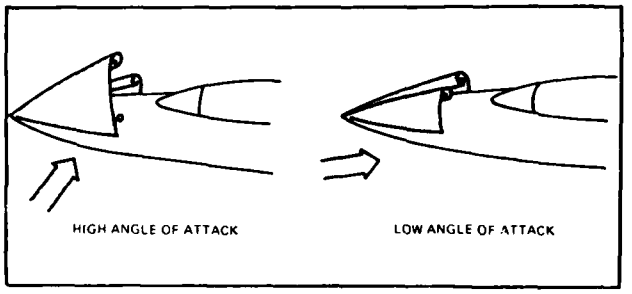


FOREBODY VORTEX PATTERNS

Fig. 18 (Extrait de CP 235 papier n° 19)

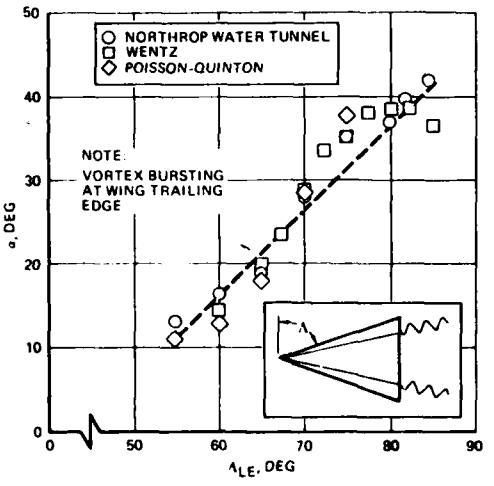


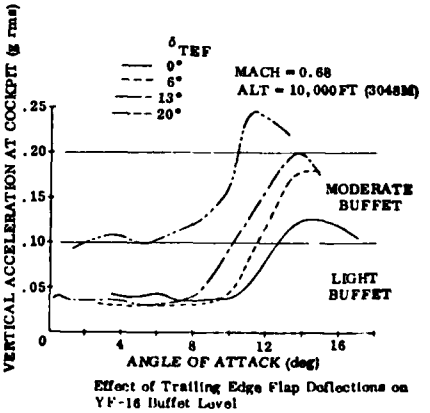


Effect of Trailing Edge Flap Deflections on YF-16 Buffet Level

Fig. 20 (Extrait de CP 260 papier n° 2)

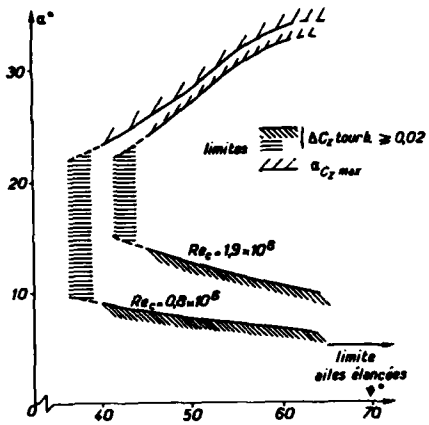


– Domaine d'existence des écoulements tourbillonnaires.

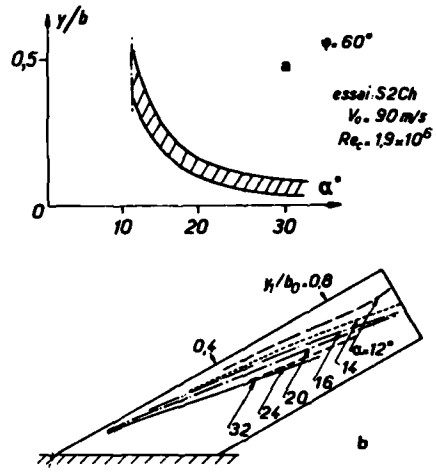


– Caractéristiques de l'écoulement tourbillonnaire
a) évolution de l'origine du tourbillon en fonction de l'incidence ;
b) positions approximatives de l'axe tourbillonnaire en fonction de l'incidence.

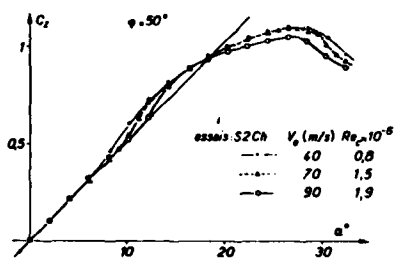


– Influence du nombre de Reynolds sur la portance.

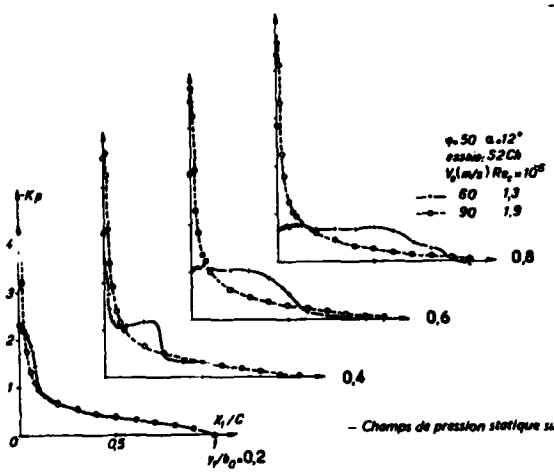


– Champs de pression statique sur l'extrados. Effet du nombre de Reynolds.

**Fig. 19 (Extrait de CP 247 papier n° 12)**

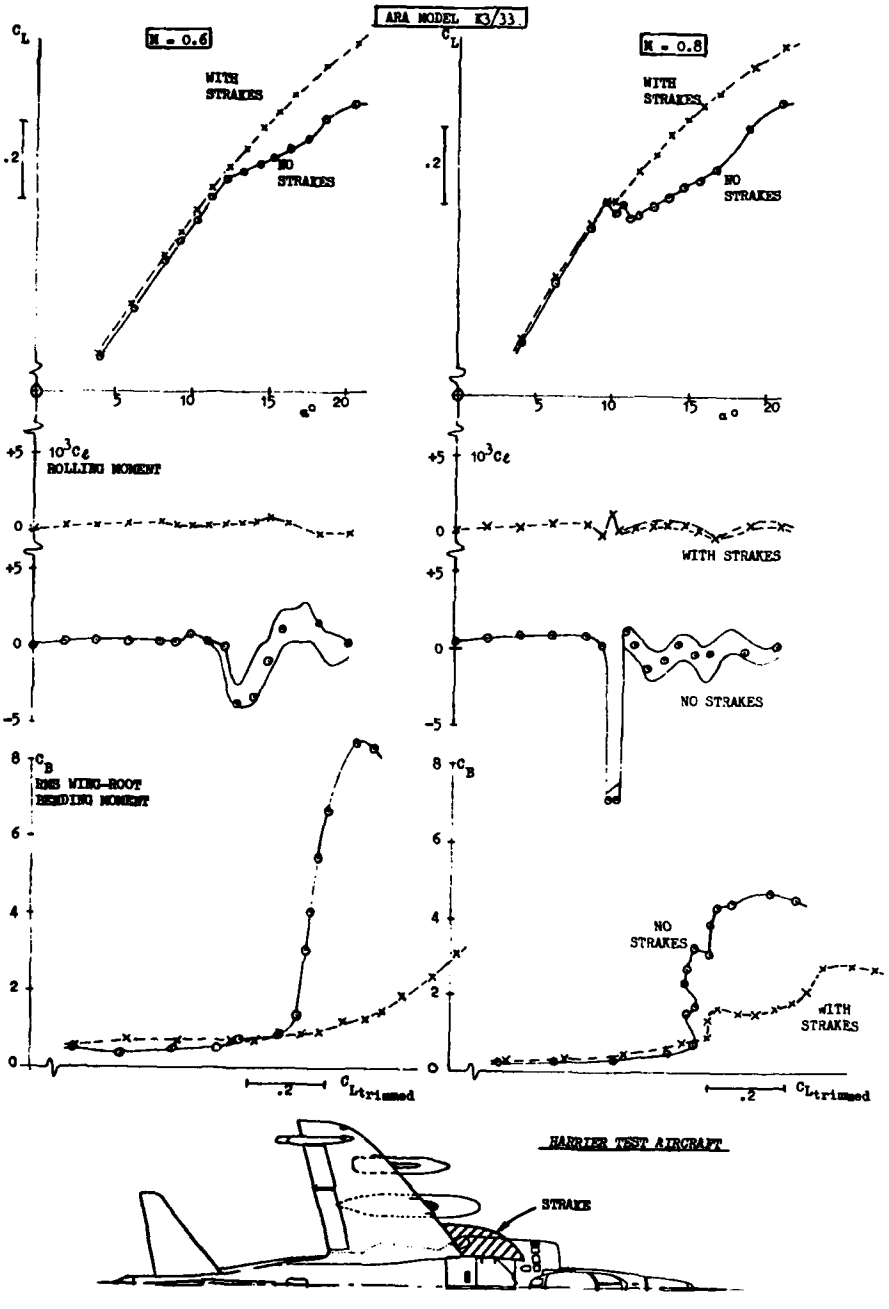


Effect of strakes on wing buffeting and unsteady rolling

Fig. 21 (Extrait de CP 247 papier n° 4)

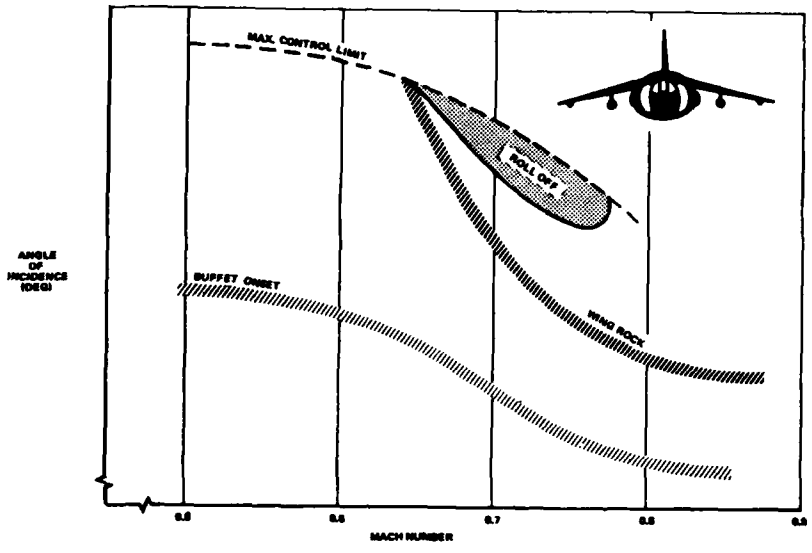


FLIGHT HANDLING LIMITS

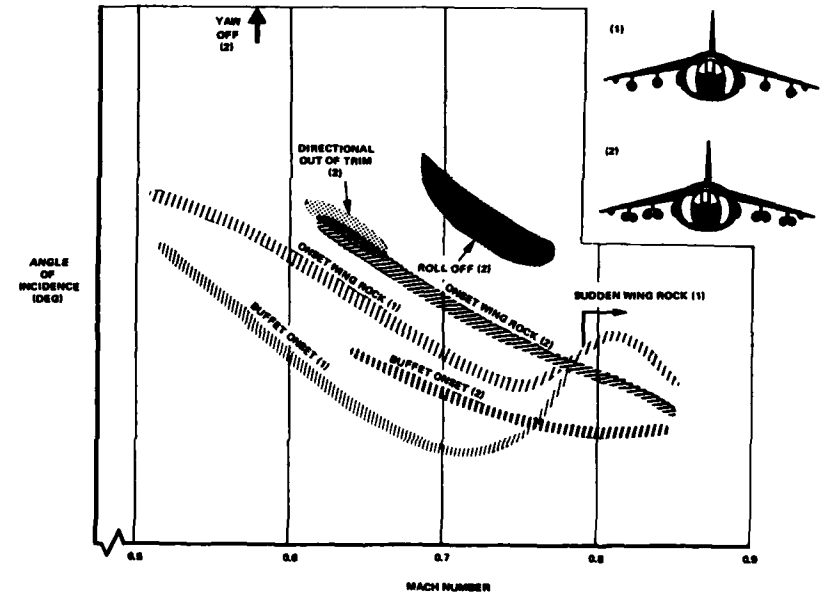


FLIGHT HANDLING LIMITS

Fig. 22 (Extrait de CP 187 papier n° 20 A)

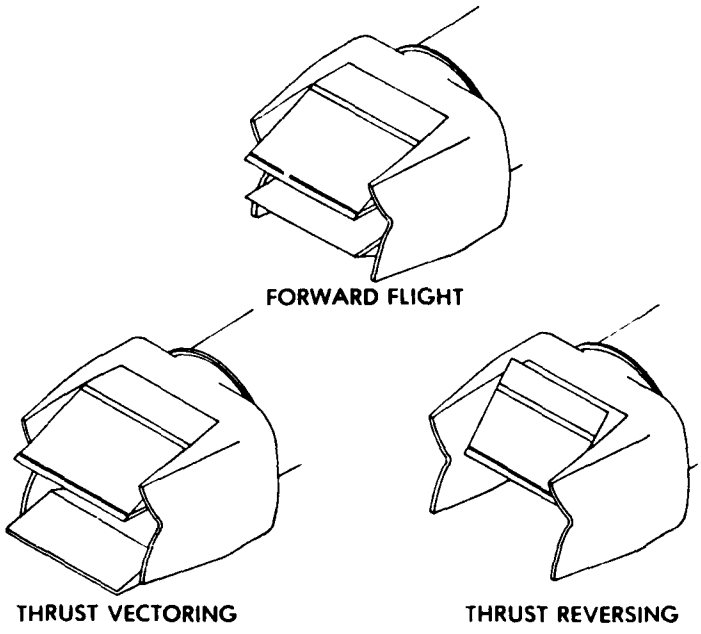


Two-Dimensional, Convergent-Divergent Nozzle

Fig. 23 (Extrait de CP 241 papier n° 17)

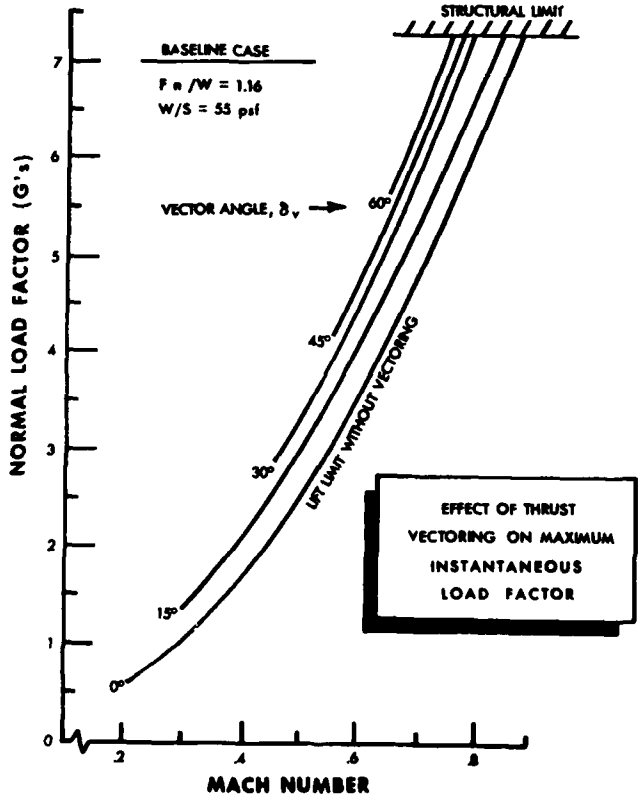


Effect on Instantaneous Normal Load Factor

Fig. 24 (Extrait de CP 241 papier n° 17)

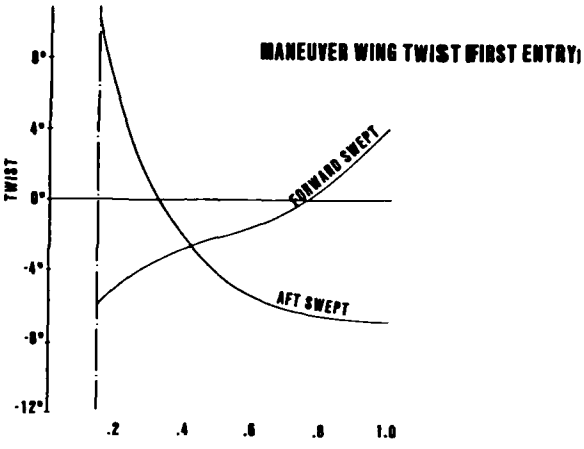


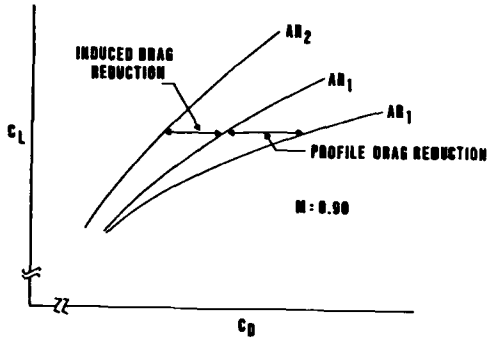


FORWARD SWEPT WING DRAG ADVANTAGE

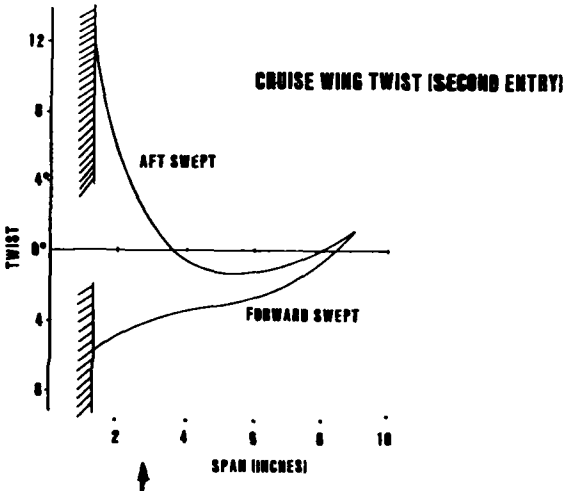


Fig. 25 (Extrait de CP 285 papier n° 21)

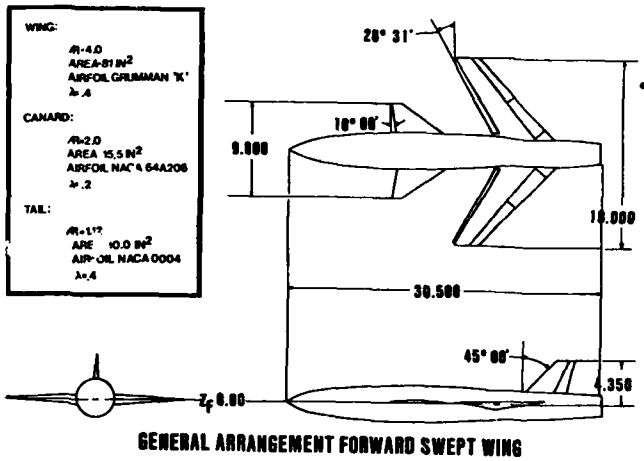


GENERAL ARRANGEMENT FORWARD SWEPT WING

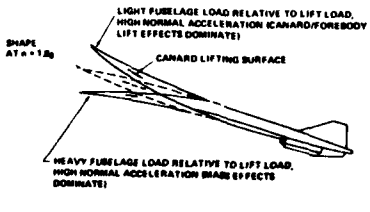


*Aeroelastic Effects of Canard in Maneuvering Flight*

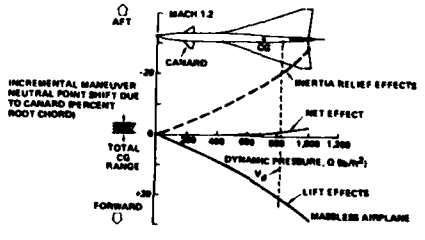


*Effect of Aeroelasticity on Canard Contribution to Longitudinal Stability*

Fig. 26 (Extrait de CP 262 papier n° 5)

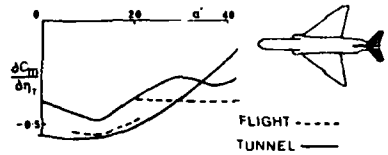


Variation of pitching moment derivative due to tailplane with angle of attack; F-4E

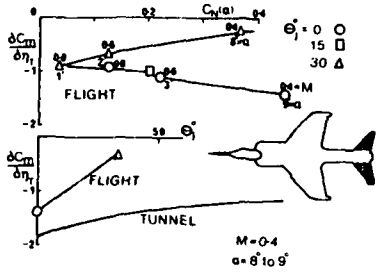


Variation of pitching moment derivative due to tailplane with normal force coefficient and with thrust deflection; Kestrel

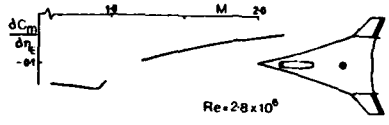


Variation of pitching moment derivative due to elevons with Mach number; supersonic fighter concept

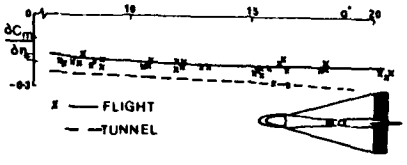


Variation of pitching moment derivative due to elevons with angle of attack; HP 115

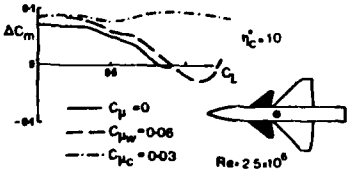


Effect of spanwise blowing on incremental pitching moment due to canard deflection and angle of attack; research canard model

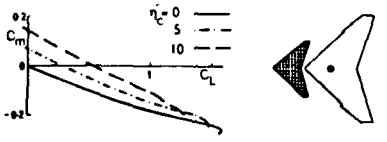

Pitching moment due to deflected canard and angle of attack; swept-wing canard configuration

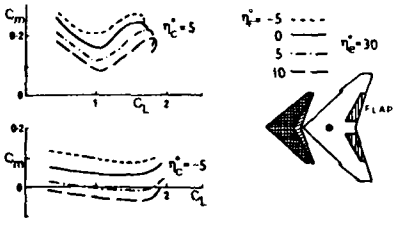


Effect of canard setting on pitching moment due to trailing edge flap and angle of attack; swept-wing canard configuration

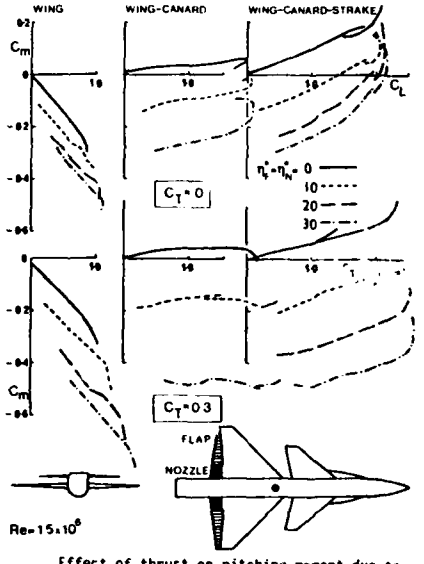


Effect of thrust on pitching moment due to trailing edge and nozzle flaps, and angle of attack; wing-canard-strake configurations

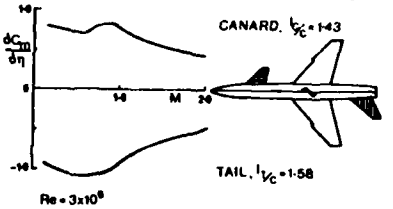


Variation of pitching moment derivative due to canard or tailplane with Mach number; research configuration

**Fig. 27 (Extrait de CP 262 papier n° 2)**

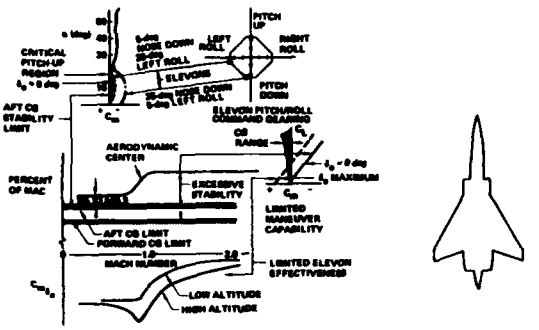


*Tailless Aircraft Control and Stability Limitations*

**Fig. 28 (Extrait de CP 262 papier n° 5)**

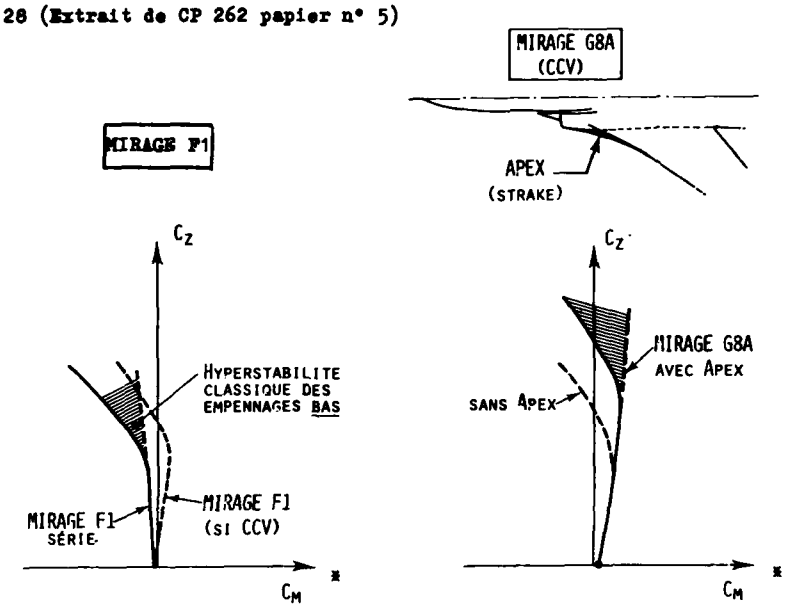


* CONVENTION DE SIGNE INVERSE AUX U.S.

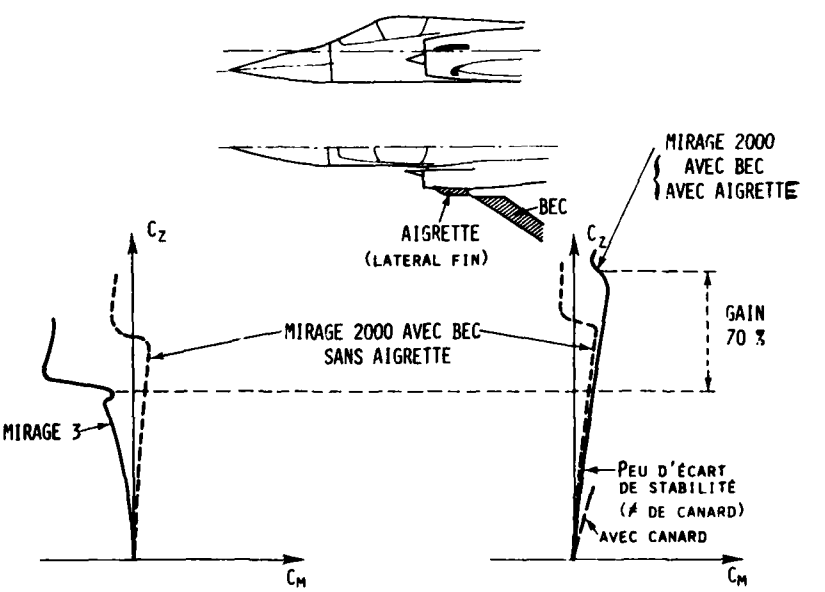


**Fig. 29 (Extrait de CP 241 papier n° 11)**

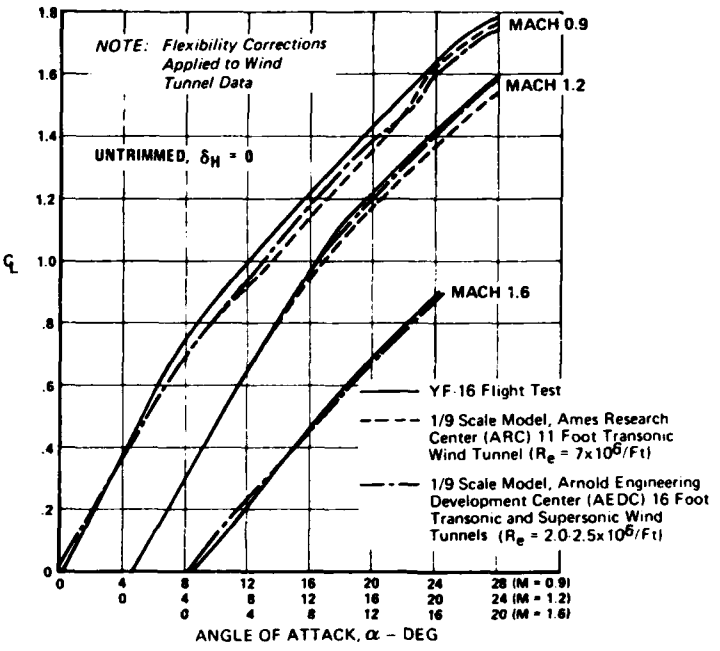


Comparison of Flight Test With Wind Tunnel Lift Curves for YF-16

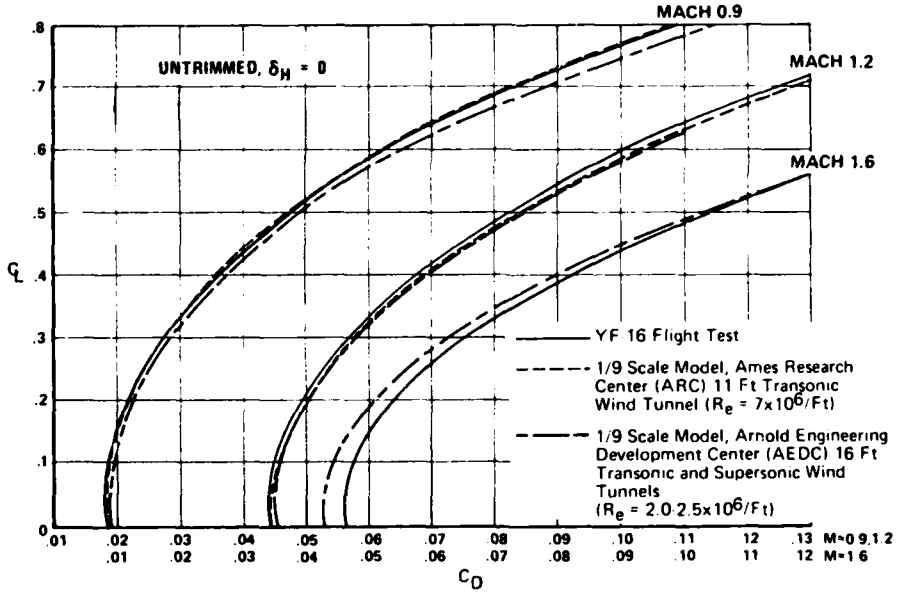


Comparison of Flight Test With Wind Tunnel Drag Polars for YF-16

Fig. 30 (Extrait de CP 242 papier n° 19)

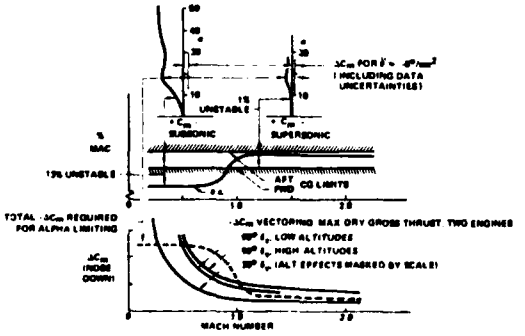


Fig. 33 (Extrait de CP 262 papier n° 5)

*Thrust Vectoring Pitch Control for Alpha Departure Prevention Unstable Tailless Aircraft*

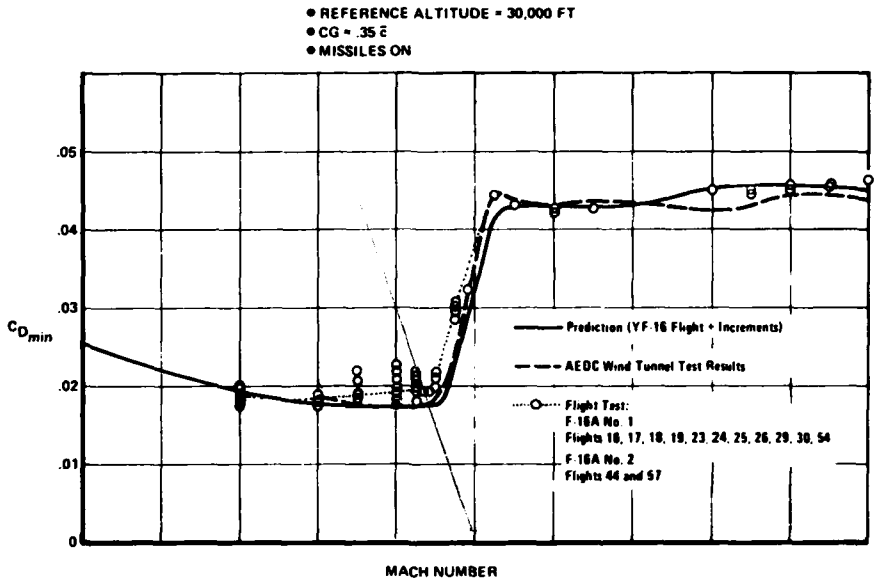


Apparent Minimum Drag from Steady-State Level Flight

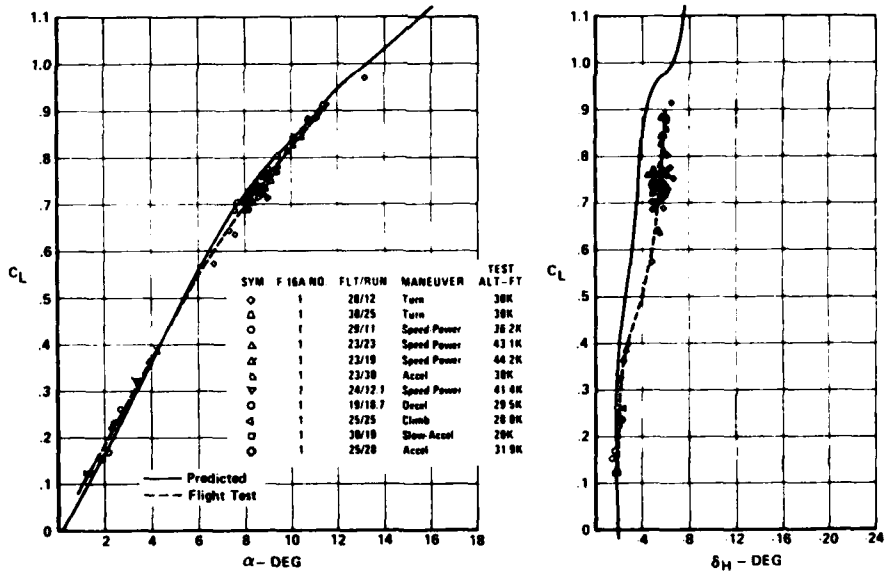


Comparison of Predicted With Flight Test for Trimmed Lift vs Alpha and Tail Deflection at Mach 0.9

Fig. 31 (Extrait de CP 242 papier n° 19)

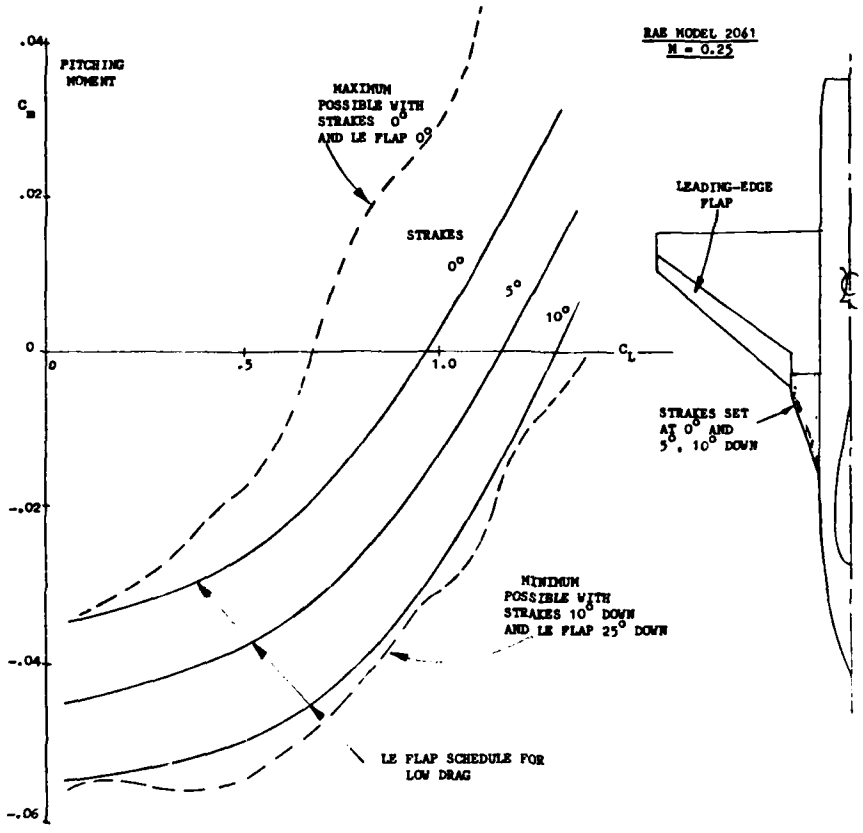


Possible use of strake droop as a pitch control

Fig. 32 (Extrait de CP 247 papier n° 4)

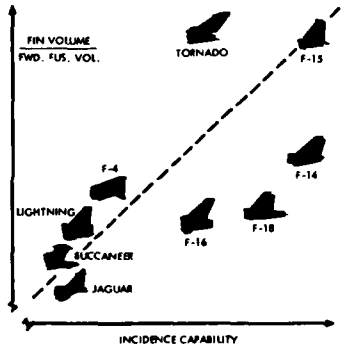


FIN GROWTH WITH INCIDENCE CAPABILITY

Fig. 34 (Extrait de CP 262 papier n° 12)

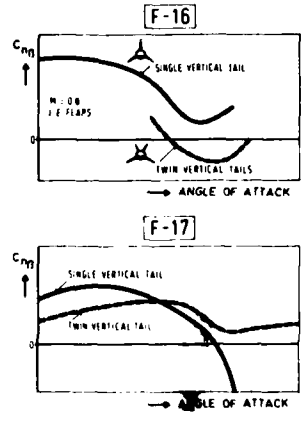


LAY-OUT CRITERIA FOR SINGLE OR TWIN VERTICAL TAIL

Fig. 35 (Extrait de CP 241 papier n° 8)

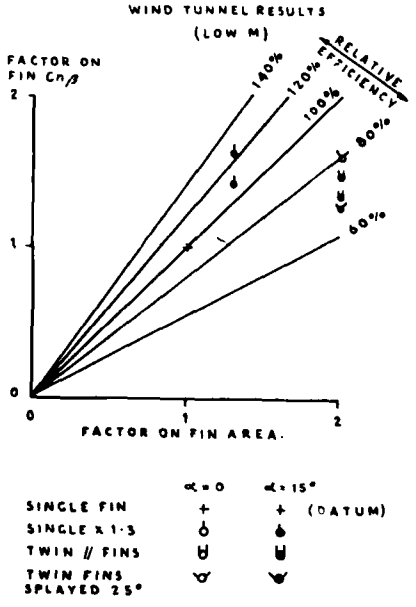


COMPARISON OF SINGLE AND TWIN FIN CONTRIBUTIONS TO DIRECTIONAL STABILITY

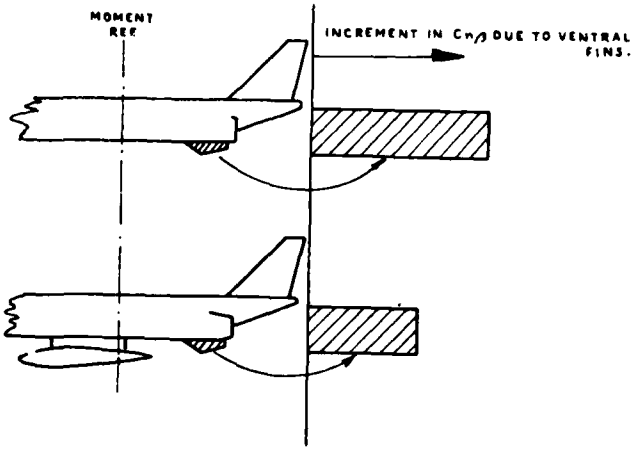


REDUCED EFFECTIVENESS OF VENTRAL FINS IN THE PRESENCE OR A VENTRAL STORE

Fig. 36 (Extrait de CP 119 papier n° 7)

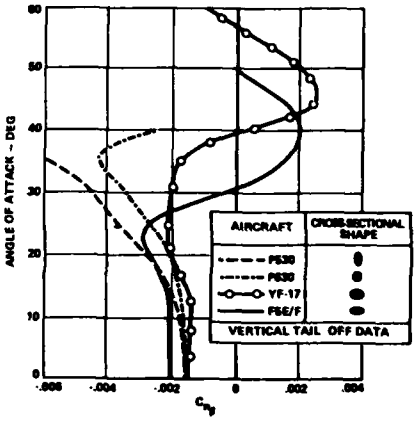


EFFECT OF NOSE SHAPE ON STABILITY

Fig. 38 (Extrait de CP 247 papier n° 6)

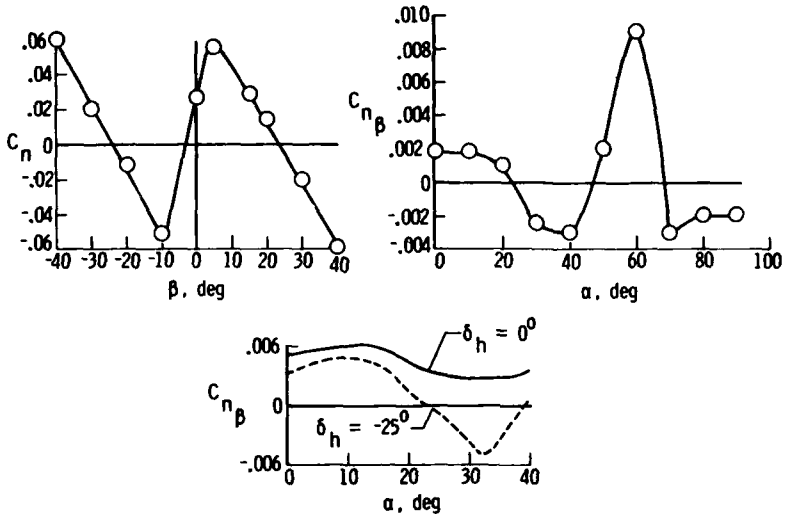


Typical variations of static aerodynamic data at high angles of attack.

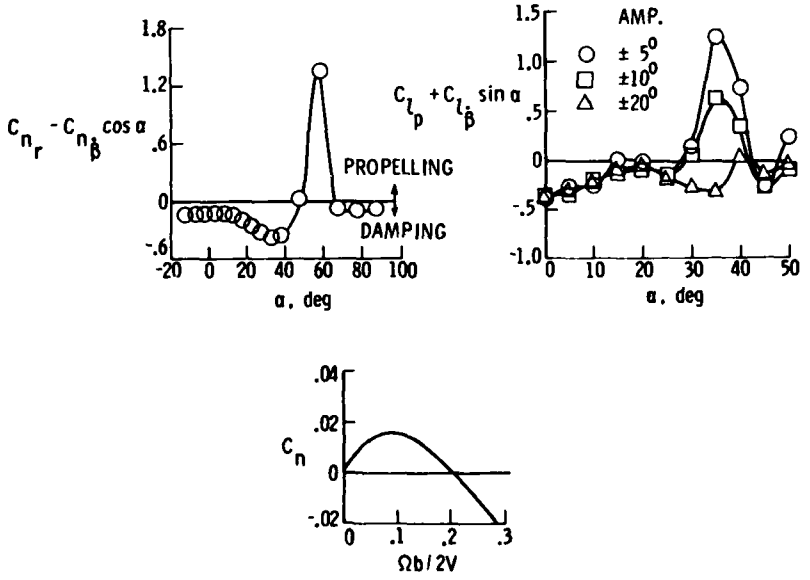


Typical variations of dynamic aerodynamic data at high angles of attack.

**Fig. 37 (Extrait de CP 235 papier n° 33)**

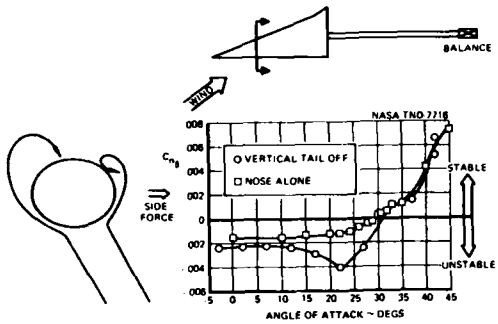


NOSE EFFECT ON STABILITY

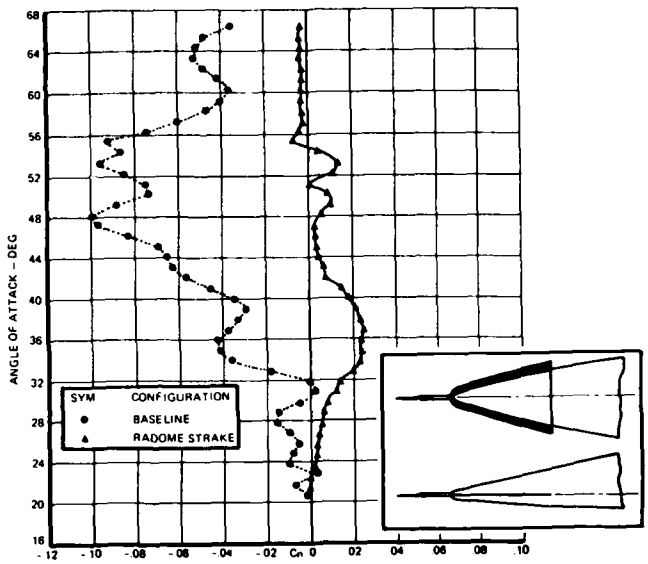


STRAKE EFFECT ON AERODYNAMIC ASYMMETRIES

**Fig. 39 (Extrait de CP 235 papier n° 19)**

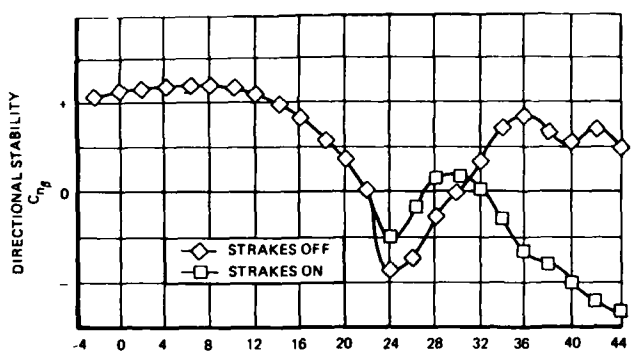


STRAKE EFFECT ON STABILITY

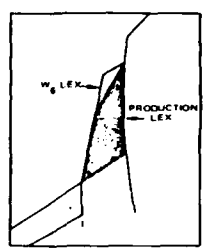


$W_6$ LEX GEOMETRY

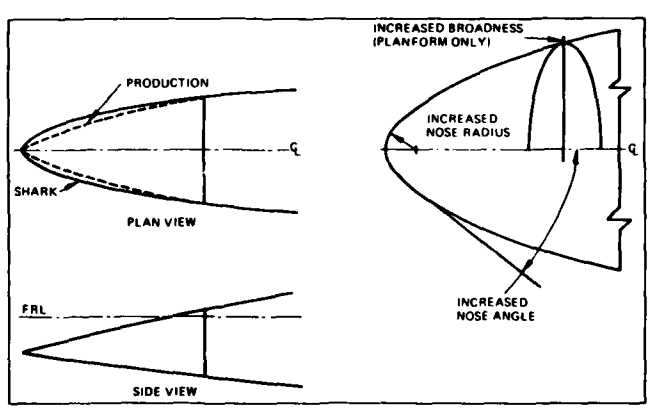


SHARK NOSE GEOMETRY

**Fig. 40 (Extrait de CP 235 papier n° 19)**

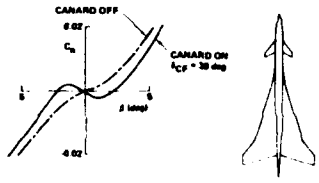


Canard Effect on Subsonic Directional Stability

Fig. 41 (Extrait de CP 262 papier n° 5)

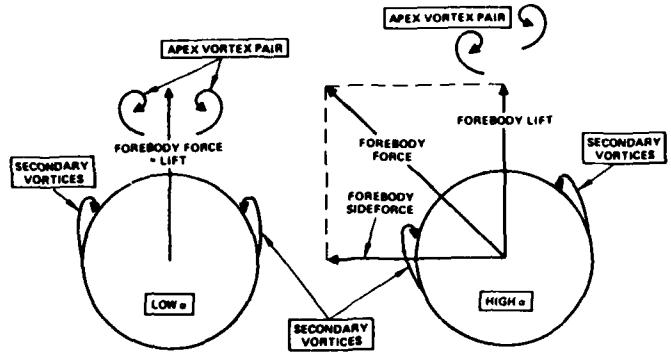


FOREBODY VORTEX PATTERNS

Fig. 42 (Extrait de CP 247 papier n° 6)

## HYSTERESIS EFFECTS

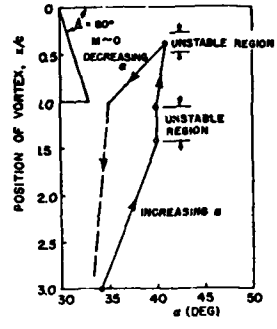


VORTEX BURST LOCATION ON A DELTA WING

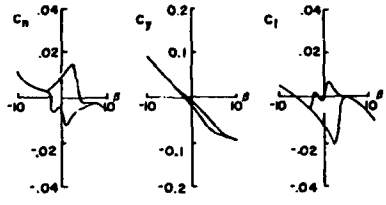


LATERAL AERODYNAMIC COEFFICIENTS AS FUNCTION OF ANGLE OF SIDESLIP

AERODYNAMIC HYSTERESIS IN A REGION OF VORTEX BREAKDOWN

Fig. 43 (Extrait de CP 247 papier n° 1)

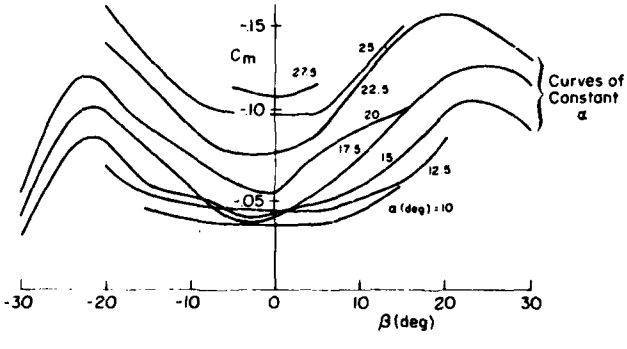


$C_m$ Versus β From F-4 Lookup Tables

Fig. 44 (Extrait de CP 235 papier n° 36)

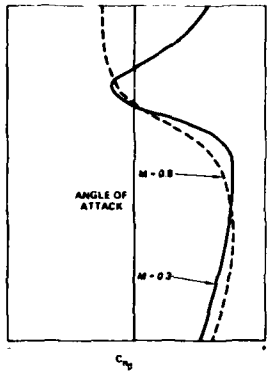


TRENDS IN DIRECTIONAL STABILITY

Fig. 45 (Extrait de CP 247 papier n° 6)

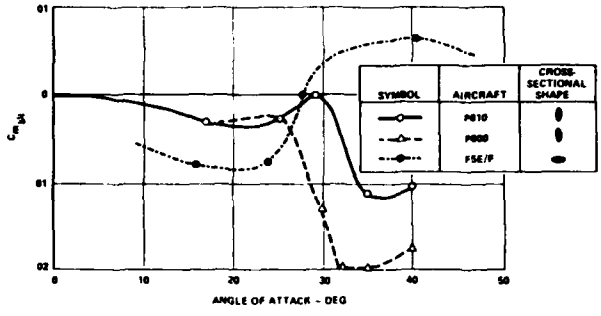


PITCHING MOMENT DUE TO SIDESLIP

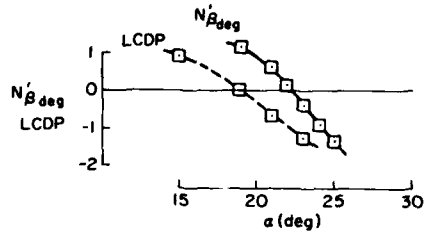


Divergence Criteria Predictions for the F-4

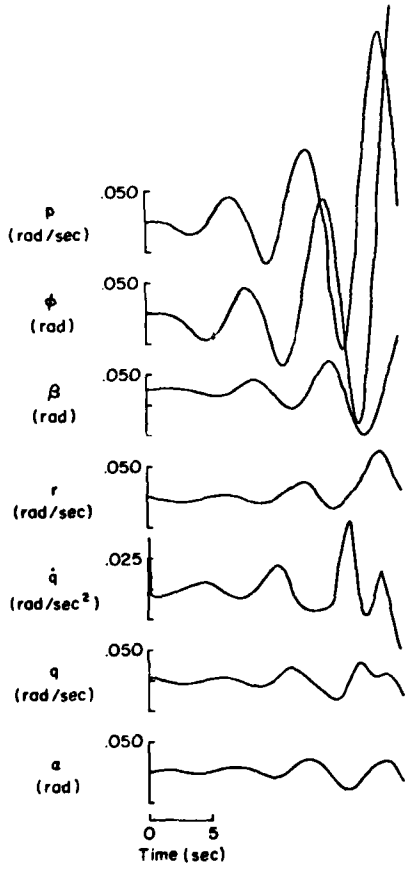


Open-Loop Nonlinear Airframe Response to Elevator Pulse; $\alpha_o$ = 21 deg; $\beta_o$ = 1.5 deg

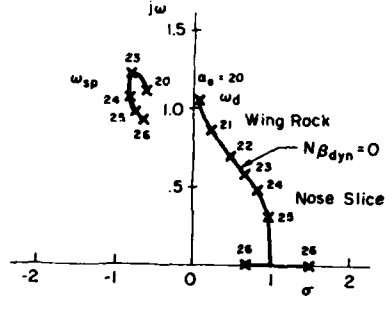


Lateral/Longitudinal Root Migration With α

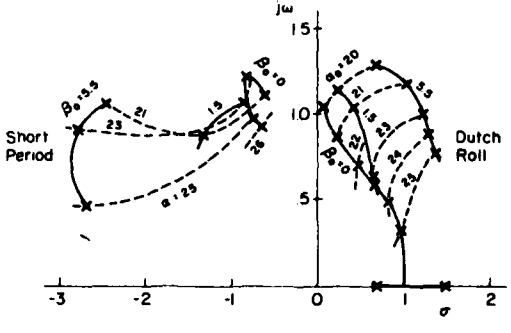


6 DOF Linearized Equation; Lateral/Longitudinal Root Migration with α and β

Fig. 46 (Extrait de CP 235 papier n° 36)

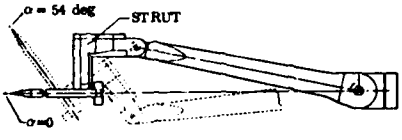


a. High Alpha Free-Oscillation Pitch Apparatus, AEDC-VKF

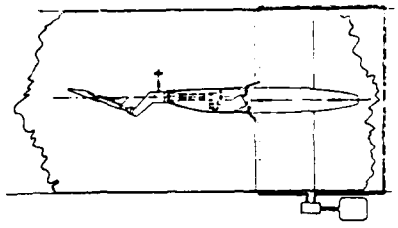

b. Steady-Roll Apparatus, NASA-Langley

High-α Model Support Systems

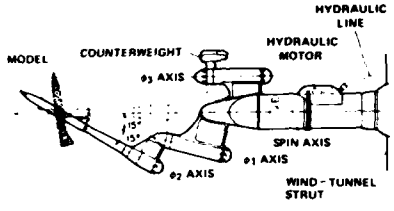


Rotary Rig of NASA-Ames RC

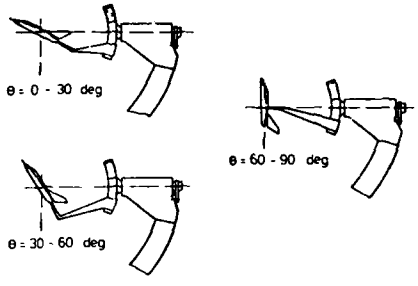


Rotary Rig of DFVLR

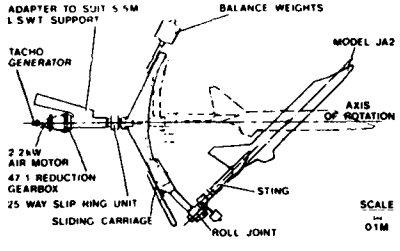


a. 5·5 LSWT Rotary Derivative Rig

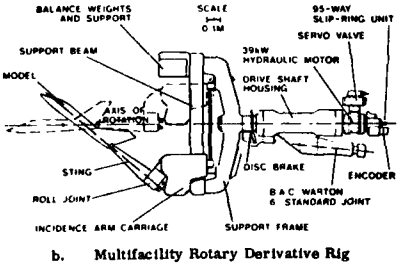


b. Multifacility Rotary Derivative Rig

Rotary Derivative Rigs, BAC, Warton Div

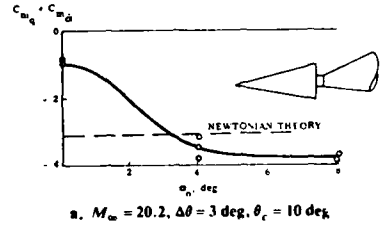


a. $M_\infty = 20.2$, $\Delta\theta = 3$ deg, $\theta_c = 10$ deg

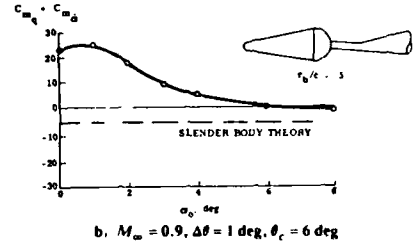


b. $M_\infty = 0.9$, $\Delta\theta = 1$ deg, $\theta_c = 6$ deg

Sting Interference Effects

Fig. 47 (Extrait de CP 260 papier n° 2)

## β-DERIVATIVES

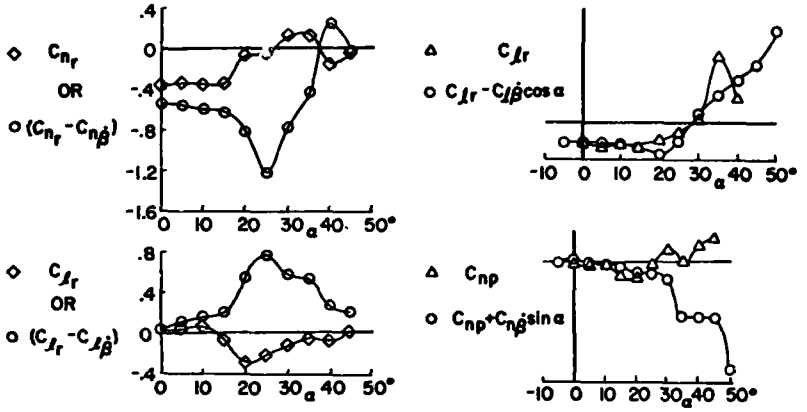


Fig. 48 (Extrait de CP 247 papier n° 1)

DIFFERENCE BETWEEN PURELY ROTARY AND OSCILLATORY DERIVATIVES REPRESENTING DERIVATIVES DUE TO TIME RATE OF CHANGE OF ANGLE OF ATTACK OR SIDESLIP.

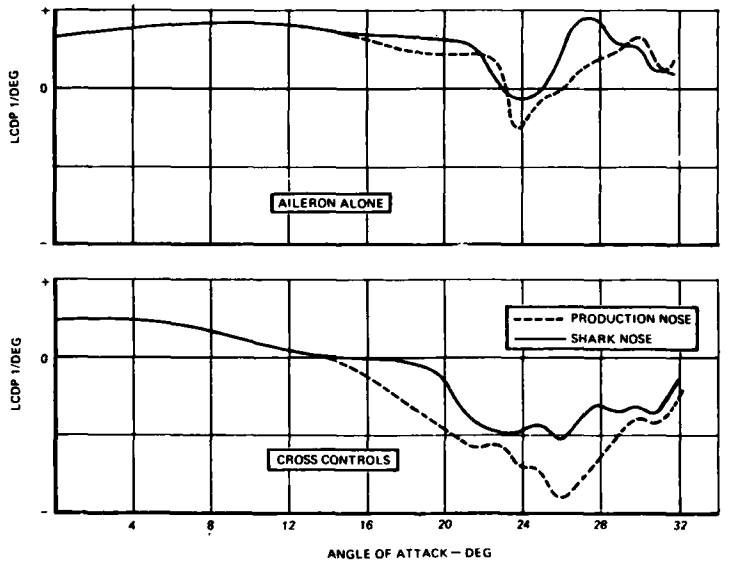


SHARK NOSE EFFECT ON LCDP

Fig. 49 (Extrait de CP 235 papier n° 19)

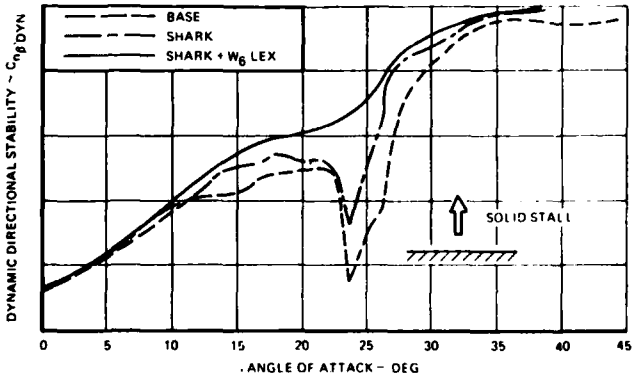


DYNAMIC STABILITY COMPARISON

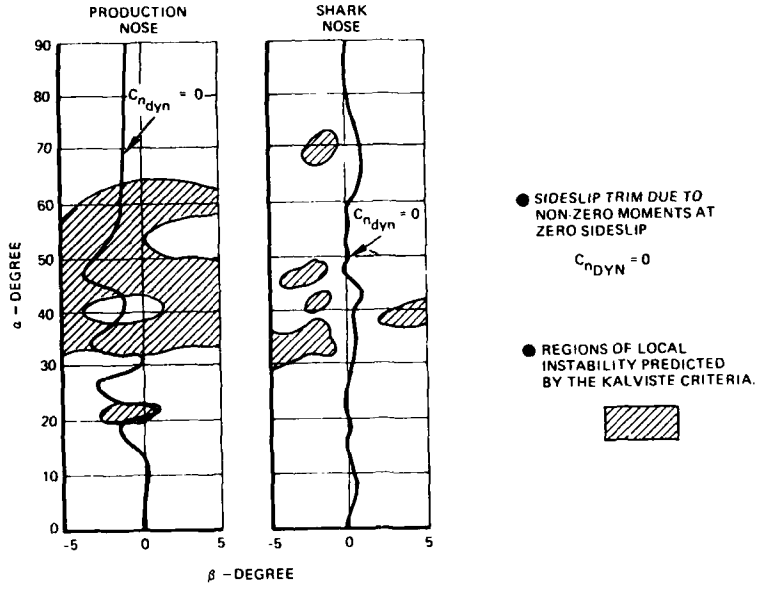


EFFECT OF SHARK NOSE ON COUPLED STABILITY PARAMETERS

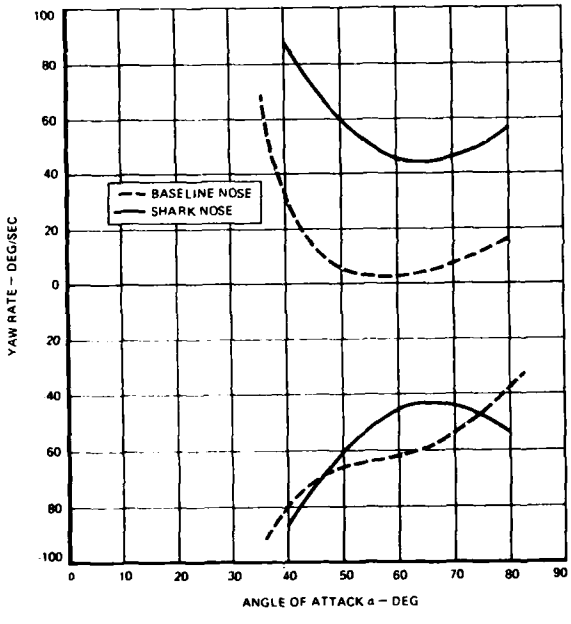


SHARK NOSE EFFECT ON ANALYTICAL SPIN ENTRY BOUNDARY

Fig. 50 (Extrait de CP 235 papier n° 19)

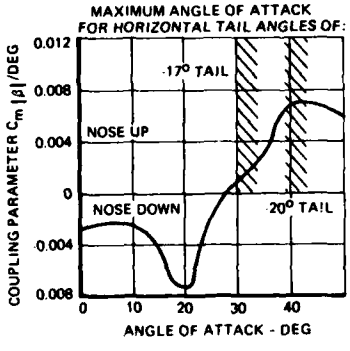


EFFECT OF LIMITING TAIL AUTHORITY ON SIDESLIP/ANGLE-OF-ATTACK COUPLING PARAMETER

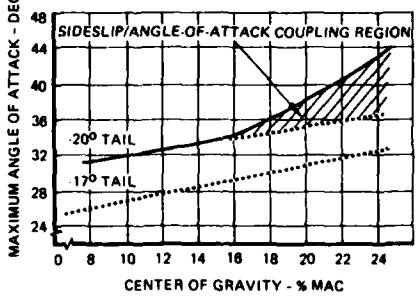


EFFECT OF LIMITING TAIL AUTHORITY ON MAXIMUM ANGLE OF ATTACK

Fig. 51 (Extrait de CP 235 papier n° 19)

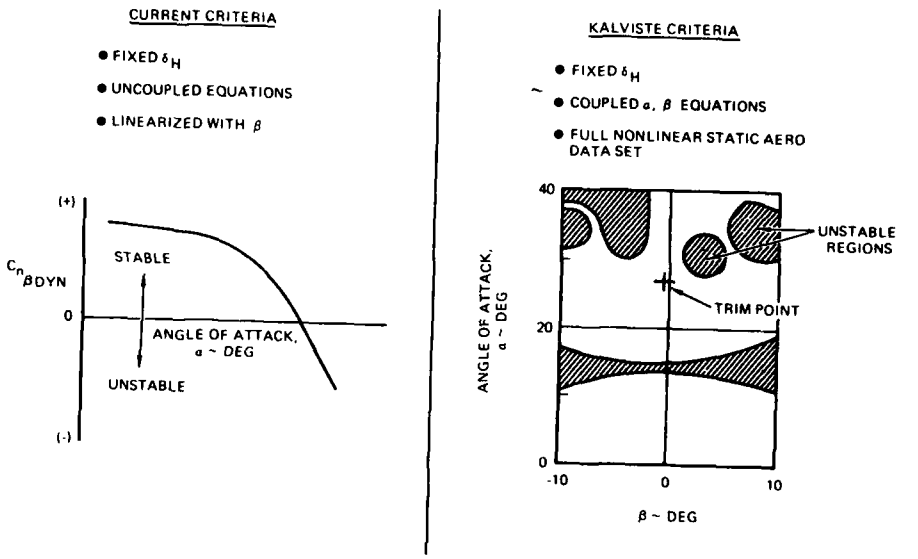


COMPARISON OF KALVISTE CRITERIA WITH $C_{n_{DYN}}$ CRITERIA

CHARACTERISTIC POLYNOMIAL

$(S^4 + AS^2 + B)(S) = 0$

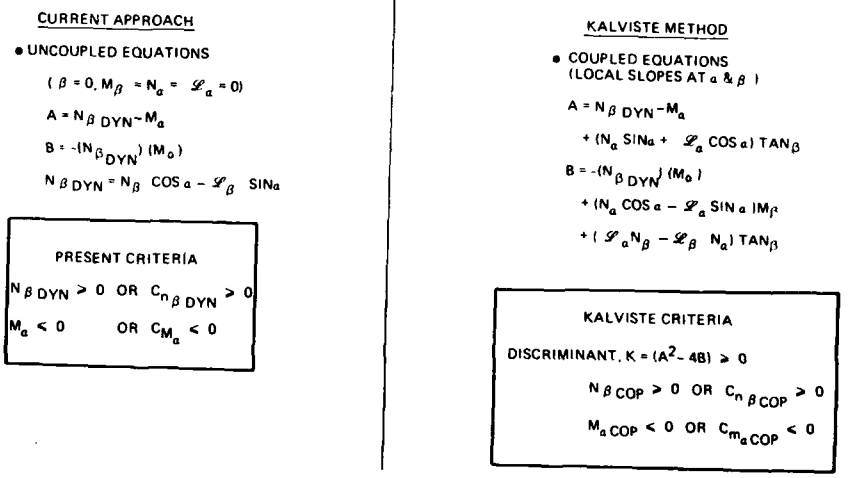


AIRCRAFT STATIC STABILITY PERTURBATION EQUATIONS

**Fig. 52 (Extrait de CP 235 papier n° 19)**

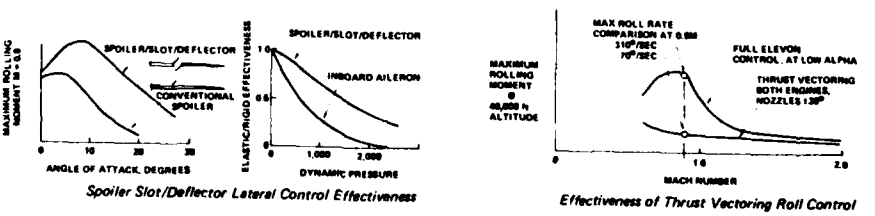


*Spoiler Slot/Deflector Lateral Control Effectiveness*

*Effectiveness of Thrust Vectoring Roll Control*

**Fig. 53 (Extrait de CP 262 papier n° 5)**

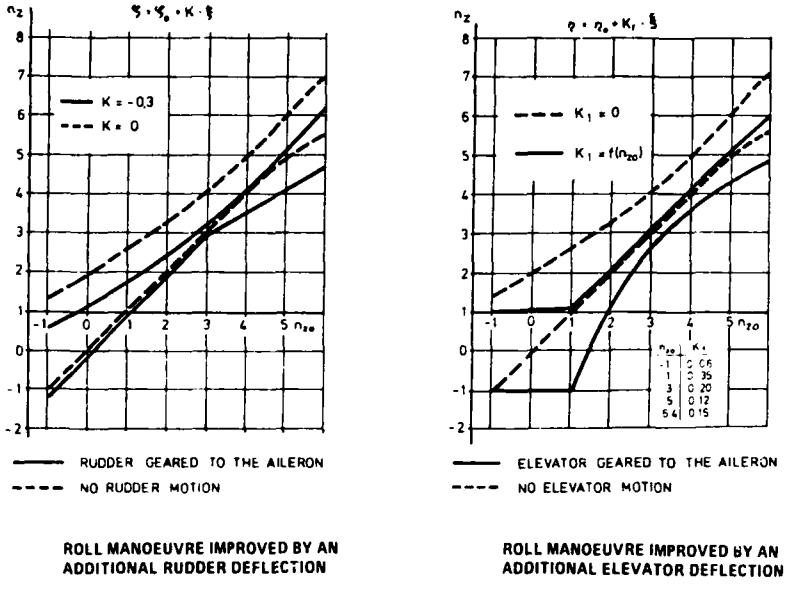


Fig. 54 (Extrait de CP 241 papier n° 20)

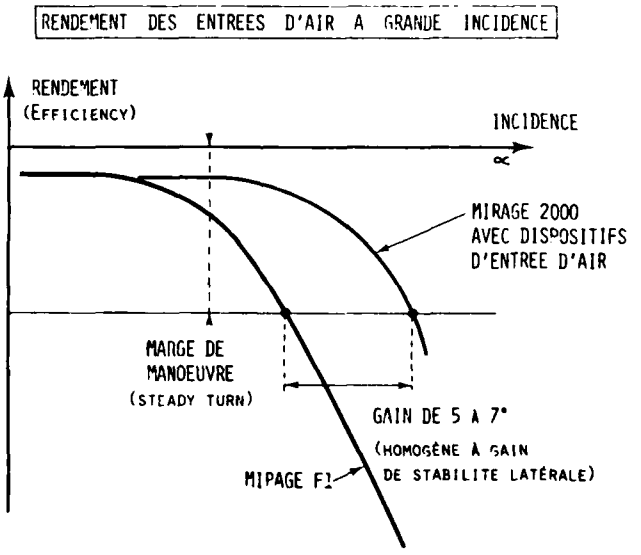


Fig. 55 (Extrait de CP 241 papier n° 11)

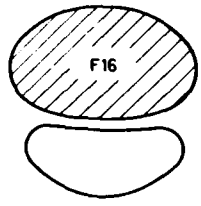


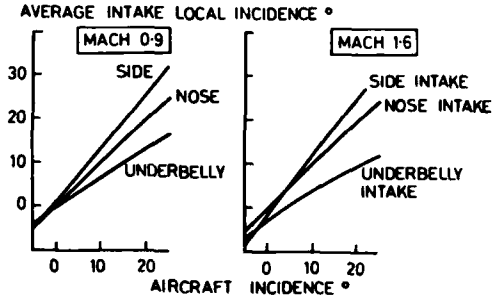


Underbelly location

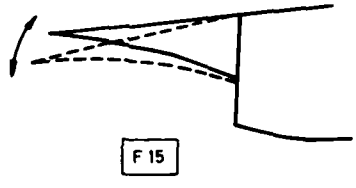


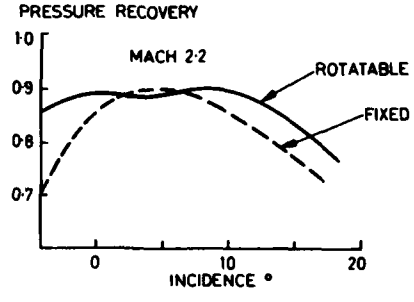


Rotatable intake

Fig. 56 (Extrait de CP 241 papier n° 16)

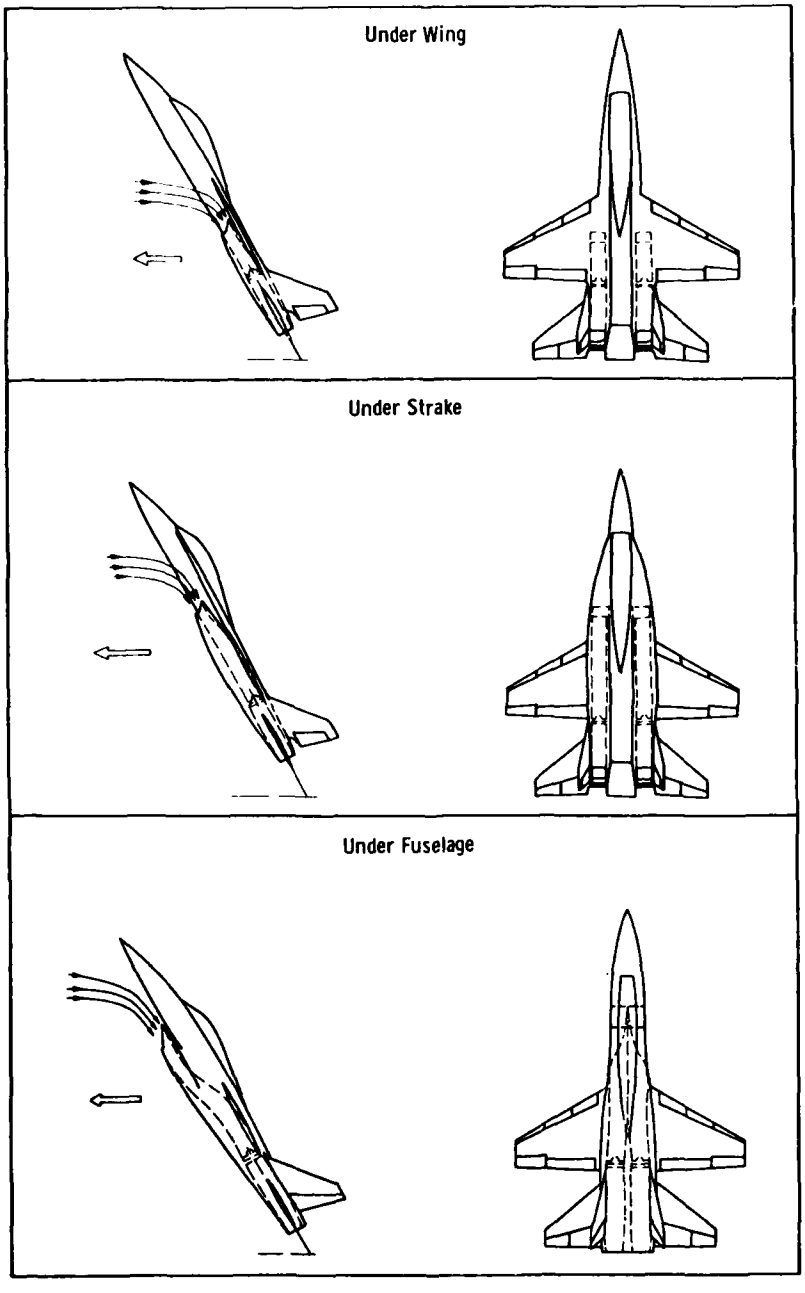


Fig. 57 (Extrait de CP 247 papier n° 32)

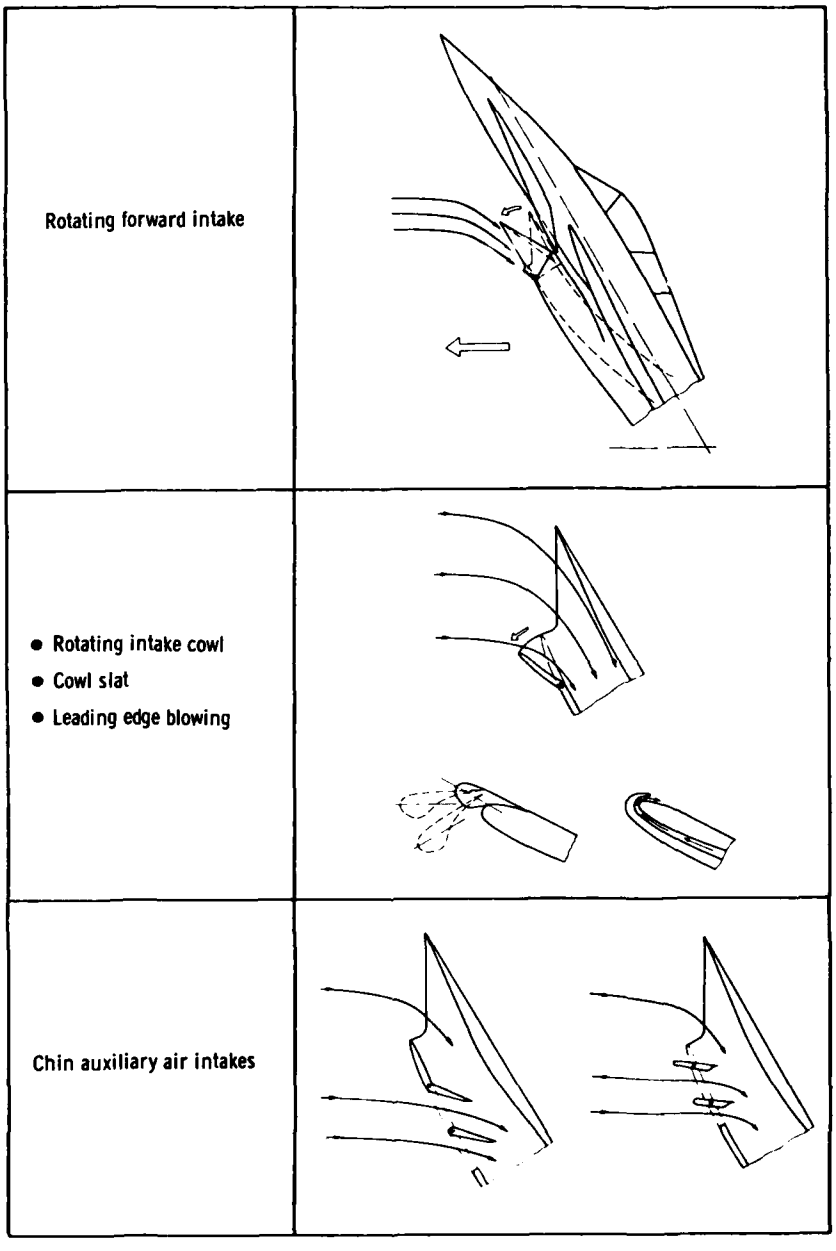


Intake concepts for high angles of attack

**Fig. 58 (Extrait de CP 247 papier n° 32)**

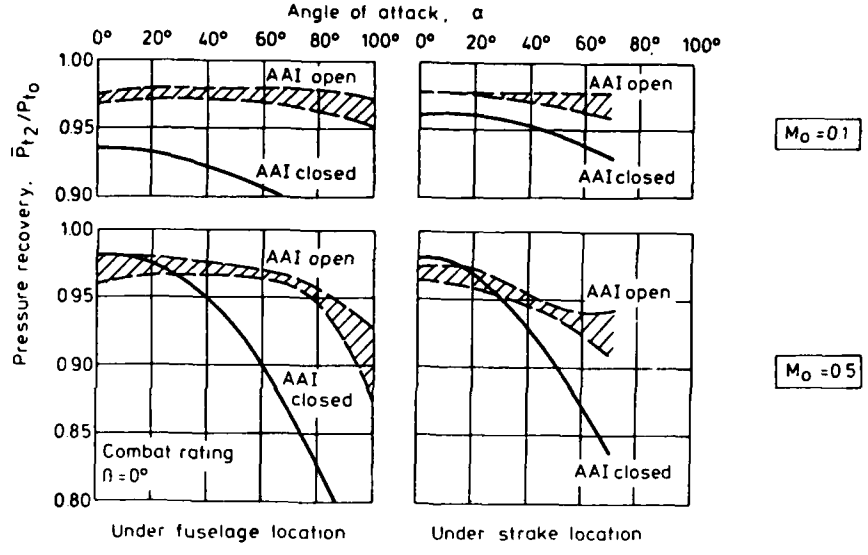


Effect of angle of attack on pressure recovery

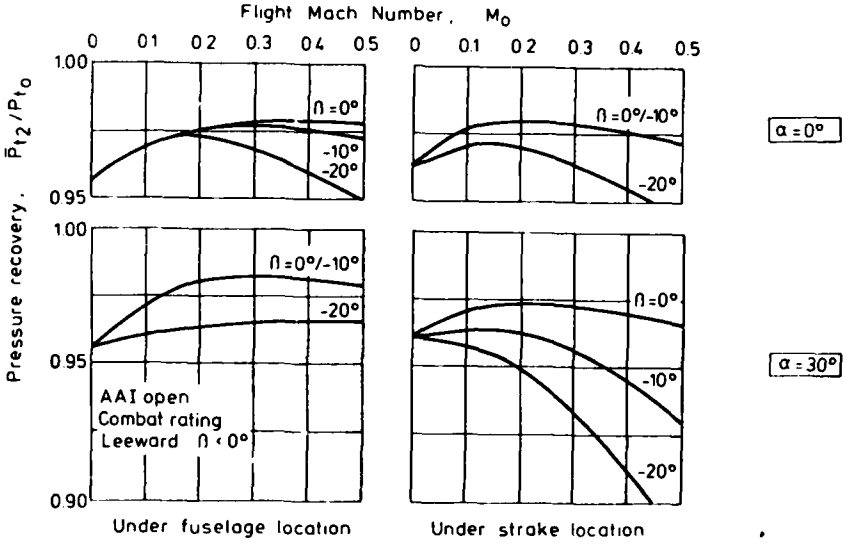


Effect of yaw angle on pressure recovery

**Fig. 59 (Extrait de CP 247 papier n° 32)**

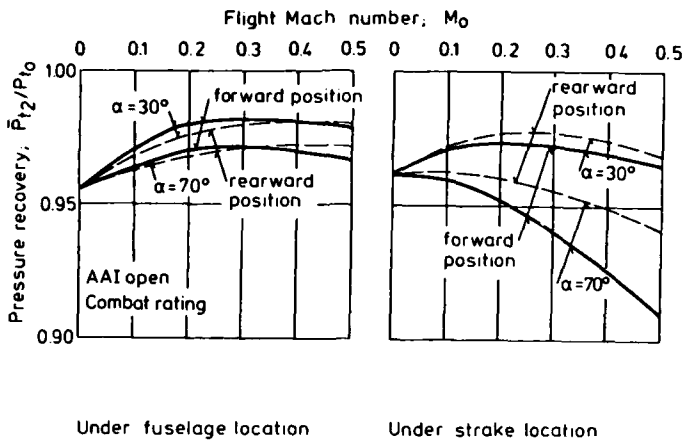


Effect of axial inlet position on pressure recovery

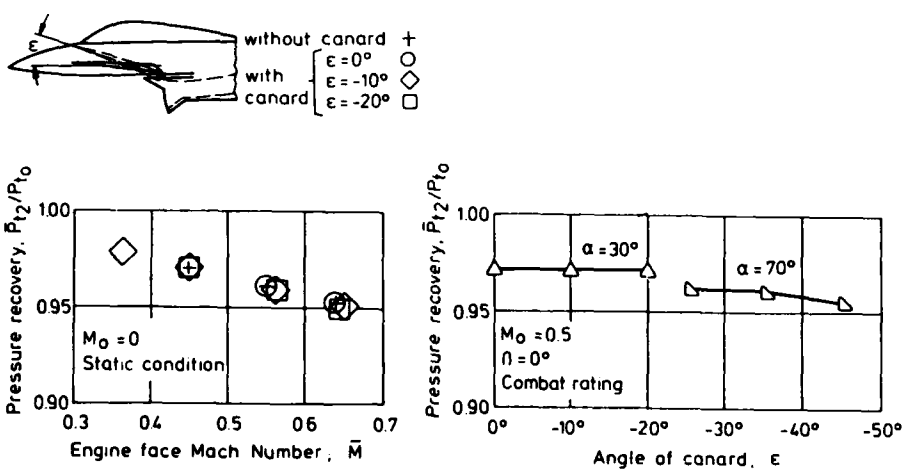


Effect of canard on pressure recovery

**Fig. 60 (Extrait de CP 247 papier n° 32)**

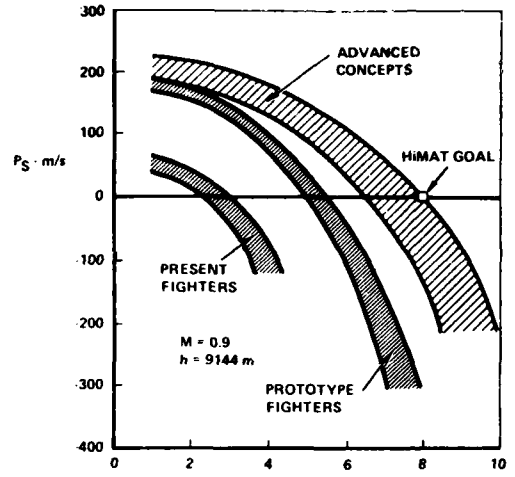


HiMAT Maneuvering Performance Objective

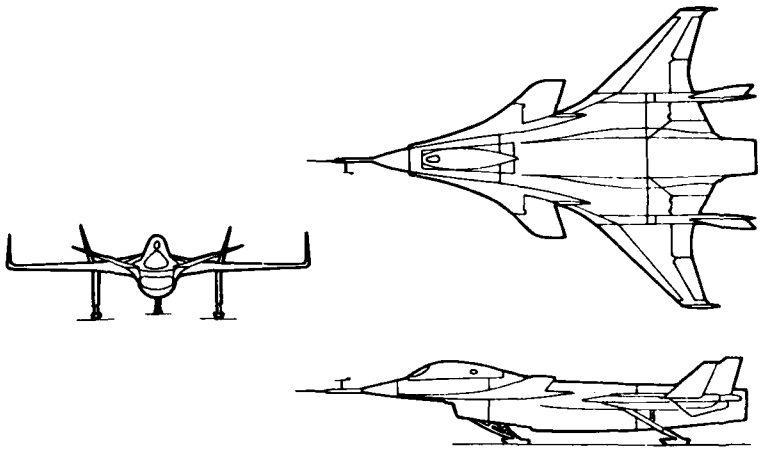

RPRV, -17A

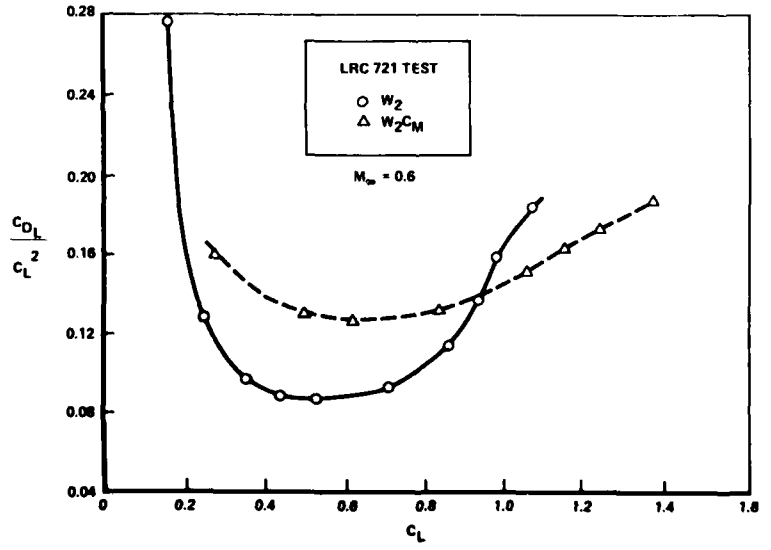


Effect of Canard on Maneuver Configuration (-17A) Drag Due to Lift

**Fig. 61 (Extrait de CP 280 papier n° 17)**

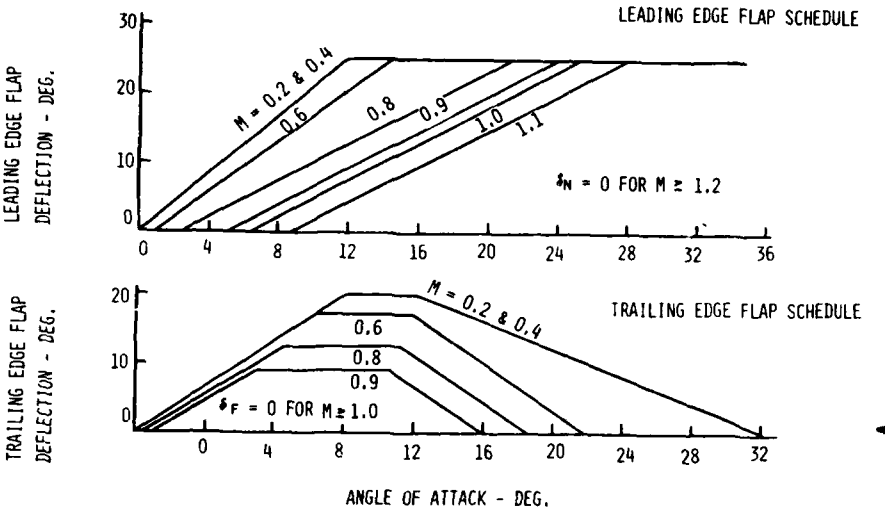


F-18 Flap schedules

Fig. 63 (Extrait de CP 241 papier n° 14)

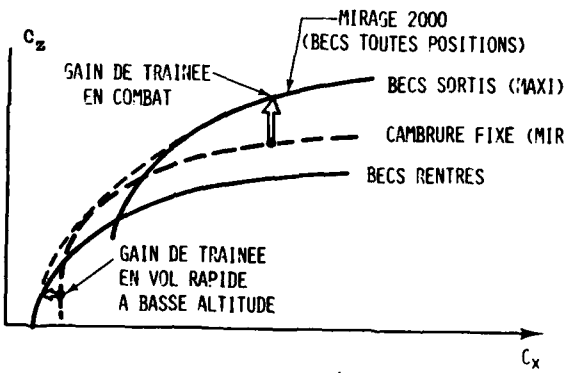


Fig. 62 (Extrait de CP 241 papier n° 11)

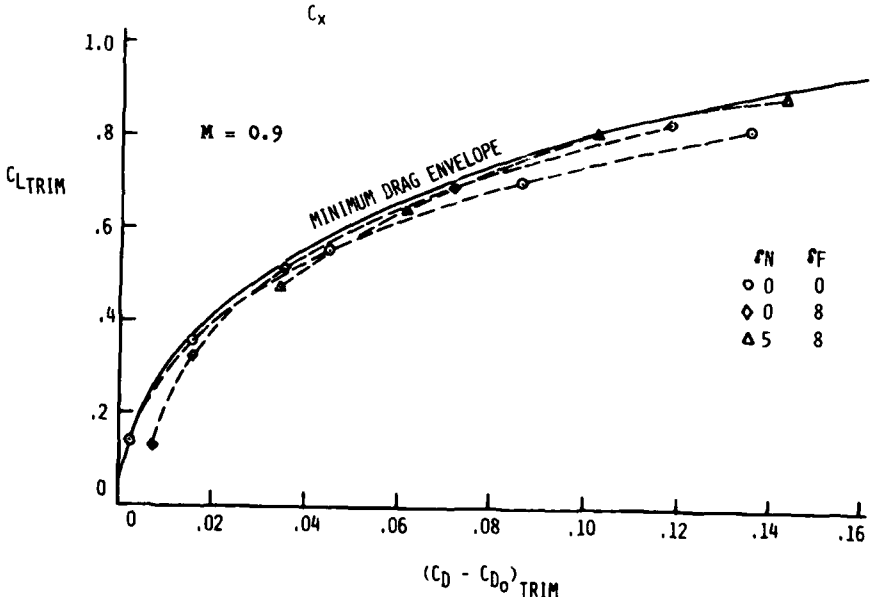


F-18 Trimmed drag due to lift, M = 0.9

Fig. 64 (Extrait de CP 241 papier n° 14)

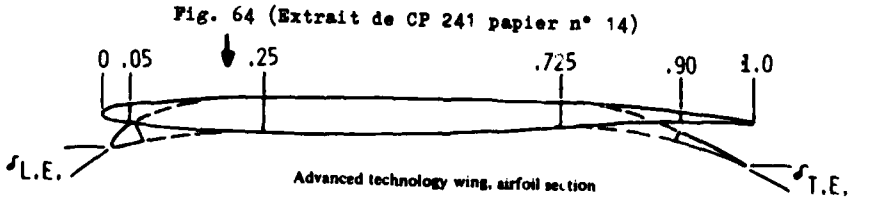


Advanced technology wing, airfoil section

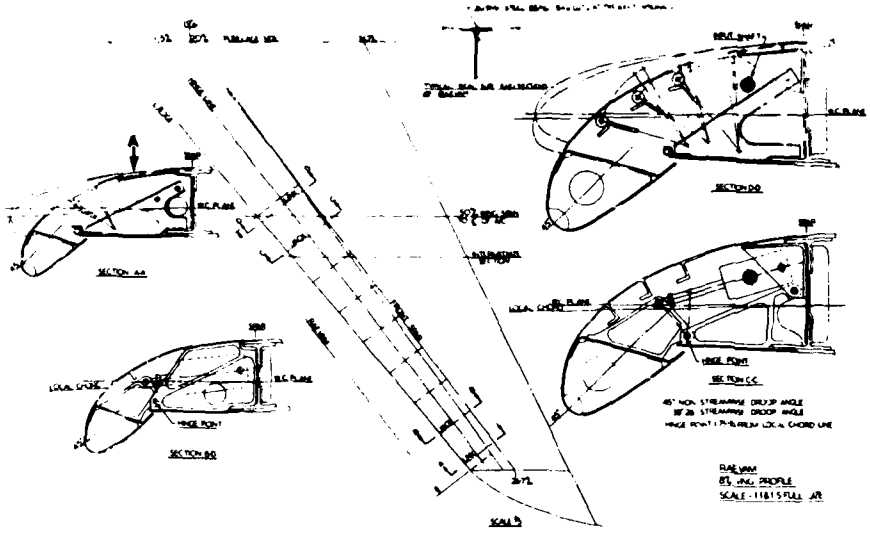

Typical RAEVAM mechanism for a strike fighter wing

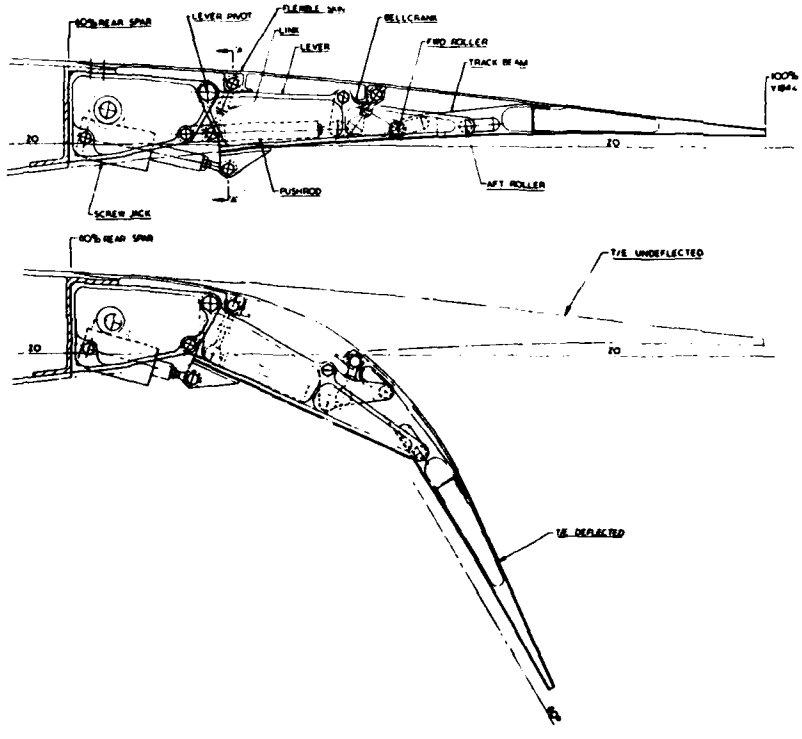


Typical contour flap mechanism

**Fig. 65 (Extrait de CP 262 papier n° 4)**

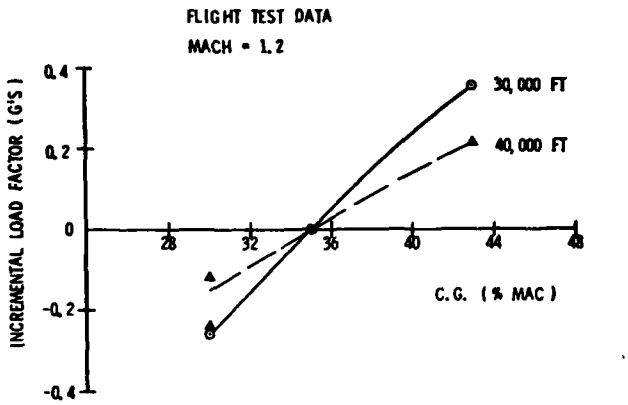


Effect Of C.G. Location On Maximum Sustained Load Factor

**Fig. 66 (Extrait de CP 235 papier n° 16)**

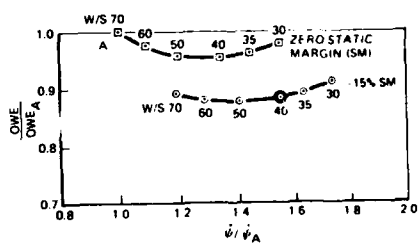


. EFFECT OF STATIC MARGIN ON OPERATIONAL WEIGHT EMPTY AND SUSTAINED TURN RATE AT M 0.9, 30,000 FT

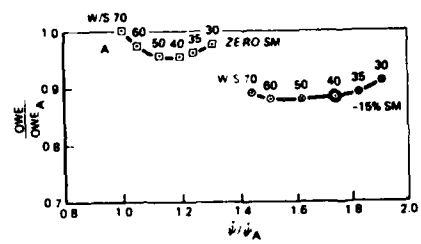


. EFFECT OF STATIC MARGIN ON OPERATIONAL WEIGHT EMPTY AND SUSTAINED TURN RATE AT M 1.2, 30,000 FT

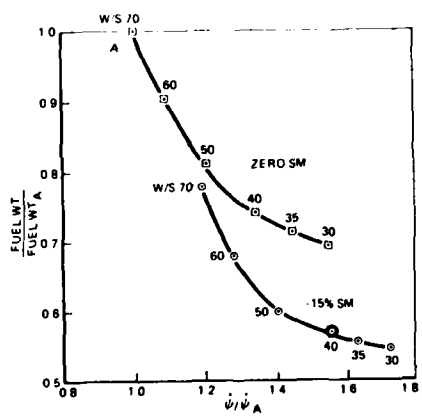


. EFFECT OF STATIC MARGIN ON FUEL WEIGHT AND SUSTAINED TURN RATE AT M 0.9, 30,000 FT

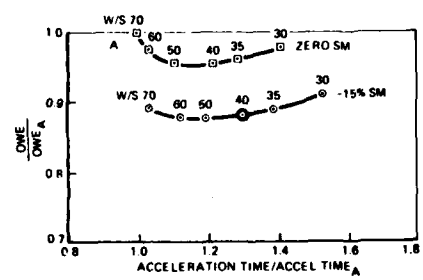


. EFFECT OF STATIC MARGIN ON OPERATIONAL WEIGHT EMPTY AND ACCELERATION TIME FROM M 0.9 TO M 1.8 AT 30,000 FT

**Fig. 67 (Extrait de CP 260 papier n° 7)**

| FUNCTION | | SEVERITY OF SITUATION WITH FUNCTION DEGRADATION | MEANS AVAILABLE FOR MODIFYING RISKS PRESENTED BY FAILURES |
|---|---|---|---|
| Relaxed Inherent Stability Augmentation | | Moderate-Very | Redundancy + Authority distribution<br>Reduced operating envelope<br>CG management |
| Load Control | Maneuver | Negligible-Moderate | Redundancy + Authority distribution<br>Reduced operating envelope |
| | Gust | Negligible-Moderate | Redundancy + Authority distribution<br>Reduced operating envelope |
| | Fatigue Damage | Negligible | Reduced operating envelope |
| Flutter Control | | Very-Extreme | Redundancy + Authority distribution<br>Reduced operating envelope |
| Ride Quality Control | | Negligible-Moderate | Redundancy + Authority distribution<br>Reduced operating envelope |
| Envelope Limiting | | Negligible-Moderate | Redundancy<br>Reduced operating envelope |
| CG Control | | Negligible | Reduced operating envelope |

Degraded situation impact

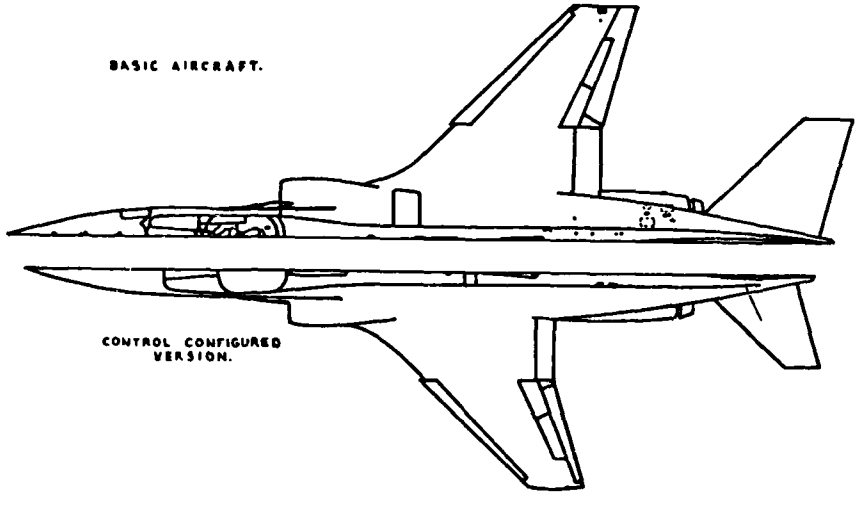


Effect of artificial stability on aircraft size

Fig. 68 (Extrait de CP 260 papier n° 1)

Fig. 69 (Extrait de CP 262 papier n° 5)

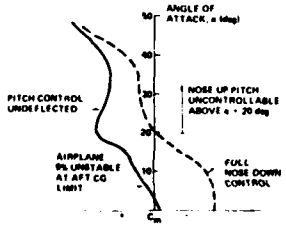


*Excessive Instability*

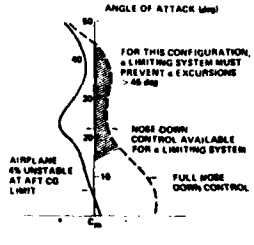


*Controllable Instability*

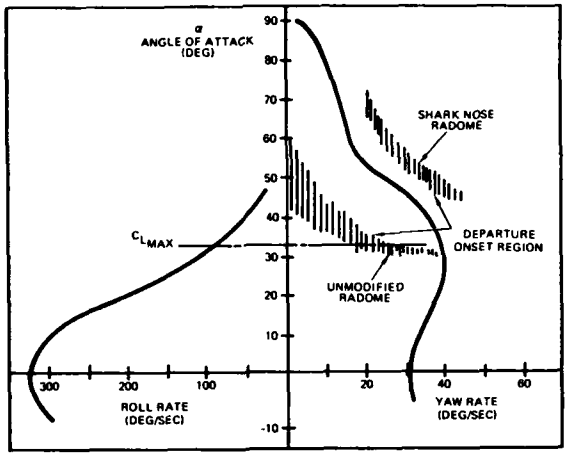


EFFECT OF IMPROVED AERODYNAMICS ON DEPARTURE RESISTANCE

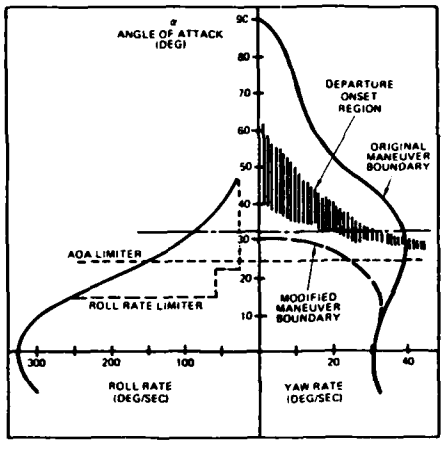


EFFECT OF CONTROL LIMITERS ON DEPARTURE RESISTANCE

Fig. 70 (Extrait de CP 262 papier n° 24)

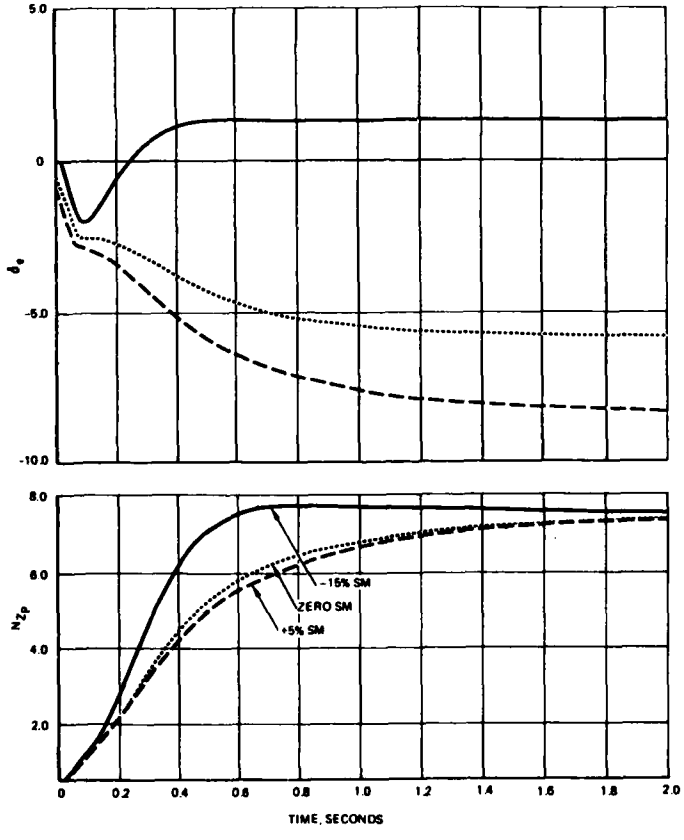


EFFECT OF STATIC MARGIN ON RESPONSE AT M 0.9, 500 FT

Fig. 71 (Extrait de CP 260 papier n° 7)

| CCV Flight Control Mode | Recommended Authority |
|---|---|
| Maneuver Enhancement | Fighter CCV |
| Direct Lift | 1,0 to 2,0 X Fighter CCV |
| Direct Sideforce | |
| Air Combat | Greater than Fighter CCV ; 2g offensively and 3g defensively |
| Air-to-Ground | Same as Fighter CCV (Approximately 1g) |
| Pitch Pointing | 2 X Fighter CCV ($\pm$ 5 degrees) |
| Yaw Pointing | Fighter CCV ($\pm$ 5 degrees) |
| Vertical Translation | Equal to or Greater than Fighter CCV (1500 fpm) |
| Lateral Translation | |
| Formation, Aerial Refuel | 10 Knots |
| Landing in Crosswind | 30 Knots |
| Air-to-Ground Weapon Delivery in Crosswind or Against Moving Target | 50 to 80 Knots |

Typical Fighter CCV Capability : 30 Knots

Control Mode Authorities

Fig. 73 (Extrait de CP 260 papier n° 18)

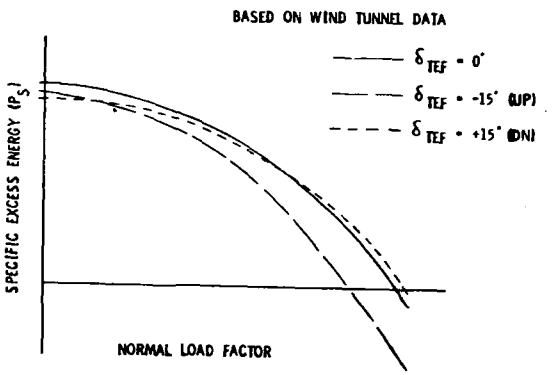


Effect Of DLC On Subsonic Maneuver Potential

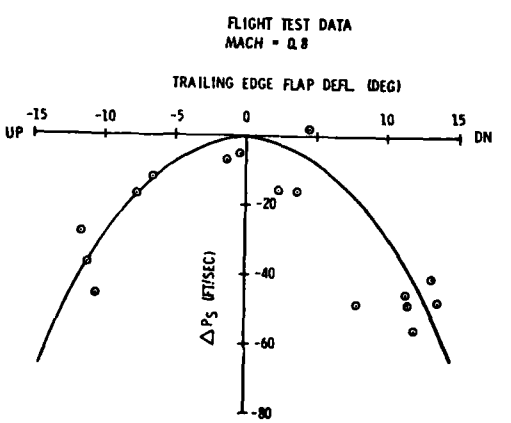


Effect Of Pitch Pointing On Aircraft Energy

Fig. 75 (Extrait de CP 235 papier n° 16)

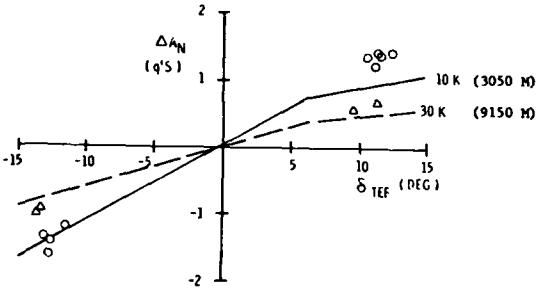


CCV YF-16 Flight Test Data vs. Predictions - Direct Lift Mode - M=0.8

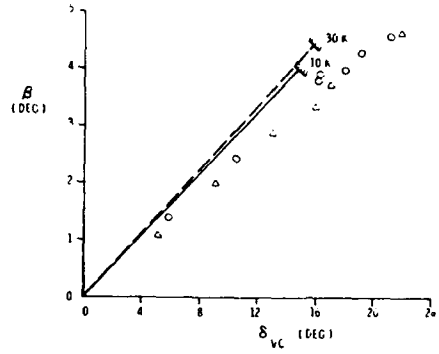


**CCV YF - 16 Flight Test Data vs Predictions YAW POINTING MUDE M.0.8**

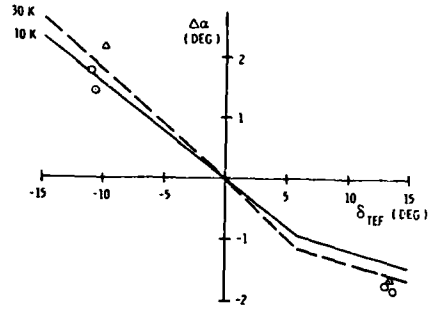


CCV YF-16 Flight Test Data vs. Predictions
Pitch Pointing Mode - M=0.8

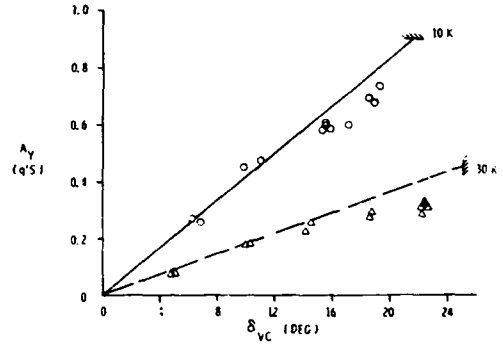


CCV YF-16 Flight Test Data vs. Predictions
Direct Sideforce Mode - M=0.8

**Fig. 74 (Extrait de CP 260 papier n° 18)**

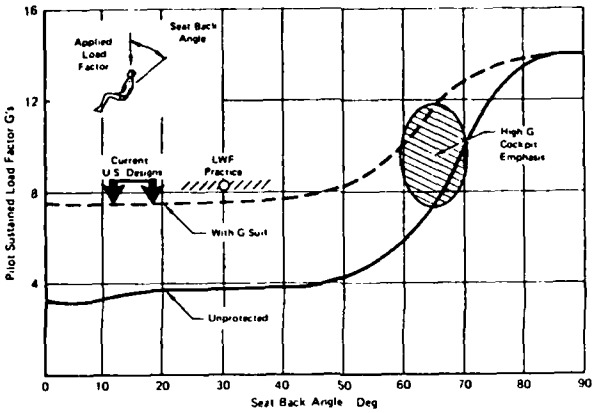


Pilot sustained G-tolerance as a function of seat back angle

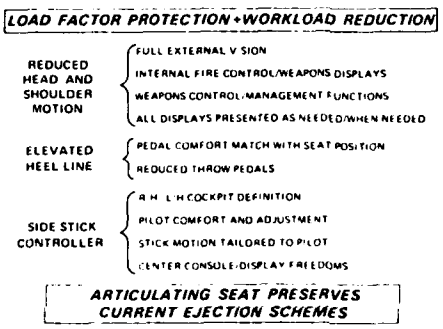


Pilot/vehicle interface problems addressed in the high acceleration cockpit design studies

**Fig. 76 (Extrait de CP 212 papier n° 22)**

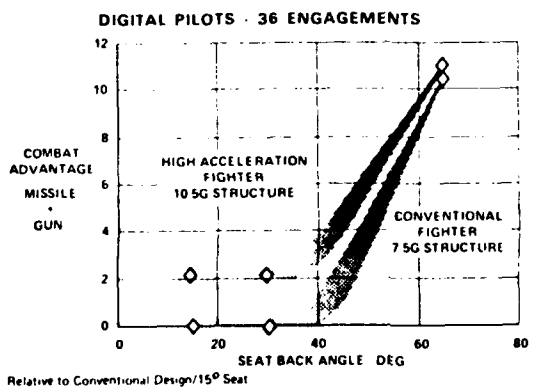


Air combat maneuvering modeling results. (The 36 engagements were for both fair fight and biased initial conditions.) The combat advantage over a conventional fighter without reclining seat (high acceleration cockpit) is shown

**Fig. 77 (Extrait de CP 212 papier n° 22)**

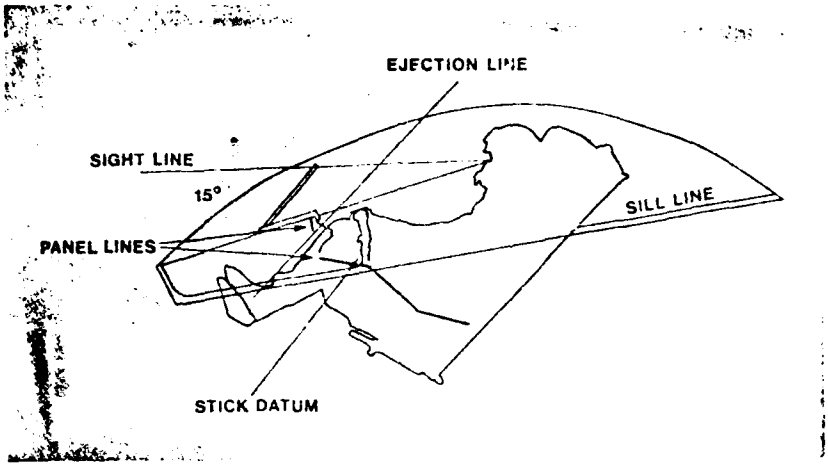


Advanced cockpit

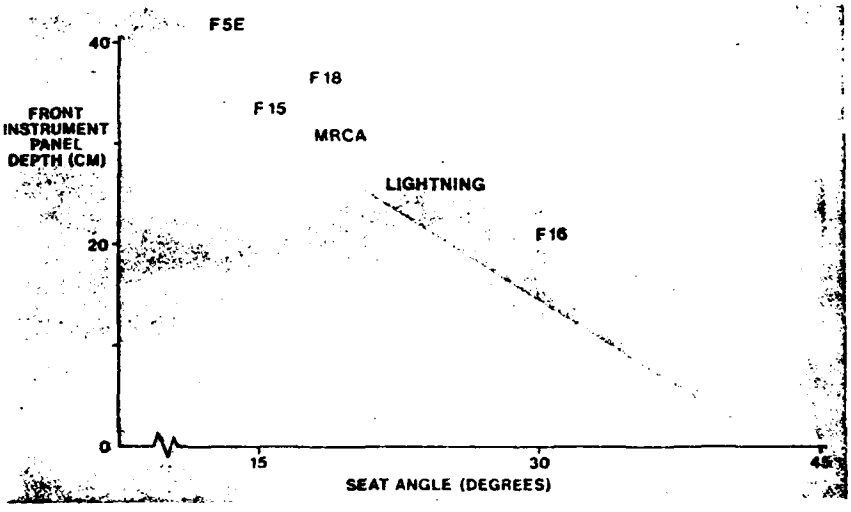


Influence of seat tilt on panel space

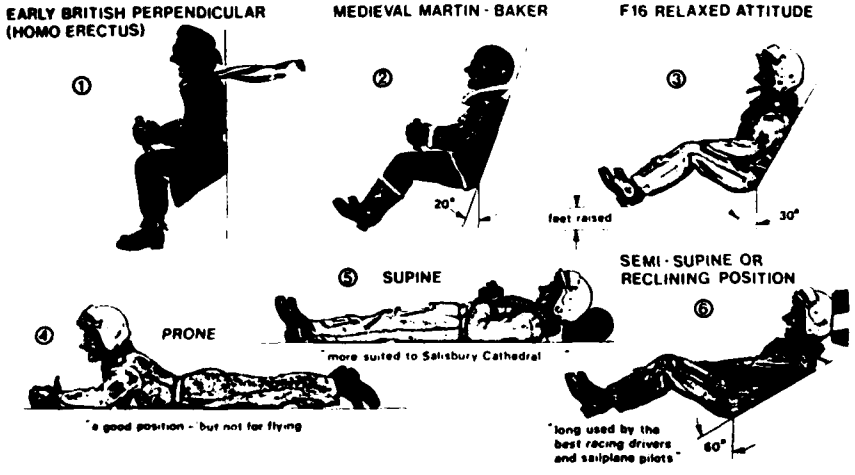


Pilot's seating postures

Fig. 78 (Extrait de CP 241 papiers n°2 et 27)

# REVIEW OF PRACTICAL EXPERIENCE ON COMBAT AIRCRAFT MANOEUVRABILITY

by

Major A.W.Henni, RNLAF
Hartmarlaar 30
3760 XJ Soest
The Netherlands

SUMMARY

Based upon practical experience in both air-to-air and air-to-ground operations with F-84F, F-104G and NF-5 fighter aircraft, an assessment is given of the importance of combat aircraft manoeuvrability.

In air-to-ground operations the effect of limited manoeuvrability on tactics is treated in terms of speed/altitude and manoeuvrability requirements during ingress/egress and weapon delivery, in relation to attack effectiveness and survivability against enemy defences. Present shortcommings are identified.

For air-to-air operations the parameters that influence the outcome of a manoeuvring fight are identified. The relation between manoeuvrability and tactics is discussed. It is concluded that the impact of manoeuvrability on mission effectiveness becomes less prominent at increasing total number of air-to-air capable aircraft, fighting in a limited airspace.

Dependent on the type of operation, desirable improvements in manoeuvrability are discussed with emphasis on turn performance (at low speeds), rapid speed changes and direct force generation. In this context human tolerance limits are taken into account. It is stressed that the main problems confronting a fighter pilot in the Central European environment are not related to manoeuvrability but to the availability of military subsystems.

## INTRODUCTION

1. The mission of fighter type aircraft in a conflict in broad terms is to participate in achieving a favourable air situation and to contribute to the land, sea and air battle. In the Central European theatre air superiority, the freedom to fight and to use aircraft where and when desired without significant hostile interference from the air, has to include not only the suppression of the effectiveness of the enemies air-potential but also his surface-to-air weapons. Therefore air superiority has to include air-to-air engagements, counter air and counter-SAM operations. The latter being partly a fight of technology, partly an air-to ground operation in which tactics play an important part. Further support of the battle by fighter type aircraft is done by air-to-ground missions.

2. Potential mission effectiveness of combat aircraft is determined by a number of factors, such as the pilot's ability, avionics, weapons and related systems and the performance characteristics of the aircraft Manoeuvrability, the ability to change direction and magnitude of an aircraft's velocity vector, is the factor in the performance of fighters to be dealt with in this paper. Basing myself upon practical experience as an operational pilot on F-84F and F-104G and as an Air Combat Tactics instructor on F-104G and NF-5, I will give my personal view on the importance of combat aircraft manoeuvrability both in air-to-ground and air-to-air missions, followed by some thoughts on desirable improvements. In conclusion, some possibilities will be mentioned where improved weaponry and related subsystems can compensate for lack of manoeuvrability.

## THE IMPORTANCE OF MANOEUVRABILITY IN THE AIR-TO-GROUND ROLE

3. In an operational mission manoeuvrability is an asset, used by the pilot in order to accomplish a task to the best of his abilities. He thereby has to take into consideration the posibilities, or rather, the impossibilities of his aircraft. Unless protected by perfect ECM and IRCM, high speed and low level flight is what an air-to-ground pilot wants in the Central European high threat environment during ingress and egress and, if possible, also during weapon delivery;this in order to reduce the time he will be exposed to enemy defences. During a mission the manoeuvring qualities of an aircraft in relation with air

speed is one of the factors determining how closely terrain can be followed in low level flight when the pilot wants to avoid detection by enemy radar or I.R. SAM systems. In this respect there is a difference between e.g. the NF-5 and the high wingloaded F-104. It is noticeable that the average F-104 pilot takes more care (=altitude) in performing recoveries from a pitch-down attitude than his colleague in a low wingloaded airplane at the same speed. This is caused by the fact that the F-104 pilot has to "pull" more angle of attack than his NF-5 colleague in order to achieve the same amount of altitude loss in dive recovery at equal speed. The F-104 reaches the point of high-speed stalling at a certain speed earlier than a low wingloaded aircraft. This in combination with the F-104's pitch rate limiting system, which is easily activated when pulling G following a so-called bunt manoeuvre where the pilot applied negative G to follow the downslope of a hill, makes the F-104 or a high wingloaded aircraft in general less suitable for low level terrain-following flight. However, in my opinion improved manoeuvrability in manually-flown high speed low level missions in the relatively flat Central European theatre will only lead to minor improvements in the attainable minimum altitude because of the predominancy of the pilot's ability to detect, interprete, decide and react, versus speed. In a threat environment with sharp ridges, however, enhanced manoeuvrability, especially when this leads to reduction of the time between control input and the required change in aircraft trajectory, will be very helpful. In the context of terrain following, speed is a very important factor. It is a known fact that with speed the average altitude above terrain depending on pilots experience increases in manually flown low level missions. Both high speed and low altitude serve the purpose of avoiding detection and tracking by enemy weapon systems, so that the pilot is faced with conflicting requirements. To fly really low level, the pilot will have to cut down his speed considerably, thus sacrificing manoeuvring potential which makes this option less attractive. In fig. 1 the required and available amount of positive G (for W/S=120 and 90 lbs/ft$^2$) is presented for an aircraft following a sinus shaped contour with a wavelength of 1200 m and an amplitude of 30 m at different speeds, assuming $C_{L_{max}}$=1.

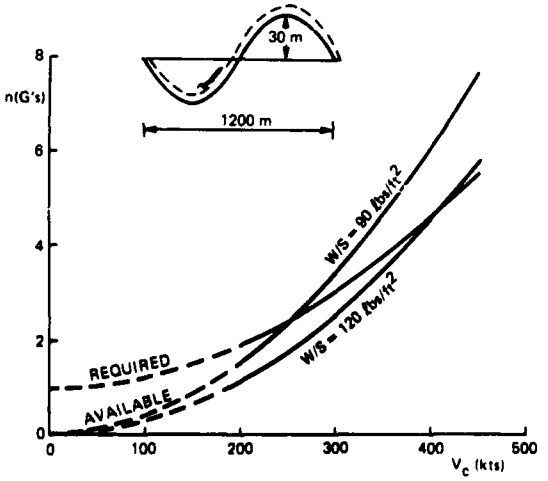


Figure 1

The figure shows that at speeds below 415 kts an aircraft with a wing loading of 120lbs/ft$^2$ is not able to follow the contour. Flying high speed at a higher average altitude makes the aircraft detectable, which is not attractive either. Systems like Radar Warning Receivers, ECM, IRCM and in the future Missile Launch and Approach Detectors (MLAD) may be able to compensate for the enhanced vulnerability caused by increased detectability. To find an optimum trade-off between speed and altitude requirements is a difficult task, in which flight test against ground-to-air weapon systems and subsequent computer simulations, as performed by the National Aerospace Laboratory in Amsterdam for example, are helpful. Another factor that has to be taken into account is that low level ride qualities usually are better with high wingloaded aircraft, thus creating diverging demands for the wing loading of fighters that have to perform low level missions at high speeds.

4. In the weapon delivery phase of the air-to-ground mission manoeuvrability related problems are of the same nature as described above: high speed and low level flight reduce the time available for target acquisition and weapon aiming, inducing the need for fierce last second manoeuvres where the danger of high speed stalling is ever present. Here too reducing speed or flying at a higher altitude to enlarge the time available for target acquisition and weapon aiming, results in an increased detectability by enemy defences. Moreover, reducing the speed of an aircraft that was designed to fly fast, will greatly reduce manoeuvring potential. For this reason this option is not a viable one.

5. A problem in itself is the significant degradation of performance, including manoeuvrability, when aircraft are loaded with external stores. This degradation is especially felt when defensive manoeuvring -as a precaution or defence against tracking hostile aircraft or SAM's- is necessary. Weight and aerodynamic degradation, especially at higher angles of attack, reduce instantaneous and sustained turn performance and handling qualities to such an extent that stores will often have to be jettisoned in evasive manoeuvres, thus leading to an ineffective mission.

6. In conclusion it can be said, that in the air-to-ground mission, apart from defensive manoeuvring against SAM's and other threats, the main difficulty in fulfilling the requirements for avoiding enemy ground-to-air systems is the dilemma between desired speed, altitude and pilot reaction-time. In these missions enhanced manoeuvrability at high speeds will naturally be welcomed by pilots because it gives them more opportunities to allow for late reactions and last second corrections but will not overcome afore said dilemma. Better manoeuvrability at low speeds - A-10 like - will make the option to fly low and slow to achieve timely acquisition of targets that are difficult to find, more viable than it is with most of present generation conventional ground attack or multirole fighters. In my opinion however the fact remains that, especially in relatively flat Central Europe fighters that have to perform air-to-ground missions will need high speed performance in order to survive in the present high threat SAM/AAA environment facing NATO. Therefore an aircraft that has to perform in various types of air-to-ground missions, to meet the demands for ingress and egress and to leave open the option of flying at low speeds for target acquisition, retaining the capability for defensive reactions, needs manoeuvrability over a wider speed band than is presently the case.

## THE IMPORTANCE OF MANOEUVRABILITY IN THE AIR-TO-AIR ROLE

7. In air-to-air combat gaining or losing advantage can be expressed as changes in range, relative position (angle off tail) and angle between longitudinal axes of the opponents. Performance characteristics that are important in bringing about those changes are handling qualities, Specific Excess Power (Ps), the limits of the flightenvelope and related to the previous factors: turn performance.

8. Good handling qualities, especially at high angles of attack , like spin and departure resistance, enable the pilot to perform manoeuvres up to the edges of the flight envelope without the risk or fear of losing control. Attainable pitch and roll rate are important factors in the initiation and execution of manoeuvres. Ps in itself and in relation with angle of attack and load factor is a parameter of paramount importance in the manoeuvrability problem. It not only enables an aircraft to climb and accelerate but also provides the energy to turn. Favourable Ps figures give the pilot the opportunity to change range, relative position and angle between longitudinal axes relative to his opponent favourably. The Ps figures for a given airplane are very dependent upon the load factor. If, under set circumstances, an airplane has advantageous Ps figures in 1 G conditions, the balance might shift considerable when pulling G's. This effect is shown in fig. 2.

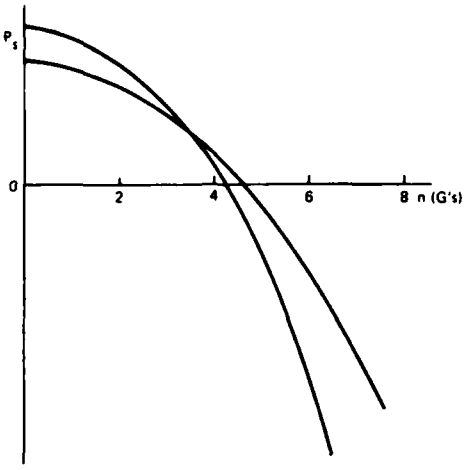


Figure 2

Wing loadings and aerodynamic properties such as $C_L$ - $C_D$ characteristics are accountable for this phenomenon. Another factor that influences turn performance is the relationship between speed and available sustained and instantaneous G. Attainable turn rate and radius are directly related to these figures. Available G at a certain speed is dependent upon design load limit and stalling speed ($V_s$). An often used way to present the relationship between turn rate ($\omega$), radius, Ps, load factor and speed at a certain altitude is presented in figure 3.

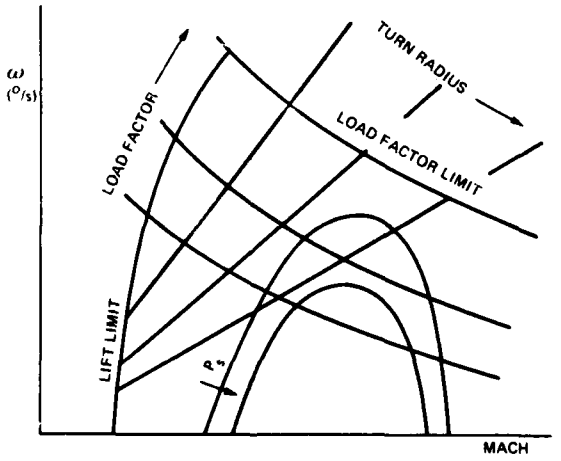


Figure 3

From graphs like this we can learn that a fighter pilot who wants to change the relevant parameters in an air-to-air engagement to his advantage would like:

a. The lift limit at a lower speed than his opponent. This enables him to turn at small radii and manoeuvre inside of his opponent's turn, thus reducing the range by "cutting corners". The resulting higher instantaneous turn rate enables the pilot to gain "angles" on his opponent. Lowering the lift limit speed will also bring the manoeuvre point, the point where maximum turn rate and nearly minimum radius can be reached simultaneously, at more favourable values.

b. A higher design load factor than his opponent. This results in better turn rate and radius at high speeds.

c. Higher Ps values than his opponent. This enables the pilot to manoeuvre with less energy bleed off allowing him to continue a manoeuvring fight longer.

Fulfilment of these wishes paired with good handling qualities theoretically enables a pilot to gain advantage in any one versus one engagement. However, other factors, like visibility from the cockpit, aircraft size, engine smoke, weapon system and avionics play an important part too. When we compare the $n$-speed graphs of various airplanes, relative strong and weak points in the performance of adversaries and own aircraft can be found. This provides opportunities to compensate for lack of manoeuvrability by using proper tactics.

TACTICAL PRINCIPLES AND TACTICAL DOCTRINES

9. In WW I the Red Baron was alleged to have said "When your opponent fires at the zig, you have to be in the zag and when he fires at the zag, you have to be in the zig". This still is the basis of defensive manoeuvring. Take care never to be co-located with the opponent's projectiles or missiles. Another maxim of the old days still holds: try to manoeuvre for your opponent's deep six o'clock. This means try to get low behind the opponent because he cannot see you there and it is a good position from which to close in for the use of short range weapons. In air-to-air engagements the sun and clouds are still used for the same purpose as in WW I. A rule like "never be predictable" is still valid. Modern fighters look quite different from their predecessors and the flight envelopes have shifted to higher speeds, altitudes and load factors, but the manoeuvres they can perform are still the same:hard turns, breaks, scissors, loopings, barrel-rolls etc. The entity of general rules, use of meteorological conditions, use of the sun and the available two and three dimensional manoeuvres are called Tactical Principles. Basically these principles have not changed in the history of air combat.

10. When we look at a one versus one engagement between an F-104 G and an NF-5 we are dealing with an aircraft with a relatively high thrust to weight ratio and ditto wing loading and one with a low thrust to weight ratio and wing loading. On top of that the NF-5 has better handling characteristics and a lower Vs than the F-104 G. Design load factors are equal. These performance characteristics and interpretation of the respective $n$-speed graphs (not included in this paper for classification reasons) lead to the conclusions that the NF-5 has an advantage in roll and pitch initiation and in instantaneous and sustained turns at lower speeds. At higher speeds the NF-5 and F-104 are equal qua instantaneous turn and the F-104 gains some advantage in Ps, an advantage that is largely reduced, or even changed into a disadvantage, under high G conditions because of the rather drastic increase in induced drag (see fig. 2). For these reasons the NF-5 pilot will try to conduct a manoeuvring engagement against an F-104 - like aircraft at speeds below the transonic region, whereas the F-104 pilot has to keep his speed, or better, the sum of potential and kinetic energy up to avoid entering the zone where his opponent is superior. However, as a turning fight progresses, both aircraft, trying to gain angle and range, will lose energy, because the required turn rate and radius will force the pilots to pull more than sustainable G. This will cause both aircraft to slow down, eventually leading the F-104 into an area of the flight envelope where the NF-5 is superior. Before this occurs, the F-104 pilot will have to leave the fight because continued manoeuvring will bring him in the situation where his only advantage over the NF-5, a higher Ps at transonic speeds, is lost. Here we see that although both aircraft are capable of using the same tactical principles, each of them will tend to use only those that do not bring at risk the aircraft's relevant superiorities. In general, for an NF-5 this means: do not try to run away from a fast F-104, but force an overshoot. The F-104 pilot will refrain from pursuing an NF-5 if this means sacrificing energy to a point where his ability to run away - disengage - is in danger.

11. Where in a one versus one environment - weapon systems and pilot ability being about equal - manoeuvrability and flight envelope are the factors dominating the outcome of the engagement, things change when more air-to-air capable aircraft enter the scene. A numerial superiority can compensate for lack of performance and manoeuvrability because it is very difficult to respond adequately to the manoeuvring of two aircraft simultaneously. Manoeuvring against one will give the other opponent the opportunity to gain an advantageous position. When we consider more aircraft in a relatively small piece of sky the factor "situation awareness" has to be mentioned too. In my experience the maxim "it's the one you don't see that kills you" becomes frightfully true. Once the opponents know each others whereabouts the outcome of the fight is dominated by relative numbers and performance. In my opinion, however, situation awareness - to get to know the whereabouts of threats, targets and friends - in a multi aircraft air-to-air engagement is the more important factor provided that all participants use the right tactics. Of course, also in the air-to-air environment enhanced manoeuvrability adds to an aircraft's offensive and defensive abilities; to know when to go into the offense or defense, however, is especially in a crowded air-to-air arena of more importance.

## DESIRED IMPROVEMENTS

12. Introduction. In the previous paragraphs I reached the conclusions that in an air-to-ground mission in the high threat environment to be expected in Central Europe the dilemma between pilot-reaction time, speed and altitude and the problem of target acquisition are the main factors hindring the achievement of the high speed - low level profile that is desired during ingress and egress in order to avoid enemy ground-to-air defenses. Enhanced manoeuvrability in this mission will help the pilot to fly slightly lower at the same speed and will be useful in the weapon delivery phase to make aiming corrections. In the air-to-air mission and also in the air-to-ground mission during reactions to air or surface-to-air threats, enhanced manoeuvrability will enlarge the offensive and defensive capability of fighter aircraft. Situation awareness, however, is the prerequisite to offensive or defensive reactions and as such, in a complex air-to-air arena, predominant to a high degree of manoeuvrability because the use of suitable tactical doctrines can compensate for lack of it. In the following part of this paper I will go into desired improvements in manoeuvrability. Aspects like training, avionics, displays, weapons and weapon systems, however, cannot remain unmentioned.

13. Improved manoeuvrability. In the air-to-ground mission during ingress and egress through dense SAM defenses manoeuvrability is used for the purpose of terrain following, avoiding obstacles, following valleys and up- and down slopes of hills. A desirable improvement in this area is to allow for high instantaneous pitch rates (reducing the risk or pilot's fear for high speed stalls and subsequent altitude loss). Possibly highly responsive automatic manoeuvring flaps and less detrimental aerodynamical effects of external stores at high angles of attack can offer solutions here. The use of direct force generation in my opinion is a promising development in this field. Altitude variations for the purpose of avoiding obstacles and closely following the terrain, with this technique can be obtained without changing aircraft attitude. Direct force generation in a lateral direction offers the possibility to avoid obstacles without having to bank and turn the aircraft, a manoeuvre which is pretty scaring and dangerous for the average pilot because of the limited realistic very low level flight training attainable in Central Europe. In the target acquisition and weapon delivery phase, especially in the high threat areas near the front lines and around important targets, enhanced manoeuvrability can play an important part. As mentioned before, acquiring targets, especially concealed ones, takes time. This means that a pilot has to fly higher to enlarge his acquisition range or fly slower to enlarge the time available for finding the target or a combination of these options. The first option means a higher detectability by enemy defences, the second one loss of manoeuvring potential. The main problem, acquiring targets, can only be solved by advanced sensor and display technology. Enhanced manoeuvrability can be helpful in providing the pilot with means to choose, depending on the threat and other circumstances, whether to fly higher or slower. This means that manoeuvring potential should be available also at relatively low speeds. This, however, in combination with the ability to accelerate quickly in order to retain an aircraft's prime offensive and defensive strength: the ability to change its position threedimensionally over long distances in a short time.

In the weapon aiming and delivery phase of a mission manoeuvrability plays its role in preventive jinking (irregular threedimensional changes in direction) against ground-to-air threats (provided that the weapon aiming computer can handle the resulting aiming computations) and in precise manoeuvring during the final part until weapon release. At medium and high speeds present fighters possess sufficient manoeuvring potential for jinking. At lower speeds, however, especially with external stores, improvements are desirable.

14. In the field of improved manoeuvrability for the air-to-ground mission fast responding automatic manoeuvring flaps, thrust vector control and improved aerodynamic characteristics of external stores at high angles of attack can improve instantaneous and low speed turn performance, whereas high Ps values are necessary for required accelleration and sustained performance. Variable geometry wings can take care for better low speed characteristics while retaining high speed low level cruise qualities. Direct force generation, vertical and lateral, will make terrain following more easy for the average pilot. In combination with advanced fire control computers direct force generation will add finesse to the aiming of unguided weapons.

15. In the air-to-air role design load limit as offered by aircraft such as the F-16 in my opnion touches the fringes of what the human body can endure. Improvements in manoeuvrability therefore can only be found in extending the flight envelope where the design load limit can be reached or sustained. This comes down to improving the position and course of the lift limit line in the graph shown in paragraph 8 and by enhancing the Ps values. This means low wing loading, favourable $C_L$ - $C_D$ relations and high thrust to weight ratio's. The new generation of fighter aircraft designed for air combat as well as R and D in this field show that these items get ample attention. Rightly so. New technology, associated with direct force generation and thrust vector control, will play a part in further improvements in manoeuvrability.

16. Improved systems. As stated, the main problem in the air-to-ground mission is target acquisition under conditions of high-speed low-level flight as necessitated by the ground-to-air threat in Central Europe. As long as these conditions prevail manoeuvrability helps the pilot to perform his mission. Advanced sensor and display technology can assist in target acquisition. Major improvements in the air-to-ground mission effectiveness can in my opinion, however, only be expected when fighter aircraft regain the survivable use of three dimensions, including altitude. For this, efficient ECM, IRCM and threat warning as well as offensive options against ground-to-air systems, are necessary.

17. In the air-to-air arena the basic problem is situation awareness. So far the means for situation awareness available to the fighter pilot are his forward looking radar, his eyes, a radar warning system and radio information from intercept controllers. This will do perfectly well in a surveyable situation. Manoeuvrability and weapon system in that case are predominant. In the rather unsurveyable air situation that can be expected during a conflict in the Central Region enhanced manoeuvrability will do little to improve mission effectiveness unless accompanied by means to improve the pilot's view of the situation. Improved radar coverage and better means for identification and threat warning in my opinion are more badly needed than improved manoeuvrability beyond that already offered by the new generation of fighters that were or are being designed for air-to-air work.

18. Manoeuvrability and weapons. Weapons like high energy lasers are no longer pure science fiction. In combination with sensors and fire control computers directed laser beams can become a defensive weapon that takes away most of the necessity for defensive manoeuvring against guided missiles. Precision guided air-to-ground weapons can, if delivery parameters become such that they are useful under European circumstances, overcome the need for precise manoeuvring for weapon aiming.

19. In the air-to-air mission off-bore-sight all-aspect missiles can compensate for limited manoeuvrability. Manoeuvring to bring a target within launch parameters will be an easier job with these missiles. Use of these missiles in an air-to-air engagement will also reduce the effect of defensive manoeuvring because it will be harder to stay or get out of the launch envelope. The only hope is to stay out of missile range or upset the missile's tracking or guidance systems.

20. Technological developments in the military subsystems tend to make manoeuvrability requirements less demanding. On the other hand, new weapons tend to provoke new defensive systems. It can therefore be expected that the historical trend, in which neither IR nor Radar missiles banned out the close-in manoeuvring fight, continues. Manoeuvrability therefore will continue to be a valuable asset in a fighter's mission.

CONCLUSION

21. With respect to the manoeuvrability already achieved by the new generation of fighter aircraft with an air-to-air task, main improvements leading to more effective missions are to be expected from systems that overcome the basic problems confronting the present fighter business namely:

a. *Regain the full use of the vertical dimension in the Central European threat environment with* reasonable survivability.

b. Target acquisition.

c. Situation awareness in multi aircraft engagements.

22. Technological developments in the military subsystems, however, to my expectation will not fully overcome the problems and manoeuvrability will continue to play its important part. Enhancements in manoeuvrability therefore deserve continued attention. Bearing in mind human limitations, fields where improvements can be found are low speed sustained and instantaneous turn performance, direct force generation and enhanced ability to change speed.

# THE MILITARY FLYING QUALITIES SPECIFICATION, A HELP OR A HINDRANCE TO GOOD FIGHTER DESIGN?

by

RALPH C. A'HARRAH
NAVAL AIR SYSTEMS COMMAND HEADQUARTERS
Washington D.C. 20502

and

ROBERT J. WOODCOCK
AIR FORCE WRIGHT AERONAUTICAL LABORATORIES
WRIGHT-PATTERSON AFB, OH 45433

## SUMMARY

Based on recent experience with Air Force and Naval aircraft, the current flying qualities specification is evaluated for application on a future fighter design.

The recent experience includes analog and digital fly-by-wire flight control systems having multiple redundancy levels, and significant control law variations. Some specific observations are shared on the following topics with regard to the flying qualities in general and the specification in particular:

- time delays
- force commands
- forward-loop integration
- high gains
- signal blending
- equivalent systems
- pilot location
- high angle of attack
- roll performance
- systems integration

In addition, some general observations are made on the use of MIL-F-8785B, and a Navy conducted survey on the effectiveness of the flying qualities specification is discussed.

## 1. INTRODUCTION

We have noticed a signficant erosion in confidence with our flying qualities specification in recent years. And with this erosion in confidence has come a lack of commitment to understand the specification, and to actively utilize the specification guidance during the evolution of the design. For a number of designers, MIL-F-8785B or C has essentially become and after-the-fact check list that is often perceived to be more of a burden than an asset.

There are several reasons for this situation. First, the specification is derived from data on simple airplanes with simple control systems but our airplanes with advanced flight controls constitute complex systems. The relevancy and the adequacy of the specification to handle these complex systems appropriately is therefore brought into question.

Second, the specification used to be the primary tool for evaluating the flying qualities prior to first flight. Flight simulators, of increasing sophistication as the design progresses, are now utilized as an integral part of the design process. The computational capabilities available to support simulation hardware can model the complex aircraft and flight control systems for pilot evaluation. Indeed, the design of advanced aircraft today is virtually unthinkable without substantial flight simulation support. Because of its sophistication and direct involvement with pilots, the simulator may be more readily believed than the specification, whether warranted or not.

The third major reason is resource limitations. The pressure to produce, at a reasonable risk, a satisfactory fighter design with the minimum investment of resources is the essence of the competitive aircraft business. This concern is not conducive to supporting the significant effort required to continuously cycle the latest design parameter through a comparison with the specification while, in parallel, supporting a flight simulation effort. The commitment of resources will inevitably be further confounded by a significant aerodynamic or flight control redesign. The specification effort will characteristically suffer even further under these conditions.

Acknowledging that the above reasons and others have been used to justify deemphasis of the flying qualities specification, let us now examine some reasons for reemphasizing the specification.

First, the specification is the most complete compilation of flying qualities criteria available. The criteria contained in the specification have evolved as aircraft technology has evolved. The supporting data is unrivaled.

Second, our more recent aircraft designs with their flight control systems designed on flight simulators have been disappointing. Advanced control system technology is recognized to have great potential for providing enhanced flying qualities, but our new aircraft are approaching first flight with some fundamentally bad flying qualities. One recent design has required three years, several signficant control law changes, and a complete change in design philosophy before approaching satisfactory flying qualities characteristics. The A-9, A-10, F-16, F-17, F-18 and Space Shuttle have all had fundamental and significant flying qualities deficiencies which were undetected until early flights, or were exposed during in-flight simulations prior to first flight. A more active involvement of the specification during the design and development could have prevented many of the problems encountered.

The purpose of this paper is to communicate our feeling that the flying qualities specification needs to be more instrumental in guiding the advanced control system design, and to discuss some of the subtleties involved.

## 2. NAVY EXPERIENCE

The applications of 8785 to aircraft utilizing advanced flight control systems have certainly been limited in number. However, this admittedly limited exposure to advanced flight control characteristics has shown no examples of satisfactory flying qualities which the specification indicates to be unsatisfactory. In that sense our flying qualities specification has not unduly restricted innovative control law implementation. Further, tailored application with an open mind has allowed even such innovations as complete reliance on fly-by-wire.

There have, however, been numerous examples of control laws which were introduced to improve the flying qualities over and above the specification, but were instead a source of flying qualities decay. Four specific examples which will be discussed are: inappropriate blending of signals to be nulled by forward-loop integration; high forward-loop gains; force rather than displacement command signal for the pilot; and forward-loop integration.

### 2.1 Time Delay

The major specification shortcoming uncovered during the Navy's most recent fighter design was the need to stipulate the allowable time delay between the pilot's command and the associated aircraft response. The latest revision to the flying qualities specification, MIL-F-8785C, contains the time delay limits shown in Figure 1, which satisfy this need.

TABLE XIV. Allowable airplane response delay.

| Level | Allowable Delay, Sec |
|---|---|
| 1 | 0.10 |
| 2 | 0.20 |
| 3 | 0.25 |

Figure 1 - MIL-F-8785C Time Delay Requirement

While the importance of the equivalent time delay as a pilot acceptance parameter was highlighted on an aircraft using a digital flight control computer, the portion of the time delay attributable to the digital computer's inherent characteristics, i.e. the computational cycle time, was a relatively small portion (less than 10%) of the total. The major contribution was the cascading effects of prefilters, structural filters, dynamic shaping, etc., etc. Thus the substantially increased capacity of digital computer to implement control laws and the innovativeness of the controls engineers to utilize this capacity produced unacceptable performance during tight tracking tasks.

Examining equivalent time delay values on previous aircraft having limited-authority augmentation and a direct command signal to the aerodynamic surfaces, we find values of equivalent time delay which exceed the 0.1 sec. Level 1 limit and even approach the Level 2 limit value. For example, the equivalent time delay for the longitudinal response of the F-14 is 0.15 seconds; for the A-7, 0.17 seconds. For these aircraft, only the surface actuator and the stick dampers contribute to the equivalent time delay. Clearly, inserting additional higher order elements in the system may ruin the tight tracking performance unless compensating changes are made to the basic elements.

The focus on time delay is critical to providing satisfactory tight tracking performance. The insidious nature of time delay is illustrated by the inability of either dynamic analysis or piloted flight simulation (at levels which would be considered adequate by any measure) to uncover significant problems with both the Shuttle and the F-18. Only with the help of in-flight simulation (references 1 and 2) were the characteristics ultimately defined and appreciated by the pilots.

## 2.2 Force Commands

The advantages of using force commands rather than displacement are the phase lead (or lack of lag) in the command path, and maintaining control after a mechanical jam. A disadvantage is the substantial filtering required to attentuate the structural mode/control system coupling. For trainer aircraft, a second disadvantage is the complex mechanization of the cockpit controls so that the instructor pilot can readily monitor the student's control strategy by viewing the motion of his own control. One of the contemporary fighters has managed nicely with a force command system implemented on a side arm controller. Another fighter/attack vehicle, which originally used force command implemented through a conventional center stick arrangement, is being modified to a displacement command center stick in order to relieve some of the required filtering. Had the required filtering been added to accomodate the force command mechanization, there would have been an associated deterioration of the tight tracking task performance, corresponding to the increased equivalent system time delay. So for this particular example, the benefits of phase lead were overcome by the required compensation to such a degree that remechanization was necessary to achieve satisfactory characteristics.

## 2.3 Forward-Loop Integration

Incorporating forward-loop integration as a means of providing constant load factor to stick force, or constant roll rate to stick force, throughout the flight envelope must appear attractive: several contemporary flight control systems utilize such mechanizations. The U.S. Navy currently does not share that view for the following reasons: forward-loop integration of normal load factor error, pitch rate error, or a weighted blend of the two produces neutral speed stability (and positive speed stability is still a Navy requirement): no significant benefits are derived from the increased complexity; and the resulting tendency for constant dynamic response characteristics over a range of flight conditions is unnatural, and deprives the pilot of information useful in monitoring the flight state of his aircraft.

Unquestionably the flying qualities specifications tailored for specific procurements have, in the past, so tightly constrained some aspects of vehicle response (such as establishing an upper limit on roll rate which is inappropriately close to the lower limit on roll rate) that use of an integrator has been encouraged if not required. However, the current acceptance regions of MIL-F-8785B and C have been and are being met without resorting to forward-loop integration. This practice is encouraged.

## 2.4 High Gains

High forward-loop gains are attractive for quickening the vehicle in regions of characteristically sluggish response. The logic is intuitively attractive. How high the forward-loop gain should be to provide the enhancement without provoking a sensitivity problem is less clear, and is not explicitly addressed in the specification.

Numerous instances of unsatisfactory control sensitivity have been experienced with the advanced flight control systems. The standard measures of sensitivity such as stick force per g, and roll performance per stick force, indicated the advanced flight control system to be nicely entrenched in the Level 1 region of the specification. However, there were significant differences in the initial response. For overly sensitive configurations, the initial acceleration values were higher than the corresponding Level 1 values for an equivalent system. For the sluggish configurations, the initial accelerations were below the equivalent-system Level 1 values. The implication here is that while advanced flight control systems provide a limitless variety of control law combinations which will satisfy the letter of the specification, consideration must be given to the fundamental response characteristics which provided the data base for the specification. For example, the bank angle response requirements were derived for control laws giving an initial roll acceleration linearly varying with command, and the combination of the values of roll acceleration and roll damping would uniquely establish the bank-angle response characteristics, Figure 2. Thus the pilot acceptance regions could justifiably have been expressed either as combinations of roll acceleration and roll damping or by the currently stipulated bank-angle response criteria. The choice was arbitraty, except perhaps for considerations of convenience or ease of interpretation. The specification can be credibly interpreted only as levels of bank angle response achieved with the associated combinations of roll damping and roll acceleration. Calling for high levels of initial roll acceleration to be quickly cancelled by feedback and forward-path integration providing the characteristics illustrated in Figure 3 is clearly outside the specification guidance. Providing modestly high forward path gains to alleviate sluggish response levels is appropriate, but both $\emptyset_1$ and $L_{F_S}$ should be within the acceptance region.

An analogous situation exists in the longitudinal mode. The specification was derived for control laws having the control anticipation parameter, $CAP = \theta_o/n_{ss}$ always equal to the variation of normal load factor to angle-of-attack sensitivity with short period frequency, $\omega_n^2/n_\alpha$. However, as a practical matter there can be significant difference between CAP and $\omega_n^2/n_\alpha$ for unsophisticated control systems, as discussed from

various viewpoints in references 3, 4, and 5, due to the lag contributions of stick dampers and actuator dynamics. The use of forward-loop integration, high forward-loop gains, and the associated additional prefiltering can cause even further distortion in the CAP, $\omega_n^2/n_\alpha$ relationship. Because of this distortion, satisfactory short-period response requires the independent consideration of both the $\omega_n^2/n_\alpha$ and CAP parameters, as illustrated in Figure 4.

Further, the existence of significantly different acceptance regions for the two parameters is suggested by DiFranco, reference 4, with comparative applications recently done by Bischoff, reference 3. Additional alternative approaches to the short-period response acceptance criteria have been recently proposed by Stengel, reference 8; Mitchell and Hoh, reference 9; and Mooij, reference 5.

The approach currently recommended for fighter type aircraft, independent of these new and different acceptance criteria, is to consider both CAP and $\omega_n^2/n_\alpha$ independently, and to consider the acceptance criteria for both to be the existing specification.

## 2.5 Signal Blending

The advantage of blending washed-out pitch rate with normal acceleration to form an error signal for a forward-loop integrator is the increased efficiency of the integrator in nulling the high-frequency error content while providing a more docile controller of subtle motions. The nulling instincts of such a blending are compatible for unbanked flight. However, during rapid rolling maneuvers the parameter mix is not compatible. Rolling about the stability axis suggests a constant normal load factor (Figure 5) and thus an oscillatory pitch rate of magnitude $\frac{g}{V}(n - \cos \phi)$. Alternatively, rolling about the body axis produces a constant pitch rate but oscillatory normal acceleration of magnitude cos $\phi$ (Figure 5). Thus the integrator would complement the stability-axis roll if the error signal were simply normal load factor; and would likewise complement the body-axis roll if the error signal were just pitch rate. The result of load factor and pitch rate blending, however, was a disconcerting level of pitch coupling during the roll maneuver. The solution was to adjust the relative gains of the two components so that more emphasis was placed on the normal acceleration errors and the pitch rate signal was de-emphasized. Figure 6 indicates the relative improvement of the load factor excursions during 360° rolls with the improved blending.

A solution would be the blending of angle-of-attack rate, rather than pitch rate, with the normal acceleration signals. These signals are compatible during rolling maneuvers about the stability axis. Alternately, the blending of pitch rate and attitude would provide compatible signals for body axis rolls.

## 2.6 Equivalent Systems

During the presentation of reference 10, there was considerable discussion on a difficulty with equivalent system parameters derived from matching the pitch rate response over a nominal bandwidth; the physical interpretation of an equivalent $n_\alpha$ significantly different than the value derived from the wind tunnel. In fact, the example of reference 10 indicated a factor of 20 difference between the two values. More recent matches, using both the pitch rate and load factor response over the same bandwidth, result in a significantly reduced migration of the equivalent $n_\alpha$ value, as indicated by the superposition of the simultaneous matched data of Figure 7. While the $n_\alpha$ values are significantly different, the control anticipation parameter is essentially the same for the two different matching techniques, and therefore the interpretation of the pilots' acceptance is unchanged. The benefit of the dual match is simply that the results will be perceived more credibly.

Application of the equivalent systems technique to the lateral-directional characteristics has progressed through an in-flight investigation on the Air Force - Calspan NT-33 (references 11 and 12). The flight-derived pilot rating obtained from evaluations of various higher-order systems was used with the corresponding equivalent system characteristics to compare with acceptance regions of the specification. The lateral-directional matching utilizes a sideslip to rudder pedal response and a bank angle to lateral stick response in order to get sufficient information for consistent identification of all the numerator and denominator parameters of the second- over fourth-order equivalent system describing function.

There are no definite "match" or "fit" criteria for the application of equivalent systems, and with the experience to date there is little likelihood of establishing such criteria in the near future. Pilot ratings of various higher-order systems, which had the same equivalent system characteristics but with significantly different levels of mismatch, indicated no significant variation of pilot rating with mismatch (reference 13).

An indepth look at equivalent system applications to several Navy tactical aircraft (reference 3) clearly indicates that the relevant information on the acceptability of flying qualities characteristics can consistently be established independent of the mismatch. In fact, example cases are shown with larger mismatches giving more intuitively reasonable parameters than do the cases with exceptionally good matches. The level of acceptability predicted from the equivalent system characteristics for the different techniques remained unchanged, however.

Based on the total equivalent system experience and the above two examples in particular, the absence of mismatch criteria is not considered crucial to the meaningful interpretation of higher-order system characteristics within the specification framework. What is clear is that without a specified equivalent system routine and a mismatch criterion, the enforcement of the specification in an adversarial confrontation may be futile. But given a mismatch limit, then the goal can easily become one of judiciously manipulating the match routine to achieve the best set of equivalent system parameters from a specification compliance viewpoint, while not exceeding the mismatch limit. An authentically useful tool would thus be compromised. The point is that without a mismatch criterion, application of the equivalent systems approach is done with the goal of getting the best match and then evaluating the acceptability of equivalent systems' characteristics.

## 2.7 Aircraft Size, Pilot Location Considerations

As a result of discussion at the October 1979 AFFDL Flying Qualities Symposium (reference 14) on the very poor correlation of large-aircraft flying qualities acceptability with the specification criteria for the short period requirements, the Navy conducted an informal survey of large-aircraft characteristics. The original control anticipation parameter (reference 15) which uses initial pitch acceleration, identified as $CAP_1$, was compared to an alternate approach (reference 16) which uses initial normal acceleration at the pilot, which will be called $CAP_2$. $CAP_2$ is simply $CAP_1$ times the distance from the pilot to the instantaneous center of rotation for pitch control inputs, i.e., $CAP_2 =$

$$\frac{\ddot{\theta}_o}{n_{ss}}\left(\frac{l_p}{g}\right) = \frac{n_{p_o}}{n_{ss}} .$$

At issue is whether the initial linear acceleration index provides clearer guidance than the current initial angular acceleration index. The essential difference between the two parameters is the sensitivity to aircraft size afforded by the consideration of the pilot's location. Forty-two data points on five different aircraft exhibited characteristics ranging from the lower Level 1 boundary to below the Level 2-3 boundary for the $CAP_1$ boundaries of the current specification as shown in Figure 8.

The aircraft had demonstrated Level 1 flight characteristics based on flight evaluations and operational experience, but would be judge marginal to unsatisfactory based on the current specification.

To compare the same 42 data points against the alternate format, the specification boundaries were translated directly using a distance from the pilot to the center of rotation of 9 ft. The 9 ft. value was utilized because, first, the upper Level 1 boundary of the specification would coincide with the upper boundary suggested by reference 15 and, second, for the modest sized aircraft providing the majority of the original data base, reference 17, an average pilot-to-rotation-point distance of 9 ft. is not unreasonable. For the large aircraft the 42 data points are shown in Figure 9 to migrate to the upper Level 1 area of the revised format. There is now consistency between flight experience and the specification alternative.

For modest sized contemporary military aircraft including the S-3, AV-8, F-14, F-15, and F-18 a comparison of the two approaches, using over one hundred data points, indicated the analysis to be unaffected relative to the acceptance regions, as illustrated in Figure 10.

The large-aircraft results of reference 18 verify the trend of the alternative suggested here, namely that pilot location far forward of the center of rotation significantly improves flying qualities acceptance.

## 3. NAVY FLYING QUALITIES SURVEY

In October of 1980, eight major U.S. aircraft companies were requested to participate in a survey on the effectiveness of the Flying Qualities of Piloted Airplanes, Military Specification MIL-F-8785.

The request stated that personal answers rather than the corporate view was desired. The request further suggested that the mix of respondees within the company be a stability and control engineer and supervisor, a flight control engineer and supervisor, and the first-level manager responsible for both the stability and control function and flight control function. The stated intent was to get a sampling of perceptions which were representative of the individuals primarily responsible for the flying qualities exhibited by the military aircraft.

Forty-six engineers from eight major U.S. aircraft companies responded to the questionnaire. Sixteen respondees had backgrounds in flying qualities; thirteen in flight control; and seventeen were experienced in both. The average level of experience with MIL-F-8785 or its predecessor was 17.2 years, with a minimum experience level of 5 years and a maximum of 30 years. Eighty-seven percent of the respondees had 10 or more years of experience; 65% had 15 or more; and 50% had 20 years or more. The mix of technical management to technical specialists was half and half.

The following are excerpts from the conclusions of the survey report, reference 19:

With respect to MIL-F-8785, a majority of the responders felt

- that the design and development of a new high technology fighter would benefit from using 8785 as the flying qualities specification.

- that 8785 was most effective as a communication aid between government and contractor engineers; the second most effective area was in providing guidance during design and development, third most effective area was that of being a specification.

- that 8785 was an important factor in achieving satisfactory flying qualities; after engineering talent, groundbased simulation, and good working relationship between flight control and flying qualities organizations.

- that 8785 was a factor in compromising flying qualities; ranked behind schedule constraints, cost constraints, inadequate aerodynamic data, and inadequate use of groundbased simulation.

- that revising 8785 was the least effective investment strategy for providing better flying qualities on the next generation military aircraft, for a fixed investment.

With respect to program management, the responses indicate

- that program management's cost and schedule constraints are perceived to be most responsible for compromising satisfactory flying qualities.

- that program management is considered to have the most potential for cost-effective improvements in flying qualities.

## 4. AIR FORCE EXPERIENCE

When MIL-F-8785B was adopted, complaints were heard on the following:

- Overly complex requirements.

- Requirements not related well to design.

- Requirements not related well to flight test.

- Requirements not related well to operational needs.

- Requirements too stringent.

These same opinions are heard today. We must acknowledge a degree of truth in these complaints. Nevertheless, as the following discussion attempts to show, on the whole we believe the current specification to be a valid, workable document. With attention to correct interpretation, this utility appears to hold for a good number of recent or suggested higher-order systems, digital mechanizations, etc. After a discussion of these questions, the direction of some future handling qualities work will be discussed.

Some current requirements are certainly complex; a prime example concerns Dutch roll, particularly roll/yaw coupling. There may be a simpler, more effective way to state design criteria for this flying quality area of universally conceded importance - but twelve years have not produced one. A number of the requirements reflect our inability to adequately meet the needs of designer, procuring agency and user simultaneously.

Flight testing is tremendously expensive, and emphasis is properly placed on relating the flight testing of a new design to operational usefulness. Thus, much of the flying qualities demonstration is becoming a validation of the analytical model, so that more detailed study can be done on the computer. With certain requirements such as those relating to atmospheric disturbances, analysis of a model and qualitative spot checks are all that flight test can accomplish. However, flight exploration of aircraft limits remains important - indeed becomes more so as we increasingly rely on the flight control system for both stability and control. Quantitative requirements are particularly difficult to establish in this area; consequently a significant portion of the specification remains qualitative.

Complaints about the effort needed to show the probability of having each flying qualities level in the many envelopes are still heard. However, a rare testimonial from industry, reference 20, is relevant here: A U.S. aerospace company discussed with the Flight Dynamics Laboratory's Handling Qualities Group their early experience in applying MIL-F-8785. The purpose of the study was to establish a set of flying qualities requirements for a weapon system development program, and to take a preliminary look at compliance. At first, defining airplane normal states, failure states, and flight envelopes appeared to be a task of monumental proportions. But defining the normal states for each flight phase was found to be more of a bookeeping problem than anything else and was necessary to assure the identification of critical combinations of configuration and loading. This success, and the improved understanding of all aspects of the total system that resulted, convinced the contractor that the effort was worthwhile. The only flight envelopes required in this documentation effort were the Operational Flight Envelopes. Since these represent the speed, altitude and load factor capability necessary to complete the mission, consideration of the effect of external stores, etc., on airplane limitations was not necessary, which simplified the task a great deal. The considerable overlap

of the envelopes led to a manageable number of envelopes to be considered. The company was very liberal in sizing, realizing that larger envelopes enhance the competitiveness of their design. They had not come to grips with the problem of providing Level 1 flying qualities within these large envelopes, and the impact on such things as system weight, cost, complexity, reliability. They acknowledged that they might have had to reduce these envelopes because of these considerations, in order to be responsive to the need for a relatively simple system. The identification and assessment of system failure consequences in terms of degraded flying qualities were found to be straightforward. Establishing the per flights probability presented no particular problem. Some failure modes identified through this evaluation would not otherwise have been recognized. There was little confidence in the accuracy of their failure probability analysis because of the inaccuracy in the system component failure rate data available in the open literature. Looking back on the application on MIL-F-8785B in this particular study, it was concluded that the benefits throughout the service life of the airplane would more than compensate for the additional design effort required. No changes were recommended to MIL-F-8785B based on their experience in this application.

More recently we have seen a tendency to avoid these probability-based requirements, relying more on an expanded list of specific failures along with the flying qualities Level to be achieved after failure. Once even a preliminary flight control system has been settled upon, such a list can be prepared with some assurance of adequacy, barring radical design change. Whichever approach is taken, critical failures must be found and their effects assessed. When overall mission-success and flight-safety reliability are specified, the procuring activity may be willing to rely on those requirements entirely. But for flight safety and mission effectiveness there is a definite need for a good failure modes and effects analysis with respect to flying qualities.

### 4.1 High Angles of Attack

Increasingly, stability and control augmentation is being used to meet flying qualities requirements, both as a result of increased performance demands and because of the availability of increasingly sophisticated flight control systems. Flight control systems designed for normal flight conditions, where aerodynamic derivatives are mostly linear and tractable, can become destabilizing near and beyond stall where, as noted, requirements remain qualitative. A control system commanding normal acceleration, as in the original F-111, was found to promote stalling. Below the minimum drag speed, normal acceleration feedback tends to promote divergence, another manifestation of the "speed instability" we normally associate with control of flight path at low speed. A pitch damper will continue to add damping beyond stall, but its stiffness contribution through the term $Z_w M_q$ becomes destabilizing for positive $Z_w$. Pitch attitude stabilization will become destabilizing for large $C_{D_\alpha}$, inhibiting nose-down to maintain airspeed as angle of attack increases. Reference 21 attempts to incorporate guidance for these and other cases. Although the qualitative high-angle-of-attack requirements of MIL-F-8785C cover such effects in a general way, the proliferation of possibilities with advanced flight control systems make more specific requirements difficult.

### 4.2 Roll Performance

Roll performance has been a controversial subject from the beginning. While a certain minimum performance is necessary, the price is significant in terms of structural weight, reduced high-lift capability and system complexity. For fighter aircraft the original pb/2V requirement was replaced by limits on time to bank through 90°, then an additional upper limit put on the roll time constant. Air Force and NASA studies (references 22 and 23) had consistently failed to show the value of roll capability over half the 100 deg. in the first second required in 1959 by MIL-F-8785; but in view of the service pilots' insistence and the excellent success achieved in Korean combat, a reduction below 90 degrees could not be justified. The requirements are intended to apply throughout the speed, altitude and load-factor dimensions of the pertinent flight envelopes, but in practice were demonstrated only at 1 g. For the F-15, the procuring activity wanted to emphasize agility and so put special emphasis on getting the most feasible roll control power at the low-speed edge of the V-n flight envelope. Reflecting experience with the F-15 and F-16, the new MIL-F-8785C has more explicit reference to flight conditions: 360° rolls are required in 1-g flight, and higher-g rolls through lesser angles somewhat related to combat usage. At low and high speed extremes the roll requirements are relaxed as a concession to the natural falloff of aerodynamic effectiveness. Below the approximate "corner speed", the lowest airspeed for limit load-factor capability, less roll capability is required. Closer to the 1-g stall speed a further reduction is allowed. One effect of this change should be to lessen the unusably high roll capability which results from attempts to meet the stringent requirement over a broader speed range. Several fighter data points - F-15 through F-18 - tend to validate the requirements, though some surveyed pilots want more low-speed roll capability than inertial coupling will permit (reference 24). The F-16 roll performance has been quite satisfactory, and has benefited from a shorter roll time constant (more roll damping) at zero control force, so that the airplane "stops on a dime". F-18 roll performance, initially below specification and considered inadequate, has been improved to meet the specification.

In a piloted simulation study of one-on-two combat conducted on the McDonnell fixed-based air combat simulator, a conclusion on the importance of roll performance from the study reported by Guthrie in Paper No. 23 was as follows:

> Rolling agility, which was formerly considered a second order effect, . . . has been shown to provide first order air combat consequences traditionally associated with large (30-50%) changes in $P_s$ or maneuvering $C_L$.

Improved rolling performance in the vicinity of 30° angle of attack through differential deflection of a variable-incidence wing was found to give much earlier kills and doubled exchange ratios. While there are no means to investigate this result in actual flight, the results do provide incentives for not reducing the roll requirements for air combat any further.

4.3 Integration With Other Subsystems

If flying qualities are overspecified, the design options are narrowed and thus overall effectiveness is degraded. How important are flying qualities to the success of new aircraft? The answer, of course, depends on which flying quality is being considered. Maintaining control is fundamental to flight as well as a prime safety consideration. Beyond that is the maneuverability needed to perform design missions well. We can argue about quantitative limits, or even the form of requirements; but we all seem agreed that these aspects must be treated in detail.

Detailed levels of requirements on dynamic characteristics, however, can be justified only to the extent that pilots actually fly the airplane. Especially in the European scenario of much interest to NATO, we hear of intense battles envisioned with dense concentrations of everything: aircraft, friendly and enemy; both human and automatic communications giving directions, updates and other information; a multitude of sensors for navigation, warning, target acquisition; and complicated onboard weapons, propulsion, fire control, etc. systems to manage. To manage all these factors effectively takes so much concentration that little time is left for flying the airplane.

As just one example of the help afforded by a more capable system, consider the AN/ARN-101 Digital Modular Avionics System (reference 27) for more accurate ground attack. With "28 indicators, 22 switches with 83 different positions and 56 pushbuttons",

> . . . the computer solves the problem regardless of release parameters . . . However, we must get in the habit of meeting specific parameters every time we drop. If we don't, (1) impact angle and impact velocity will suffer to the detriment of weapons effects, CBU patterns, etc.; (2) fuze arm and safe escape will be jeopardized; (3) LGB guidance time and envelope may be adversely affected; (4) aircrews lacking BFM skills may fly into the ground and (5) improper delivery airspeeds may degrade aircraft maneuverability.

Kinnan concludes, "The ARN-101 is capable, but it's not sophisticated. Take all of that capability and mechanize it with two or three switches and one indicator; now that would be sophisticated." That is quite a challenge for cockpit designers and systems integrators.

It is commonplace to say that the pilot has become a manager. This leaves two possibilities for unloading the pilot: make the flying task as easy as possible, or automate it. With these prospects before us, what dynamic characteristics will we need to specify? Two examples show some implications of control integration.

Recent AFWAL simulations of an integrated flight/fire control system (IFFC) have shown how a cooperative pilot-autopilot effort can improve air-to-air gunnery (reference 28). The head-up display shows the director-guided sight reticle and a box which indicates the IFFC authority in normal acceleration and roll rate. In this version the pilot can add his own pitch and roll commands to help the IFFC put the reticle on the target, and to null the authority box on the reticle so that maximum IFFC authority is available for tracking. The IFFC has complete control when the reticle is inside the authority box, the pilot then retaining only limited control in roll (ailerons, while IFFC commands the differential tail). For the simple initial conditions and target maneuvers studied, performance with the IFFC was significantly better than with just the director sight or a lead computing optical sight (and far superior to performance with a fixed sight). Performance was almost as good when roll control was given exclusively to the pilot, who could see target bank angle while the IFFC could not. The evaluation pilots wanted to keep actively involved, in order to monitor system operation. In this application we see a continuing need for satisfactory response to pilot control, and a further need to develop requirements governing the interface of manual control, displays and weapons management.

Another IFFC application being studied by AFWAL involves air-to-ground gunnery and bombing, the object being to present a more difficult target to the antiaircraft people while improving flexibility and accuracy of delivery. Rather than rolling out onto a straight-in approach, the pilot rolls into a sideslipping, rolling dive while the system keeps the guns pointed toward the designated target; similarly bombs are released at a computed point in a turn. Here again we have indications that careful attention must be given to the division of duties and interface between the pilot and the system.

These examples use only the conventional moment-producing control surfaces. Other papers presented here show some uses of direct force control as well. Mechanizations of direct force control have ranged from blended operation with other flight controls by means of the same controller through fully manual control by means of a thumb swith to fully automatic control integrated with the fire control system. Reference 30 discusses integration of flight and engine control for the Mission Adaptive Wing airplane with variable leading-edge and trailing-edge camber, so commands to the multiple surfaces must be optimized. Because of control limits, the various commands had to be prioritized according to different criteria for, e.g., maneuvering, cruise and landing approach. It has become very clear (e.g., references 31 and 32) that overall requirements must be developed and adhered to if such systems integration is to work. Handling qualities for piloted control are a subset of these overall requirements.

The combat environment is getting more hazardous as well as more complex, with terrain following/avoidance, ground- and air-launched missiles to avoid or defeat. It seems unlikely that a pilot would relinquish flight control entirely. On the other hand, our present requirements are largely predicated on his need to perform fine tracking-whether air-to-air or air-to-ground. To the extent that automatic controls or guided, standoff weapons take over this function, we can somewhat relax those requirements. But then how much can we depend upon these automatic functions? In the F-16, for example, we have already accepted reliance on electronics for control and stabilization essential to flight safety, but with great attention to reliability and invulnerability. Other systems such as fire control have not had commensurate redundancy, etc. We cannot have redundant radar dishes in the nose. In the interests of operational readiness as well as flight safety, it would seem prudent to keep up the more traditional capability as well. We also may have high attrition early on, and rapid exhaustion of supplies or stand-off weapons, advanced air-to-air missiles, deterioration of communications. After some initial engagement we may be getting back toward the basics. A number of implications result.

Automatic control must be compatible with manual control to the extent that the pilot can monitor performance effectively and insert additional commands or take over as the occasion demands. As long as stockpiles of iron bombs remain, we will need the capability to deliver them. As the burden of other duties increases (communications to or from AWACS, JTIDS, etc.; navigation at low level, monitoring automatic terrain following/avoidance; weapons management; sensor selection) automatic pilot-assist functions become essential to the mission. Do performance requirements for such modes belong in a flight control system specification as at present, on in the Flying Qualities Specification? What different choices of control modes, automatic and manual, can be incorporated without leading to confusion? It is apparent that a number of issues remain to be settled, and that flying qualities requirements are central to the integration of control.

## 5. CONCLUSIONS

1. Consideration of the equivalent time delay characteristics is fundamental to achieving satisfactory closed-loop tracking performance and should not be considered unique to digitally implemented control laws.

2. Based on the experience with "high-gain" forward loop systems to date, the benefits may turn into liabilities when the time delay and sensitivity aspects are considered.

3. For aircraft not utilizing angle-of-attack limiting, positive speed stability is still required.

4. The simultaneous matching of normal load factor and pitch rate in determining the equivalent system characteristics was found to provide values of equivalent $n_\alpha$ which are more in line with the wind-tunnel-derived values than are the pitch-rate-only match values.

5. An alternate formulization of the short-period frequency requirement, which accomodates pilot location (and thus size) as a normalizing factor in the acceptance boundaries, shows promise conceptually in more appropriately reflecting large-aircraft requirements.

6. Based on a survey of U.S. engineers, MIL-F-8785 is considered to be a reasonable and effective specification for the next generation fighter.

7. Significantly more flying qualities problems are being experienced as a result of not adhering to the specification guidance than are being caused by specification inadequacies.

8. Active utilization of the specification to guide the flight control design is necessary to assure satisfactory flight characteristics with minimum revisions.

9. Use of MIL-F-8785B in an airplane design (a) is not inordinately complex and (b) uncovers problems that might otherwise be missed.

10. At high angles of attack, with a combination of nonlinearities and more stability and control augmentation, flying qualities requirements will probably remain largely qualitative, of limited help in design.

11. Roll performance is important throughout the speed-altitude-load factor flight envelope. At low and high speed, requirements recently were reduced, in line with current satisfactory airplanes but with lingering misgivings.

12. The scope of flight control automation is expanding, to keep pilot workload manageable and also to improve mission effectiveness. A role remains, however, for piloted flight; and flying qualities requirements are central to system integration.

6. REFERENCES


1. Smith, Rogers E. — Evaluation of F-18A Approach and Landing Flying Qualities Using An In-Flight Simulator. Calspan Report No. 6241-F-1. February 1979.

2. Weingarten, Norman C. — In-Flight Simulation of the Space Shuttle Orbitor During the Landing Approach and Touchdown in the TIFS. Calspan 6339-F-1, September 1978.

3. Bischoff, David E. — Longitudinal Equivalent Systems Analysis of Navy Tactical Aircraft. Naval Air Development Center.

4. DiFranco, Dante A. — Flight Investigation of Longitudinal Short Period Frequency Requirements and PIO Tendencies, AFFDL-TR-66-163. June 1967. AD-656784*

5. Mooij, H. A., De Boer, W. P., Van Gool, J. F. C. — Determination of Low-Speed Longitudinal Maneuvering Criteria for Transport Aircraft with Advanced Flight Control Systems. National Aerospace Laboratory (NLR). The Netherlands, NLR TR 79125. 20 December 1979.

7. DiFranco, Dante A. — In-Flight Investigation of the Effects of Higher-Order Control System Dynamics on Longitudinal Handling Qualities. AFFDL-TR-68-90. August 1968. AD-840752*

8. Stengel, Robert F. — A Unifying Framework for Longitudinal Flying Qualities Criteria, AIAA Paper No. 81-1889.

9. Mitchell, David C., Hoh, Roger H. — Systems Technology Incorporated Working Paper No. 1163-1, Review and Interpretation of Existing Longitudinal Flying Qualities Criteria for Use in the MIL Standard/Handbook, December 1980.

10. A'Harrah, R. C., Lamanna, W. J., Hodgkinson, J. — Are Today's Specifications Appropriate for Tomorrow's Airplanes? AGARD Conference Proceedings No. 260. September 1978.

11. Smith, Rogers E., Hodgkinson, J., Snyder, R. C. — Equivalent System Verification and Evaluation of Augmentation Effects on Fighter Approach and Landing Flying Qualities. AFWAL-TR-81-3116, September 1981. *

12. Smith, R. E., Monagan, S. J., Bailey, R. E. — Investigation of Higher-Order Control System Effects on the Lateral Directional Flying Qualities of Fighter Aircraft. AIAA-81-1891, August 1981.

13. Wood, J. R., Hodgkinson, J. — Definition of Acceptable Mismatch Levels, Report MDC A6792, December 1980.

14 Crombie, R. B., Moorhouse, D. J. — Flying Qualities Design Criteria - Proceedings of AFFDL Flying Qualities Symposium held at WPAFB in Oct 1979. AFWAL-TR-80-3067, May 1980. AD-088066*

15. Bihrle, William — A Handling Qualities Theory for Precise Flight Path Control. AFFDL-TR-65-198. June 1966. AD-801498*

16. A'Harrah, Ralph C. — Maneuverability and Gust Response Problems Associated with Low-Altitude, High-Speed Flight. AGARD Report No. 556. October 1967.

17. Chalk, C. R., Neal, T. P., Harris, T. M., Pritchard, F. E., Woodcock, R. J. — Background Information and User Guide for MIL-F-8785B (ASG), "Military Specification - Flying Qualities of Piloted Airplanes". AFFDL-TR-69-72. August 1969. AD-860856*

18. Weingarten, N. C., Chalk, C. R. — In-Flight Investigation of Large Airplane Flying Qualities for Approach and Landing. AFWAL-TR-81-3118, September 1981. *

19. A'Harrah, Ralph C. — Results of a Survey on the Flying Qualities of Piloted Airplanes, MIL-F-8785. NAVAIR Report. June 1981.

20. Wilson, R. K, — AFFDL/FGC Weekly Activity Report. June 1971

21. Moorhouse, D. J., Woodcock, R. J. — Background Information and User Guide for MIL-F-8785C, Military Specification - Flying Qualities of Piloted Airplanes. AFWAL-TR-81-3109. June 1981.*

22. Aubin, W. M. — Some Considerations of the Effects of Mission on Roll Requirements, Aerospace Engineering Vol. 20, No. 9, Part 1, September 1961.

23. Phillips, W. H. — Analysis of Effects of Interceptor Roll Performance and Maneuverability on Success of Collision-Course Attacks, NASA TN D-952. August 1961.

24. Johnston, D. E., — Investigation of High AOA Flying Qualities Criteria and Design Guides, AFWAL-TR-81-3108*. June 1981.

27. Kinnan, Maj. T. A. — All New Digital F-4E, USAF Fighter Weapons Review, Issue 4, Winter 1980.

28. Cord, T. J. — IFFC Flying Qualities Simulation, AIAA Paper No. 81-1821-CP, AIAA Guidance and Control Conference. August 1981.

30. Vincent, J. H., Rock, S. M., Dehoff, R. L. — Application of Modern Control Theory to Design of Aircraft Flight Propulsion Control Systems, AIAA Paper No. 81-1708, AIAA Aircraft Systems and Technology Meeting. August 1981.

31. Hunter, J. E., Holdridge, R. D. — The Technical and Managerial Challenge of Integrated Flight/Fire Control, AIAA Paper No. 81-1706, AIAA Aircraft Systems and Technology Meeting. Aug 1981.

32. Martorella, P., Kelly, C. — Precision Flight Path Control in Carrier Landing Approach - A Case for Integrated Control System Design, AIAA Paper No. 81-1710, AIAA Aircraft Systems and Technology Meeting, August 1981.


* Available from NTIS, 5285 Port Royal Road, Springfield, VA 22151, U.S.A.

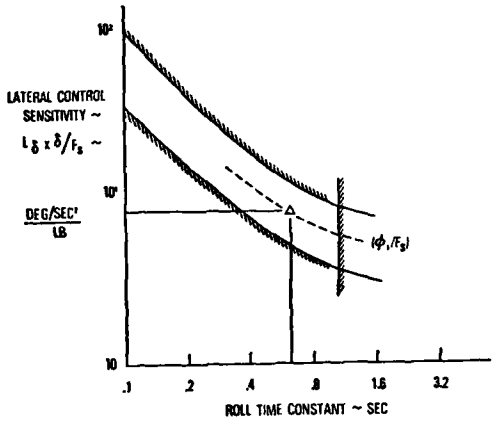


Figure 2. Typical Roll Sensitivity - Proportional

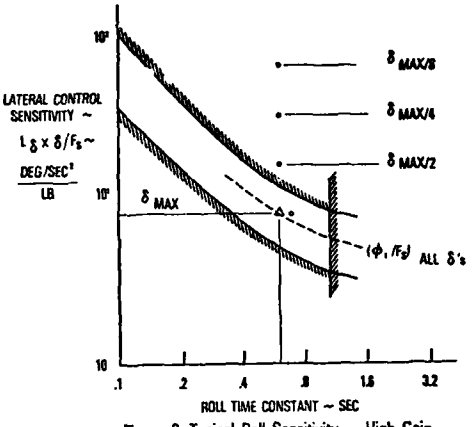


Figure 3. Typical Roll Sensitivity ~ High Gain

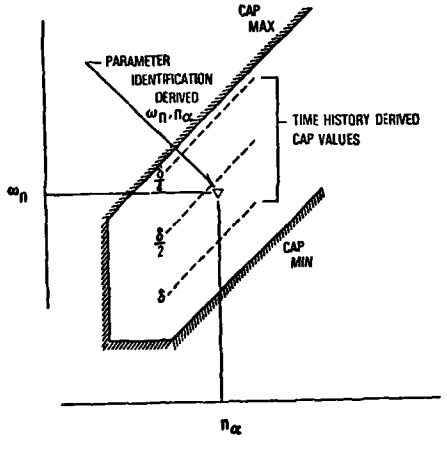


Figure 4. Typical Short Period Characteristics – High Gain

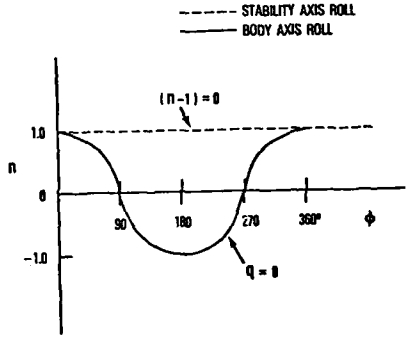


Figure 5. Normal Load Factor Variations with Bank Angle

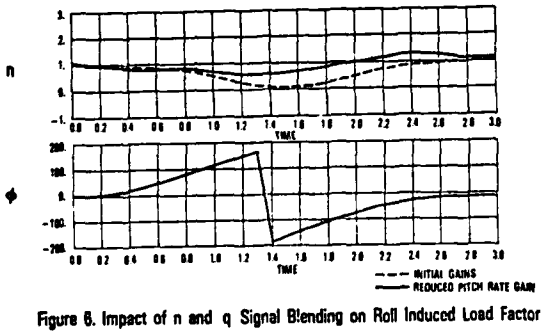


Figure 6. Impact of n and q Signal Blending on Roll Induced Load Factor

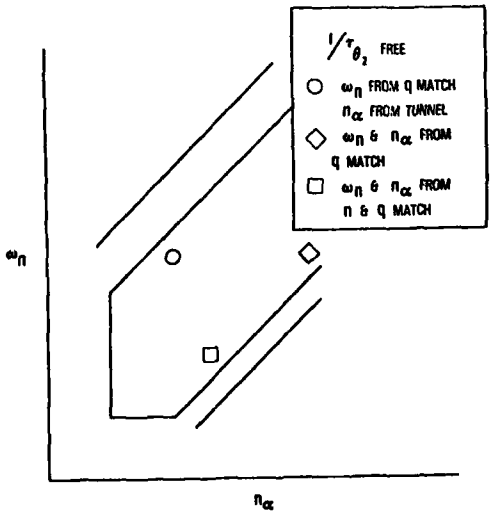


Figure 7. Equivalent System Match Effects

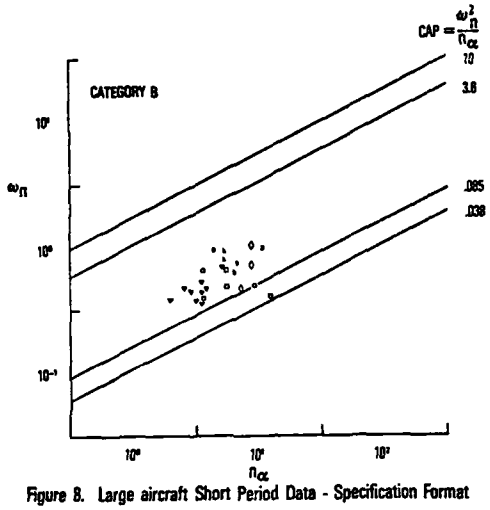


Figure 8. Large aircraft Short Period Data - Specification Format

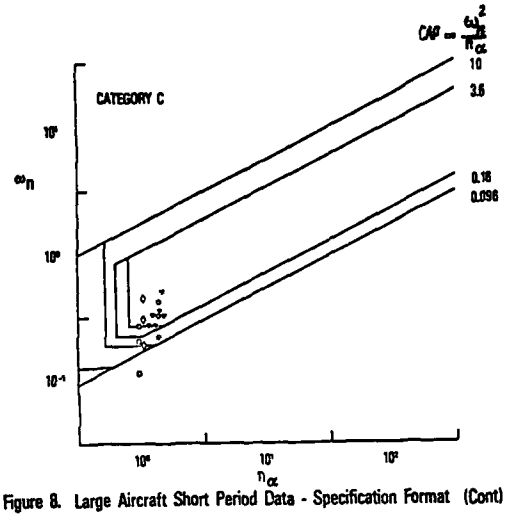


Figure 8. Large Aircraft Short Period Data - Specification Format (Cont)

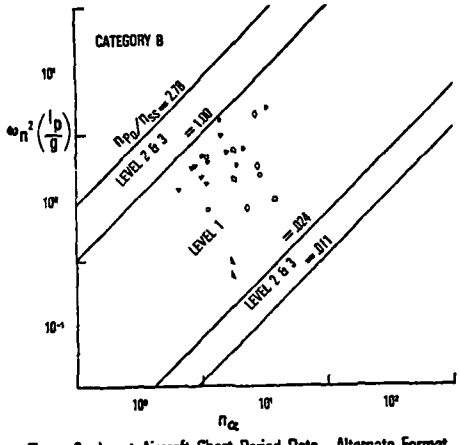


Figure 9. Large Aircraft Short Period Data - Alternate Format

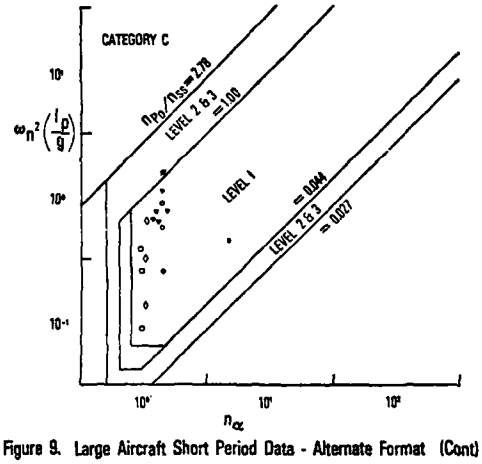


Figure 9. Large Aircraft Short Period Data - Alternate Format (Cont)

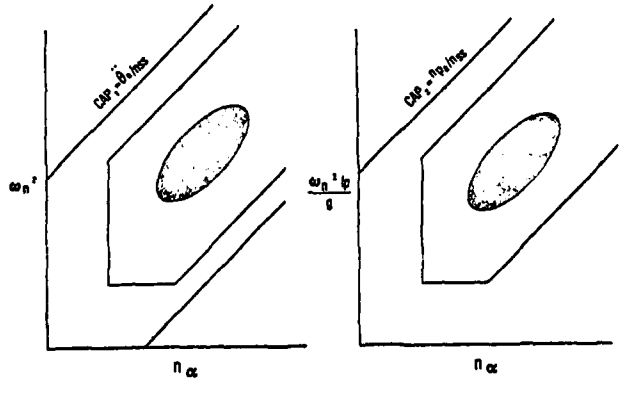


Figure 10. Modest Sized Aircraft Short Period Data - Specification vs Alternate Format

# DEVELOPMENT OF A TENTATIVE FLYING QUALITIES CRITERION FOR AIRCRAFT WITH INDEPENDENT CONTROL OF SIX DEGREES OF FREEDOM -- ANALYSIS AND FLIGHT TEST*

Roger H. Hoh, Thomas T. Myers, and Irving L. Ashkenas
Systems Technology, Inc.
13766 South Hawthorne Blvd.
Hawthorne, California 90250
U.S.A.

## INTRODUCTION

The objective of this study was to develop a tentative flying qualities specification for aircraft having direct force effectors that allow independent control over the horizontal and vertical degrees of freedom. Such aircraft are referred to here as direct force control (DFC) vehicles. The primary problem with developing flying qualities for such aircraft is their unconventional responses as reflected in a very incomplete data base including MIL-F-8785C. Accordingly, an essential part of the study involved a limited flight simulation of a DFC aircraft.

From the outset the work was not intended to evaluate various DFC modes, such as pitch pointing, wings-level turn maneuver enhancement, etc. (see for example, Refs. 1-4). Rather, the objective was to define what is and what is not acceptable, once it has been decided to use a given DFC mode of control. Once developed and validated the resulting criterion will be included in the Military Flying Qualities Standard and Handbook which is currently being developed to replace Ref. 5 (Mil-F-8785C).

## BANDWIDTH HYPOTHESIS AND GENERAL CONSIDERATIONS

The use of auxiliary control surfaces which exert large direct forces along the aircraft y and z axes allows (together with conventional surfaces) many combinations of coupling between the aircraft degrees of freedom. The coupling can be favorable or unfavorable. For example, the maneuver enhancement control mode (also termed direct lift control) utilizes direct force control in the z-axis to produce favorable coupling to augment the aircraft heave damping. Unfavorable coupling can "contaminate" an intended purified response, such as lateral translation or wings-level turn, because of inappropriate or inaccurate feedback or crossfeed gains or equalization, possibly due, in turn, to gain scheduling problems. Clearly, it would be a big job to consider and to specify flying qualities for all modes of coupling for all possible DFC combinations. Rather, we searched for and attempted development of requirements that are based on fundamental aspects of DFC pilot/vehicle dynamics and therefore are universally applicable. In fact, we did develop such a requirement based on the bandwidth hypothesis:

- Specification of bandwidth is an adequate flying quality criterion for DFC dynamics
- The dominant effect of inter-axis coupling is its effect on bandwidth
- The following characteristics must be separately specified
  - Control authority
  - Manipulator characteristics (gain, deadband, breakout, etc.)
  - Maximum pilot accelerations as a function of pilot restraint and task

The bandwidth hypothesis makes the fundamental assumption that the primary factor in the pilot's evaluation of a DFC mode is his ability to exert tight control to minimize errors and thereby achieve improved closed-loop tracking performance. The hypothesis originated from an old and well accepted idea -- namely, that a measure of the handling qualities of an airplane is its response characteristics when operated in a closed loop compensatory tracking task. The "bandwidth" ($\omega_{BW}$) as a measure of the maximum frequency at which such closed loop tracking can take place without threatening stability. It follows that airplances capable of operating at a large value of bandwidth will have superior performance. An implicit assumption here is that inter-axis coupling or contamination, regardless of type or source, affects the pilot opinion only insofar as it affects the bandwidth.

When flying a DFC mode with low bandwidth, the pilot finds that attempts to rapidly minimize tracking errors result in unwanted oscillations. He is, therefore, forced to "back off" and accept somewhat less performance (larger and more sustained tracking

*The work reported here was performed under the sponsorship of the US Air Force, Flight Dynamics Laboratory, under Contract F33615-78-C-3616. Lt. Jack Browne was the contract technical monitor.

error) or to compensate with lead equalization. It is not difficult to imagine a clear cut preference on the part of pilots for aircraft with increased bandwidth capabilities.

As mentioned above, the concept of using bandwidth is not new. The most recent utilization of bandwidth was in the Neal-Smith criterion (see Ref. 6). This criterion consists of a grid of the closed-loop pitch attitude resonance $\theta/\theta_{c_{max}}$ vs. pilot equalization for a piloted closure designed to achieve a specified bandwidth. Experience with this criterion has shown that the results can be sensitive to the selected value of closed-loop bandwidth. The criterion suggested in this paper utilizes the maximum value of bandwidth achievable without threatening stability, thereby removing the necessity for selecting a value for $\omega_{BW}$ a priori.

Another criterion utilizing bandwidth was suggested in Ref. 7. This criterion also selected a fixed value of bandwidth (1 rad/sec for power approach). It utilized the phase margin $\phi_M$ and slope of the phase curve $d\phi/d\omega$ at the selected bandwidth frequency as a correlating parameter. Again, experience has shown that the fixed value of bandwidth limited application of the criterion.

It should be noted that a given level of bandwidth will only insure satisfactory dynamics. Other characteristics of DFC airplanes, which must be separately specified, are control authority, manipulator characteristics, and maximum pilot acceleration depending on task and pilot restraint. In this paper we will concentrate primarily on specifying a boundary that separates acceptable from unacceptble dynamics for DFC aircraft.

The classical definition of bandwidth (for example, see Ref. 8) is illustrated in Fig. 1, as shown by the closed-loop response plot in the upper left corner. The generally accepted definition of bandwidth is the frequency at which the Bode amplitude is 3 dB less than the steady-state amplitude of the system (-3 dB is equivalent to approximately 70 percent). The fundamental intention of the bandwidth parameter is to separate frequencies at which a system will follow the input from frequencies where it will not. In the simple example attitude system of Fig. 1, the pitch attitude $\theta$ is approximately equal to the commanded value, $\theta_c$, at frequencies below 1/T (the bandwidth), but rapidly decreases beyond 1/T. The point here is that the bandwidth is a fundamental measure of the ability of the system output to follow the system input. The connection between the frequency response and the time response is also shown in the lower right side of Fig. 1. Here we can see that, for an ideal K/s shape, the bandwidth frequency and the system time constant are, in fact, identical quantities ($\omega_{BW} = 1/T$). Furthermore, for the pure K/s open-loop system of Fig. 1 the open-loop piloted "crossover frequency" is also exactly the classical closed-loop bandwidth (frequency at which -3 dB and 45 deg occur). The open-loop "crossover frequency" is defined by the simplified pilot loop closure gain (horizontal line) intersection with the open-loop $\theta/\delta$. Because the two quantities are nearly equal even for higher-order open-loop systems, we have taken the liberty of using the term "bandwidth" when referring to the "crossover frequency."

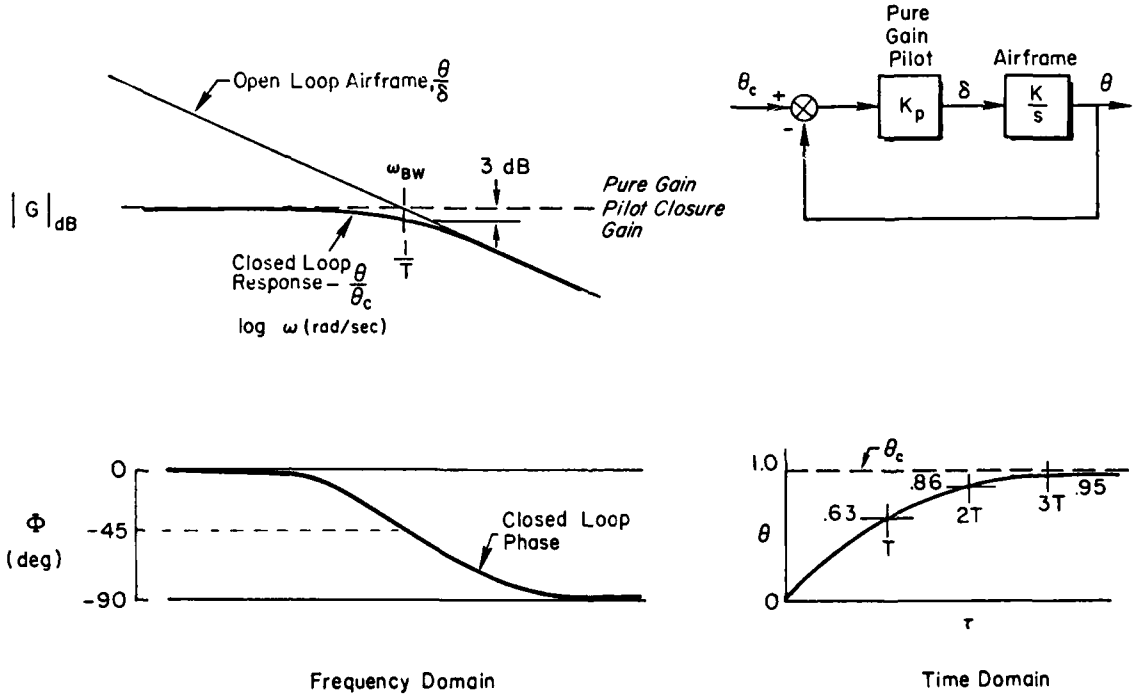


Figure 1. Classical Definition of Bandwidth

## DEFINITION OF BANDWIDTH USED IN CRITERION

In keeping with the above we define the bandwidth ($\omega_{BW}$) for handling criterion purposes as the crossover frequency for simplified pure gain pilot at which the phase margin is 45 deg or the gain margin is 6 dB, whichever frequency is lower (Fig. 2). In order to apply this definition one first determines the frequency for neutral stability from the phase portion of the Bode plot ($\omega_{180}$). The next step is to note the frequency at which the phase margin is 45 deg. This is the bandwidth frequency as defined by phase $\omega_{BW_{phase}}$. Finally, note the amplitude corresponding to $\omega_{180}$ and subtract 6 dB; the frequency at which this value occurs on the amplitude curve is $\omega_{BW_{gain}}$. The bandwidth, $\omega_{BW}$, is the lesser of $\omega_{BW_{phase}}$ and $\omega_{BW_{gain}}$. If $\omega_{BW} = \omega_{BW_{phase}}$, the system is said to be phase-margin limited. On the other hand, if $\omega_{BW} = \omega_{BW_{gain}}$, the system is gain-margin limited; that is, the aircraft is driven to neutral stability when the pilot increases his gain by 6 dB (a factor of 2). Gain-margin-limited aircraft may have a great deal of phase margin, $\phi_M$, but increasing the gain slightly causes $\phi_M$ to decrease rapidly. Such systems are characterized by frequency response amplitude plots which are flat, combined with phase plots which roll off rapidly, such as shown in Fig. 2.

## PHYSICAL SIGNIFICANCE OF BANDWIDTH

The considerations that are implicit in using bandwidth as a flying quality criterion are summarized as follows:

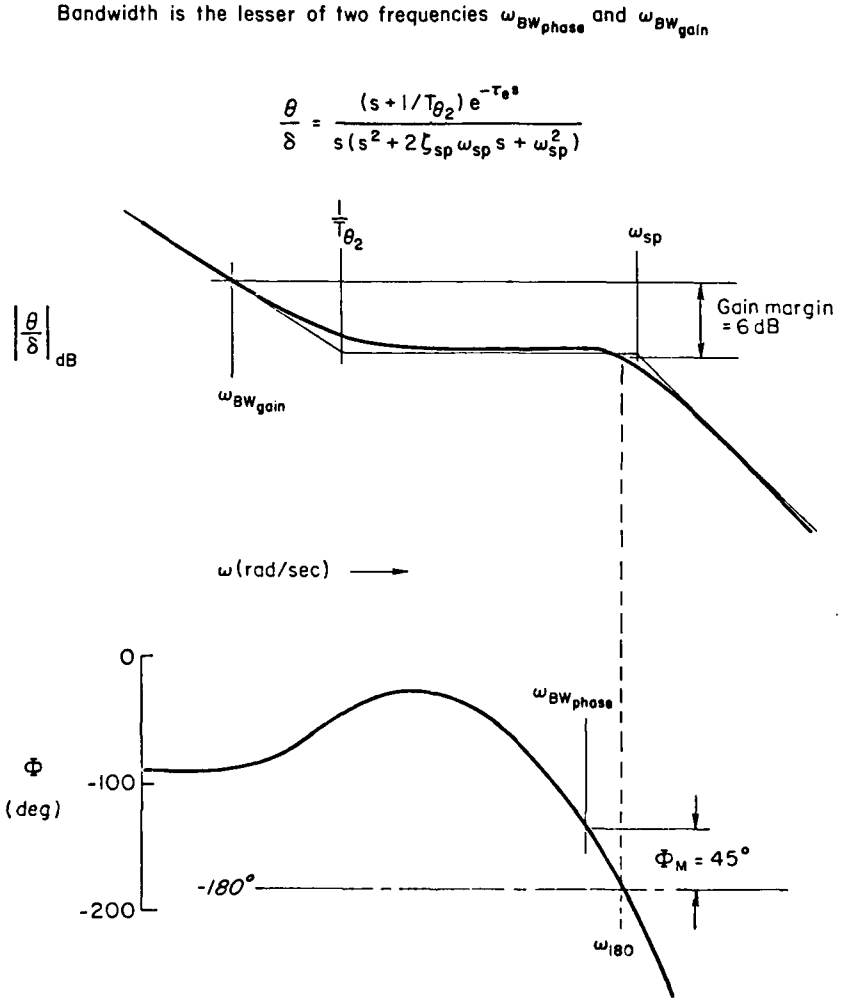


Figure 2. Definition of Bandwidth Frequency, $\omega_{BW}$

- Bandwidth is a measure of risetime or speed of response.
- The closed-loop system bandwidth is approximately equal to the crossover frequency for a pure gain pilot.
- Low values of bandwidth are indicative of a need for pilot lead equalization and hence poor ratings.
- The bandwidth is limited by stability considerations.
- Stability can be threatened by:
  - Inherent phase lags in the desired region of crossover
  - Adverse coupling or unfavorable zero locations

Requiring a minimum value of bandwidth is equivalent to insisting on rapid responses to control inputs without overshoots or any other undesirable characteristics of low damping. If such characteristics are not available through the basic airframe, it will be necessary to achieve them via stability augmentation. If the basic values of the limiting aerodynamic derivatives are low, high feedback and/or crossfeed gains will be required. The implications of this are listed below:

- If the basic values of the limiting aerodynamic derivatives are low:
  - High feedback and/or crossfeed gains will be required.
  - Failures will tend to be violent.
  - Redundancy requirements will be high.
  - High authority controls will be required to avoid saturation.
- The feedback sensors should be gustproofed, e.g., $a_y$ instead of $\beta$, etc.

The limiting forms for the DFC response modes shown in Table 1 were derived (in Ref. 9) by assuming infinitely high gain feedbacks, which of course is not practical in a real-world situation. However, the results are of similar form to those for more practical, lower gains. Hence, the following observations based on the limiting forms in Table 1 are generally applicable:

- Even when the feedback and crossfeed gains are ideal, the DFC response characteristics are limited by certain inherent aerodynamic derivatives. For example, the bandwidth of the vertical translation mode is limited by $Z_w$ (aircraft heave damping), even if the aircraft is perfectly decoupled.
- The longitudinal and lateral modes are symmetrical, that is, the form for normal acceleration and wings-level turn are identical, as they are for pitch pointing and yaw pointing and for vertical translation and lateral translation. Given that these forms are identical, results obtained for lateral DFC modes may possibly be extended to the longitudinal axis (and vice versa) assuming that the piloting tasks are similar.

## FLIGHT TEST EXPERIMENT

The purpose of the flight test phase of this program was to fill in gaps in the data base as required to develop a handling qualities criterion. The scope of the flight test program was quite limited and hence a systematic variation of parameters to define certain boundaries was well beyond the resources available. A more practical approach was to take the hypothesis and disprove, validate, extend, or modify it based on the results obtained in the flight test program.

### 1. Description of Flight Test

The primary task selected for the flight test was air-to-air tracking. This task was ideal because the target motions could be tailored to exercise a broad spectrum of frequencies in the tracking aircraft.

Due to structural limitations of the side force generators, the Princeton University Variable Response Research Aircraft (VRA) has a maximum maneuvering speed of 105 kt -- well below typical air-to-air combat speeds. It was therefore necessary to adjust the range between the target and attacker to make the fixed gunsight dynamics consistent with a typical air combat encounter (see Ref. 9, page 20 for details).

The primary disadvantage of testing at speeds well below typical air combat speeds (M = 0.8) is that it is not possible to correctly simulate the 0.8 M aircraft dynamics and the pilot acceleration cues simultaneously. This may be seen from the equation for sensed lateral acceleration (Ref. 8):

$$a_{y_{cg}} = U_o(\dot{\beta} + r) - g\phi$$

TABLE 1. IDEAL RESPONSES FOR DIRECT FORCE CONTROL MODES

| MODE | CONSTRAINTS | LIMITING FORMS OF RESPONSES |
|---|---|---|
| Normal Acceleration ($\alpha = 0$) ($A_N$) | $w \rightarrow \delta_e$, $u \rightarrow \delta_T$ | $\frac{a_z}{\delta_L} \rightarrow \frac{N^{a_z w}_{\delta_L \delta_e} N^{u}_{\delta_T}}{N^{w}_{\delta_e} N^{u}_{\delta_T}} = Z_{\delta_L}$ |
| Pitch Pointing ($\alpha_1$) | $a_z \rightarrow \delta_L$, $u \rightarrow \delta_T$ | $\frac{\theta}{\delta_e} \rightarrow \frac{N^{\theta}_{\delta_L} N^{a_z u}_{\delta_e \delta_T}}{N^{a_z}_{\delta_L} N^{u}_{\delta_T}} = \frac{M_{\delta_e}}{[s^2 - M_q s - M_\alpha]}$ |
| Vertical Translation ($\alpha_2$) | $\theta \rightarrow \delta_e$, $u \rightarrow \delta_T$ | $\frac{w}{\delta_L} \rightarrow \frac{N^{w}_{\delta_L} N^{\theta u}_{\delta_e \delta_T}}{N^{\theta}_{\delta_e} N^{u}_{\delta_T}} = \frac{Z_{\delta_L}}{(s - Z_w)}$ |
| Wings-Level Turn ($A_y$) | $\beta \rightarrow \delta_R$, $\varphi \rightarrow \delta_A$ | $\frac{a_y}{\delta_{SF}} \rightarrow \frac{N^{a_y}_{\delta_{SF}} N^{\beta \varphi}_{\delta_R \delta_A}}{N^{\beta \varphi}_{\delta_R \delta_A}} = Y_{\delta_{SF}}$ |
| Yaw Pointing ($\beta_1$) | $a_y \rightarrow \delta_{SF}$, $\varphi \rightarrow \delta_A$ | $\frac{\psi}{\delta_R} \rightarrow \frac{N^{\psi}_{\delta_R} N^{a_y \varphi}_{\delta_{SF} \delta_A}}{N^{a_y \varphi}_{\delta_{SF} \delta_A}} = \frac{N'_{\delta_R}}{[s^2 - N'_r s + N'_\beta]}$ |
| Lateral Translation ($\beta_2$) | $\psi \rightarrow \delta_R$, $\varphi \rightarrow \delta_A$ | $\frac{\beta}{\delta_{SF}} \rightarrow \frac{N^{\beta}_{\delta_{SF}} N^{\psi \varphi}_{\delta_R \delta_A}}{N^{\psi \varphi}_{\delta_R \delta_A}} = \frac{Y^*_{\delta_{SF}}}{(s - Y_v)}$ |

If the $\dot{\beta}$ and r responses are correct, the lateral acceleration will be scaled down by the inertial speed $U_o$. In the present experiment we elected to maintain the integrity of the sideslip and yaw rate responses at the expense of side acceleration cues, which were about a factor of 5 less than those corresponding to M = 0.80. This was done in accordance with the notion that visual cues are more dominant than acceleration cues in air-to-air tracking, and with the VRA's maximum lateral acceleration (0.5 g) capacity. Lateral accelerations as high as 0.5 g were utilized frequently during the experiment. This would translate to about 2.5 g at M = 0.8. There is a requirement for additional work to determine: 1) if 2.5 g lateral $a_y$ is reasonable with any kind of practical restraint; and 2) the effect of reduced authority on pilot opinion. An informal discussion with an Air Force pilot who flew the YF-16 evaluation up to $a_y$ = 0.9 g indicated that large $a_y$ might be acceptable if the pilot could be appropriately restrained. Also, McAllister noted (Ref. 10) that a 1 g command was acceptable, but a 1 g failure transient was objectionable.

The air-to-air tracking scenario was developed to maximize the probability of exposing deficiencies in the tracking aircraft. This exposure was obtained by tracking a target aircraft whose heading varied in a random-appearing fashion corresponding to a power spectrum concentrated in, but evenly spaced over, the frequency range of interest. I. A. M. Hall developed such a signal in Ref. 11 for the purpose of identifying the frequency response characteristics of aircraft in flight. The signal developed in Ref. 11 is shown in Fig. 3. The frequency content of this input signal as given in Ref. 11 is shown in Fig. 4. This signal was selected because it has adequate power at and above the roll mode time constant of most fighter aircraft. The square wave was introduced as a hard-over signal into the target aircraft lateral autopilot servo via a left/right command switch controlled by the target aircraft pilot. This signal resulted in approximately three-quarters of full aileron travel at the testing speed of 105 kt resulting in roll rates of approximately 30 deg/sec. The pilot of the target aircraft selected le[illegible]d

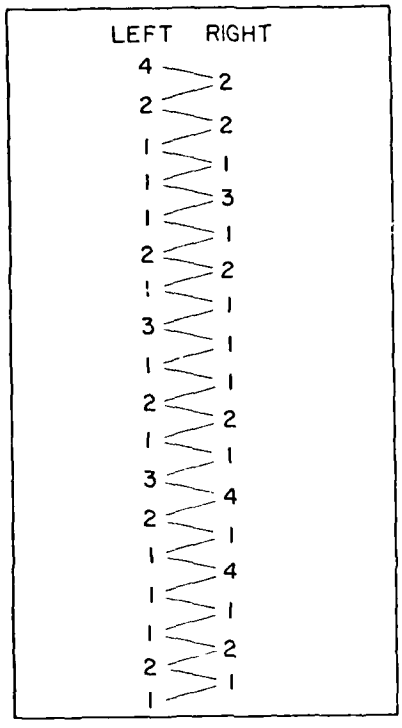


Figure 3. Typical Pilot Switching Program

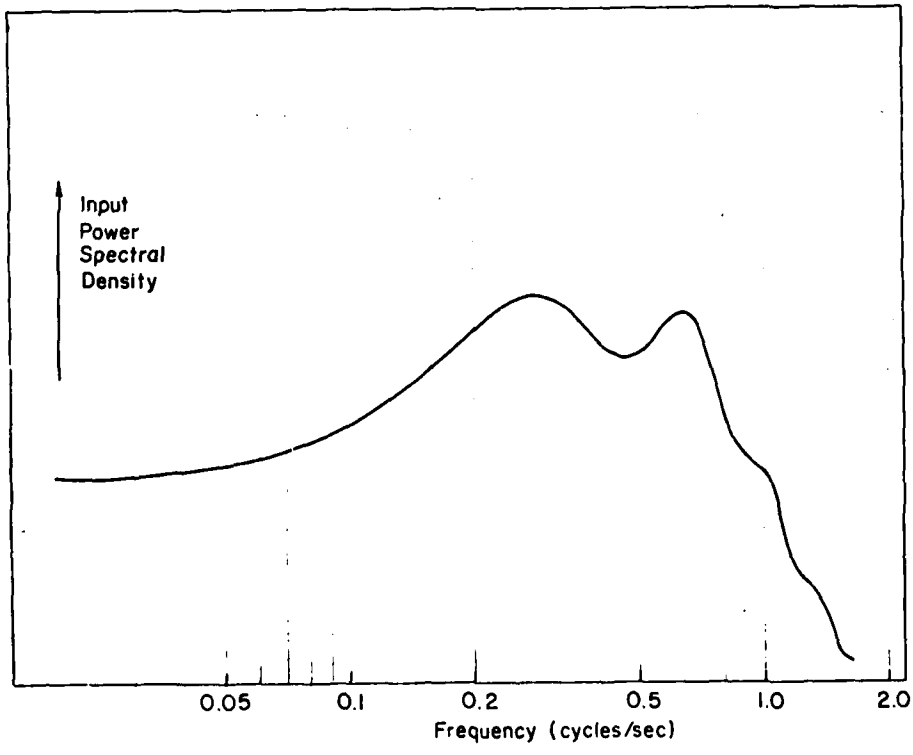


Figure 4. Frequency Content of Input Used for Target Aircraft

right signals via the schedule in Fig. 3 where the numbers are the length of time in seconds that the switch was held in the left or right position. This was accomplished by taping the sequence as audible right/left commands and playing it back to the target pilot during each run.

The primary mode selected to test the bandwidth hypothesis was the wings-level turn ($A_y$ mode). This mode was chosen primarily because it has considerable potential for future DFC aircraft in air-to-air and air-to-ground application.

The approach taken to test the bandwidth hypothesis was to generate a series of configurations with adverse and proverse roll and yaw coupling in the wings-level turn mode. If the bandwidth hypothesis is valid, the pilot ratings should correlate with bandwidth regardless of the type or magnitude of coupling. The configurations shown in Table 2 were developed based on this line of reasoning.

**2. Measurement of Bandwidth From Flight Data**

The Variable Stability Research Aircraft (VRA) was mechanized to have response characteristics identical to those of the YF-16 control-configured vehicle (CCV) at a flight condition of M = 0.80 at 20,000 ft. The dynamic characteristics of the configurations listed in Table 2 were identified using a pilot-generated frequency sweep input through the DFC controller. A typical DFC control input and the yaw rate response are shown in Fig. 5. The DFC controller for the wings-level turn mode was rudder pedals in this experiment. The yaw-rate-to-pedal transfer functions were obtained via Fast Fourier Transforms with typical results as shown in Figs. 6-8 for the baseline case, as well as the adverse and proverse yaw cases, respectively. The bandwidth of these configurations was obtained by simply noting the frequency at which 45 deg phase margin or 6 dB gain margin occurs. The measurement of heading to DFC controller input was extremely simple, requiring only a pedal position transducer and a rate gyro.

The Cooper-Harper pilot ratings from the flight test experiment are plotted versus heading bandwidth in Fig. 9 for the air-to-air tracking task using the wings-level turn mode. The open symbols in Fig. 9 signify that variations in heading bandwidth were achieved via yaw coupling, that is, the crossfeed gain from the DFC controller (pedal) to the rudder was increased above its nominal value to achieve favorable yaw coupling and below its nominal value to achieve unfavorable yaw coupling. The closed symbols in Fig. 9 signify that the heading bandwidth was varied via changes in roll coupling (e.g., pedal to aileron gain). To the pilot, favorable yaw coupling appears as a tendency for the nose to abruptly move in the direction of the commanded turn; whereas unfavorable yaw coupling appears as a tendency for the nose to initially swing away from the commanded turn. When flying a configuration with favorable roll coupling, the pilot will observe a tendency for the aircraft to roll in the direction of the commanded wings-level turn.

TABLE 2. LIMITED FLIGHT TEST EXPERIMENT

Purpose

To check the validity of the bandwidth hypothesis.

Configurations (Total - 17)

- Wings-level turn (WLT) with minimal coupling (1 configuration)
- WLT with favorable roll coupling (2 configurations)
- WLT with favorable yaw coupling resulting in similar bandwidth to the above roll coupling cases (2 configurations)
- WLT with unfavorable roll coupling (3 configurations)
- WLT with unfavorable yaw coupling resulting in similar bandwidth to the above roll coupling cases (5 configurations)
- Lateral translation:
  - Bandwidth less than F-16 ($Y_v$ = 0.2) (1 configuration)
  - Greater than F-16 in bandwidth due to proverse yaw coupling (1 configuration)

Tasks

- Air-to-air tracking using discrete series of inputs on target roll rate to excite all DFC modes (Fig. 3)
- Formation flying -- lateral translation only

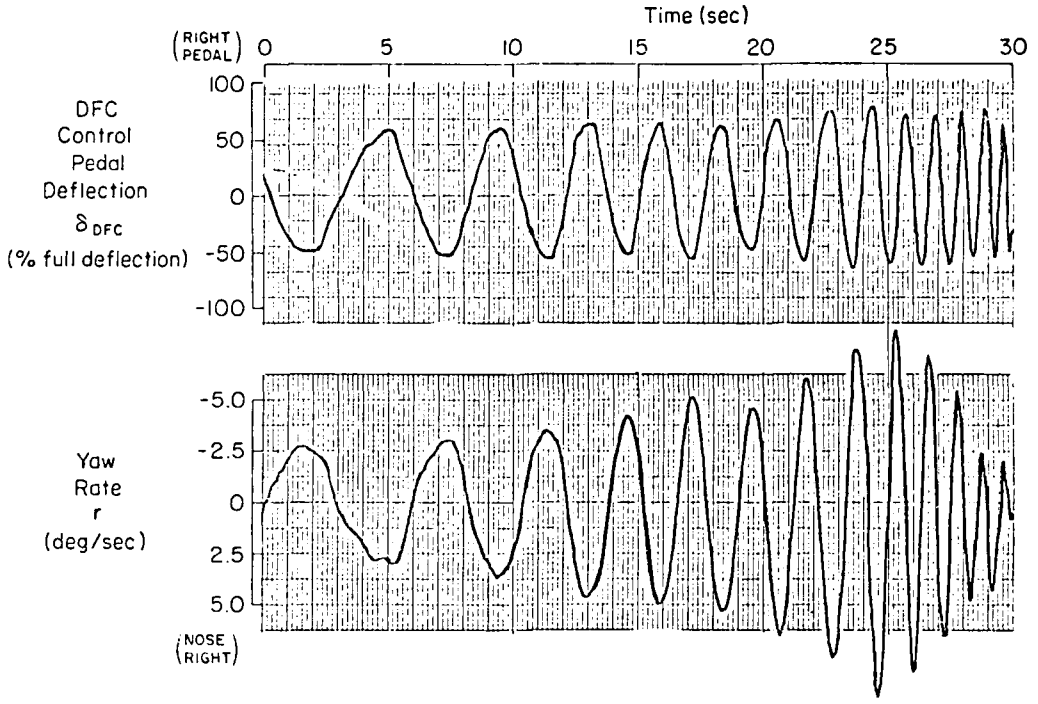


Figure 5. Typical DFC Control "Hand Generated Frequency Sweep" and Response for Configuration Identification (Configuration WLT 2)

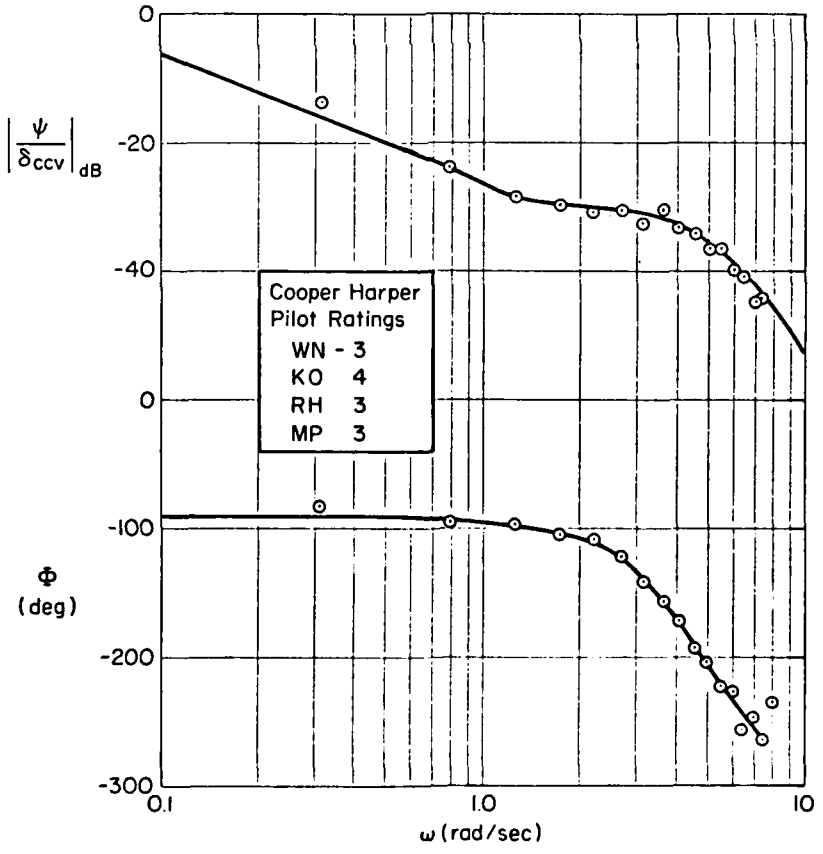


Figure 6. Fourier Transformed Hea ng Response -- Configuration WLT 1 (Minimal Coupling)

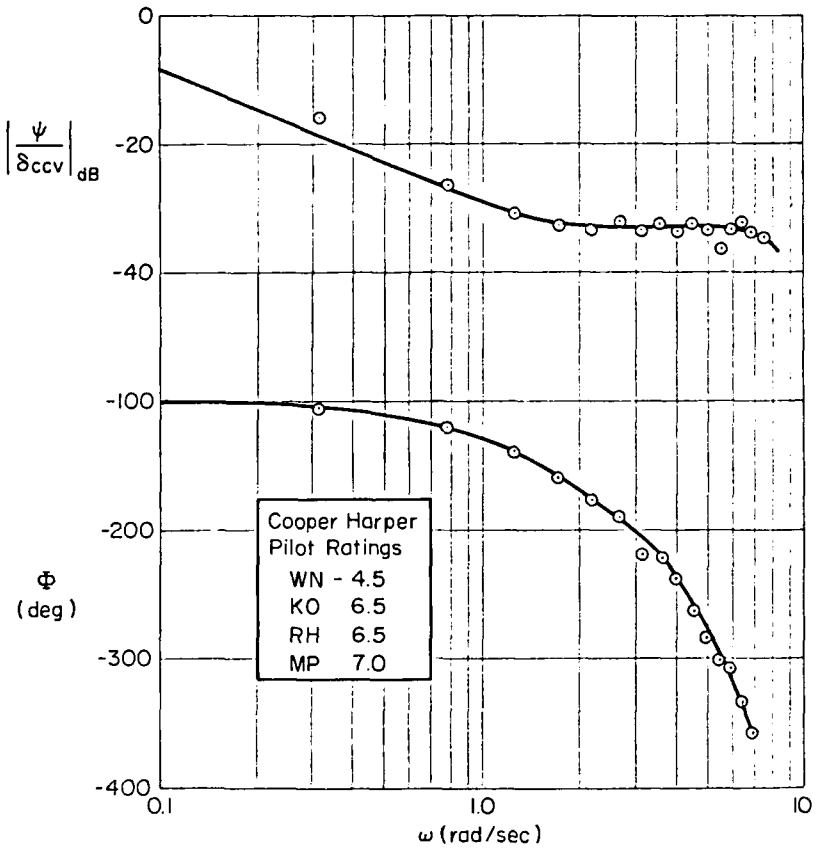


Figure 7. Fourier Transformed Heading Response -- Configuration WLT 4 (Adverse Roll Coupling)

Configurations with adverse roll coupling tend to roll away from the commanded wings-level turn. On the whole, the data in Fig. 9 support the bandwidth hypothesis. That is, the pilot ratings are similar for aircraft with approximately equal values of heading bandwidth regardless of the secondary aircraft motions (coupling). For example, the pilot rating for Configurations WLT4 and WLT15 (adverse yaw coupling) are approximately the same as the pilot ratings for Configuration WLT13 (adverse roll coupling). As can be seen from Fig. 9, all three of these configurations have approximately the same heading bandwidth of between 0.7 and 0.8 rad/sec.

The rating data in Fig. 9 indicate that even the best wings-level-turn configurations barely met the classical definition of Level 1 flying qualities (e.g., Cooper-Harper pilot rating equal to or better than 3.5). However, when one considers that the task involved tracking a target which was undergoing large and rapid bank angle reversals, it is difficult to conceive of any configuration that would correspond to the description of a pilot rating of 3 ("minimal pilot compensation required for desired performance").

A summary of the flight test results is given below:

- The bandwidth hypothesis appears to be valid, e.g.,
  - Yaw and roll coupling are rated equally when they occur at the same bandwidth.
  - Favorable coupling results in little rating degradation.
- Control sensitivity was found to be critical at elevated levels of favorable coupling.
- Pilot acceleration was noted to be a problem for favorable coupling even at the reduced levels of lateral acceleration used in this flight test.
- The bandwidth required for Level 1 flying qualities was 1.25 and for Level 2 was 0.55 rad/sec.*

*Level 1 implies a Cooper-Harper Piloting Rating of 3-1/2 or better and Level 2 implies a rating range between 3-1/2 to 6-1/2.

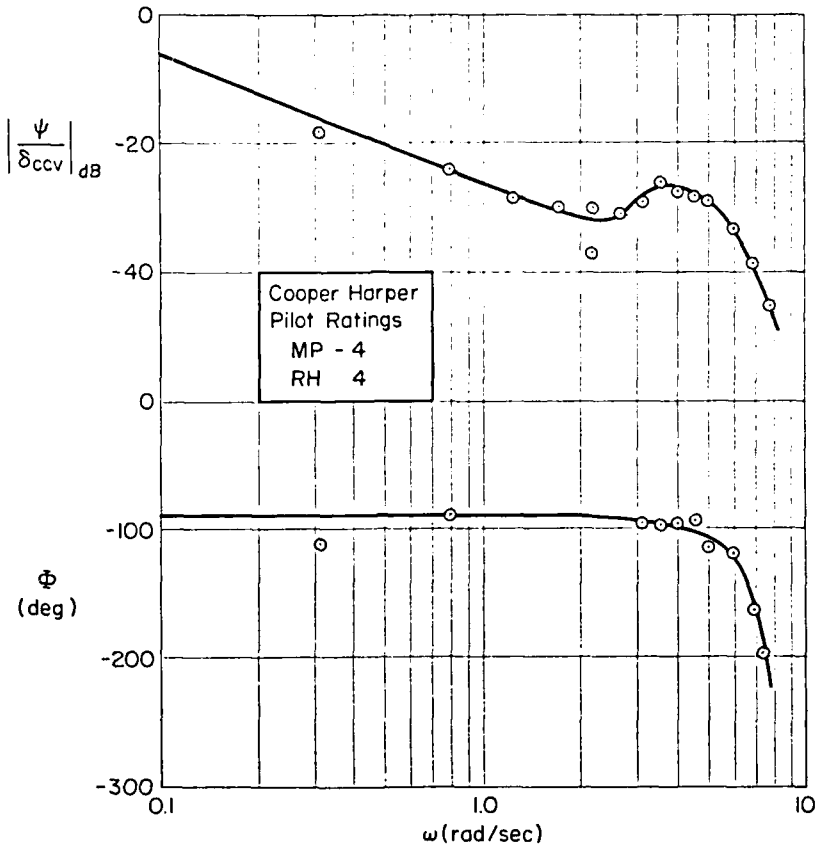


Figure 8. Fourier Transformed Heading Response -- WLT 10 (Proverse Roll Coupling)

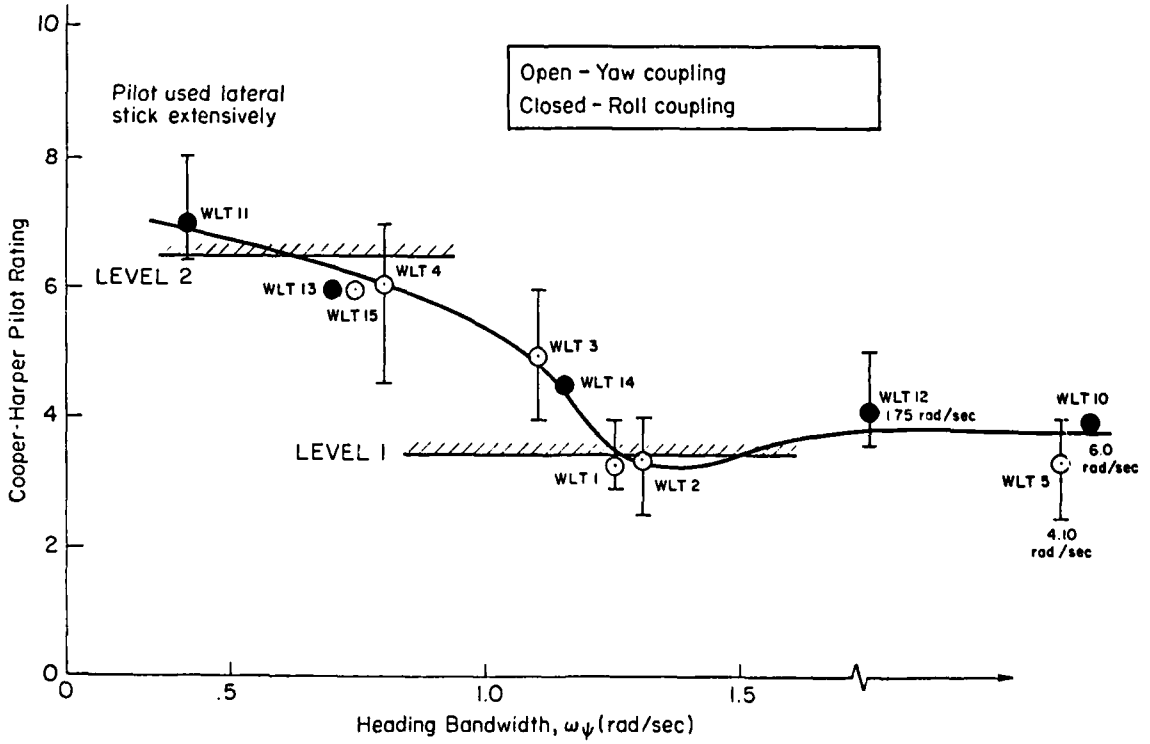


Figure 9. Correlation of Pilot Rating with Heading Bandwidth; Wings-Level Turn Mode: Air-to-Air Tracking Task

- Use of conventional controls for gross maneuvering and DFC control for fine tuning was found to be acceptable and even desirable.

- The bandwidth required for the path deviation task was 0.3 rad/sec (formation). This is consistent with previous conventional mode results as well as with the F-16 lateral translation results.

As noted above, the issue of control sensitivity had to be addressed especially at elevated levels of favorable coupling. The pilots were allowed to vary the control sensitivity during the experiment. It was found that for the favorable coupling cases (both yaw and roll) non-optimal levels of control sensitivity led to severe degradations in pilot rating. When the coupling was small or adverse there did not appear to be a noticeable dependence of pilot rating on control sensitivity.

Pilot acceleration was noted to be a factor, especially for favorable roll coupling. This was a consequence of the pilot's head being above the roll axis and hence would not scale with flight speed. Some pilots objected to this more than others.

**TENTATIVE SPECIFICATION**

A tentative flying qualities specification based on the results discussed above is given in below:

Dynamics

The response of the control variable defined in Table 4 shall have at least 6 dB of gain margin and 45 deg of phase margin at $\omega >$ __ rad/sec (from Table 3) for Level 1 and __ rad/sec (from Table 3) for Level 2.

Control Authority

The control variable defined in Table 3 shall achieve a value equal to or greater than for full CCV control input.

Acceleration of Pilot

Abrupt DFC inputs shall not produce pilot head or arm motions that interfere with the appropriate tasks as defined in Table 3. Pilot restraints shall not obstruct his normal field of view or interfere with manipulation of any cockpit control.

A study of control authority was beyond the scope of this program, and hence has not yet been determined. Values of bandwidth, which were shown to be limiting in the flight test experiment, are presented in Table 3. The variable for which bandwidth is to be specified depends on the task being performed. An initial attempt to define the appropriate variables based on the piloting tasks is presented in Table 4.

TABLE 3. BANDWIDTH REQUIREMENT IS TASK DEPENDENT

| Task | Required Bandwidth (rad/sec) | |
|---|---|---|
| | Level 1 | Level 2 |
| Tracking (CAT A)<br>• Air to air gunnery<br>• Strating<br>• Photo<br>• Dive bombing | 1.25 | 0.55 |
| Path Deviation (CAT C)<br>• Formation<br>• Air to air refueling<br>• Approach | 0.30 | 0.10 |
| Short Final and Landing ("CAT D") | 1.0 | ? |

TABLE 4. CONTROL VARIABLE DEPENDS ON DETAILS OF TASK

| Task | Control Variable |
|---|---|
| Air to air tracking | Pipper error for $\frac{U_0}{R} > 0.4$<br>$\theta$ or $\psi$ acceptable if $\frac{U_0}{R} \leq 0.4$ |
| Air to ground tracking<br>• Pointing tasks<br>— Strafing<br>— Photo<br>• Flight path tasks<br>— Dive bombing | <br>$\theta$ or $\psi$<br><br><br>Path angle |
| Path Deviation Tasks and Landing | Path angle |

## REFERENCES


1. Billue, S. K., and C. P. Senn, NATC, Evaluation of the Direct Lift Control System Installed in the F-8C Airplane, 1969, Tech. Rept. FT-69R-69.

2. Lorenzetti, R. C., "Direct Lift Control for Approach and Landing," paper presented at AGARD Guidance and Control Panel Symposium, Cambridge, Mass, 1969.

3. Brulle, R. V., W. A. Moran, and R. G. Marsh, AFFDL, Direct Side Force Control Criteria for Dive Bombing. Vol. I: Summary. Vol. II: Analysis and Results, 1976, TR-76-78.

4. McAllister, J. D., et al., AFFDL, Fighter CCV Phase IV Report. Vol. II: Flight Test Data Evaluation. Vol. III: Test Phase Data Summary, Parts 1 and 2, 1978, TR-78-9.

5. Flying Qualities of Piloted Airplanes, MIL-F-8785C, 1980.

6. Neal, T. Peter, and Rogers E. Smith, AFFDL, An In-Flight Investigation to Develop Control System Design Criteria for Fighter Airplanes, 1970, TR-70-74, Vol. I and II.

7. Ashkenas, Irving L., Roger H. Hoh, and Samuel J. Craig, AFFDL, Recommended Revisions to Selected Portion of MIL-F-8785B (ASG) and Background Data, 1973, TR-73-76.

8. McRuer, Duane, Irving Ashkenas, Dunstan Graham, "Aircraft Dynamics and Automatic Control," Princeton University Press, Princeton, N.J., 1973.

9. Hoh, Roger H., Thomas T. Myers, Irving L. Ashkenas, et al, AFWAL, Development of Handling Quality Criteria for Aircraft with Independent Control of Six Degrees of Freedom, 1981, TR-81-3027.

10. Black, G. Thomas, David J. Moorhouse, and Robert J. Woodcock, eds., AFFDL, Proceedings of AFFDL Flying Qualities Symposium Held at Wright State University 12-15 September 1978, 1978, TR-78-171.

11. Hall, I. A. M., British Aircraft Corp., Frequency Response Method for Measuring Aircraft Dynamic Characteristics, 1964, Ae. 217.

# EXPERIMENTAL FLIGHT TEST PROGRAMS FOR IMPROVING COMBAT AIRCRAFT MANOEUVRABILITY BY MANOEUVRE FLAPS AND PYLON SPLIT FLAPS

by

D. JACOB, D. WELTE, H. WONNENBERG

DORNIER GMBH
Postfach 1420
799 Friedrichshafen

SUMMARY :

The paper describes two flight test programs which are currently in progress with the Alpha-Jet as test vehicle.

In the first program the standard wing of the aircraft is replaced by a transonic wing with manoeuvre flaps. Wind tunnel and flight test results are presented which show the increase in performance and manoeuvrability based on the improved drag polars and buffet limits.

In the second program pylon split flaps are used to provide flat turn and side step manoeuvres by an alternating deflection of the four left or right split flaps. A drag modulation mode is realized by symmetrical deflection of all eight flaps.

## 1. INTRODUCTION

The German Ministry of Defense is currently sponsoring two aerodynamics and flight mechanics oriented experimental flight test programs at Dornier which are based on the Alpha-Jet as a test vehicle. The purpose of the programs is to show the improvements in manoeuvrability and performance which can be obtained by replacing the standard wing by a transonic wing with manoeuvre flaps and by installing pylon split flaps for direct side force control and drag modulation.

In the first program, called TST (Transsonischer Tragflügel = Transonic Wing),which incorporates a transonic wing with manoeuvre flaps (Fig. 1), part of the flight testing has already been completed, so that first flight test results can be shown.

The flight tests of the second program called DSFC (Direct Side Force Control) will start later this year. The pylon split flaps to be investigated in this program are attached to pylons on the standard Alpha-Jet wing.

## 2. THE T S T - PROGRAM

### 2.1 General Information

The TST-program consists of the design, manufacturing and flight testing of a transonic wing with manoeuvre flaps. The main purpose of the program is the investigation of the improvements in performance and manoeuvrability obtainable by a transonic wing on a subsonic/transonic combat aircraft and the development and testing of theoretical and experimental methods required for the design of future transonic combat aircraft.

Specific points of interest are:

- 3-D effects on moderate aspect-ratio wings
- performance of a transonic wing in a broad $C_L$-M-region
- effectiveness of manoeuvre flaps on a transonic wing
- the behaviour at and beyond the buffet boundary

Since a complete description of the design philosophy and the theoretical and experimental work up to 1976 is published in reference /1/, only a short review of the background of the program is given here.

The program started in 1974 when the German Ministry of Defense (BMVg) awarded a contract to Dornier as prime contractor and VFW-Fokker as subcontractor. It was joined by ONERA in 1975. Fig. 2 shows the participating agencies and their main contributions. The DFVLR supported the program by a series of wind tunnel tests.

Flight testing began in December 1980 and is currently continuing as a joint effort of Dornier and the German Flight Test Center (BWB AFB LG IV and E-Stelle 61) in Manching. Since not all configurations have been flown so far and since the already available data have not yet been completely evaluated, only preliminary results can be presented. A final evaluation will be available next summer.

## 2.2 Design Description

Compared with a conventional wing a transonic wing offers the following advantages either alternatively or in combination:

- increased maximum flight velocities
- increased lift coefficients at a given Mach number

  results in: - increased tationary and non-stationary load factors

  consequence: - improved manoeuvrability
  - reduced vulnerability

- increased wing thickness

  results in: - lower structural weight
  - increased tank volume

  consequence: - increased radius of action

- reduced sweep angle of wing

  results in: - lower structural weight
  - improved stall behaviour

  consequence: - reduced landing velocity

The selection of the optimum design parameters depends on the requirements. In the TST-program the choice was limited due to the following restrictions:

- Cost and airplane availability considerations allowed only a replacement of the wing and no further modifications. Since the tail could not be modified, the wing planform (sweep angle) had to be kept constant (Fig. 3).
- An increased drag-rise Mach number could not be fully utilized due to thrust restrictions. Therefore, a thicker profile was selected which could be generated without changing the existing wing spar (Fig.4).

Based on these considerations, the TST experimental wing shows the following differences to the wing of the standard Alpha-Jet (Fig. 5):

- Transonic profiles
  (thickness, approximately 20 % increased)
- Extended wing leading edge
  (to improve area distribution)
- Manoeuvre flaps
  (consisting of slats and 25 % single-slotted fowler-flaps).

Fig. 6 shows a comparison of the new TST-profile with the profile (modified RAE 103) of the standard Alpha-Jet. With a thickness of 12.4 % at the root and 10.3 % at the tip it is approximately 20 % thicker than the standard profile. It is designed such that the drag rise Mach number is not decreased at low lift coefficients and increased at high $C_L$-values.

The different slat and flap positions are described in Figures 7 and 8. The standard Alpha-Jet has no slats and 30 % single-slotted landing flaps with a fixed hinge-line. In the $\eta_k = 32^0$-position both flaps have the same extension of the wing planform.

On the current experimental flight test wing the flaps and slats cannot be moved in flight. Due to funding restrictions it was decided to use fixed flap positions, which can be changed on the ground corresponding to the five positions shown in Figures 6 - 8.

## 2.3 Results

The configurations described in the previous section have been designed by a series of theoretical and experimental investigations. Most of the low speed tests have been performed by the DFVLR. In addition to 2D-transonic tests in the S3-Wind tunnel the ONERA contributed high-speed tests with a 1:10 model in their S2-wind tunnel at a Reynolds number $Re = 2.5 \cdot 10^6$ (based on mean aerodynamic chord) and a full scale half-model test in the S1-tunnel at $Re = 4 \div 25 \cdot 10^6$. In the transonic S1-tunnel with its 8 m diameter test section the actual half-wing of the airplane attached to a simplified fuselage could be tested. The wing (Fig. 5) was equipped with the same devices used in the flight tests:

- static pressure tubes at 4 sections
  (48 pressures in each section)
- 20 kulite dynamic pressure probes in 4 sections on the upper side of the wing

- a rotating pitot-rake for wake measurements at the trailing edge

- 5 accelerometers for buffet analysis

- 24 strain gages for load and buffet analysis

Flight tests began on December 12, 1980 with the clean configuration (flaps and slats retracted) and were continued with the configurations $\eta_V = 5^o/\eta_K = 32^o$ (Fig. 8) and $\eta_V = 0^o$ extended / $\eta_K = 5^o$ (Fig. 7). The test data have only been partially evaluated, so that the following results describe mainly the clean configuration with some additional data for the $\eta_V = 5^o/\eta_K = 32^o$ configuration.

As shown in Fig. 2, the flight tests are performed in cooperation with the German Flight Test Center (E-61) in Manching. The flight envelopes for each configuration are opened by Dornier, while the majority of the flights for performance and control evaluations is carried out by E-61.

In Fig. 9 flight test results for the TST and the standard Alpha-Jet are compared for the clean configuration at Mach number M = 0.50, M = 0.70 and M = 0.825. The drag polars $C_L(C_D)$ of the TST were obtained from steady flight data. Additional flight test points, derived from non-stationary manoeuvres, will be added later on. As expected from wind tunnel tests the difference between TST and Alpha-Jet polars is small at M = 0.5 but increases with increasing Mach number. At M = 0.825, which is close to the design Mach number for the TST, the transonic wing has a considerably lower drag than the standard wing.

Fig. 10 shows good agreement of drag rise curves from flight tests and wind tunnel tests for the clean configuration. As pointed out previously, the transonic wing was designed such that there is only a small increase of the drag rise Mach number at small lift coefficients $C_L$ and a larger increase at larger $C_L$. It has to be kept in mind that the improved drag rise characteristic of the TST has been obtained with a 20 % thicker wing!

In Fig. 11 the lift coefficient $C_L$ for buffet onset (or light buffet) is plotted as function of $M_\infty$. In this figure buffet onset is defined as the point ($\alpha$, $C_L$) where the root mean value of the wing root bending moment $C_F$ reaches twice the value it has at small angles of attack. The results were obtained in the S2 wind tunnel at $Re = 2.5 \cdot 10^6$. The thicker transonic wing can reach higher buffet-free lift coefficients than the standard wing. The additional increase which can be realized by manoeuvre flaps is considerable.

Buffet curves derived from flight test results are shown in Fig. 12. The absolute values of these buffet onset curves are somewhat lower than the values presented in Fig. 11. The difference between transonic and standard wing is, however, similar in both figures. Aiming and manoeuvre limits lie, of course, at higher lift coefficients for both wings.

The TST flight test curves based on pilot perception are supported by data obtained from wing tip accelerometer. The divergence point of the wing tip accelerometer agrees closely with the pilots impression of buffet onset. A more detailed analysis of different buffet indicators is in progress.

In Fig. 13 the maximum lift coefficients for both wings are compared. For the clean configuration the maximum lift coefficient of the transonic wing is increased by $\Delta C_L = 0.04$ relative to the standard wing, while for the landing configuration the increase is $\Delta C_L = 0.37$ which is mainly due to the slat on the TST. Similar to the Alpha-Jet the stall behaviour for both configurations is very good with early stall-warning, symmetrical stall and full control in the stall region.

After the major aerodynamic results obtained from wind tunnel and flight tests have been described the corresponding improvements in performance and manoeuvrability have to be discussed.

Fig. 14 shows the radius of action of the Alpha-Jet-TST and the standard Alpha-Jet. The transonic wing increases the radius of action considerably because of the following reasons:

- reduced drag

- increased wing thickness (increases internal tank volume)

- wing leading edge glove (also increases internal tank volume)

The maximum stationary load factors reached with the TST in flight tests are increased by approximately 1 g in the complete altitude range (see Fig. 15).

Fig. 16 gives a comparison of non-stationary manoeuvre limits for a load factor of n = 7.5 at buffet onset. The curves describe the maximum altitude for buffet-free flight at n = 7.5 as function of the Mach number. They are based on the buffet onset curves of Fig. 12 for the clean wing and Fig. 11 for manoeuvre configurations. It is clearly seen that the transonic wing with and without manoeuvre flaps allows n = 7.5 manoeuvres at much higher altitudes or vice versa considerably larger non-stationary load factors at a constant altitude.

The improved maximum lift coefficients at low speeds discussed in Fig. 13 lead to reduced corner speeds, increased turn rates and reduced turn radii as shown in Fig. 17. The major improvement is obtained by deflecting the TST manoeuvre flaps. Comparable figures for the standard wing in landing configuration are non included because the flaps of the standard wing are not designed for loads corresponding to n = 4 g.

## 2.4 Conclusion

The flight test results described in the previous section indicate that a transonic wing with manoeuvre

flaps offers substantial improvements in performance and manoeuvrability compared with the standard wing.

A more detailed analysis including a comparison of the complete flight test results with theoretical results and experimental data obtained in different wind tunnels will be presented after completion of the flight test program. The theoretical and experimental experience gained in the TST program will facilitate the effective design of future subsonic/transonic combat aircraft.

It is planned to continue the TST program with manoeuvre flaps which are automatically positioned in flight such that an optimum increase in manoeuvre performance in the entire flight envelope can be realized.

## 3. THE DSFC - PROGRAM

Another research program, which is realized with an Alpha-Jet as test aircraft, will investigate the effectiveness of pylon split flaps for direct side force and drag control purposes. When proposing this paper to the program committee, we expected that first flight test results could be presented at this meeting, too. But due to some additional unforeseen tasks of the provided test aircraft, one of the prototypes, the begin of the flight tests is retarded. Therefore, only some of the aims and technical aspects of the program can be shortly discussed here; a detailed description was given already at an AGARD-FDP Symposium /2/.

The pylon split flap arrangement at the Alpha-Jet enables the aircraft to use some CCV-techniques with only few modifications and without a complex control system. Fig. 18 shows the arrangement which consists of two flaps at each pylon. Using the first 15 mm of the rudder pedals travel for control of either the four left or the four right flaps to produce left or right DSF. A control of all eight flaps simultaneously produces an effective drag control.

Fig. 19 shows the operational modes which can be realized with the system:

- side slip free change of the course with constant bank angle, which is faster than the conventional heading change and does not disturb the moments equilibrium;
- side step manoeuvre at constant attitude for crosswind compensation and formation flight control improvement;
- drag modulation for sudden decelerations in air combat, steeper approaches at sufficient engine thrust, quicker deceleration from cruising to approach speed and glide-path control.

Different configurations of DSFC control surfaces were analyzed in the theoretical and experimental study (Fig. 20):

- special control surfaces under the wing
- split flaps and spoilers at the pylons
- vertical canards

Fig. 20 shows the effectiveness measured in the wind tunnel of the different configurations.

The criterium to achieve an effectiveness as great as possible with small coupling moments and low technical complexity finally led to the decision to pursue the configuration with split flaps at the four external store pylons.

Since the center of pressure of the pylon split flaps is situated near the aircraft center of gravity with respect to the z and x-direction, it could be expected that with DSFC flap deflection no or only inconsiderable coupling moments will occur, so that a coupling between DSFC and the conventional control surfaces is not necessary for the compensation of these moments.

Two configurations of the flaps, a longer and a short one, have been investigated by wind tunnel tests with an 1:5 Alpha-Jet model. Fig. 21 shows the effectiveness of two representative flaps at the inner station. The difference between flap 1 and 2 is caused by induced side-wash effects at the pylon, which enlarges the effectiveness of flap 1 and reduces it for flap 2. The interference effects in roll, second diagram of the Fig. 21, shows that both flaps are producing an opposite rolling moment. This fact has been used to compensate the remaining coupling moments internally by a proper adjustment of the different deflections of the four flaps. Furthermore, the absolute values of the coupling moments are significantly smaller for the shorter flaps and as the next Fig. 22 shows, also the hinge moments, which would cause less hydraulic power for actuation.

A final evaluation of the wind tunnel results showed that with the shorter flaps even the same overall effectiveness than for the longer could be realized with the control law of Fig. 23 including the combined rudder deflection due to the corresponding pedal travel. The effective maximum side force coefficient corresponds to a lateral acceleration of 0.4 g at VC = 400 kts.

The remaining coupling moments, due to non-linearities, request a simple artificial yaw, roll and pitch damping equipment. The next Fig. 24 shows the effectiveness of the split flaps in drag producing which creates twice the value of the normal air brakes with the same small nose-up pitch coupling moment.

The flight test program, which is envisaged to start in the very near future, should demonstrate the expected improvement in manoeuvrability and aiming capacity. The flight tests are planned in two phases:

one is to check-out and optimize the system itself and give some first qualitative results, the second phase will include gun firing and weapon release tests using this new equipment to show whether the advantage are quantitatively significant enough to discuss a possible installation into the series Alpha-Jets.

REFERENCES

/1/ M. Lotz, B. Monnerie — The Franco-German Experimental Program for the Evaluation of a Supercritical Wing for a Combat Aircraft Application ICAS-Paper No. 76 - 21, 1976

/2/ P. Esch, H. Wünnenberg — Direct Side Force and Drag Control with the Aid of Pylon Split Flaps AGARD CP No. 262

FIG. 1

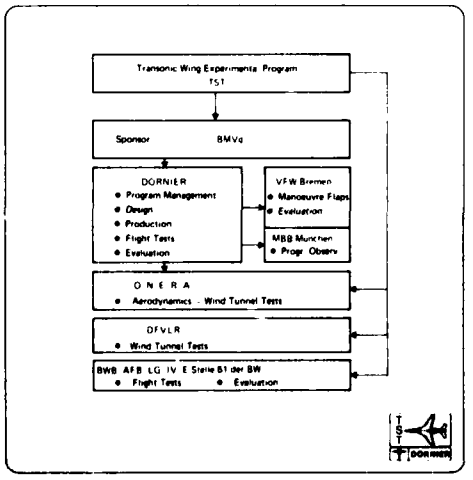


FIG. 2

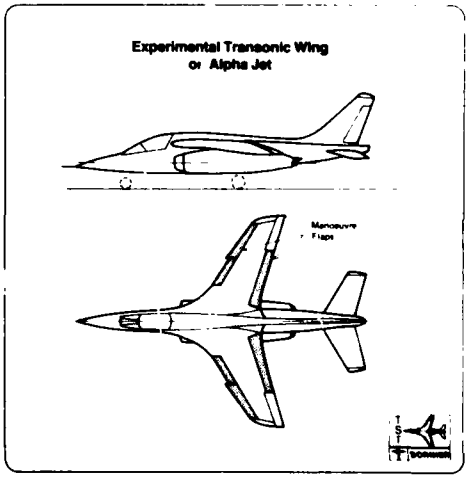


FIG. 3

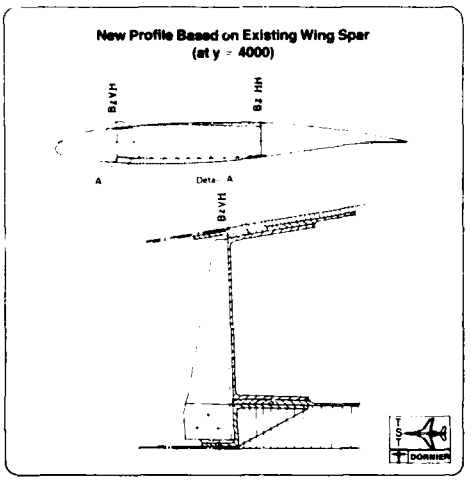


FIG. 4

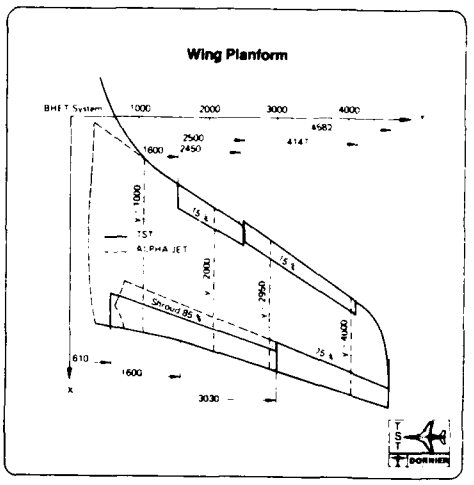


FIG. 5

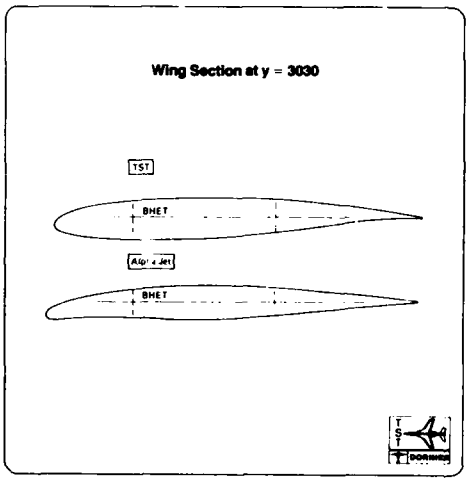


FIG. 6

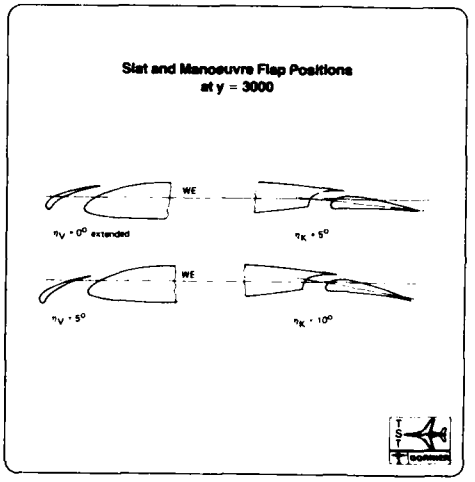


FIG. 7

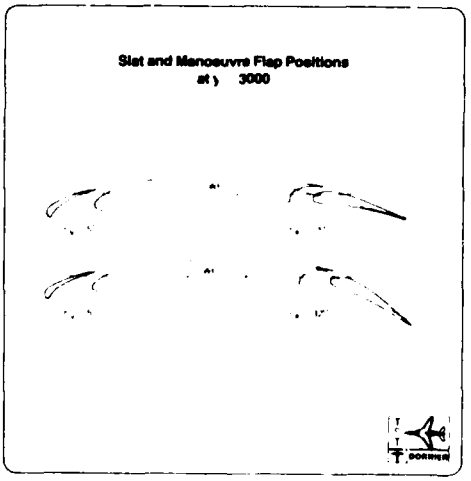


FIG. 8

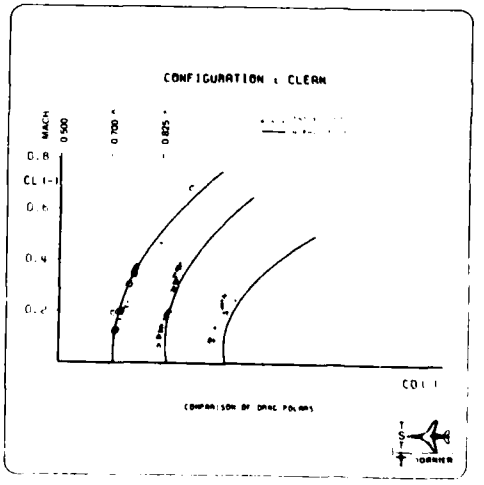


FIG. 9

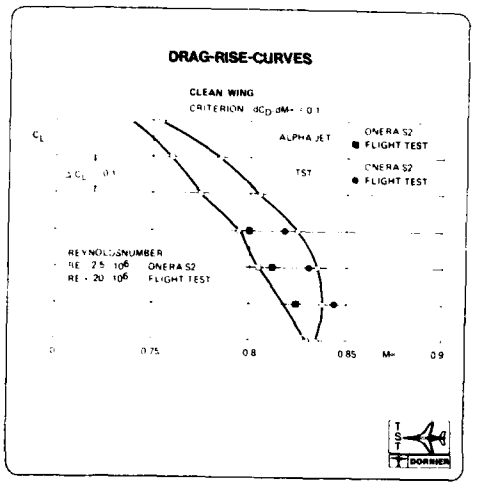


FIG. 10

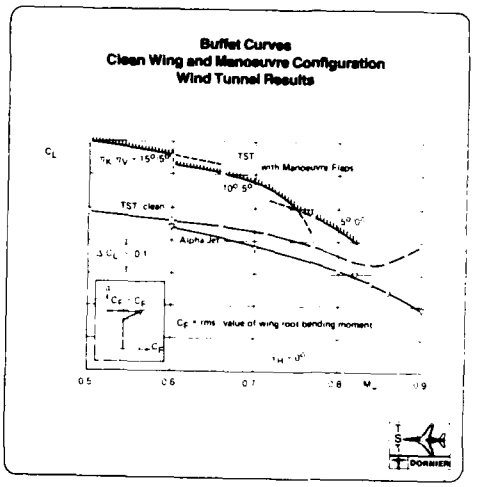


FIG. 11

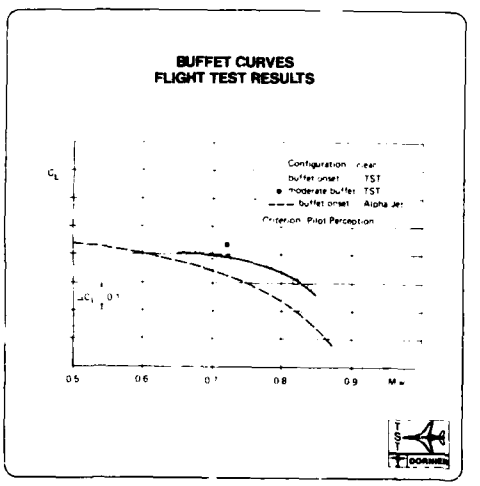


FIG. 12

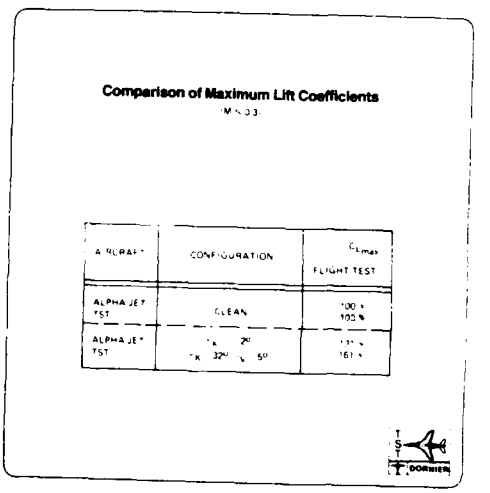


FIG. 13

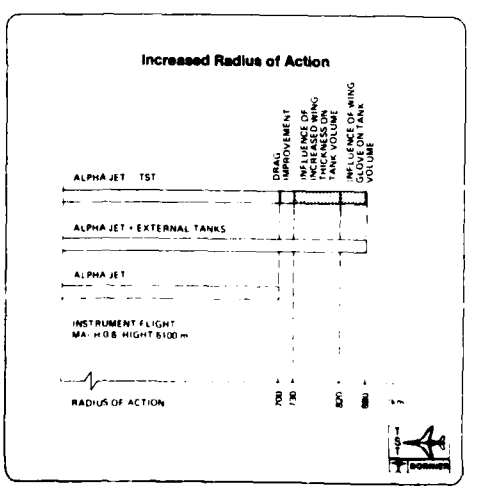


FIG. 14

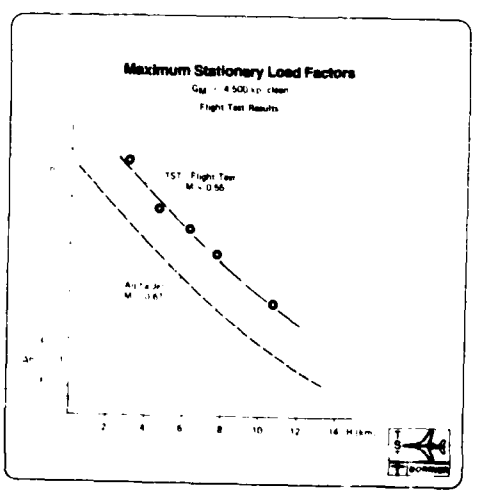


FIG. 15

AD-A112 310 ADVISORY GROUP FOR AEROSPACE RESEARCH AND DEVELOPMENT--ETC F/G 1/2
COMBAT AIRCRAFT MANOEUVRABILITY.(U)
DEC 81
UNCLASSIFIED AGARD-CP-319 NL

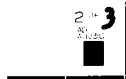

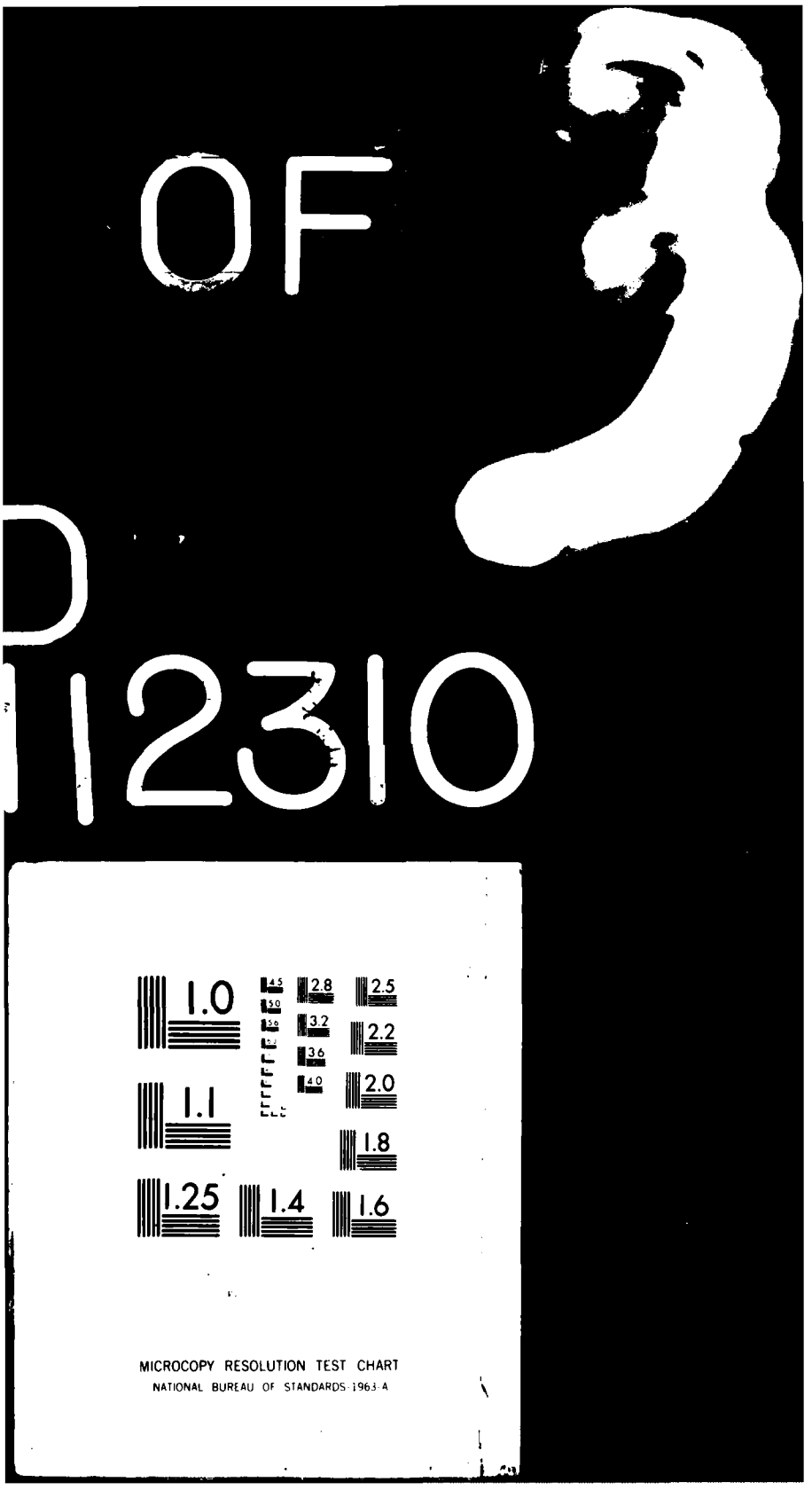
OF
12310
1.0
1.1
1.25
1.4
1.6
2.8
3.2
3.6
4.0
2.5
2.2
2.0
1.8
MICROCOPY RESOLUTION TEST CHART
NATIONAL BUREAU OF STANDARDS-1963-A

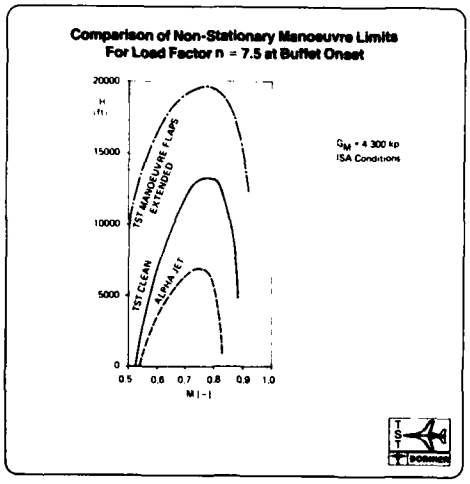


FIG. 16

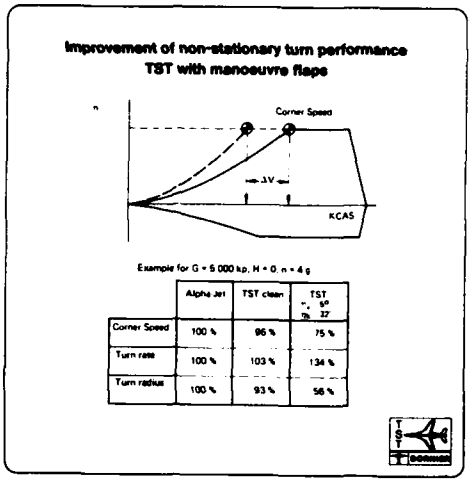


FIG. 17

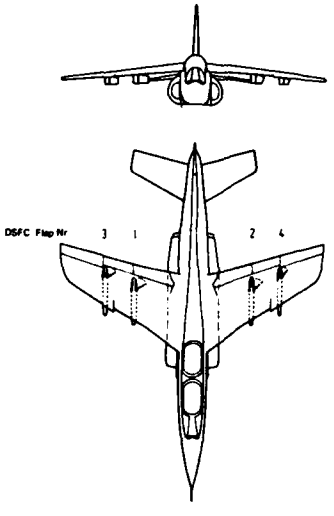


Pylon Split Flap Arrangement at Alpha-Jet

FIG. 18

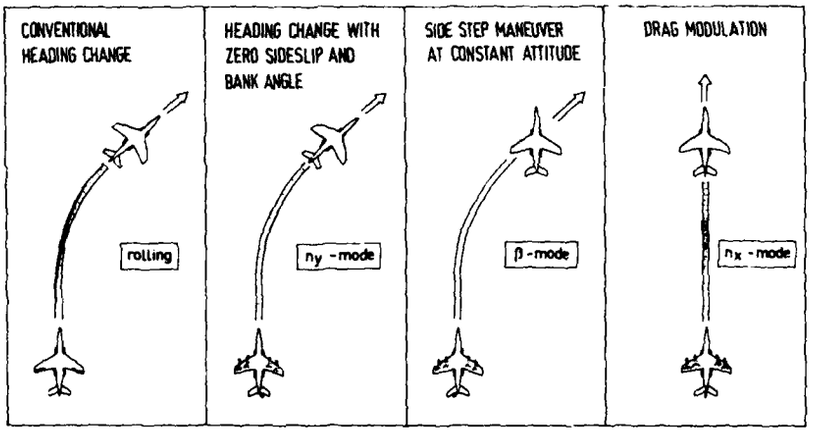


OPERATIONAL POSSIBILITIES BY DSFC-MODES

FIG. 19

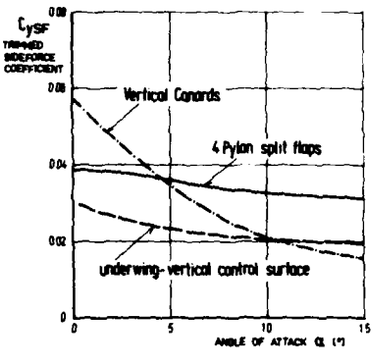


THE EFFECTIVENESS OF DIFFERENT METHODS TO GENERATE DIRECT SIDE FORCES

FIG. 20

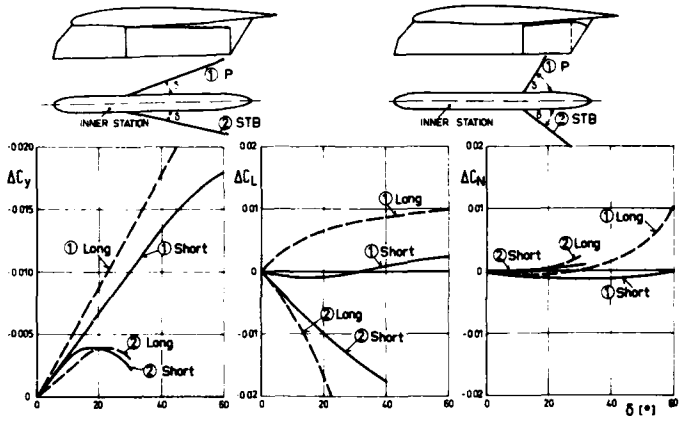


EFFECTIVENESS AND COUPLING MOMENTS COMPARISON BETWEEN LONG AND SHORT FLAP CONFIGURATION

FIG. 21

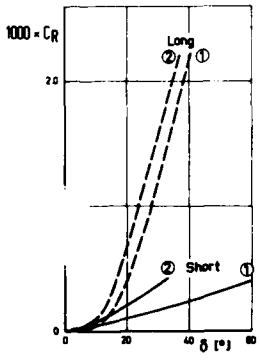


HINGE MOMENTS COMPARISON BETWEEN LONG AND SHORT FLAP CONFIGURATION

FIG. 22

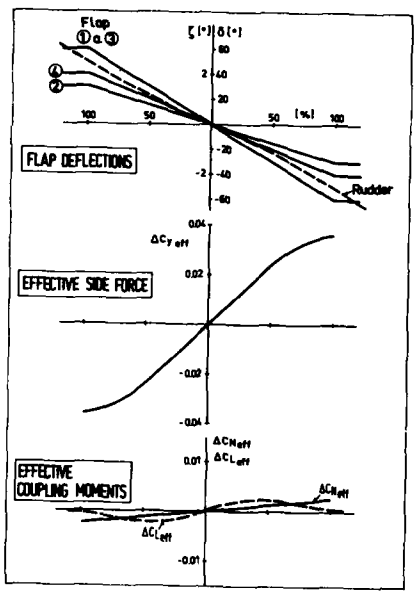


or CONTROL LAW

FIG. 23

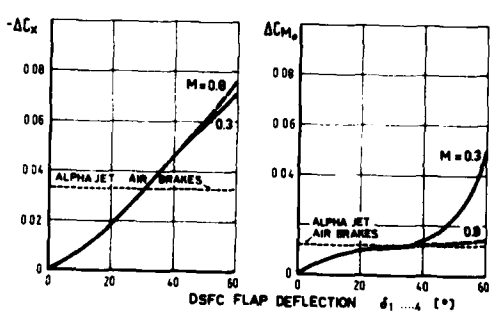


EFFECTIVENESS OF DRAG MODULATION BY THE PYLON SPLIT FLAPS

FIG. 24

# MULTIVARIABLE CLOSED-LOOP CONTROL ANALYSIS AND SYNTHESIS FOR COMPLEX FLIGHT SYSTEMS

by
David K. Schmidt
School of Aeronautics and Astronautics
Purdue University
West Lafayette, IN 47907
U.S.A.

## SUMMARY

In this paper, a flight control system analysis and synthesis method is presented that is intended to be especially suitable for application to vehicles exhibiting complex dynamic characteristics. For such vehicles quantitative handling qualities specifications are not usually available. However, handling qualities objectives are specifically introduced in this method via the hypothesis of correlation between pilot ratings and the objective function of an optimal control model of the human pilot. Further, since augmentation and pilot operate in parallel, simultaneous determination of the augmentation and pilot-model gains is required. Desirable augmented dynamics are obtained for a variety of complex systems and the method is experimentally verified in the case of simple pitch-damper gain selection for optimum pitch tracking performance.

## PREFACE

Clearly, in the design of flight vehicles, the piloted performance of these man-machine systems and the difficulty of the piloting task is extremely important. The ultimate measure of merit in this regard is the pilot opinion ration (P.O.R.) of the vehicle's handling qualities. By means of an established rating method (i.e. the Cooper-Harper[1] rating system), the pilot's subjective rating, considering performance and difficulty factors, is quantified through flight tests and/or man-in-the-loop simulation. The overall objective of this paper is to present a unified methodology for achieving desirable man-in-the-loop performance of advanced, complex flight vehicle systems.

The two fundamental problems to be discussed here, generally stated, are

- On what quantitative factors does the pilot rating depend and how can the pilot's opinion rating be analytically predicted?
- If a proposed vehicle is predicted to be unacceptable to the pilot, how should the vehicle be modified to achieve maximum pilot acceptance or performance?

A multitude of vehicle-dependent factors are ultimately involved. They include

1. Instrumentation availability and information quality, or the machine-to-man information interface
2. Control manipulator design or the man-to-machine information interface and
3. The inherent dynamic properties of the pilot-vehicle system

In this paper we are primarily concerned with the latter very important area dealing not only with the human element, but also with the aeronautical systems areas of flight vehicle control systems analysis and synthesis with emphasis on systems of high order.

## 1. BACKGROUND

Historically, the pilot's opinion rating was almost completely dependent on the vehicle's rigid body dynamics. The approach taken to solve the two fundamental problems stated above was to correlate a host of pilot opinion data with these rigid body dynamic characteristics (e.g., the frequency and damping of the various modes).[2] Acceptable open-loop vehicle dynamic characteristics have then provided the vehicle designer the specifications or design objectives.

This approach has been appropriate for vehicles exhibiting conventional dynamic properties dominated by these rigid body modes. However, quantitative specifications based on pilot opinion data are almost nonexistant for vehicles with non-conventional dynamics resulting from foreign operating environments or radically new designs; for example, control-configured vehicles (CCV's). Furthermore, the effects of dynamic modes previously ignored, such as aeroelastic and control or display augmentation, have been found to significantly alter pilot opinion ratings from that "predicted" by simple rigid body handling qualities specifications.[3-4] These effects become extremely important when considering new large, flexible and/or highly augmented vehicles of the future.

An alternative approach to the open-loop method described above is that of analytically predicting the pilot rating by means of a pilot-vehicle model. The most notable of these techniques, originally applied to a VTOL hover task, was the "paper pilot" proposed by Anderson.[5] In this approach, as well as in later applications of the "paper pilot", parameters in a describing-function pilot model of assumed form were chosen to minimize a pilot rating metric, and this metric was empirically related to the pilot opinion rating. This rating metric consisted of a measure of performance (e.g., rms tracking error) and a measure of pilot work load expressed, in this case, in terms

of "lead" required in the pilot's describing function (see McRuer[6]). In an assessment of this technique[7], it was found that a pilot rating metric based on easily-measured, closed-loop performance parameters correlated well with pilot rating in certain cases. Other more recent efforts have been reported by Smith[8], Onstott[9,10], and Brulle & Anderson[11]. These approaches also utilized a frequency response approach to modeling the man-machine system dynamics, or a pilot describing function.

This fact is the fundamental difficulty with using these approaches for higher order systems applications. The form of the pilot's describing function must be specified a priori. For "conventional" vehicles and "conventional" piloting tasks this may be possible. However, for radically new multivariable vehicles such as those cited previously, the analytical pilot model is not well established. The pilot is known to adapt his gain and form of equilization to the vehicle and task, and clearly, the accuracy of any analytical pilot rating prediction will depend on the validity of the pilot-vehicle model. A much more general model is required, a model which determines the pilot gains, equilization, etc. for the vehicle and task in question.

## 2. PREDICTING PILOT RATING

Due to the multi-variable aspects of these new system concepts, an optimal-control pilot model[12] appears appropriate. This modeling approach has been utilized successfully to predict piloted vehicle performance in numerous tasks, including low visibility landings[13], piloted aircraft system stability[14], and to investigate display design.[15]

The model[12] is based on the assumption that the well-trained, well-motivated human pilot adjusts his gains and compensation for the vehicle and task such that an objective function, $J_p$, is minimized subject to human limitations. Where

$$J_p = E\left\{\lim_{T\to\infty}\frac{1}{T}\int_0^T (\bar{x}^T\ Q\bar{x}\ +\ \bar{u}_p^T\ R\bar{u}_p\ +\ \dot{\bar{u}}_p^T\ G\dot{\bar{u}}_p)dt\right\};\ E(\cdot)\ \text{denotes expected value} \qquad (1)$$

and Q, R, and G are selected weighting matrices, and the plant dynamics are modeled by the linear relation

$$\dot{\bar{x}} = A\bar{x} + B\bar{u}_p + \text{noise} \qquad (2)$$

The pilot's control vector is $\bar{u}_p$, and the pilot's vector of (delayed) observations is

$$\bar{Y}_p = C\bar{x}\ (t-\tau) + \text{noise} \qquad (3)$$

Furthermore, Hess[16] has shown that the optimal control model may be used for predicting pilot opinion for simple vehicle (plant) dynamics and for the helicopter hover task. He convincingly argues that if pilot opinion is driven by performance and work load, the index of performance in the optimal-control pilot model, $J_p$, should reflect this, due to the fact that $J_p$ is expressed as rms (or quadratic) performance, control activity, and control rates. The use of this modeling approach for pilot rating prediction allows for a natural pilot rating metric via the pilot-model objective function. Proper selection, based on a careful definition of the task, of the state and control weights (Q, R, and G) in the objective function ultimately predicts a dynamic model for the pilot plus a pilot rating. Since this objective-function/rating correlation provides a valuable tool for handling qualities research and flight control synthesis, as used in the methodology to be presented, validating it over a wide range of tasks and plant dynamics is appropriate.

To this end, an analysis of Arnold's (Ref. 17) simulation results for fourteen aircraft configurations flight tested earlier by Neal and Smith (Ref. 3) has been completed.[18] A fixed set of pilot model parameters were found for all cases in modeling the simulated regulation task, and a strong correlation, shown in Figure 1, was obtained between the cost function and rating. Furthermore, modeling the same fourteen configurations in the tracking task used by Neal and Smith indicated reasonable correlation as well, considering no experimental data is available from the Neal and Smith tests to check the pilot model parameters in this case. Other results presented in Ref. 18 indicate that with the vehicle and task properly modeled, an objective function/rating correlation is evident for highly augmented aircraft and very flexible vehicles as well.

## 3. SYNTHESIS METHODOLOGY

Utilizing this rating hypothesis, a methodology for augmenting the man-machine system dynamics to improve pilot acceptability has been proposed by Schmidt[19] based on the following analysis. Recalling the previous discussion on pilot ratings, if the smaller the value of the pilot's objective function the better the pilot rating, then the best augmentation will minimize the pilot's objective function $J_p$ (defined in the optimal control pilot model) as given in Eq. (1), or

$$J_p = E\left\{\lim_{T\to\infty}\int_0^T (\bar{x}^T Q\bar{x}\ +\ \bar{u}_p^T\ R\bar{u}_p\ +\ \dot{\bar{u}}_p^T\ G\dot{\bar{u}}_p)dt\right\} \qquad (4)$$

We shall choose then, as a reasonable performance index or objective function for the vehicle augmentation system

$$J_{Aug} = J_p + E\left\{ \lim_{T\to\infty} \int_0^T \bar{u}_c{}^T F \bar{u}_c dt \right\} \tag{5}$$

or the pilot's objective function subject to a "penalty" on augmentation control energy, $\bar{u}_c$. The pilot-optimal control problem, as posed, is to determine the augmentation control input that minimizes the above $J_{Aug}$ subject to the "constraint" that the pilot will be choosing $\bar{u}_p$ to minimize $J_p$. Note that in solving this problem, two controls, $\bar{u}_p$ and $\bar{u}_c$, minimizing two different objective functions are to be found. The plant dynamics described in terms of these two control inputs are

$$\dot{\bar{x}} = A\bar{x} + B_p\bar{u}_p + B_c\bar{u}_c + \text{noise} \tag{6}$$

To be presented now is the original solution approach, along with a summary of previous results, after which an extension will be presented. Finally, we will conclude with an experimental verification of this extended methodology.

## 3.1 ORIGINAL METHOD

Now the result obtained from the optimal control pilot model is that the pilot's control input may be expressed as

$$\tau_N \dot{\delta}_p = -K_p\hat{\bar{x}} - \delta_p + \text{noise} \tag{7}$$

when the scalar control is taken as stick deflection, for example, and $\tau_N$ is the pilot's neuromuscular time constant (nominally 0.1 - 0.2 sec.), adjusted by adjusting the weighting (G) on $\bar{u}_p$ in the objective function. Further, $\hat{\bar{x}}$ is the pilot's best estimate of the system state vector. Now under the assumption that the pilot's control input could be approximated by

$$\tau_N \dot{\delta}_p = -K_p\bar{x} - \delta_p + \text{noise} \tag{8}$$

where $\bar{x}$ is now the actual state vector rather than the estimate state, the solution to the pilot-optimal augmentation control problem stated previously is (as in Ref. 19)

$$\bar{u}_c = -K_x\bar{x} - K_\delta \delta_p \tag{9}$$

This system structure may be represented as in Figure 2. Further, it was shown[19] that the gains $K_p$, $K_x$, and $K_\delta$ may be determined by simultaneously solving two coupled Riccati equations, one yielding the augmentation gains $K_x$ and $K_\delta$ and one yielding the pilot gains $K_p$ in the optimal control pilot model. It can also be shown that the above control law is globally optimal via the theory of cooperative, non-zero-sum differential games. The control strategy, known as a Nash equilibrium solution to the cooperative control problem, or game, is known to minimize its cost function $J_{Aug}$ subject to the constraint that $\bar{u}_p$ is chosen to simultaneously minimize its cost function $J_p$. Since the optimal-control model is based on exactly this assumption, we may claim this to be the case for the prediction of $\bar{u}_p$, and refer to this augmentation as "pilot-optimal".

In recent applications of this methodology[20,21], the problem addressed was the analysis and augmentation synthesis of the plant dynamics of the (air-to-air) tracking task. The system included not only the flight vehicle rigid body and actuator dynamics, but the display dynamics of lead-computing sights with a heads up display (HUD). In the cases investigated, these display dynamics introduced primarily "numerator dynamics" in the error-to-elevator ($\varepsilon(s)/\delta_E(s)$) transfer function.

The objective of the investigation was to determine the augmentation of the high order system, with the absence of handling qualities specification, to improve the tracking performance, and maintain or improve pilot acceptance. In the process of doing so, a perhaps more important and fundamental objective was to determine the most desirable high-order plant or "controlled element" dynamics. Although improved pilot acceptance has not been completely verified experimentally yet, correlation with previous work (Ref. 22) and proper trends in parameters known to affect pilot rating (objective function magnitude, amount of pilot lead required) were obtained. Also, based on linear systems analysis techniques, rms tracking error, stick deflection, and stick rate (work load) was significantly reduced. By parametrically varying the level of augmentation, we were also able to establish trends in the desirable plant characteristics, and to relate these trends to the asymptotic properties of linear, optimally-controlled systems. Simultaneously, we were able to predict the changes in the human operator characteristics associated with varying high-order plant characteristics.

The schematic for the display is shown in Figure 3, where the line of sight to the target, $\bar{\beta}$, and the displayed lead angle, $\bar{\chi}$, are as shown. With the linearized equations of motion for the vehicle, the line of sight and displayed lead angle, and colored noise representing the target motion, the model may be represented in the usual vector-matrix, differential equation

$$\dot{\bar{x}} = A\bar{x} + B\delta_{st} + \text{noise} \tag{10}$$

with stick deflection $\delta_{st}$ the control. For pitch tracking the state vector may be taken as

$$\bar{x}^T = [\gamma_T,\ \beta,\ \lambda,\ \alpha,\ \theta,\ \dot{\theta},\ \delta_e]$$

and the system model is summarized in the table below.

Table 1
SYSTEM MODEL
PITCH TRACKING

| | |
|---|---|
| Rel. Line of sight, $\dot{\beta} = f_1(\theta, \alpha, \gamma_T]$ | |
| Target flight path, $\dot{\gamma}_T = f_2(a_{T_n})$ | Error, $\varepsilon = \lambda - \beta$ |
| Target Acceleration $a_{T_n}$ - noise | obs. Vector, $\bar{y}_p^T = [\varepsilon, \dot{\varepsilon}, \lambda, \dot{\lambda}]$ |
| Lead Angle, $\lambda = f_4(\dot{\lambda}$ or $\dot{\beta}, \dot{\theta}, \alpha, a_T)$ | $Q_{ii} = [16, 1, 0, 4]$ |
| Vehicle Dynamics - F-4E Short-period dynamics M = .9; 10,000Ft | $\tau_N$ = .1 sec. |

To aid in the system characterization we may note that the transfer function compatible with that of the controlled element in a compensatory task is in this case

$$\varepsilon(s)/\delta_{st}(s) = \frac{K(N_1 s^3 + N_2 s^2 + N_3 s + N_4)}{s^2(T_f s + 1)(\tau_a s + 1)(s^2 + 2\xi\omega_{sp} s + \omega_{sp}^2)} \tag{11}$$

where $N_1$ - $N_4$ are functions of vehicle characteristics as well as display characteristics. Note in the denominator the vehicle short period and actuator dynamics, and a display time constant $T_f$ that depends on the type of sight considered.

Now, the empirically determined pilot's objective function for this task for a variety of system dynamics was found[23] to be

$$J_p = E\left\{\lim_{T\to\infty} \frac{1}{T} \int_0^T (\bar{y}^T Q_y \bar{y} + g\ \dot{\delta}_{st}^2)dt\right\} \tag{12}$$

with $Q_{ii} = [16, 1, 0, 4]$ and $\bar{y}$ defined above. In addition, the stick-rate weighting g was selected to yield an effective neuromuscular time constant, $\tau_N$, of 0.1 seconds.

Now, the pilot-optimal augmentation $u_c$, is chosen to minimize the cost function

$$J_c = J_p + E\left\{\lim_{T\to\infty} \frac{1}{T} \int_0^T f u_c^2 dt\right\} \tag{13}$$

where in this case, $u_c$ is an effective stick deflection. So for various selected values of control weighting, or f above, we generate a family of augmented systems.

The resulting system eigenvalues for an unaugmented and (various) augmented systems with one particular lead computing sight equation are shown in Figure 4. The roots (denoted by X's) vary from the unaugmented (labeled U) through augmented levels A, B, and C(C being the highest augmentation gains considered). When the pilot closes the loop on these systems, the resulting closed-loop system eigenvalues are denoted by the circled data points. We have found that these trends are explainable, at least qualitatively, in terms of the asymptotic properties of the eigenvalues of optimally-controlled systems. Further, with this methodology, we are able to quantitatively determine these specific trends. Finally, predicted tracking performance for this case is shown in Table 2 below.

Table 2. AUGMENTED PERFORMANCE (rms)

| | Unaugmented | Level A | Level B | Level C |
|---|---|---|---|---|
| Tracking Error, $\varepsilon$(deg) | 3.05 | 2.50 | 1.12 | 0.31 |
| Stick Deflection, $\delta_{st}$(deg) | 3.71 | 3.64 | 3.51 | 3.68 |
| Stick Rate, $\dot{\delta}_{st}$(deg/sec) | 7.33 | 6.64 | 5.36 | 5.10 |

$\sigma_{a_T}$ = 5 g's, D = 1000 ft.

Consider now the application of this methodology to a vehicle system with a different display. In this case, the sight equation results in a much less dynamic display almost representative of a fixed sight. This is closer then to pure pitch tracking with only airframe dynamics included. The trend in augmented short-period eigenvalues in this case is shown in Figure 5. Note the difference in this trend from that in the previous figure, or the effect of the sight dynamics on the optimum vehicle dynamics! Also shown is the comparison of these (vehicle short period) results with those of Hollis.[22] In his analysis, Hollis determined the vehicle augmentation yielding the best pilot rating via the "paper-

pilot". Pitch rate and plunge acceleration were used for augmenting only the vehicle with a fixed sight (with no display dynamics). It is seen that the results are in general agreement with the trend determined by Hollis' consideration of several sets of vehicle dynamics.

The more challenging problem of pilot-vehicle analysis and augmentation for a multi-axis air-to-air tracking task has also been considered.[21] The dynamics of the system, as in the pitch tracking analysis in the previous section, include both vehicle and display dynamics. However, the flight condition to be considered is a highly banked turn with a normal load factor of four (i.e., 4 g turn). This involves several issues not frequently, and in some cases never, considered in previous investigations of pilot-vehicle dynamics. These extenuating issues result from the significant amount of unsymmetrical coupling between the elevation and azimuth axes of the system and the multiple control inputs involved (i.e., elevator, aileron, and rudder).

The open- and closed-loop root loci as augmentation level increases from unaugmented (denoted by U) to higher levels of augmentation (denoted 1→4) are shown in Figures 6 and 7. The first figure shows the (primarily) longitudinal eigenvalues (recognizing this system actually has coupled longitudinal and lateral-directional modes), with the second figure depicting the (primarily) lateral-directional roots. As with the pitch tracking results above, the augmented system roots are denoted as "X" and the piloted closed-loop roots are denoted as "O". Finally, the sight equation is that resulting in the less dynamic display, as previously discussed.

Examination of the longitudinal root locus shows that the trends are changed only slightly from those obtained in the single-axis pitch-tracking analysis. However, the close proximity of the open-loop roots to the closed-loop roots for the unaugmented plant (U), as well as the level-two augmented plant (2), indicate less compensation being introduced by the pilot than in the single-axis case, due to his limited bandwidth and a much more complex task.

Finally, note again that the predicted improvement in tracking performance due to Level 2 augmentation is significant, as shown in the table below.

Table 3

AUGMENTED SYSTEM

RMS PERFORMANCE

| | Tracking Error (deg) | | Control Inputs (in) | | | Lateral Accelerational ($ft/sec^2$) |
|---|---|---|---|---|---|---|
| | Elevation $\varepsilon_{EL}$ | Azimuth $\varepsilon_{AZ}$ | $\delta_{E_{st}}$ | $\delta_{A_{st}}$ | $\delta_{R_{ped}}$ | $a_y$ |
| Unaugmented | 1.78 | 1.72 | 0.23 | 0.15 | 0.10 | 0.78 |
| Augmented | 0.54 | 0.20 | 0.19 | 0.11 | 0.06 | 0.25 |

## 3.2 EXTENDED METHOD

The above encouraging results were obtained under two important assumptions

1) The pilot's compensation resulting from state estimation has little effect on the optimal augmentation

and

2) The augmentation implementation allows full-state feedback

Now assumption 2 is never true. A much more realistic control law is linear feedback of easily measured outputs such as pitch rate and accelerations, or a control law of the form

$$\bar{u}_{aug} = E\bar{y}_{output}$$

and (14)

$$\bar{y}_{output} = C\bar{x}_{vehicle}$$

Furthermore, we will show that assumption 1 is untrue as well. Finally, correlation with this extended approach with fixed-base simulation results will be demonstrated.

As shown in Ref. 24, the solution is as follows. Recall that the control pilot's input is given (from the optimal control model) as

$$\dot{\bar{u}} = -K_x\hat{\bar{x}} - K_u\hat{\bar{u}} + \bar{v}_m$$

or (15)

$$\dot{\bar{u}}_p = -[K_x : K_u]\,\hat{\bar{x}} + \bar{v}_m$$

where $\bar{v}_m$ is the motor noise vector with zero mean and intensity $V_m$ and $\hat{x}$ is col $[\hat{x}, \hat{u}_p]$.

If the original system is $\dot{\bar{x}} = A\bar{x} + B\bar{u} + Dw$, the dynamics of the plant with the pilot's control included is given by:

$$\dot{\bar{x}} = \begin{bmatrix} A & B \\ 0 & 0 \end{bmatrix} \bar{x} + \begin{bmatrix} 0 & 0 \\ K_x & K_u \end{bmatrix} \hat{x} + \begin{bmatrix} B \\ 0 \end{bmatrix} \bar{u}_s + \begin{bmatrix} D & 0 \\ 0 & I \end{bmatrix} \begin{matrix} \bar{w} \\ \bar{v}_m \end{matrix} \tag{16}$$

$$\bar{y}_s = [C_s \; 0]\bar{x} \quad \text{(augmentation measurement)}$$

Also, the state estimation dynamics of the pilot is represented by

$$\dot{\hat{x}} = \begin{bmatrix} A_s & B \\ K_x & K_u \end{bmatrix} \hat{x} + \begin{bmatrix} M_1 \\ M_2 \end{bmatrix} C_p(\bar{x} - \hat{x}) + \begin{bmatrix} 0 \\ \bar{v}_m \end{bmatrix}; \quad Y_p = C_p\, \bar{x}(t-\tau) + \bar{v}_p \tag{17}$$

where $A_s = A + BEC_s$, and $M_{1,2}$ are Kalman filter gains. So we wish to find the optimal controller $u_s = Ey_s$ which minimizes the index of performance:

$$J_s = J_p + E\left\{\lim_{T\to\infty} \frac{1}{T} \int_o^T \bar{u}_s^T F \bar{u}_s \, dt\right\} \tag{18}$$

and $J_p$ as given previously, subject to the constraints

$$\dot{\bar{q}} = \begin{bmatrix} \dot{\bar{x}} \\ \dot{\hat{x}} \end{bmatrix} = \left[\begin{array}{cccc} A & B & 0 & 0 \\ 0 & 0 & K_x & K_u \\ \hline M_1C_p & 0 & A_s+M_1C_p & B \\ M_2C_p & 0 & K_x-M_2C_p & K_u \end{array}\right] \bar{q} + \left[\begin{array}{c} B \\ 0 \\ \hline 0 \\ 0 \end{array}\right] \bar{u}_s + \left[\begin{array}{ccc} D & 0 & 0 \\ 0 & I & 0 \\ \hline 0 & 0 & M_2 \\ 0 & I & M_2 \end{array}\right] \begin{bmatrix} \bar{w} \\ \bar{v}_m \\ \bar{v}_p \end{bmatrix} \tag{19}$$

$$\bar{Y}_s = [C_s \quad 0 \quad 0 \quad 0]\bar{q}$$

with $\bar{v}_p$ the pilot's oberservation noise vector.

Now $J_s$ can be written as

$$J_s = E\left\{\lim_{T\to\infty} \frac{1}{T} \int_o^T (\bar{q}^T \begin{bmatrix} Q_1 & 0 \\ 0 & Q_2 \end{bmatrix} \bar{q} + \bar{u}_s^T F \bar{u}_s)dt\right\} \tag{20}$$

with

$$\begin{bmatrix} Q_1 & 0 \\ 0 & Q_2 \end{bmatrix} = \left[\begin{array}{cccc} Q & 0 & 0 & 0 \\ 0 & R & 0 & 0 \\ \hline 0 & 0 & K_x^T G K_x & K_u^T G K_x \\ 0 & 0 & K_x^T G K_u & K_u^T G K_u \end{array}\right]$$

And more compactly, we have

$$\dot{\bar{q}} = \begin{bmatrix} A_{11} & A_{12} \\ A_{21} & A_{22} \end{bmatrix} \bar{q} + \begin{bmatrix} B_2 \\ 0 \end{bmatrix} \bar{u}_s + \begin{bmatrix} D_1 & 0 \\ D_o & D_2 \end{bmatrix} \bar{w} \tag{21}$$

$$\bar{y}_s = [C_2 \quad 0]\bar{q}$$

where the newly introduced matrices have obvious structures from the above relationships.

This system of equations with the constraint

$$u_s = Ey_s \tag{22}$$

defines the suboptimal output feedback problem.[25,26] The necessary conditions for optimality based on first variation principles gives the following expression for the gain matrix E

$$E^* = -F^{-1} [B_2^T \; 0] H^* L^* \begin{matrix} C_2^T \\ 0 \end{matrix} ([C_2 \quad 0]L \begin{matrix} C_2^T \\ 0 \end{matrix})^{-1} \tag{23}$$

with $H^*$ and $L^*$ positive definite unique solutions of

$$A_c^T H^* + H^* A_c + \begin{bmatrix} Q_1 & 0 \\ 0 & Q_2 \end{bmatrix} + \begin{bmatrix} C_2^T E^T F E C_2 & 0 \\ 0 & 0 \end{bmatrix} = 0 \tag{24}$$

and

$$A_c L^* + L^* A_c^T + \begin{bmatrix} D_1 & 0 \\ D_o & D_2 \end{bmatrix} \bar{W} \begin{bmatrix} D_1^T & D_o^T \\ 0 & D_2^T \end{bmatrix} = 0 \tag{25}$$

where $\bar{W}^T$ = diag [W, $V_m$, $V_p$] (the noise covariance matrices)

and

$$A_c = \begin{bmatrix} A_{11} + B_2 E C_2 & A_{12} \\ A_{21} & A_{22} \end{bmatrix} \tag{26}$$

The matrix L is the covariance matrix for the entire system and it is given by:

$$L = \begin{bmatrix} L_{11} & L_{12} \\ L_{12} & L_{22} \end{bmatrix}, \quad \begin{aligned} L_{11} &= E[xx^T] \text{ (state covariance)} \\ L_{12} &= E[x\hat{x}^T] = L_{22} = E[\hat{x}\hat{x}^T] \text{ (state estimate covariance)} \end{aligned} \tag{27}$$

Rewriting $E^*$ in partitioned form we get

$$E^* = -F^{-1} B_2^T H_{11} L_{11} C_2^T (C_2 L_{11} C_2^T)^{-1} - F^{-1} B_2^T H_{12} L_{12} C_2^T (C_2 L_{11} C_2^T)^{-1} \tag{28}$$

or

$$E^* = E_1 + E_2 \tag{29}$$

As we can see, two terms contribute to the total augmentation gain matrix. The first term is due to the plant (vehicle) dynamics, where the second is due to the plant and (pilot's) estimator dynamics. This shows that we can not a priori neglect the presence of the pilot's estimator in the synthesis of the optimal stability augmentation system, or assumption 1 stated previously is false. Furthermore, if we assume that the augmentation has a full-state feedback structure (or assumption 2 were true) we would have

$$C_2 \equiv I \text{ (identity)}$$

and the gain matrix $E^*$ becomes

$$E = -F^{-1} B_2^T H_{11} - F^{-1} B_2^T H_{12} L_{12} L_{11}^{-1} \tag{30}$$

Only the first term on the right hand side of the relation is the result from the original method. The second term represents the contribution to the total gain ($E^*$) of the estimator in the pilot model.

This extended methodology is now applied to "predict" the optimal pitch rate feedback gain for a T-33 aircraft in a position tracking task. The results will be compared to experimental data obtained from fixed-base digital simulations.[27]

The short period dynamics of the aircraft in level flight at Mach = 0.5 and altitude 15,000 ft, is given in state variable form as

$$\dot{\bar{x}} = \begin{bmatrix} -0.1 & 0 & 0 & 0 \\ 0 & 0 & 1. & 0 \\ 0 & 0 & -1.0524 & -3.01 \\ 0 & 0 & 1. & -1.384 \end{bmatrix} \bar{x} + \begin{bmatrix} 0 \\ 0 \\ -14.5164 \\ -0.843 \end{bmatrix} \delta + \begin{bmatrix} 1 \\ 0 \\ 0 \\ 0 \end{bmatrix} \omega \tag{31}$$

where the commanded pitch angle is given by the relation:

$$\begin{aligned} \dot{\theta}_c &= -w_b \theta_c + \omega, \quad \omega \text{ white noise process, zero mean, intensity } \sigma_\omega^2 \\ w_b &= 0.1 \text{ (break frequency)} \end{aligned} \tag{32}$$

The state vector is $x^T = [\theta_c, \theta, \dot{\theta}, \alpha]$ and the total elevator control is the sum, $\delta_p + \delta_s$, of pilot's and augmentation inputs, respectively.

The indices of performance to be minimized by $\delta_p$ and $\delta_c$ are

$$\begin{aligned} J_p &= E\left\{\lim_{T\to\infty} \frac{1}{T} \int_o^T [(\theta_c - \theta)^2 + 0.002\, \dot{\delta}_p] dt\right\} \\ J_s &= J_p + E\left\{\lim_{T\to\infty} \frac{1}{T} \int_o^T 0.01\, \dot{\delta}_s^2 dt\right\} \end{aligned} \tag{33}$$

The pilot is able to perceive position error information ($\theta_c - \theta$) and the augmentation measurement is pitch rate $\dot{\theta}$ only, thus:

$$\bar{y}_p = [1. \ -1. \ 0 \ 0]\ \bar{x} + v_p$$
$$\bar{y}_s = [0 \ 0 \ 1. \ 0]\bar{x} \qquad (34)$$

The table contains the augmentation gains predicted with and without inclusion of the pilot's state estimation.

Table 4. PITCH RATE FEEDBACK GAIN

| Predicted Gain with Estimator in Pilot Model | Predicted Gain Without Estimator In the Pilot Model |
|---|---|
| -0.24 | 0.09(!) |

The importance of the effect of state estimator is underscored. The optimal gain obtained by neglecting the estimator actually decreases pitch damping. As it can be seen from Figures 8 and 9, the predicted gain and the gain obtained from experimental data produce very good agreement for the best pilot rating. Finally, note the correlation between pilot rating (Figure 8) and the sum of the rms error plus stick rate-or "quadratic objective function"-obtained from simulation (Figure 9).

REFERENCES


1. Cooper, G.E. and Harper, R.P., Jr., The Use of Pilot Rating in the Evaluation of Aircraft Handling Qualities, NASA TN D-5153, 1969.

2. Chalk, C.R. et. al., Background and User Guide for MIL-F-8785(ASG), "Military Specification-Flying Qualities of Piloted Airplanes," AFFDL-TR-69-72, August, 1969.

3. Neal, T.P. and Smith, R.E., An In-Flight Investigation to Develop Control System Design Criteria for Fighter Airplanes, Vols. I and II, AFFDL-TR-70-74, 1970.

4. Swaim, R.L., and Yen, W.Y., "Effects of Dynamic Aeroelasticity on Handling Qualities and Pilot Rating," AIAA Paper 78 - 1365, Presented at the AIAA Atmos. Flight Mech. Conf., Palo Alto, Calif., Aug., 1978.

5. Anderson, R., A New Approach to the Specifications and Evaluation of Flying Qualities, AFFDL-TR-69-120, 1969.

6. McRuer, D.T. and Krendel, E.S., Mathematical Models of Human Pilot Behavior, AGARD-AG-188, AGARD, NATO, 1974.

7. Teper, G.L., An Assessment of the "Paper Pilot" - An Analytical Approach to the Specification and Evaluation of Flying Qualities, AFFDL-TR-71-74, June, 1972.

8. Smith, R.H., "A Unified Theory for Pilot Opinion Rating," Proceedings of the 12th Annual Conf. on Man. Control, Univ. of Illinois, NASA TMX-73,170, 1976. See Also AFFDL-TR-75-119, 1976.

9. Onstott, E.D., "Task Interference in Multi-Axis Aircraft Stabilization," Proc. of 12th Annual Conf. on Manual Control, Univ. of Illinois, NASA TMX-73, 170, 1976.

10. Onstott, E.D. and Faulkner, W.H., "Discrete Maneuver Pilot Models for Flying Qualities Evaluation," AIAA, Journal of Guidance & Control, Vol. 1, No. 2, 1978.

11. Brulle, R.V. and Anderson, D.C., Design Methods for Specifying Handling Qualities for Control Configured Vehicles, Vol. 1, AFFDL-TR-73-142, 1973.

12. Kleinman, D.L. Baron, S., and Levison, W.H., "An Optimal Control Model of Human Response" Parts I and II, Automatica, Vol. 6, pp. 357-383. 1970.

13. Harrington, W.W., Capt., "The Application of Pilot Modeling to the Study of Low Visibility Landing," 12th Annual Conf. on Manual Control, NASA TMX-73, 170, 1976.

14. Broussard, J.R. and Stengel, R.F., "Stability of the Pilot-Aircraft System in Maneuvering Flight," 12th Annual Conf. on Manual Control, NASA TMX-73, 170, 1976.

15. Hess, R.A., "Analytical Display Design for Flight Tasks Conducted Under Instrument Meteorological Conditions," IEEE Trans. on Sys., Man, and Cyber., Vol. SMC-7, No. 6, June, 1977, pp. 453-462.

16. Hess, R.A., "Prediction of Pilot Opinion Ratings Using an Optimal Control Pilot Model," Human Factors, pp. 459-475, 1977. Also see NASA TMX-73, 101, 1976.

17. Arnold, J.D., "An Improved Method of Predicting Aircraft Longitudinal Handling Qualities Based on the Minimum Pilot Rating Concept," AFIT Thesis GGC/MA/73-1, Wright Patterson AFB, Ohio, 1973.

18. Schmidt, D.K., "On the Use of the OCM's Objective Function As a Pilot Rating Metric," Presented at the 17th Annual Conf. on Manual Control, Los Angeles, CA, June, 1981.

19. Schmidt, D.K., "Optimal Flight Control Synthesis via Pilot Modeling," AIAA Journal of Guidance and Control, Vol. 2, No. 4, July-Aug., 1979.

20. Schmidt, D.K., "Pilot Optimal Augmentation of the Air-to-Air Pitch Tracking Task," AIAA Journ. of Guid. and Cont., Vol. 3, No. 5, Sept-Oct. 1970.

21. Schmidt, D.K., "Multivariable Closed-Loop Analysis and Flight Control Synthesis for Air-to-Air Pitch Tracking," Final Report for AFOSR Grant 79-0042, by Purdue University, West Lafayette, IN, June, 1980.

22. Hollis, T.L., "Optimal Selection of Stability Augmentation---for the Pitch Tracking Task," AFIT M.S. Thesis, GGC/EE/71-10, Wright-Patterson AFB, Ohio, 1971.

23. Harvey, T.R., "Application of an Optimal Control Pilot Model to Air-to-Air Combat," AFIT Thesis GA/MA/74M-1, March 1974.

24. Schmidt, D.K. and Innocenti, M., "Pilot-Optimal Multivariable Control Synthesis by Output Feedback," NASA CR 16312, July, 1981.

25. Levine, W.S., and Athans, M., "On the Determination of the Optimal Constant Output Feedback Gains for Linear Multivariable Systems," IEEE Trans. AC-15, No. 1, Feb. 1970, pp. 44-48.

26. Joshi, S.M., "Design of Optimal Partial State Feedback Controllers for Linear Systems in Stochastic Environments," Paper 6D-4. Proc. 1975, IEEE Southeastern, Charlotte, N.C.

27. Webb, Thomas P. and Schmidt, David K., Determination of Aircraft Augmentation Rate Feedback Gain Using Flight Simulation, A&AE Report 81-1, School of Aeronautics and Astronautics, Purdue University, July, 1981.

ACKNOWLEDGEMENT

Much of the work presented herein constitutes the M.S. Thesis of Mr. S. N. Prasad and the Ph.D. Dissertation of Mr. Mario Innocenti, both with the School of Aeronautics and Astronautics, Purdue University. Their diligent efforts are appreciated.

This research was supported by the Air Force Office of Scientific Research, Grant 79-0042, and by the NASA Dryden Research Center, Grant NAG4-1.

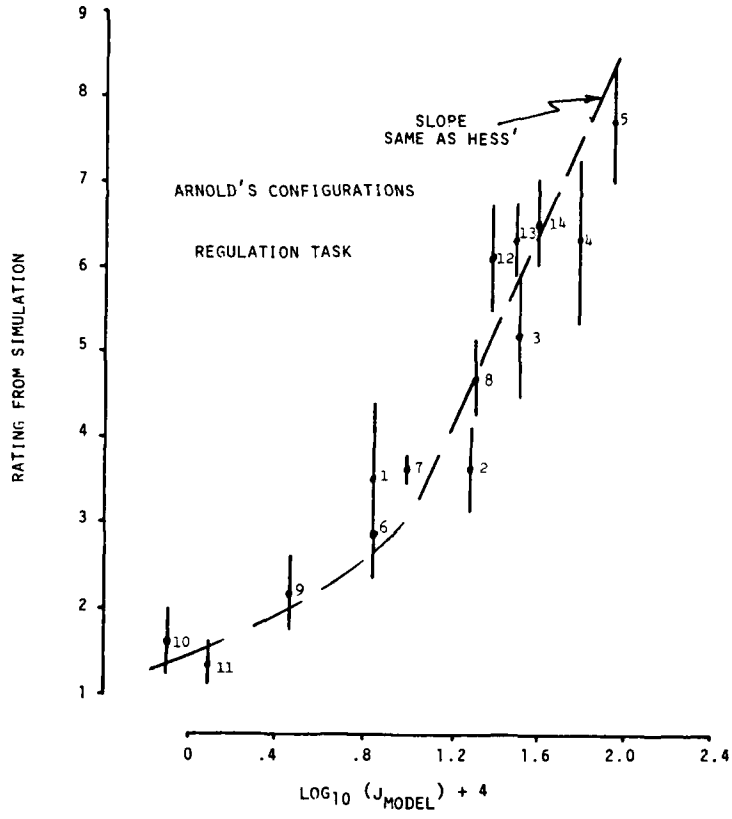


Fig. 1 Pilot Rating/Objective Function Correlation

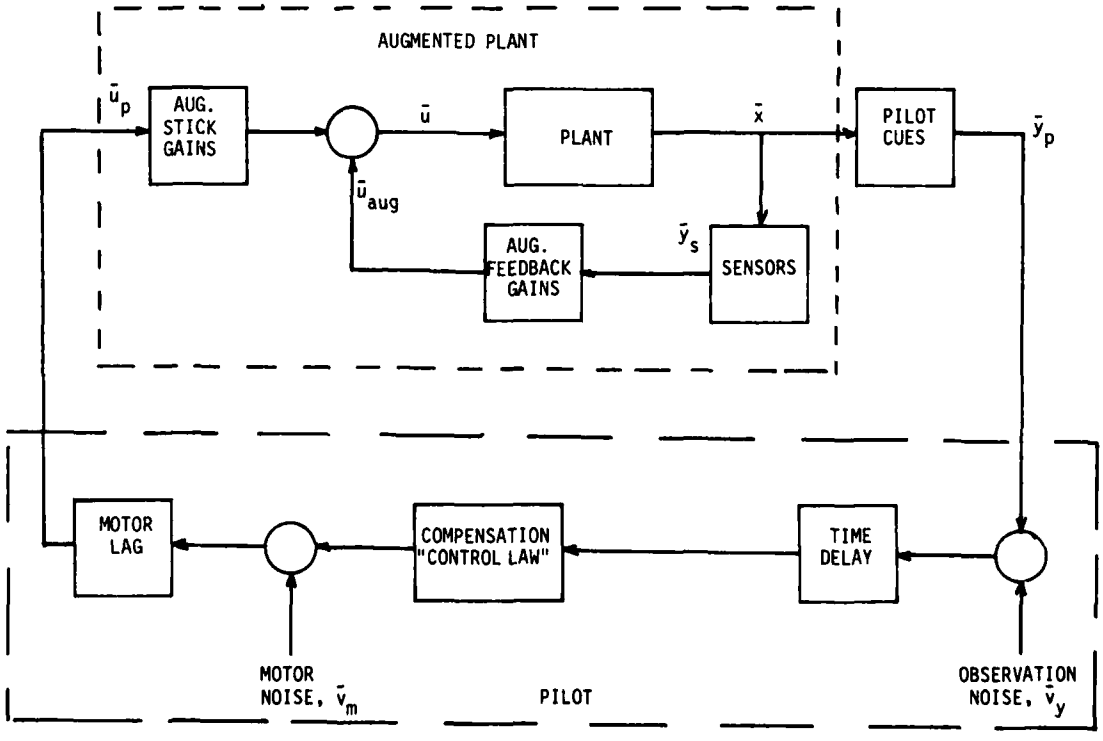


Fig. 2 Pilot/Vehicle System Architecture

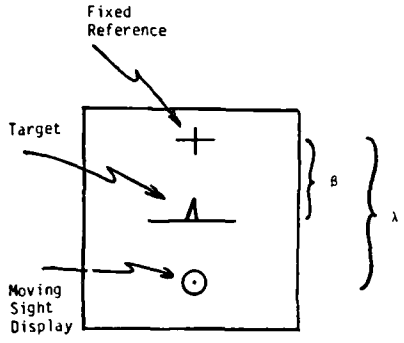


Fig. 3 Heads-Up Sight Display Schematic

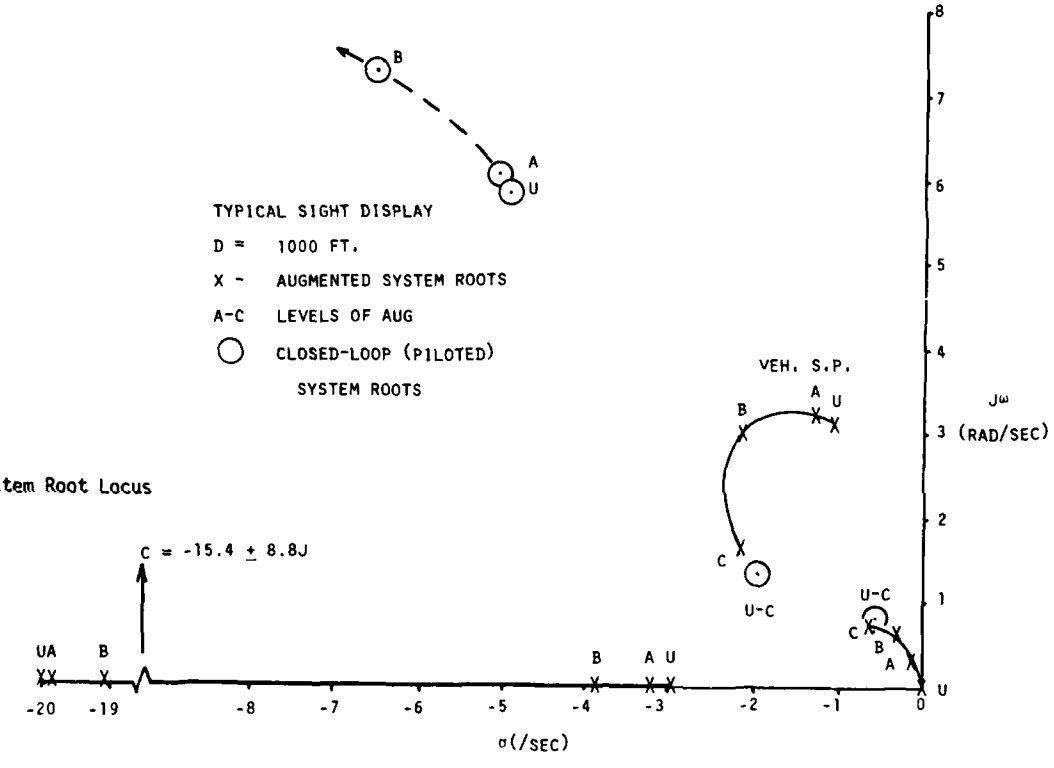


Fig. 4

Augmented System Root Locus

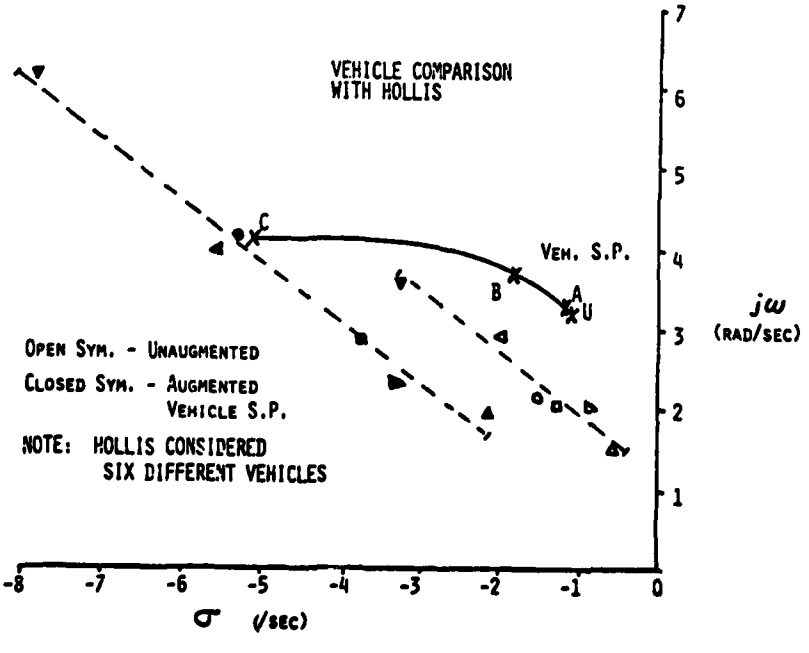


Fig. 5

Comparison of Results-Fixed Sight

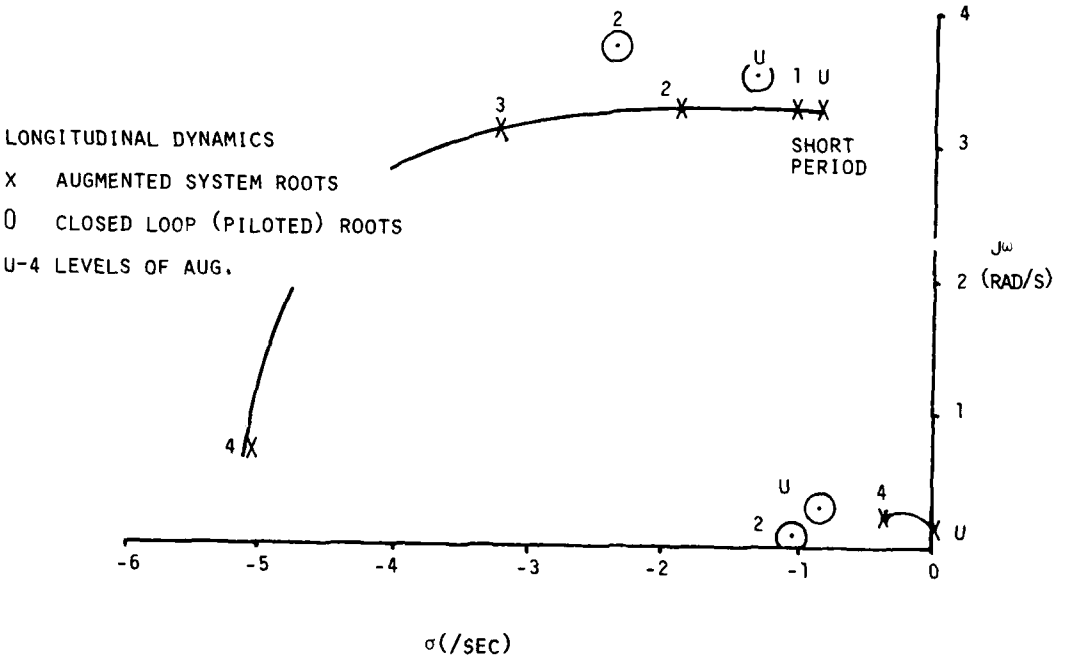


Fig. 6 Longitudinal Root Locus

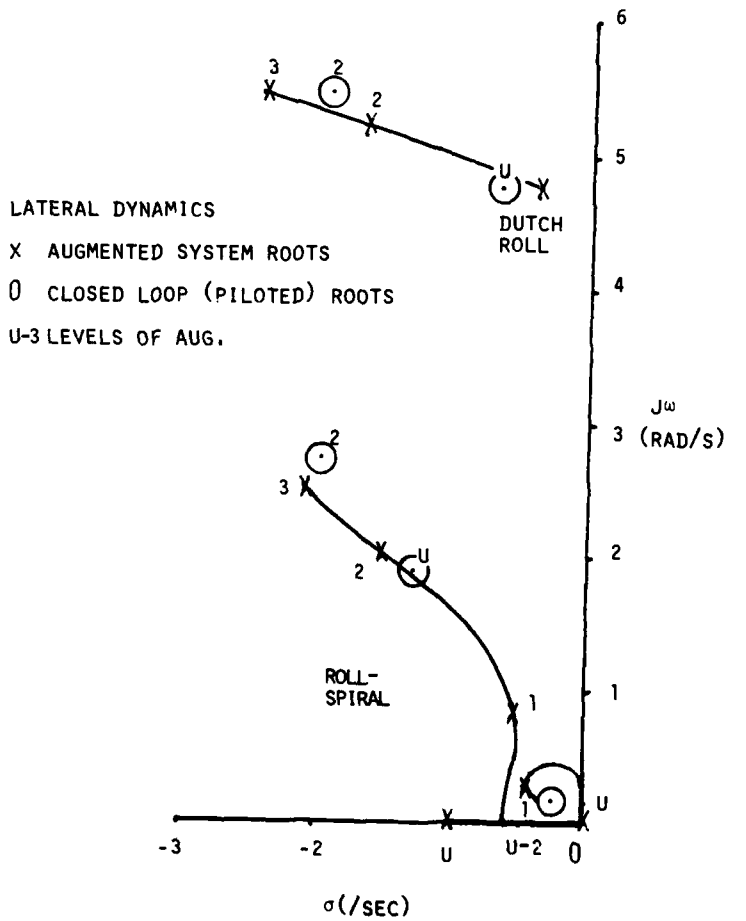


Fig. 7 Lateral-Directional Dynamics

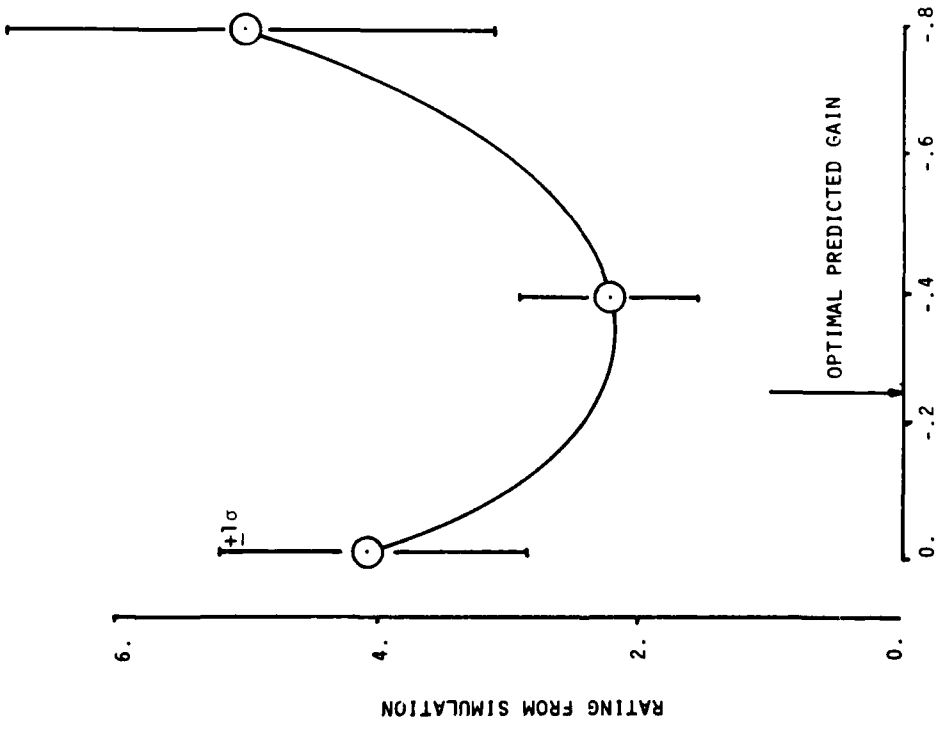


Fig. 8 Optimum Gain-Predicted and Experimental

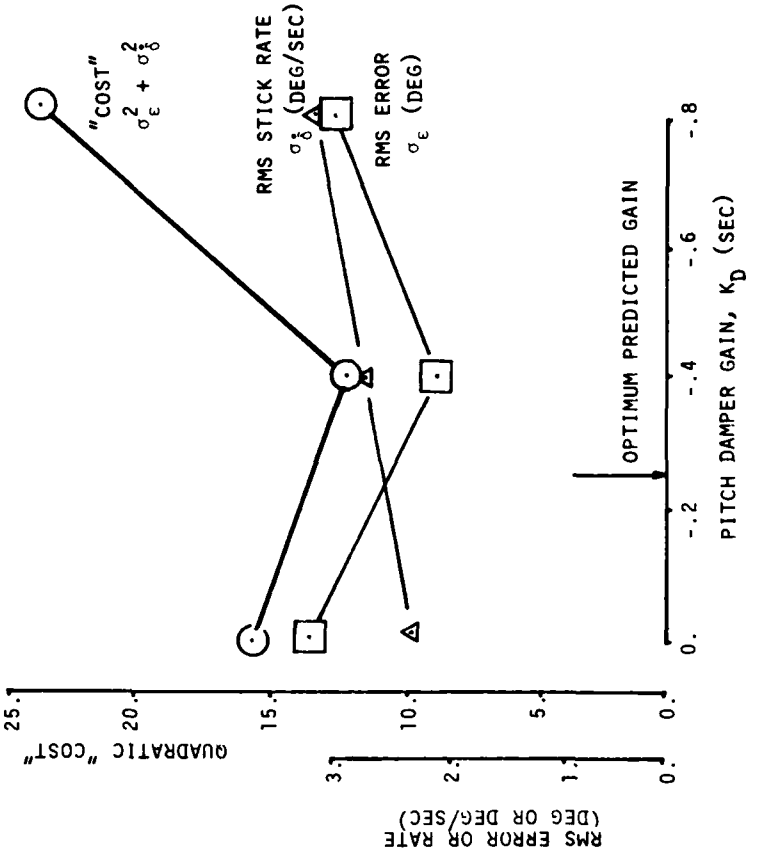


Fig. 9 Experimental "Cost Function"

# INTEGRATION OF AVIONICS AND ADVANCED CONTROL TECHNOLOGY

by
M. E. Waddoups
Director, Technology Demonstrations
and
C. A. Anderson
Vice President, Engineering
General Dynamics
Fort Worth Division
P. O. Box 748
Ft. Worth, Texas 76101

SUMMARY

Two seemingly exclusive requirements, low-cost tactical fighters and night under-the-weather operations, are being merged by means of advanced technology. The key operational problem is forced by the extremely difficult timeline for low-altitude, high-speed, air-to-surface weapon delivery. The inherent economy of single-seat operation can be developed by automation. The key technological problems are caused by the lack of volume in a small fighter. In order to achieve automation of the required tasks, flight path control and sensor interfaces must be developed. Based upon emerging hardware and software technology, flight control and avionic subsystems can be optimized and integrated to achieve capability previously unavailable in small fighters. The AFTI/F-16 test-bed aircraft, in which the subject technology will be flown as a subset, is now approaching first flight.

(NOTE:The complete text of this presentation was not available at the time this Proceedings was sent for printing.)

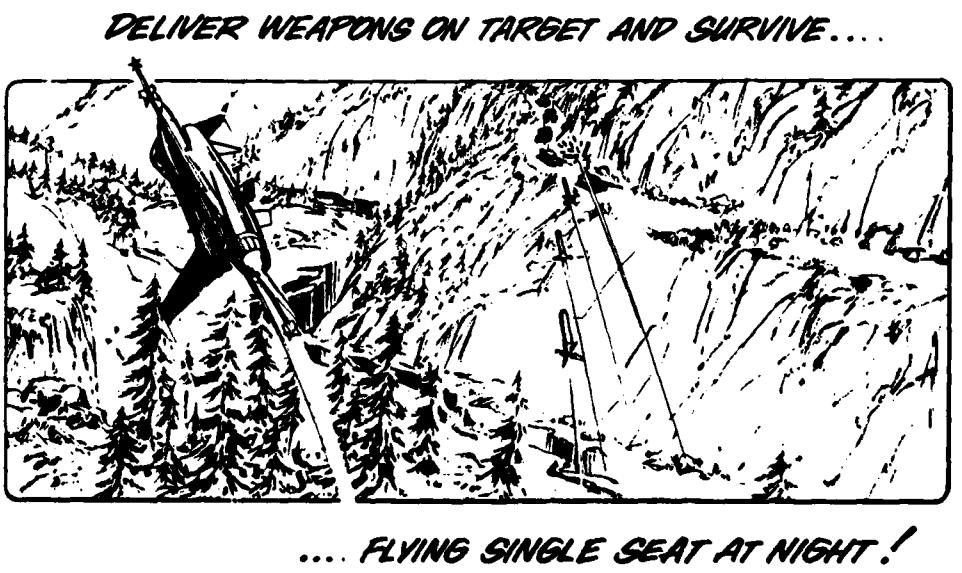


FIGURE 1

## TECHNOLOGY PROVIDES THE TOOLS

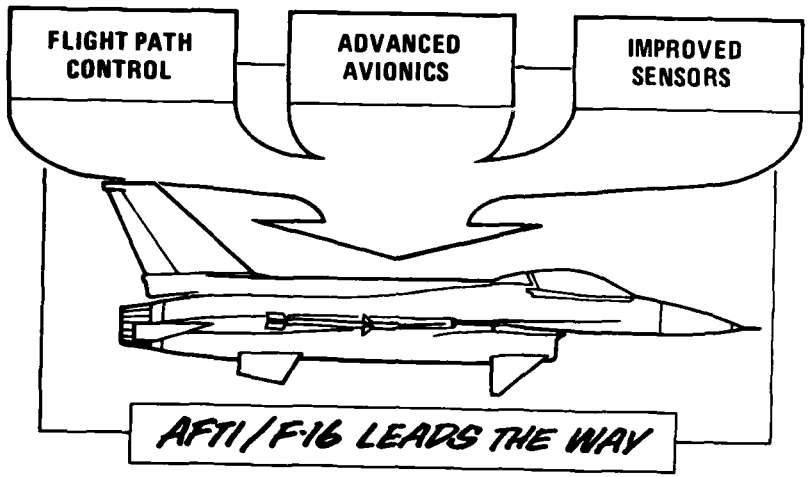


FIGURE 2

## THE BASIS OF AFTI/F-16 . . .

- *FULL AUTHORITY DIGITAL FLIGHT CONTROL*

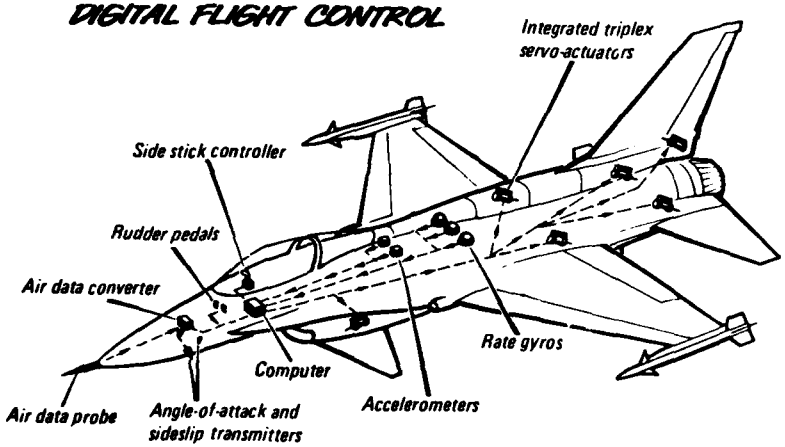


FIGURE 3

## AFTI/F-16 ADDS ANOTHER DIMENSION . . .

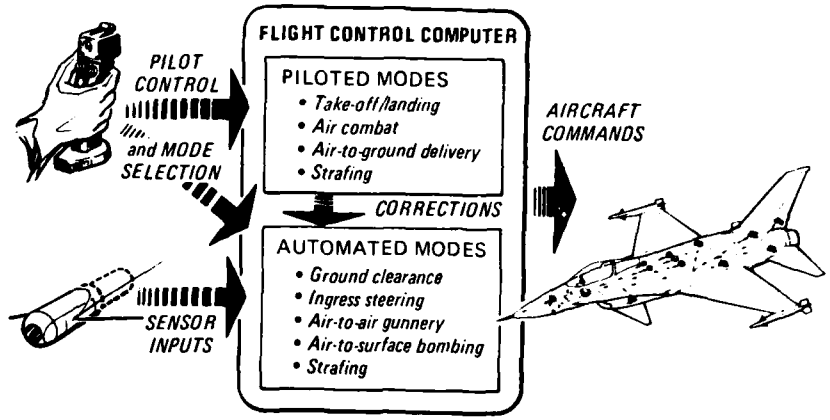


*. . . . DIGITAL MISSION-ORIENTED CONTROL MODES*

FIGURE 4

## MICROELECTRONICS ARE REVOLUTIONIZING AVIONICS CAPABILITIES

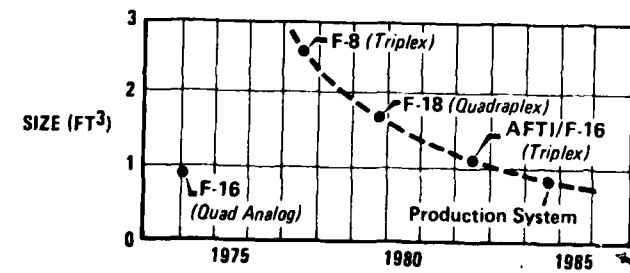


*10 FOLD INCREASE IN FLIGHT CONTROL COMPUTER CAPABILITY*

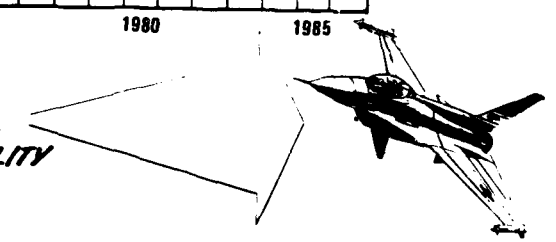

FIGURE 5

## FLIGHT CONTROL MONITORING OF CRUCIAL SINGLE THREAT AVIONICS GUARANTEES SAFETY

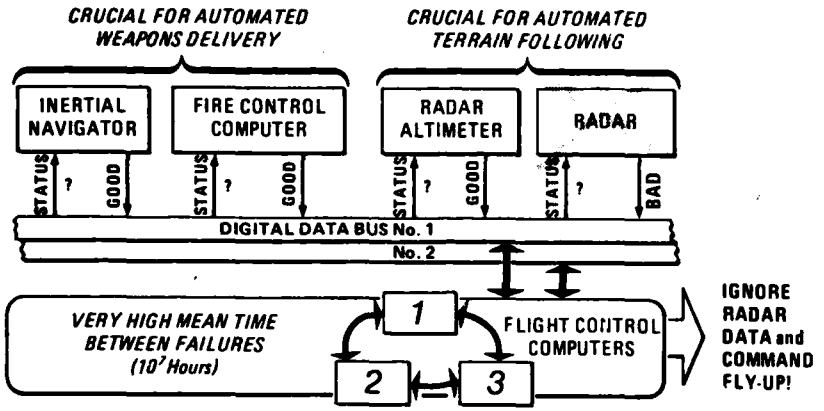


*CATASTROPHIC FAILURES DRAMATICALLY REDUCED*

FIGURE 6

## DIGITAL FLIGHT CONTROL AND INTEGRATED MISSION AVIONICS ARE THE KEY

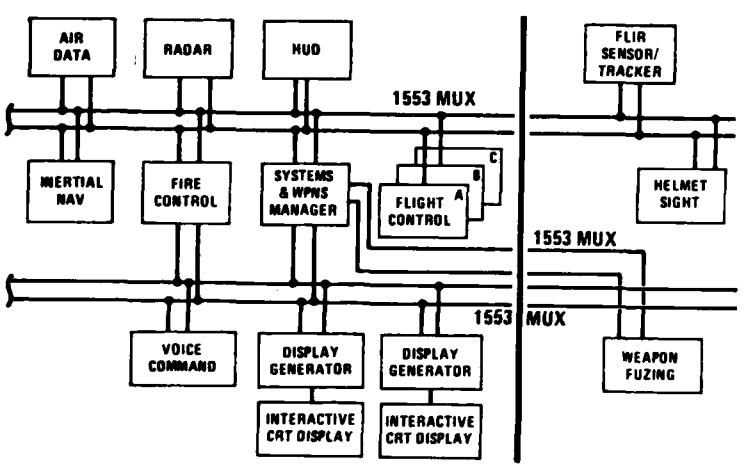


FIGURE 7

## AUTOMATED MANEUVERING ATTACK SYSTEM (AMAS)

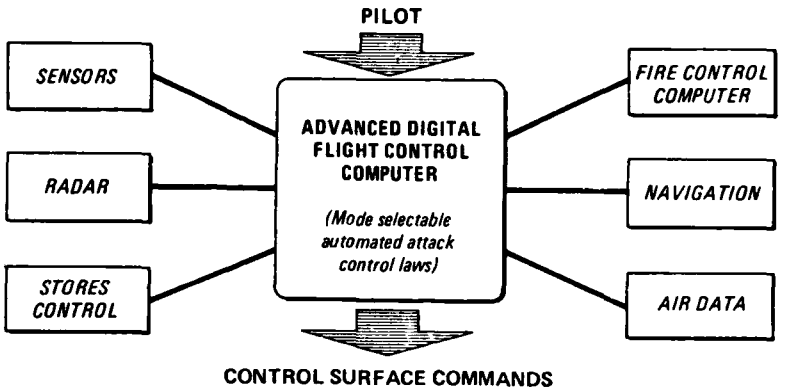


*ADVANCED AVIONICS AND MISSION MODE SOFTWARE PUT AFTI/F-16 RIGHT ON TARGET!*

FIGURE 8

## CONFORMAL FLIR/LASER SENSING PODS...

*THE NEXT STEP IN TARGET LOCATION AND TRACKING*

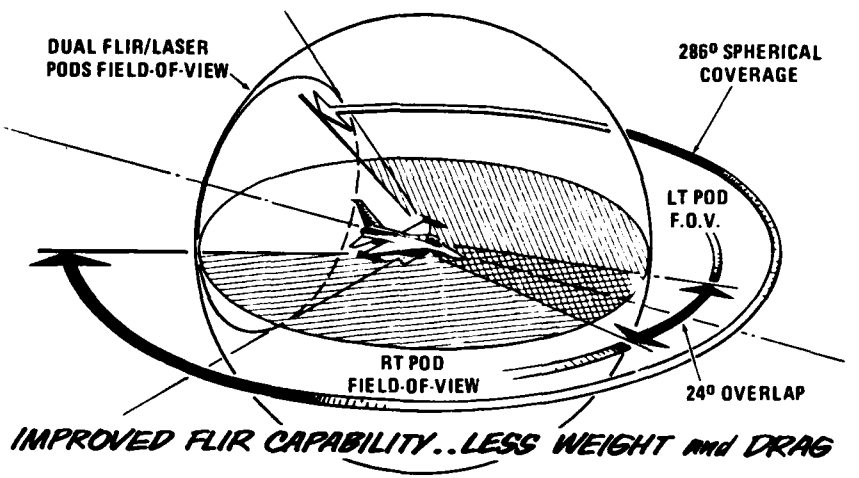


*IMPROVED FLIR CAPABILITY..LESS WEIGHT and DRAG*

FIGURE 9

# TOMORROW'S DEMONSTRATOR IS PREPARING TODAY FOR FIRST FLIGHT!

FIGURE 10

## AFTI/F-16 PROVIDES CRITICAL DEMONSTRATIONS LEADING TO . . .

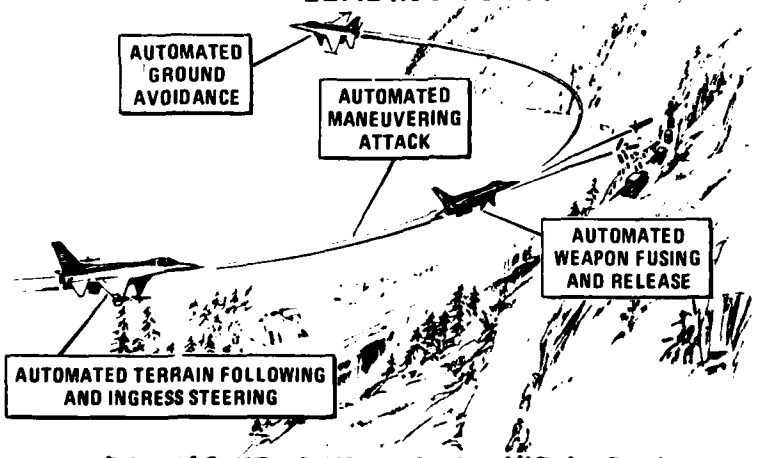


*AUTOMATED SINGLE SEAT NIGHT ATTACK*

FIGURE 11

# Enhanced Piloting Control Through Cockpit Facilities and A.C.T.

by

D.J.Walker
British Aerospace P.L.C.
Kingston-Brough Division
Brough, North Humberside
U.K.

and

P.W.J.Fullam
Flight Systems Department
Royal Aircraft Establishment
Farnborough, Hampshire
U.K.

## 1. SUMMARY

The last decade has seen major developments for directly improving combat manoeuvrability in the field of aerodynamics, avionics, thrust vectoring and control systems. Unchanged however, is the pilot and to make the most of these technological improvements the relationship between man and machine must receive particular attention. It was with this aspect in mind that, as part of its studies into future aircraft design, BAe Brough embarked on a flight programme with the RAE using their A.C.T. Hunter to complement the ground based advanced cockpit evaluation facility at Brough.

This paper concentrates on the manoeuvring aspects of this work and covers total loop control, advanced cockpit, flight control programme and specific activities.

The latter item elaborates on the following activities from the flight programme: General manoeuvring, force sidestick, depressed roll axis, non-linear pitch controller and carefree manoeuvring.

## 2. INTRODUCTION

A joint RAE/BAe flight research programme has been stimulated by a desire to improve, through flight control, the performance of the pilot aircraft combination in carrying out the range of tasks demanded of a modern combat aircraft.

Although the joint activity specifically concerns RAE's ACT aircraft Hunter XE 531, it is the intention here to show how this work relates to advanced cockpit programmes such as the one being pursued at BAe Brough. Futhermore the concept of total loop control (see Section 2) has been an important consideration in the design and implementation of the experiments. A cockpit programme covers many areas of study including seat design, switches, displays, safety etc. but the primary areas of commonality with the Hunter programme concern inceptors and HUDs (Fig.1).

The scope of this paper is thus total loop control, advanced cockpits and the Hunter flight programme with emphasis on manoeuvrability aspects.

## 3. TOTAL LOOP CONTROL

It is important to recognise that to give a pilot proper control of his aircraft in a maneouvring sense, then design of the control system must encompass the entire loop around the pilot or, more correctly around the piloting task (Fig.2). This is particularly so with modern control systems which can be tailored to suit the task under consideration - which itself can be automatically sensed by the system in numerous ways, both directly and indirectly.

Total loop control begins with a broad specification of the piloting tasks in terms of manoeuvrability, handling and display requirements. The inceptor with its variable shaping, the control laws which convert direct and feedback signals into the desired response, and the visual displays are all then related; they can each be varied electrically and strictly should all be tuned together. However, despite this ability to optimise the control system for any given task, so numerous are the tasks demanded of a modern combat aircraft that the main objective of flight testing is to achieve an efficient yet tolerant system which needs as few mode changes as possible so as not to over complicate the software. There are inevitably compromises, but from the work done so far on Hunter XE 531 it would appear that some of these can be surprisingly acceptable.

It should be noted that the combat task will inevitably involve control of the vehicle at the boundaries of the flight and structural envelopes where the pilot needs to be aware of his proximity to these limits. The control system design must ensure both desirable handling and departure protection in order that all possible combat advantages may be achieved.

## 4. ADVANCED COCKPIT

The cockpit is the pilot's interface with his aircraft and the outside world (Fig.3). Clearly there are basic ground rules to be used to ensure that it is suitable for the tasks of a combat aircraft. Manoeuvrability, the subject of this symposium is of prime consideration and obviously field of view, displays, seating, operational systems, inceptors and handling are all important factors (Fig.4). (The relationship between manoeuvrability and handling seen here is that the manoeuvring potential of the aircraft cannot be properly exploited by the pilot without good handling.)

An active control system contributes to the cockpit design in several ways. It is important that the pilot's attention is not dominated by having to fly the aircraft, and this is particularly important in air to air combat. Here ACT is able to automatically prevent the aircraft from manoeuvring beyond safe limits, whether they be aerodynamic or structural. Care has to be taken, however, that the envelope provided is not more restrictive than an experienced pilot could use merely because of ill chosen laws. As indicated above, good handling is just as essential near to the manoeuvre boundary as in any other part of the flight envelope. ACT is able to provide this.

As demonstrated so well by the F16, ACT also gives the designer freedom to locate what can now be a miniature inceptor either in the centre or at the side of the cockpit thus greatly assisting in display location. Results from the Hunter flight programme indicated that a force stick in particular can offer improvements in manoeuvre response.

Displays are another cockpit facility which sould integrate with the flight control system. The many parameters involved in, for example, energy management make this a difficult subject to present and there are many candidates. In any type of guidance or management system however, experiments have shown that the best results are obtained when the influential parameters on the display are under direct rather than indirect control of the pilot.

What could be considered as an extreme case of control complementing display requirements is in air to air combat when in fact the pilot has not the time to refer to a display; here the control system can provide him with a safe flight envelope i.e. carefree manoeuvring.

## 5. FLIGHT CONTROL PROGRAMME

A joint RAE/BAe programme was set up between Farnborough Flight Systems Dept. and Brough to research into flight dynamics aspects of an actively controlled aircraft Hunter XE 531 (Fig.5). This aircraft is a two seater, the experimental right hand cockpit (Fig.6) area having been provided with a quadruplex full authority analogue active system in all three axes. A safety pilot with conventional controls is retained in the left hand seat and this makes a versatile research and demonstration vehicle.

The programme so far has comprised of an initial piloting evaluation, force sidestick and conventionally shaped centre stick evaluation, and currently new control laws and other stick configurations are being assessed (Fig.7). With the addition of discrete micro-processors, the programme will then move onto research into more new control laws including those necessary for carefree flying, some of which will be related to system architecture. It is quite wrong to suppose that with the advent of high agility wide envelope fighters that flight control work is necessary only at the boundaries. The majority of the tasks will still be within the broad 'centre' of the envelope (see Figure 8).

The programme has a recognised experimental procedure (Fig.9) in which ideas are processed through various stages of simulation to become suitable for flight. The analysis is carried out using a combination of classical control theory and time plane responses. The first stage of piloted simulation is an 'ergonomic' rig (Fig.10) based at Farnborough in which much preliminary optimisation can be carried out before moving on to the full simulation facility. Some examples of the rig work are shown in Figure 11 which shows the crosstalk generated when a pilot tries to apply pure single axis inputs with a fixed sidestick. Also shown are typical force signatures to operate the stick switches. It should be noted that these effects do not always appear to cause significant problems in the air because of the extra feedback available to the pilot in the real situation. They do however represent a spurious compensation task which can be minimised by careful inceptor design.

Full pilot-in-loop simulation is carried out on the general purpose facility at BAe Hatfield (Fig.12). Although the cockpit is not fully representative of the Hunter, the HUD facility is common and efforts are made to make the seat/stick geometry close to that on the aircraft. The simulation tasks are matched as closely as possible to those of the aircraft, which itself is representative of a combat aircraft (see Figure 13).

## 6. SPECIFIC ACTIVITIES

In this section, results relevant to the subject of this symposium will be discussed.

### 6.1 General Manoeuvring

Hunter XE 531 has a rate demand flight control system in the primary 'up and away' axes of pitch and roll, with in effect direct rudder and limited authority yaw damping. Thus the aircraft basically obeys gyrometric control laws and as such will manoeuvre differently from a conventional aircraft. This fact has been commented upon by the pilots (Ref. 1), and as a generalisation the effect seems to be nether good nor bad, just different. There are exceptions and a purpose of the flight programme is to identify possible problem areas. For the control designer there is a conflict of choice for roll axis between that to optimise fine tracking and the usual axis alignment for gross manoeuvring (see 6.3). Also, and common for any combat aircraft, there is a conflict between the desired pitch response for fine tracking and for gross manoeuvring (see 6.4).

### 6.2 Force Sidestick

A Lear Siegler force sidestick with a General Dynamics specified grip has been flown in the side position on Hunter XE 531. This equipment is identical with that of the early models flown in the production F16, having minimal compliance. Initial testing tended to support the critics of this type of controller and a PIO on take off was experienced (see Fig.15), though this was readily recovered by the safety pilot. An intensive simulation exercise followed which eventually resulted in improved stick signal electrical shaping, but to satisfy the need for effectiveness over the range of tasks tabled previously two sets of curves emerged - one more suited to take-off and landing, the other to 'up and away' flight (see Fig.16). In addition there still remained a tracking versus manoeuvring conflict in terms of stick sensitivity and absolute forces. Primarily because most of the flying would be 'up and away', that shaping was selected but such was its acceptability in flight (compared with more critical simulation results) that it was eventually successfully used for takeoff and landing. Thus

with this force stick, shaping is critical, but a single shape solution was found that was linked and tolerant to the range of tasks.

6.3 Depressed Roll Axis

A simple gyrometric roll demand system with its axis approximately parallel to fuselage datum will result in marked pendulous motion of the target when fine tracking with a depressed aiming point (necessary because of factors such as lead time and gravity drop). However, for normal manoeuvring a roll axis may be achieved close to wind axis by means of roll/yaw crossfeeds etc. In the current Hunter programme a control law is being assessed which constrains the aircraft to roll about an axis depressed some 4 deg. below flight path datum, limited to small perturbations only. This limitation is due in part to surface limitations (see below) but primarily avoids the large variations in lateral acceleration which would otherwise occur during rapid full rolls.

The programme is still being flown, and the initial results are encouraging (see Fig.17). However, because the means of implementation which is through a roll rate demand to rudder crossfeed, one has to be aware of structural limitations due to the increased sideslip and rudder angle required (see Figure 18).

6.4 Non-Linear Pitch Response

For gross manoeuvring a rapid aircraft normal acceleration response is required, whereas for fine tracking a relatively sluggish response is required - and this has emerged as a somewhat fortuitous benefit of limited authority autostabilisers, but only around 1g. It is intended that the non-linear pitch filter currently being flown on Hunter XE 531 provides a response which not only varies with size of fore and aft stick input but is able to operate about a datum which shifts during a steady manoeuvre. Simulated responses are shown in Fig.15.

Although the control law is undergoing some optimisation in the current flight programme, acquisition and tracking during air to air manoeuvres has been significantly improved.

6.5 Carefree Manoeuvring

This is an important area which has been referred to earlier in this paper.

Although a simulator programme has been carried out, this feature is not due for implementation on the aircraft until next year. Of the candidate systems considered, the one selected incorporates an angle of attack limiter based upon that produced for the NASA F8 programme (Ref. 2). Briefly, the limiting system operates full time in parallel with the normal pitch control system, and that which demands the greater nose down elevator is automatically selected. Some changes from the F8 system have been made to improve handling near to the manoeuvre boundary. The main advantages of this system are considered to be its relatively hard limit and constant handling qualities up to the limit.

Flight assessments will also include any possible boundary penetration, a facility offered by the well known depature and recovery characteristics of the Hunter, and will provide opportunities to compare different handling characteristics in this region.

## 7. CONCLUDING REMARKS

The need for interrelated cockpit/displays/controls design aimed at optimising pilot task performance is seen as the basic for an experimental programme encompassing pilot inceptor, cockpit display and control law design and flight assessments. The programme described offers valuable insight into task control problems widely applicable to modern aircraft.

Refs. 1 RAeS Lecture, London 1979
A.J. Leng and R. Searle

2 F8 Digital CCV Control Laws
G.L. Hartman, J.A. Hange, R.L. Hendrick
NASA CR-2639 (1976)

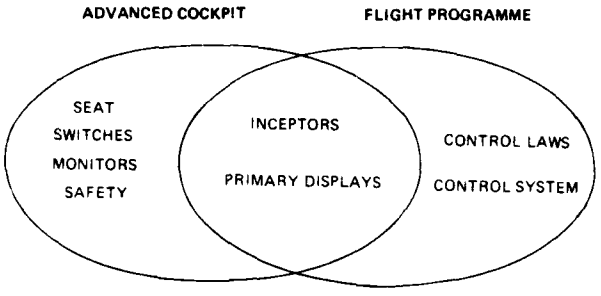


Fig.1. STUDY AREAS

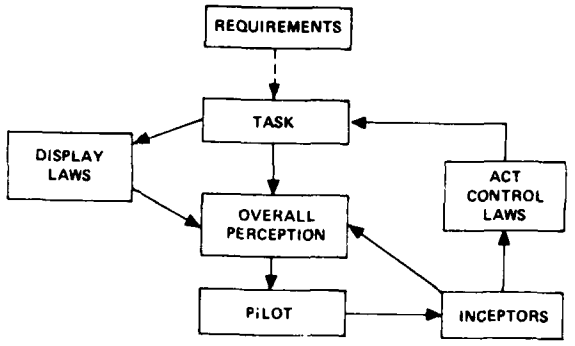


Fig.2. TOTAL LOOP APPROACH

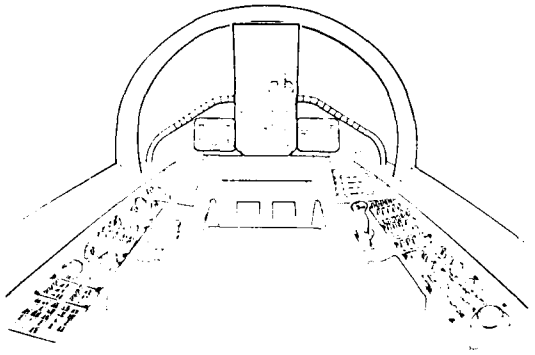

Fig.3. BAe BROUGH ADVANCED COCKPIT

FACILITIES
- INCEPTORS
- DISPLAYS
- SEATING
- FIELD OF VIEW
- OPERATIONAL SYSTEMS

CONTROL LAWS
- CAREFREE MANOEUVRING
- TASK ORIENTATED

Fig.4. ADVANCED COCKPIT - MANOEUVRING ASPECTS

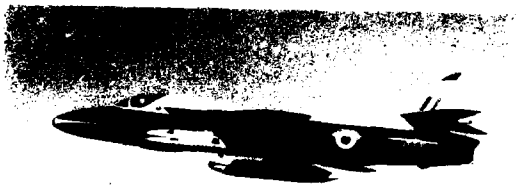

Fig.5. HUNTER XE531

Fig.6. HUNTER XE531 - EXPERIMENTAL COCKPIT

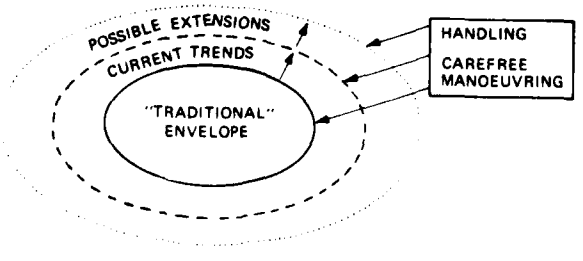


Fig.7. HUNTER JOINT PROGRAMME

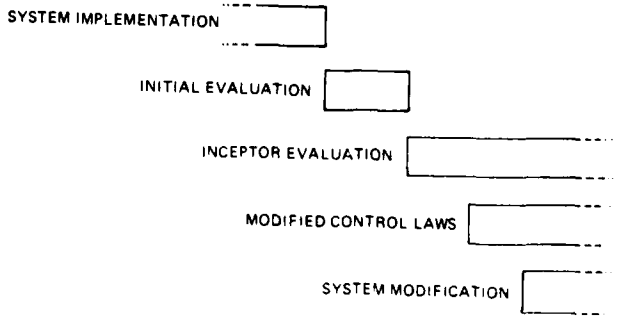


Fig.8. ROLE OF ACT

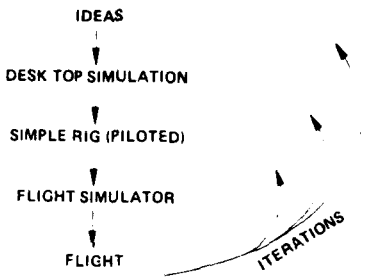


Fig.9. EXPERIMENTAL PROCEDURE

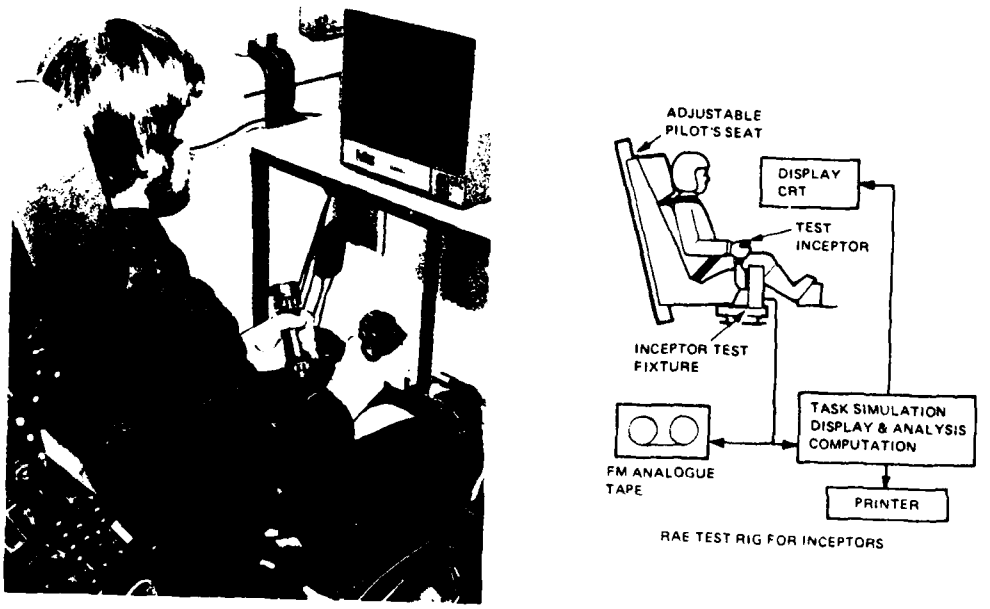


Fig.10. FARNBOROUGH RIG

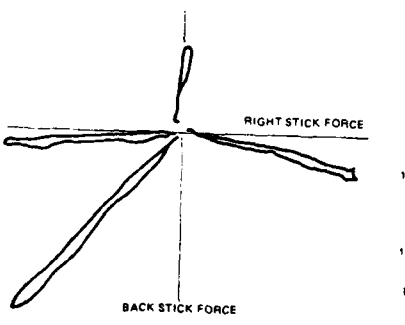


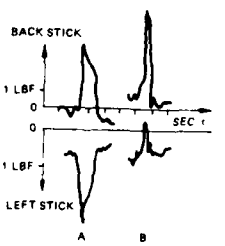


Fig.11. OPEN LOOP TEST CHARACTERISTICS OF FORCE STICK (RAE TEST RIG)

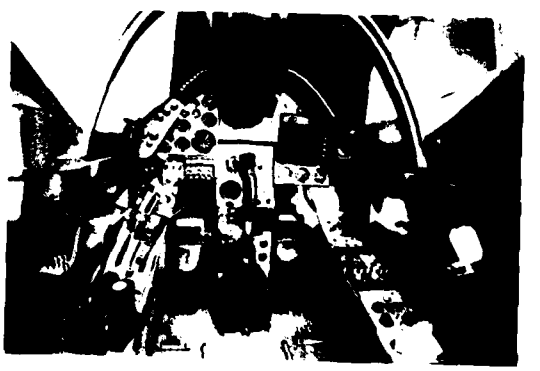

Fig.12. BAe FLIGHT SIMULATOR (HATFIELD)

- TAKE OFF
- AIR TO GROUND
- AIR TO AIR
- GENERAL MANOEUVRING
- LANDING

Fig.13. SIMULATION/FLIGHT TASKS

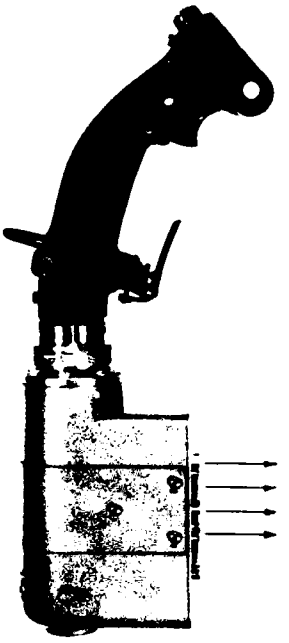

Fig.14. FORCE STICK

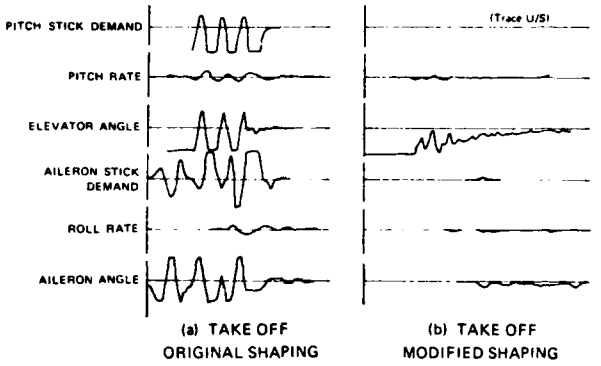


Fig.15. FORCE SIDESTICK-TAKE OFF

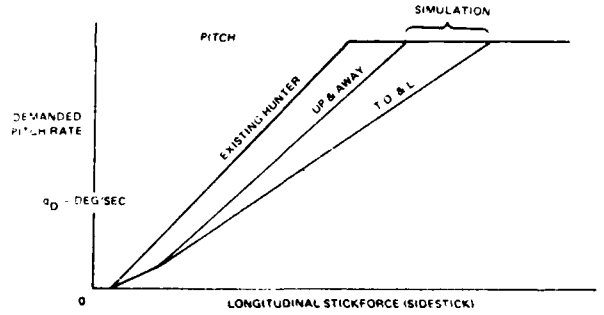


Fig.16. STICK SHAPING - PITCH

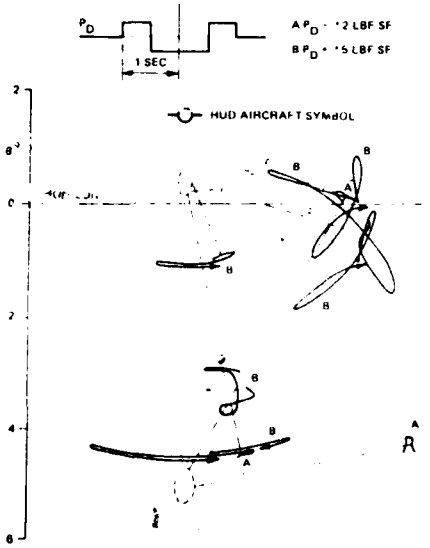


Fig.17. DEPRESSED ROLL AXIS GROUND POINT LOCI FROM SIMULATION

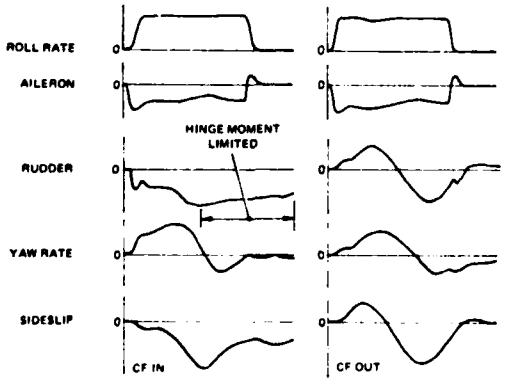


Fig.18. MANOEUVRING LIMITATIONS

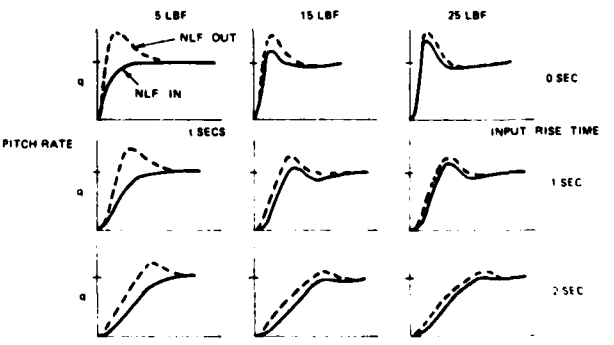


Fig.19. PITCH RESPONSES TO RAMPED STEP INPUT WITH NON-LINEAR FILTER

# THE DEVELOPMENT OF CRYOGENIC WIND TUNNELS AND THEIR APPLICATION TO MANEUVERING AIRCRAFT TECHNOLOGY

by
E. C. Polhamus and R. P. Boyden
NASA Langley Research Center
Hampton, VA 23665 U.S.A.

## SUMMARY

Because of the strong influence of Reynolds number, Mach number, and aeroelasticity on the aerodynamics of combat aircraft in the high angle-of-attack range encountered during maneuvers, the unique capabilities of the new cryogenic wind tunnels offer the aircraft designer important new capabilities for validation of his design methodology as well as the ability to isolate various effects. This paper, therefore, discusses the cryogenic wind tunnel relative to its potential for advancing maneuvering aircraft technology.

The first portion of the paper consists of a brief overview of the cryogenic wind-tunnel concept and the capabilities and status of the Langley cryogenic facilities. Included in this part is a review of the considerations leading to the selection of the cryogenic concept such as capital and operating costs of the tunnel, model and balance construction implications, and test conditions and will be related to requirements specifically associated with maneuvering aircraft technology. Typical viscous, compressibility and aeroelastic effects encountered by maneuvering aircraft are illustrated and the unique ability of the cryogenic wind tunnels to isolate and investigate these parameters while simulating full-scale conditions is discussed. The status of the Langley cryogenic wind-tunnel facilities is reviewed and their operating envelopes described in relation to maneuvering aircraft research and development requirements.

The final portion of the paper reviews the status of cryogenic testing technology development specifically related to aircraft maneuverability studies including force balances and buffet measurement techniques. Included are examples of research carried out in the Langley 0.3-meter Transonic Cryogenic Wind Tunnel to verify the various techniques.

## SYMBOLS

| | |
|---|---|
| A | aspect ratio |
| A/C | aircraft |
| b | wing span, meters |
| $\bar{c}$ | mean geometric chord, meters |
| $c_{root}$ | root chord, meters |
| $C_A$ | axial-force coefficient |
| $C_L$ | lift-force coefficient |
| $C_m$ | pitching-moment coefficient |
| $C_N$ | normal-force coefficient |
| $C_{B,D}$ | dynamic wing-root bending-moment coefficient, $\frac{M_D}{qS\bar{c}}$ |
| D | balance diameter, centimeters |
| f | frequency, hertz |
| g | acceleration due to gravity |
| k | reduced frequency parameter, $\frac{\omega\bar{c}}{V}$, radians |
| $\ell$ | wind-tunnel reference size, meters |
| M | free-stream Mach number |
| $M_D$ | time averaged rms value of dynamic wing-root bending moment, newton-meters |
| $\sqrt{nF(n)}$ | nondimensional fluctuating pressure parameter |
| NF | normal force, newtons |
| $P_t$ | stagnation pressure, newtons/meter$^2$ or atmospheres |
| q | free-stream dynamic pressure, newtons/meter$^2$ |
| $R_{\bar{c}}$ | Reynolds number based on $\bar{c}$ |
| S | reference wing area, meter$^2$ |
| S.L. | sea level |
| $T_t$ | stagnation temperature, kelvin |
| V | free-stream velocity, meters/second |
| W | airplane weight, newtons |
| $\alpha$ | angle of attack, degrees |
| $\beta$ | angle of sideslip, degrees |
| $\omega$ | angular frequency, $2\pi f$, radians/second |

## 1. INTRODUCTION

In recent years interest in greatly expanded maneuvering envelopes of combat aircraft has increased as a result of technology advances that provide both controllability and

high levels of maneuver lift at angles of attack well beyond the normal stall limit of earlier generations of aircraft. Representative of the technology advances involved are automatic departure and spin prevention systems, the development and exploitation of the "controlled separation" concept by various forms of vortex lift maneuver devices, applications of advanced variable camber concepts, use of thrust vectoring and direct lift and side-force generation, and various "multiple lifting surface" concepts. The expansion of the operational angle-of-attack range of combat aircraft associated with these technology advances is accompanied by an increased exposure to flows that are highly Reynolds number dependent such as, for example, fuselage forebody cross-flows particularly with respect to noncircular cross-sectional shapes, symmetric and asymmetric vortex breakdown phenomena associated with vortex maneuver lift concepts, and a variety of induced flows resulting from the interactions of vortices shed from various components. The complexity of the high angle-of-attack flow phenomena is increased further by the fact that the high thrust-to-weight ratios of most modern combat aircraft allow the high angle-of-attack penetrations to be performed at high subsonic speeds introducing strong shock boundary-layer interactions.[1,2]

In order to fully exploit the concepts for improved combat maneuverability, improved design capabilities are needed with regard to both computational and experimental aerodynamic methods of simulating the full-scale Reynolds number characteristics of the complicated flows. The new cryogenic wind tunnels with their high Reynolds number capabilities and unique operating envelopes offer the possibility of greatly improved experimental capabilities. The purpose of this paper is to describe the development of cryogenic wind tunnels, to indicate some of the ways in which they may be used for combat maneuverability research and development, to illustrate some of the developments in cryogenic wind-tunnel technology, and to describe some of the remaining problem areas.

## 2. THE CRYOGENIC TUNNEL CONCEPT

Ten years ago, in October of 1971, a small group of researchers and technicians at the NASA Langley Research Center began a cryogenic wind-tunnel technology development program that led to the current interest and application of the concept to new transonic facilities having high Reynolds number capabilities and unique operating envelopes. The primary advantages of the cryogenic concept can be described with the aid of figure 1 where three methods of increasing the Reynolds number capability of a wind tunnel are shown in relation to the drive power required. For transonic tunnels, increasing size alone to obtain full-scale Reynolds number capability is prohibitive from both the drive power requirements and the cost of the tunnel. The pressure tunnel approach, while somewhat less prohibitive, also requires large drive power increases as well as undesirably large dynamic pressures which translate into large model and balance loads. The problems associated with these two approaches result from the fact that they increase the Reynolds number by increasing the inertia force. The cryogenic approach avoids these problems by providing large decreases in the viscous force while the inertia force, for a constant Mach number, remains constant. With regard to drive power it can be seen that the reduced velocity at constant Mach number resulting from the reduction in sound speed with decreasing temperatures actually reduces the power requirements as Reynolds number increases. This characteristic makes the highly desirable continuous-flow fan-driven tunnel a practical option in place of the intermittent "stored energy" approaches previously being considered for new high Reynolds number transonic tunnels.

Because of these and other advantages, researchers at Langley initiated an extensive cryogenic wind-tunnel technology program resulting in the National Transonic Facility (NTF) which is nearing completion. The research and development program leading to this new facility can be briefly summarized with the aid of figure 2 which presents photographs and basic characteristics of the three Langley cryogenic wind tunnels.

Shortly after the initial analytical studies of the concept in the autumn of 1971, an existing scale model of a low-speed wind tunnel was insulated and modified for cryogenic operation which began in January 1972. It was in this model tunnel that the basic concept for cooling, that of spraying liquid nitrogen ($LN_2$) at about 78 K directly into the tunnel circuit was developed and complete evaporation of the $LN_2$ demonstrated down to a tunnel temperature of 80 K. Many of the practical considerations associated with the development of a cryogenic wind tunnel were investigated and a few critical aerodynamic experiments were made in such areas as, for example, boundary-layer simulation in cryogenic gaseous nitrogen and the use of a water-jacketed strain-gage balance for force measurements.

The encouraging results of the analytical and experimental studies were reported during the AIAA 7th Aerodynamic Testing Conference in September of 1972,[3] and following additional analytical studies, including the investigation of "real gas" effects and its important conclusion that gaseous nitrogen is a valid transonic test medium,[4,5] a decision was made in late 1972 to build a pressurized transonic cryogenic "proof-of-concept" tunnel[6] shown by a recent photograph in the center of figure 2. This highly successful "proof-of-concept" tunnel began operation in the autumn of 1973 and later was converted to a research facility and designated as the 0.3-meter Transonic Cryogenic Tunnel. This facility, which can operate at pressures up to 6 atmospheres, was designed and constructed "in-house." After a series of critical aerodynamic proof-of-concept tests[7] and a broad cryogenic wind-tunnel technology program, the cryogenic wind-tunnel concept was selected in 1975 for the new U.S. National Transonic Facility shown in the lower photo-

graph of figure 2. This unique high Reynolds number facility, which is to serve the needs of NASA, DOD, industry, and universities, is nearing completion at its Langley site and is expected to begin shake-down runs in early 1982.

## 3. THE NATIONAL TRANSONIC FACILITY

The National Transonic Facility[8,9] is being constructed on the site of the deactivated 4-foot supersonic pressure tunnel to take advantage of existing variable speed induction drive motors, drive control system, cooling towers, and office building. Because of the pressure requirement of the NTF (8.8 atm.), a synchronous motor has been added to the drive system bringing the total drive horsepower to 120,000. Although similar to most fan-driven tunnels there are certain features of the NTF that are dictated by the ability to operate at high stagnation pressures and cryogenic temperatures. For example, to reduce both the cost of the pressure shell and the consumption of liquid nitrogen, the volume of the circuit has been minimized, with the major contributing feature being the wide-angle diffuser located immediately upstream of the settling chamber which considerably shortened the circuit length. Directly related to the cryogenic operation are, of course, the liquid nitrogen injection nozzles located, for efficiency reasons, upstream of the fan and the internal thermal insulation which shields the relatively thick pressure shell from the tunnel flow, thereby reducing liquid nitrogen consumption required for cooldown and avoiding thermal cycling of the pressure shell. To further reduce operational cost by maintaining tunnel pressure and temperature during model changes, test section isolation valves and a tunnel access system which provides a "room temperature" work environment in the test section are provided.

A further indication of the construction status of the National Transonic Facility can be seen in figure 3 where photographs of a portion of the control room and of the tunnel test section, taken in August 1981, are shown. The control room, which is completed and equipped, houses the data system complex which includes subsystems for facility and model control, aerodynamic data acquisition, process monitoring, data management, etc.[10] In the interest of high productivity and reduced operational cost, four identical computers with switchable peripherals have been provided. In addition, the system provides for real-time displays, on-site data analysis, a link to the Langley data reduction center, and national user access for pretest planning, software development, and debugging. An additional feature related to reducing the high cost of full-scale Reynolds number testing is the development of a completely automatic system to control temperature, pressure, and Mach number. Experience gained with the successful automatic control of temperature and pressure of the 0.3-m TCT has added confidence that the NTF control requirements will be achieved.

The photograph of the test section shows three of the four walls in place, the angle-of-attack strut, and the high-speed diffuser. The test section has all four walls slotted and is 2.5 meters square which will allow models large enough for good construction fidelity to be tested at the high angles of attack of interest for highly maneuverable combat aircraft. Information has been recently published[11] to provide potential users of the NTF with the information necessary for preliminary planning of test programs and for preliminary layout of models and model supports.

An indication of the degree to which the NTF will simulate the full-scale characteristics of maneuvering combat aircraft can be seen in figure 4 in terms of the Mach number-Reynolds number envelope for a typical combat aircraft.[8] Because of the increase in wall interference effects at the high angles of attack of interest for maneuvering combat aircraft, the model size has been reduced such that the mean aerodynamic chord, $\bar{c}$, is only 6 percent of the square root of the test section area. This results in a $\bar{c}$ of 15.0 cm being used to define the Reynolds numbers of the NTF envelope. The full-scale aircraft Mach number-Reynolds number envelope derived from its altitude-Mach number combat arena (3g and above maneuvering envelope) is shown by the shaded area. The comparison indicates that for this aircraft the NTF should be capable of simulating the complete subsonic portion of the combat arena and the higher altitude portions of the transonic region. Also shown is a composite envelope derived from the maximum capabilities of existing U.S. tunnels. The large increase in the Reynolds number capability afforded by the NTF is readily apparent.

With the NTF described and its capabilities in simulating the combat arena indicated, the remainder of the paper will describe some of the aerodynamic research and development testing capabilities associated with the cryogenic pressure tunnel concept and review selected portions of the Langley cryogenic wind-tunnel technology program, particularly with regard to high angle-of-attack combat aircraft applications. Some of the operating envelopes will be described followed by discussions of portions of the cryogenic testing technology program related to force and moment testing, and buffet testing.

## 4. SOME UNIQUE OPERATING ENVELOPES

Because of the ability to independently control stagnation temperature, pressure, and Mach number the cryogenic pressure tunnel offers some unique operating envelopes that allow new freedoms in aerodynamic testing.[12] For example, figure 5 illustrates a constant Mach number operating envelope in terms of Reynolds number and test section dynamic

pressure. This envelope is bounded by the maximum and minimum stagnation pressures and temperatures. The maximum stagnation temperature line is representative of conventional, noncryogenic, pressure tunnels and illustrates the large variations in dynamic pressure that accompany Reynolds number sweeps in these tunnels. These large variations in dynamic pressure, in addition to restricting the useful Reynolds number due to excessive model, balance and support system loads, result in aeroelastic effects accompanying the Reynolds number effects. However, as indicated by the arrows, the cryogenic tunnel allows large Reynolds number sweeps at a constant dynamic pressure and dynamic pressure, or aeroelastic sweeps at constant Reynolds number. The large reductions in dynamic pressure at a constant Reynolds number that accompanies the reduced temperature is also an important test consideration that will be discussed later.

The ability to adjust dynamic pressure in the cryogenic pressure tunnel while holding Reynolds number constant has implications with regard to both aeroelastic model testing and model loads considerations. For example, figure 6 shows the variation in wind-tunnel dynamic pressure associated with the simulation of aircraft aeroelastic distortion and Reynolds number over an altitude range. The left part of the figure illustrates the conditions encountered in conventional pressure tunnels. The symbol represents an aeroelastic model designed to match both the full-scale aircraft aeroelastic distortion and the Reynolds number for the sea-level condition and the lines represent the variation in tunnel dynamic pressure associated with matching these conditions as the altitude is increased. Since temperature changes with altitude, the conventional pressure tunnel cannot match both Reynolds number and the variation in the dynamic pressure required for simulation of aeroelastic distortion. At a simulated altitude of 12,000 meters, the difference in dynamic pressure associated with matching the two conditions is about 27 percent. However, as shown on the right side of figure 6, the cryogenic pressure tunnel provides a Reynolds number matching envelope that encompasses the dynamic pressure required for aeroelastic matching and therefore has the capability for matching Reynolds number and aeroelastic distortion over the altitude range with a single aeroelastic model and at a much lower dynamic pressure. Advanced model construction technology will, of course, be needed to handle the cryogenic aspects of an aeroelastic model.

The above capability also has implications in relation to model loads encountered over the Reynolds number range as illustrated in figure 7. In this figure, the lift force in newtons generated by a typical combat aircraft model for a Mach number of 0.9 and for an aircraft wing loading of 2870 newtons per square meter is presented as a function of $R_{\bar{c}}$ for a $C_L$ of 2.0 at an ambient temperature condition and for a series of $C_L$'s at the minimum cryogenic temperature set by a local Mach number of 1.4 from condensation considerations. First, by comparing the model lift force at a constant $C_L$ the large reductions in model loads, for a given Reynolds number, resulting from cryogenic operation can be seen. Of additional interest for highly maneuverable combat aircraft is the fact that in the cryogenic mode the dynamic pressure ratio matching capability illustrated previously by figure 6 results in the model lift load ($C_L \times q$) for a given maneuver load factor remaining essentially constant with Reynolds number (or equivalent altitude) just as for the aircraft.

Also of interest is the fact that in the cryogenic condition, a full-scale Reynolds number simulation of a 7g maneuver at an altitude of 12,600 meters can be provided with a tunnel stagnation pressure of only 2 atmospheres. Since several of the existing conventional pressure tunnels of the NTF size operate up to 2 atmospheres, it is pertinent to note that if the model strength is sufficient in those tunnels at the lift coefficient corresponding to the 12,600-meter altitude, it will be sufficient at cryogenic temperatures where full-scale Reynolds numbers can be simulated all the way to sea-level conditions.

These new capabilities provided by cryogenic pressure tunnels to isolate Reynolds number, Mach number, and aeroelastic effects and to match conditions over the aircraft operating envelope promises to provide greatly improved research and development capability and is of particular importance for maneuvering combat aircraft.

## 5. FORCE AND MOMENT TESTING

The majority of aerodynamic testing related to maneuvering combat aircraft consists of conventional force and moment measurements to establish the aerodynamic performance, stability, and control over the wide range of flight conditions expected to be encountered. A major portion of the extensive cryogenic wind-tunnel technology program being carried out at Langley deals with this type of testing and selected portions will be described.

### 5.1 Model Technology

Even though cryogenic operation provides large reductions in model loads relative to an ambient temperature tunnel of the same size at the same Reynolds number, the combination of relatively high loads and the effects of cryogenic temperature on the mechanical properties of materials has resulted in sizable model design and construction challenges for complicated scale models of combat aircraft.

Although 0.3-m TCT cryogenic technology and airfoil research programs are developing experience in such areas as material selection, machinability, new construction concepts

(including orifice installation), heat-transfer effects, etc., the size of the 0.3-m TCT precludes much of the practical experience required for the large three-dimensional NTF models. This primarily two-dimensional model program, which includes in-house research and development, contracts with model construction firms, and a metallurgical research project at the University of Southampton, has indicated that for the current state of the art, model construction time and cost is considerably greater than for the lower Reynolds number ambient temperature tunnels. While indicating that satisfactory airfoil models can be constructed, it has been shown that "non-handbook" metallurgical changes must be carefully considered with regard to material selection, machining, etc.

In order to identify and solve additional problem areas associated with the highly stressed and complicated NTF combat aircraft models, an extensive research and development program directed towards model design and construction is underway with both in-house and contract efforts. Focal points for this study are the in-house design and construction of a "pathfinder" model and its support sting and the development of an NTF "users criteria" document.

## 5.2 Strain-Gage Balance Technology

In general, the laboratory studies and operational experience of the 0.3-m TCT during the past 8 years have indicated that the basic instrumentation technology developed for cryogenic testing is generally satisfactory and should be directly applicable to maneuvering combat aircraft studies in the NTF.

An indication of the type of cryogenic instrumentation development programs being carried out and an illustration of the manner in which the 0.3-m TCT is utilized in conjunction with other laboratory types of evaluation equipment can be derived from a review of the strain-gage balance development program.

As with most of the testing to be carried out in the NTF, the research and development testing associated with maneuvering combat aircraft will require internal strain-gage balances capable of accurately measuring large aerodynamic loads over a wide temperature range. The development of such balances has been a continuing part of the Langley cryogenic technology program with the initial studies concentrated on thermal control using standard balances. A water jacketed balance was tested in the low-speed cryogenic tunnel in 1972, and in 1974 a conventional balance with the addition of resistance heaters was investigated in the 0.3-m TCT. In 1975 the program was expanded[13] to develop design technology in the areas of balance material, strain gages, solder, wiring, and moisture-proofing to allow the effects of the cryogenic environment on strain-gage output to be minimized. This extensive research program has provided new technology information that has been applied to the design and construction of successful cryogenic balances of both thermal controlled and nonthermal controlled types. Both types utilized strain gages that were developed so the gage factor and the balance material modulus temperature effects were compensated such that the sensitivity shift over the entire temperature range was only -0.7 to -1.0 percent, greatly minimizing heater and calibration requirements. The nonthermal controlled balance design resulted from the development of a technique in which a computer system matches experimentally determined gage characteristics to select companion gages in a four-active arm bridge circuit such that there is essentially no zero shift with temperature. Further, by installing two gages transverse to the principal stress axis the sensitivity shift due to temperature was reduced to -0.3 percent or less.

Following extensive laboratory tests, both balance types were tested under aerodynamic load over the complete NTF temperature range in the 0.3-m TCT. Photographs of the balances tested as part of the evolution of the NTF-101 balance are shown in figure 8 along with the respective aerodynamic bodies used during the tests. The two small balances of the High Reynolds Number Cryogenic series are designated HRC-1 and HRC-2 with the HRC-1 being the conventional balance with resistance heaters added that was tested in 1974. The HRC-2 balance was the first balance completely designed for cryogenic operation and was tested in both thermally controlled and nonthermally controlled versions with satisfactory results. The NTF-101 is the first full-scale NTF balance and is a nonthermally controlled design based on the gage-to-balance material and gage-to-gage balancing technology described above. It is a high capacity type balance providing a normal force of 28,910 newtons with only a 6.03-centimeter diameter and was designed to meet the force and size requirements of a planned NTF model. The tests of this balance in the 0.3-m TCT verified the previous findings, in laboratory experiments, that this type of balance produces reliable, repeatable, and predictable data from 300 K down to 110 K under steady-state conditions. Recent tests have shown that the improved gaging techniques provide equally good results during temperature transients on five of the components. Research directed towards improving the axial component transient temperature response is continuing.[13] Although temperature transients can be greatly minimized in a continuous flow tunnel such as the NTF, improvements in the axial response could increase data acquisition rate.

An example of types of balance data obtained from tests that have been carried out in the 0.3-m TCT is presented in figure 9. The example shown is for the nonthermally controlled version of the HRC-2 balance installed in a delta-wing model. The sample shown is for a Mach number of 0.30 with the measured model normal-force, pitching-moment, and axial-force coefficients presented over an angle-of-attack range up to approximately $30^{\circ}$. Tests were made at three tunnel stagnation temperature conditions, a cryogenic condition of 100 K, an intermediate temperature of 200 K, and an ambient temperature condi-

tion of 300 K. To maintain a constant Reynolds number of $4.85 \times 10^6$ the tunnel stagnation pressure was varied as the temperature was varied. The main strut angle of attack was determined by an accelerometer, maintained at ambient temperature, located on the turntable. The effect of the varying dynamic pressure on model angle of attack was accounted for by sting and balance bending calibrations. Aeroelastic effects on the model shape were negligible due to the short span and extreme thickness. For this unheated balance sensitivity corrections due to temperature were applied as determined from the laboratory tests. As mentioned previously the later NTF-101 balance utilizes new gaging techniques which automatically compensate for temperature. The results shown in figure 9 indicate excellent agreement between the results for the three tunnel stagnation temperatures, particularly for the normal-force and pitching-moment coefficients. What appears to be poorer agreement for the axial-force coefficient is associated with the fact that the axial load provided by the model was a very small fraction of the axial capacity. These and other data obtained during the balance studies demonstrate that accurate force data can be obtained using unheated strain-gage balances.

An indication of the current status with regard to the sizes of one-piece balances required to develop various load capacities, a consideration of particular importance for high angle-of-attack testing, is given in figure 10. Here the normal-force capacity in newtons is presented as a function of balance diameter in centimeters. The curves represent three balance capacity levels. The lower curve represents the upper bound of Langley's existing conventional noncryogenic six-component balances, the center curve represents a "high-capacity" balance capability that has been obtained without degrading performance, and the upper curve indicates the additional load capability that can be provided in three-component balances. With regard to cryogenic balances three six-component designs covering a normal-force range up to $90 \times 10^3$ newtons have been completed and the mid-size balance, the NTF-101, which has been constructed and successfully tested in the 0.3-m TCT is indicated by the upper solid symbol. The two cryogenic three-component balances, the HRC-1 and HRC-2, are shown as the two lower solid symbols.

Although research and development is continuing to provide further balance improvements it appears that the current technology should provide balances suitable for the high angle-of-attack testing associated with maneuvering aircraft.

## 6. BUFFET TESTING

A phenomenon which can degrade the maneuver capability of a combat aircraft is the onset of buffet and the rate at which it builds up with increasing angles of attack. Since buffet is a separated flow phenomenon, it is, of course, often highly dependent on Reynolds number. The new cryogenic wind tunnels offer unique opportunities to improve the ground-based simulation of full-scale buffet characteristics. In addition to the obvious Reynolds number advantage, the cryogenic pressure tunnel offers advantages such as increasing the ratio of aerodynamic-to-structural damping and providing a certain degree of control over the reduced frequency parameter with a single model stiffness. These characteristics of the cryogenic pressure tunnel will be discussed in the following sections.

A precursor study, in preparation for buffet measurements in the NTF, has been carried out in the 0.3-m TCT[14] to determine if an existing buffet testing technique, the measurement of the unsteady wing-root bending moment, can be used successfully at cryogenic temperatures. The aerodynamic configurations utilized for the study, shown in figure 11, were selected as a result of discussions with Dennis G. Mabey of the British Royal Aircraft Establishment in connection with a lecture on dynamic aeroelastic model tests in cryogenic tunnels which he presented at Langley.[15]

The aspect ratio 3 rectangular wing with its "peaky" type airfoil provides the opportunity to investigate the shock induced separation type of buffet while the 65° delta wing with its sharp leading edge generates the leading-edge vortex flow typical of supercruiser type of combat aircraft and provides the opportunity to investigate the effects of vortex breakdown on buffet. The semispan wing models were cantilevered from a turntable in the sidewall of the two-dimensional test section of the tunnel. It is recognized there are sidewall interference effects because of the relatively large size of these three-dimensional models compared to the size of the test section. However, for the purpose of comparing results at ambient and cryogenic temperatures the wall interference effects are of little importance.

### 6.1 Model Construction and Instrumentation

The semispan buffet wing models were constructed from the same type of aluminum alloy, 7075-T6, as the turntable to which they were mounted. This was done in order to eliminate any possible effects of differences in thermal expansion characteristics between the model and the turntable over the range of test temperatures in order to provide a rigid model mounting to keep the structural damping as low as possible. A strain-gage bridge and two thermocouples were bonded with cement into recesses machined into the upper and lower surfaces of the wings near the root chord. The remaining void was then filled back to the original surface with the same cement which is rated for use over the temperature range of interest of 100 K to 300 K. No artificial transition was used to trip the boundary layer on either of the models for these tests. The first natural frequency

in bending at ambient temperatures for the rectangular wing is about 270 hertz and for the delta wing the frequency is about 492 hertz.

The buffet data system used for these tests is a two-channel integrated unit designed by personnel of the Instrument Research Division at Langley. The system determines the average root-mean-square values of the unsteady voltage signal from the bending-moment gage by integrating the time-varying portion of the signal for a preselected time interval which may be varied from 1 to 99 seconds. For this test an integration time of 20 seconds was used. The unsteady bending-moment signal was recorded on magnetic tape for later off-line analysis.

### 6.2 Test Procedure

Before the actual wind-tunnel test, the models were loaded statically while in an environmental chamber in order to determine the effect of the large temperature range on the strain-gage sensitivity. The variation in the sensitivity with temperature was found to be linear and to increase by 21 percent for the delta wing and 24 percent for the NPL-9510 wing over a range of temperature from 300 K to 110 K. This rather large change in sensitivity with temperature is apparently the result of the strain gages not being well matched to the aluminum alloy used for the models. The calibration curve for each of the two models as a function of temperature was used to correct the gage sensitivity in the data reduction.

After the wind tunnel had reached the required test conditions and the angle of attack had been set, the gain of the buffet system was adjusted to maximize the output of the unsteady wing-root bending-moment signal. This signal was monitored with an oscilloscope and a recording oscillograph for amplifier overload and for the allowable input range for the analog tape recorder. The unsteady bending-moment signal was then integrated for the 20-second time interval chosen for this test and then recorded on the tunnel data system. Afterwards a 20-second segment of the unsteady signal was recorded on magnetic tape for later analysis. A separate desk-top calculator was used to compute and plot the dynamic coefficients for on-line display.

### 6.3 Buffet Test Results

The range of test conditions for the delta-wing model is shown in figure 12 for a Mach number of 0.35 by the envelope of the Reynolds number and the reduced frequency parameter combinations. The stagnation pressure and temperature are indicated along the boundaries of the envelope. The ability to provide this unique envelope in a cryogenic tunnel with a single model is a result of the wide range of temperature control and its effect on the speed of sound and thereby on the reduced frequency parameter at a given Mach number.

As shown in figure 13, results were obtained at the same free-stream velocity, which gave almost the equivalent reduced frequency parameter, and the same dynamic pressure by adjusting the Mach number and the stagnation pressure. At these low Mach numbers any Mach number effect should be small. Good agreement for the unsteady bending moment was obtained over the entire range of angle of attack using this procedure. This good agreement in the dynamic root bending moment is considered to demonstrate that the root bending-moment strain-gage technique operates satisfactorily at cryogenic temperatures. The variation in the reduced frequency parameter in figure 13 from 5.71 to 6.01 radians for the ambient and the cryogenic data, respectively, is a result of the frequency of the first natural bending mode increasing with a decrease in temperature because of an increase in modulus of elasticity of the aluminum alloy. As will be seen later, it is possible that the small difference in reduced frequency parameter could conceivably account for the small differences in the data.

The unique capability of the cryogenic tunnel in which control of the speed of sound can be utilized to provide a range of reduced frequencies while maintaining constant Mach and Reynolds numbers is illustrated by the results presented in figure 14. Shown are the data for a Mach number of 0.35 and a constant Reynolds number for two values of the reduced frequency parameter obtained by temperature variation. Also indicated is the angle of attack at which vortex breakdown has reached the wing trailing edge as obtained from the study of reference 16. The buffet measurements indicate that the onset of buffet coincides with vortex breakdown at the trailing edge and that the intensity, which increases as the vortex breakdown moves toward the wing apex, is highly dependent upon the reduced frequency. At a given angle of attack beyond buffet onset the buffet intensity is seen to increase greatly as the reduced frequency parameter is increased from 3.49 to 6.01. It has been suggested by Mabey[17] that the reduced frequency effect shown in figure 14 is consistent with the increased magnitude of the excitation spectrum with increases in reduced frequency observed by Keating in an analysis of oscillating surface pressures on a model of the BAC 221 slender wing research airplane. These effects were attributed to the frequency content induced by the vortex flow in which breakdown had occurred at about the one-half root chord longitudinal station. To illustrate this possible correlation figure 15 has been prepared. The data by Keating are shown on the left side of figure 15 with the nondimensional fluctuating pressure parameter plotted against the frequency parameter. On the right side of figure 15, the buffet coefficient for the delta-wing model is plotted for vortex breakdown at about 50-percent root chord and for breakdown at 25-percent root chord. The leading-edge vortex type of flow on these two types of slender wings should be similar even though the detailed geometry of the planforms is different. The increase in excitation for values of $fb/V$ of 0.78 to 1.34 is considered analogous to the increase in the buffet coefficient over the same range of

frequency parameter. The demonstrations of the capability of utilizing a conventional buffet test technique at cryogenic temperatures, and of the benefits of temperature control over a wide range with regard to controlling various buffet parameters, along with the research results obtained, should be of value in assuring efficient use of the NTF for combat aircraft buffet studies utilizing simple wing-root bending gages.

## 7. CONCLUDING REMARKS

During the past decade a great deal of progress has been made in the development of high Reynolds number cryogenic wind tunnels and in the testing technology required to utilize the unique capabilities of these facilities. Subsequent to the U.S. decision, in 1975, to construct the National Transonic Facility, interest in the concept has grown throughout the world and, at present, there are at least 10 small and moderate size cryogenic tunnels in operation or under construction in the U.S., Europe, and Japan in addition to the Langley tunnels.[18-20] Besides the national programs, there is also a four-Nation program in Europe to develop a large European Transonic Wind-tunnel (ETW).[18] The operational experience and cryogenic technology programs associated with these programs will augment the Langley experience.

With the NTF scheduled to begin operation in 1982, experience will be gained in a cryogenic tunnel large enough to carry out full-scale Reynolds number research and development at the high angles of attack applicable to maneuvering combat aircraft aerodynamic technology.

If these new transonic high Reynolds number facilities live up to their unique potentials, they will provide outstanding capabilities for improving maneuvering combat aircraft technology.

## 8. REFERENCES


1. The Proceedings of the AGARD Fluid Dynamics Panel Symposium on High Angle of Attack Aerodynamics. AGARD CP 247, January 1979.

2. Polhamus, Edward C.: Technical Evaluation Report on the Fluid Dynamics Panel Symposium on High Angle of Attack Aerodynamics. AGARD-AR-145, August 1979.

3. Goodyer, Michael J.; and Kilgore, Robert A.: The High Reynolds Number Cryogenic Wind Tunnel. AIAA Paper 72-995, 7th Aerodynamic Testing Conference, Palo Alto, California, September 13-15, 1972. Also AIAA Journal, vol. 11, no. 5, May 1973, pp. 613-619.

4. Adcock, Jerry B.; Kilgore, Robert A.; and Ray, Edward J.: Cryogenic Nitrogen as a Transonic Wind Tunnel Test Gas. AIAA Paper No. 75-143, January 1975.

5. Adcock, Jerry B.: Real-Gas Effects Associated with One Dimensional Transonic Flow of Cryogenic Nitrogen. NASA TN D-8274, December 1976.

6. Kilgore, Robert A.: Design Features and Operational Characteristics of the Langley 0.3-Meter Transonic Cryogenic Tunnel. NASA TN D-8304, 1976.

7. Ray, Edward J.; Kilgore, Robert A.; and Adcock, Jerry B.: Analysis of Validation Tests of the Langley Pilot Transonic Cryogenic Tunnel. NASA TN D-7828, 1975.

8. McKinney, Linwood W.; and Howell, Robert R.: The Characteristics of the Planned National Transonic Facility. Paper presented at the AIAA 9th Aerodynamic Testing Conference, Arlington, Texas, June 7-9, 1976.

9. Igoe, William B.: Characteristics of the U.S. National Transonic Facility. Paper No. 17, AGAPD Lecture Series No. 111, 1980.

10. Russell, Charles H.; and Bryant, Charles S.: Instrumentation Complex for Langley Research Center's National Transonic Facility. Instrument Society of America. 23rd International Instrumentation Symposium, May 1977.

11. Fuller, Dennis E.: Guide for Users of the National Transonic Facility. NASA TM 83124, July 1981.

12. Polhamus, Edward C.; Kilgore, Robert A.; Adcock, Jerry B.; and Ray, Edward J.: The Langley Cryogenic High Reynolds Number Wind-Tunnel Program. Astronautics and Aeronautics, vol. 12, no. 10, October 1974, pp. 30-40.

13. Ferris, Alice T.; and Moore, Thomas C.: Force Instrumentation for Cryogenic Wind Tunnels. Presented at 27th International Instrumentation Symposium, Instrumentation Society of America, Indianapolis, Indiana, April 27-30, 1981.

14. Boyden, Richmond P.; and Johnson, William G., Jr.: Preliminary Results of Buffet Tests in a Cryogenic Wind Tunnel. NASA TM 81923, July 1981.

15. Mabey, Dennis G.: Some Remarks on Dynamic Aeroelastic Model Tests in Cryogenic Wind Tunnels. Transcript of an Informal Lecture and Discussion. NASA CR 145209, 1975.

16. Wentz, William H., Jr.; and Kohlman, David L.: Wind-Tunnel Investigation of Vortex Breakdown on Slender Sharp-Edged Wings. NASA CR 98737, 1968.

17. Mabey, Dennis G.: Some Remarks on Buffeting. RAE Technical Memorandum Structures 980, February 1981.

18. Cryogenic Wind Tunnels. AGARD Lecture Series No. 111, May 1980.

19. Maurer, Franz; Viehweger, Guenther; and Lorenz-Meyer, Wolfgang: Arbeiten der DFVLR auf dem Gebiet der Kryo-Windkanaltechnik. DFVLR-Nachrichten, No. 13, November 1980, pp. 8-12.

20. Goodyer, Michael J.: Cryogenic Wind Tunnel Activities at the University of Southampton. NASA Contractor Report 159144, September 1979.

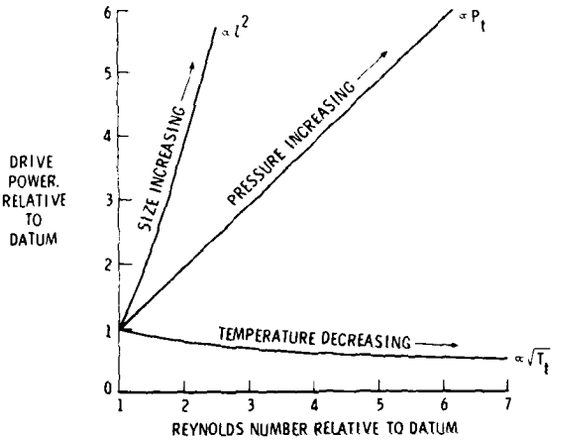


Figure 1.- Drive power requirements for three methods of increasing Reynolds number. M = Constant.

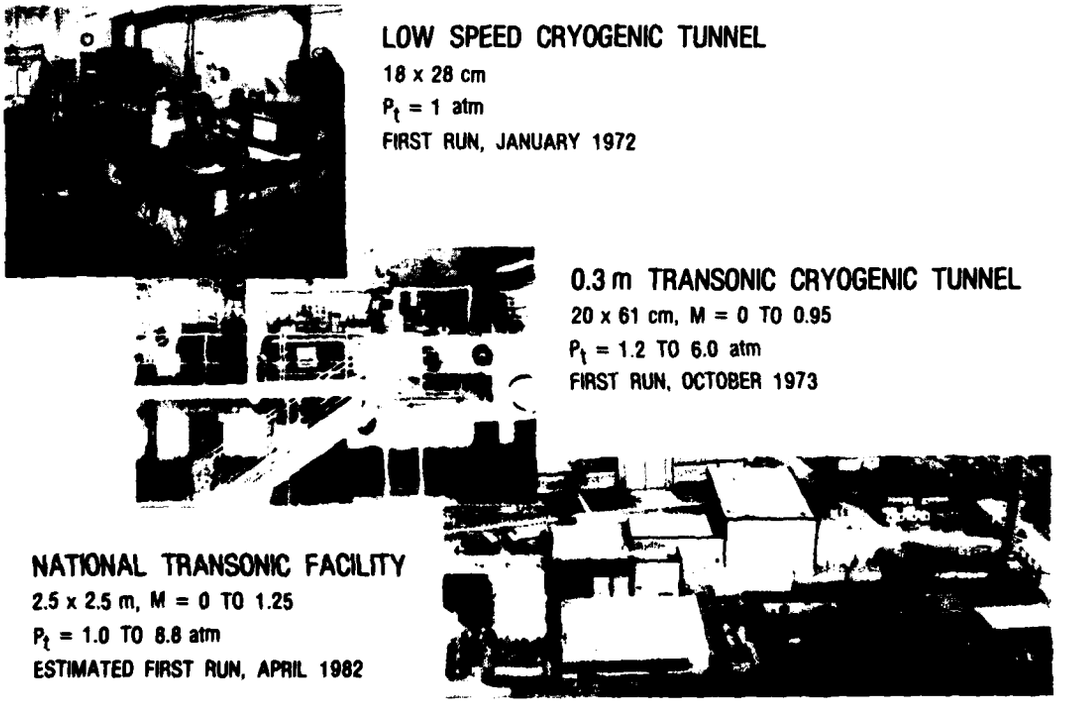


Figure 2.- Evolution of the National Transonic Facility.


Figure 3.- Photographs of the National Transonic Facility. August 1981.

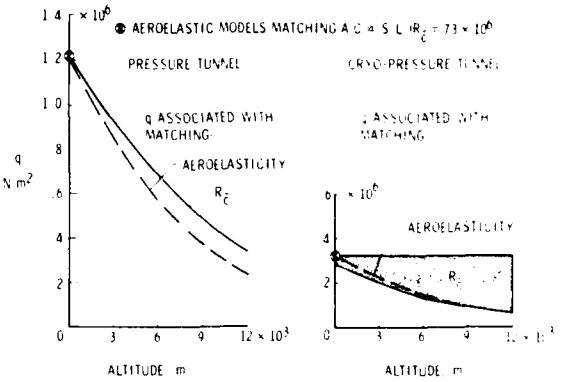


Figure 6.- Effect of altitude on simulation of aeroelastic distortion and Reynolds number. M = 0.9, 2.5 meter tunnel, $\bar{c}$ = 0.142 meter.

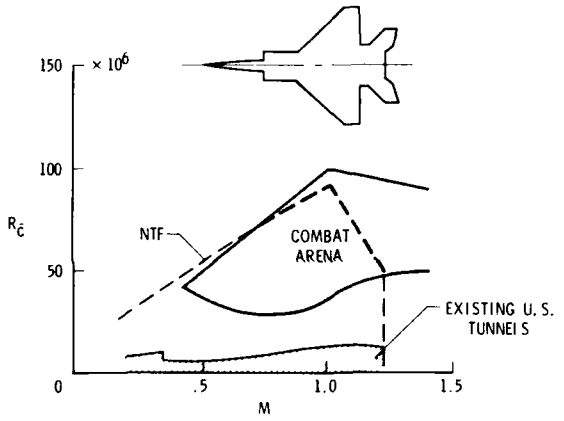


Figure 4.- National Transonic Facility simulation of typical fighter combat arena.

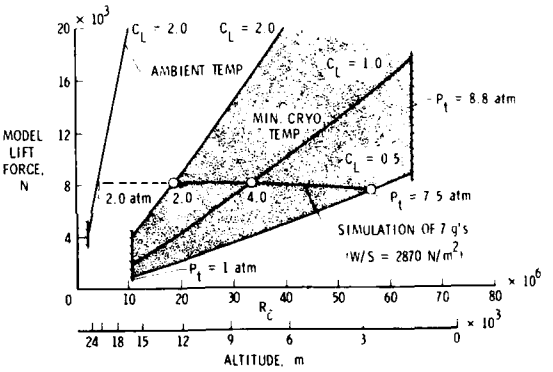


Figure 7.- Effect of cryogenic wind-tunnel operation on model loads for a typical fighter at M = 0.9, 2.5 meter tunnel, model $\bar{c}$ = 0.142 meter.

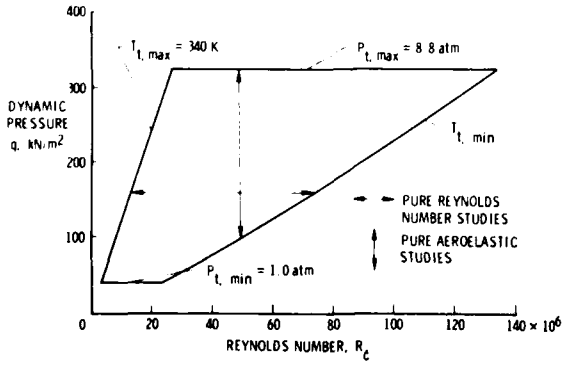


Figure 5.- Constant Mach number operating envelope for a pressurized cryogenic wind tunnel. M = 1.0, 2.5 by 2.5 meter test section.

Figure 8.- Evolution of cryogenic strain-gage balances.

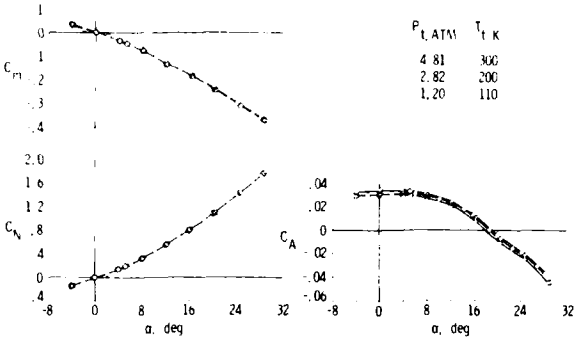


Figure 9.- Balance data at ambient and cryogenic temperatures in the 0.3-meter Transonic Cryogenic Tunnel. M = 0.30, $R_{\bar{c}} = 4.85 \times 10^6$.

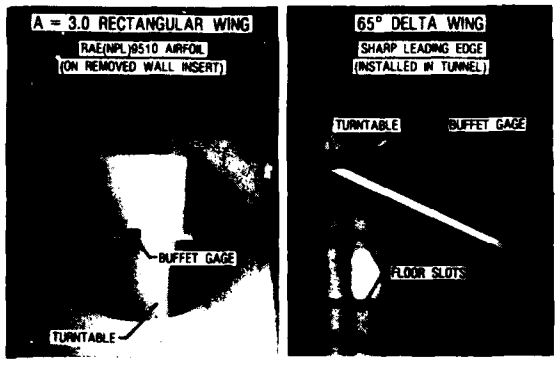


Figure 11.- Buffet models tested in 0.3-meter Transonic Cryogenic Tunnel.

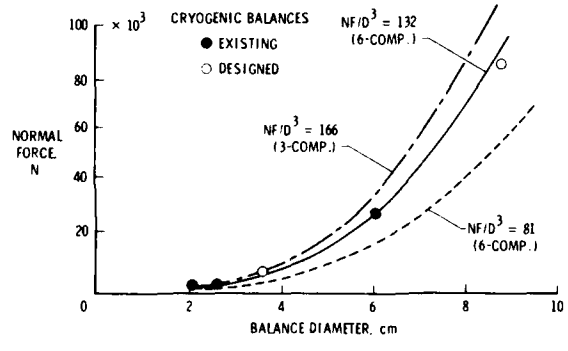


Figure 10.- Balance capacity variation with size.

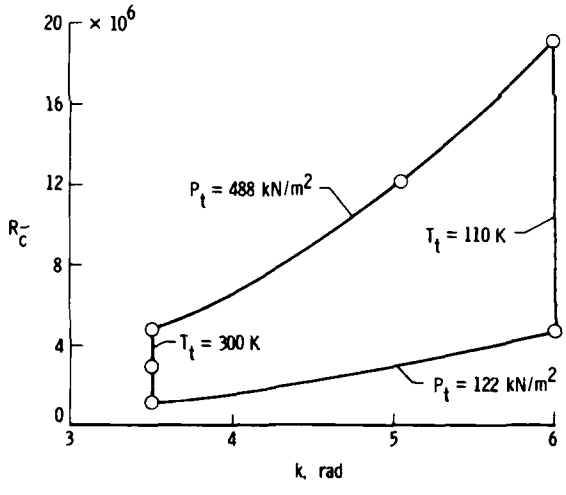


Figure 12.- Reynolds number-reduced frequency envelope for buffet tests of the delta-wing model in the 0.3-meter Transonic Cryogenic Tunnel. M = 0.35, $\bar{c}$ = 0.1355 meter.

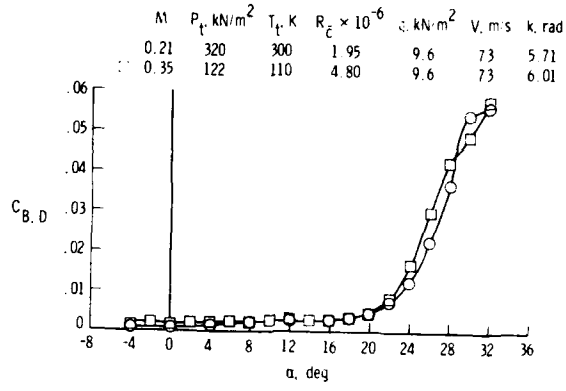


Figure 13.- Comparison of ambient and cryogenic buffet data for the delta-wing model.

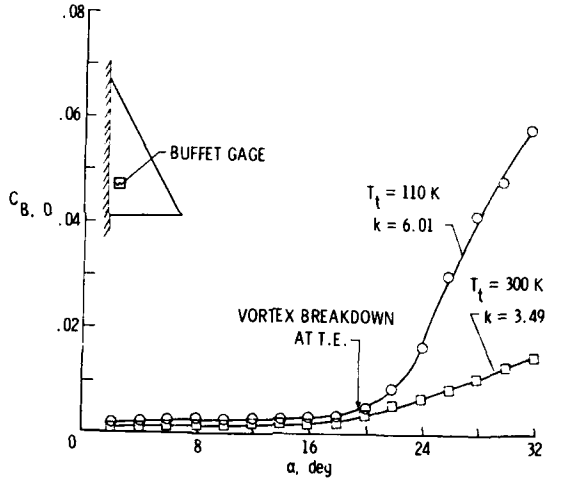


Figure 14.- Effect of reduced frequency on buffet response for the delta-wing model. M = 0.35, $R_{\bar{c}} = 4.80 \times 10^6$.

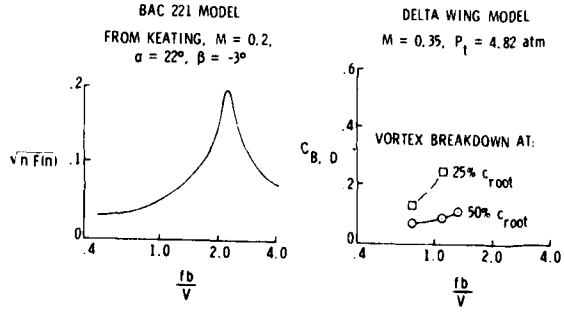


Figure 15.- Effect of frequency parameter on excitation of the BAC 221 model and on buffet results for the delta-wing model.

# ETAT DE L'ART ET PERSPECTIVES NOUVELLES RELATIVES A L'ETUDE DE LA PERTE DE CONTROLE ET DES VRILLES

M.G.VANMANSART et D.R.TRISTRANT

Institut de Mécanique des Fluides
I.M.F.L.(France) 5 bd Painlevé, Lille

*ABSTRACT.-*

During these last years, integration of new technologies was in permanent and rapid evolution, concerning the design of modern fighters, and has considerably enhanced its potential area of use. In a more complex and synthetic manner, we are dealing today with problems connected to flight qualities, manoeuvrability, performance and security.

Under atmospheric disturbances and pilot orders, the dynamic response of the airplane system can be considered as the behaviour result of four sub-systems highly interactive :

- mechanical : mass and inertial aspect
- structural : elastic aspect
- aerodynamic : both high angles and rotations field
- automatic control : concepts, new control-surfaces.

The strong connection in these systems also depends on the airplane configuration and approached flight domain. In particular, it is in the high angles evolutions domain that these connections are the most significant and the requirements in stability and manoeuvrability prediction matter are particularly important from the point of view of security problems. On another hand, in this field, we have to focus the loss of control or spin prevention systems.

The definition of these active or passive means during the design stage, and their reliability require an improved knowledge of the airplane behaviour at the limits of its evolution domain.

Taking into account the complexity of encountered problems for the prediction of the airplane behaviour in high angles, departure or spin domain, there is no unique solution for obviously covering the whole needs. A diversification of complementary methods has to be developed in association with synthesis works which could involve as more as possible components influencing the airplane dynamic response.

The aim of this paper is to present some of these experimental or analysis methods, particularly developed in the I.M.F.Lille, which contribute to the airplane behaviour prediction at high angles and stall/spin. The presentation cannot be exhaustive ; it proposes a brief review of the method, its contribution to the study of considered problem illustrated by a few examples, its limitations and the expected development prospects.

## *1 - INTRODUCTION.-*

Au cours des dernières années,l'intégration de technologies nouvelles en constante et rapide évolution dans la conception de l'Avion d'Armes Moderne a considérablement élargi son domaine potentiel d'emploi et pose aujourd'hui, de façon plus complexe et synthétique, les problèmes liés aux qualités de vols, à la manoeuvrabilité, à la performance et à la sécurité.

La réponse dynamique du système avion soumis aux perturbations atmosphériques et aux ordres pilote peu être considérée comme la résultante du comportement de quatre sous-ensembles aujourd'hui fortement interactifs (planche 2) :

- Mécanique : aspect massique et inertiel
- Structural : aspect élastique
- Aérodynamique : domaine des grands angles et de fortes rotations
- Commande automatique : concepts, gouvernes nouvelles.

L'intensité des couplages entre ces systèmes dépend aussi de la configuration de l'avion et du domaine de vol abordé. C'est singulièrement dans le domaine des évolutions aux grands angles que ces couplages sont les plus marqués et que les besoins en matière de prédiction de stabilité et de manoeuvrabilité, associés aux problèmes de sécurité, sont particulièrement importants. En outre, dans ce domaine, une attention nouvelle est portée sur les systèmes de prévention de perte de contrôle ou de vrille. La définition de ces moyens actifs ou passifs au stade du projet, ainsi que l'évaluation de leur robustesse, nécessitent une connaissance accrue du comportement de l'avion aux limites de son domaine d'évolution.

Compte-tenu de la complexité des problèmes rencontrés pour la prédiction du comportement de l'avion dans les domaines du vol aux grandes incidences, de la perte de contrôle ou de la vrille, il est clair qu'aucune technique ne peut couvrir l'ensemble des besoins. Une diversification de méthodes complémentaires doit être développée, associée à des travaux de synthèse permettant la prise en compte du plus grand nombre de composantes intervenant dans la réponse dynamique de l'avion.

L'objectif de ce papier est de présenter un certain nombre de ces méthodes expérimentales ou d'analyses, en développement notamment à l'I.M.F.Lille, contribuant à la prédiction du comportement de l'avion aux grands angles, perte de contrôle et vrille. La présentation ne peut être exhaustive, réf.{1} et {2} ; elle propose un bref exposé de la méthode, sa contribution à l'étude du problème considéré illustrée par quelques exemples, ses limitations et les perspectives de développement envisagées.

## 2 - *TECHNIQUES EXPERIMENTALES APPLIQUEES A L'ETUDE DE LA PERTE DE CONTROLE, GRANDES INCIDENCES ET VRILLES.-*

### 2.1 - *Remarques générales - Présentation d'ensemble des diverses approches expérimentales.*

Les techniques d'essais sur maquettes, applicables à l'étude des grandes incidences-vrille, recouvrent, d'une part les méthodes classiques de soufflerie : détermination des caractéristiques aérodynamiques statiques et dynamiques et, d'autre part, des techniques spécifiques en constant développement faisant appel aux maquettes libres ou semi-libres.

La figure 3 présente une classification d'ensemble des techniques expérimentales mises en oeuvre.

Compte-tenu du nombre de variables à considérer et de l'amplitude du domaine de variation des paramètres, les essais en soufflerie sur maquettes captives feront appel à des montages variés sollicitant les divers degrés de liberté et seront coordonnés par un programme expérimental général très étroitement connecté à la structure considérée de la modélisation mathématique du torseur aérodynamique (voir réf.{3}).

L'apport des essais sur maquettes libres est fondamental dans ce domaine d'étude car ils représentent une approche synthétique indispensable à la validation des travaux de base relatifs à l'élaboration de modèles mathématiques de représentation, et qu'ils constituent une voie directe quasi-unique de prédiction globale de comportement dans le domaine de la perte de contrôle, de l'efficacité des systèmes de prévention et des techniques de récupération. Ces méthodes permettent également d'établir des corrélations directes avec les essais grandeur.

Sur la validité de ces techniques et leur représentativité, un commentaire généralement formulé est celui des effets de Reynolds et de Mach. Les essais classiques en soufflerie apportent sur ce point des éléments de réponse et un certain apaisement. Les effets du nombre de Reynolds sont étroitement liés à la configuration géométrique. Pour les avions d'armes, la configuration voilure fléchée et bord d'attaque mince est relativement insensible au nombre de Reynolds jusqu'à des valeurs basses d'environ $0.5\ 10^6$, notamment pour les caractéristiques de décrochage et de stabilité latérale aux grands angles : perte de contrôle, vrille débutante. Dans le domaine de vrille proprement dit, les effets les plus significatifs du nombre de Reynolds sont attribués au rôle déterminant du fuselage, en particulier de la géométrie de l'avant. Les sections circulaires de fuselage-avant sont réputées peu sensibles au nombre de Reynolds alors que l'effet est déterminant pour des sections plus anguleuses.

De manière générale, la fiabilité de la prédiction des vrilles en soufflerie est bonne. Elle est illustrée par la corrélation avec les résultats grandeurs (§1.4) : les cas de vrille sont plus nombreux en soufflerie que sur avion, mais incluent toujours les cas réels. Les essais à tendance pessimiste de la soufflerie peuvent être imputés aux conditions initiales et à l'environnement calme de la maquette.

Les effets du nombre de Mach sont aujourd'hui encore très difficiles à apprécier car le domaine d'incidence dérapage à étudier n'est pas suffisamment couvert par les souffleries trans ou supersoniques.

### 2.2 - *Essais sur maquettes captives en soufflerie.*

#### 2.2.1 - *Aspects généraux - réf.{4}, {5}, {6}, {7} et {8}*

Ces techniques sont aujourd'hui très répandues et en constant développement. Leur diversification, en particulier dans les montages dynamiques, résulte du double souci d'une simulation dynamique représentative des évolutions variées de l'avion et de l'observabilité des coefficients de stabilité dynamique sur la base d'un modèle de représentation approprié.

Les essais statiques en soufflerie jusqu'aux très grands angles d'incidence-dérapage, et les efficacités statiques des gouvernes, constituent la base de l'identification aérodynamique de l'avion. Ces essais doivent être menés avec de particulières précautions compte-tenu des fortes non linéarités et des grandes amplitudes de variations, associées à de forts couplages des composantes du torseur aérodynamique (variations de $\alpha$, $\beta$ par pas très faible ou excursion en continu dans le domaine ( $\alpha$, $\beta$ ). En préalable aux essais et à l'analyse des contributions dynamiques, la modélisation du torseur statique doit être envisagée avec une attention spéciale. Elle contribue notamment de façon déterminante à la recherche d'états ou de domaines probables d'équilibre de vrille stationnaire en y adjoignant, ultérieurement, l'effet de $\Omega$ continu (avec $\vec{\Omega}$, $\vec{V} = 0$) ainsi qu'à une prédétermination des domaines d'instabilité permettant d'apprécier les tendances à la perte de contrôle.

Au stade préliminaire, ce caractère est usuellement apprécié par des critères du type $C_{n_{\beta\ dyn}}$ ou LCDP > 0. Quelques remarques sur l'aspect modélisation du torseur statique sont formulées plus loin.

En addition à la reconnaissance du torseur statique, l'identification de la contribution des paramètres dynamiques, introduits par des évolutions du type grands mouvements amples et rapides (perte de contrôle, récupération), oscillations, ou rotations continues avec superposition éventuelle d'agitations (vrilles stationnaires ou agitées), nécessite le développement en soufflerie de moyens de simulation dynamique.

Les principales caractéristiques de ces techniques expérimentales sont proposées planche 5.

De même que pour les essais statiques, les techniques dynamiques ne couvrent pas à l'heure actuelle simultanément le domaine ( $\alpha$ , $\beta$ , M, Re) souhaité. Ces techniques peuvent être classées selon trois types principaux de mouvements simulés :

- Technique d'oscillations forcées autour d'un état moyen
- Technique de balance dynamique en rotation uniforme
- Technique des grands mouvements non périodiques

permettant notamment de décrire des trajectoires dans l'espace d'état.

Certains montages en soufflerie permettent une superposition de ces mouvements.

Mentionnons l'apport déterminant de ces expériences dans des études paramétriques : effet de Re, M, gouvernes, amplitude et fréquence réduite et l'excellente adaptation à une instrumentation extensive. Cependant, les interférences aérodynamiques ou mécaniques de la soufflerie et du montage créent de délicats problèmes dans le traitement des informations {voir réf. 9}.

*2.2.2 - Technique des oscillations forcées et des grands mouvements.*

Ces méthodes sont bien connues car exploitées depuis près de vingt ans, et demeurent d'une grande actualité dans le domaine des grands angles. Leur contribution associée aux résultats statiques fournit des informations précieuses dans le régime du décrochage et du début de la perte de contrôle, car les facteurs d'amortissement dépendent fortement des variables d'état et de leurs dérivées. Dans le domaine de la vrille, leur contribution est plus douteuse. On ne connait pas en effet aujourd'hui le rôle joué par le caractère hélicoïdal de l'écoulement lié à la rotation uniforme vis-à-vis des amortissements provenant des oscillations autour de cet état moyen. Des équipements spécifiques permettant de superposer oscillations en roulis ou lacet et rotation uniforme sont en développement à l'I.M.F.L. afin de valider cette hypothèse {réf.10} (planche 10).

Un montage typique destiné aux mesures par oscillations forcées est présenté planche 6.

Il prend place dans la soufflerie horizontale de l'I.M.F.L. (diamètre 2,5 m, 55 m/s).

Il permet le positionnement de la maquette dans le domaine $\alpha$ , $\beta \pm 90°$ et d'établir des rotations autour des axes maquette selon p, q et r indépendamment ou de façon combinée.

Les modes de fonctionnement en p r et p q sont représentés sur cette planche.

Ce montage est animé autour des 3 axes par des moteurs hydrauliques pilotés par servo-valves et générateurs de fonctions. La maquette est portée par une balance six composantes.

Le mode de fonctionnement usuel de ce montage est celui d'oscillations forcées pour lesquelles un découplage des divers degrés de liberté a été recherché, associé à un domaine extensif d'incidence dérapage. Des exemples de résultats sont présentés planche 7 et planche 8 : effet classique amortisseur-moteur du $C_{lp+\dot{\beta}}(\alpha)$, effet de l'amplitude et de la fréquence sur $C_Y(\beta)$ en oscillation forcée de lacet.

Un autre mode de fonctionnement du montage est actuellement étudié pour permettre de réaliser des trajectoires dans l'espace d'état (p, q, r) à partir de lois représentatives d'un mouvement type perte de contrôle, identifié par ailleurs (maquette de vol libre), et reproduit en soufflerie. Cette procédure devrait permettre d'étudier la stabilité du phénomène autour de cette trajectoire nominale {10}.

Une deuxième possibilité serait également offerte, Elle consisterait, pour les mouvements autour du centre de gravité, à réaliser une loi de $\vec{\Omega}(t)$ calculée en temps réel en fonction des mesures instantanées du torseur réduit à L M N de telle sorte que celui-ci soit nul pour une maquette en similitude dynamique de l'aérodyne. Il est indispensable d'associer à cette procédure les entrées du type gouvernes. Ces méthodes très attractives sont néanmoins très délicates de mise en oeuvre.

Un autre dispositif expérimental de la même famille et de plus forte capacité fonctionnant dans la même soufflerie est représenté planche 9. Il est utilisé à la fois pour les mesures en statique, en oscillations forcées : tangage ou lacet ou roulis dans une variante du montage non représentée, et permet, dans le domaine ($\alpha$ , $\beta$ 45°), des mouvements selon des lois variées pour des maquettes de plus grande taille (1,5 m).

*2.2.3 - Balance rotative de l'I.M.F.L.*

La balance rotative de l'I.M.F.L. permet la mesure de caractéristiques aérodynamiques dans un très large domaine d'incidence-dérapage pouvant présenter des mouvements de rotation élevés et continus. Ainsi,ce montage a été conçu pour couvrir deux grandes gammes d'essais : d'une part,l'étude du domaine de vol jusqu'aux grandes incidences avec la possibilité d'y adjoindre un taux de rotation, d'autre part : l'étude de la vrille avec la possibilité de simuler un tel mouvement avec de nombreux degrés de liberté.

*Description du montage.*

La balance rotative est installée dans la soufflerie verticale de l'I.M.F.L. La planche 10 présente un schéma du montage avec ses différents degrés de liberté et les limitations cinématiques sur chacun d'eux.

Pour un descriptif complet et détaillé, nous renvoyons le lecteur à {11} mais nous rappellerons toutefois que :

- la vitesse maximum de la soufflerie est de 40 m/s
- la taille maxi des maquettes est de 1,5 m
- les gouvernes de la maquette peuvent être éventuellement motorisées
- les originalités de ce montage vis-à-vis d'autres balances rotatives résident dans l'existence des paramètres suivants :
  - $\lambda$ = angle entre la vitesse $\vec{V}$ du vent et l'axe de la rotation principale du montage (en $\Omega$ ou $\dot{\psi}$)
  - R = rayon vrille : distance entre le centre de gravité et l'axe de vrille
  - $\psi_r$ = cap relatif : angle sous lequel le nez de l'avion regarde l'axe de vrille
  - et, lorsque $\lambda = 0$, l'axe de rotation est vertical, ce qui annule l'effet pulsatoire de la pesanteur sur les mesures en rotation et donc les vibrations du système.

Deux motorisations existent aujourd'hui sur ce montage permettant les rotations continues en $\Omega$ et en $\dot{\phi}$ suivant les deux sens de rotation.

Plus de détails quant aux possibilités cinématiques du montage sont fournis dans {12}. En particulier, cette balance rotative peut, grâce au paramètre $\lambda$, dissocier les coefficients aérodynamiques du type $C_{mq}$ ou $C_{nr}$ de ceux du type $C_{m\dot{\alpha}}$ ou $C_{n\dot{\beta}}$ dans le domaine des petits angles.

*Mesures - Traitement.*

La chaîne d'acquisition associée au montage dispose de 30 voies de mesures permettant ainsi d'obtenir des informations simultanées de la pression cinétique, des différentes voies balance et des différents paramètres cinématiques. Chaque information est codée sur 12 bits ; d'autre part l'échantillonnage des signaux peut être effectué jusqu'à la fréquence maximale de 780 Hz. Toutes les informations sont stockées sur bande magnétique et font l'objet d'un traitement différé {12} qui comporte un filtre numérique passe-bas optionnel précédant un second échantillonnage. Cette nouvelle discrétisation réside dans une procédure de moyennes à l'intérieur de fenêtres découpées sur l'angle de rotation $\psi$. L'analyse spectrale du signal périodique est obtenue par FFT et permet ensuite d'effectuer dans le domaine fréquentiel la réjection des raies résultant de bruits structuraux ou électriques, celles-ci ayant été préalablement identifiées.

*Résultats.*

Des essais en rotation continue sur avion d'armes ont été effectués à l'I.M.F.L.. Quelques résultats de ces essais sont présentés planches 11 et 12. Celles-ci représentent, sur une période en $\psi$, la variation des coefficients aérodynamiques, de l'incidence et du dérapage, p, q et r étant constants au cours d'un essai.

La planche 11a correspond à un essai à $\lambda = 0$, c'est-à-dire avec $\alpha$ et $\beta$ constants, aux corrections de soufflerie près.

L'analyse des résultats de ces essais (à $\dot{\alpha}, \dot{\beta}$ nuls) pour diverses valeurs de $\Omega$ dans le domaine des angles "normaux" débouche sur l'identification des coefficients dérivés liés à p, q, r.

Puis, dans un second temps, le basculement du montage par rapport à la direction du vecteur vitesse permet d'effectuer des rotations où incidences et dérapages varient au cours d'un tour. Ce type d'essai introduit donc la contribution des variables supplémentaires que sont $\dot{\alpha}$ et $\dot{\beta}$. Sur la planche 11b figure le résultat d'un essai de ce type, à p, q, r constants.

Tant qu'incidence et dérapage restent dans le domaine des petits angles, le modèle linéaire classique de mécanique du vol reste valide, et de tels essais permettent alors d'identifier les coefficients aérodynamiques liés aux dérivées $\dot{\alpha}$ et $\dot{\beta}$.

Puis, sur les figures 12a et 12b, nous avons représenté deux résultats d'essais similaires (l'un sans, l'autre avec $\lambda$) mais dans une gamme d'incidences beaucoup plus élevée ($\alpha_{moyen} = 45°$). On peut noter alors l'apparition d'oscillations sur les coefficients de moments (surtout sur le $C_n$), même pour l'essai à $\alpha$ constant et $\beta$ nul. Un peu plus loin, nous essayerons de donner une interprétation de ce phénomène.

Quant à l'essai à $\lambda = 20°$, où l'incidence varie entre 65° et 25° (fig.12b), alors que le dérapage varie entre -20 et 20°, on voit de très fortes variations des coefficients. Cet essai, très riche en informations, est toutefois très difficile à interpréter.

*2.3 - Essais sur maquettes libres en laboratoire.*

Les méthodes expérimentales sur maquettes libres contribuent de façon déterminante et fiable à la prédiction de comportement de l'avion aux grands angles, tout particulièrement du fait d'une représentation globale du système avion et des évolutions caractéristiques. Elles permettent aussi d'établir des corrélations directes avec l'avion.

Ces méthodes sont développées à l'I.M.F.Lille depuis 1965 et sont exploitées dans des domaines variés : identification de paramètres{réf. 13} (stabilité et contrôle, qualités de vol aux grands angles, techniques du contrôle actif, ainsi qu'à l'étude du comportement en turbulence ou pour des études d'impact (atterrissage). Le domaine d'applications considéré ici est présenté planche 13.

Les aspects spécifiques de cette méthode sont rappelés planche 14. Elle bénéficie notamment des conditions de laboratoire en ce qui concerne l'environnement, et de possibilités de sollicitations variées introduites aux conditions initiales et au cours du vol libre.

La méthode expérimentale est simple. Des maquettes non propulsées, en similitude dynamique, sont mises en vol libre au moyen d'une catapulte, le vol libre recouvrant un parcours de 35 à 50 m selon les installations, avant récupération de la maquette.

Les principales spécifications relatives à la maquette, à son instrumentation, aux entrées, aux conditions initiales ainsi qu'aux équipements sol sont présentées planche 15.

Cette technique en constante évolution permet l'intégration dans les maquettes de capteurs et d'actionneurs de hautes performances associés à des systèmes de télémétrie et de télécontrôle numériques, ainsi que la mise en oeuvre de microprocesseurs embarqués pour la génération de lois de commande et la création de boucles de pilotage internes. Des logiciels spécifiques sont développés pour l'acquisition et la génération de boucles de contrôle en temps réel, pour l'élaboration des variables d'états et la restitution du torseur aérodynamique à partir des données trajectographiques et dynamiques, ainsi que pour l'identification de paramètres (on trouvera, en réf.{13}, plus de détails sur ces méthodes).

Deux laboratoires de vol libre sont exploités à l'I.M.F.L. Une vue générale de ces installations est présentée planche 16 et planche 17.

La première d'entre elles est utilisée pour l'identification de paramètres, coefficients stationnaires, paramètres de stabilité dynamique ou efficacité de gouvernes à partir de vols libres. Des études de qualités de vol y sont réalisées : vol aux grands angles, stabilité et manoeuvrabilité, études de gouvernes nouvelles, technologie du contrôle actif. Elle est par ailleurs équipée de générateurs de rafales et d'une table d'impact, pour des études de vol en turbulence et d'atterrissage.

La seconde installation est spécifiquement destinée aux études de décrochage, perte de contrôle, vrille débutante, prévention de perte de contrôle ou de vrille. Cette installation, en cours de développement, sera opérationnelle courant 1982. Des essais de vrille débutante viennent d'y être réalisés et les premiers résultats obtenus sont particulièrement démonstratifs.

Nous illustrons les possibilités de ces méthodes expérimentales par un exemple simple présenté planche 18. Les résultats se rapportent à des essais d'efficacité d'une commande automatique de stabilisation de facteur de charge normal avec ou sans superposition d'ordre pilote. L'ordre pilote est ici un double créneau à la direction superposé à la commande automatique. De tels essais sont réalisés en paramétrant notamment les conditions initiales : incidence, dérapage, en installant des conditions dynamiques au largage (p, q, r, $\Delta n_z$ ...) etc. Ils contribuent à l'ouverture d'un domaine de vol, à l'examen de la manoeuvrabilité en liaison avec la simulation.

*2.4 - Les essais sur maquettes libres en soufflerie verticale.*

*2.4.1 - Essais classiques.*

Les essais de vrille libre ont commencé à l'I.M.F.L il y a plus de 30 ans et, à ce jour, près de 200 maquettes d'avions de tous types (armes, transport, légers) ont été essayées, et les nombreuses corrélations des vrilles maquette et avion ont montré l'utilité de ces essais en soufflerie verticale.

La soufflerie verticale permet, en premier lieu, d'étudier la vrille stabilisée et la récupération à partir de cette vrille ; dans certains cas, il est également possible d'obtenir des renseignements sur l'établissement de la vrille. Cependant, il est bien évident que la soufflerie verticale ne peut pas couvrir la phase d'entrée en vrille. Celle-ci sera analysée par des méthodes de vol libre en laboratoire ou par maquettes atmosphériques télépilotées (M.A.T.).

La soufflerie verticale présente l'avantage de pouvoir étudier avec le meilleur rapport efficacité/coût l'influence de tout paramètre sur la vrille et la sortie de vrille d'un avion :

- Paramètres massiques : masse, centrage, inerties, chargement dissymétrique, altitude
- Paramètres géométriques : volets, becs, aérofreins, train d'atterrissage ...
- Paramètres massiques et géométriques : charges externes.

De plus, lors de l'étude de l'avion à l'état de projet (alors que sa géométrie n'est pas encore totalement figée), il est facile de prévoir sur la maquette des éléments amovibles permettant de représenter plusieurs géométries du projet.

Par ailleurs, la soufflerie verticale permet de définir les caractéristiques d'un moyen de secours (parachute, fusée, arêtes) approprié au type de problème éventuellement rencontré.

Enfin, comme nous le verrons ultérieurement, certaines maquettes de vrille (suffisamment dimensionnées) sont instrumentées afin de définir avec précision les caractéristiques cinématiques de la vrille (planche 23).

En dehors des études propres aux aviors existants ou en projet, des études à caractère général sont entreprises : études paramétriques faites sur des maquettes démontables et permettant de représenter de nombreuses et diverses géométries de la voilure et/ou du fuselage et/ou des empennages. A ce sujet, citons une étude récente relative à la vrille des avions d'armes actuels. Ces avions sont caractérisés, entre autres, par un avant de fuselage très long, générateur de fortes asymétries d'écoulement aux grands angles, susceptibles notamment de créer des difficultés de récupération de vrille. C'est le problème dit de "longs nez" dont l'importance est mise en évidence, ne serait-ce que par l'abondance des travaux effectués sur le sujet.

Nous nous proposons ici de décrire comment s'est présenté l'un des problèmes liés aux "longs nez" lors des essais dans la soufflerie verticale de l'I.M.F.L.

Au cours d'une étude à caractère général, nous avons représenté sur une maquette d'avions d'armes des nez de formes diverses et parfois même non réalistes (planche 19).

A la suite des résultats de cette campagne d'essais, nous avons pu classer les nez en 3 groupes (planche 20) :

- nez dits "bons"
- nez dits "moyens"
- nez dits "mauvais".

Précisons maintenant ce que nous entendons par nez bon et nez mauvais : un nez est dit "bon" si, pour une certaine géométrie de la maquette, à partir d'une vrille stationnaire, en amenant les gouvernes pour la récupération, cette dernière est obtenue systématiquement. Par contre, avec un nez mauvais, la récupération peut ne pas être obtenue : nous observons alors une vrille très lente, souvent oscillatoire, qui peut se maintenir longtemps, à la limite se perpétuer.

Il faut préciser qu'avec un "nez mauvais" le problème de sortie n'apparaît pas systématiquement. En début d'étude, l'évolution de la vrille vers une franche sortie ou vers une vrille maintenue nous a paru aléatoire ; mais,par la suite,nous nous sommes aperçus que le caractère du phénomène final dépendait uniquement de la géométrie de l'extrême pointe du nez. Ainsi, une faible imperfection de cette pointe pouvait conditionner le phénomène et il suffisait de déplacer (par rotation du nez autour de son axe) cette imperfection pour transformer une franche récupération en refus de sortie, et inversement. Par contre, pour un nez dit bon, sa rotation n'a aucune influence sur la sortie.

De même, dans la suite des essais, il nous suffisait de placer une petite singularité sur la pointe du nez, au bon endroit, pour obtenir systèmatiquement une bonne sortie, ou au mauvais endroit pour obtenir systématiquement une sortie douteuse.

Précisons que ce dernier résultat peut être obtenu même avec les gouvernes à fond pour la sortie ; ainsi l'effet des gouvernes devient secondaire en regard de celui de la petite déformation du nez.

Une autre remarque est également à signaler : à priori nous aurions pu envisager que plus le nez est long, plus le problème de sortie serait marqué. Cela n'est absolument pas le cas (planche 20).

En soufflerie, nous avons pu réduire l'importance du problème "long nez", voire même le supprimer par divers moyens dont le plus sûr semble être des virures (planche 21).

La question qui se posait alors était de savoir si le problème long nez trouvé en soufflerie pouvait apparaître également sur l'avion. Après analyse de documents relatifs à diverses campagnes d'essais en vol et à certains incidents ou accidents de vrille, il est apparu que le problème pouvait être rencontré sur avion ; nous avons pour exemple des enregistrements de vrille que nous présentons (planche 22):

Dans le 1er cas de vrille (vrille très agitée mais à agitations organisées), les gouvernes sont recentrées pour obtenir la sortie ; cette dernière est obtenue mais très tardivement : c'est un exemple de sortie douteuse du type de celle trouvée en soufflerie, mais rappelons que les gouvernes ne sont que recentrées.

Dans le 2ème cas, le gauchissement (gouverne en principe prépondérante sur cet avion) est amené à fond pour la sortie. Cette manoeuvre n'a pas d'influence sur la sortie qui reste très longue : comme en soufflerie, l'effet des gouvernes devient secondaire.

Dans le 3ème cas, l'avion est équipé de virures. La vrille est nettement moins agitée et la durée de sortie est divisée par deux. Comme en soufflerie, les virures ont un effet favorable vis-à-vis de la récupération.

*2.4.2 - Instrumentation des maquettes de vrille libre.*

Jusqu'à une époque récente, les essais de vrille libre en soufflerie se faisaient à l'aide de maquettes dynamiquement semblables à l'avion (masse, inerties, altitude) dont les gouvernes pouvaient être radio-télécommandées, d'abord par tout ou rien, puis par commande proportionnelle. Les caractéristiques principales des phénomènes étaient relevées à vue, avec recours éventuel à des dépouillements de film pris à cadence accélérée pour analyser plus finement, en différé, certaines évolutions très rapides et/ou complexes. Cependant, les valeurs retenues ne portaient uniquement que sur les paramètres fondamentaux de description géométrique et cinématique de la vrille, à savoir :

- vitesse angulaire $\Omega$ et linéaire V
- attitudes $\theta$ et $\phi$,
- rayon de vrille R, et éventuellement le cap relatif associé $\psi_r$ (planche 10).

Notons que, pour des essais classiques, cette procédure reste actuelle.

Cependant, nous verrons plus loin, que, pour des études générales, ou pour des recoupements avion-maquette plus complets (notamment pour les vrilles agitées), ou encore pour les besoins de "la visualisation de la vrille " au pilote sur simulateur ou console graphique, il est apparu indispensable d'instrumenter la maquette de façon plus complète.

L'instrumentation des maquettes de vrille devient possible avec l'incessante miniaturisation de capteurs embarquables performants et de leur électronique associée, moyennant - dans un premier temps - une adaptation de la taille des maquettes (+ 30 %, soit au total près d'un mètre pour la longueur du fuselage), ainsi que de leur type de construction (thermo-formage, fibres de verre, de carbone, Kevlar) afind'accroître au maximum les capacités d'emport du fuselage qui se trouve ainsi creux et très léger tout en gardant un maximum de solidité pour subir au mieux les essais.

Ainsi, des maquettes d'avions d'armes récents et même des maquettes d'avions légers ont pu être équipées en partie des installations suivantes :

- recopies de gouvernes
- accéléromètres
- gyromètres (3)
- asservissements de gouvernes à des gyromètres
- asservissements de dispositifs de secours à des accéléromètres et gyromètres
- motorisation (couple gyroscopique, et éventuellement - pour les avions légers à hélice - effets séparés de la traction, couple de renversement, sans oublier l'effet global)
- soufflage de l'extrados de la voilure, etc ...

Un exemple de résultats est donné planche 23.

Par ailleurs, au travers du concept CAG, la résistance de l'avion au départ en vrille est l'objet d'une attention spéciale. Il est donc hautement souhaitable de pouvoir instrumenter les maquettes de vrille de façon la plus complète possible. Ces maquettes seraient utilisables à la fois en soufflerie verticale et dans le laboratoire de vrille débutante déjà décrit. Les essais actuellement réalisés permettent d'augurer d'une telle faisabilité.

*2.5 - Essais sur maquettes libres atmosphériques télépilotées.*

Une nouvelle technique complémentaire pour l'étude de la vrille des avions légers, développée à l'I.M.F.L., est rapidement mentionnée dans cette communication.

Elle utilise comme support d'expérience des maquettes atmosphériques télépilotées (MAT). La maquette pour ces essais est en similitude de Froude, à l'échelle d'environ 1/5, motorisée et instrumentée, la masse variant de 5 à 6 kg suivant l'équipement.

Pour la première campagne d'essais, l'objectif de base a été d'évaluer la validité de ce moyen d'essai. Pour cela, nous avons mené parallèlement, sur une même maquette, des essais de vrille en soufflerie verticale et des vols atmosphériques télépilotés. Une bonne corrélation entre ces deux moyens d'essais a pu être mise en évidence :

- démonstration de modes de vrille différents selon le sens de rotation
- effet de la présence d'arêtes ventrales sur ces deux modes.

Les MAT se présentent comme un moyen d'essais offrant la possibilité d'étude du phénomène global : perte de contrôle, vrille, récupération, à des Reynolds plus favorables vis-à-vis de la perte de contrôle avec prise en compte de la motorisation.

*3 - AUTRES METHODES D'ETUDES.-*

*3.1 - Figuration animée des mouvements aux grands angles.*

Au cours des essais en vol, lors des premiers tours de vrille, surtout pour un avion dense, la trajectoire n'est pas verticale et l'évolution des valeurs des assiettes ne ressemble en rien à celle observée en soufflerie lors de phénomènes identiques.

Les planches 24 et 25 mettent en évidence la divergence de résultats sur les attitudes pour des mouvements absolument identiques mais décrits autour de trajectoires différentes. Les essais grandeur et ceux de soufflerie ne sont donc généralement pas directement comparables, du moins en ce qui concerne les paramètres géométriques de description de la vrille identifiés en soufflerie et les mêmes perçus par le pilote.

A ce propos, à partir des enregistrements effectués en vol lors de la campagne d'essais de vrille d'un avion d'armes, un logiciel a été mis au point, permettant la représentation des évolutions de l'avion, au cours de l'essai, telles qu'elles sont observées en soufflerie verticale (vrille avion → vrille soufflerie). Autrement dit, l'originalité de cette animation électronique (sur console graphique) réside dans le fait que la description des mouvements de l'avion a lieu dans un repère lié à la trajectoire moyenne (l'axe de l'hélicoïde de la vrille), qui correspond alors à l'axe de la soufflerie verticale.

Il y a donc similitude des paramètres géométriques de description de la vrille.

D'autre part, une méthode de figuration permet de représenter aux pilotes, à partir des enregistrements de soufflerie (paramètres cinématiques), une visualisation directe de leur horizon et/ou d'instruments de bord (boule pilote entre autres) (vrille soufflerie → vrille avion). Cette "visualisation pilote" contribue de façon avantageuse à la formation des pilotes par la reconnaissance des différents mouvements de la vrille envisageables sur l'avion considéré, et ce après transposition du mouvement autour d'une trajectoire tendue, comme c'est le cas pour l'avion.

Très démonstratives, ces méthodes d'animation peuvent contribuer à :

- faciliter la comparaison des résultats avion et maquette
- démontrer rapidement la validité d'une modélisation mathématique de la vrille
- avertir le pilote d'essais du genre de phénomènes qu'il rencontrera sur son avion
- former les pilotes et leur permettre de reconnaître les divers mouvements (ce qui n'est souvent pas évident) afin d'appliquer la consigne adéquate.

L'intérêt pédagogique de la figuration animée de la vrille n'est plus à démontrer, surtout pour les phénomènes très agités et, de surcroit, lorsque l'entraînement volontaire sur avion est interdit.

### *3.2 - Comparaisons vols-soufflerie de vrille.*

La transposition des résultats de soufflerie et leur validation, la prise en compte de l'opinion du "pilote" rendent indispensable un rebouclage des informations entre la soufflerie et les vols avant les essais grandeur, et entre les vols et la soufflerie après ces mêmes essais. En particulier, avant les vols, les discussions échangées entre souffleurs et pilotes présentent deux intérêts majeurs :

- illustration aux pilotes des phénomènes attendus,
- optimisation des consignes avec prise en compte de la charge du pilote et de sa propre expérience.

Après les essais grandeur, la comparaison vols-soufflerie est systématiquement envisagée. Pour être valable, elle ne peut s'appuyer que sur les enregistrements des paramètres dynamiques et des gouvernes. Afin de s'affranchir de la pente de la trajectoire réelle, les enregistrements sont alors traités afin de procéder notamment à la figuration animée vols → soufflerie exposée précédemment. Celle-ci s'avère parfois indispensable comme on peut le constater en se reportant à la planche 26. Sur cette planche, figurent les simulations de 4 vrilles agitées différemment:

La première est agitée seulement selon "l'angle de gîte" $\Phi$ , celui observé autour d'une trajectoire verticale ou redressée verticalement : les composantes p et q sont agitées.

La deuxième vrille est agitée seulement selon "l'assiette longitudinale" $\Theta$ : les trois composantes p, q et r sont cette fois oscillées.

Or, les trois composantes de $\Omega$ sont également agitées si la vrille est agitée à la fois en $\Theta$ et $\Phi$ et, de plus, les phases sont les mêmes que précédemment. La seule différence "visible" est dans l'amplitude balayée par p : plus forte maintenant que dans le deuxième cas.

Le quatrième exemple montre qu'un déphasage affectant une des deux voies $\Theta$ ou $\Phi$ peut affecter l'amplitude des trois voies de mesure en laissant supposer une vrille à agitations sur $\Theta$ et $\Phi$ plus ou moins fortes, alors qu'elles sont inchangées.

Dans de tels cas, la figuration animée (vols → soufflerie) de la vrille rend de précieux services.

Parmi d'autres traitements des informations grandeur, citons la restitution des coefficients aérodynamiques et leurs recoupements avec les résultats de la balance rotative, pour des mêmes conditions d'essais.

La comparaison vols/soufflerie, qui est effectuée chaque fois que possible, a fait que la méthode d'essais a évolué sans cesse et que l'interprétation des résultats et les conclusions ont ainsi été améliorées.

Quant aux éventuels "écarts" entre la soufflerie et les vols, ils sont de deux sens :

- en ce qui concerne les avions légers, la soufflerie est parfois optimiste, c'est-à-dire qu'un résultat trouvé marginal en soufflerie peut se détériorer et devenir mauvais en grandeur ;

- en ce qui concerne les avions d'armes, la soufflerie est parfois pessimiste, c'est-à-dire que des mauvais résultats trouvés en soufflerie peuvent ne pas être retrouvés lors des essais en vol (planche 4).

Par contre, et en ce qui concerne tous les avions, les résultats trouvés francs en soufflerie (franchement mauvais ou franchement bons), restent francs en grandeur. Aussi, lorsque l'on étudie toute modification géométrique de la maquette ou un dispositif de secours, s'arrange-t-on pour obtenir alors des résultats francs pour assurer la même efficacité en grandeur.

*3.3 - Etude statistique - corrélation avions ⟷ vrilles.*

La banque de données et l'expérience que possède l'I.M.F.L. depuis plus de 30 ans avec l'étude de près de 200 maquettes d'avions de tous types lui a permis d'envisager une étude de corrélation entre les caractéristiques des aérodynes et celles de leurs vrilles. Cette étude a pour but principal d'orienter les avionneurs vers des formules de géométries saines avec la meilleure probabilité possible ; elle n'a pas la prétention de prédire les caractéristiques de la vrille au vu de la géométrie. Par ailleurs, il est évident que plus la population sera grande, plus il en sortira de renseignements ; aussi, il serait souhaitable d'y ajouter toutes les données complémentaires provenant de l'Etranger sur ce sujet.

La population d'avions a été divisée en trois grandes catégories afin de regrouper éventuellement des géométries ayant un caractère commun dans leur allure générale :

- avions légers : 41 % actuellement
- avions de transport : 13 %
- avions d'armes : 46 %

Pour l'instant, une quarantaine de paramètres géométriques et massiques ont été utilisés pour représenter au mieux les caractéristiques de tous les avions (masse, inerties, surfaces, bras de levier de surfaces, positions relatives, singularités, ...). Bien entendu, toutes ces grandeurs sont ramenées sans dimension.

Huit paramètres géométriques et cinématiques de description de la vrille ont été pris en considération (assiettes longitudinale et transversale, vitesses de rotation et de chute, rayon de vrille, intensité des agitations, leur type et leur mode). Pour la plupart d'entre eux, ces paramètres ont été estimés en vrille libre à la soufflerie verticale et ont été décomposés en classes de modalités ordonnées.

Dans son ensemble, la base de données peut être sondée pour déterminer des familles de départ. Par exemple, peut être recherché le sous-ensemble des avions d'armes à forte flèche qui ont une vrille plate et rapide, et l'étude de corrélation est menée sur cette famille.

Dans un premier temps, des corrélations simples et intuitives entre les caractéristiques de la vrille ont été recherchées. Par exemple, la corrélation entre une vrille à la fois plate et rapide a été vérifiée. Ceci permettrait de réduire sous certaines conditions, par une première analyse multidimensionnelle des variables de vrille, le nombre de variables indépendantes. Ces premières corrélations n'étaient pas le but recherché initialement, mais en observant la planche 27, montrant une matrice de corrélation simple entre les caractéristiques de vrille, on comprendra facilement que l'interprétation des résultats futurs nécessitera une analyse approfondie. Cette planche nous indique en effet deux corrélations vraiment bonnes (tous avions) et à priori évidentes :

$\Theta$ et $V_Z$ : plus l'attitude est piquée, plus la vitesse de chute croît ;
$\Omega$ et $R^Z$ : plus la rotation est rapide, plus la vrille est centrée.

La corrélation est déjà plus faible sur $W$ et $\Omega$ : plus la rotation est rapide, plus la vrille est calme, mais il y a aussi beaucoup de vrilles lentes qui sont calmes. Même chose pour $\Theta$ et $\Phi_1$ : la corrélation serait ici meilleure si l'on prenait en compte le gauchissement.

Dans un second temps, des corrélations sur trois paramètres ont été calculées. Elles englobent la corrélation simple, en étant plus fines et plus détaillées.

Faisant suite à ces premières étapes, une analyse multidimensionnelle sera effectuée sur l'ensemble des caractéristiques avions. La méthode à priori la plus apte à traiter des données à la fois qualitatives et quantitatives est une méthode dite de segmentation : elle réalise, sur la famille de départ, une partition par dichotomies successives, en sous-familles le plus distinctes possible, tout en étant le plus homogènes possible vis-à-vis des caractéristiques de la vrille. Apparemment, cette méthode se prête assez bien à l'interprétation des résultats. Par exemple, reprenons la planche 27 et examinons la corrélation $\Theta$ - $\Omega$ . Celle-ci est relative à l'ensemble des avions et au domaine de $\Theta$ compris entre -90° et 0°.

La corrélation faible observée peut vouloir dire deux choses :

- soit que $\Omega$ est absolument indépendant de $\Theta$
- soit que la courbe $\Omega = f(\Theta)$ présente une symétrie.

Si maintenant nous subdivisons l'axe $\Theta$ en différentes tranches, et que pour chacune d'entre elles nous calculons la corrélation $\Omega - \Theta$, nous allons obtenir :

- soit à nouveau une valeur très faible pour toutes les tranches $\Theta$, ce qui prouverait que $\Omega$ est effectivement indépendant de $\Theta$ (chose improbable)

- soit des corrélations beaucoup plus fortes, ce qui montre bien que la courbe $\Omega(\Theta)$ est symétrique (en l'occurrence par rapport à $\Theta = -45°$).

Nous voyons donc, par un exemple simple à la planche 27, que les corrélations très faibles peuvent être d'un intérêt aussi grand que les corrélations très fortes ; il suffit pour s'en convaincre de pratiquer la méthode de segmentation.

D'autres méthodes d'analyse peuvent être envisagées pour l'étude statistique de la vrille, par exemple celle dite canonique. Cette méthode recherche, à partir des deux ensembles de caractéristiques avions ($x^j$) et vrilles ($y^k$), les deux variables $a^1$ et $b^1$ respectivement combinaisons linéaires des $x^j$ et $y^k$ et telles que le carré de la corrélation entre $a^1$ et $b^1$ soit maximum. De même, sont recherchées $a^2$ et $b^2$ à carré de corrélation maximum, mais telles que $a^1$ et $a^2$, ainsi que $b^1$ et $b^2$, soient non corrélées. Cette méthode présente néanmoins l'inconvénient de mal se prêter aux variables qualitatives.

En résumé, les divers objectifs des études de corrélation sont :

- effectuer d'abord une synthèse de ce que possède l'I.M.F.L. en vue de vérifier la validité d'un certain nombre de critères généralement admis pour classer les vrilles en fonction des géométries et/ou inerties des avions (T.D.P.F., ...) ;

- chercher de nombreux critères permettant une meilleure estimation des caractères de la vrille avec une probabilité suffisamment grande ;

- fournir à l'avionneur des indications sur les choix à porter au moment du projet de son avion ;

- dégager les tendances en vrille à priori principales d'un avion nouveau à géométrie et inerties données ;

- constituer un support à une modélisation ultérieure en indiquant ce sur quoi il est important d'insister.

### 3.4 - *Aérodynamique et modélisation.*

*Modélisation.*

La détermination des qualités de vol, des performances, des évolutions d'un avion de combat nécessite, dans la résolution des équations d'équilibre, la connaissance la plus exacte possible des efforts aérodynamiques exercés sur l'avion. Or, l'ensemble des moyens d'essais dont dispose l'I.M.F.L. contribue justement à déterminer ces efforts dans un large domaine de vol. Des campagnes d'essais sont réalisées et permettent la constitution d'une banque de données où figurent les valeurs des diverses composantes du torseur aérodynamique en fonction de celles du vecteur d'état, c'est-à-dire généralement $\alpha$ , $\beta$ , p, q, r, ...

Ici apparaît le problème de la modélisation, notamment dans le domaine des grands angles. Le modèle linéaire très largement appliqué pour les petites incidences n'est alors pas satisfaisant. Quelques résultats expérimentaux réalisés à l'I.M.F.L. en statique sur avions d'armes sont présentés planche 28. La figure 28a nous montre l'apparition, avec l'incidence, d'un fort coefficient de lacet présentant lui-même de fortes discontinuités et donnant lieu, déjà au niveau de la modélisation du torseur statique, à la découverte de sérieux problèmes...

Plusieurs méthodes de modélisation pourraient essayer de prendre en compte de tels phénomènes : l'une d'entre elles consisterait, à partir d'un ensemble de résultats expérimentaux, de représenter l'évolution d'un coefficient aérodynamique en fonction de toutes les variables d'état. Ceci revient alors à déterminer l'équation d'un hyperplan dans un espace de dimensions $n+1$ où $n$ est le nombre total de variables dans le modèle. Cependant, ce genre de méthode présente néanmoins deux inconvénients principaux : d'une part, elle nécessite, pour être exploitable, un nombre d'essais très important ; d'autre part, comme elle ne fait pas intervenir la compréhension des phénomènes, toute extrapolation effectuée en dehors du domaine investigué lors des essais semble hasardeuse.

De plus, si l'on observe plus précisément cette même planche (28a), on remarquera que la densité de points mesurés est nettement plus importante au voisinage des maxima et des minima que dans les phases intermédiaires. Ceci semble accréditer l'hypothèse de l'existence d'états d'équilibre stables pour l'écoulement autour de la maquette.

Cette remarque débouche alors sur une seconde idée de modélisation qui consisterait à considérer l'incidence et le dérapage comme étant les paramètres fondamentaux du modèle, ceux qui fixent l'état d'équilibre de l'écoulement, les autres paramètres comme p, q et r n'intervenant que comme des facteurs de variation autour de cet état d'équilibre. On peut voir d'ailleurs que les variations du $C_n$ obtenues à $\alpha = 45°$ et $\beta = 0°$ (planche 12a) peuvent s'expliquer simplement à la vue du résultat de

l'essai statique (28a) qui comporte une forte discontinuité vers 45°. Ceci souligne donc l'importance d'effectuer aux grands angles des essais statiques où l'exploration en incidence est effectuée avec un pas très fin. L'essentiel des campagnes d'essais consisterait alors à effectuer une série d'essais statiques de façon à distinguer les différents régimes d'écoulement.

Mais le problème de la modélisation se complique encore un peu si l'on observe le résultat suivant : sur la figure 28b, nous présentons un essai effectué exactement dans les mêmes conditions que celui de la figure 28a, mis à part qu'une petite discontinuité géométrique (en l'occurrence une aspérité) a été posée au préalable sur le nez de la maquette. On peut alors observer que l'allure de la courbe de $C_n$ s'en trouve fortement modifiée (voir § 2.4.1). Ceci montre donc qu'une légère modification en un endroit bien précis de la maquette peut changer notoirement l'écoulement et peut conduire à une autre forme de modélisation. Celle-ci pourrait reprendre l'idée des états d'équilibre mais, au lieu de prendre en compte un torseur au niveau du centre d'inertie de la maquette, elle pourrait considérer cette maquette comme un ensemble de plusieurs éléments (nez, voilure, dérive, ...) sur lesquels incidence et dérapage ont des effets distincts. Ceci conduit alors dans la procédure d'essais à mesurer des torseurs sur chacun de ces différents éléments.

Toutes ces méthodes visent à construire un modèle de représentation des efforts aérodynamiques de façon à pouvoir les prendre en compte dans les équations de la mécanique du vol. Alors la reconnaissance de tous les mouvements types rencontrés aux grands angles sur avions d'armes (comme la vrille, les autotonneaux, etc ...) peut être pleinement effectuée grâce à une méthode d'analyse comme, par exemple, celle dite des bifurcations que Monsieur GUICHETEAU (14) a développée à l'O.N.E.R.A. et dont il présente un exposé dans le cadre de ce colloque.

*CONCLUSION.-*

Un bref panorama des principales méthodes mises en oeuvre à l'I.M.F.L. pour l'étude de la perte de contrôle et des vrilles a été présenté.

En regard de la complexité des phénomènes, notamment du point de vue aérodynamique, les efforts à développer, en vue d'une prédiction efficace des comportements aux grands angles devraient être orientés dans les directions suivantes :

- Développement accru de méthodes de simulations dynamiques représentatives en soufflerie ou en vol libre (aspect représentation des phénomènes).

- Analyse du point de vue aérodynamique expérimentale et théorique (aspect compréhension des phénomènes).

- Recherche et développement de modèles de représentation fiables fondés sur des concepts nouveaux (choix de paramètres d'état réellement descriptifs, prise en compte de phénomènes locaux dans le cadre d'une modélisation par éléments ...) (aspect prédiction du comportement).

Ces remarques sont particulièrement fondées pour traiter efficacement de la prévention de la perte de contrôle et des vrilles ainsi que des limites de manoeuvrabilité aux grands angles.

*REFERENCES.-*


(1) ORLIK RUCKEMANN, K.J.
Techniques for dynamic stability testing in wind tunnels
AGARD n° 235 - Athens 1978

(2) CHAMBERS, J.R.
Overview of stall/spin technology
A.I.A.A. Paper 80 - 1580

(3) THOMAS, H.H.B.M. and EDWARDS, G.
Mathematic models of aircraft dynamics for extreme flight conditions (theory and experiment)
AGARD n° 235 - Athens 1978

(4) MATTHEWS, A.W.
Experimental determination of dynamic derivatives due to roll at British Aerospace Warton Division
AGARD n° 235 - Athens 1978

(5) HAFER, X.
Wind tunnel testing of dynamic derivatives in W.Germany
AGARD n° 235 - Athens 1978

(6) DECKEN, J. - SCHMIDT, E. and SCHULZE, B.
On the test procedures of the derivative balances used un W. Germany
AGARD n° 235 - Athens 1978

{7} ORLIK RÜCKEMANN, K.J. - HANFF, E.S.
Experiments on cross-coupling and translational acceleration derivatives
AGARD n° 235 - Athens 1978

{8} HANFF, E.S. and ORLIK RÜCKEMANN, K.J.
A generalized technique for measuring cross-coupling derivatives in wind tunnels
AGARD n° 235 - Athens 1978

{9} SCHERER, M.
Determination dans les installations au sol des paramètres aérodynamiques de stabilités d'aéronefs
AGARDOGRAPHIE 242 - 1979

{10} VANMANSART, M.G.
Application des mesures de coefficients aérodynamiques statiques et dynamiques à des recoupements par calcul des vrilles obtenues en soufflerie
AGARD n° 199 - Bruxelles Rhode-Saint-Genèse 1975

{11} VERBRUGGE, R.A.
Balance rotative de l'I.M.F.L. et techniques associées
A.A.A.F. Nov. 1979

{12} TRISTRANT, D.R.
Logiciels balance rotative
Rapport IMFL 81/07 - Fév. 1981

{13} VERBRUGGE, R.A. and CHARON, W.
Wind tunnel and free flight model identification experience
AGARD - Lectures Series 104 - Oct. et Nov. 1979

{14} GUICHETEAU, P.
Application de la théorie des bifurcations à l'étude de la perte de contrôle sur avion de combat
AGARD - Florence 1981.

## ETUDES DE PERTE DE CONTROLE ET DE VRILLE

### SCHEMA DE L'EXPOSE

TECHNIQUES EXPERIMENTALES

- Présentation de l'ensemble des méthodes
- Maquettes captives
- Maquettes libres en laboratoire
- Maquettes libres en soufflerie verticale
- Maquettes atmosphériques télé-pilotées

AUTRES METHODES D'ETUDES

- Figuration animée des mouvements aux grands angles
- Comparaison vol-soufflerie.
- Etude statistique : corrélation
- Aérodynamique et modélisation
- Documentation

*Planche 1*

## REPRESENTATION CLASSIQUE DU SYSTEME AVION

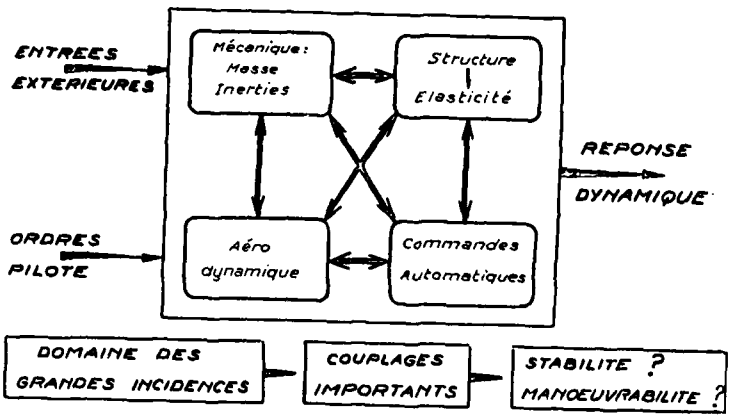


*Planche 2*

## DOMAINE DES GRANDES INCIDENCES PRINCIPALES TECHNIQUES EXPERIMENTALES

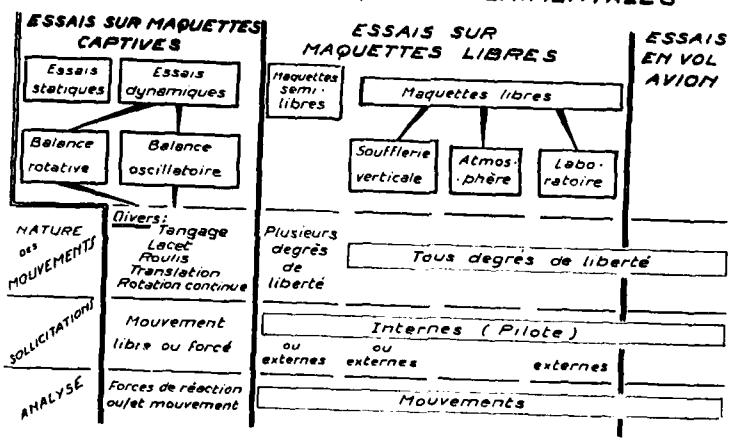


*Planche 3*

## COMPARAISON DES VRILLES SOUFFLERIE -AVION

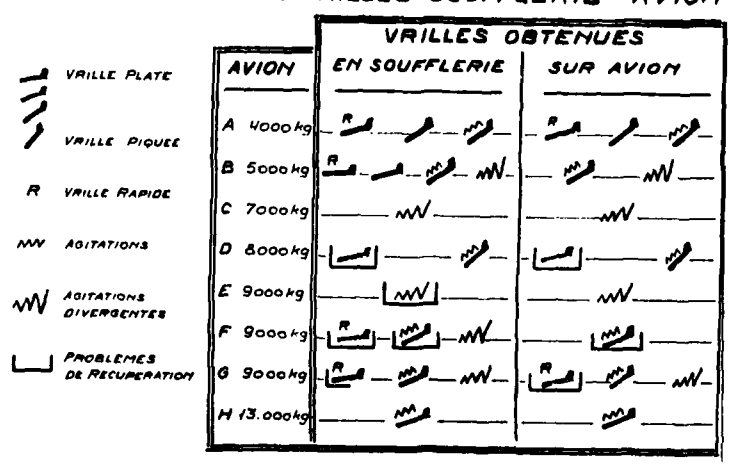


*Planche 4*

# ESSAIS SUR BALANCE DYNAMIQUE
## PRINCIPALES CARACTERISTIQUES

- Domaine extensif du nombre de Reynolds ou du nombre de Mach
- Domaine extensif des angles d'attaque et de dérapage (90°)

} non combinés

- Mouvements séparés ou combinés (3 degrés de liberté) possibles.
- Possibilité de larges variations du domaine de fréquence réduite et amplitude independemment
- Essai avec instabilités aérodynamiques

} Oscillations forcées

- Entrées gouvernes possibles.
- Instrumentation extensive : balance à 5 ou 6 composantes
  accéléromètres dans la maquette
  mesures de fréquence et d'amplitude
  visualisations
  pression etc.....
- Bonne adaptation aux études paramétriques

---

- Interférence de la soufflerie et du montage : aérodynamique et mécanique
- Mouvement libre non simulé.

Planche 5

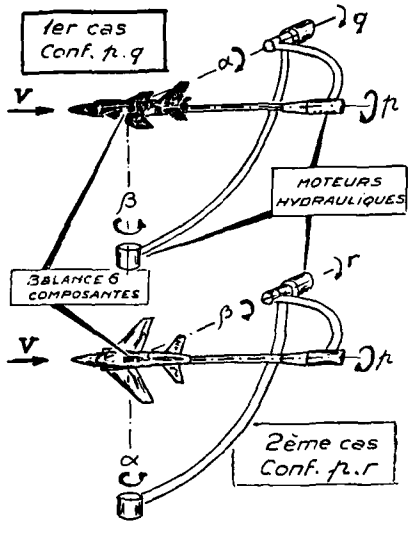


Planche 6

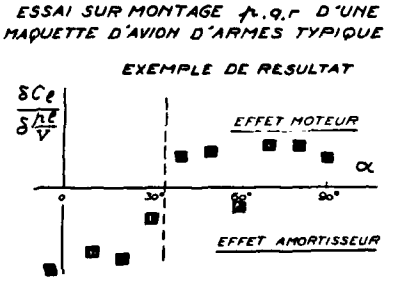


Planche 7

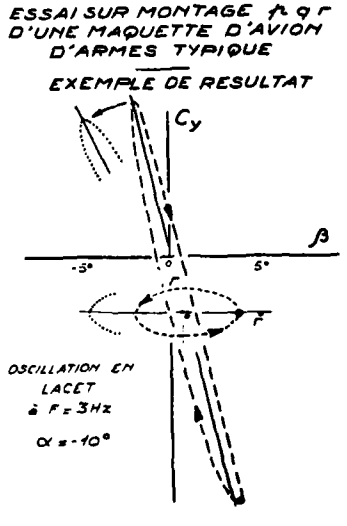


Planche 8

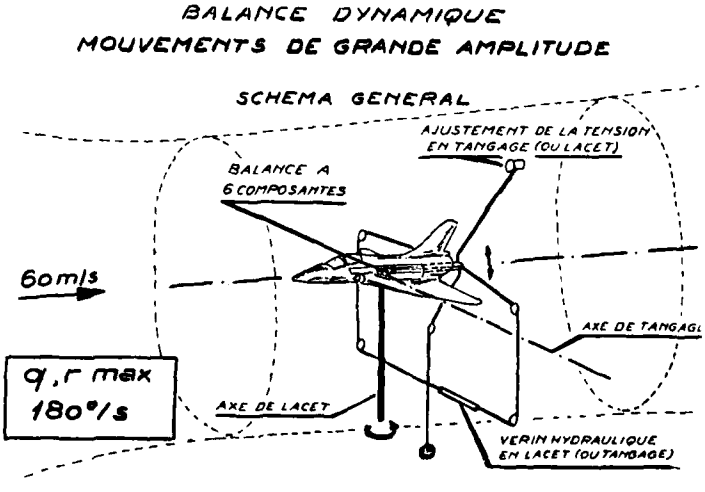


Planche 9

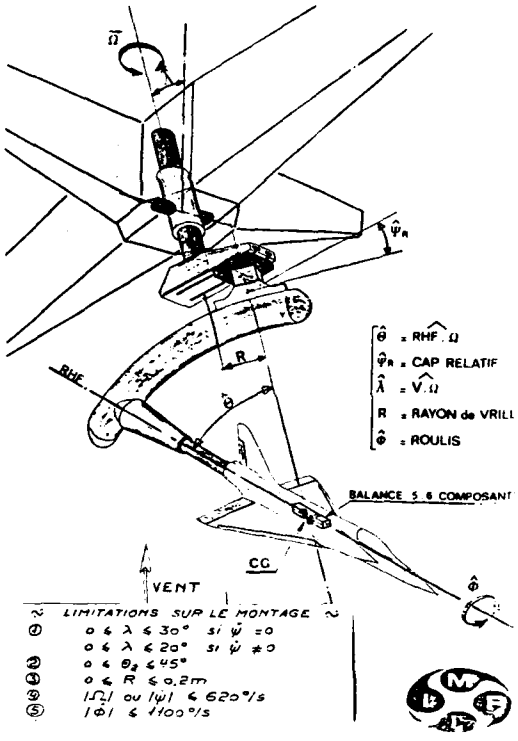


Planche 10

ESSAIS SUR BALANCE ROTATIVE

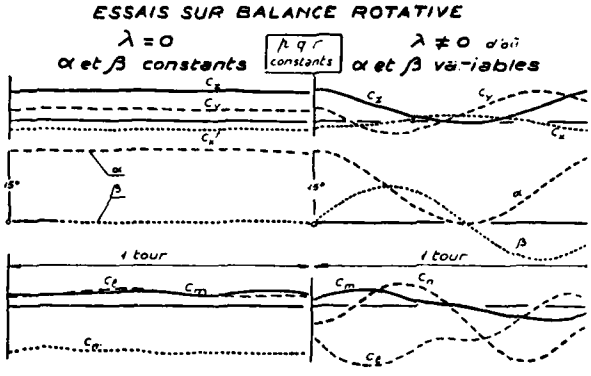


Planche 11

ESSAIS SUR BALANCE ROTATIVE AUX TRES GRANDS $\alpha$

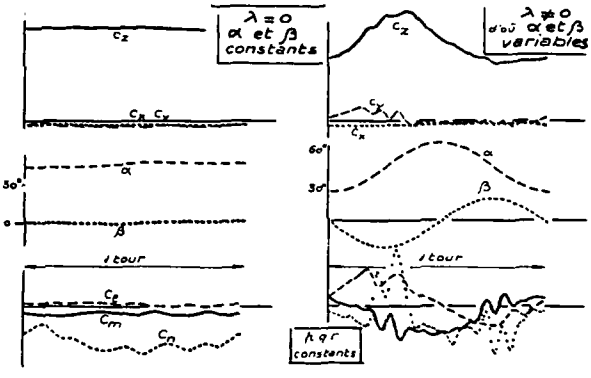


Planche 12

MAQUETTES DE VOL LIBRE EN LABORATOIRE
DOMAINE GENERAL D'APPLICATIONS

ECOULEMENT INCOMPRESSIBLE
NOMBRE DE REYNOLDS $10^5 < \mathcal{R} < 5.10^6$
rapporté à la corde moy. aéro.

**IDENTIFICATION DE PARAMETRES** (Tous degrés de liberté)
- Coefficients stationnaires
- Paramètres de stabilité dynamique
- Efficacité des gouvernes.

**ETUDE DES QUALITES DE VOL**
- Grands $\alpha$, étude des basses vitesses.
- Technique des commandes actives.
- Perte de contrôle · Vrille stabilisée · Récupération.

Planche 13

TECHNIQUE D'ESSAIS SUR MAQUETTES LIBRES EN LABORATOIRE
ASPECTS SPECIFIQUES

- Essais à basse vitesse ≈ Nombre de Reynolds dans la gamme de $10^6$
- Tous degrés de liberté représentés
- Bonne connaissance de l'environnement (conditions de laboratoire)
- Grande précision sur les masse, inerties et caractéristiques structurales de la maquette
- Enveloppe de vol incluant : grands $\alpha$, décrochage, vrille débutante
- Grande diversité des entrées: gouvernes, conditions initiales
- Instrumentation extensive :
  - embarquée : gyros, accéléros, pression ($V, \alpha, \beta$....)
  - au sol : système de trajectographie optique
  - embarquée ou au sol : boucle commandes automatiques
- Application des techniques d'identification de paramètres
- Courte durée de l'essai (5 à 10 s. valeur avion)
- Complémentarité avec souffleries basse vitesse

Planche 14

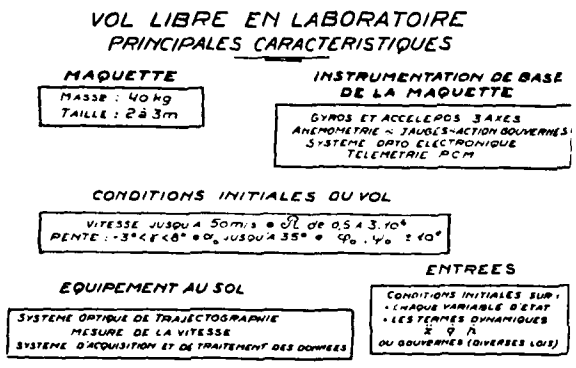


Planche 15

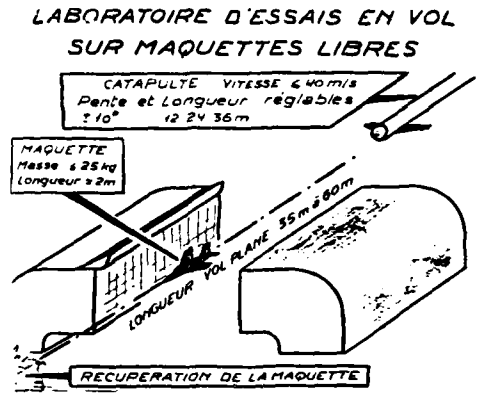


Planche 16

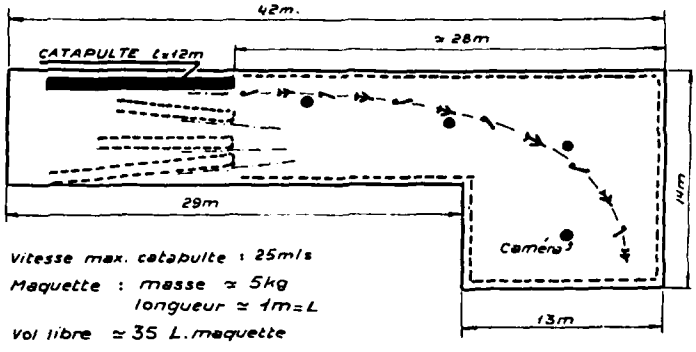


## STATION D'ESSAIS DE VOL LIBRE
### ETUDE DE LA MISE EN VRILLE

Planche 17

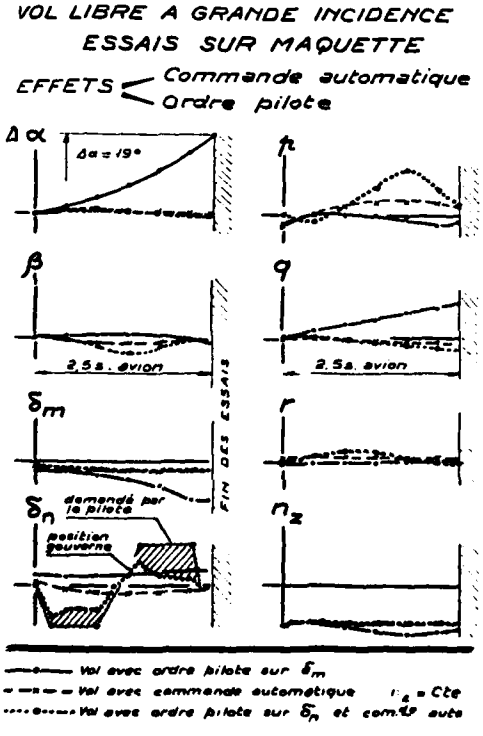


Planche 18

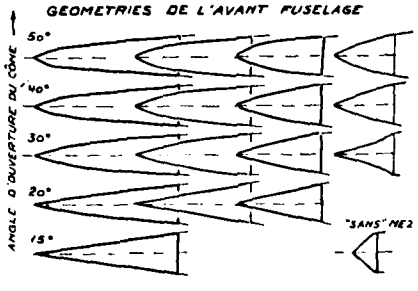


Planche 19

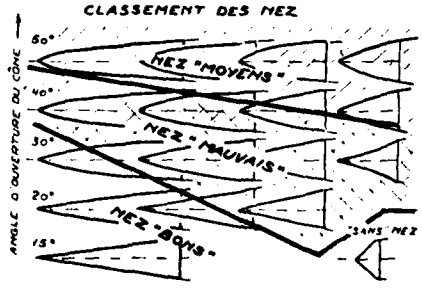


Planche 20

VIRURES

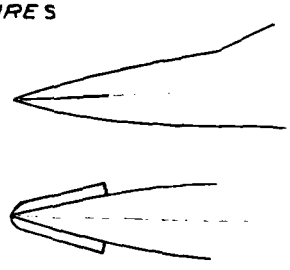

Planche 21

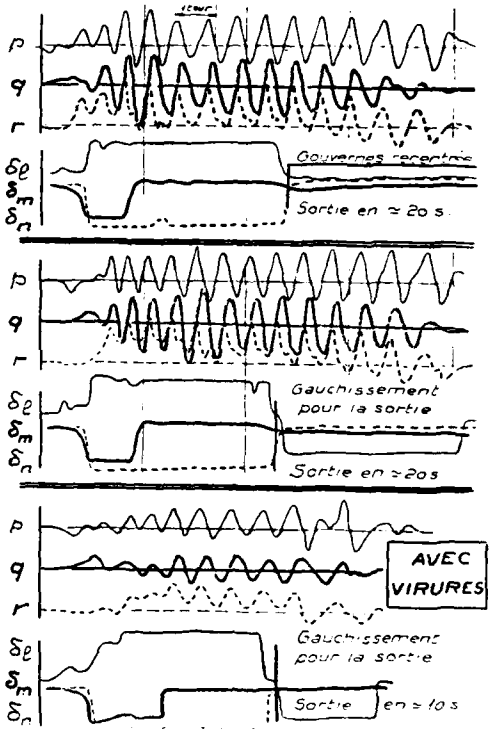


Planche 22

ESSAIS DE VRILLE LIBRE
MAQUETTE INSTRUMENTÉE d'UN AVION D'ARMES CONVENTIONNEL

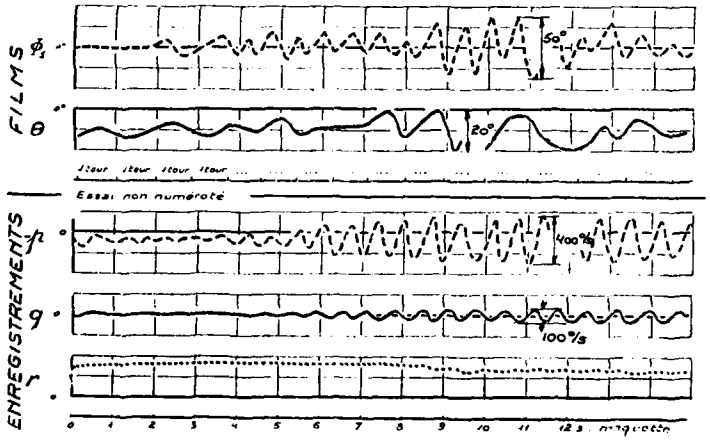


Planche 23

VRILLE CALME
ASSIETTE LONGITUDINALE SELON LA TRAJECTOIRE

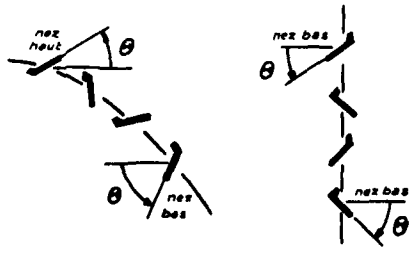


Planche 24

DESCRIPTION DE LA VRILLE
ANGLES D'EULER

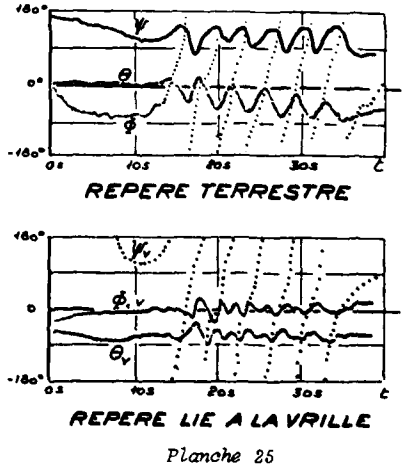


Planche 25

EFFETS SEPARES ET SIMULTANES DES OSCILLATIONS SUR θ ET φ AU COURS D'UNE VRILLE AGITEE

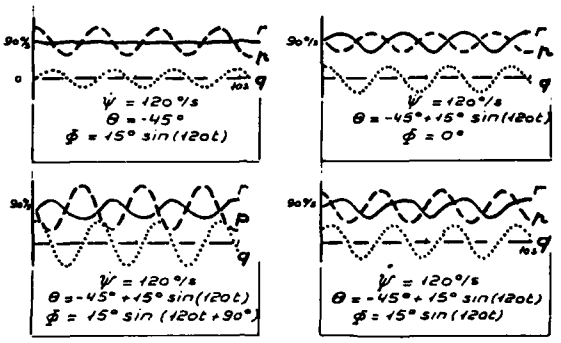


*Planche 26*

CORRELATIONS SIMPLES SUR LES CARACTERISTIQUES DE LA VRILLE

| | θ | $\phi_1$ | Ω | R | $V_z$ | W | $T_y$ | Mod |
|---|---|---|---|---|---|---|---|---|
| θ | | 0,39 | 0,04 | -0,24 | -0,58 | -0,14 | -0,12 | -0,06 |
| $\phi_1$ | | | -0,10 | -0,05 | -0,24 | -0,06 | -0,06 | -0,05 |
| Ω | | | | -0,62 | -0,17 | 0,33 | 0,34 | 0,26 |
| R | | | | | 0,25 | 0,24 | 0,27 | 0,20 |
| $V_z$ | | | | | | -0,05 | -0,09 | -0,07 |
| W | | | | | | | | |
| $T_y$ | | | | | | | | |
| Mod | | | | | | | | |

θ : Assiette longitudinale
$\phi_1$ : Assiette transversale
Ω : Vitesse de rotation de vrille
R : Rayon de vrille
$V_z$ : Vitesse de chute
W : Intensité des agitations
$T_y$ : Type des agitations (ordonnées ou non)
Mod : Mode des agitations (p,q,r)

*Planche 27*

ESSAIS STATIQUES SUR MAQUETTE D'AVION D'ARMES à α > 35° et β ≈ 0°

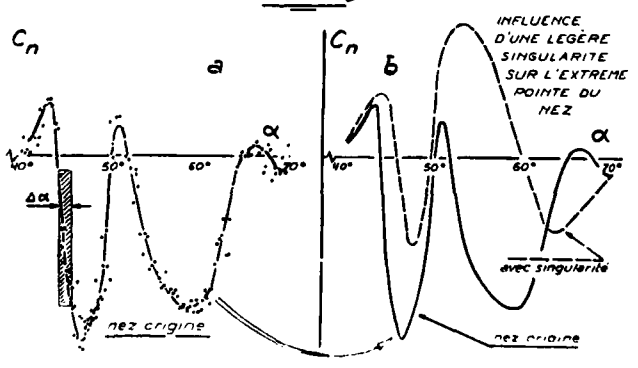


*Planche 28*

# APPLICATION DE LA THEORIE DES BIFURCATIONS A L'ETUDE DES PERTES DE CONTROLE SUR AVION DE COMBAT

par
Philippe Guicheteau
ONERA
92320 Châtillon, France

RESUME

Le mouvement d'un avion peut être décrit de manière rigoureuse par un système différentiel non linéaire, dépendant de paramètres, liant les variables d'état (incidence, dérapage, vitesse...) et les variables de commande (braquages des gouvernes) par l'intermédiaire des équations de la mécanique du vol et du modèle aérodynamique.

La méthode proposée ici consiste à déterminer les limites de stabilité du système et à prédire l'évolution de celui-ci lorsqu'il devient instable. Elle fait appel à la théorie des bifurcations des systèmes différentiels non linéaires.

## 1. INTRODUCTION

Depuis de nombreuses années, l'étude des pertes de contrôle et des vrilles sur avion de combat est un domaine de recherches très important. Malgré les efforts déployés, l'analyse de tels phénomènes reste encore très délicate en raison de leur complexité, de leur caractère apparemment aléatoire et des faibles connaissances dont on dispose en aérodynamique à grande incidence.

Pourtant, l'examen attentif de nombreux résultats d'essais en vol sur des avions très différents révèle d'étonnantes similitudes de comportement qu'il semble difficile d'attribuer au hasard. D'autre part, des études de vrilles en simulation ont montré qu'il était possible, avec un modèle adéquat, d'effectuer des recoupements satisfaisants avec des essais en soufflerie ou en vol, suggérant ainsi que la vrille est une caractéristique du système différentiel utilisé dans les simulations.

Par opposition aux évolutions à faible incidence, le comportement des avions à grande incidence est caractérisé par des mouvements de grande amplitude pour lesquels l'analyse linéarisée de la stabilité ne fournit que des renseignements très limités.

Pour toutes ces raisons, une étude déterministe du comportement des avions dans le domaine non linéaire a été entreprise. On a utilisé des résultats mathématiques très importants relatifs aux applications différentiables et regroupés sous le nom de théorie des bifurcations. Grâce à l'outil numérique, la méthode proposée ici offre l'avantage de traiter des équations complètes. Pour illustrer cette nouvelle approche des phénomènes non linéaires de la mécanique du vol, on présente deux applications.

La première traite le phénomène bien connu de l'auto-tonneau avec un modèle d'avion à coefficients constants et des équations simplifiées. Malgré la simplicité du système étudié, on met en évidence l'existence d'états d'équilibre multiples associés à un braquage donné de gouvernes.

Dans la seconde, on étudie le comportement à grande incidence d'un modèle aérodynamique non linéaire d'avion de combat, en utilisant les équations complètes de la mécanique du vol, sans aucune hypothèse simplificatrice. Grâce à l'étude des bifurcations du système ainsi construit, on prévoit par le calcul et on retrouve en simulation des phénomènes très généraux de saut, d'hystérésis et de cycle limite qui présentent de grandes analogies avec des comportements qu'il est classique d'observer en vol.

## 2. BIFURCATIONS ET THEORIE DES CATASTROPHES

### 2.1 - Avertissement

Il n'est pas dans l'esprit de cette communication de se substituer aux ouvrages spécialisés exposant les fondements mathématiques de la théorie des catastrophes (1). Toutefois, il semble indispensable d'en exposer quelques aspects, illustrés par des exemples, pour faciliter la compréhension des chapitres suivants.

### 2.2 - Premier exemple : la catastrophe de Riemann - Hugoniot

Considérons l'équation différentielle scalaire

$$\frac{dx}{dt} = -(x^3 + ax + b)$$

dans laquelle $x$ représente l'état d'un système et (a,b) des paramètres de commande lentement variables. Cette équation scalaire peut être considérée comme représentative de l'évolution de la variable x dans un champ de gradient dont la fonction potentielle est définie par les relations :

$$\dot{x} = -\text{grad}\,(\varphi(x))$$

et $$\varphi(x) = \frac{x^4}{4} + \frac{ax^2}{2} + bx$$

Par conséquent, l'étude des minima et des maxima de la fonction $\varphi(x)$ renseigne sur la stabilité ou l'instabilité des états d'équilibre du système.

Supposons que l'on fixe a (a = - 3), que l'on fasse varier lentement b de - 3 à + 3 de telle sorte que la variable x atteigne un état d'équilibre pour chaque valeur de b (fig 1), et que x soit en $x_1$ au début de la variation de b. Pour b = +2, le minimum de la fonction $\varphi(x)$ devient un point d'inflexion et, pour une petite varation de ce paramètre, x passera rapidement de l'état $x_1$ à l'état $x_2$. De même, si l'on change le sens de variation de b, x restera en $x_2$ jusqu'à ce que b atteigne la valeur -2 et "sautera" ensuite à l'état $x_1$.

On note au passage que l'on vient de mettre en évidence un hystérésis dû au fait que le saut de $x_1$ vers $x_2$ ou de $x_2$ vers $x_1$ dépend de l'histoire de la variation du paramètre b.

Représentons dans l'espace (x,a,b), la surface (M) des points d'équilibre définie par $\dot{x} = 0$ et sa projection (C) sur le plan (a,b) (fig.2). Dans ce plan, le lieu des points tels que l'équation $\dot{x} = 0$ admet trois racines est à l'intérieur d'une courbe en forme de pointe. La frontière entre les régions de l'espace (a,b) ayant un nombre différent d'états d'équilibre est appelée surface de bifurcation. Sur cette surface, la superposition d'un minimum et d'un maximum crée un point d'inflexion pour lequel les dérivées première et seconde de $\varphi(x)$ s'annulent. Par conséquent, en éliminant x des équations

$$\frac{\partial \varphi}{\partial x} = x^3 + ax + b = 0$$

$$\frac{\partial^2 \varphi}{\partial x^2} = 3x^2 + a = 0$$

on obtient l'équation de la surface de bifurcation

$$\frac{1}{27} a^3 + \frac{1}{4} b^2 = 0$$

De cette dernière, il vient immédiatement que si a est négatif, il sera possible de se trouver sur cette surface et donc d'être sur un point de bifurcation. Aussi, pour éviter cette situation que l'on qualifie de "catastrophique", il sera nécessaire que a soit positif (fig.2).

2.3 - Deuxième exemple : bifurcation de Hopf. (fig.3)

Considérons un système de dimension 2 en coordonnées polaires $(r, \theta)$ dans lequel

$$r^2 = x_1^2 + x_2^2 \qquad \theta = \text{Arctg} \frac{x_2}{x_1}$$

$$\begin{cases} \dot{\theta} = -1 \\ \dot{r} = r(c - r^2) \end{cases}$$

Les solutions correspondant à un équilibre doivent satisfaire l'équation $r(c - r^2) = 0$ ce qui entraine $r = 0$ ou $r = \sqrt{c}$ avec $c \geq 0$. Pour $c < 0$, seule la solution $r = 0$ existe (foyer stable).
Pour $c \geq 0$, la solution $r = 0$ devient instable (foyer instable) et une nouvelle solution $r = \sqrt{c}$ apparait. Cette dernière correspond à un cycle limite dont le rayon croit comme $\sqrt{c}$. Le point C est un attracteur vague et représente le point de bifurcation de Hopf.

3. BIFURCATIONS ET MECANIQUE DU VOL

3.1 - Modèles d'avions utilisés.

L'application de la théorie des bifurcations portera sur deux modèles d'avions.

L'avion A possède un modèle aérodynamique linéaire et à coefficients indépendants de l'incidence. Il est utilisé pour traiter l'exemple simplifié de l'auto-tonneau (& 4).

L'avion B possède un modèle aérodynamique non linéaire sans hystérésis, dont la validité s'étend à des incidences $-10° \leq \alpha \leq +90°$ et des dérapages $-40° \leq \beta \leq +40°$.
Il est utilisé dans le deuxième exemple d'application de la théorie des bifurcations qui concerne certaines pertes de controle à grande incidence.

Le modèle B est celui d'un avion de combat fictif à aile haute et empennage arrière. Il est cependant réaliste car il est issu d'une synthèse de nombreux essais de soufflerie. Ses caractéristiques sont résumées à la figure 4.

La formulation du modèle B a été adaptée aux besoins des calculs de mécanique du vol. Chacun des six coefficients globaux : $C_\ell$, Cm, Cn, Cx, Cy, Cz, s'exprime de façon indépendante en fonction des paramètres d'influence : $\alpha$, $\beta$, $p$, $q$, $r$, gouvernes.
Ainsi les non-linéarités et les couplages aérodynamiques s'expriment dans un développement en série de Taylor autour des valeurs de référence (état nominal) définies de la façon suivante :

$$\alpha = \bar{\alpha} \quad , \quad \beta = 0 \quad , \quad p = q = r = 0 \quad , \quad \delta\ell = \delta m = \delta n = 0$$

L'expression générale des coefficients est de la forme :

$$C = C_0(\bar{\alpha}, \beta = 0, p = q = r = 0, \delta\ell = \delta m = \delta n = 0) + \Delta C(\bar{\alpha}, \beta) + \Delta C(\bar{\alpha}, \delta\ell) + \cdots + \Delta C(\bar{\alpha}, p) + \cdots$$

- Les coefficients $C_0$ sont appelés coefficients nominaux. Ils sont non linéaires en fonction de l'incidence. En particulier, les coefficients nominaux latéraux n'ont pas été choisis systématiquement nuls, aux incidences supérieures à 20°, en vue de simuler les dissymétries aérodynamiques identifiées sur de nombreux avions à grande incidence.

- Les termes $\Delta C$ expriment la variation par rapport à sa courbe nominale, du coefficient C, en fonction du paramètre x. Ce sont des fonctions paires ou impaires du paramètre x suivant la nature du coefficient $\Delta C$ et de x.

3.2. - Equations du mouvement.

Le système d'équations adopté représente un modèle complet puisqu'on y trouve :

- les trois équations de moment, en supposant D = F = 0

$$A\dot{p} - E\dot{r} + (C - B)qr - Epq = \frac{1}{2} \rho S \ell V^2 C_\ell$$

$$B\dot{q} + (A - C)rp + E(r^2 - p^2) = \frac{1}{2} \rho S \ell V^2 C_m$$

$$C\dot{r} - E\dot{p} + (B - A)pq + Erq = \frac{1}{2} \rho S \ell V^2 C_n$$

- les trois équations de force,

$$m[\dot{V}\cos\alpha\cos\beta - V(\sin\alpha\cos\beta\,\dot{\alpha} + \cos\alpha\sin\beta\dot{\beta}) + V(q\sin\alpha\cos\beta - r\sin\beta)]$$
$$= -mg\sin\Theta + \frac{1}{2}\rho SV^2C_x + F_x$$

$$m[\dot{V}\sin\beta + V\cos\beta\dot{\beta} + V(r\cos\alpha\cos\beta - p\sin\alpha\cos\beta)]$$
$$= mg\cos\Theta\sin\Phi + \frac{1}{2}\rho SV^2C_y$$

$$m[\dot{V}\sin\alpha\cos\beta + V(\cos\alpha\cos\beta\,\dot{\alpha} - \sin\alpha\sin\beta\dot{\beta}) + V(p\sin\beta - q\cos\alpha\cos\beta)]$$
$$= mg\cos\Theta\cos\Phi + \frac{1}{2}\rho SV^2C_z + F_z$$

- deux équations cinématiques. L'équation cinématique d'Euler en cap $\Psi$ , n'est pas prise en compte.

$$\dot{\Phi} = p + tg\Theta(q\sin\Phi + r\cos\Phi)$$
$$\dot{\Theta} = q\cos\Phi - r\sin\Phi$$

Les non-linéarités de ce système sont nombreuses et peuvent être classées en deux catégories :

- La première renferme celles qui sont intrinsèques au système et qui sont dues à l'écriture des équations du mouvement d'un solide dans l'espace (lignes trigonométriques et couples gyroscopiques).

- La seconde contient celles qui proviennent du modèle aérodynamique de l'avion considéré. Dans cette catégorie, il convient de faire une distinction entre :

  . les non-linéarités de courbure des coefficients aérodynamiques,

  . les non-linéarités de couplage, comme certains coefficients aérodynamiques qui dépendent de deux variables. ex : $Cl_{pr}$

Cette distinction n'est pas évidente à priori, mais elle est justifiée par l'expérience.
En effet, les premières conduisent à des évolutions brutales, pour une variation"douce" des braquages de commandes, les autres à des oscillations plus ou moins entretenues.

3.3 - Mise en oeuvre de la théorie des bifurcations

3.3.1 - Calcul des états d'équilibre

Bien que dans certains cas particuliers (auto-tonneau) une solution analytique soit envisageable, la méthode utilisée consiste à rechercher numériquement tous les états d'équilibre du système différentiel non linéaire ci-dessus pour chaque combinaison du triplet de braquages de gouvernes ( $\delta\ell$ , $\delta m$ , $\delta n$ ).

Le système différentiel non linéaire des équations de la mécanique du vol se ramène à la forme générale :

$$\dot{X} = F(X,C)$$

dans laquelle

X est un vecteur de dimension n appelé vecteur d'état

C est un vecteur de dimension m appelé vecteur de commande

F est un ensemble de n fonctions continues dérivables non linéaires dépendant à la fois de l'état et de la commande.

On se propose d'étudier l'ensemble des états d'équilibre (X) du système définis par $\dot{X} = 0$ lorsque le vecteur de commande varie.

Lorsqu'on fait l'hypothèse classique selon laquelle le système est linéaire, il n'existe qu'un seul état X vérifiant la relation $F(X,C) = 0$, pour une valeur donnée du vecteur de commande. Par contre, lorsque le système est non linéaire, il peut exister plusieurs états d'équilibre différents vérifiant la relation $\dot{X} = 0$ pour une valeur donnée du vecteur de commande.

Le traitement numérique de ce problème recèle de nombreuses difficultés. La méthode employée vise à décrire la surface d'équilibre du système à l'aide d'une variable descriptive. Cette idée, due à Klopfenstein [6], a donné naissance à de nombreux algorithmes améliorant la précision, la rapidité du calcul et pouvant traiter de nombreux cas de bifurcations. Ils sont dus principalement aux travaux de Davidenko, Keller [7] et Kubicek [8].

Dans le cas présent, on a repris en le modifiant légèrement l'algorithme proposé par Kubicek [8].

3.3.2 - Détermination de la surface de bifurcation

Il s'agit de rechercher l'ensemble des états d'équilibre tels que une (ou plusieurs) valeur propre (considérée comme un nombre complexe) de la matrice jacobienne du système $\dot{X} = F(X,C)$ possède une partie réelle nulle. Cette condition sépare en effet les domaines des équilibres stables et instables.

Dans la suite de cette étude, on ne s'intéresse qu'aux bifurcations associées à une (ou plusieurs) valeur propre nulle.

La résolution rigoureuse de ce problème peut être faite en utilisant l'algorithme utilisé dans le paragraphe précédent en adjoignant, au système différentiel initial, une condition sur le déterminant de la matrice jacobienne (Det = 0). L'adjonction de cette dernière condition pénalise beaucoup le temps de calcul. Pour cette raison, on a choisi de construire la surface de bifurcation à partir d'un maillage de la surface d'équilibre. Bien que moins précise, cette façon de procéder procure non seulement les points de bifurcation mais aussi les points d'équilibre qui existent au-delà, et vers lesquels le système tend après avoir traversé une bifurcation.

3.3.3 - Prédiction du comportement à grande incidence

La démarche présentée ci-dessus correspond à une description statique de l'ensemble des états d'équilibre possibles, stables ou non. La prédiction a pour objet de définir l'évolution dynamique qui se produit au franchissement d'une surface de bifurcation.

Elle est réalisée en interprétant les résultats obtenus ci-dessus. Cette étape de la méthode est assurément la plus délicate car il s'agit de passer d'informations quantitatives à une description qualitative d'un comportement dynamique. Elle ne doit pas être faite en se guidant aveuglément sur les valeurs propres des états d'équilibre. Bien que cela soit très schématique, il est possible de dégager quatre règles de prédiction qui ne s'excluent pas mutuellement :

a) Les surfaces d'équilibre présentent des propriétés de symétrie en raison de la symétrie du modèle. Dans ce cas, les perturbations extérieures agissant sur l'avion le font tendre vers un état d'équilibre ou l'état symétrique.

b) Les manoeuvres sont exécutées rapidement, ou bien la vitesse de l'avion est importante. Dans ce cas, l'avion peut présenter des pertes de contrôle partielles non prévisibles par les calculs précédents. Pour ce type de manoeuvre, les calculs négligeant l'influence de la pesanteur permettent la prédiction.

c) Pendant la manoeuvre, tous les états d'équilibre vers lesquels tend le système sont stables. Dans ces conditions, la prédiction ne présente pas de difficulté.

d) Après une bifurcation, les états d'équilibre en présence sont instables oscillatoires. Dans ce dernier cas, la prédiction se déroule en deux temps. En faisant provisoirement abstraction des valeurs propres imaginaires conjuguées on détermine l'état d'équilibre théorique défini par $\dot{X} = 0$ vers lequel tendrait le système dans l'hypothèse où il serait stable. Puis, on précise la prédiction en intégrant le mouvement du système autour de cet état d'équilibre, après l'avoir soumis à une petite perturbation afin de mettre en évidence l'existence éventuelle d'un cycle limite ou d'autres phénomènes oscillatoires non linéaires qui ne sont pas traités actuellement par la méthode exposée plus haut.

Malgré la brièveté de cette classification, la méthode est efficace, comme le démontrent les paragraphes 4 et 5.

3.3.4 - Vérification par simulation

L'expérience acquise par le traitement d'un grand nombre de cas est très précieuse pour prédire correctement le comportement d'un avion au-delà d'une bifurcation. Grâce à cette expérience, et dans de nombreux cas, il n'est pas indispensable de simuler la manoeuvre étudiée pour connaître le comportement de l'avion.

Mais pour les cas difficiles cités à l'alinéa d) ci-dessus, ou si un doute se présente, il faut effectuer quelques simulations. Un avantage considérable de la méthode est que les diagrammes de bifurcations permettent d'ajuster les manoeuvres de pilotage à coup sûr, et ainsi de n'exécuter que les cas de calcul pertinents. Ces simulations sont réalisées au moyen d'un programme d'intégration du mouvement qui prend en compte des équations complètes et toutes les non-linéarités.

On justifie ainsi, a postériori et si nécessaire, les hypothèses simplificatrices qui auraient pu être faites dans les calculs de bifurcations et dans la prédiction.

## 4. APPLICATION A L'ETUDE DE L'AUTO-TONNEAU

Cette première application est un exemple simplifié de l'utilisation de la théorie des bifurcations à l'étude du phénomène d'auto-tonneau qui est connu depuis fort longtemps et dont l'étude a été reprise récemment par Schy, Hannah et Mehra [2,3,4].

### 4.1 - Hypothèses

L'expérience et les calculs antérieurs [5] ayant montré que l'auto-tonneau se produit à faible incidence, que la vitesse de l'avion varie peu et que l'influence de la pesanteur est négligeable, le système différentiel complet des équations de la mécanique du vol a été simplifié de la façon suivante :

- le modèle d'avion est à coefficients constants (incidence faible)

- l'équation de traînée est absente (vitesse constante)

- on suppose que les termes renfermant la quantité g/V sont toujours petits et constants. Cette dernière hypothèse présente l'avantage de découpler les deux équations en $\Theta$ et $\Phi$ et de ne pas contraindre le mouvement de l'avion à s'effectuer autour d'un axe vertical.

### 4.2 - Etude de l'auto-tonneau

Les hypothèses ci-dessus conduisent à écrire un système différentiel simplifié dont on cherche l'ensemble des états d'équilibre ( $\dot{\alpha} = \dot{\beta} = 0$, $\dot{p} = \dot{q} = \dot{r} = 0$).

En supposant $\dot{\alpha} = \dot{\beta} = 0$ et $\dot{q} = \dot{r} = 0$ et en négligeant l'influence du terme $qr$, le système se met sous la forme :

$$\dot{p} = f_6 p^5 + f_5 p^4 + f_4 p^3 + f_3 p^2 + f_2 p + f_1$$

qui, par un changement de variable $x = p + \frac{f_5}{5f_6}$, se ramène à l'équation différentielle

$$\dot{x} = x^5 + dx^3 + cx^2 + bx + a$$

Ainsi, on met en évidence la forme canonique d'une singularité de $\mathbb{R}^4 \to \mathbb{R}^4$ appelée "catastrophe papillon" dont l'étude fait apparaître des points de bifurcation pouvant entraîner des sauts pour certaines valeurs des paramètres (a,b,c,d).

En effet, pour un braquage de profondeur à piquer effectué à partir de la position de trim correspondant à l'incidence choisie ($\alpha = 5°$), et gouvernes transversales au neutre, il existe 5 états d'équilibre possibles repérés A1 et A5 sur la figure 5, et non pas un seul comme le prévoit l'approximation linéaire. Les états A1, A3 et A5 sont stables ; A2 et A4 sont instables. Partant de l'état nominal A3, un braquage progressif du gauchissement correspondant à une manoeuvre bénigne de roulis à droite, effectuée sous facteur de charge légèrement négatif, déplace le point de fonctionnement jusqu'en A'3, puis le fait "sauter" vers A'1. Précisément, la vitesse de roulis répond tout d'abord à peu près linéairement (c'est-à-dire intuitivement) à la sollicitation du pilote, puis, brusquement, elle "saute" à une valeur excessivement élevée par rapport à la commande. Le pilote décide immédiatement de ramener le gauchissement au neutre. Cette manoeuvre est à peu près sans effet, et le demeure même s'il braque le gauchissement en sens opposé. Ces deux phénomènes apparaissent nettement en simulation (figure 6) . Ces simulations, réalisées avec des équations complètes, suggèrent deux remarques :

- l'influence de la pesanteur se traduit par une oscillation des variables d'état autour d'une valeur moyenne sans modifier les phénomènes,

- la prise en compte de la pesanteur fait piquer l'avion et le fait accélérer. Il s'ensuit que la vitesse de roulis ne se stabilise pas à la valeur calculée précédemment. En fait, on remarque qu'on peut réécrire le système étudié en utilisant la variable réduite $p^* = Pl/V$. On vérifie alors que, malgré l'accroissement de la vitesse de l'avion et de la vitesse de roulis, la valeur de $p^*$ est parfaitement stabilisée à la valeur prévue par les calculs d'équilibre.

De la même façon, une action à piquer à la profondeur peut provoquer le saut spontané d'un équilibre de type A3 vers un équilibre de type A1 (figure 7).

Enfin, sur ce réseau de courbes d'équilibre on observe que, partant du point A1, gauchissement au neutre, on pourra retrouver l'état d'équilibre initial à $p = 0$ par un nouveau saut obtenu en ramenant la profondeur à sa position de trim (simulation figure 8).

4.3 - Conception d'une loi de pilotage pour éviter l'auto-tonneau

Outre la description du comportement de l'avion, le calcul des états d'équilibre et des points de bifurcation procure de précieux renseignements sur les moyens d'éviter les sauts. Dans le cas présent, le calcul de la surface de bifurcation dans le plan ( $\delta l$ , $\delta m$ ) pour un braquage de profondeur donné montre qu'il existe une zone privilégiée dans laquelle on ne rencontre pas de bifurcation (figure 9). Il s'ensuit que si l'on astreint le système à demeurer dans cette région du plan, l'avion aura un comportement quasiment linéaire par rapport aux commandes $\delta l$ et $\delta m$. En pratique un tel système est un couplage gauchissement-direction, dont de nombreux exemples existent. Bien qu'ils ne modifient pas les réseaux de courbes de bifurcation qui sont intrinsèques à l'avion, ils en modifient l'apparence, car les équilibres accessibles ne sont plus les mêmes, et plus aussi variés, comme en témoigne la figure 10. En simulation le saut a disparu (figure 11).

4.4 - Remarques de synthèse sur l'auto-tonneau

Cet exemple simple montre l'efficacité de la méthode .

En effet, au-delà de la mise en évidence de l'importance des termes de couplage par inertie grâce à un modèle simple et linéarisé, le phénomène de l'auto-tonneau a reçu une explication claire et rigoureuse. Par ailleurs, on a pu ébaucher une méthodologie pour la recherche de lois de commande qui protègent les avions de combat contre les pertes de contrôle.

5. APPLICATION AU COMPORTEMENT D'UN AVION A GRANDE INCIDENCE

On rappelle que la méthode proposée conduit théoriquement à étudier les multiples infinités d'états d'équilibre possibles d'un modèle entièrement non linéaire. On a donc choisi de présenter les résultats de la manière suivante :

- 1ère partie : mouvements de pilotage transversal à position fixe de la profondeur

- 2ème partie : mouvements de profondeur pure (le modèle d'avion est dissymétrique).

Le souci de richesse de l'exposé a conduit à insister dans la première partie sur la méthodologie, en décomposant les différentes étapes du raisonnement. Dans la seconde, on insiste plus largement sur les aspects "qualités de vol".

5.1 - Pilotage transversal à $\alpha = 13°$, $\delta m$ = cte

Il s'agit d'étudier le comportement du modèle B lorsqu'on effectue des braquages d'ailerons et de direction autour du vol en palier à partir d'une incidence de 13°. Le problème étant ainsi posé, le système différentiel étudié ne dépend plus que de deux paramètres ( $\delta\ell$ , $\delta n$ ).

La première étape du calcul consiste à déterminer la surface d'équilibre du système lorsque $\delta\ell$ et $\delta n$ varient. Par exemple, si l'on fait un balayage des braquages de direction, à gauchissement nul, on observe qu'il existe de nombreux états d'équilibre qui correspondent à des valeurs très différentes des variables d'état (figure 12).

On note, au passage, qu'au dessus de 20° d'incidence, les courbes de l'état en fonction de la commande perdent leur propriété de symétrie, en raison des dissymétries incluses dans le modèle pour simuler l'aérodynamique à grande incidence.

Ensuite, pour chaque état d'équilibre, on calcule les valeurs propres de la matrice jacobienne. Actuellement, on distingue trois types de points d'équilibre, suivant les valeurs propres :

- ceux qui ont toutes leurs valeurs propres à partie réelle négative,

- ceux qui ont une ou plusieurs valeurs propres réelles positives,

- ceux qui ont leurs valeurs propres réelles négatives mais qui possèdent au moins 2 valeurs propres imaginaires conjuguées à partie réelle positive.

Les premiers sont stables, les seconds sont instables et inaccessibles, les troisièmes, instables eux aussi, peuvent conduire à l'apparition d'oscillations non linéaires entretenues (cycle limite).

Ensuite, on détermine la projection dans l'espace des commandes ( $\delta\ell$ , $\delta n$ ) de l'ensemble des points pour lesquels la partie réelle des valeurs propres passe par zéro. Dans la suite de cette communication, on ne raisonnera que sur les points de bifurcation correspondant au changement de signe des valeurs propres réelles ( figure 13). En effet, le cas des valeurs propres imaginaires à partie réelle positive nécessite un traitement particulier non encore mis en oeuvre, et dont la portée pratique n'est pas encore clairement établie. Sur la figure 13, le nombre d'états d'équilibre est indiqué par zones. La traversée d'une ligne de bifurcation se traduit par l'apparition (ou la disparition) de deux états d'équilibres.
Il est à noter que la surface de bifurcation n'est pas symétrique par rapport au centre du diagramme.

L'étape suivante consiste à prédire le comportement de l'avion lorsque le pilote agit sur les gouvernes de gauchissement et de direction. Pour cela, et compte tenu de la configuration du diagramme de la figure 13, on choisit d'étudier deux manoeuvres symétriques par rapport au point d'équilibre initial défini plus haut. La première est constituée par un braquage du manche à gauche ( $\delta\ell$ = + 10°) suivi d'un braquage du pied à gauche de $\delta n$ = 0° à $\delta n$ = + 20° exécuté en deux temps, en s'arrêtant quelques secondes à mi-braquage ( $\delta n$ = 10°). D'après les courbes d'équilibre quasi-statique correspondant à cette manoeuvre (figure 14), le système ne traverse pas de point de bifurcation. Malgré cela, au voisinage de $\delta n$ = 10°, la variation des paramètres d'équilibre est importante en raison de la proximité de la bifurcation, et peut entraîner une perturbation sur le mouvement de l'avion. La seconde manoeuvre est symétrique de la première. Le pilote agit sur le manche à droite ( $\delta\ell$ =-10°) puis sur la direction à fond à droite de $\delta n$ = 0° à $\delta n$ = - 20° en s'arrêtant quelques instants à mi-braquage. L'analyse des courbes d'équilibre (figure 16) montre que, partant d'un état stable, le système traverse une bifurcation pour $\delta\ell$ = - 10° et $\delta n$ = - 12°. De plus, au-delà de $\delta n$ = - 12°, le système tend vers une branche d'équilibre instable oscillatoire. En intégrant les équations du système lorsque l'on perturbe l'état d'équilibre donné par la résolution de l'équation $\dot{X} = 0$ pour $\delta n$ = - 20°, on prédit l'existence d'une oscillation non linéaire entretenue sur toutes les variables du système.

La dernière étape, facultative, de l'application de la méthodologie est destinée à démontrer l'exactitude des prédictions par la simulation. La première manoeuvre (figures 14 et 15) montre que le mouvement de l'avion est perturbé par le passage à proximité d'une bifurcation. Dans la seconde (figures 16 et 18), on observe que le comportement du système est "quasiment linéaire" jusqu'à la combinaison de braquages ( $\delta\ell$ = - 10°, $\delta n$ = - 10°) ; puis, apparaît le saut sur les variables d'état et le développement du cycle limite escompté (figure 17).

5.2 - Mouvements de profondeur à partir de $\alpha = 13°$

Il s'agit de déterminer les différents comportements que peut présenter un avion lorsque le pilote agit seulement sur la profondeur à cabrer ou à piquer à partir d'une incidence de 13° avec le gauchissement et la direction au neutre ; compte tenu que le modèle aérodynamique B est dissymétrique au-delà de $\alpha$ = 20° (figure 20). Les calculs de la surface d'équilibre et de la stabilité de chacun des états mettent en évidence de nombreux points de bifurcation (figure 19) que l'on va étudier.

Partant des conditions d'équilibre à l'incidence de 13° et cabrant légèrement, on rencontre une première bifurcation à $\delta m$=-0,5°. Elle correspond approximativement à l'apparition de l'instabilité spirale prévue par les critères traditionnels. Le retour à la stabilité se situe vers $\delta m$ = - 4°. Entre ces deux valeurs, l'avion est instable en vol rectiligne et, sur une perturbation transversale, il tend vers un vol en virage dont les caractéristiques sont déterminées par les deux branches d'équilibre stable situées entre $\delta m$ = - 0,5° et $\delta m$ = - 4° (figure 21).

Lorsque l'action à cabrer est plus importante ( $\delta m$ = - 18°),on trouve une [illegible] de 3 bifurcations très proches dont l'existence semble être liée à la dissymétrie du modèle à grande incidence. De plus, lorsqu'on étudie la stabilité des différentes surfaces d'équilibre en présence, on s'aperçoit qu'elles sont soit instables, soit instables oscillatoires. D'une manière générale, les simulations montrent que la conjonction de bifurcations et de surfaces instables entraîne un comportement très agité de l'avion (figure 22)

En effet, lorsque le pilote tire sur le manche suffisamment pour se placer au voisinage de des bifurcations l'avion commence par subir une excursion très rapide en dérapage en raison de l'instabilité oscillatoire qui correspond à la divergence du roulis hollandais. Ensuite, en continuant le braquage à cabrer, l'avion entre dans une vrille très agitée. Il serait hasardeux de généraliser mais ce comportement du système n'est pas sans rappeler des pertes de contrôle transversal, réelles, obtenues gouvernes transversales au neutre, lorsque le pilote exécute une forte montée en incidence ou une cloche.

Au-delà de $\delta m = -22°$, on observe une bifurcation importante. En effet, pour les braquages extrêmes, il ne reste plus qu'une seule surface d'équilibre, très éloignée de la bifurcation qui entraîne un saut et une grande variation des paramètres d'équilibre. En outre, cette surface est instable oscillatoire et, pour $\delta m = -25°$, elle admet un cycle limite que l'on retrouve en simulation (figure 23). En ce point, on peut montrer que si l'on continuait à cabrer, l'avion tendrait vers une vrille plate, très stable ($\alpha \simeq 80°$), dont il ne sortirait pratiquement pas, sauf si certains mouvements de gouvernes pouvaient restaurer un niveau d'agitations permettant la sortie.

Par contre, si l'on ramène la profondeur au neutre, le cycle limite se transforme en oscillation divergente, le système s'éloigne de la surface de vrille et vient converger vers l'état stable initial à $\alpha = 13°$. Grâce à la grande efficacité de la profondeur du modèle B, il est donc possible de sortir de la vrille (figure 24).

Lorsque l'action sur la profondeur est à piquer, deux surfaces quasiment symétriques par rapport à l'axe $r = 0$ apparaissent. Dans ce cas, si l'on compare la forme et l'évolution de la vitesse de roulis réduite (P1/V) avec celle obtenue au paragraphe 4 et figure 7, on constate une grande similitude, malgré les hypothèses simplificatrices utilisées dans l'étude de l'auto-tonneau et la différence entre les modèles d'avions (figure 25).

Dans le cas présent, il s'agit des surfaces correspondant à l'état d'équilibre vers lequel tend l'avion après avoir effectué des auto-tonneaux, enchaînés autour d'une trajectoire semi-balistique.

Ces surfaces peuvent être atteintes en sortie de vrille comme le montre la simulation (figure 26).

Cette rapide revue des différentes bifurcations dues à l'action sur la gouverne de profondeur montre un des aspects de la puissance de cette analyse.

En effet, une étude de simulation pure des pertes de contrôle serait longue et hasardeuse alors que le calcul des caractéristiques de la surface d'équilibre permet de conclure rapidement. De plus, pour vérifier les prédictions, il suffit d'effectuer quelques simulations cruciales.

## 6. CONCLUSION

Les résultats présentés dans cette communication montrent la richesse des renseignements fournis par la théorie des bifurcations appliquée à la mécanique du vol.

Cette technique ne dispense cependant pas de la recherche d'un bon modèle aérodynamique de l'avion étudié, valable dans une large gamme d'incidence et de dérapage autour des manoeuvres envisagées. Sa première mise en oeuvre est un peu lourde, mais par la suite, grâce à la finesse de l'ingénieur, elle apporte une moisson de renseignements qui compense largement les inconvénients mentionnés ci-dessus.

Le potentiel de cette technique est considérable. Elle constitue un outil efficace et rigoureux pour l'étude de l'influence des non-linéarités sur le vol de l'avion. Outre les indications qu'elle fournit évidemment sur la limite de validité des calculs linéarisés, elle permet d'envisager sérieusement une approche déterministe des problèmes de pertes de contrôle. Il reste entendu que la qualité du résultat sera directement fonction de la qualité du modèle aérodynamique. Mais la constitution du modèle requis est peut-être un problème moins difficile qu'on pourrait le craindre.

En effet, certains des résultats d'application mentionnés dans ce texte tendent à montrer qu'un modèle statique -même à très grande incidence- suffit déjà à rendre compte de comportements irréguliers et agités, qui eussent été qualifiés de pseudo-aléatoires dans un contexte essais en vol, par exemple.

Enfin, la théorie des bifurcations constitue le premier pas, décisif, dans l'établissement d'une méthodologie pour la conception de systèmes de commandes de vol qui puissent offrir à coup sûr une protection contre les pertes de contrôle.

## 7. REFERENCES

[1] R. THOM
Stabilité structurelle et morphogénèse

[2] A.A. SCHY, M.E. HANNAH
"Prédiction of jump phenomena in Roll Coupling manoeuvers of airplanes"
Journal of Aircraft, Vol. 14, April 1977

[3] A.A. SCHY, J.W. YOUNG, K.G. JOHNSON
"Pseudo-state analysis of nonlinear aircraft manoeuvers"
NASA TP 1758, Dec. 1980

[4] MEHRA, KESSEL, CARROL
"Global Stability and Control Analysis of aircraft at high angle of attack"
Scientific systems Inc-AD-AO 51850-SSI-TR-77-1

[5] T. HACKER et C. OPRISIU
"A discussion of the roll coupling problem"
Progress in Aerospace Sciences, Vol 15, Pergamon Press, Oxford 1974

[6] R.W. KLOPFENSTEIN
"Zeroes of nonlinear functions"
J. ACM, 8 (1961)

[7] H.B. KELLER
"Numerical solution of bifurcation and nonlinear Eigenvalue problems"
Application of Bifurcation Theory
Academic Press New York (1977)

[8] M. KUBICEK
"Algorithm 502, Dependance of Solution of nonlinear Systems on a Parameter"
ACM-TOMS, 2 (1976) pp. 98-107

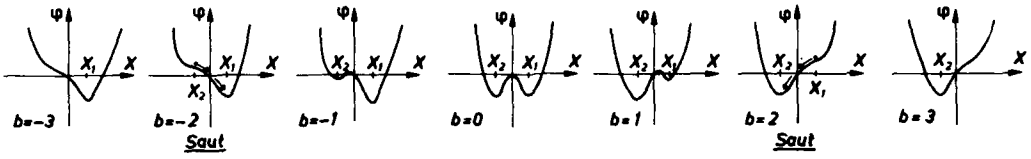


*Fig. 1 – Catastrophe de Riemann Huguoniot : fonction potentielle $\varphi(x) = (x^4/4) + (ax^2/2) + bx$ (avec $a = -3$).*

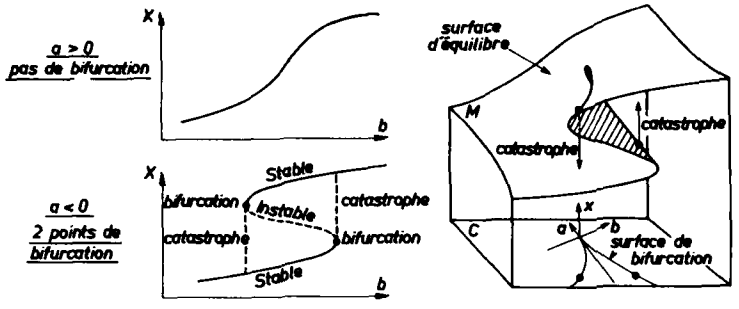


*Fig. 2 – Catastrophe de Riemann Huguoniot : Surfaces d'équilibre et de bifurcation.*

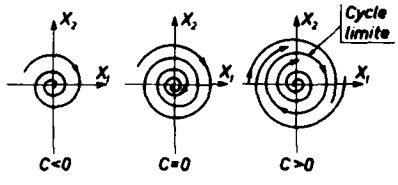


*Fig. 3 – Bifurcation de Hopf.*

*Retour à l'équilibre en fonction de C*

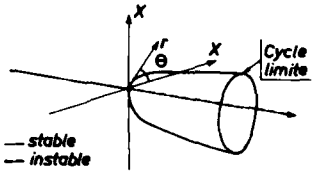


*Evolution des attracteurs en fonction de C*

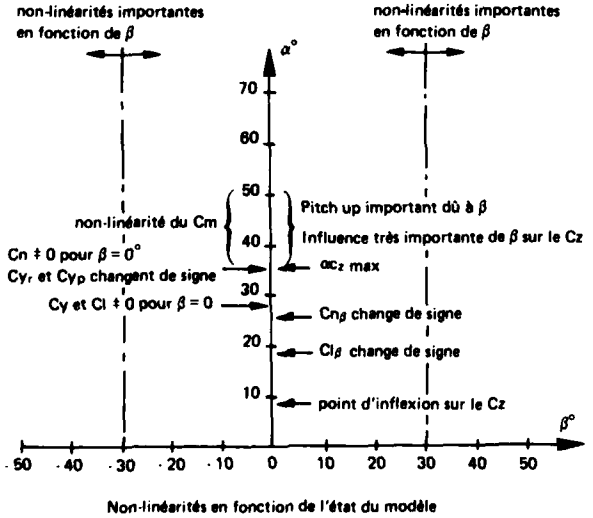


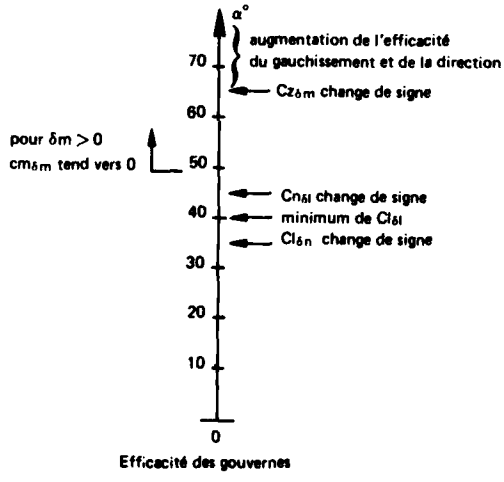


*Fig. 4 – Planche récapitulative des principales non-linéarités du modèle B.*

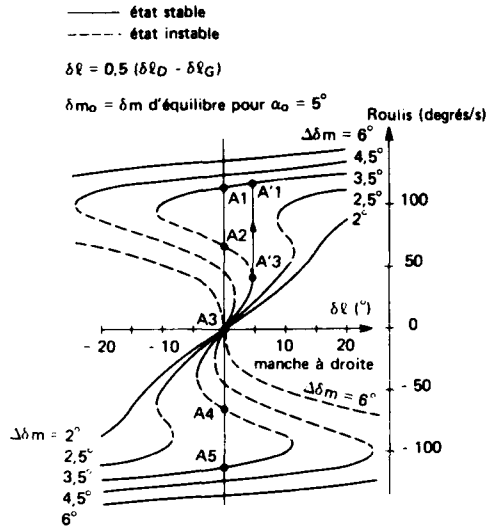


*Fig. 5 – Avion A : Evolution de la vitesse de roulis d'équilibre en fonction du braquage du gauchissement.*

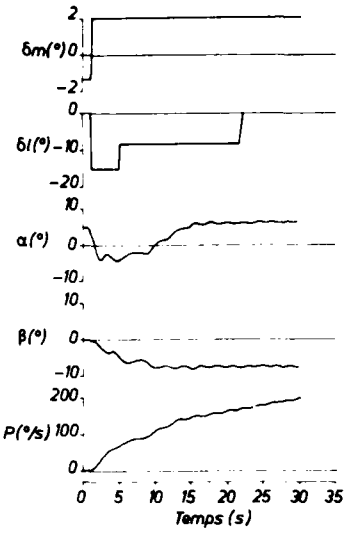


*Fig. 6 – Avion A : Simulation.*

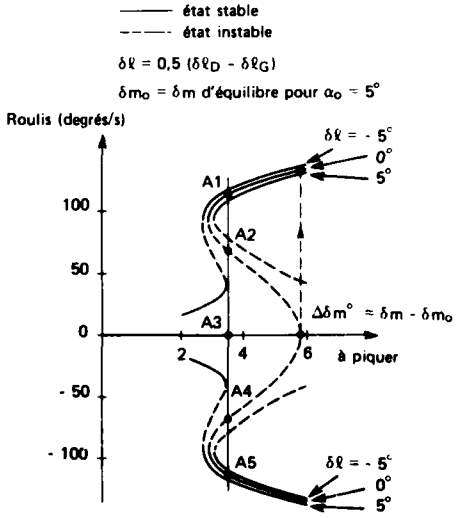


*Fig. 7 – Avion A : Influence de la profondeur.*

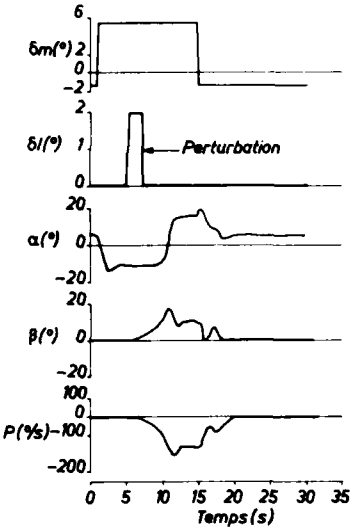


*Fig. 8 – Avion A : Simulation.*

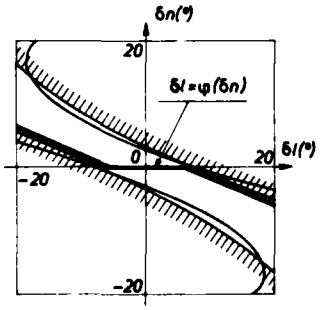


*Fig. 9 – Avion A : Surface de bifurcation. Loi de pilotage δl = φ (δn).*

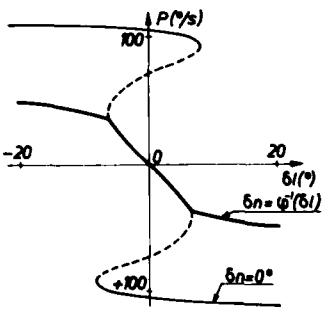


*Fig. 10 – Avion A : Influence de la loi de pilotage sur la vitesse de roulis*

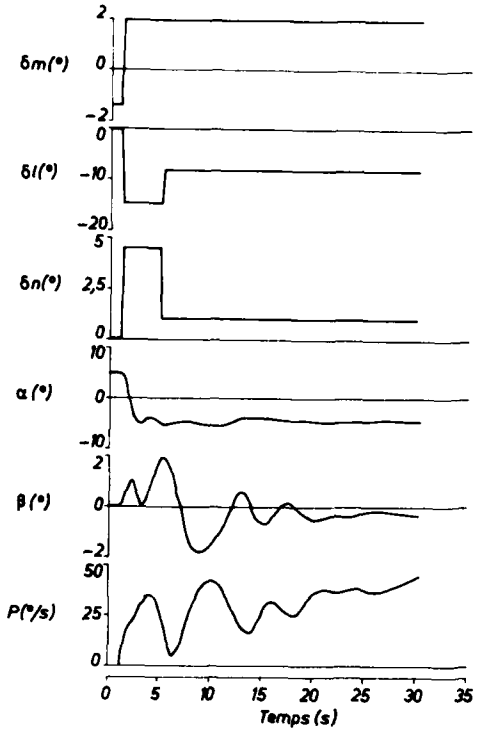


*Fig. 11 – Avion A : Simulation.*

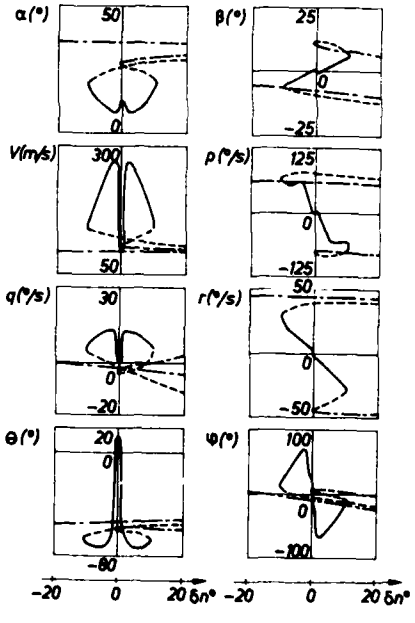


*Fig. 12 – Extrait de la surface d'équilibre de l'avion B ($\delta m \approx 0{,}4°$, $\delta l = 0°$).*

—— *stable*
------ *instable*
– – – *instable oscillatoire.*

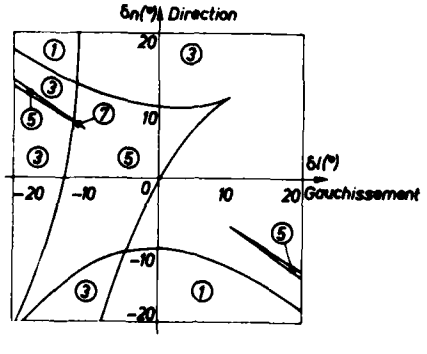


*Fig. 13 – Avion B : Surface de bifurcation ($\delta m = 0{,}4°$).*
*(n) n états d'équilibre.*

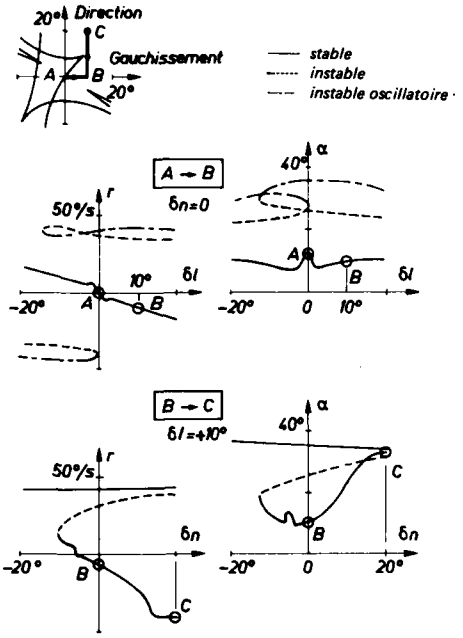


Fig. 14 – Avion B : Manoeuvre n° 1 : Prédiction

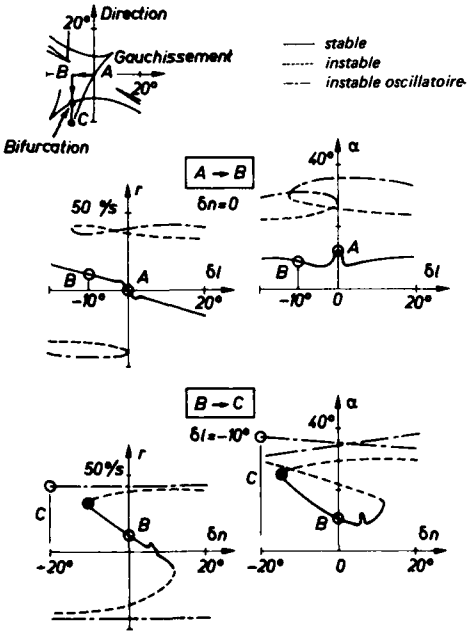


Fig. 16 – Avion B : Manoeuvre n° 2 : Prédiction.

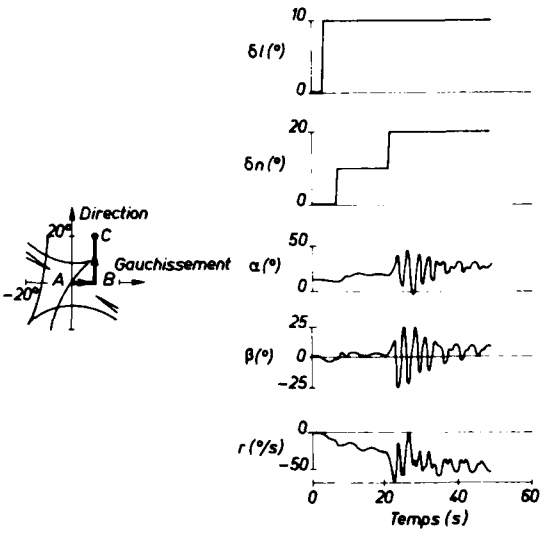


Fig. 15 – Avion B : Manoeuvre n° 1 : Simulation.

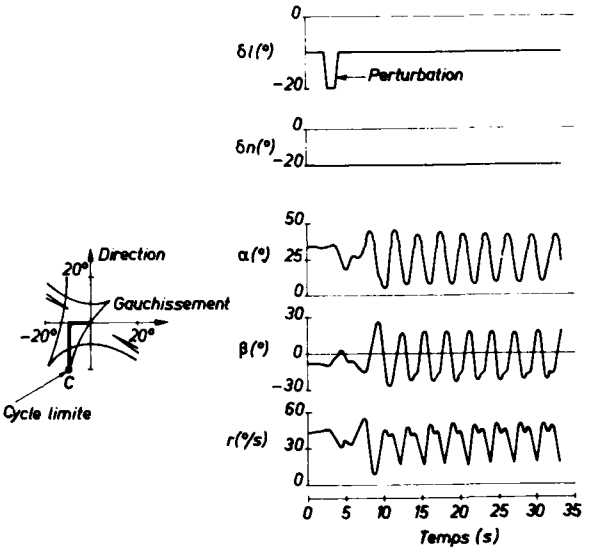


Fig. 17 – Avion B : Manoeuvre n° 2 : Prédiction du cycle limite.

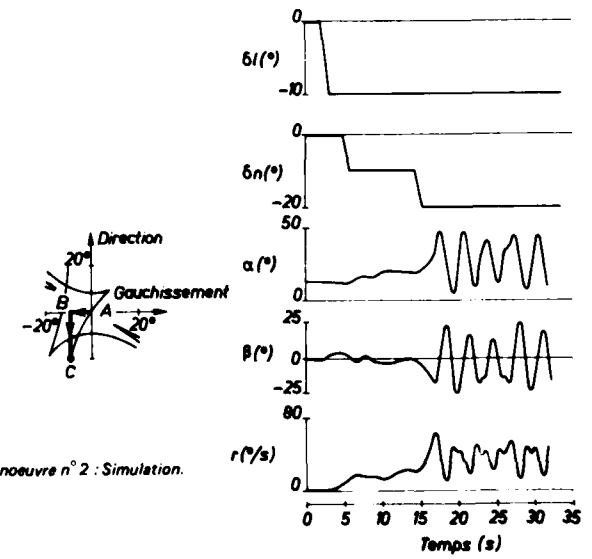


Fig. 18 – Avion B : Manoeuvre n° 2 : Simulation.

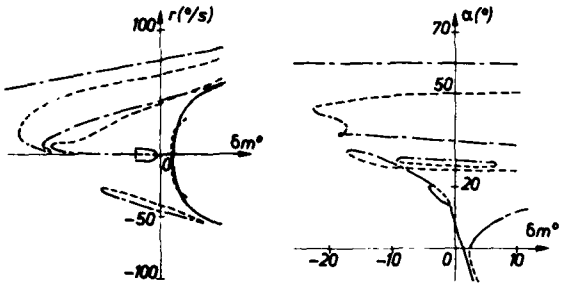


*Fig. 19 – Avion B : Influence de la profondeur (Extrait de la surface d'équilibre).*

—— *stable*
------ *instable*
-·-·- *instable oscillatoire.*

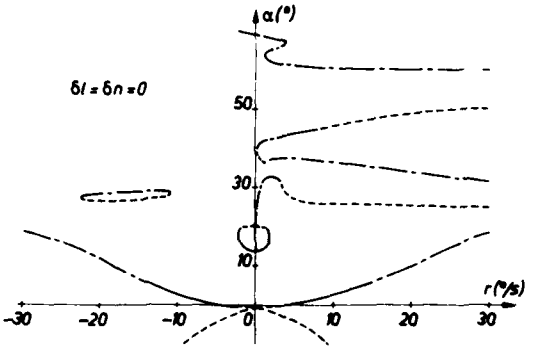


*Fig. 20 – Avion B : Influence de la profondeur. Diagramme (α, r).*

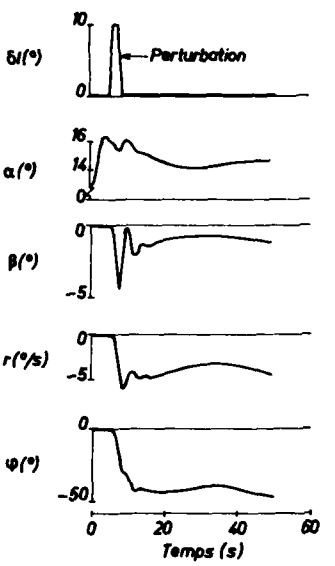


*Fig. 21 – Avion B : Simulation de l'instabilité spirale.*

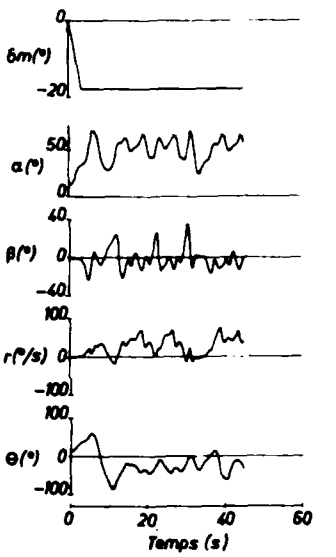


*Fig. 22 – Avion B : Perte de contrôle transversale.*

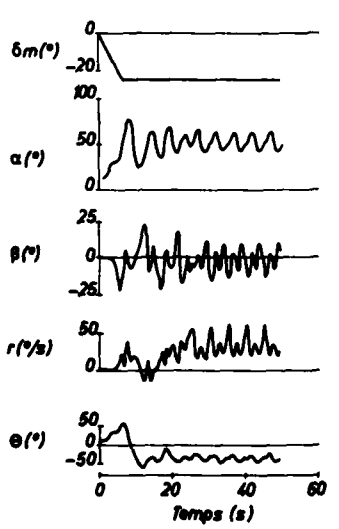


*Fig. 23 – Avion B : Mise en vrille.*

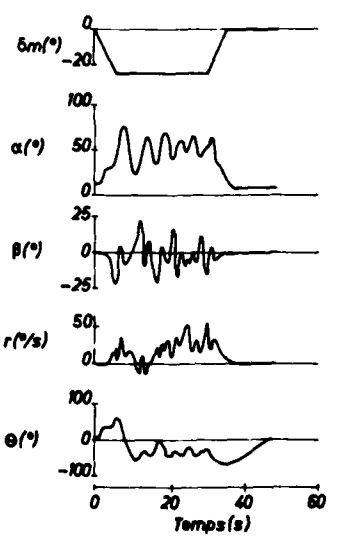


*Fig. 24 – Avion B : Sortie de vrille. Manche au neutre.*

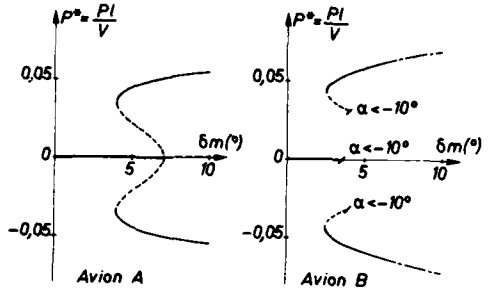


Fig. 25 – Auto-tonneau. Comparaison des avions A et B.

—— stable
····· instable
–·– instable oscillatoire.

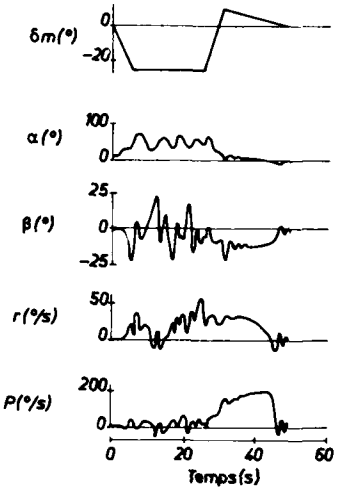


Fig. 26 – Avion B : Sortie de vrille par auto-tonneau.

# PREDICTIONS OF AERODYNAMIC CHARACTERISTIC OF HIGHLY MANEUVERABLE CONFIGURATIONS

by

W. B. Brooks
Senior Staff Engineer, Aerodynamics
and
T. D. Beatty
Senior Engineering Specialist, Aerodynamics

Vought Corporation
Box 225907
Dallas, Texas 75265

SUMMARY

Vought has surveyed the ability of a variety of currently available engineering type methods to predict the lateral/directional characteristics of arbitrary configurations. The programs surveyed generally had either non- linear or arbitrary body capability, but not both. Published comparisons between the Hypersonic Arbitrary Body program and experimental data suggested a direct extension of the commonly used Allen-Jorgenson cross flow analogy to arbitrary bodies. Though useful, however, this extension of the Allen-Jorgenson method did not include dynamic pressure losses on aft lifting surfaces.

Vought has recently begun examination of a non-linear approach which computes the forces on a combined body/separated region contour and corrects these forces by an empirical momentum deficit in the separated region. For axisymetric bodies the method reduces to the standard Allen-Jorgenson cross flow approach. Two potentially major advantages over the Allen-Jorgenson method are that the method does provide a model for predicting body-fin interaction and that the method is extendable to arbitrary bodies.

NOMENCLATURE

$A_R$ is the reference area
$A_1$ = Area of Physical Body
$A_2$ = Area of Combined Body
a is semi width
b is semi height
$C_d$ is the length adjusted cross flow drag coefficient
$(C_n/C_{n_0})$ is the shape adjustment based on Newtonian Newtonian theory
$C_\Delta$ is the coefficient of momentual deficit
F = Y + i N
L is the body length
N = the normal force
R is the equivalent radius
q = v + i w
V is the free stream velocity
v is the lateral velocity component
W is the complex potential
w is the vertical velocity component
$\Delta X$ is the distance between cross sections
Y = the side force

$\zeta$ = y + i z
$\alpha$ is the angle of attack
$\beta$ is the angle of side slip
$\rho_\infty$ is the free stream density
$\gamma_c$ is ARC TAN $\alpha^a/\beta b$

## 1. INTRODUCTION

The preliminary design assessment of the maneuverability of advanced configurations requires adequate predictions of aerodynamic characteristics. Many of these configurations, such as those shown in Figure 1, blend the propulsive, lifting, and load carrying, elements to form an efficient air frame. To analyze such configurations Vought has combined many of the currently available methods into an analysis system called VAAAS. A modular construction philosophy allows new methods to be easily incorporated as acquired. This system has permitted a systematic examination of current methods that predict lateral directional characteristics of advanced configurations. Of the methods examined only the Hypersonic Arbitrary Body Program (HABP) had even limited non-linear aerodynamic predictive capability for arbitrary geometries. Good agreement between prediction and experimental data from the Aerodynamic Configured Missile (ACM) study (e.g., Reference 1) initially suggested a Newtonian flow modification to the Allen-Jorgenson cross flow analogy. This modification has been accomplished and has proven useful in predicting lateral directional characteristics of arbitrary lifting body configurations. For complete configurations the Newtonian modification did not provide adequate estimation of body-fin interaction.

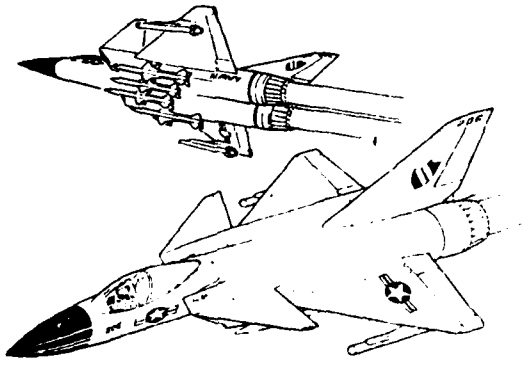

**FIGURE 1 Advanced Configuration**

Recently Vought has been investigating an approach suggested by work performed at the Naval Weapons Center (NWC) in which the potential flow is computed based on the physical body and the separated flow region to the lee of the body. A simple separated flow model is then applied to the flow inside the separated region. The method reduces to the Allen-Jorgenson analogy as a special case but is expected to also estimate the body-fin interactions so critical to the prediction of lateral directional characteristics.

## 2. VOUGHT AUTOMATED ANALYSIS SYSTEM (VAAAS)

VAAAS is divided into three basic parts. These parts, illustrated in Figure 2, are the geometric input, analysis, and output display. The input and display functions of the system are common to all analysis methods. To maintain this commonality, an input pre-processor and an output post-processor for each method are included in the system. This serves two purposes. First it maintains the basic systems structure, and second each analysis methods maintains a stand alone capability.

A primary task in the analysis of an arbitrary configuration is the formulation of the digitized computer input. In the VAAAS system, configurations are formed and stored as components using a Hess-Smith quadralateral representation (Reference 2). Three options are available for inputting these components; cards, digitizing tablet and utilization of specified shapes. Early in a design, a digitizing tablet input is inefficient since accurately scaled cross sections are required. An example of the geometry input is illustrated in Figure 3.

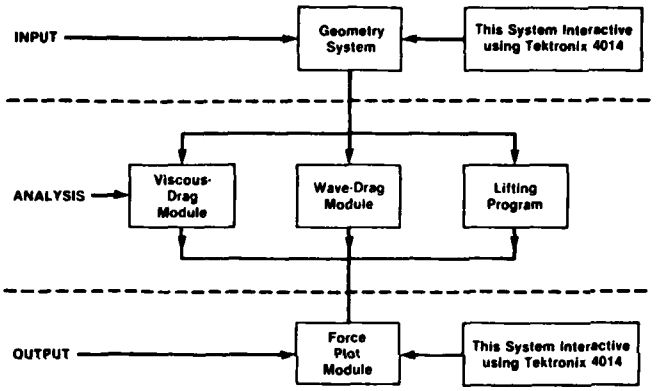


FIGURE 2 Program Organization

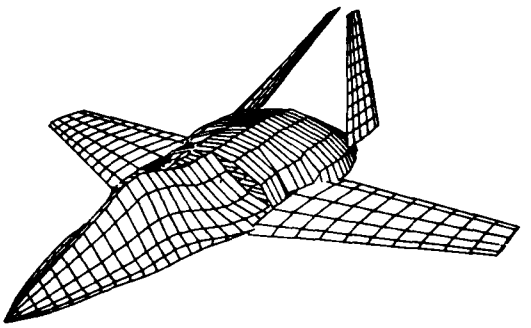

FIGURE 3 Typical Panel Geometry

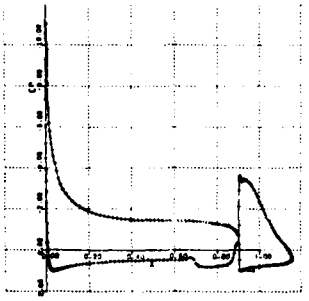

FIGURE 4 Terminal Output

Because each analytical method maintains its orginial form, the standard program output is available. But for most evaluation purposes graphical presentations are more convenient. It is desirable that these presentations include not only analytical configuration analysis, but comparisons with experimental data, when possible. To aid in both purposes the VAAAS output post processors store the results of the analytical programs on index sequential files in the same form as results stored from wind tunnel test examinations. Consequently, both analytical and experimental files can be accessed through computer procedures for either interactive presentation using the Tecktronix 4014 or hard copy Calcomp type plots for formal presentations. Examples are shown in Figure 4.

## 3. ANALYTICAL METHODS SURVEYED

At present VAAAS contains the analytical routines illustrated in Figure 5. Of these only the "ADVANCED" routines have significant arbitrary body capability, and only the Hypersonic Arbitrary Body Program (HABP) has both arbitrary body on non-linear capability. This particular program has been extensively compared with experimental data for arbitrary configurations, for example the aerodynamic configured missile (ACM studies reported in Reference 1). The results obtained to date are quite encouraging; however, the limitation of the program to higher Mach numbers limits its usefulness. Previous experience indicated non-linear capability and particularly a procedure for the shadowing of one component by another is of critical importance for determining lateral directional characteristics.

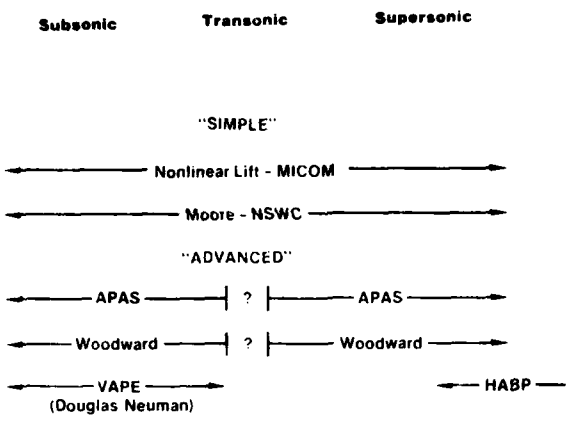


FIGURE 5 VAAAS Methods

Recently a number of groups, such as the Naval Surface Weapons Center and Nielsen Engineering, have initiated research efforts to develop non-linear methods for non-circular bodies. These efforts, however, are still in the development stage. As these or other new codes reach "production" status Vought intends to incorporate the more appropriate ones into the VAAAS system. However, until such codes are available, some modification of existing methods is required. Both the MICOM and the Moore-NSWC programs, illustrated in Figure 5, estimate the non-linear effects through variations on the axisymetric version of the Allen-Jorgenson method, Reference 3. Because of the nature of this method, the proper way to extend the approach to non-circular configurations (and particularly to the prediction of lateral directional characteristics) is not obvious. Jorgenson, in Reference 3, suggested an approach in which the Newtonian force on a given cross section is ratioed to that of a circular cross section. This ratio is then used to modify the empirical cross flow drag coefficient in the non-linear computation.

This results in the expansion (taken directly from Reference 3).

$$\Delta\left(\frac{d/C_N}{d/L}\right)_{NONLINEAR} = \frac{2n\ C_d\ SIN^2}{A_R} \int_0^L \left(\frac{C_n}{C_{n_o}}\right)_{NEWTONIAN} R\ dx$$

4. NEWTONIAN EXTENSION OF ALLEN-JORGENSON ANALOGY

While Jorgensen's original suggestion is limited to angle of attack variation, the conceptual idea of computing the Newtonian force on a section and then empirically correcting the results based on test data for circular cylinders is at least feasible. (In practice the task is simpler if the angle of attack/side slip dependence is included in the Newtonian factor.) Indeed the ACM experience, Reference 1, with the Hypersonic Arbitrary Body program suggests this extension of the Allen-Jorgenson method may produce satisfactory results at least at the higher Mach numbers. Such a computation has been carried out explicitly for an elliptic cross section. The resulting side force factor is

$$\frac{dCy}{dx} \propto 2b \left\{ \frac{4\ b/a}{[1-(b/a)]^{3/2}} TAN^{-1}\left[\sqrt{\left(\frac{a}{b}\right)^2 - 1}\ \cos\eta_o\right](\beta^2 - \alpha^2) - \frac{2\cos\eta_o}{1-(b/a)^2}\left[(b/a)^2\beta^2 - \alpha^2\right] - \alpha\beta\ \frac{4\ b/a\ \sin\eta_o}{1-(b/a)^2} + \alpha\beta \frac{4\ b/a}{[1-b/a]^{2/3}}\ TANH^{-1}\left[\sqrt{1-(b/a)^2}\ \sin\eta_o\right]\right\};\quad a>b$$

The constant of proportionably is somewhat arbitrary. The direct adaptation of Jorgenson's work would be to use a proportionably factor of $3/8\ 1/\sqrt{ab}$, but Vought experience suggests the $\sqrt{ab}$ not be included and appropriate changes be made in the Allen-Jorgenson integral. The complexity of this explicit relation illustrates the necessity of machine computational procedures for evaluating the Newtonian factor for truly arbitrary bodies. Experience with the Hypersonic Arbitrary Body Program suggests the required coding procedures are already available.

In carrying out his Newtonian computations, Jorgenson assumed that the lee side of the section approached vacuum conditions. The ACM studies of Reference 1 found this assumption was only satisfactory at very high Mach numbers. In the ACM studies a modified pressure relation was required for good data correlation. Also, Jorgenson did not address the shielding problem.

5. ANALYTICAL COMPARISONS

For evaluation of potential procedures Vought has relied heavily on the experimental data for the configuration shown in Figure 6. This configuration offers a variety of cross sectional variations and has been extensively tested by NASA at supersonic speeds.

The body inlet side force characteristics of the three configurations at a Mach number of 2.50 are shown in Figure 7. Also shown is the Newtonian extension of the Allen-Jorgenson method for configuration $B_1I_1$. (In performing this computation the inlet/body cross section was assumed to be elliptical.) The general shape of the curve is encouraging. It is interesting to note the effect of inlet orientation on the shape of the curves. Both the $I_2$ and $I_3$ inlet curves show a far more complex dependency on angle of attack. The dotted line across the curves illustrates the attitude at which the windward inlet is aligned with the cross flow. Each curve tends to be linear for an angle of attack

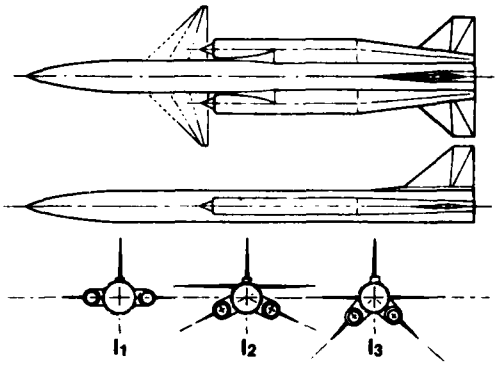


FIGURE 6 Test Configuration

increment that is "roughly symmetric" about this point. At the higher angle of attack end "linearity" of this region there is a noticeable reduction in the slope of the curve. (Indeed the side force declines locally for the $I_2$ inlet.) After readjustment the curves are roughly parallel to the $B_1I_1$ inlet. This behavior is consistent with the Newtonian approach since, at large angle of attack the separation pattern for each cross section would be similar.

A component build up for the $I_2$ configuration is shown in Figure 8. Of particular interest is the full component characteristics. Note that the side force begins to drop off around 3 degrees probably due to shielding of the vertical fin. This side force decline continues up to around 14 degrees at which time the fin should be totally blanked. At this point the side force again picks up and maintains a slope roughly parallel to that produced by the wing effects. As would be expected the data appears to confirm the need for shadowing effects in any good lateral directional computational procedure. Thus, while the Newtonian extension of the Allen-Jorgenson method contains several potentially useful features, additional improvements are necessary. Current work along these lines are discussed in the next section.

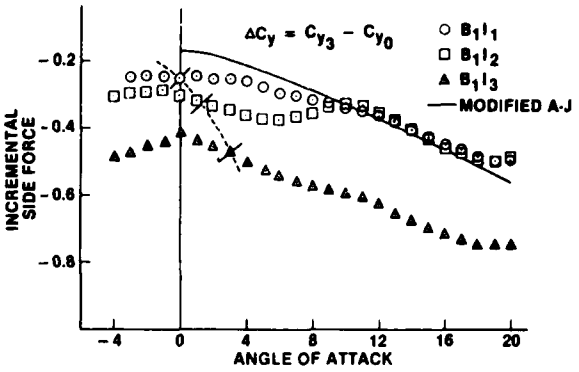


FIGURE 7 Body Inlet Comparisons

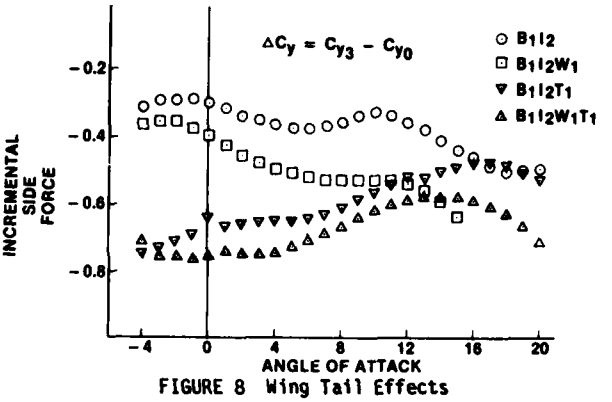


FIGURE 8 Wing Tail Effects

## 6. PROJECTED IMPROVEMENTS

A principle shortcoming of the methods considered is their inability to predict the vortex and separated flow regions which develop at angle of attack. These flow regions have significant impact on the lateral/directional characteristics primarily because of effects on the vertical tails. Even with computer advances, the adequate representation of these regions is still beyond the current practical state of the art. The most ambitious efforts involve the Reynolds averaged Navier Stokes Equations. Not only are these codes large and time consuming, but also success is critically dependent on the turbulence model used. Unfortunately an effective universal turbulence model does not now exist. A second approach is the multi vortex codes procedured by Wardlow and Nielsen. To date these codes have been limited to simple geometry. The codes have a fundamental problem in that a "cloud" of discreet vortex elements, no matter how carefully choosen, do not represent the physical flow phenomena within the bound of the cloud. For example, axial momentum deficits within the separable region are not easily represented within the region while the vortex "swirl" flows are locally exaggerated. Thus, the model is overly complex for predicting flow fields outside the separated region without offering a physically meaningful model within the separated region. The shortcomings of this finite vortex model have suggested a simpler approach which may be equally valid physically and a good deal more efficient computationally. This is to treat the potential flow around a composite body/separated region and then treat the separated region in a comparatively simple fashion. Vought has made some preliminary estimates within slender body theory using a conceptual approach. In these estimates, the boundary of the separated region is assumed to be generated by lines parallel to the free stream velocities as shown in Figure 9. While this is an obvious over-simplification, it does include many of the critical features of the comparison.

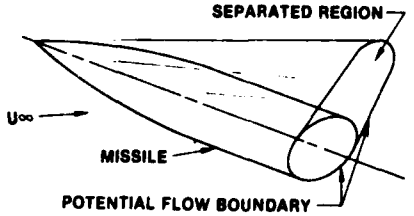


FIGURE 9 Conceptual Model

From slender body theory, Reference 4 the complex force on an element of the combined body/separated region is:

$$F = -i \rho_\infty V_\infty \oint W \, dz - \rho_\infty V_\infty \bar{q}_\infty A_1$$

Altering the expression to included the momentum deficit gives the expression.

$$F = -i \rho_\infty V_\infty \oint W \, dz - \rho_\infty V_\infty \bar{q}_\infty [A_1 + C_\Delta (A_2 - A_1)]$$

For a simple illustration of the conceptual approach, consider a circular body with an approximately, elliptic combined body. (Similar to that shown in Figure 9.) Because of the geometry it is sufficient to consider only angle of attack.

$$F = i N$$
$$q = - i w$$

For an ellipse the appropriate Laurent expansion of the complex potential is

$$W - i w_\infty \left( z - b \frac{(a + b)}{2z} + \ldots \right)$$

Therefore around a closed contour:

$$W \, dz = -w_\infty \frac{b(a + b)}{2} (2 \pi)$$

Similarly the areas are:

$$A_1 = \pi b^2$$
$$A_2 = \pi a b$$

This leads to a force estimation:

$$N = \rho_\infty V_\infty w_\infty (C_\Delta \pi b^2 + (1 - C_\Delta) \pi (ab)$$

For a body lamina

$$\frac{d C_n}{dx} = 2 \left( C_\Delta \frac{d}{dx} (\pi b^2) + (1 - C_\Delta) \frac{d}{dx} (\pi a b) \right.$$

Simplifying to a high fineness ratio body:

$$a = b + x \alpha / 2$$

Hence;

$$\frac{dC_n}{d\alpha} = 2 \alpha \frac{d}{dx} (\pi b^2) + (1 - C_\Delta) 2\alpha^2 b + \ldots$$

Note this is identical in form to the Allen-Jorgenson cross flow method with

$$C_{dc} \sim 1/2 (1 - C_\Delta)$$

This approach has two major advantages over classical Allen Jorgenson theory. First separated flow/fin interference is estimated since the region of influence is bounded. Second, at least conceptually, the approach is directly extended to arbitrary cross sections at arbitrary roll orientations. Both these advantages stem a methodology that is nearer to a rational perturbation philosphy (e.g. related to boundary layer theory) than to an analogy. Indeed by employing an "inner" model to the separated flow a fully rational iteration scheme might be possible.

Vought has adapted this preliminary model to the APAS slender body method, etc. Starting at the nose, an initial cross section is projected back along the free stream velocity vector. This is accomplished by the simple translation.

$$y_1 = \Delta X_i \sin \beta$$
$$Z_1 = \Delta X_i \cos \beta \sin \alpha$$

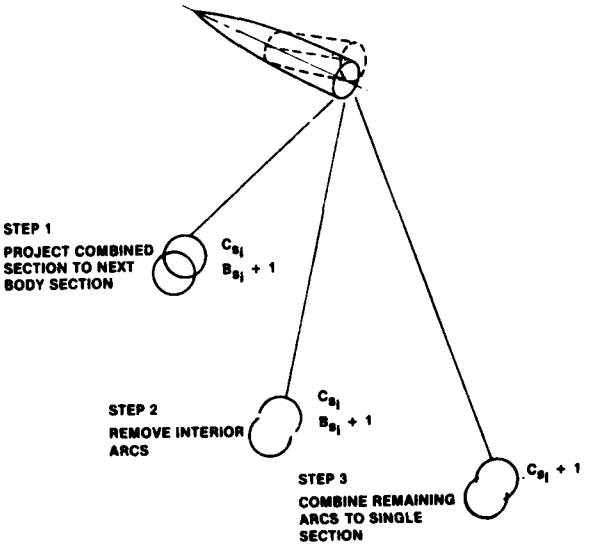


FIGURE 10 Composite Cross Section Development

At the next station this produces possibly two overlapping cross sections, as shown in the first part of Figure 10. A Cauchy integral criteria is used to remove interior arcs and then sequentially connects the remaining segments, as illustrated by the middle part of Figure 10. These cross sections are combined into a single cross section, a shown schematically in the second part of Figure 10.

The flow around the combined cross section is computed using the slender body subroutines of APAS. The computation is continued by projecting the combined section back to the next body segment, etc. The computation of the momentum deficit correction to the force involves only the determination of the difference in the cross sectional area of the combined and body cross sections and the coefficient of momentum deficit. For present purposes the $C_{Dc}$ curve of MOORE in the NSWC program is used to infer $C_a$. While the basic methods are linear, a non-linear result is produced since the cross sectional geometry of the combined flow field now changes with angle of attach as well as side slip.

The procedure is still in the early stages of evaluation. Because of the close connection with more conventional cross flow methods, several of the more prominent shortcomings of the Allen-Jorgenson method will likely remain in the present formulation. Because of the tendency of the current approach toward a rational perturbation procedure, several potential avenues to correcting these shortcomings are open. This would include a more rational selection of separation boundary and/or improved model of the separated region.

## REFERENCES

1. Krieger, R. J., Gregoire, J. E., Hood, R. F., Eiswirth, E. A. Taylor, M. L., "Aerodynamic Configured Missile - Final Report", Technical Report AFWAL-TR-80-3071, March 1980.

2. Gentry, Ervil E., Smyth, Douglas N., Oliver, Wayne R., "The Mark IV Supersonic-Hypersonic Arbitary Body Program", Technical Report AFFDC-TR-73-1959, November 1973.

3. Jorgenson, L. H., "Prediction of Static Aerodynamic Characteristics of Slender Bodies Alone and with Lifting Surfaces to Very High Angles of Attack", NASA-TR-R-474, September 1977.

4. Ashley, Holt, Landahl, Marten, Aerodynamics of Wings and Bodies, Addison Wesley, 1965.

# AEROELASTIC TAILORING FOR CONTROL AND PERFORMANCE - ARE REQUIREMENTS COMPATIBLE?

by
D. Booker
Principal Aerodynamicist
British Aerospace Public Limited Company,
Aircraft Group
Warton Division
Warton Aerodrome
Preston, Lancs., PR4 1AX
England

## SUMMARY

The variations of camber and twist along a wing required for optimum performance in low 'g' (cruise) and high 'g' (combat) flight are discussed. It is shown that a wing with active leading-edge and trailing-edge manoeuvre devices scheduled with angle of attack, and structurally tailored to control aeroelastic bending and torsion, can approach optimum performance. However the torsional stiffness of such a wing may be too low for satisfactory roll control at high airspeeds in supersonic flight. Some compromise to performance is implied if torsional stiffness has to be increased to provide adequate control capability.

## 1. INTRODUCTION

The advent of transonic three-dimensional computational flow prediction methods, together with more powerful computers, affords the wing design aerodynamicist with the means for a far more accurate determination of the optimum wing shape for best performance over a range of important design points. At each condition the aerodynamicist will define camber and twist distributions along the span of the wing. These requirements are to be met by a combination of mechanical means - appropriately scheduled leading-edge and trailing-edge manoeuvre devices - together with aeroelastic distortion of the structure under the loads applied to it. Structural tailoring is carried out to achieve the required aeroelastic properties, use of carbon fibre composite materials increasing the scope for change.

Besides aiming for the wing shape offering optimum performance the structural designer must respect other aerodynamic requirements. In particular roll control effectiveness must be retained at high speed, and margins from flutter must be provided. This paper considers the compatibility of the control and performance requirements for an aeroelastically tailored wing. It is assumed that flutter considerations are fully accounted for during tailoring. Data presented is based on the results of a parametric investigation of aeroelastic tailoring on a family of wings covering planform variables applicable to a fighter aircraft.

## 2. QUASI-STATIC AEROELASTICS

To aid understanding of later parts of the paper a brief introduction to the mechanics of aeroelastic distortion is given.

Figure 1 shows the undistorted and equilibrium distortion positions of a swept back wing carrying load. Twisting of the wing due to loads applied ahead of or behind the flexural axis is easily understood. What is perhaps less obvious is that while loads applied on the flexural axis by definition cause pure bending of that axis i.e. zero twist in planes normal to it, in the free stream direction nose down twist (wash out) results on wings with swept back flexural axes. Figure 1 illustrates this case. Deflection of a trailing edge control causes nose down twist from both torsion and bending.

Nose down twist reduces the local angle of attack on the wing section and therefore aerodynamic loads are reduced. Hence flexible wing lift curve slopes are less than rigid wing values (unless the flexural axis is designed to be well aft and/or unswept) and trailing-edge control effectiveness is reduced by flexibility.

In the case of a swept forward wing bending along the flexural axis causes nose up twist (wash in). This effect reduces, or even reverses the torsional nose down twist due to deflection of a trailing edge control. This situation is quite attractive but careful design (using carbon fibre composite materials) is needed to achieve a satisfactory wing free from divergence at high speed and to avoid excessive mass. Such matters are beyond the scope of the present paper.

## 3. OPTIMUM CAMBER AND TWIST

Figure 2 shows typical section profiles for optimum performance (maximum lift/drag ratio) at low 'g' and high 'g'. The required change in camber with 'g' is essentially confined to the extremities of the aerofoil and this change can be matched approximately by progressive deflection of leading-edge and trailing-edge manoeuvre devices.

Figure 3 shows lift/drag ratios for a wing with various manoeuvre device settings. These lines could be derived theoretically for attached flow but more likely result from wind tunnel testing of a rigid model. Optimum performance is achieved by scheduling the manoeuvre device settings with angle of attack such that the envelope shown by the dashed line is followed. Typical schedules are illustrated in Figure 4. Additional decambering at low angle of attack might be applied for supersonic speeds.

Twist is used to achieve the optimum spanwise distribution of lift at given design points. Requirements are almost always defined by calculation but spot point testing of a 'bent wing' model can be used to verify the final design. Typical twist requirements at low 'g' and high 'g' are illustrated in Figure 5. The twist at 1g is largely built in during wing manufacture but the additional twist at high 'g', which can approach $10^{o}$ at the wing tip, must be achieved aeroelastically. Figure 6 shows that the required twist distribution can be obtained inboard of about $3/4$ semi-span on wings constructed from composite materials. In the tip region the twist requirement is not achievable due to reduced loading and the need to maintain torsional stiffness to prevent tip flutter. The comparison shown in Figure 6 is typical of that for a range of planform parameters applicable to fighter aircraft.

## 4. AEROELASTIC RATIOS

The flexible wing to rigid wing aeroelastic ratios for the wing described in the previous Section are now considered. Figure 7 shows the lift curve slope ratio at Mach numbers of 0.9 and 1.2. The subsonic values are a natural consequence of the twist design requirements for subsonic conditions. At supersonic speeds it is likely that specific high 'g' twist requirements have not been specified and the lift curve slope ratios are therefore fall-out from the subsonic design cases. Both subsonic and supersonic values are acceptable.

Trailing-edge (flaperon) roll control effectiveness ratios are shown in Figure 8 at the same Mach numbers. Subsonically the situation is just satisfactory but supersonically flaperon reversal occurs at relatively low airspeeds even when only the inner half of the flaperon is used. To meet the subsonic twist requirement this wing was tailored to have a well forward flexural axis so that the significant increase in torsional stiffness needed to restore acceptable roll control capability at supersonic speeds would reduce aeroelastic twist and therefore introduce a performance penalty. The penalty at high 'g' (combat) could be reduced by building in additional twist during manufacture though this would be at the expense of low 'g' (cruise) performance.

Aeroelastic tailoring studies for other planforms suitable for fighter aircraft show that the results of Figure 8 are some of the more severe. Increasing aspect ratio and reducing taper ameliorates the roll control situation though not to a sufficient extent to make it acceptable.

The implications on performance of non-optimum camber and twist distributions are briefly discussed in Reference 1.

## 5. OTHER CONSIDERATIONS

In the foregoing part of this paper interactions between the flaperon roll controls and other parts of the airframe have not been considered. The downwash change over the tailplane and sidewash induced over the fin can significantly reduce the rolling moment available from flaperon deflection. These effects were discussed at the 'Aerodynamic Characteristics of Controls' Conference in 1979 (Reference 2).

## 6. CONCLUSIONS

The advent of transonic three-dimensional computational flow prediction methods allows spanwise camber and twist distributions to be defined which will maximise performance over a range of flight conditions including cruise and combat. Wind tunnel testing of conventional and 'bent wing' models provides a complementary means for checking out the theoretical predictions and extending results into regions where the theory is not applicable.

Camber requirements can be met by actively scheduling leading-edge and trailing-edge manoeuvre device settings with angle of attack. Twist variations must be achieved aeroelastically.

Aeroelastic tailoring enables the separate twist distributions needed at low 'g' and high 'g' to be approached through built in twist at low 'g', aeroelastic distortion at high 'g'. However the resulting torsional stiffness of the wing may be low and trailing-edge roll control effectiveness unacceptable at high airspeeds in supersonic flight. Increasing torsional stiffness to provide satisfactory roll control effectiveness implies performance must be compromised.

## 7. REFERENCES

1. Holt, D. R. and Probert, B. : Some Particular Configuration Effects on a Thin Supercritical Variable Camber Wing : Paper 15 of AGARD-CP-285, 1980.

2. Moynes, J. F. and Nelson, W. E. Jr. : Flaperon Control - The Versatile Surface for Fighter Aircraft : Paper 9 of AGARD-CP-262, 1979.

## 8. ACKNOWLEDGEMENT

In preparing this paper the writer has drawn liberally on results from work carried out by colleagues in the Advanced Projects, Aerodynamics, Dynamics, Structural Engineering and Weights Departments of BAe Warton.

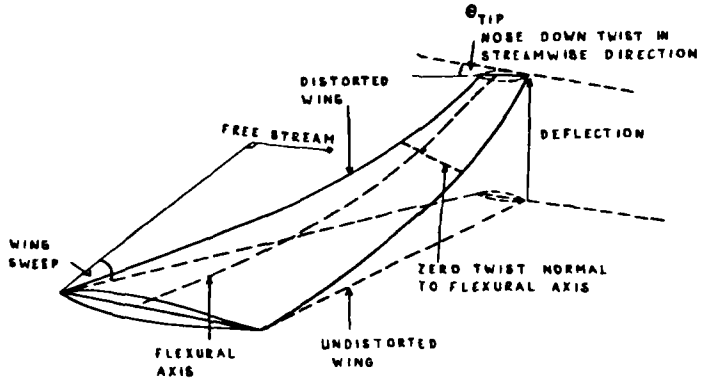


FIG.1 WING AEROELASTICALLY DISTORTED BY LOADING ALONG THE FLEXURAL AXIS

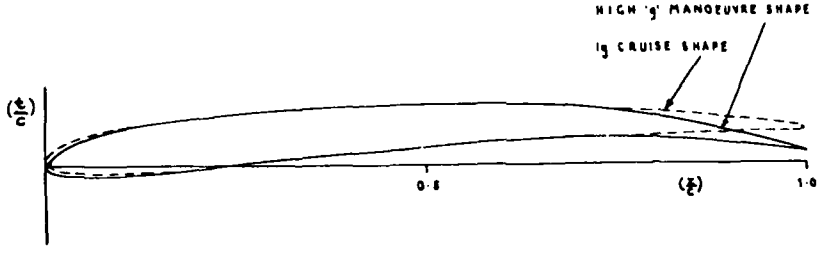


FIG. 2 SECTION PROFILES FOR OPTIMUM PERFORMANCE AT LOW 'g' AND HIGH 'g'.

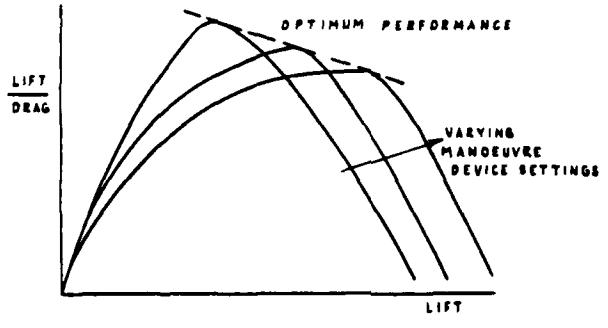


FIG 3. LIFT/DRAG RATIOS FOR VARYING MANOEUVRE DEVICE SETTINGS

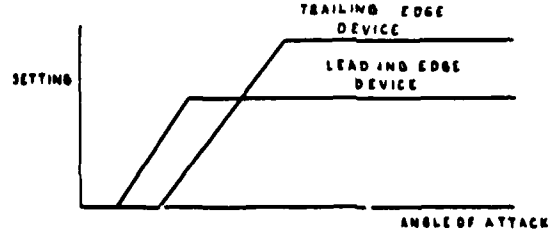


FIG.4. TYPICAL MANOEUVRE DEVICE SCHEDULES FOR OPTIMUM LIFT/DRAG RATIO.

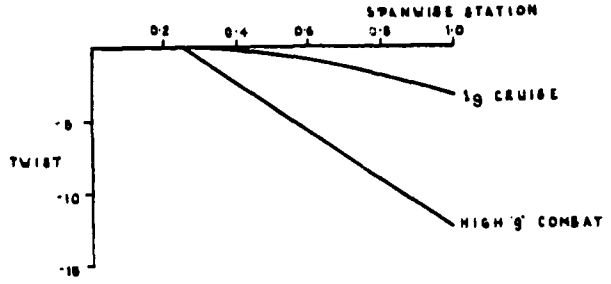


FIG.5. TYPICAL TWIST REQUIREMENTS AT LOW 'g' AND HIGH 'g' FOR OPTIMUM PERFORMANCE

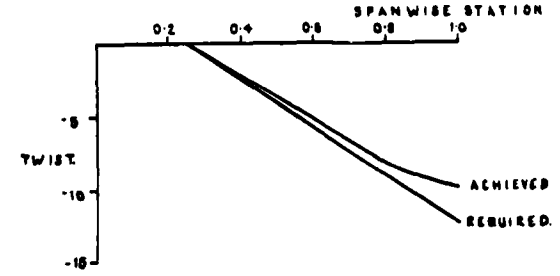


FIG.6. COMPARISON OF REQUIRED TWIST DISTRIBUTION WITH THAT ACHIEVED BY AEROELASTIC TAILORING

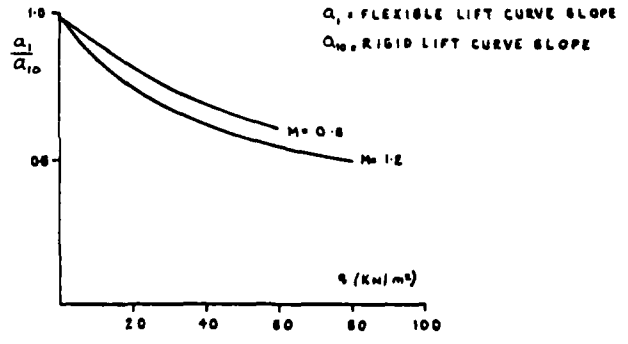


FIG.7 WING LIFT CURVE SLOPE AEROELASTIC RATIOS

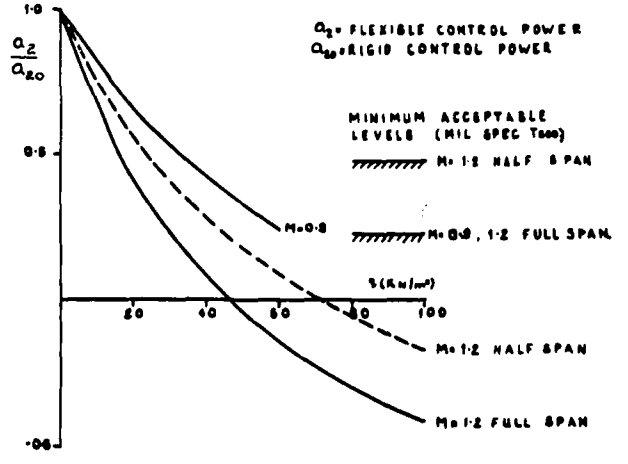


FIG.8 FLAPERON CONTROL POWER AEROELASTIC RATIOS

# TAIL CONFIGURATIONS FOR HIGHLY MANEUVERABLE COMBAT AIRCRAFT

W. E. Fellers, W. S. Bowman, P. T. Wooler
Northrop Corporation, Aircraft Division
One Northrop Avenue, Hawthorne, California, 90250
U.S.A.

## SUMMARY

An evaluation is presented of the drag-due-to-lift, maximum lift, and stability and control characteristics of tailless, canard, and aft tail configurations of highly maneuverable combat aircraft, using both aerodynamic surfaces and vectored thrust for pitch control. The same low aspect ratio wing planform was used on all the configurations. Control configured vehicle concepts were employed. Variable wing camber employing leading edge and trailing edge flaps was used to reduce profile drag. The center of gravity was located as far aft as allowed by the stability and control criteria, in order to reduce subsonic and supersonic trim drag.

The critical pitch control criterion was found to be the providing of adequate nose-down pitch acceleration in the angle of attack region near maximum lift. The aft center of gravity limits for both tailless and canard configurations without pitch thrust vectoring were required to be forward of the optimum location for minimum subsonic maneuver trim drag. The aft-tail configuration was not limited in this manner. In addition it could attain a higher subsonic maximum lift. It also had a greater design flexibility since the aft center of gravity limit could be influenced by the tail area. For these reasons it was the preferred configuration.

The addition of pitch thrust vectoring to the canard and aft-tail configurations was considered inappropriate. In both cases it is redundant since both configurations already have a control capability separate from the wing, and in both cases it cannot be used to improve the subsonic trim drag. Addition of pitch thrust vectoring to the tailless configuration improved the subsonic and supersonic trim drag to the extent that the combined configuration could be considered comparable to the aft-tail configuration. Additional design studies would be required in order to make a decision.

## SYMBOLS AND ACRONYMS

| | |
|---|---|
| AOA, $\alpha$ | Angle of attack |
| a.c. | Aerodynamic center |
| c.g. | Center of gravity |
| c.p. | Center of pressure |
| $\delta$ | Deflection |
| L/D | Lift/drag ratio |
| LEF | Leading edge flap |
| MAC | Mean aerodynamic chord |
| PTV | Pitch thrust vectoring |
| SM | Static margin |
| TEF | Trailing edge flap |

## Introduction

Combat aircraft maneuverability is an important aspect of the total air combat effectiveness. Performance and flying qualities characteristics are the prime ingredients in maneuverability. These characteristics can be studied in aerodynamic terms by an evaluation of drag-due-to-lift at low angle of attack, maximum lift capability, and stability and control parameters over a wide angle of attack range.

The paper describes an evaluation of the longitudinal stability and control, maximum lift, and drag-due-to lift characteristics of tailless, canard and aft tail configurations using both aerodynamic surfaces and vectored thrust for pitch control. The main objective was to understand the basic principles of the configurations, rather than to examine them in great detail, so approximations were used in order to simplify and clarify the presentation. Also it must be recognized that many other factors will influence the choice of a tail configuration, such as arrangement integration, mission requirements, cost, etc., but these are beyond the present scope. The same basic wing planform having a low aspect ratio, high leading edge sweep and low taper ratio was used on all the configurations. The rationale for this was that the trend is in this direction for future

fighters. In addition, the tailless configuration requires low aspect ratio to obtain adequate control moment arm, so a low aspect ratio is the only planform that can be used on all three configurations. Also the comparison of aft-tail and canard configurations is essentially independent of the wing planform.

The configurations are shown in Figures 1, 2, and 3. The canard is close-coupled to the wing and slightly above it. A low aspect ratio highly swept canard is used to provide a large stall angle of attack with no abrupt lift loss. No canard flaps were considered. All three configurations have the same canted twin vertical tails.

Control configured vehicle concepts were employed. An active control system was assumed with the primary control provided by elevon, canard or aft tail, with and without pitch thrust vectoring. A variable camber wing employing leading edge and trailing edge flaps was used for all the configurations. Lateral-directional stability and control characteristics were assumed to be satisfactory in order to limit the scope of the study.

The aerodynamic performance criterion was to minimize drag for the primary combat region which is at subsonic speed, with angle of attack (AOA) below about 15°. A secondary consideration was to maximize lift for instantaneous turns. This consideration does not permit limiting the angle of attack below that for maximum lift.

For supersonic performance, no direct evaluation of lift/drag ratio was attempted. Instead, for comparison purposes, an approximation to the level of trimmed drag-due-to-lift was used. This was the difference, in percent of the mean aerodynamic chord (MAC), between the allowable aft center of gravity (c.g.) and the optimum c.g. at supersonic speed. The optimum c.g. was based on the assumption that for a tailless configuraion, zero elevon deflection is optimum, and for a tailled configuration, the tail lift coefficient should equal that of the wing. In other words, the optimum c.g. for a tailless configuration is at the supersonic aerodynamic center (a.c.), and for a tailied, at the tail-on supersonic a.c.

Stability and control criteria were established relative to AOA ranges for maneuvers and relative to aft center of gravity (c.g.) limits. Pitch trim capability and fast response to controls were required to angles of attack of 30° to 40° which is greater than the AOA for maximum lift. The capability of trimmed post-stall operation to about 60° AOA was evaluated as an option. Positive aerodynamic stability at higher AOA was provided to preclude departures during inadvertent pitch transients at low airspeeds.

Three aft c.g. limit criteria were applied, in order to provide adequate nose-down stall recovery pitch acceleration and to avoid excessive complexity in the flight control system. An accurate determination of the required nose-down pitch acceleration would require an assessment of the lateral-directional stability and control characteristics which is beyond the present scope. The lateral-directional characteristics are important due to the influence of kinematic and inertial coupling, which can produce unwanted nose-up pitch rate and acceleration, which must then be overcome ty the longitudinal control. The value of pitch acceleration used here in the cases without pitch thrust vectoring (PTV) corresponds to about 0.3 rad/sec$^2$ at a low flight dynamic pressure with full nose-down aerodynamic control deflection.

PTV can supply a large nose-down acceleration at high thrust settings which would allow the c.g. to be far aft. However consideraion must be given to lesser thrust settings, including idle. This is because the tactical situation may call for a defensive "break," and the desire to slow down and force the opponent to overshoot. Also in the case of engine failure at high AOA, it is required that the aircraft be recovered to low AOA. The criteron used here in the cases with PTV is that at zero thrust the pitching moment at any AOA may not be positive, but can be allowed to be essentially zero. Note that in this study the only use of PTV was to provide pitch control power; its use to augment lift is not addressed.

The third aft c.g. limit criterion imposed related to avoiding excessive complication in the flight control system. Other studies have indicated that the control system rate required increases rapidly as negative static margin is increased when flight in turbulence is considered. Specialized high response actuators are required as the static margin becomes increasingly negative. In this study a value of approximately 15% MAC negative static margin, tail-on, was established as the limit.

The appropriate negative static stability level defined with flaps and controls fixed was selected for each configuration to optimize performance while satisfying the stability and control criteria.

Basic Data Common to All Configurations

For the wing-body configuration, subsonic wind tunnel test data were to determine the optimum leading and trailing edge flap deflection schedules to minimize drag at angles of attack up to 15°. In practice, an iterative process is used to select the deflections of the leading edge and trailing edge flaps. However, to simplify the presentation we will: first, determine the optimum leading edge and trailing edge flap deflection schedules to minimize drag at angles of attack from 0 to 15°; second, above 15° angle of attack, select flap deflections from stability and trim considerations; third, determine the wing/fuselage pitching moments with these flap schedules; and fourth, evaluate the

stability and control of the three complete configurations, first using either elevon control, canard control or aft-tail control, and then adding pitch thrust vectoring in combination with the aerodynamic control where appropriate.

Drag-due-to-lift is comprised of induced drag, profile drag and trim drag. The induced drag of all the configurations is the same, because the same wing planform is used. The profile drag is also the same for the three configurations, because the same airfoil and flap schedules are used. The trim drag then constitutes the primary difference among the three tail configurations.

The subsonic wing profile drag is significantly reduced by deflecting the leading edge and trailing edge flaps with varying angle of attack. This is shown in Figures 4 and 5. Figure 4a shows subsonic drag polars for three leading edge flap (LEF) deflections, 0°, 20°, and 30°. It indicates as expected that as AOA is increased, the minimum drag is obtained with progressively larger LEF deflections. If the LEF is scheduled automatically with AOA, the envelope drag polar indicated can be obtained. Figure 4b shows the resulting LEF deflection schedule with AOA. Figure 5 indicates that the same process can be carried out with the trailing edge flap (TEF) to obtain minimum drag at all lift coefficients, with the LEF deflection scheduled according to Figure 4b.

At supersonic speeds, trailing edge flaps generally do not reduce drag, so it is assumed they are not deflected. Leading edge flaps at very low deflections may provide some benefit, depending on leading edge sweep and Mach number.

The slope of scheduled LEF and TEF deflection with AOA is shown in Figure 6 as a function of Mach number, showing that the scheduling is reduced at transonic speed, and no scheduling above some supersonic speed.

In determining subsonic trim drag, the primary factor is the tail-off pitching moment which determines the magnitude and basic direction (up or down) of the tail load required for trim. The tail-on pitching moment characteristics are only used to determine the local flow field direction and tail deflection needed to achieve the required trim load, and are secondary factors in trim drag.

Optimum subsonic trim drag occurs at zero or very low positive tail loads. Therefore it is desirable to locate the center of gravity (c.g.) to operate at the tail-off center of pressure with scheduled leading edge and trailing edge flaps.

The pitching moments obtained at various LEF deflections are shown in Figure 7 as well as with scheduled LEF. The moment center was chosen to produce a negative static margin (SM) of -15% of the mean aerodynamic chord (MAC). This selection is arbitrary at this point. The reason for that amount of negative SM is shown in Figure 8, which shows pitching moments for various TEF deflections with scheduled LEF deflections. Also superimposed is the data for TEF deflections scheduled for minimum drag. The flap incremental lift, drag, and pitching moments are such that when flaps are scheduled for minimum drag, there results an effective increase in "stability" at low angle of attack equivalent to about 15% MAC for this class of planforms. Therefore, the optimum subsonic trim drag (zero tail load) at low angle of attack is achieved when the aircraft is 15% MAC unstable with the tail off and flaps fixed at low AOA.

Optimum supersonic trim drag occurs at slightly positive tail load; therefore, optimum supersonic trim drag is achieved with approximately neutral aircraft stability with tail on and flaps zero.

This aft c.g. location associated with the scheduled flaps at subsonic speed significantly improves the supersonic drag-due-to-lift. With this type of wing planform, the aft shift of the aerodynamic center (a.c.) from subsonic to supersonic speed is approximately 15% MAC, as shown in Figure 9, so that the c.g. would be located approximately at the supersonic a.c., tail-off, providing a low level of trim drag.

The lift curves are shown in Figure 10, showing that maximum lift is attained at about 25° AOA.

The other basic data required is the effectiveness of the pitch thrust vectoring (PTV) to be applied where appropriate. Engine size is assumed to produce a take-off thrust to weight ratio of 1.1. A maximum thrust vector angle of 30° is used. The resulting pitching moment coefficient available from PTV is shown in Figure 11 as a function of Mach number. The values shown are those available from the gross thrust; no interference effects are included.

The previous discussion has related to the basic wing-body aerodynamics and PTV. Now these data will be used in applications to each of the three tail configurations: tailless, canard, and aft tail. For each configuration the stability and control considerations will dictate an allowable aft c.g. limit. Since -15% SM with tail off has been shown to be the value for minimum subsonic trim drag, the extent to which each configuration can approach that value will determine its level of trim drag compared to the minimum.

Tailless Configuration

The tailless configuration subsonic stability and control characteristics are shown in Figure 12. Figure 12a shows data at the same c.g. as that at which the wing-body data were presented, that for -15% SM, the optimum location for drag. It will be seen that there is a large range of AOA at which the configuration cannot be trimmed, even with full TEF deflection of 30°. 30° deflection of a simple hinged TEF produces the maximum available nose-down moment. It is clear that the c.g. must be moved somewhat forward of the optimum aft location. The degree of c.g. movement is determined by the minimum required amount of nose-down pitch acceleration. The criterion applied here is to provide 0.3 rad/sec$^2$ nose-down, as discussed previously.

The data in Figure 12b has been transferred to a farther forward c.g. to produce the nose down pitching moment required. Instead of the desired -15% SM, it has only -7% SM. The resulting effect on trimmed L/D at a maneuver lift condition is shown in Figure 13 as a function of SM. At the allowable aft c.g. the L/D is 11% less than the optimum.

Considerations relating to supersonic trim drag are indicated in Figure 14, showing the a.c. variation with Mach number. Optimum c.g. locations for minimum trim drag are shown for subsonic and supersonic speeds. As discussed above, the optimum subsonic c.g. location is that corresponding to -15% SM. At supersonic speed, neglecting considerations of wing twist and camber to vary the pitching moment at zero lift, the optimum c.g. location is that at which zero elevon deflection is required for trim; that is, at the supersonic a.c. The subsonic nose-down pitching moment criterion requires that the c.g. be 8% MAC forward of the optimum supersonic location also. Trailing-edge-up elevon deflections will be required for trim, and increased trim drag will result.

The configuration is stable above the critical AOA region as indicated by the elevon deflection required for trim shown in Figure 15. The sense of the deflection is shown as "Forward Stick" and "Aft Stick," as though the pilot's control stick were directly connected to the control surface.

Noted at the right of the figure is the maximum instability in terms of the control deflection per degree of aircraft AOA. This derivative is proportional to the amount of static instability and inversely proportional to the control effectiveness. It can be considered as an indication of the rate of control deflection required to overcome the aircraft tendency to diverge. The value will be used in comparing the three configurations. Also shown is the maximum deflection required to provide a varying AOA capability. This is summarized in Figure 16, showing, for example, that if it is desired to provide an AOA operating region approaching 60°,the required total elevon deflection capability is 60°.

The maximum trimmed lift capability is shown in Figure 17 as a function of SM. The lift and moment characteristics of the flaps place the highest value at -10% SM. This value of -10% SM can be obtained by interpolating between the data in Figures 12a and 12b, and setting to zero the pitching moment at the critical AOA. This produces the c.g. at which the wing-body aerodynamic data is self-trimmed and incorporates the LEF and TEF deflection for maximum lift. Because of the nose down pitch control requirement, the tailless configuration with -7% SM can attain only about 95% of the aerodynamic lift capability.

In summary, for the tailless configuration, without the use of pitch thrust vectoring, the center of gravity must be moved 8% MAC forward of the optimum position for subsonic trim drag. This is necessary to provide for trim and pitch-down control at medium angle of attack. With this center of gravity location, the tailless configuration is 7% MAC unstable at low AOA, but becomes stable above 25° angle of attack. Trimmed post-stall operation can be achieved up to higher angles of attack, if desired.

Adding pitch thrust vectoring permits the use of a farther aft c.g. location and more nearly optimum trailing edge flap deflections for minimizing drag-due-to-lift at subsonic and supersonic speeds. The criterion for allowable aft movement of the c.g. has been discussed above: at zero thrust, the power-off pitching moment is not required to be negative, but can be allowed to be essentially zero.

The allowable aft c.g. movement can be estimated by interpolating between the -15% SM data in Figure 12a and the -7% SM of Figure 12b. This indicates that the c.g. can be allowed to move about 3% MAC farther aft than in the case without PTV. The tailless configuration with PTV then has -10% SM and its maneuver L/D is within 7% of the optimum. Using the PTV to furnish trim capability could provide an even higher aerodynamic L/D but at some loss of thrust component in the flight direction. By appropriate scheduling, the proper combination of PTV and TEF for maximum thrust-minus-drag could be provided for all maneuver conditions.

In terms of supersonic trim drag, the c.g. location is within 5% MAC of the optimum. Relative to subsonic maximum lift without thrust effects, the c.g. location produces the highest value obtainable. Trimmed post-stall operation to high angle of attack is again possible, if desired.

Canard Configuration

For the canard configuration, the pitch control limits are shown in Figure 18a for the optimum c.g. which has 15% negative SM with canard off and flaps fixed. Again a large AOA region is shown to be untrimmable. The critical AOA is about 60°, where the canard has very little nose-down trim capability. To provide AOA capability to 60°, increasing the canard size is very ineffective, so the c.g. must be moved forward. The resulting pitching moments are shown in Figure 18b, showing that the required nose-down moment is provided. The c.g. is again 8% MAC forward of the optimum, so that the negative SM, canard off, flaps fixed is -7%. The canard increment in stability is -10% MAC, so with the canard on, the configuration is 17% unstable at low AOA with flaps fixed. This instability is marginal with regard to the -15% SM limit established by flight control system considerations. The L/D at a maneuver lift condition is shown in Figure 19a as a function of tail-off SM. Data are plotted as a function of tail-off SM in order to maintain a more constant reference in comparing the three configurations. I' also is a direct indication of the c.g. location. The data are then re-plotted in Figure 19b as a function of tail-on SM as a reminder that with the tail located forward, the degree of instability is greater with the tail on. The canard configuration at its aft c.g. limit has 7% less L/D than the optimum.

Relative to supersonic trim drag, the a.c. variation with Mach number is shown in Figure 20 for canard on and off. The optimum c.g. locations for subsonic and supersonic speeds are shown. The optimum subsonic location is again with negative 15% SM with tail off. The supersonic location shown is based on the assumption that at the optimum location, the canard lift coefficient should equal that of the wing. This corresponds approximately to the canard-on a.c. The c.g. location established by the nose-down pitching moment criterion is seen to be very close to the supersonic optimum.

The reason for the small nose-down trim capability of the canard is indicated in Figure 21, showing that there is considerable upwash at the canard over the 25° to 60° AOA range. This makes the AOA of the canard very large; for example, at 60° aircraft AOA the canard AOA is about 75°. A canard deflection of -75° is required to just reduce the canard lift to zero. As the canard is deflected farther in the negative direction, the canard lift vector passes close to the aircraft c.g., producing little pitching moment.

Canard effectiveness data is shown in Figure 22, and canard deflection for trim in Figure 23. The configuration is unstable at all AOA to 60°. The required total canard control deflection to provide varying AOA operating capability is shown in Figure 24. 90° total canard deflection is required to operate over a 60° AOA region.

The maximum trimmed lift capability is shown in Figure 25 as a function of tail-off SM. Whereas at forward c.g., with positive SM, the canard adds lift, as the c.g. is moved back resulting in negative SM, the canard increment decreases. At -10% SM where the tail-off data are self-trimmed, the canard must provide zero pitching moment, and test data indicates that it adds no maximum lift.

In summary of the canard configuration, for trim and pitch-down control at high angle of attack, the center of gravity must be moved 8% forward of the optimum center of gravity for minimum trim drag at subsonic speed. Then with fixed flaps and controls, the canard configuration was 7% unstable tail-off and 17% unstable tail-on at low angle of attack. The canard configuration becomes aerodynamically more unstable above 15° angle of attack and only becomes stable above 60° angle of attack. Trimmed post-stall operation at 60° angle of attack required -60° of canard deflection. Due to the instability, at 60° angle of attack, 20° additional canard deflection was required for pitch-down control (total = -80°). At the aft c.g. the canard added 7% in maximum lift capability to that available with the tailless configuration.

Adding pitch thrust vectoring could permit a more aft c.g. location except that this would violate the aft c.g. limit criterion relating to flight control system complexity; the configuration is already marginal with -17% SM tail-on. The canard size could be decreased to permit the aft c.g. movement, but it would soon become unrepresentative of a canard concept. Also PTV is redundant when applied to a configuration which already has a control capability independent of the wing. Thus the addition of PTV to a canard configuration does not appear to be a desirable concept.

Aft Tail Configuration

Pitch control limits for the aft tail configuration are shown in Figure 26 at the c.g. for minimum drag. In this case the tail was sized to produce the required nose-down moment at stall, so the optimum c.g. for drag can be used. The configuration then had -15% SM with tail off, flaps fixed, and -11% SM with tail on, flaps and controls fixed. The flow field at the tail is shown in Figure 27 showing that the downwash developed by the wing below stall gradually reduces to zero at high AOA. This permits a large nose-down moment to be developed with only moderate tail deflections.

The resulting tail effectiveness data is shown in Figure 28. The static stability is shown in Figure 29 and the total pitch control deflection is shown in Figure 30. Approximately 80° total deflection was required to provide a 60° AOA operating capability.

The trimmed L/D at a maneuver lift condition is shown in Figure 31a as a function of tail-off SM. The aft tail configuration can attain the maximum value. The data are then re-plotted as a function of tail-on SM in Figure 31b. With the tail located aft, the degree of instability is less with the tail on. Relative to supersonic trim drag, the a.c. variation with Mach number is shown in Figure 32, tail on and off. The optimum c.g. locations for subsonic and supersonic speeds are shown, based on considerations presented above. To carry positive lift on the tail to trim at supersonic speed, the c.g. would need to be aft of the subsonic optimum. This would indicate some trade-off between subsonic and supersonic performance could be considered by moving the c.g. aft.

The maximum trimmed lift capability is shown in Figure 33 as a function of tail-off SM. The highest value occurs at -18% SM for the tail area used. This might provide additional incentive to move the c.g. farther aft.

In summary, the aft-tail aircraft can use the center of gravity for optimum performance at subsonic speed. With fixed flaps and controls, the aft-tail aircraft was 15% unstable tail off and 11% unstable tail on at low angle of attack. The aft-tail configuration became stable above 25° angle of attack. Trimmed post-stall operation at 60° angle of attack could be achieved with -50° of tail deflection, and the required nose-down response could be achieved with +30° deflection.

The use of pitch thrust vectoring as an additional pitch control is not necessary to minimize trim drag with an aft tail, but may reduce the tail size required. However as discussed in the case of the canard configuration, this would make the configuration less representative of an aft-tail concept and PTV is redundant since there is already a control capability independent of the wing. Thus the addition of PTV to an aft-tail configuration does not appear to be a desirable concept.

## Configuration Comparisons

Since we have discarded the application of PTV to the canard and aft-tail configurations as being redundant and undesirable, the comparisons will be of the three configurations without PTV and the tailless with PTV.

In the case without PTV, both the canard and aft tail configurations have an advantage over the tailless in that they both provide a control capability separate from the wing. This provides the possibility of considering various concepts to improve the aircraft capability. The concepts include fuselage pointing, direct lift control and ride qualities improvement.

Another general consideration relates to the level of confidence inherent in each configuration that the aerodynamic characteristics obtained during the design development stage can be carried over into the actual aircraft. For both the tailless and canard configurations, determining the aft c.g. limit depends strongly on an accurate knowledge of the absolute value of the wing-body-flap pitching moments at moderate and high AOA. This is not true of the aft tail configuration, since its aft c.g. limit can be varied by changing the tail area. Absolute values of pitching moment are very difficult to obtain from wind tunnel testing. Therefore in the case of the tailless and canard configurations, there is somewhat less confidence that the desired aft c.g. limit can be obtained on the actual aircraft. This is especially crucial in the case of the tailless configuraion. Figure 34a compares the L/D values for the three configurations as a function of the tail-off SM. The symbol denotes the aft c.g. limit for each. It can be seen that the tailless configuration has a greater sensitivity to c.g. location and therefore loses performance more rapidly if it is found that the c.g. must be moved forward to obtain the required stall recovery moment. In the case of the aft tail, an additional design flexibility is available in that the tail area can be increased if necessary to maintain the desired SM.

Figure 34a compares the L/D as a function of tail-off SM. Figure 34b shows the same values of L/D but as a function of tail-on SM. It will be noted that the aft-tail and canard L/D values are essentially the same, but they are obtained at considerably different levels of tail-on SM, -11% MAC for the aft tail, and -17% MAC for the canard. Thus the canard configuration has considerably greater risk in terms of developing a satisfactory control system.

Figure 35 contains a comparison of maximum trimmed lift coefficient without thrust effects. The aft-tail has the highest value. Again the tailless configuration has a greater sensitivity to the level of stability.

Figure 36 compares the values at the respective aft c.g. limits of the parameters which have been quantified. As indicated, the subsonic performance parameters favor the aft tail; supersonic performance, the canard; stability and control parameters, the tailless. When the various additional considerations are accounted for, there is a preference for the aft tail.

Figure 37 compares the values using PTV where appropriate. As discussed above, PTV offers added capability only in the case of the tailless configuration, allowing the aft c.g. limit to be 3% MAC farther aft. In addition it provides a control capability separate from the wing and allows consideration of the additional control modes such as fuselage pointing, direct lift control and ride quality improvement. It also relieves, to some extent, the concern about wind tunnel data accuracy. Thus the tailless configuration with PTV is competitive with the aft tail, and a decision would require more detailed design studies.

## Conclusion

Within the scope of the aerodynamic considerations included in this study, it is concluded that, without pitch thrust vectoring, the aft tail configuration is preferred. When pitch thrust vectoring is added to the tailless configuration, it becomes sufficiently comparable to the aft-tail configuration that additional design studies would be required to make a decision.

## ACKNOWLEDGEMENT

Considerable assistance was provided by our associates at Northrop Corp., especially William Chen, John Krause, Al Larson, and Henry Ziegler.

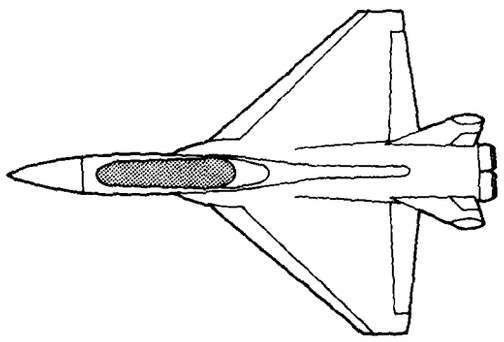

**FIGURE 1. TAILLESS CONFIGURATION**

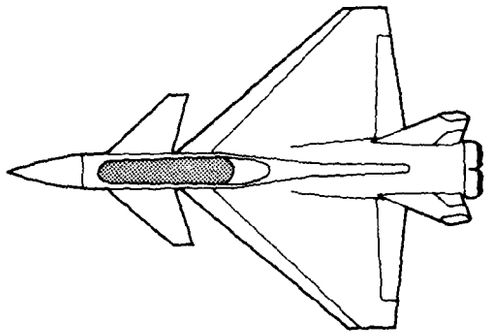

**FIGURE 2. CANARD CONFIGURATION**

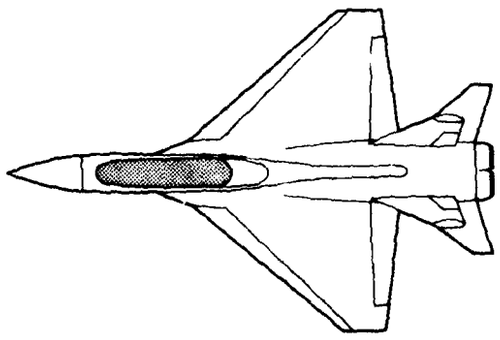

**FIGURE 3. AFT-TAIL CONFIGURATION**

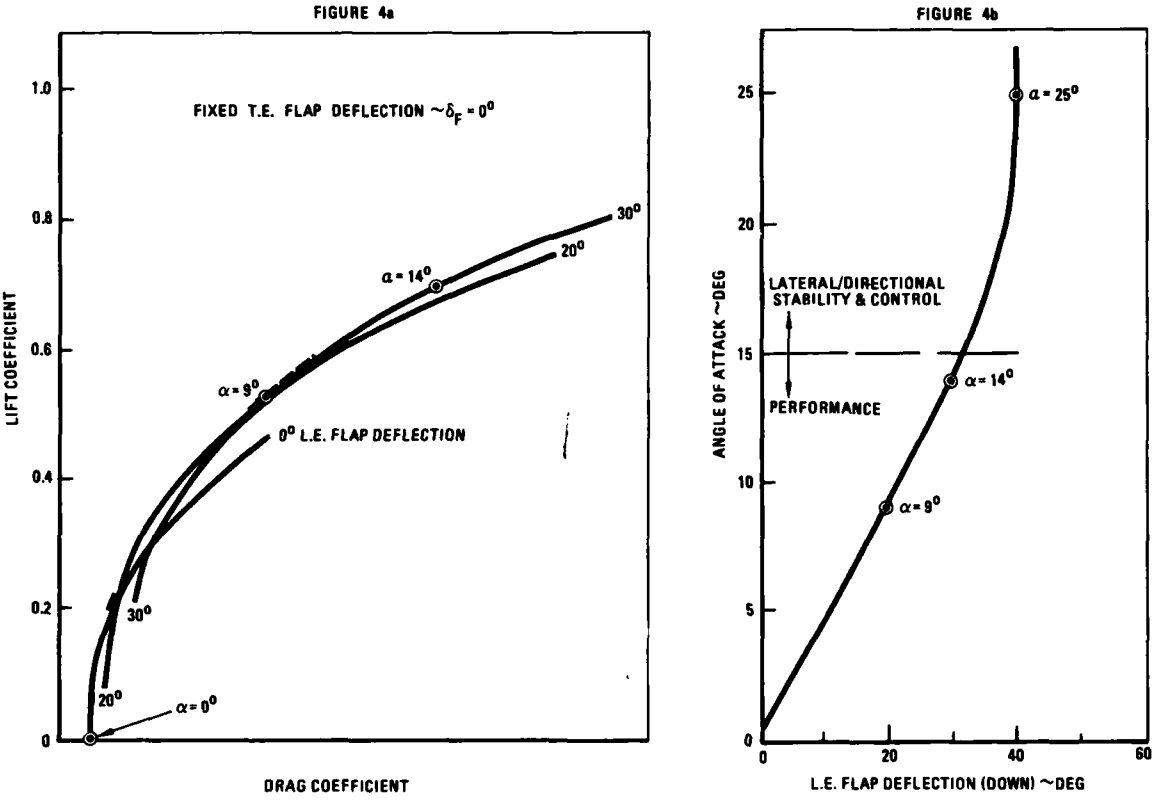


FIGURE 4. SELECTION OF LEADING EDGE FLAP SCHEDULE – SUBSONIC WING/FUSELAGE DRAG

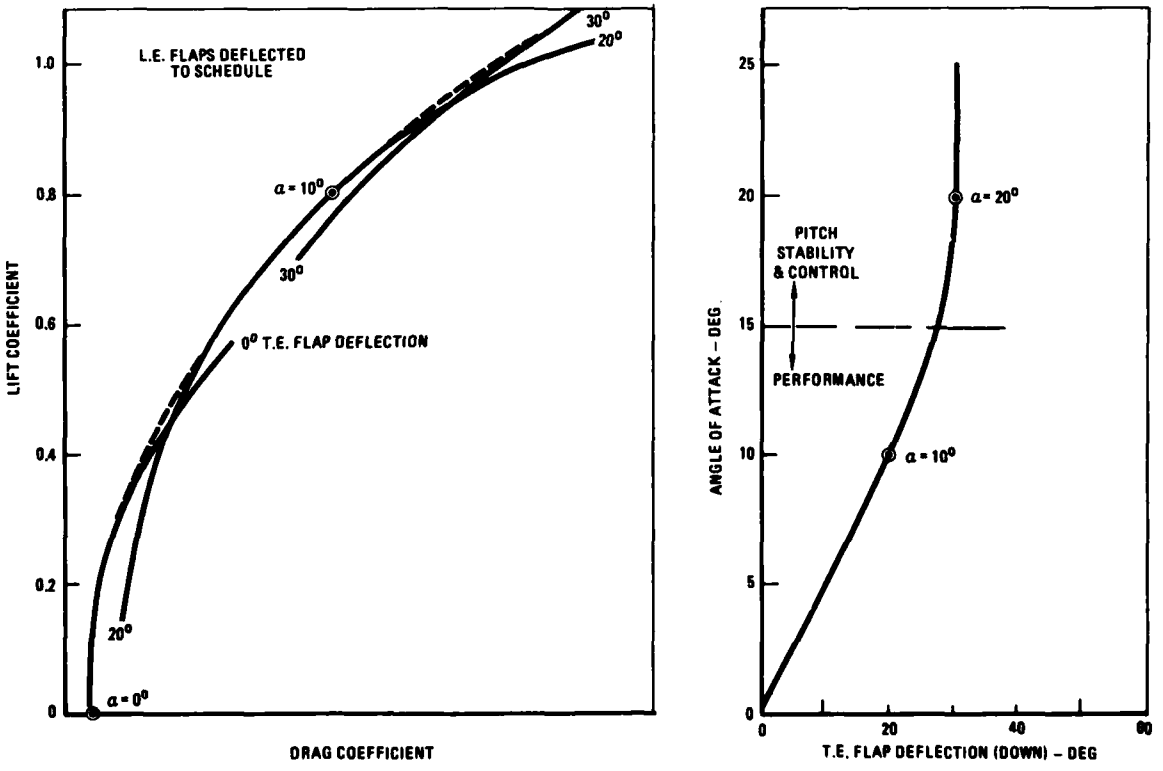


FIGURE 5. SELECTION OF TRAILING EDGE FLAP SCHEDULE – SUBSONIC WING/FUSELAGE DRAG

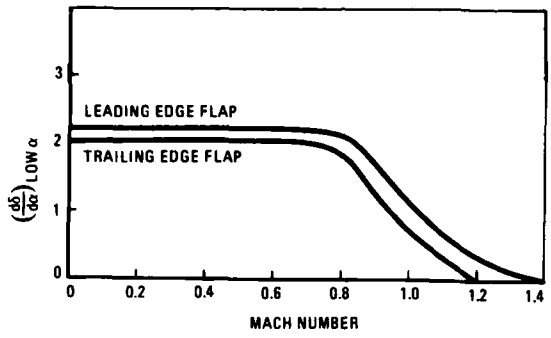


FIGURE 6. LEADING AND TRAILING EDGE FLAP SCHEDULES FOR MINIMUM PROFILE DRAG

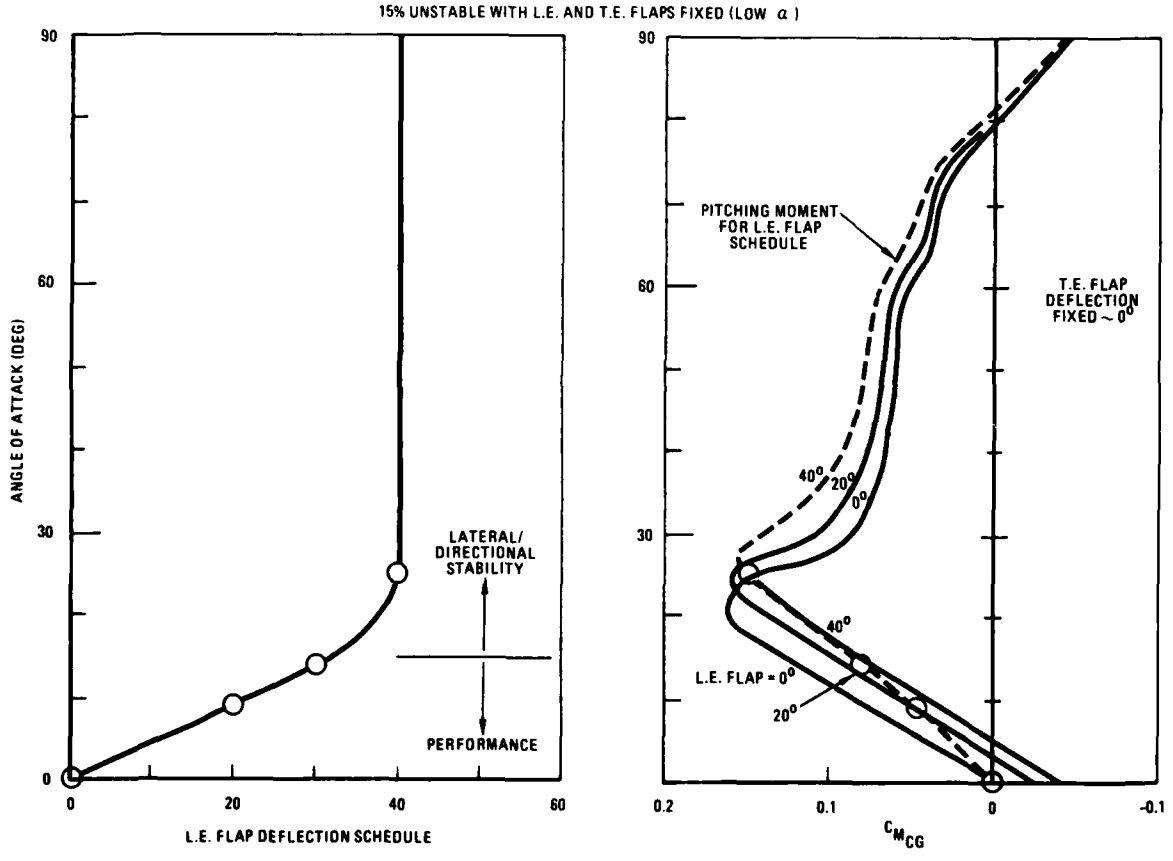


FIGURE 7. VARIABLE LEADING EDGE FLAPS, WING/FUSELAGE PITCHING MOMENT

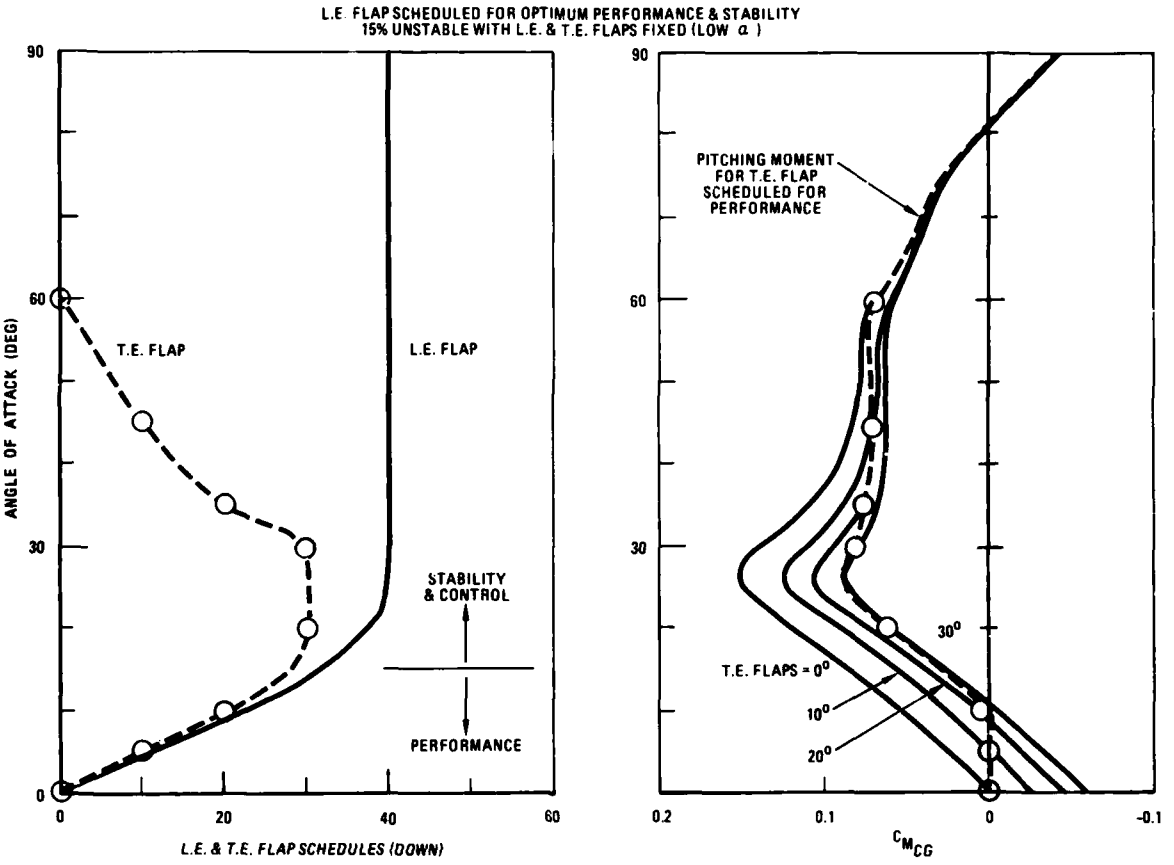


FIGURE 8. VARIABLE TRAILING EDGE FLAPS, WING/FUSELAGE PITCHING MOMENT

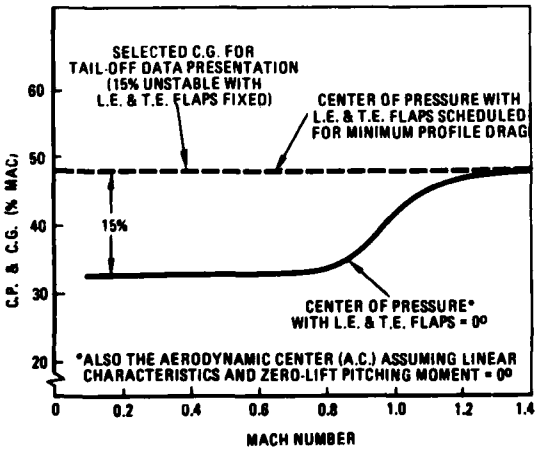


FIGURE 9. C.G. AND TAIL-OFF C.P. POSITION AT LOW $\alpha$ ($0^\circ - 10^\circ$)

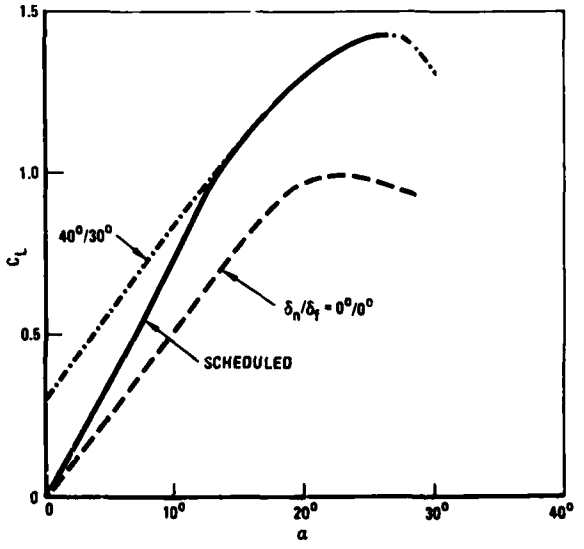


FIGURE 10. WING-BODY SUBSONIC LIFT DATA

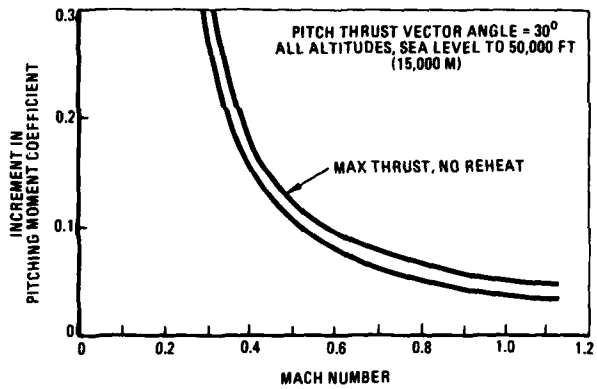


FIGURE 11. PITCH THRUST VECTORING CONTROL POWER

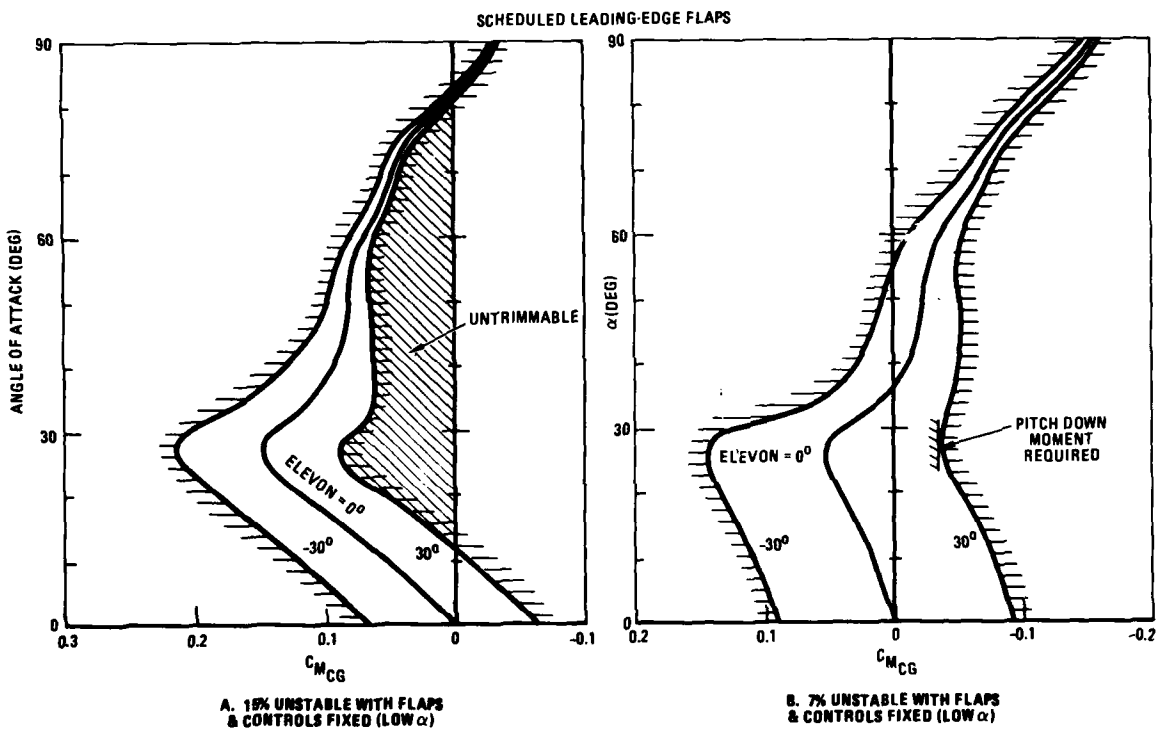


FIGURE 12. TAILLESS CONFIGURATION, EFFECT OF C.G. ON PITCH CONTROL LIMITS WITH ELEVONS

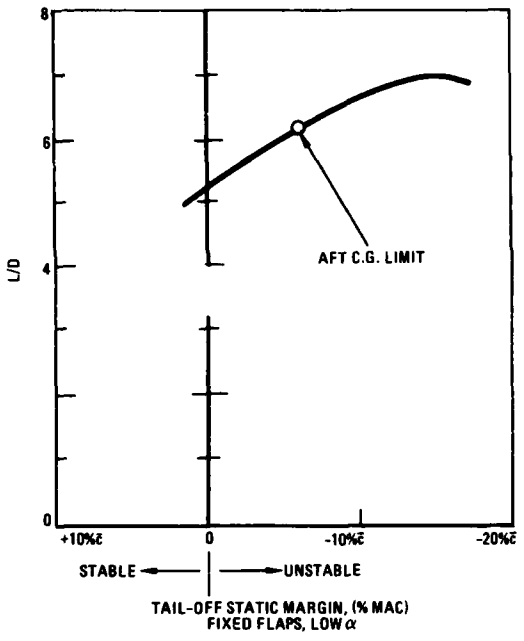


FIGURE 13. TAILLESS CONFIGURATION
LIFT/DRAG RATIO, SUBSONIC SPEED, $C_L \sim 0.7$

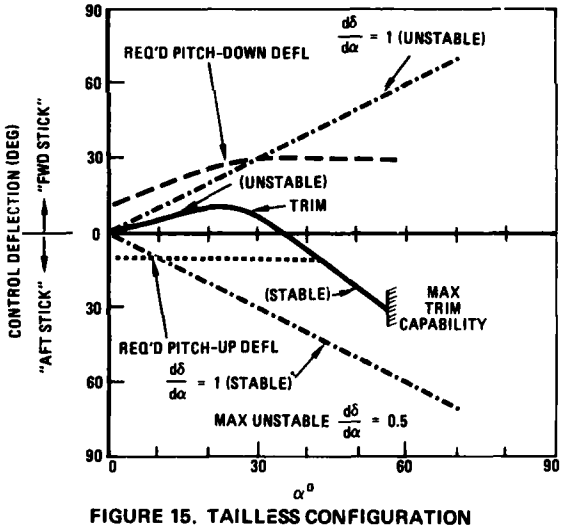


FIGURE 15. TAILLESS CONFIGURATION
ELEVON DEFLECTION

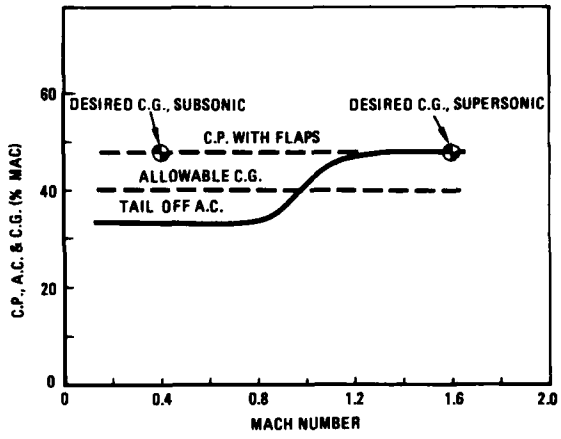


FIGURE 14. TAILLESS CONFIGURATION
AERODYNAMIC CENTER

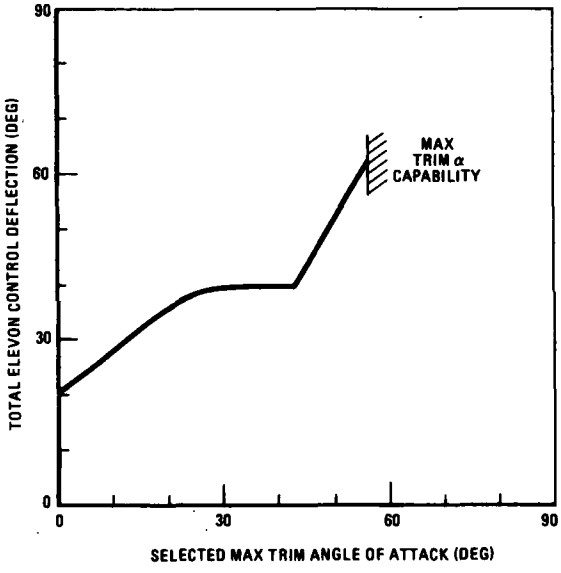


FIGURE 16. TAILLESS CONFIGURATION
TOTAL ELEVON CONTROL DEFLECTION

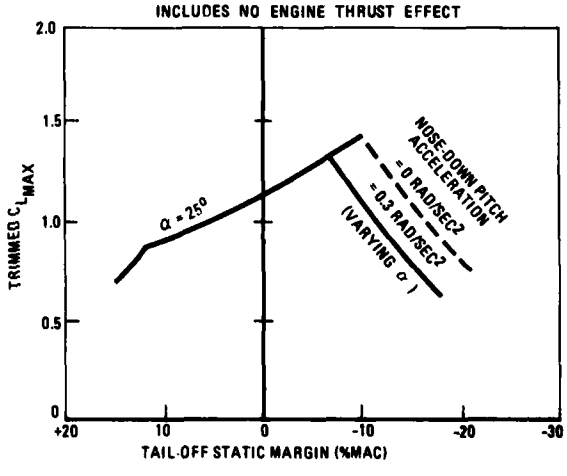


FIGURE 17. TAILLESS CONFIGURATION MAXIMUM LIFT

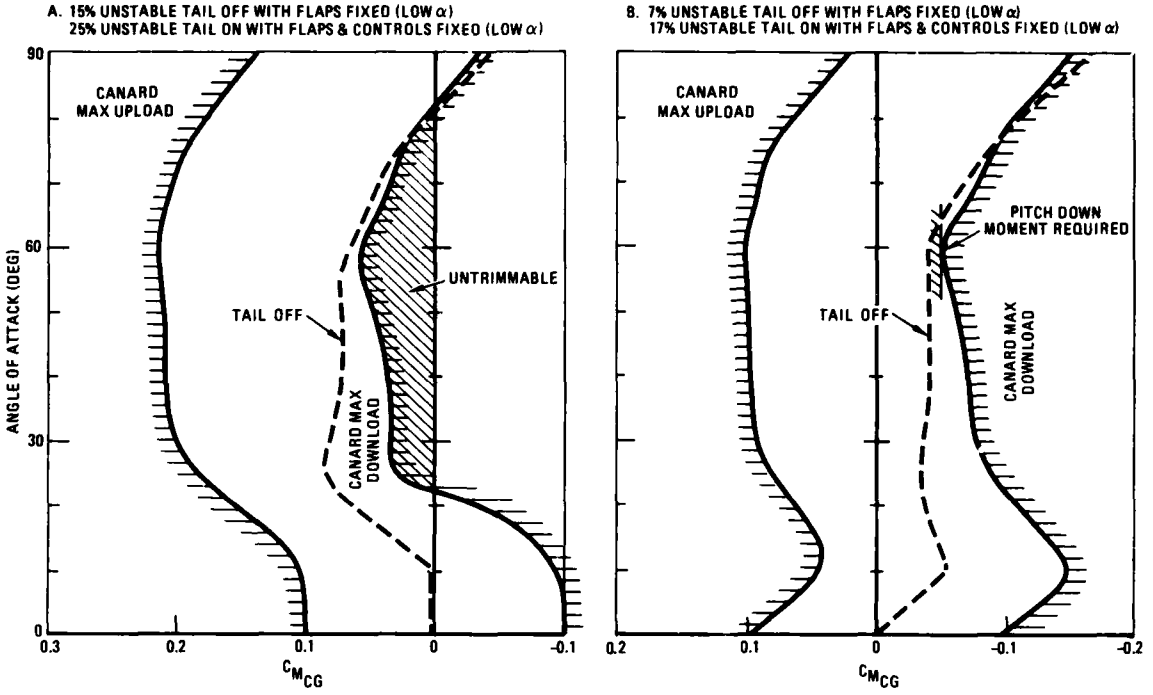


FIGURE 18. CANARD CONFIGURATION PITCH CONTROL LIMITS, SCHEDULED L.E. & T.E. FLAPS

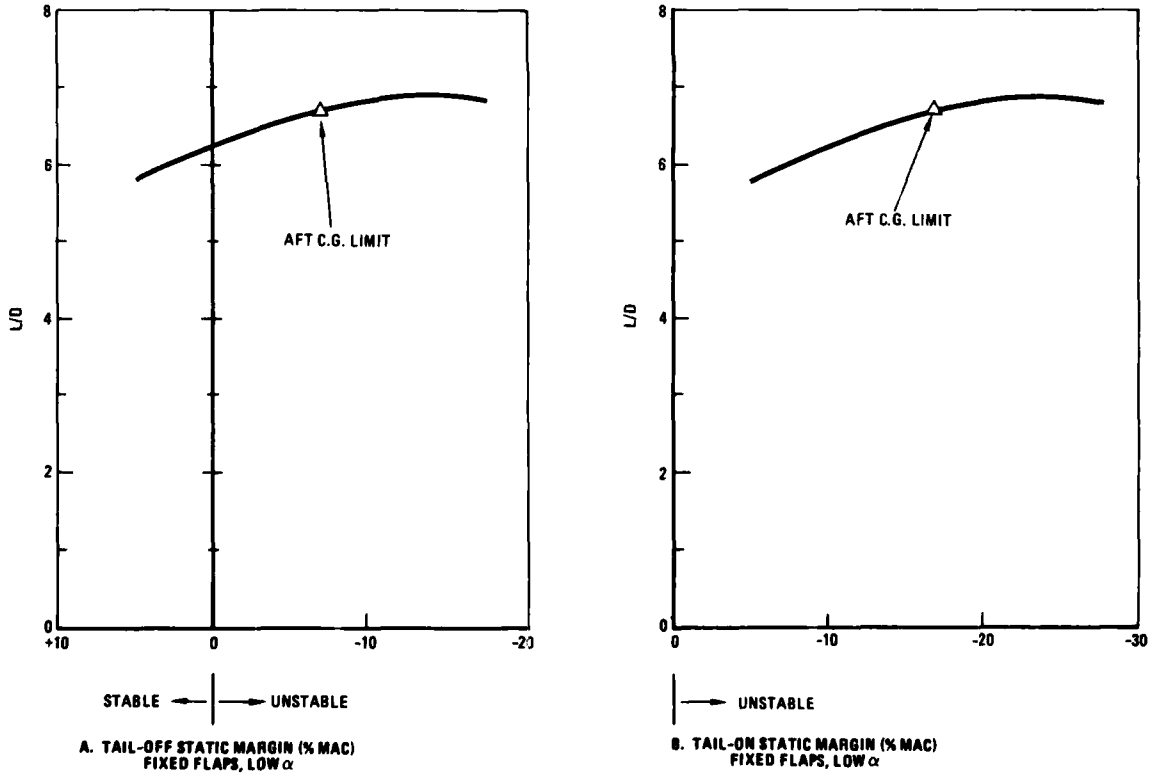


FIGURE 19. CANARD CONFIGURATION LIFT/DRAG RATIO, SUBSONIC SPEED, $C_L \sim 0.7$

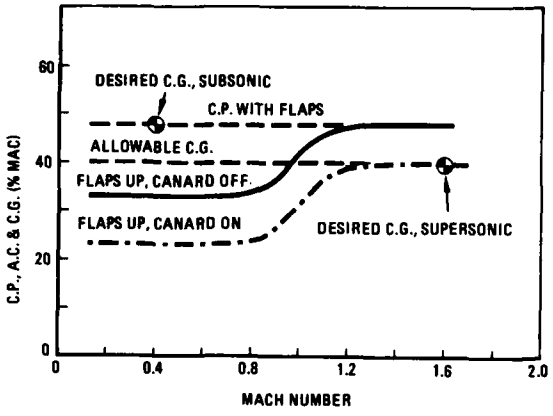


FIGURE 20. CANARD CONFIGURATION AERODYNAMIC CENTER

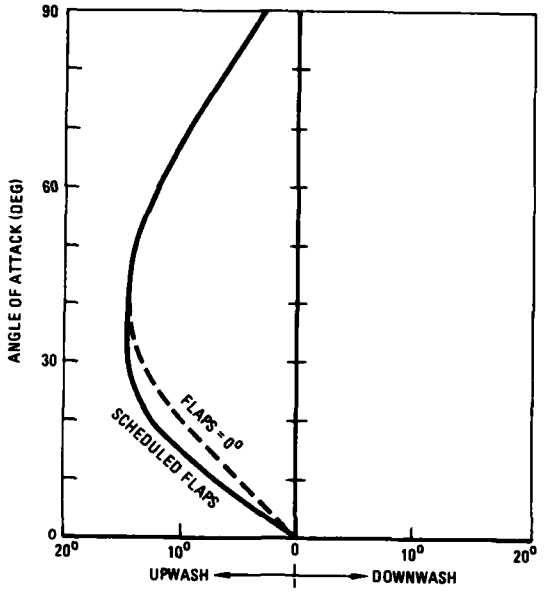


FIGURE 21. CANARD CONFIGURATION, FLOW FIELD AT CANARD

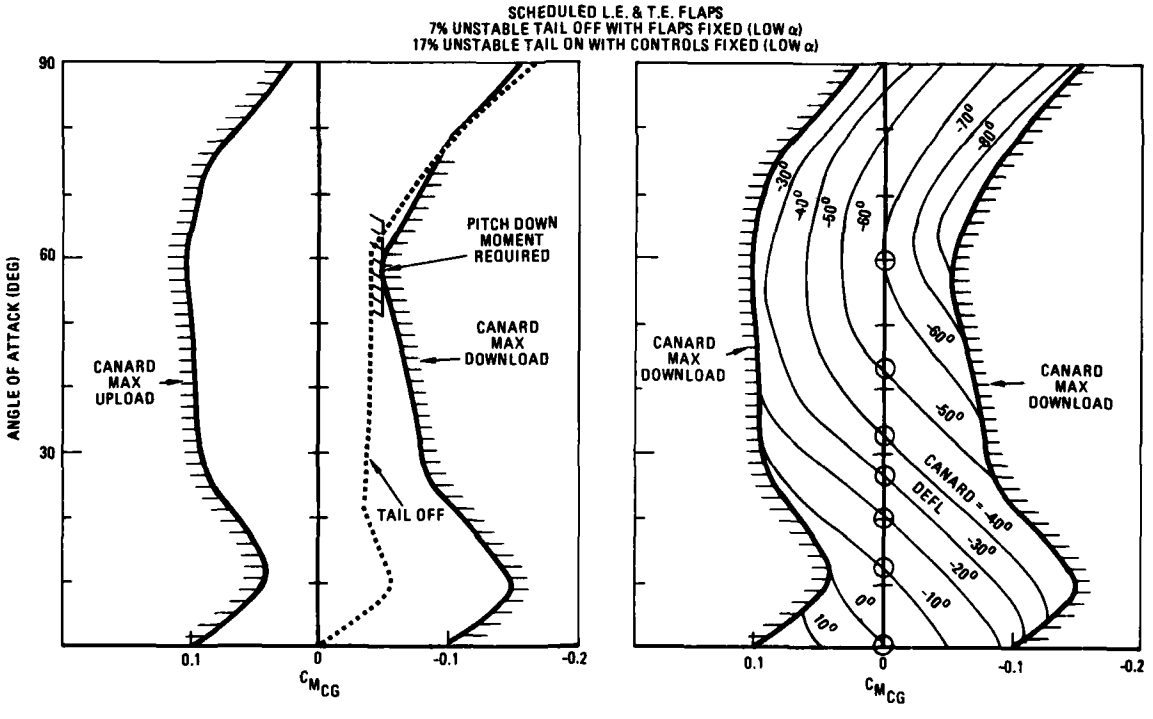


FIGURE 22. CANARD CONFIGURATION PITCH CONTROL

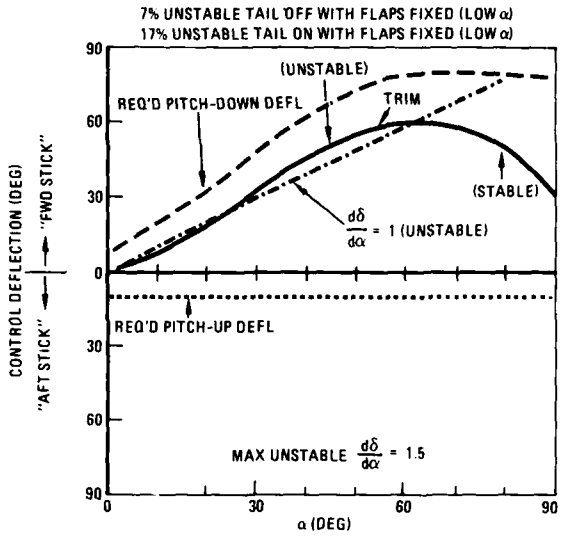


FIGURE 23. CANARD CONTROL DEFLECTION

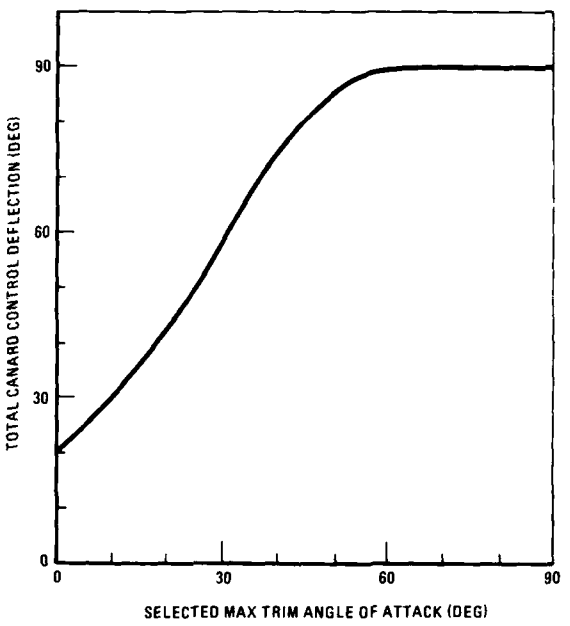


FIGURE 24. CANARD CONFIGURATION, TOTAL CANARD CONTROL DEFLECTION

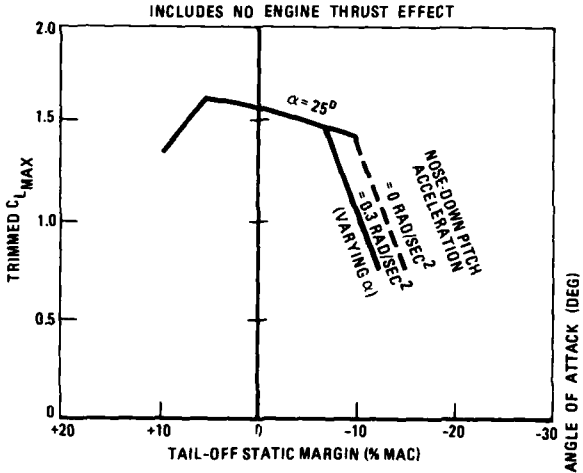


FIGURE 25. CANARD CONFIGURATION MAXIMUM LIFT

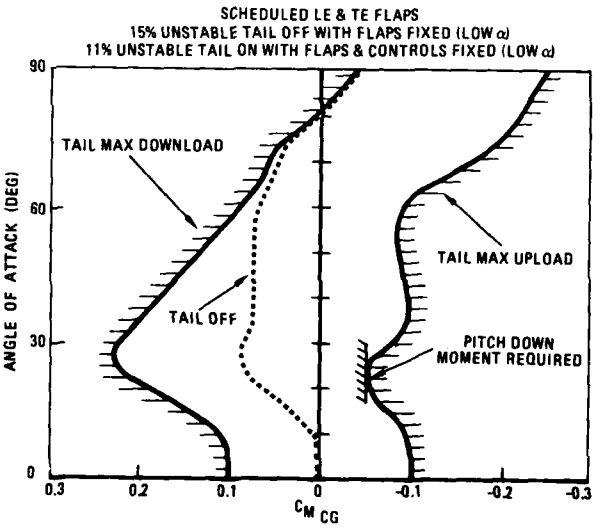


FIGURE 26. AFT-TAIL CONFIGURATION PITCH CONTROL LIMITS

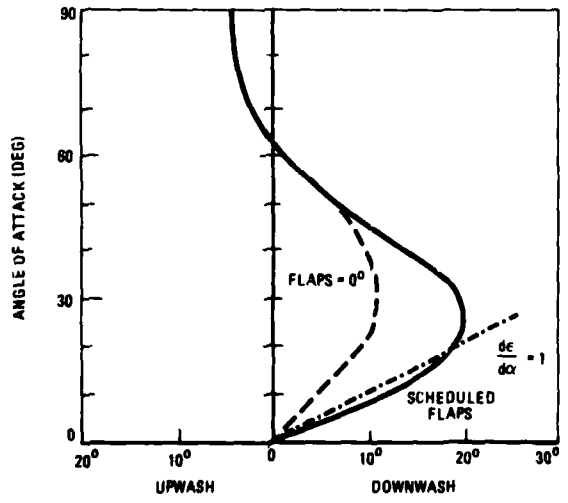


FIGURE 27. AFT-TAIL CONFIGURATION, FLOW FIELD AT TAIL

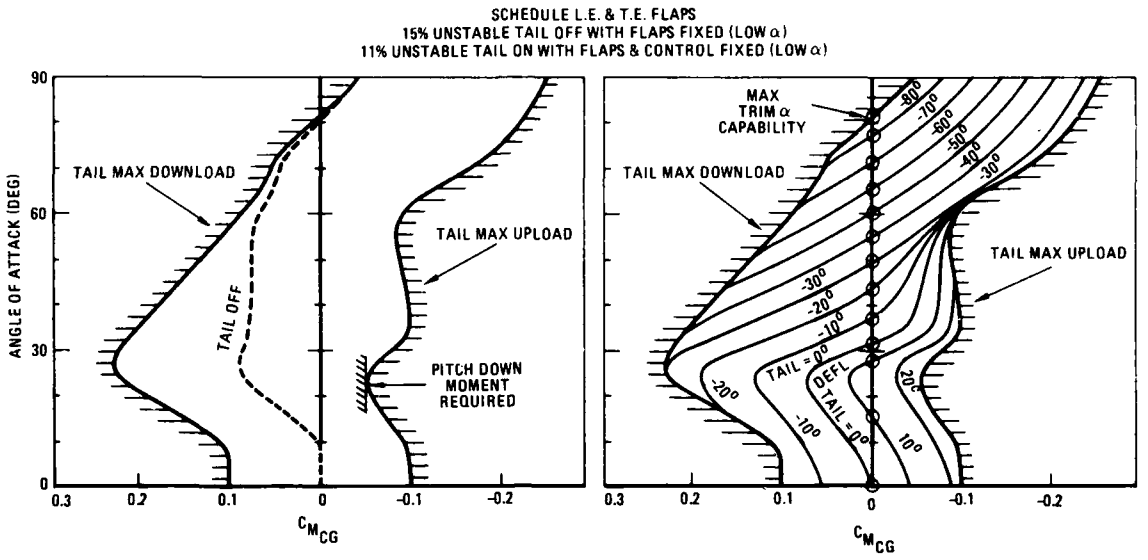


FIGURE 28. AFT-TAIL CONFIGURATION PITCH CONTROL

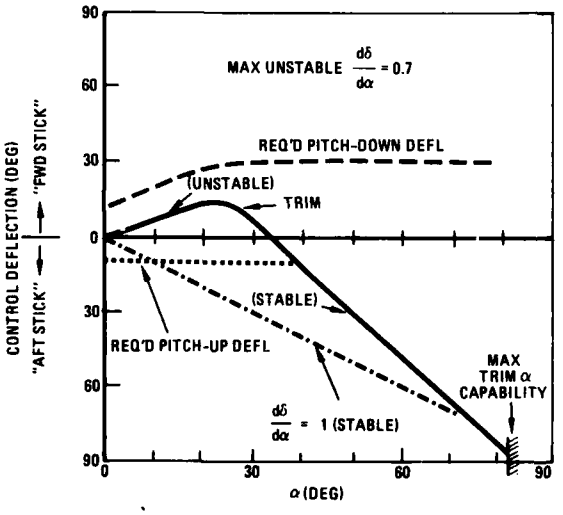


FIGURE 29. AFT-TAIL CONTROL DEFLECTION

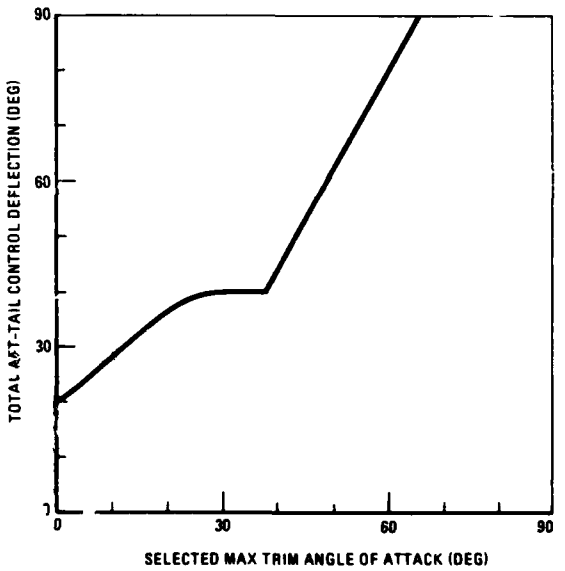


FIGURE 30. AFT-TAIL CONFIGURATION, TOTAL AFT-TAIL CONTROL DEFLECTION

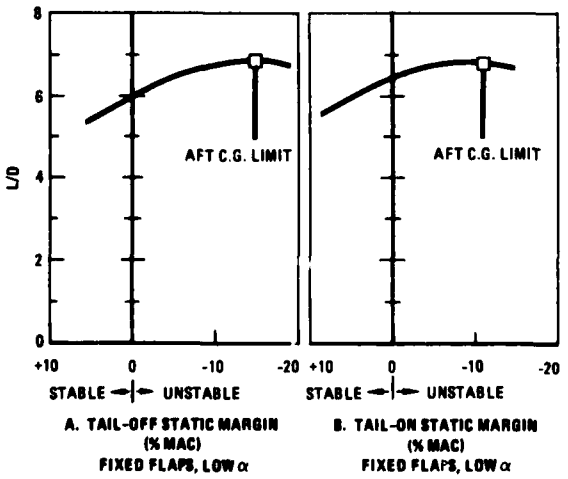


FIGURE 31. AFT-TAIL CONFIGURATION LIFT/DRAG RATIO, SUBSONIC SPEED, $C_L \sim 0.7$

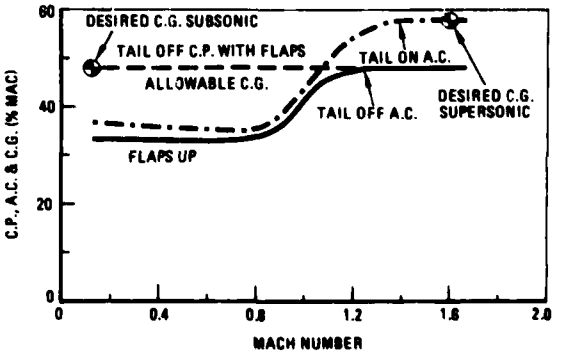


FIGURE 32. AFT-TAIL CONFIGURATION AERODYNAMIC CENTER

AD-A112 310 ADVISORY GROUP FOR AEROSPACE RESEARCH AND DEVELOPMENT--ETC F/G 1/2
COMBAT AIRCRAFT MANOEUVRABILITY.(U)
DEC 81
UNCLASSIFIED AGARD-CP-319 NL

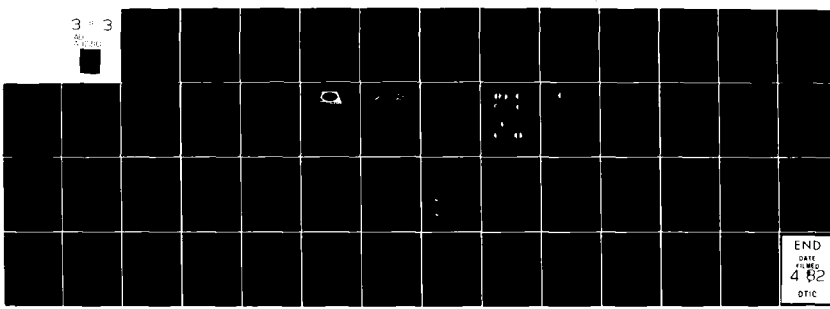

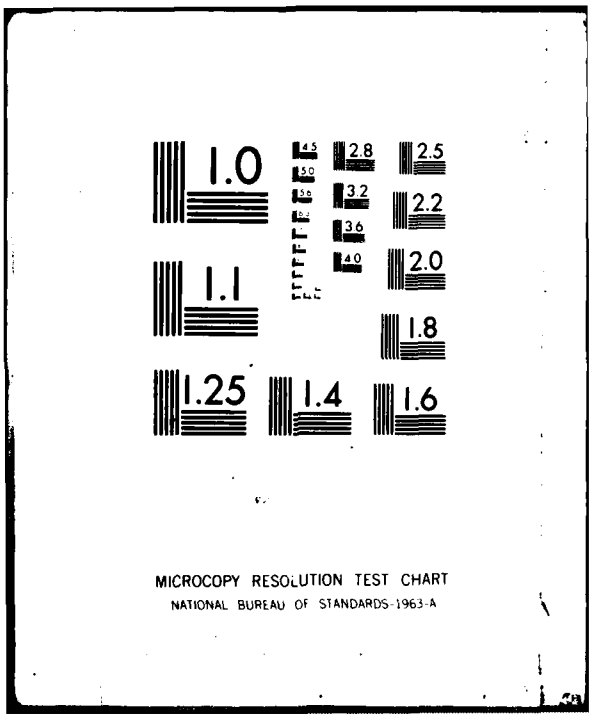
1.0
1.1
1.25
1.4
1.6
1.8
2.0
2.2
2.5
2.8
3.2
3.6
4.0
MICROCOPY RESOLUTION TEST CHART
NATIONAL BUREAU OF STANDARDS-1963-A

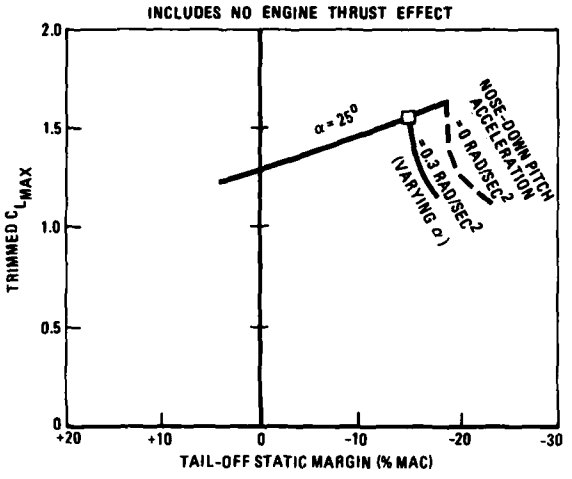


FIGURE 33. AFT-TAIL CONFIGURATION MAXIMUM LIFT

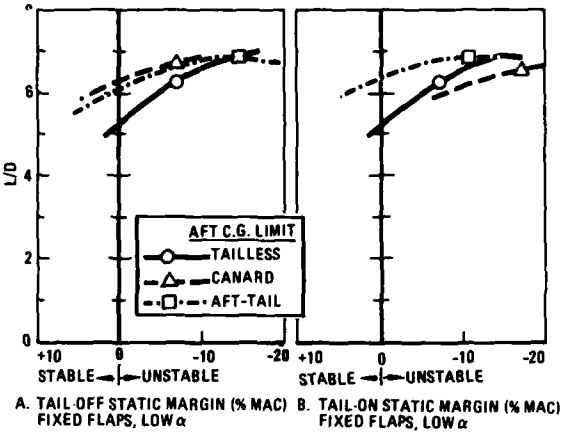


FIGURE 34. COMPARISON OF MANEUVER L/D WITHOUT PTV

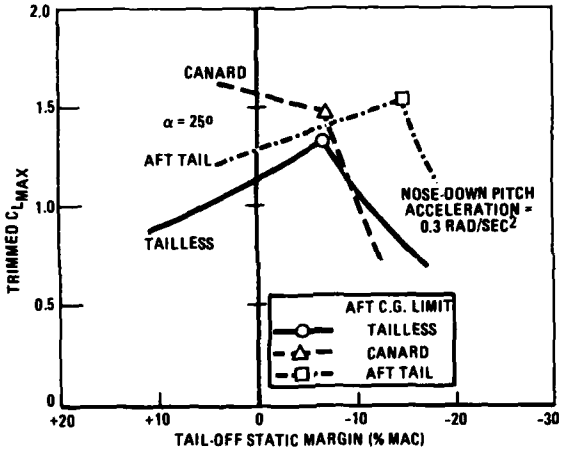


FIGURE 35. COMPARISON OF MAXIMUM TRIMMED LIFT

| PARAMETER | DESIRED VALUE | TAILLESS | CANARD | AFT TAIL |
|---|---|---|---|---|
| PERFORMANCE | | | | |
| SUBSONIC MANEUVER L/D | LARGE | 6.2 | 6.7 | 6.9 |
| SUPERSONIC TRIM DRAG (C.G. – OPTIMUM C.G.), % MAC | SMALL | -8 | 0 | -10 |
| SUBSONIC MAXIMUM LIFT COEFFICIENT | LARGE | 1.35 | 1.45 | 1.55 |
| L/D SENSITIVITY TO SM | SMALL | LARGE | SMALL | SMALL |
| SENSITIVITY TO ABSOLUTE PITCHING MOMENT | SMALL | LARGE | LARGE | MODERATE |
| STABILITY & CONTROL | | | | |
| -SM, SUBSONIC, TAIL ON, % MAC | ≤15 | 7 | 17 | 11 |
| MAXIMUM UNSTABLE $d\delta/d\alpha$ | SMALL | 0.5 | 1.5 | 0.7 |
| STABLE ABOVE ___ AOA | SMALL | $25^0$ | $60^0$ | $25^0$ |
| TOTAL CONTROL TRAVEL REQUIRED TO OPERATE TO 60 DEGREE AOA | SMALL | $60^0$ | $90^0$ | $80^0$ |
| CAPABILITY OF OTHER CONTROL MODES | YES | NO | YES | YES |

FIGURE 36. COMPARISON OF CONFIGURATIONS WITHOUT PTV

| PARAMETER | DESIRED VALUE | TAILLESS (WITH PTV) | CANARD (NO PTV) | AFT TAIL (NO PTV) |
|---|---|---|---|---|
| PERFORMANCE | | | | |
| SUBSONIC MANEUVER L/D | LARGE | 6.5 | 6.7 | 6.9 |
| SUPERSONIC TRIM DRAG (C.G. – OPTIMUM C.G.), % MAC | SMALL | -5 | 0 | -10 |
| SUBSONIC MAXIMUM LIFT COEFFICIENT | LARGE | 1.45 | 1.45 | 1.55 |
| L/D SENSITIVITY TO SM | SMALL | LARGE | SMALL | SMALL |
| SENSITIVITY TO ABSOLUTE PITCHING MOMENT | SMALL | MODERATE | LARGE | MODERATE |
| STABILITY & CONTROL | | | | |
| -SM, SUBSONIC, TAIL ON, % MAC | ≤15 | 10 | 17 | 11 |
| MAXIMUM UNSTABLE $d\delta/d\alpha$ | SMALL | 0.7 | 1.5 | 0.7 |
| STABLE ABOVE ___ AOA | SMALL | $25^0$ | $60^0$ | $25^0$ |
| TOTAL CONTROL TRAVEL REQUIRED TO OPERATE TO 60 DEGREE AOA | SMALL | $50^0$ | $90^0$ | $80^0$ |
| CAPABILITY OF OTHER CONTROL MODES | YES | YES | YES | YES |

FIGURE 37. COMPARISON OF CONFIGURATIONS USING PTV WHERE APPROPRIATE

# EVALUATION D' AVIONS EN COMBAT SIMULE CALCULATEUR CONTRE CALCULATEUR OU CALCULATEUR CONTRE PILOTE HUMAIN

par

**J. PEDOTTI**
AVIONS MARCEL DASSAULT-BREGUET AVIATION
78, Quai Carnot - 92214 ST CLOUD - France

**Y. HIGNARD**
CENTRE ELECTRONIQUE DE L' ARMEMENT
35170 BRUZ - France

**Résumé**

Un programme de simulation du combat aérien à un contre un a été développé. Ce modèle LAMA (Logique Adaptative de Manœuvre Aérienne) a été validé par des études théoriques et par des essais pilote/modèle sur le simulateur du CELAR.
Il permet soit une modélisation entièrement numérisée, soit une simulation d'hostile interactif opposé à un pilote sur simulateur.
LAMA est à la fois un moyen d'étude de nouveaux systèmes d'armes et un hostile performant pour l'entraînement des pilotes.

## 1. INTRODUCTION

Compte tenu de la part de plus en plus grande donnée à la fonction "Supériorité Aérienne" pour les avions de combat modernes et de l'évolution résultante des capacités de manoeuvre de ces avions, il a paru nécessaire de développer un programme de simulation de combat aérien.

Il est en effet indispensable de pouvoir comparer au stade avant-projets l'efficacité en combat aérien des divers compromis réalisables compte tenu des autres contraintes. Or cette comparaison avec les moyens classiques de calculs de performances est rendue difficile, voire impossible pour au moins deux raisons :

a) l'aspect compromis conduit à envisager des projets plus performants dans certaines zones du domaine de vol ou de la polaire, moins dans d'autres, ce qui ne permet pas de conclure au vu de simples tableaux de chiffres.

b) l'efficacité de dispositifs permettant de découpler attitude et forces (CAG, tuyères orientables, voilures pivotantes, etc...) est impossible à juger en termes de performances pures.

Ce moyen d'étude, par sa simplicité de mise en oeuvre (calculs sur ordinateur) présente une souplesse qui en fait un outil complémentaire des études sur simulateur. Il permet, d'une part, de dégager des premières conclusions qui orienteront les essais sur simulateur et les rendront plus efficaces ; d'autre part, un tel programme peut être opposé à un pilote sur simulateur : il constitue alors un hostile de référence intéressant car les combats pilote/ordinateur sont plus répétitifs donc, en général, plus faciles à interpréter que les combats pilote/pilote.

C'est de plus un moyen pour l'ingénieur d'acquérir l'expérience qui lui permet de mieux appréhender ce qui se passe lors d'un engagement air-air, et donc de dialoguer plus aisément avec les pilotes opérationnels.

Telles sont les réflexions qui nous ont poussé à mettre au point un tel outil.

Notre premier objectif a été de réaliser un programme limité au combat à un contre un : c'est le programme LAMA (Logique Adaptative de Manœuvres Aériennes) qui sera présenté ici. Historiquement il a d'abord été développé en version ordinateur/ordinateur. Il a été, par la suite, créé une version adaptée au temps réel pour permettre sa validation contre des pilotes sur les installations de simulation du CELAR à Rennes.

Il a été basé au départ sur :

- l'analyse des programmes existants dans ce domaine
- des interviews de pilotes opérationnels pour modéliser au mieux le processus décisionnel du pilote
- l'analyse de déroulements de combats sur simulateur et en vol.

Il s'est enrichi au fur et à mesure par deux voies différentes :

a) la voie théorique : apports de la théorie des jeux différentiels, qui assure l'optimalité de la solution

b) la voie expérimentale : analyse critique des combats calculés et des combats pilote/ordinateur enregistrés lors des phases de validation.

## 2. LE MODELE LAMA

### 2.1 - Principe général

A un instant $t_o$ donné, les vecteurs état des deux adversaires sont connus. On en déduit leur situation en considérant les aspects stratégiques et énergétiques, ainsi que les autres éléments pouvant intervenir dans la décision.

De cette situation, on déduit un certain nombre de manœuvres possibles pour chacun. Ces manœuvres sont calculées sur un intervalle de temps $\Delta t_1$. Les positions obtenues pour un avion sont alors comparées à la position prédite de l'adversaire au bout de ce même temps. La manœuvre retenue sera celle qui correspond à la position la plus favorable au bout de $\Delta t_1$. Elle est alors intégrée sur un intervalle de temps $\Delta t_o$ (fig. 1).

### 2.2 -Analyse de la situation

Pour caractériser la situation de chacun des adversaires à un instant $t_o$ du combat, LAMA prend en compte les aspects stratégiques, énergétiques et les autres éléments liés aux contraintes imposées aux systèmes.

#### 2.2.1 - La situation stratégique

Cette partie de l'analyse de la situation a pour but de déterminer, en fonction de la position relative des adversaires et de leur armement, si l'un ou l'autre bénéficie d'un certain avantage.

Pour cela, on a défini un certain nombre de rôles basés sur une schématisation du domaine de tir. Pour la définition des rôles, on utilise un angle $\lambda$, angle but, angle que fait la référence avion avec la droite joignant les 2 adversaires (fig. 2).

La partie géométrique d'un domaine du tir d'un armement quelconque peut être basée sur les angles $\lambda_A$ et $\lambda_B$ et sur la distance D entre avions. Par exemple :

$$\begin{cases} \lambda_A < \lambda_{Amax} \\ \lambda_B > \lambda_{Bmin} \\ Dmin < D < Dmax \end{cases} \quad \text{(fig.3)}$$

On caractérise alors neuf rôles différents basés aussi sur ces grandeurs (fig. 4) :

Rôle Très Attaquant : les conditions géométriques du domaine de tir sont satisfaites

Rôle Très Attaquant Proche : les conditions angulaires sont satisfaites mais $D < Dmin$

Rôle Attaquant : situation favorable mais conditions de domaine non satisfaites

Par exemple : $\lambda_{Amax} < \lambda_A < 2\lambda_{Amax}$
$Dmax < D < 2\ Dmax$

Rôle Attaquant Très Proche : comme très attaquant proche mais avec une vitesse de rapprochement qui laisse prévoir un dépassement imminent.

Rôle Très Défenseur, Très Défenseur Proche, Défenseur, Défenseur Très Proche : rôles symétriques des précédents

Rôle neutre : toutes les autres situations

La détermination du rôle fixe la stratégie à adopter, c'est-à-dire l'éventail de manœuvres à essayer et les critères de choix.

#### 2.2.2 - La situation énergétique

Elle concerne plusieurs aspects :

- l'évitement sol : dès que la pente est négative, on compare l'altitude à une altitude plancher dépendant de la pente. Dès que l'avion passe sous ce plancher, les manœuvres conduisant à rendre la pente plus négative sont éliminées du choix ; plus l'altitude diminue et plus le choix de manœuvres se restreint pour ne laisser finalement que des manœuvres de ressource au facteur de charge maximal.

- les vitesses faibles : les zones de vitesse faible sont surveillées par le biais des facteurs de charges maximaux praticables. Ce sont les zones (A) et (B) du domaine de vol (fig. 5).

  Dans la zone (A), le choix des manœuvres en compétition est restreint aux manœuvres permettant de regagner de l'énergie, et d'autant plus sévèrement que la pente est plus grande en valeur algébrique.

  Dans la zone (B), on se limite aux manœuvres à $dH/dt \geqslant 0$ quelle que soit la pente.

- les vitesses élevées : la zone (C) correspond aux vitesses supérieures à la "corner speed" (vitesse où nmax = n structure, donc de manœuvrabilité optimale). En fonction de la situation stratégique, on tient compte dans cette zone de l'intérêt qu'il y a à se rapprocher de cette "corner speed".

- la situation énergétique relative : l'écart d'énergie entre les deux adversaires est pris en compte essentiellement pour décider de réduire ou non la poussée.

2.2.3 - Les autres éléments de la situation

D'autres éléments sont pris en compte pour juger de la situation instantanée. Les principaux sont :

- les limitations structurales avion : Mach, $V_C$,...
- les limitations pilote : le facteur de charge maximum praticable est automatiquement réduit dès que le temps passé à fort facteur de charge atteint une certaine valeur.
- le temps de réponse moteur : si la poussée est réduite, on tient compte du temps qu'il faut pour atteindre la poussée maximale.

2.3 - Les manœuvres élémentaires

Les manœuvres élémentaires sont essayées à vitesse constante pour gagner du temps de calcul. Elles sont caractérisées par le plan dans lequel elles se déroulent et un facteur de charge.

2.3.1 - Les plans de manœuvre

Ce sont des demi-plans passant par le vecteur vitesse de l'avion considéré et définis par l'angle $\rho$ que fait ce demi-plan avec le demi-plan vertical haut passant par ce vecteur (fig. 6).

Parmi ces plans, on en distingue deux particuliers :

- le plan d'interception, plan passant par la position prédite de l'adversaire ($\rho = \rho_i$)
- le plan précédent, plan contenant l'accélération de l'avion considéré (plan osculateur à la trajectoire au point considéré) ($\rho = \rho_p$)

Les diverses manœuvres essayées s'effectuent dans des demi-plans choisis, suivant la situation, parmi les suivants :

$$\rho = 0°\ ,\ \rho_p\ ,\ \rho_i\ ,\ \rho_i \pm 45°\ ,\ \rho_i \pm 90\ ,\ \pm 60°$$

2.3.2 - Le facteur de charge

Les diverses manœuvres essayées sont calculées là aussi à des facteurs de charge choisis suivant la situation dans une liste comprenant :

- n maximum autorisé (compte tenu de toutes les limitations)
- n marge de manœuvre
- des fractions de n marge (en cas de vitesse faible)
- $n = n_i$ tel que la trajectoire passe par la position prédite de l'adversaire
- $n = n_t$ tel que la trajectoire projetée soit tangente au cercle instantané projeté pratiqué par l'adversaire.

A titre d'exemple, dans une situation très attaquant sans problème d'énergie, les manœuvres essayées sont :

| | |
|---|---|
| $\rho = 0°$ | pente constante |
| $\rho = \rho_i$ | $n_{max}$ |
| $\rho = \rho_i$ | $n = n_i$ |

Dans le cas symétrique (rôle très défenseur) :

| | |
|---|---|
| $\rho = \rho_p$ | $n_{max}$ |
| $\rho = \rho_i$ | $n_{max}$ |
| $\rho = \rho_i \pm 45°$ | $n_{max}$ |

Si dans ces situations stratégiques se posent des problèmes de faibles vitesses, les facteurs de charge sont limités à n marge ou à une fraction de n marge suivant la pente.

2.4 - Le choix de la manœuvre

Ce choix est basé sur l'appréciation de la situation à l'issue de la manœuvre. Pour ce faire, on dispose d'une liste de 11 questions posées de telle façon que l'on peut répondre par oui ou par non et que la réponse oui soit favorable. Ces questions sont du type de celles que se pose un pilote (fig. 7).

Les questions posées sont là encore fonction de la situation : selon le cas, on utilise entre 3 et 9 questions. Une réponse oui vaut un point ; une réponse non zéro.

La manœuvre qui obtient le maximum de points est retenue.

2.5 - Les commandes

Pour l'intégration de la trajectoire, on applique alors à un modèle avion complet, 3 commandes :

- le facteur de charge retenu
- la gîte aérodynamique telle que la trajectoire se déroule dans le plan de manœuvre retenu
- la manette des gaz qui est commandée pour réduire la poussée dans certains cas bien précis :

  a) en poursuite pour rester à distance de tir

  b) pour éviter le dépassement

  c) pour se rapprocher de la corner speed.

2.6 - Exemples de combats

Les figures 8 et 9 donnent deux exemples de combats calculés par le programme LAMA.

Ces combats opposent deux avions A et B identiques à la masse près. Les conditions initiales avantagent l'avion A : il est pointé sur l'avion B ( $\lambda_A = 0°$, à M = 1.1 et 9000 m). L'avion B est à la même altitude, à un Mach plus faible (M = 0.9) et orienté tel que $\lambda_B = 110°$.

La distance initiale entre les avions est de 3500 m.

Les figures 9 et 10 donnent pour chacun de ces deux combats :

- la projection des trajectoires dans le plan x, y
- la projection des trajectoires dans le plan x, z

Ces trajectoires sont graduées en temps par un point chaque 5 secondes. Ces combats sont limités à 120 secondes.

- l'évolution des angles $\lambda_A$ et $\lambda_B$ en fonction du temps.

Dans le premier cas (fig. 8), l'avion B, désavantagé en position initiale, l'est aussi en masse (masse $_B$ = masse $_A$ + 10 %). Il est donc moins performant que l'avion A qui, dans un engagement en spirale descendante, conserve son avantage initial et a des opportunités de tir missile.

Dans le second cas (fig. 9), c'est au contraire l'avion A qui est pénalisé en masse. Le combat se déroule à peu près de la même manière que précédemment, mais après une minute environ, c'est l'avion B qui reprend l'avantage et tire.

## 3. VALIDATION DU MODELE

Avant de pouvoir utiliser un tel modèle, et de croire aux conclusions qui en ressortent, il faut être certain de deux choses :

1 - que les manœuvres effectuées sont bien les meilleures possibles

2 - que le comportement global du modèle est comparable à celui d'un pilote doté du même avion et face au même adversaire.

Nous avons donc mené en parallèle deux types de travaux :

1 - création d'un programme de combat utilisant la théorie des jeux différentiels

2 - réalisation de campagnes de combats pilote/LAMA sur le simulateur du CELAR.

Ces deux types de travaux ont permis, outre la validation, l'amélioration du modèle par l'analyse des différences observées.

3.1 - La théorie des jeux appliquée au combat aérien

Le combat aérien à un contre un est caractérisé par :

- deux joueurs
- dont la victoire de l'un exclut la victoire de l'autre
- dont les évolutions sont régies par des équations différentielles.

Il entre donc dans la catégorie des jeux différentiels à somme nulle qui ont fait l'objet d'études approfondies.

D'une façon générale, le principe d'un tel jeu peut s'exprimer de la façon suivante :

Soit :

- A et B deux joueurs
- X et Y les vecteurs état de A et B
- u et v les vecteurs commande de A et B.

Les équations d'état sont de la forme :

$$\frac{dX}{dt} = F(X,u,t) \qquad \frac{dY}{dt} = G(Y,v,t)$$

On définit une fonction coût $J(X,Y)$ que doit minimiser A et maximiser B.

Il faut trouver un couple de stratégies $(u^*,v^*)$ tel que

$u^*$ minimise J

$v^*$ maximise J

3.1.1 - Formulation du problème du combat aérien

a) Les équations d'état

Le combat se déroulant dans 3 dimensions, le vecteur état a six composantes (on suppose les masses constantes)

Les équations d'état sont donc les équations de la mécanique du vol, à savoir :

$$\dot{x} = v\cos\gamma\cos\chi \qquad \dot{v} = (\eta F\cos\alpha - R_x)/m - g\sin\gamma$$
$$\dot{y} = v\cos\gamma\sin\chi \qquad \dot{\gamma} = (R_z + \eta F\sin\alpha)\cos\mu/mv - g\cos\gamma/v$$
$$\dot{h} = v\sin\gamma \qquad \dot{\chi} = (R_z + \eta F\sin\alpha)\sin\mu/mv\cos\gamma$$

où x, y, h sont les coordonnées dans le repère absolu

v la vitesse aérodynamique — F la poussée maximale

$\gamma$ la pente — $\alpha$ l'incidence

$\chi$ l'azimut — $\mu$ l'angle de gîte

$\eta$ la commande de poussée

$R_x$, $R_z$ les composantes de la résultante des forces aérodynamiques.

b) Les commandes

- l'incidence $\alpha$ sur laquelle s'exerce une contrainte non linéaire qui pose de grandes difficultés dans la résolution du problème :

$$V \leqslant Vc \qquad \alpha \leqslant \alpha_{max}$$
$$V \geqslant Vc \qquad \alpha_{max} \text{ tel que } n \leqslant n_{max}$$

- L'angle de gîte $\mu$ $\qquad -180° \leqslant \mu \leqslant +180°$
- La commande de poussée $\eta$ $\qquad 0 \leqslant \eta \leqslant 1$

c) La fonction coût

La fonction coût retenue est de la forme

$$J = C_1 \sin^2\frac{\theta_A(t_f)}{2} + C_2\sin^2\frac{\theta_B(t_f)}{2} + C_3 D(t_f) + \int_0^{t_f}\left(k_1\sin^2\frac{\theta_A(t)}{2} + k_2\sin^2\frac{\theta_B(t)}{2}\right)dt$$

où $C_1$, $C_2$, $C_3$, $k_1$, $k_2$ sont des constantes et $\theta_A$, $\theta_B$ les angles définis sur la figure n° 10.

On peut remarquer que cette fonction est composée de deux termes :

- un terme caractérisant la situation à l'instant final $t_f$ du jeu (termes $C_1$ $C_2$ $C_3$)
- un terme intégral tenant compte de la façon dont le jeu s'est déroulé entre $t = 0$ et $t = t_f$.

On peut noter aussi que si $C_3 = 0$, cette fonction est totalement symétrique, c'est-à-dire qu'au départ du jeu il est inutile de fixer qui est le poursuivant et qui est le défenseur (si $C_1 = C_2$ et $k_1 = k_2$).

3.1.2 - Algorithmes de résolution

La résolution analytique d'un problème aussi complexe est évidemment impossible. Il a donc été fait appel aux techniques de l'analyse numérique développées pour résoudre les problème d'optimisation (Réf. 1).

Deux voies s'offrent alors :

1) La recherche d'une solution point-selle par un algorithme type Arrow-Hurwicz. On cherche alors deux stratégies $u^*$, $v^*$ telles que

$$J(u^*,v) \leqslant J(u^*,v^*) \leqslant J(u,v^*) \qquad \forall\ (u,v)$$

L'inconvénient de cette méthode est que le point-selle n'existe pas forcément.

2) La recherche d'un Min-Max (ou d'un Max-Min) par un algorithme type Uzawa faisant appel à l'optimisation non différentiable (Réf. 2) et où la contrainte non linéaire est traitée par des techniques de Lagrangien augmenté (Réf. 3).

Pour un Min-Max, on va en effet chercher deux stratégies $u_1$ et $v_1$ telles que

$$J(u_1, v_1) = \min_u \left[ \max_v J(u,v) \right]$$

Cette méthode est plus puissante et conduit plus sûrement à une solution, mais avec des temps de calcul plus importants.

On peut noter qu'on démontre que, si un point-selle $(u^*, v^*)$ existe, alors :

$$\max_v \left[ \min_u J(u, v) \right] = J(u^*, v^*) = \min_u \left[ \max_v J(u, v) \right]$$

### 3.1.3 - Techniques et exemple de calcul

Une première technique consiste à calculer le jeu de 0 à $t_f$. Un exemple de cette technique est donné sur la figure n° 11.

Il s'agit d'un engagement entre deux avions identiques calculé en Min-Max

- dans les conditions initiales

| | |
|---|---|
| Z = 9000 m | $(\theta_A)_o = 0$ |
| D = 3000 m | $(\theta_B)_o = 45°$ |
| $M_A$ = 0.9 | $M_B$ = 0.8 |

- sur un temps de 7 secondes avec modification des commandes toutes les secondes

- avec $C_1 = C_2 = 1$ $\qquad C_3 = k_1 = k_2 = 0$

La figure 11 présente les trajectoires de chacun des adversaires projetées dans les plans xy et yz, l'évolution en temps des 3 commandes, de la fonction coût totale et de ses deux termes en $C_1$ et $C_2$.

L'avion B effectue un break en descente vers son adversaire ; l'avion A ajuste ses commandes pour à l'instant $t_f$ être pointé sur son adversaire ($\theta_A \approx 0$) tout en essayant de minimiser $\theta_B$ en ouvrant sa trajectoire vers l'extérieur.

La grosse difficulté de cette méthode réside dans le fait que la convergence est d'autant plus difficile que le temps $t_f$ est plus long et ceci est fonction des conditions initiales.

La seconde technique consiste à effectuer des séquences de sous-jeu d'une durée limitée, dont la convergence est pratiquement assurée.

La figure 12 présente le même engagement que précédemment, mais calculé selon cette seconde technique sur une durée totale de 20 secondes.

Le principe est le suivant : à l'instant $t_o$ on calcule un sous-jeu de 4 secondes, sur $t_o$, $t_o + 4$ sec . On retient les commandes obtenues sur l'intervalle $t_o$, $t_o + 1$ sec . On recalcule un sous-jeu de 4 secondes à partir de $t_o + 1$ sec, dont on retient les commandes sur $t_o + 1$, $t_o + 2$ , et ainsi de suite ....

On ne peut plus certifier que la trajectoire soit optimale de 0 à $t_f$, mais par contre les décisions prises chaque seconde sont toujours les meilleures possibles à l'horizon des 4 secondes.

## 3.2 - L'expérimentation Pilote/LAMA

La première version de LAMA était ordinateur/ordinateur. Elle a été adaptée et implantée sur le simulateur de combat du CELAR pour être validée contre des pilotes.

### 3.2.1 - Description du Simulateur de Combat Aérien

#### 3.2.1.1 - Généralités

Le Centre d'Electronique de l'Armement (CELAR), implanté à BRUZ près de RENNES, possède un simulateur de combat aérien équipé de trois cabines pilotables. Chaque cabine, munie de ses commandes de vol, possède son matériel électronique et optique nécessaire à la projection de l'image sol et de la cible adverse et constitue un système pilotable pouvant fonctionner soit indépendamment, soit couplé à l'une des deux autres cabines ; dans un avenir proche, il est prévu un fonctionnement simultané des trois systèmes pour des études de combat à deux contre un. Ces trois ensembles de pilotage sont complétés par des consoles de visualisation permettant le contrôle des combats.

#### 3.2.1.2 - L'environnement pilote et les moyens de contrôle du combat

En combat aérien, les évolutions des avions étant d'une grande amplitude, nous avons renoncé à tous mouvements des cockpits, par contre les images sont projetées sur 360 degrés. Chacun des 3 systèmes comprend :

- un cockpit et une planche de bord,
- un écran sphérique de 6,40 mètres de diamètre entourant totalement la cabine,
- un système de projection de l'horizon tournant en roulis, tangage, lacet, et donnant sur 360° une image du sol issue de 6 diapositives fish-eye, obtenues par photographie aérienne d'un terrain à différentes altitudes,
- un système de projection de l'avion adverse,
- un système de génération de l'image avion soit à base de segments, soit à partir d'une génération synthétique d'images,
- pour l'une des cabines une combinaison anti-g et un gravi-siège (g-seat) muni de 2 mouvements sur le fond, 1 mouvement sur le dossier, un coussin de siège et 1 coussin de dossier.

Le contrôle des combats se fait en temps réel et en play-back sur des consoles graphiques. En permanence, la console centrale fournit une vue perspective du combat avec trace spatiale et au sol des avions. Le cadrage est automatique. On peut y lire également des renseignements indispensables tels que altitude, vitesse, incidence .... Les autres consoles sont réservées soit à des vues perspectives spéciales identiques à celles qu'aurait un observateur occupant la place pilote, soit à l'étude des systèmes d'armes (pénétration à l'intérieur des domaines de tir des missiles, trajectographie des missiles que l'on peut voir évoluer en temps réel).

3.2.1.3 - Les moyens de calcul

Les équations de la mécanique du vol, les calculs des systèmes d'armes et du programme LAMA sont résolus dans un calculateur, bi-processeur, d'une puissance de cinq millions d'opérations par seconde, ce qui permet une cadence d'échantillonnage de trente millisecondes. Les images de contrôle du combat sont générées par un second calculateur associé à des consoles graphiques. La fabrication des images avions projetées à l'intérieur des simulateurs est réalisée par une électronique spécialisée qui génère synthétiquement l'avion sélectionné décrit par une suite de facettes dont les coordonnées sont contenues dans une base de données.

Le programme LAMA est appelé toutes les secondes et envoie ses décisions au modèle avion.

3.2.2 - Les résultats obtenus

Les combats de validation ont opposé de nombreux pilotes d'essais et opérationnels au programme LAMA.

Les premières campagnes ont tout de suite mis en évidence les qualités manœuvrières du modèle, ainsi que quelques lacunes auxquelles il a pu être remédié.

La possibilité de suivre les combats, soit du poste de directeur de vol, soit de la cabine "pilotée" par LAMA, a montré le réalisme du comportement et la qualité des décisions de LAMA.

Les pilotes dans leur ensemble ont conclu à la validité du modèle dans tout le domaine de vol et, ceci, quelles que soient les conditions d'engagement. LAMA peut donc être qualifié d'adversaire valable en combat air-air à un contre un, ce qui valide sa logique de décision.

Pour quantifier cette appréciation, la figure 14 présente les résultats d'une des campagnes d'essais au cours de laquelle :

- 4 pilotes ont été opposés à LAMA, les pilotes et LAMA disposant du même avion
- dans 11 conditions d'engagement différentes choisies par les pilotes.

Cette figure donne la durée moyenne par vol de présence dans les conditions de tir pour LAMA et pour le pilote et, ceci, pour chaque condition initiale. Elle montre sur l'ensemble une légère supériorité du modèle.

La figure 15 montre à titre d'exemple un combat pilote-modèle enregistré lors de cette campagne. Les conditions d'engagement sont rigoureusement symétriques : mêmes avions à la même masse se présentant à même vitesse (M = 0.9) et même altitude (Z = 6 km), en face à face décalé de 3 km. Dans le cas présenté, c'est l'avion B qui est piloté par LAMA.

Les 5 premières secondes sont neutralisées pour permettre au pilote d'apprécier sa situation ; l'engagement débute réellement au moment du croisement. Les deux adversaires virent alors l'un vers l'autre au maximum des possibilités de l'avion et s'engagent dans une spirale descendante. Il n'y a pas de prise d'avantage avant le temps 70 s ; à cet instant le pilote doit mal apprécier la meilleure manœuvre à effectuer, LAMA prend l'avantage et l'améliore progressivement jusqu'à être en bonne position pour tirer au temps 120 s.

## 4. CONCLUSION

*Aujourd'hui on peut affirmer que les objectifs poursuivis au départ ont été atteints.*

LAMA est un programme qui a été reconnu valable pour juger de l'efficacité d'un avion en combat aérien à un contre un. C'est donc un outil qui permet de comparer différents systèmes, soit ordinateur/ordinateur, soit pilote/ordinateur sur simulateur.

C'est à ce titre qu'il fait maintenant partie intégrante des moyens de recherche de nouvelles formules d'avion ou de nouveaux systèmes d'armes, et ceci quel que soit le type d'armement envisagé.

Pour les comparaisons de systèmes, deux processus ont été utilisés, suivant le problème posé ; on peut :

- soit opposer chacun des systèmes en compétition à un adversaire de référence donné
- soit les opposer systématiquement deux à deux.

Les pourcentages de combats gagnés, nuls et perdus, permettent alors de les classer et de conclure (fig. 16).

Cette utilisation de LAMA en fait un instrument de mesure dont l'emploi, comme tel, nécessite quelques précautions. Il est, entre autres, indispensable de s'assurer que ni les conditions initiales, ni le critère de gain choisi ne peuvent fausser les résultats.

De plus, le succès des phases de validation sur simulateur a fait apparaître une autre utilisation possible pour LAMA : cet hostile performant, pouvant simuler n'importe quel système connu, peut être utilisé comme moyen d'entraînement des pilotes. Cette nouvelle fonction de LAMA nécessite de développer autour du modèle des moyens d'information sur la stratégie qu'il adopte, afin d'accroître ses qualités pédagogiques.

Signalons, enfin, que des travaux sont actuellement en cours pour adapter ce modèle au combat multi-avions pour prendre en compte le contexte opérationnel.

## REFERENCES


(1) B. ENJALBERT : Résolutions numériques pour des problèmes de jeux différentiels - Thèse de 3e Cycle (PARIS 1980)

(2) C. LEMARECHAL : On a bundle algorithm for non smooth optimization (presented at NPS4, MADISON 1980).

(3) M. FORTIN, R. GLOWINSKI : Résolution numérique de problèmes aux limites par des méthodes de Lagrangien augmenté (DUNOD, à paraître).

Fig. 1 **PRINCIPE DU PROGRAMME LAMA**

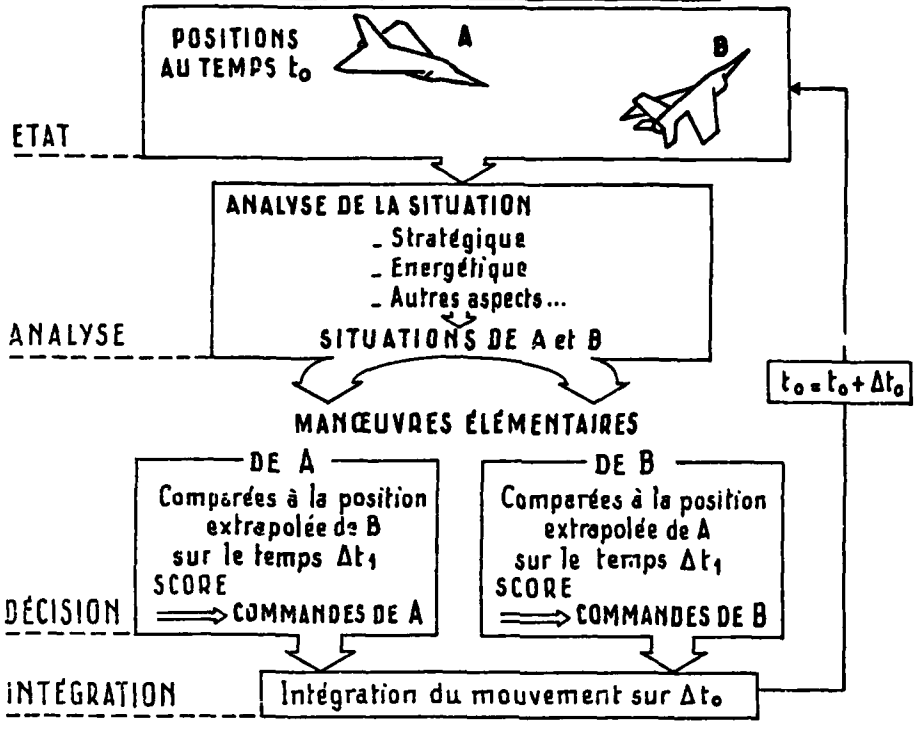


Fig. 2 **DÉFINITION DES ANGLES CARACTÉRISTIQUES**

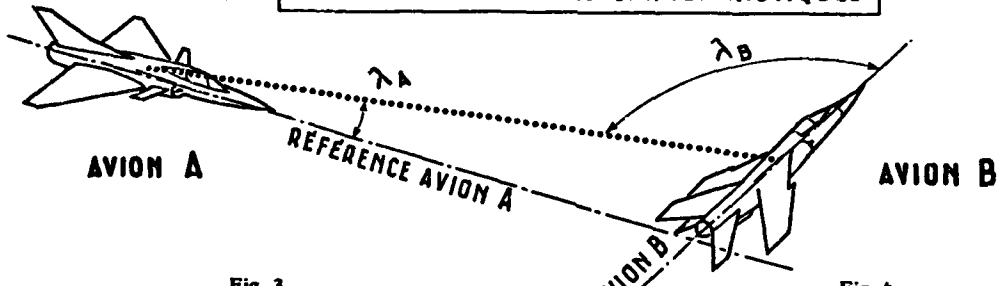


Fig. 3 **CARACTÉRISTIQUES DU DOMAINE DE TIR**

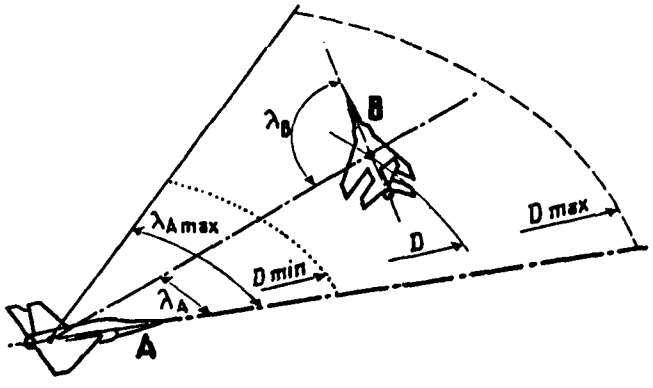


Fig. 4 **SITUATION STRATÉGIQUE**

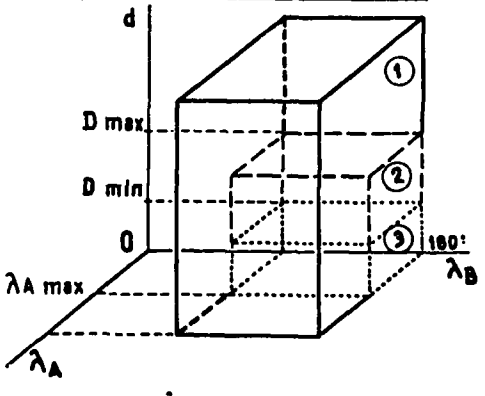


**RÔLES**

Zone ① Attaquant / Défenseur
② Très Attaquant / Très Défenseur
③ Attaquant proche / Défenseur proche
④ Zone 3 et $V_R > 0$ - Très proche

Fig. 6

## LES PLANS DE MANŒUVRE

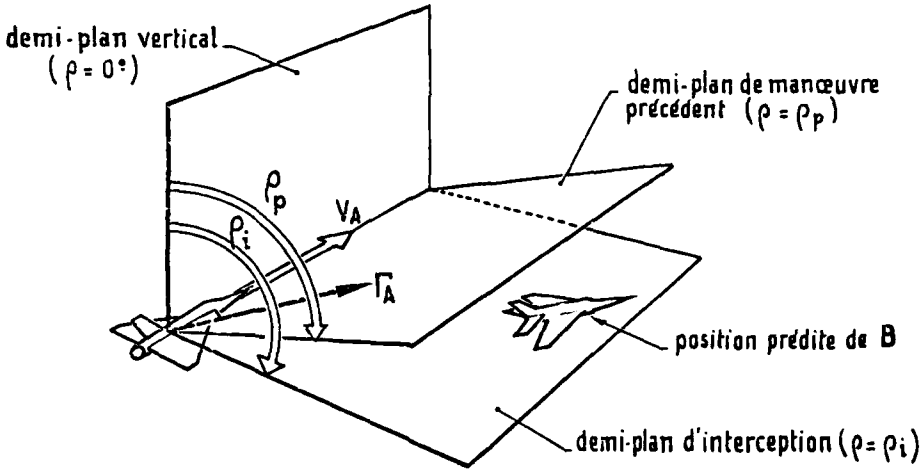


Les demi-plans envisagés sont choisis suivant la situation parmi :
$\rho = 0°$ ; $\rho_P$ ; $\rho_i$ ; $\rho_i \pm 45°$ ; $\rho_i \pm 90°$ ; $\rho = \pm 60°$

Fig. 5

## SITUATION ÉNERGÉTIQUE

1 . VITESSE

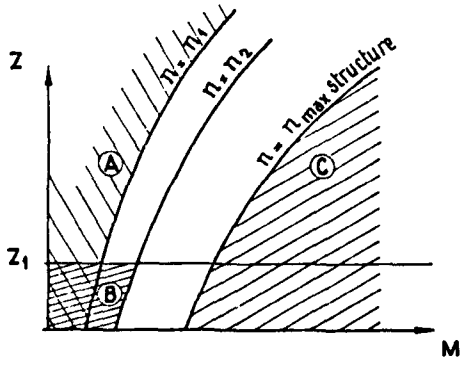


2 . ALTITUDE

Evitement sol prioritaire .

Fig. 7

## SCORE

QUESTIONS CHOISIES SUIVANT LA SITUATION PARMI :

1 . $\lambda_A < 90°$
2 . $\lambda_B > 90°$
3 . A voit B
4 . B ne voit pas A
5 . A peut tirer
6 . B ne peut pas tirer
7 . $\frac{d\lambda_A}{dt} < 0$
8 . $\frac{d\lambda_B}{dt} > 0$
9 . A améliore sa situation stratégique
10 . A ne dégrade pas sa situation stratégique
11 . $\frac{d\lambda_A}{dt} < \frac{d\lambda_B}{dt}$

Fig. 8

## EXEMPLE DE COMBAT
## MODÈLE / MODÈLE

### CONDITIONS INITIALES :

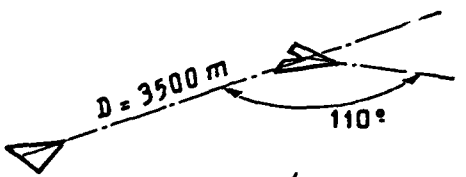


A { $m_A$ ; M = 1.10 ; Z = 9000 m }  B { $m_A$ + 10% ; M = 0,9 ; Z = 9000 m }

### TRAJECTOIRES

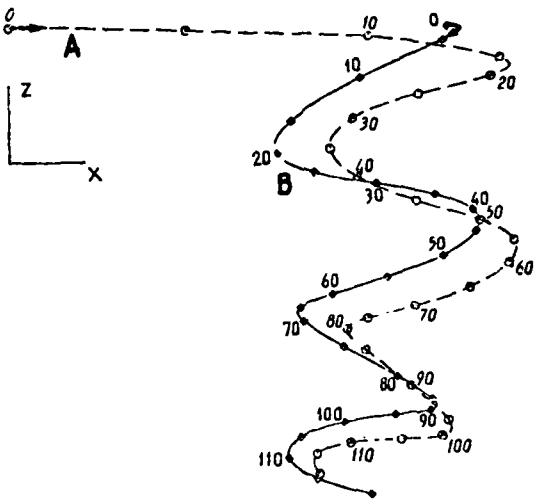


### ANGLES BUT

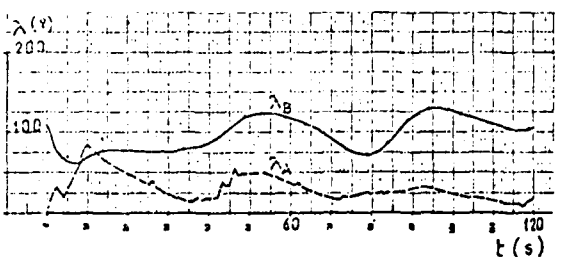


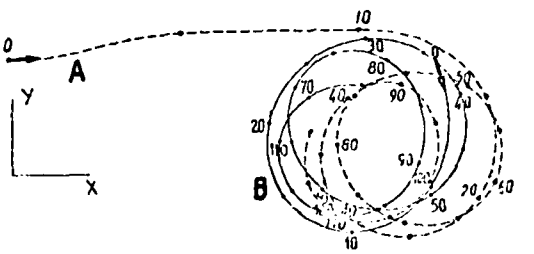


Fig. 9

## EXEMPLE DE COMBAT
## MODÈLE / MODÈLE

### CONDITIONS INITIALES :

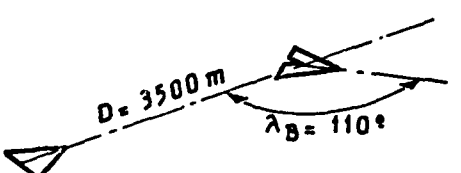


A { $m_B$ + 10% ; M = 1.1 ; Z = 9000 m }  B { $m_B$ ; M = 0,9 ; Z = 9000 m }

### TRAJECTOIRES

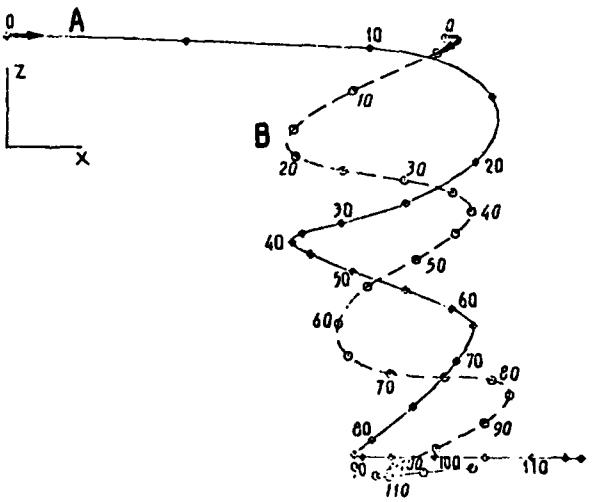


### ANGLES BUT

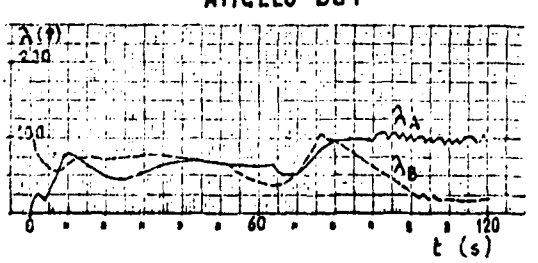


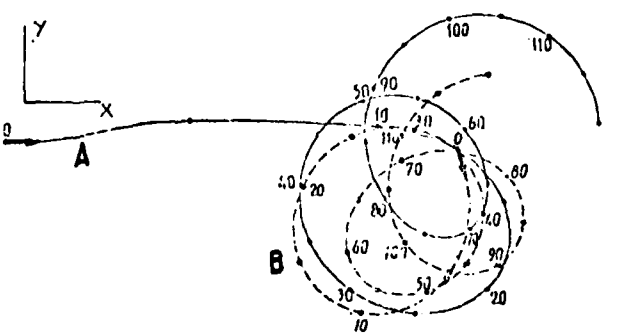

Fig. 10

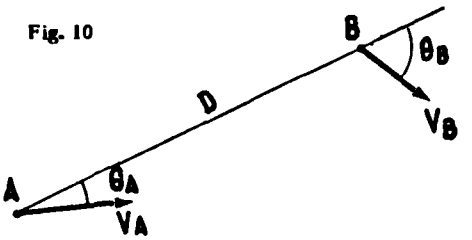


Fig. 11

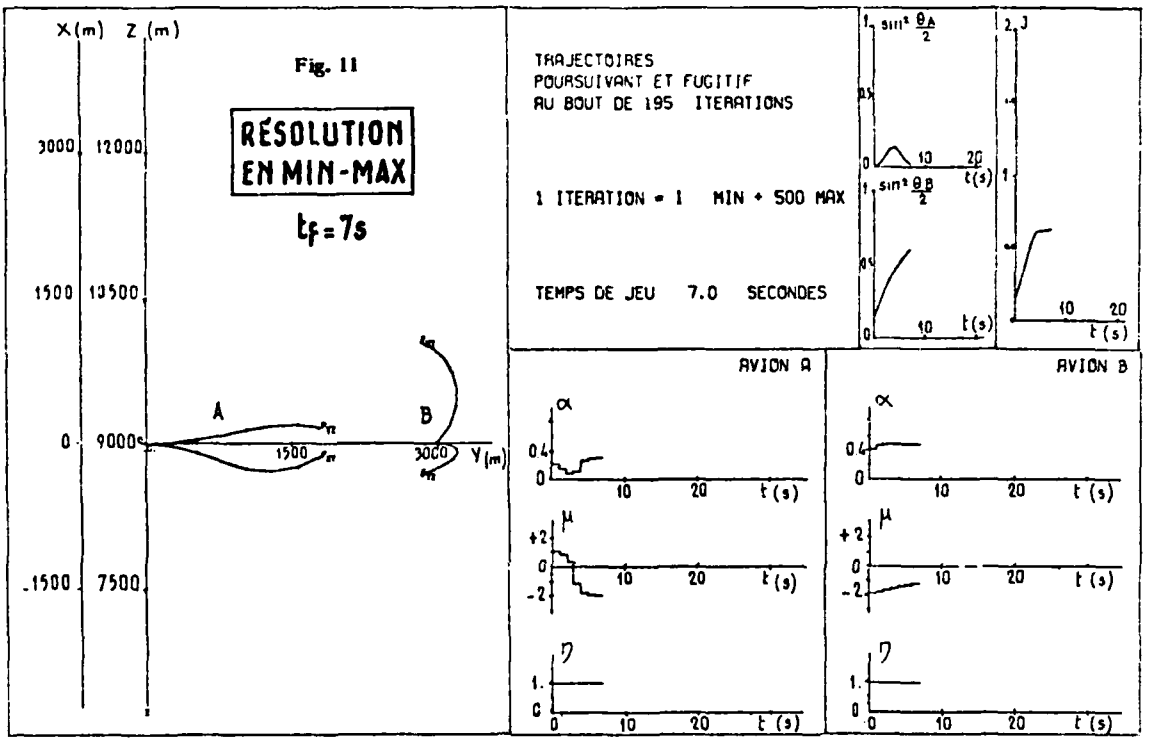


Fig. 12

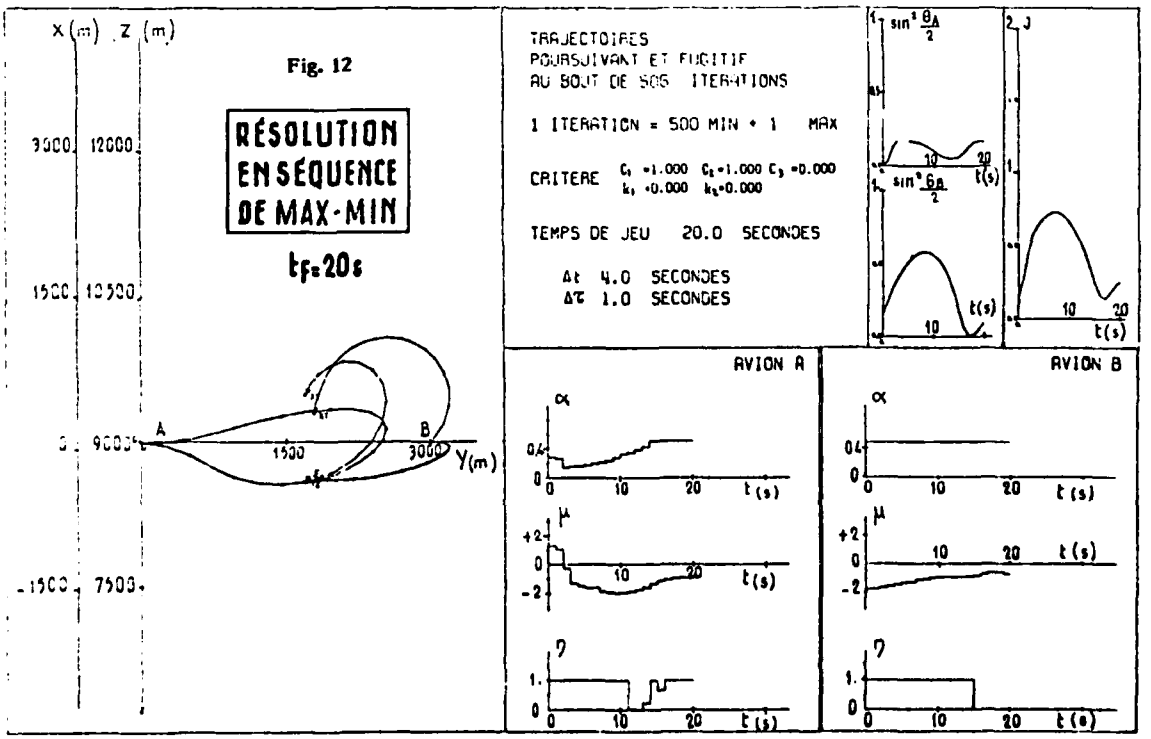

Fig. 13

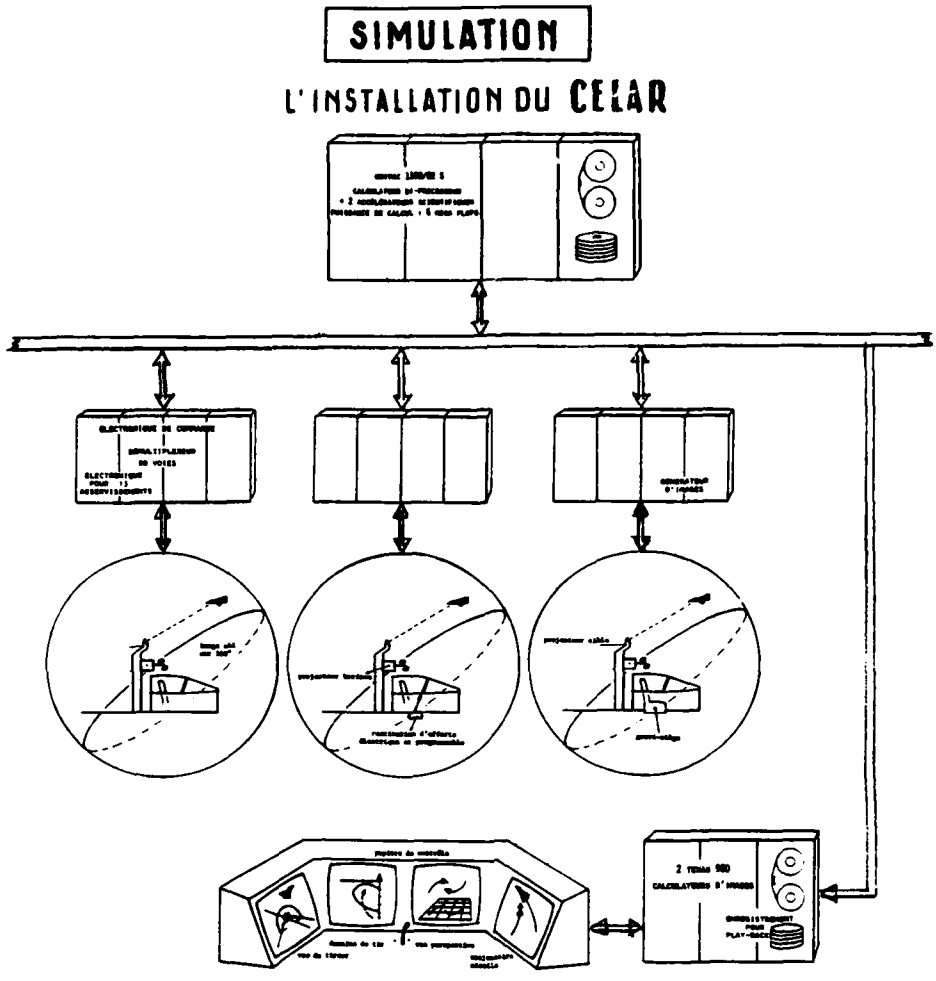
SIMULATION
L'INSTALLATION DU CELAR

Fig. 14

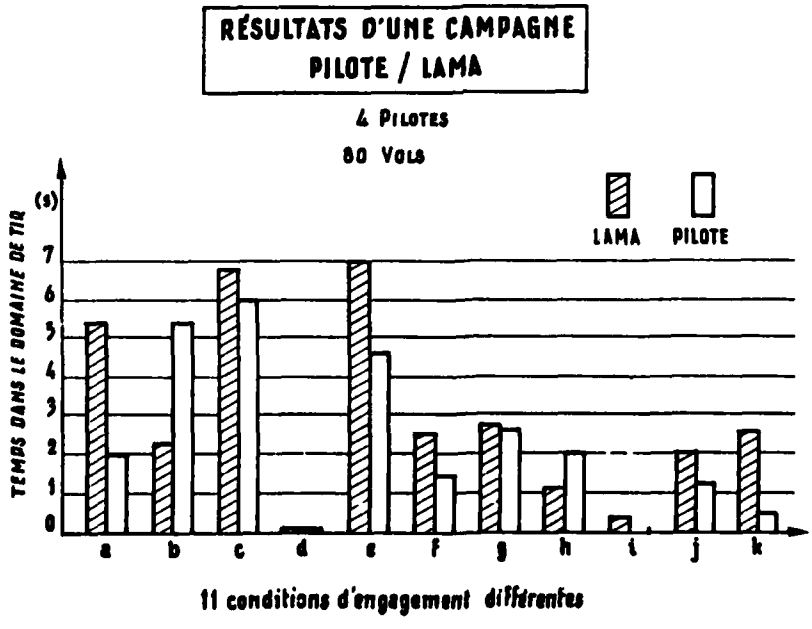
RÉSULTATS D'UNE CAMPAGNE
PILOTE / LAMA
4 PILOTES
80 VOLS
LAMA
PILOTE
TEMPS DANS LE DOMAINE DE TIR
(s)
0
1
2
3
4
5
6
7
a
b
c
d
e
f
g
h
i
j
k
11 conditions d'engagement différentes

Fig. 15

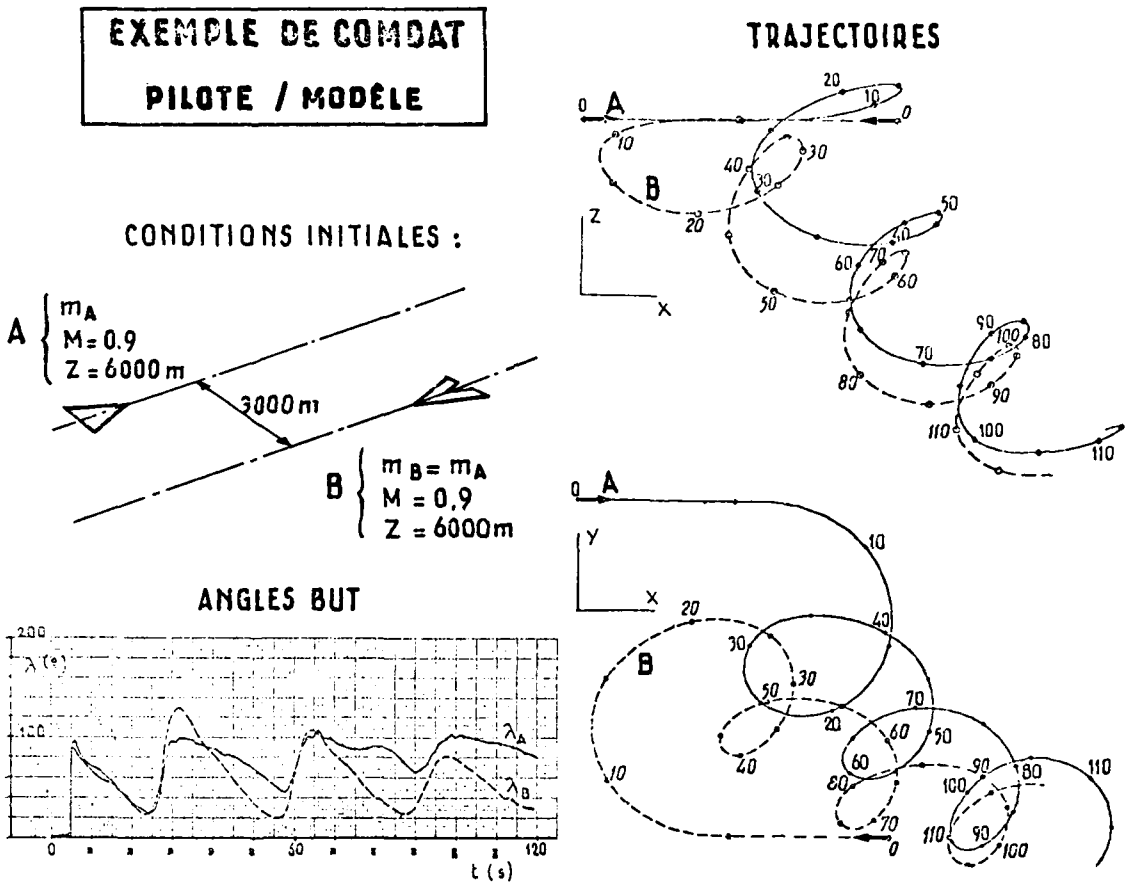
EXEMPLE DE COMBAT
PILOTE / MODÈLE
TRAJECTOIRES
CONDITIONS INITIALES :
A
$m_A$
M = 0.9
Z = 6000 m
3000 m
B
$m_B = m_A$
M = 0,9
Z = 6000m
ANGLES BUT
λ (°)
$\lambda_A$
$\lambda_B$
t (s)
Z
X
Y

Fig. 16

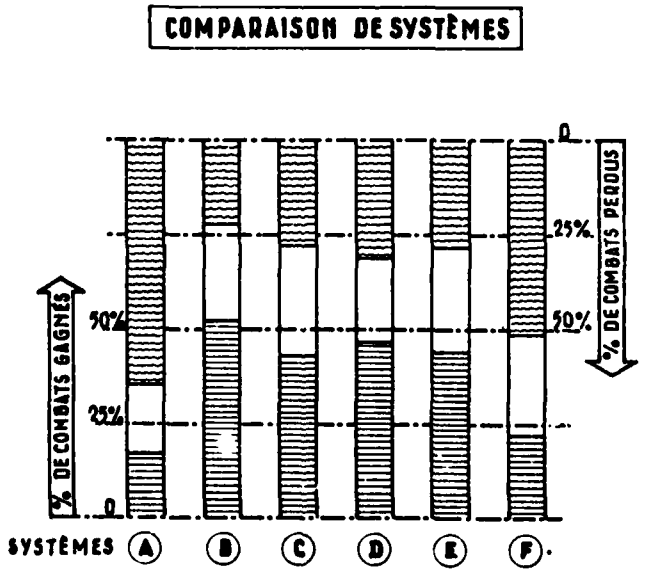
COMPARAISON DE SYSTÈMES
% DE COMBATS GAGNÉS
% DE COMBATS PERDUS
50%
25%
0
SYSTÈMES
A
B
C
D
E
F

# THE ASSESSMENT OF AIRCRAFT COMBAT EFFECTIVENESS USING A NEW COMPUTATIONAL METHOD

by

Michael Falco and Gilbert Carpenter
Research Department M.S. A08-35
Grumman Aerospace Corporation
Bethpage, NY 11714, USA

## SUMMARY

This paper presents a synopsis of the experience gained using a newly developed computational method for the assessment of aircraft combat effectiveness in the design concept phase. The approach employs a stochastic learning method, in conjunction with dynamic simulation, to derive aircraft maneuver strategies in the form of a feedback control based upon a discretized set of threat visual or warning system cues. The derived strategies maximize either survival probability or kill probability in the one-on-one setting. Computational results are presented for selected aircraft designs in missile and gun combat.

## INTRODUCTION

In the early phases of combat aircraft design, there is a need for a methodology to better quantify combat effectiveness in terms of such aircraft system attributes as maneuver performance, threat warning capability, weapon lethality, and countermeasure capability. The associated models are required to be of high fidelity in terms of dynamical similitude and yet flexible enough to allow an orderly evaluation of the sensitivity of the effectiveness measure to changes in the system attributes. To be meaningful, it is necessary to have a methodology that utilizes kill probability as the effectiveness measure and develops an "optimal" effectiveness solution for each parametric case of the combat model considered. Moreover, the optimal effectiveness solutions for each case must be computed for all relative geometries for which combat can be initiated. Solution optimality is important for consistent comparisons between systems, and to minimize maneuver strategy prejudgements and bias factors introduced by the analyst.

Application of modern optimal control and differential game theory methods seem well suited to these problems at first sight. However, the pioneering effort of Isaacs (Ref. 1), followed by those of Breakwell and Merz (Ref. 2), indicate that there does not appear to be a general systematic method for solution of even some simply structured pursuit-evasion games. This difficulty has led applications-oriented investigators (Ref. 3,4), toward consideration of discrete game approximations which circumvent the analytical problems of the continuous theory, and still offer some form of sub-optimal solution in more realistic combat models.

This paper presents a partial summary of recent computational experience gained in aircraft design applications using variations of a stochastic learning method first reported in Ref. 4. These applications are more fully reported in Ref. 5 through 11. Computational results are summarized for three important categories or air combat: 1) aircraft avoidance of air to air missiles, 2) avoidance of surface to air missiles, and 3) visual range gun combat. An explanation of the maneuver strategy development and combat effectiveness assessment methodology is given in the discussion of the air-to-air missile avoidance case.

The same approach has been extended to problems of land warfare, particularly armored vehicle maneuver effectiveness and survivability against anti-tank missile threats (Ref. 8, 10, 11). Corroboration of the computer derived solutions for specific threat cases has been obtained in independent field trials with the actual systems.

## HELICOPTER MANEUVERABILITY/AIR-TO-AIR MISSILE THREAT

One of the important questions impacting combat helicopter advanced concepts concerns quantifying the survivability gains that may be achieved by lightweight, high performance, high agility designs. The question being addressed is whether high performance and maneuver capability can impart strong survivability against selected threats, thereby minimizing dependence on countermeasure equipment and terrain masking tactics.

The threat missile in this survivability study is an anti-tank guided missile (ATGM) of 4 km maximum range capability employed in the air-to-air mode by a threat helicopter. Earlier investigations have postulated the need for evading aircraft to be equipped with a threat warning system in order to achieve a reasonable measure of survivability against missile threats. The aircraft in these investigations is assumed to employ an active radar warning system supplying relative range and azimuth information regarding the incoming threat. The baseline configuration for this warning receiver model employs 12 azimuth gates and 7 range gates from 0.25 km out to a maximum detection range of 5 km, as shown in Fig. 1. This configuration is indicative of the warning receiver performance levels that are projected for operational systems in the near future. At each threat warning contingency (represented by one of the 7 x 12 = 84 range/azimuth cells), the aircraft is allowed a choice from a finite number of elemental maneuvers. Five elemental maneuver choices are shown in Fig. 1. The choices may be comprised of maximum performance turns, climbs, dives, acceleration, deceleration, and a straight ahead constant speed policy. An aircraft evasive maneuvering strategy is the selection of an elemental maneuver for each threat warning cell. An optimal strategy is a strategy which maximizes aircraft survivability for all launch initial conditions.

The stochastic learning method is comprised of two phases: a reinforcement learning phase, in which the optimized evasive strategy is ultimately derived, and a statistics phase. The learning phase involves the development of a decision table that consists of a probability distribution used in the selection of an elemental maneuver for each warning contingency. That table is shown in its initial form at the upper right of Fig. 2. The column indices 1, ....5 under the control caption are the five elemental maneuver choices. The row indices, labeled R, ranging from 1, ...., 84 represent the threat warning contingencies. Initially, the choice of maneuver for each contingency is governed by sampling from the equally likely discrete distribution, as shown.

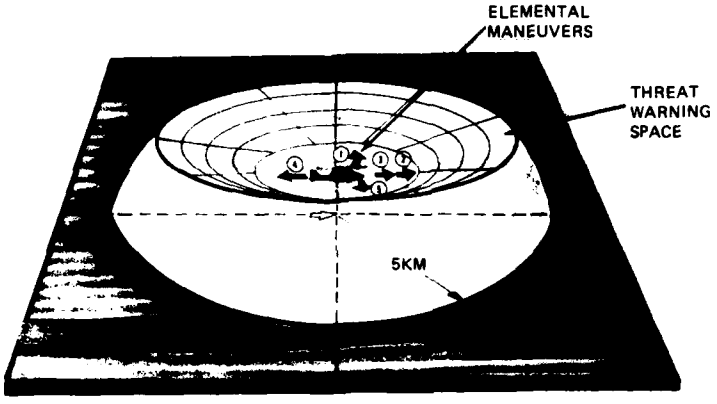


Fig. 1 Aircraft Warning System & Maneuver Strategy

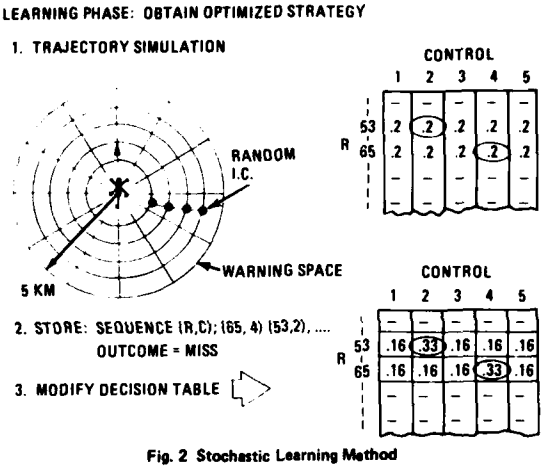


Fig. 2 Stochastic Learning Method

A random initial condition for the combat is selected and both aircraft and threat trajectories dynamically simulated. The aircraft employs a selected maneuver within the initial contingency cell until a second cell is entered and another maneuver choice is made. Threats may be launched outside the range of the warning space. In this case, the aircraft maintains its current speed and heading until the threat first enters the warning space at which time the control selection process begins. This simulation process is continued until warhead detonation or flyby, and a kill or survival event is calculated using the probability of kill distribution derived from the warhead lethality function. In the process of simulating the trajectories, the sequential contingency/control pairs employed by the aircraft are temporarily stored. Based upon the kill/survival event, the probability associated with those control choices made for each contingency are modified by a reinforcement rule. For the survival event, the probability of employing the same elemental maneuver for each stored contingency is increased, and is decreased for the kill event. The trajectory simulation and table modification process is repeated over all possible threat launch range and azimuth initial conditions using a random selection method. Approximately 100 launches per warning cell or 8400 total trajectories are numerically simulated to produce a converged decision table. The 8400 trajectories require approximately 20 minutes computer (CPU) time on IBM 370/168 systems.

In the statistics phase the converged decision table is fixed. Random starting conditions are then selected and trajectories dynamically simulated. In a manner typical of Monte Carlo approaches, the averaged probability of kill and missile warhead detonation distance statistics are computed for each warning (or launch) cell.

In this paper, the helicopter maneuver choices are restricted to those which maintain a low constant altitude. The combat altitudes were dependent upon helicopter initial speed and ranged between 15 meters at hover to 26 meters at maximum speed. Both vertical and composite vertical/horizontal maneuver models can also be investigated with this methodology, but are not reported here.

The maneuver vectorgram, labeled control set I in Fig. 3, is aimed at quantifying the impact of longitudinal and turn maneuver capability in constructing an effective evasive maneuvering strategy throughout the whole speed range from hover to maximum level flight speed. At forward speed, the helicopter can command maximum transient (or sustained) load factor turns, labeled (1) and (5); maximum longitudinal acceleration, (2); or maximum longitudinal deceleration, (4); as well as maintaining the current speed and heading, (3). At very low forward speeds including hover, the load factor turns are replaced with maximum rate pedal turns.

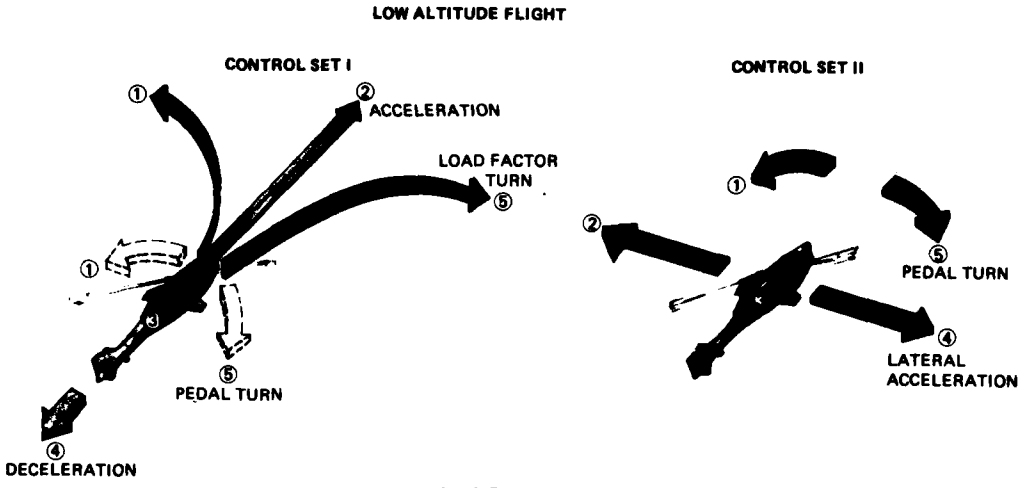


Fig. 3 Elemental Maneuvers

The maneuver vectorgram at right, captioned control set II, is aimed at quantifying the impact of lateral acceleration (sideward flight) and pedal turn capability in constructing a maneuver strategy at or near hover speeds only. Choices (1) and (5) represent maximum performance pedal turns; choices (2) and (4) maximum performance lateral accelerations; and choice (3) maintains current lateral speed at the current aircraft heading.

Figure 4 graphically summarizes the sea level maximum maneuver capability data associated with the elemental maneuver models of Fig. 3, for a conceptual enhanced performance version of a current helicopter design. The maximum commanded turn capabilities shown at upper left are employed for choices (1) and (5) in control sets I and II. For the case of maximum transient turn, the associated longitudinal transient deceleration is shown at the upper right. The maximum longitudinal acceleration and deceleration capabilities utilized for choices (2) and (4) in control set I, are given in the two lower diagrams. The lateral acceleration required for choices (2) and (4) of control set II is given in the diagram at lower left. These studies employ first order models for the aircraft transient response to the maximum acceleration and rate commands.

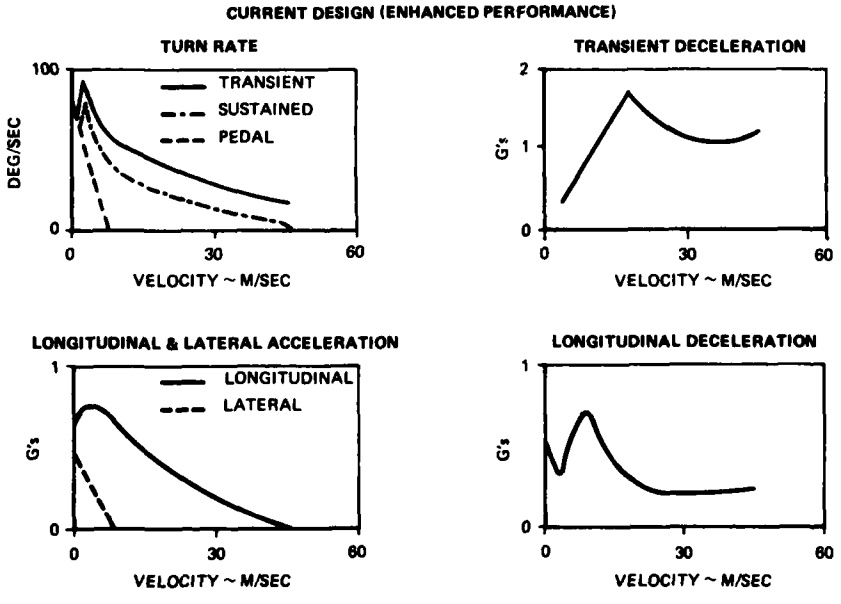


Fig. 4 Maximum Maneuver Capability

The threat is an optically tracked, wire guided missile employing a semi-automatic command to line of sight guidance system. This threat was originally designed for launch against ground combat vehicles, but has air-to-air application as well. It is assumed to have a 245 m/sec sustainer velocity, maximum range of 4 km, and maximum flight time of 16.3 seconds. In addition, it is assumed to have a 4 g maximum lateral maneuver capability, and that the launch aircraft is at co-altitude with the target. The low altitude of the target allows the survivability results to be safely extrapolated to ground launched cases as well. This threat is normally equipped with a shaped-charge contact fuze warhead for armor penetration.

However, proximity fuze warheads employing expanding rod or fragment kill mechanisms are also indicated to be adaptable to this missile airframe, and two of these types were considered in this investigation. The contact fuze warhead lethality model utilizes a probability of kill, $P_k = 1.0$ for missile contact anywhere on the helicopter fuselage envelope. Two proximity fuze warhead models are described in Fig. 5. Warhead A denotes an expanding rod warhead as used in short range air-to-air missiles. Warhead B is the largest blast/fragment warhead that can be accommodated by the missile airframe and propulsion configuration. The kill effectiveness, $P_k$, of these two warheads is given as a function of detonation distance $R_{DET}$ (from the target cg). The data shown represent an average of all warhead/target detonation aspects; however, functional dependence upon aspect is considered in the studies.

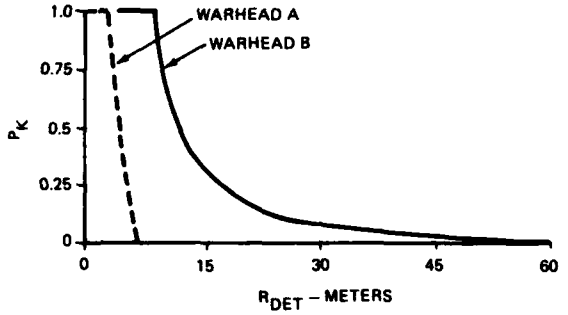


Fig. 5 Warhead Lethality

The aircraft survivability or equivalently the missile kill effectiveness results ($P_k$) for the ATGM threat for all launch conditions are calculated and presented in the helicopter warning space coordinate system for convenience. In this case the maximum effective launch range of the threat [4 km] was less than the maximum detectable range of the warning system [5 km]. (The results could also be presented in a space relative to the launch aircraft and would represent the effective launch envelope for that missile against an optimally maneuvered evader.) Threat launches were initiated from 72 of the 84 range/azimuth cells within the 5 km maximum range in both learning and statistics phases. No launches were simulated from the 12 cells making up the inner range ring (range less than 0.25 km) due to severe missile guidance transients at very short target ranges. It should be noted that in all results presented, the attacking aircraft is assumed to maintain a speed equal to the initial speed of the target, and fly a pure pursuit navigation course toward the target during missile flyout.

Figure 6 shows the kill effectiveness of the ATGM equipped with the expanding rod type warhead. Because of left-right symmetry considerations, only half of the warning space need be shown. Four levels of kill effectiveness ($P_k$) are given to simplify the presentation. The legend at lower center is employed throughout this section. The origin of each semicircular plot corresponds to the helicopter position at missile launch, and the aircraft initial heading (0°) is shown by the helicopter symbol. Head-on launches correspond to 0° to 30° azimuth sectors, and tail aspect launches 150° to 180°, respectively. The kill results are presented for four helicopter initial speed condition groups, beginning with hover at upper left, and progressing clockwise to maximum speed at the lower left. Within each of the four speed groups, the left semicircle, labeled nonmaneuver, represents missile kill effectiveness when the aircraft maintains its current speed and heading. This case is important for quantifying target speed effects without maneuver, and is useful for establishing baseline survivability measures without use of threat warning and optimal maneuver. Clearly, a scan of the nonmaneuver cases for the four initial speeds indicates improving survivability in longer range rear aspect launches with increasing speed, but at the expense of reduced survivability in the corresponding forward launch cases. In addition, a small window of improving survivability for short range beam launch cases can be seen developing with increased speed; this is due to guidance transients associated with high line of sight rate targets. The nonmaneuver cases show that speed alone (equivalent to no threat warning) does not provide sufficient survivability against the ATGM with Warhead A. The semicircles labeled OPT I in each of the four speed groups quantifies the survivability improvements that can be achieved with the 84 cell warning system, together with an optimal maneuvering strategy drived from control set I. In the four results labeled OPT I, the helicopter employed its maximum transient load factor turn performance for choices (1) and (5). One can see that survivability is still poor with combat initiated at hover, although small improvements exist for tail launches at the 4 km range. This is due to helicopter acceleration away from the oncoming missile and the missile maximum range limitation. However, at higher initial speeds, optimal maneuvering, employing transient load factor performance can provide high survivability. The lack of effectiveness of control set II (lateral acceleration and pedal turns) in constructing an optimal maneuver strategy from hover is shown by the shaded semicircle labeled OPT II. This result, together with that for OPT I to the immediate left, indicate the low survivability afforded by maneuver against the ATGM with warhead A at hover flight speeds.

The sensitivity of survivability of the enhanced performance helicopter to variations in ATGM warhead type and lethality is shown in Fig. 7. The three warhead types: contact, proximity Warhead A, and proximity Warhead B, have been examined at the helicopter minimum power required initial speed. The helicopter employs control set I with maximum transient turns for elemental maneuvers (1) and (5) in the optimal strategy development. The nonmaneuver and optimal survivability results for Warhead A are repeated at lower left. Corresponding survivability results for the contact fuzed warhead are shown upper center; those for Warhead B are shown at the lower right. The nonmaneuver results are statistically equivalent in all cases and typify the small miss distances achievable by the missile guidance system against constant velocity targets. The helicopter can be made completely survivable against the contact fuzed ATGM using optimal maneuvering at this initial aircraft speed. However, the corresponding result for Warhead B indicates that optimal maneuver would be completely ineffective. These results indicate the strong interplay between missile warhead lethality and guidance, and the need for carefully timed deployment of the aircraft's maximum maneuver capability to generate adequate miss distances.

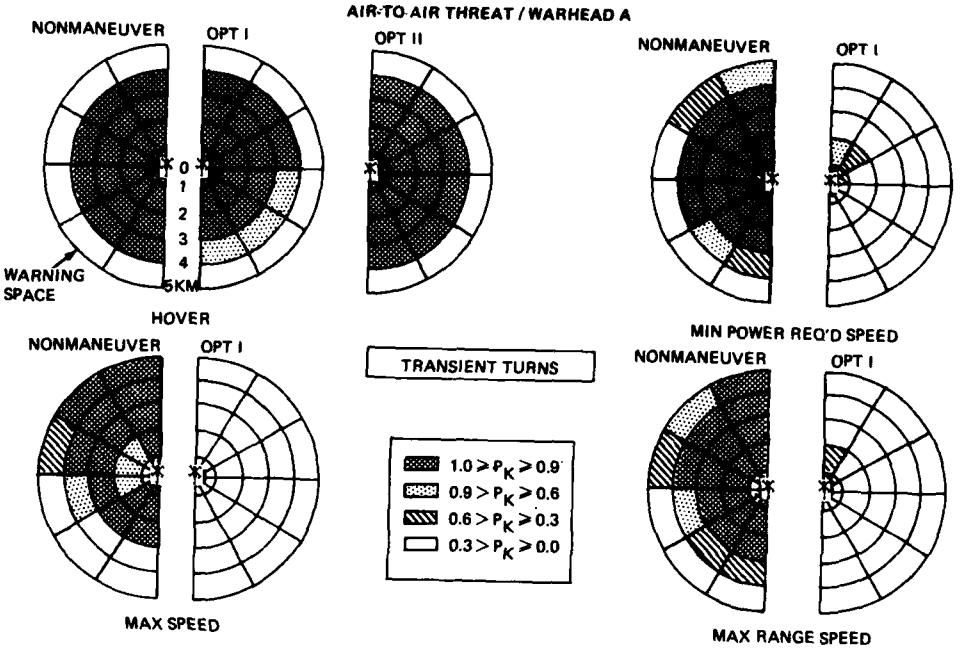


Fig. 6 Helicopter Survivability

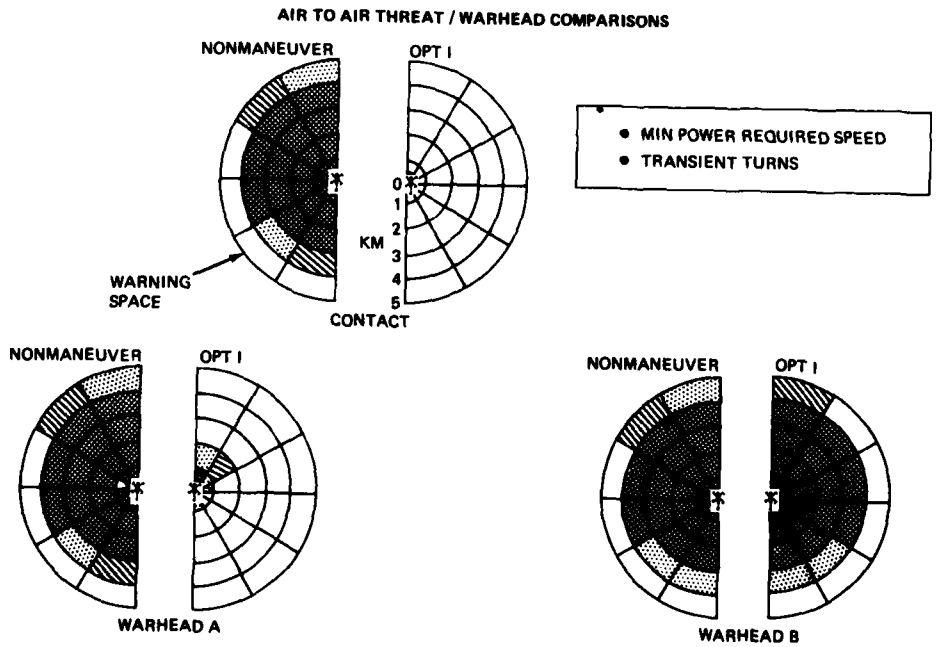


Fig. 7 Helicopter Survivability

Three optimal evasive trajectories from hover using maneuver set I against the contact fuzed warhead are shown in Fig. 8. The survivability results for nonmaneuver and optimal maneuver are presented at the upper left of the figure. For each case illustrated, only the terminal portion of the missile path and the entire helicopter path are shown because of scale effects. The head-on case at upper right and beam aspect case at lower right illustrate pedal turns immediately following launch, followed by straight accelerated flight and finally, a maximum performance load factor turn near termination. The tail aspect launch at lower left employs only the acceleration segment followed by the load factor turn at termination. In all cases shown, the aircraft maneuvers to achieve a tail aspect to present its minimal fuselage envelope dimension at missile flyby. Launches within 2 km cannot be made highly survivable because the missile flight time termination is too short to permit adequate forward acceleration and load factor turn maneuvers to avoid fuselage hits.

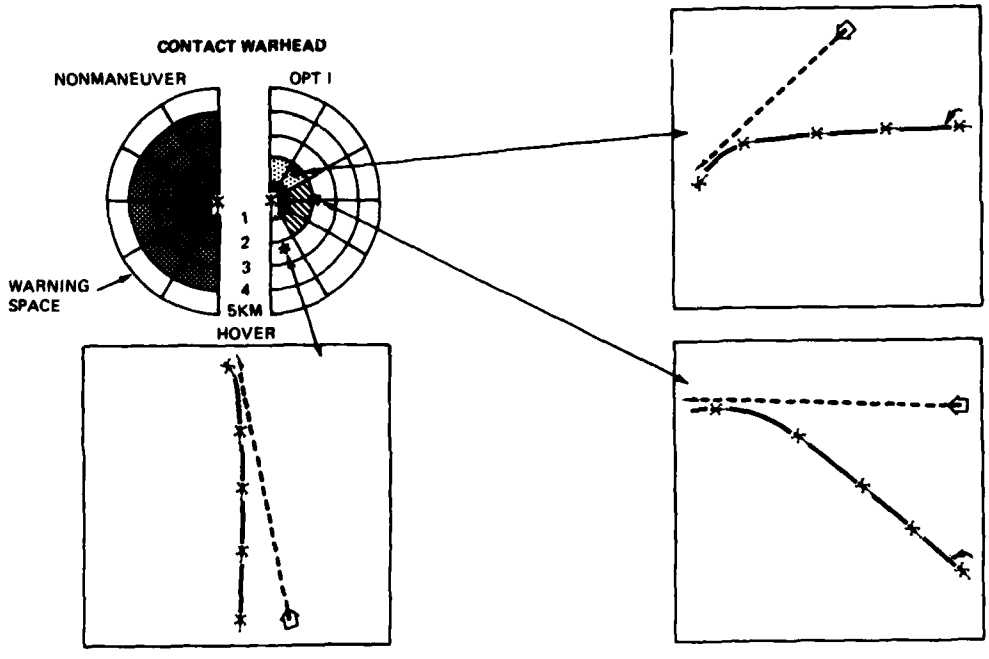


Fig. 8 Evasive Maneuvers (From Hover)

## TACTICAL FIGHTER MANEUVERABILITY/SURFACE TO AIR MISSILE THREAT

The second combat category concerns the assessment of survivability of a tactical aircraft designed expressly for supersonic cruise and weapon delivery against surface to air missile (SAM) threats. The effectiveness of supercruiser penetration speed/altitude and optimal maneuvering against a representative SAM are the main questions of interest in this study. Figure 9 shows the supercruiser threat warning and elemental maneuver models employed in the computational development; the construction closely parallels that employed in the preceding case study. The aircraft is assumed to be equipped with an active warning receiver comprised of 12 azimuth and 11 range thresholds with a maximum threat detection range of 14.6 km. The aircraft maximum maneuver choices comprise transient (or sustained) turns, maximum symmetrical climbs, dives, and straight flight. The performance capability of the supercruiser for which survivability assessments are to be presented is shown in Fig. 10. A structural limit load factor constraint of 6.5 g's was observed in the maneuver development.

The representative SAM threat is launched by a rocket booster from a transporter vehicle and is sustained in flight by a ramjet engine. The missile employs proportional navigation guidance with variable gain and has a maximum range of approximately 23 km. The missile lateral maneuver capability is summarized in Fig. 11. The aircraft terminal vulnerability to the proximity fuzed missile warhead is shown in Fig. 12. Here the kill probability is dependent upon the detonation distance $R_{DET}$, and aspect angle $\beta$. The angle $\beta$ is measured in the plane containing the aircraft velocity vector and the translated missile velocity vector.

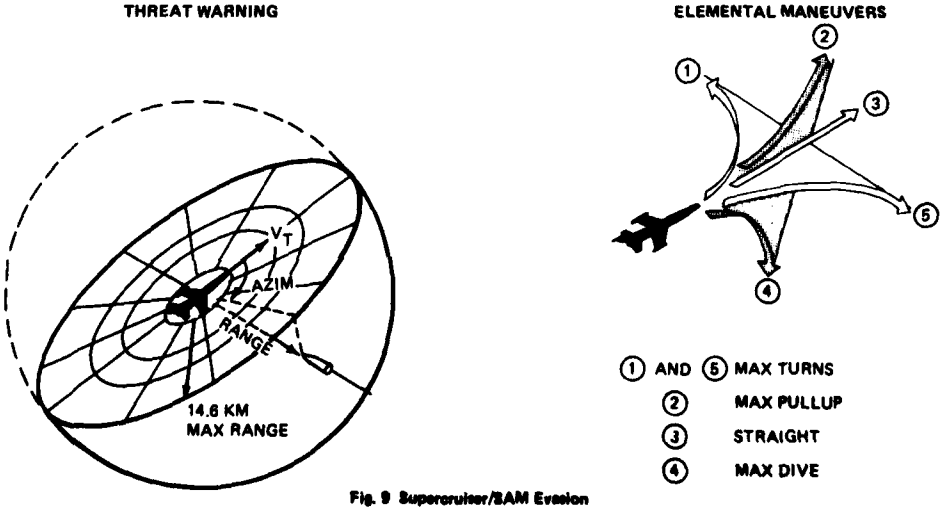


Fig. 9 Supercruiser/SAM Evasion

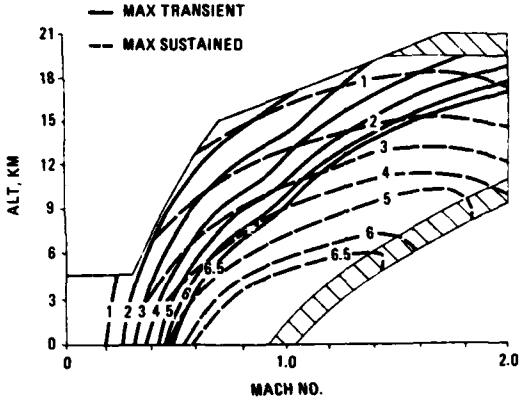


Fig. 10 Aircraft Maneuver Capability

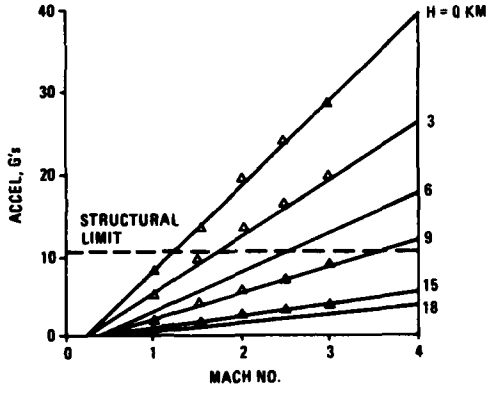


Fig. 11 Threat Maneuver Capability

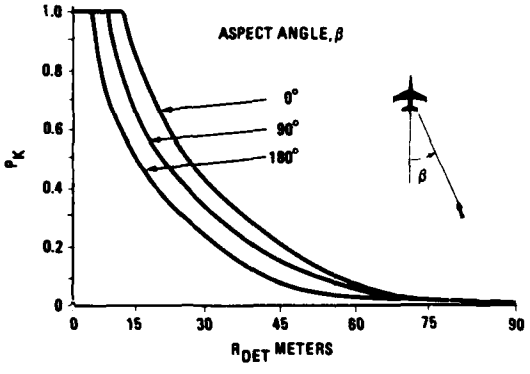


Fig. 12 Warhead Lethality

For this computational study, the missile effectiveness results will be presented for all initial conditions in a coordinate space centered at the missile launcher, as shown in Fig. 13. The two coordinates comprising this space are target ground range $R_{XY}$, and target azimuth $\omega_L$. The space is arbitrarily divided into 6000 ft. (1.83 km) range increments out to 78,000 ft. (23.8 km) and 30 degree increments in azimuth to simplify the presentation of results. The target aircraft always begins the combat with its velocity vector parallel and codirectional with $\omega_L$ = 180° azimuth. Head-on launches are specificed by $\omega_L$ between 0° and 30° and tail launches, 150° to 180°.

Five aircraft penetration speed/altitude conditions with/without optimal maneuvering have been assessed against this threat: three supersonic and two subsonic. Figure 14 shows the missile kill effectiveness for each of the penetration conditions. The left hemisphere for each condition shows missile kill effectiveness for the nonmaneuvering case, and reflects survivability without any threat warning. The right hemisphere results indicate what survivability gains may be achieved with the 14.6 km warning system and optimal evasive maneuvering. As a reminder, the $P_K$ in each Rxy, $\omega_L$ cell is an average kill effectiveness of the missile when the aircraft is in that cell at the time of launch.

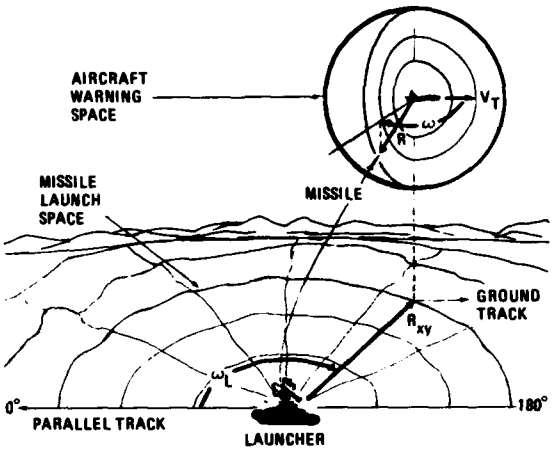


Fig. 13 Initial Condition Format

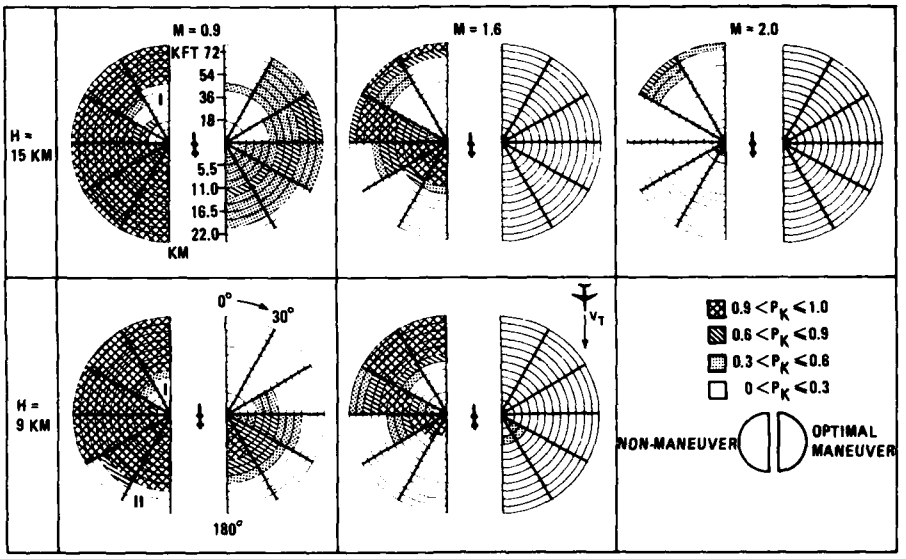


Fig. 14 Supercruiser Survivability

The results against this threat indicate that survivability for this aircraft design is extremely low for subsonic penetrations in the nonmaneuvering case. Two sections of the launch space where this is not true are indicated by numerals I and II in Fig. 14. Low kill effectiveness in I is due to missile launch elevation constraints, and in II, due to the aircraft being able to outdistance the missile range capability by maintaining its penetration speed. Optimal maneuvering in the subsonic case improves survivability dramatically, but does not exhibit low kill effectiveness for the entire missile launch space. The Mach 1.6 penetration case at both altitudes indicates the need for threat warning and optimal maneuver to achieve satisfactory survivability. The Mach 2.0 penetration indicates that the aircraft can basically outrun the missile over most of its launch space without the need for maneuvering.

Other parametric studies involving supercruiser control response and threat warning requirements for successfully implementing evasive maneuvers against SAM threats are reported in Ref. 8.

## FIGHTER MANEUVERABILITY/VISUAL RANGE GUN COMBAT

The one-on-one gun combat problem requires that one determine the domains of combat initial conditions (positions, velocities) for which each of the combatants has a unilateral capability in deciding the outcome of the combat. The comparative size of these domains furnishes a quantitative measure of superiority of one vehicle over the other. To determine these domains, the computational method was first employed with each side maximizing his kill probability, and secondly, with one combatant maximizing kill probability with the other maximizing survivability. These separate solutions determine domains where each vehicle is best operated offensively, and where each should operate with survivability as the main goal.

The threat cueing model employed in the maneuvering strategy construction for the gun combat studies is depicted in Fig. 15. The threat cueing visual sphere contains two volumes in which two distinctly different maneuvering policies are defined. The tactical volume contains maximum maneuver sequences comprised of the elemental maneuver choices shown in Fig. 16. The gun tracking volume employs lead-pursuit tracking maneuver commands. The optimal maneuver strategies are computed for each combatants tactical volume by the stochastic learning method. The kill or survival probabilities for all initial conditions are calculated by simulation, as before, using the respective optimal strategies.

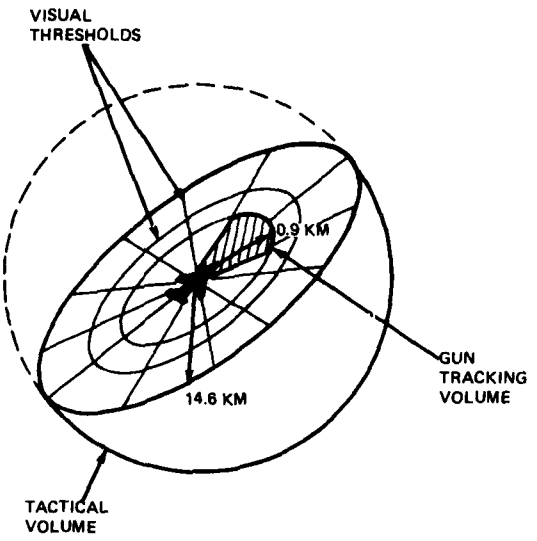


Fig. 15 Visual Model

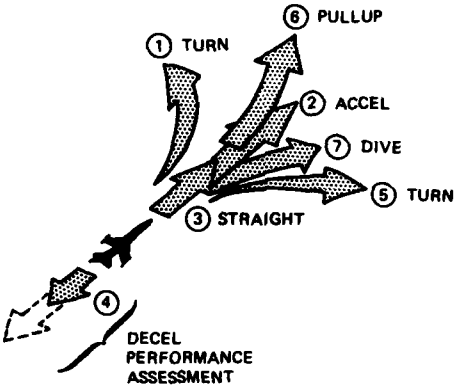


Fig. 16 Maximum Maneuvers

The case study reported here quantifies the improved domain of superiority in gun combat of aircraft with high deceleration capability (as might be obtained by in-flight thrust reversing) against conventional opponents. For the representative study, the maximum visual detection range for the tactical volume was assumed to be 48,000 ft. (14.6 km). The lead pursuit tracking volume was assumed to have a ±10° off axis capability with maximum range 3000 ft. (0.9 km). In this tactical volume, each combatant can be provided with relative range, azimuth, elevation, heading, and speed cues relative to his adversary in a manner consistent with realistic visual threshold capabilities. Only three threat cues have been assumed in the computational results presented: relative range, azimuth and heading. It was assumed that the opponent's relative heading was not detectable beyond 17,000 ft. (3.7 km). For this specific presentation, a kill event was determined by a simplified criteria: a 3 second cumulative time spent within the adversaries tracking volume. Along with the simplified kill criteria, lead pursuit tracking commands were not employed in the tracking volume, but maximum maneuver choices determined by the stochastic learning method instead. More detailed kill representations including aircraft ballistic vulnerability, gun, fire control, and projectile characteristics can be incorporated within the framework of the computational method, but are beyond the intent of this paper. Both aircraft are assumed to possess identical normal load factor and longitudinal acceleration capabilities. The Blue aircraft will be given a longitudinal deceleration capability of 3 g's greater than Red for the combat altitude examined. The 3 g differential represents a hypothetical design limit condition and was selected to determine how sensitive the optimal effectiveness solutions are to large between-aircraft deceleration parameter differences. In the results to be shown, both aircraft begin combat at M=0.9 at sea level and do not employ vertical plane maneuvers in the strategy development. Both aircraft have a maximum level speed capability of M=1.2 at the selected altitude.

The plot at the upper left of Fig. 17 shows the gun kill effectiveness of Blue and Red (see legend at lower left) for all Red range and azimuth combat initial conditions relative to the Blue aircraft. In this baseline case, Blue has identical longitudinal deceleration capability as Red (1.5 g's) and both combatants maximize kill probability. All results in Fig. 17 only apply for the case when Red has initial headings within ±45° to that of Blue, as depicted by the inset arc diagram. All other initial relative heading cases did not produce solutions of measureable effectiveness for either combatant.

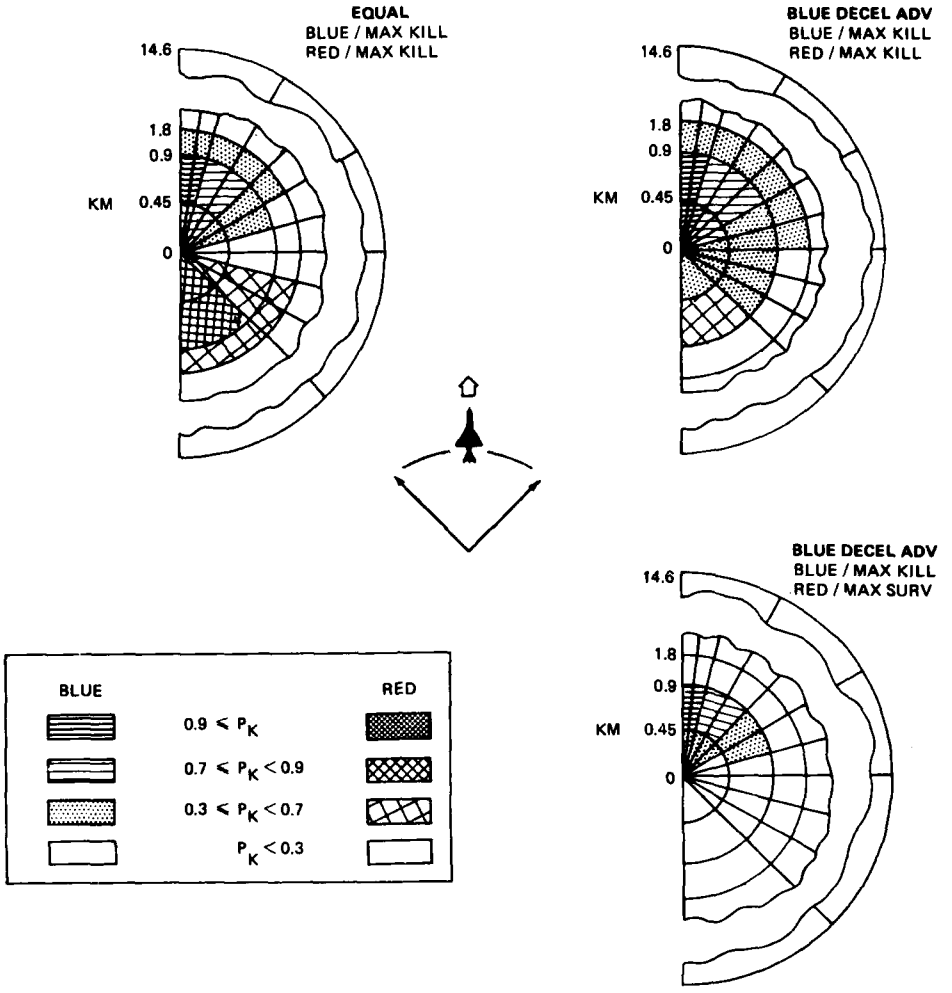


**Fig. 17 Gun Combat Effectiveness**

The result at upper right indicates the extent of the gain in effectiveness to the rear and side by the improved performance Blue when engaging an "aggressive" Red combatant. Kill effectiveness is also improved in the forward sectors at short range (0.45 km). In this latter case, the deceleration advantage is employed by Blue to maintain Red in the outer portion of his tracking volume. As in the plot at the upper left, both combatants maximize kill probability. The maneuver tactic by Blue for the side and rear initial conditions is to force Red to "overshoot." In this case, the computer generated Blue tactic is a "scissors" maneuver employing rapid turn reversals with interspersed deceleration segments. The corresponding aggressive tactic employed by Red is also a scissors maneuver.

The result at lower right indicates the effectiveness of the improved Blue aircraft when Red maximizes his survival probability. The fact that Blue loses so much capability in the rear and side sectors is due to Red "breaking off" or turning away to force a draw outcome. The disparity in computer aggressive/survival solutions can be paralleled to the "learning effect" noticed in mock-combat flight tests. Both combatants generally employ aggressive tactics at the outset of the trials until the superior maneuver capabilities of one opponent begin to dominate for certain starting conditions. The inferior aircraft then switches to defensive maneuvering tactics to reduce the effectiveness of the superior aircraft. This learning effect is accelerated when the same pilots are given rotating assignments operating each of the aircraft.

One can see from the collective solutions of Fig. 17 that the set of initial conditions for unilateral gun combat superiority for each aircraft are contained within a relative range of 6000 ft. (1.83 km) and within relative headings within ±45°. These results also suggest that the improved Blue aircraft can deny Red any offensive capability in gun combat except for rear attacks within the 0.45 and 0.9 km range sector and within ±45° angles-off the tail. Although the corresponding results are not shown here, Blue should operate defensively only within these rear sectors.

## CONCLUDING REMARKS

This paper has sketched the development and application of a digital simulation technique incorporating optimization and game theory concepts for assessment of combat aircraft maneuver effectiveness. The numerical experience to date suggests that a respectable amount of model detail regarding the integrated use of maneuver, threat warning, countermeasure and weapon capability can be considered in design studies, and that system effectiveness assessments can be accomplished within reasonable computer time budgets.

The solutions generated by this approach can also be of value when used in conjunction with manned simulation and mock combat flight experiments, by providing preliminary evaluations of the more sensitive aircraft/weapons parameters and by locating the envelopes of combat initial conditions of maximum effectiveness or greatest sensitivity. The discrete optimal maneuver solutions may be of value in training device applications (computer adversary using optimal maneuver) and in the development of effective maneuver/countermeasure tactics at the operational level.

In the future, additional effort must be dedicated to flight trial verification of the mathematical model approximations and the authenticity of the computed optimal solutions. Continued research is warranted in the application of the theory of modern optimal control, differential games, and stochastic processes, to provide improved or alternative solution concepts and rapidly convergent numerical procedures in both the one-on-one and m-on-n combat models.

## REFERENCES


1. Issacs, R., Differential Games, John Wiley, New York, 1965.

2. Breakwell, J. V. and Merz, A. W., "Toward a Complete Solution of the Homicidal Chauffeur Game", Proceedings of the First International Conference on Theory and Applications of Differential Games, Amherst, Mass., October 1969.

3. Baron, S., Kleinman, D., Serben, S., "A Study of the Markov Game Approach to Tactical Maneuvering Problems", NASA Report CR-1979, February 1972.

4. Falco, M., Cohen, V., "Strategy Synthesis in Aerial Dogfight Game Models", AIAA 11th Aerospace Sciences Meeting, Washington D.C., AIAA Paper 73-233, January 1973.

5. Falco, M., Carpenter, G., Kaercher, A., "The Analysis of Tactics and System Capability in Aerial Dogfight Game Models", Grumman Research Department Report RE-474, May 1974.

6. Carpenter, G., and Falco, M., "Analysis of Aircraft Evasion Strategies in Air to Air Missile Effectiveness Models", Grumman Research Department Report RE-506, August 1975.

7. Carpenter G., and Falco, M., "Supercruise Vulnerability to Surface to Air Missile Threats", Proceedings of Conference on Operational Utility of Supersonic Cruise, Wright-Patterson AFB, Ohio, April 1977, and Grumman Research Department Report RE-546J, October 1977.

8. Falco, M., and Carpenter, G., "Survivability Analysis of Air and Land Vehicles to Missile Threats", 4th Symposium on Vulnerability and Survivability, American Defense Preparedness Association, Tyndall AFB, Florida, March 1979, (and Grumman Research Department Memorandum)

9. Falco, M., Hinz, H., and Sobieszajski, F., "Combat Performance for Light Helicopter Concepts", Grumman Research Department Report RE-616, December 1980.

10. Falco, M., Carpenter, G., "Development and Analysis of Tank Evasion Strategies in Missile Effectiveness Models", Grumman Research Department Memorandum, August 1979.

11. Falco, M., Carpenter, G., "Tank Survivability Analysis, Anti-Tank Missile Threat, Maneuver/Smoke Countermeasures", Grumman Research Department Memorandum, April 1980.


## ACKNOWLEDGMENTS

The authors would like to acknowledge the support received during the course of these studies by the U.S. Army Aviation Research and Development Command (Directorate of Advanced Systems); the U.S. Air Force Office of Scientific Research; and the U.S. Army Tank Automotive Command.

# EVALUATION OF DIRECT FORCE MODE FIGHTERS BY COMBAT SIMULATION

C. H. Guthrie
Lead Engineer - Operations Analysis
McDonnell Douglas Corporation, P.O. Box 516, St. Louis, MO 63166, USA.

## SUMMARY

The development of advanced fighter concepts at McDonnell Aircraft Company has been significantly influenced by air combat simulation. Both man-in-the-loop and digital combat simulation are excellent tools for developing and screening advanced fighter concepts. One important application, discussed in this paper, is the evaluation of fighters with high authority aerodynamic and propulsive controls. Manned and digital air combat simulations showed that high authority controls substantially increase combat effectiveness when used both to enhance large scale maneuverability and for automatic pointing of the fuselage.

Digital simulation has shown that fighters with high authority direct force modes require lower sustained load factors than conventional designs for a constant level of effectiveness in close-in combat. Therefore, fighters with direct force modes can be lighter and less expensive than conventional aircraft.

In a recent manned simulation of close-in combat, single fighters with several levels of aerodynamic and propulsion control authority were flown against two threat fighters of equal instantaneous and sustained turn rate capability and with identical avionics and armament. For the fighter configured with the highest authority controls, many measures of engagement control and effectiveness were double those of the conventional (baseline) fighter.

## INTRODUCTION

Digital and manned simulation has been used for several years, Figure 1, as an effective tool to investigate the combat benefits of fighter aircraft with high authority aerodynamic and propulsive controls ("control configured fighters"). These simulations were an integral part of studies which showed that attention to aerodynamic and propulsion controls and direct force modes early in the design of new fighters can significantly increase effectiveness and reduce cost. Also the simulations played an important role in developing control configured fighters by screening a large number of concepts and identifying plateaus of direct force magnitudes.

Control configured fighters are capable of producing lift, drag, side force, yaw rate, roll rate, and pitch rate independent of angle-of-attack, bank angle, or yaw angle, Figure 2. The new degrees of freedom (direct lift and side force) and the enhancement of drag, pitch, roll, and yaw capability provide the pilot with many advanced maneuvering modes including direct lift, direct side force, longitudinal maneuver enhancement, lateral-directional maneuver enhancement, fuselage aiming, wings-level steering, and modulated drag.

Direct lift provides body reference vertical translation without pitch rotation. In the manned simulation direct lift, as an isolated mode, had little combat utility. However, direct lift capability is the enabling force for most of the effective advanced maneuvering modes. Our analysis indicates a design goal of 5g at Mach 0.7 and 10,000 feet altitude.

Direct side force provides body reference horizontal translation without yaw rotation. Direct side force is like direct lift in that its most effective use in air-to-air combat use is as an enabling force for the coupled flight modes. Digital simulations have shown that direct translation is useful for coupled air-to-surface deliveries. A design goal of 1g of direct side force at Mach 0.7 and sea level has been established as a desired authority level based on "moving base" simulation results.

Longitudinal maneuver enhancement is the blending of direct lift with pitch in order to provide rapid, well damped coordination of the pitch rate and the velocity vector steering rate. This mode improves both maneuvering and tracking with a resultant increase both in air-to-air and air-to-surface combat effectiveness. The design goal for this mode is a buildup rate of 8g per second.

Lateral-directional maneuver enhancement is the blending of direct forces, yaw, and roll rate to provide rapid but well damped roll control (velocity reference). The key to this mode is the proper location of high authority controls and their coordinated operation. Direct side force is automatically commanded to minimize lateral acceleration at the pilot station due to roll or sideslip. This maneuvering mode has shown large benefits in close-in combat against multiple-opponents. The design goal determined for roll control is to achieve a 90 degree change in bank angle in one second at the speed, angle of attack, and load factor used for maximum instantaneous turns. The combat effectiveness of the latest generation fighters is due in part to their ability to generate high turn

rates at high trim angles of attack. However, these fighters are not capable of producing high roll accelerations at those high angles of attack. Roll acceleration at high angles of attack can be significantly improved by the coupling of aerodynamic or propulsion controls to provide directional control.

Fuselage aiming is body axis yaw and pitch rotation without changing normal load factor. In air-to-air combat, fuselage aiming operates in a coupled mode with the flight control system automatically nulling fire control aiming error signals. The flight control system commands direct lift and direct side force to maintain pilot commanded load factor and roll rate independent of body angle-of-attack and yaw angle. This mode has proven to be very effective in multiple-opponent close-in combat when elevation independence is great enough to expand the gun envelope significantly, Figure 3. The ability to lag the target and achieve firing solutions from all aspects provides pilots additional maneuvering flexibility. Pointing authority of $\pm$10 degrees elevation and $\pm$5 degrees azimuth at Mach 0.9 and 10,000 feet was established as a design goal.

Wings-level steering, sometimes called azimuth steering, uses direct side force and azimuth fuselage control to rotate the velocity vector and the body axis without sideslip or uncommanded roll. Simulations have shown significant combat benefits in the visual delivery of air-to-surface weapons as a result of the ability to make turns without banking or sideslip. The design goal is 2 degrees per second at Mach 0.7 and sea level.

Modulated drag uses direct lift and elevation fuselage control to provide large increases in drag without changing the pilot commanded load factor. The capability to rapidly change the energy state of high thrust-to-weight fighters has shown benefits in both air-to-air and air-to-surface combat. A design goal of 3g of deceleration at Mach 0.9 and 10,000 feet was established for this mode. By automatically controlling body angle-of-attack and direct lift, the lift to drag ratio can also be maximized at all pilot commanded load factors.

The key to the effective use of these new degrees of freedom is in automatically blending the direct forces to provide large scale maneuvering improvements. Direct lift and side force are the enabling capabilities needed to mechanize the advanced flight modes, Figure 4. Our analysis indicates that only the full ensemble of advanced flight modes provides significant improvements in effectiveness.

The independence of angle of attack and flight path load factor is shown in Figure 5. At a load factor of 3g for example, the fuselage angle of attack can be controlled to any value between -7 and +14 degrees. The maximum lift-to-drag value would occur at 3 degrees. At a constant angle of attack the flight path load factor can also be changed. For example, at 8 degrees angle of attack the load factor can be any value between -3 and +10g (these are structural limits).

## MANNED SIMULATION

The MCAIR Manned Air Battle Simulation Facility can simulate air-to-air combat, air-toground combat, or full missions. Surface-to-air defenses, visual weapon deliveries, and sensor aided deliveries can be simulated during air-to-ground combat. The facility's air-to-air simulation capability has recently been expanded to include twelve pilots "in the loop" plus command and control operators, Figure 6. Four pilots fly from manned air combat simulators (MACS) while the other eight pilots use manned interactive crew stations (MICS).

The manned simulations were analyzed in three parts. First, while tests were in progress, the engagements were monitored by the test conductor, pilots, and engineers, using hard copy end-of-engagement summaries, strip chart recorders, and video recordings. The end-of-engagement summaries included effectiveness measures for each fighter, and the strip recorders tracked pilot commands and flight control responses. Video tapes were used to debrief each pilot immediately after each set of runs in a test configuration.

The second step took place in the first two months after the test had been completed. Effectiveness data was analyzed from master data tapes which contained 252 parameters recorded twenty times per second. The data was analyzed with the help of several statistical programs to produce aircraft state, engagement control, and effectiveness time histories and distributions. In the third step, an intensive analysis, examining the cause and effect aspects of the manned simulations, was conducted by a multidisciplinary engineering team (operations analysis, flight controls, avionics, aerodynamics) over the twelve months following the test using the data tapes, video tapes, and strip charts.

The validity of performing the detailed analysis is contingent on the fidelity on the simulation. Manned simulation is used in the development of all aircraft flight control systems at MCAIR. After the basic work has been completed, the flight control system design is transferred to the simulator and evaluated by test pilots flying various mission phases - take-offs, air combat, weapon deliveries, landings. As the flight control system is refined, actual hardware (cockpit controls, aircraft computers, actuators, control surfaces) are substituted for digital models. Test pilots reported after the first flights of the F-15 and F-18 that the airplane flew just like the simulator.

During the manned simulations of the direct force mode fighters as many as 60,000 data entries were used to model the aircraft. Aerodynamic data resulted from high speed wind tunnel test up to Mach 3.0 and low speed test to define control derivatives up to 80°

angle of attack. The flight control interactions for good handling qualities were developed and the advanced air-to-air and air-to-ground tracking mechanizations were fine-tuned through several manned simulation phases.

In the initial phases, six air-to-air tracking mechanizations were investigated. These initial experiments ranged from engineering pilots tracking digital targets to full, one-versus-one air combat tests of the six refined mechanizations by Air Force tactical pilots. The air-to-ground tracking mechanizations were tested using both fixed and moving base simulators. Tracking errors were fifty percent lower during air-to-air gunnery and forty percent lower for air-to-ground visual deliveries for fighters with the advanced maneuvering modes when compared to advanced fighters without the advanced maneuvering modes but with the same advanced gunnery (director) and bombing sights.

Manned simulation was later used to investigate the enhanced maneuvering capabilities in close-in combat. A control configured fighter and a conventional (baseline) fighter with equal load factor capability were flown against a common high performance opponent. The advanced maneuvering modes provided the control configured fighter faster gunnery solutions, as shown in Figure 7. The coupled fuselage aiming mode makes the gun an effective all aspect weapon, thereby providing earlier firing solutions and increasing the number of gun hits. Out of more than 1,000 hits achieved during three minutes of simulated combat, 83% of the total hits and all of the hits during the first minute of the engagement were taken head-on and from the beam, as illustrated in Figure 8. The control configured fighter was also significantly better at avoiding losses than the conventional (baseline) fighter.

In the most recent manned simulation tests, one control configured fighter engaged in close-in combat with two threat fighters. All aircraft, friendly and threat, had equal turn and climb rate performance, two all-aspect short range missiles, identical gun and fire control systems. The control authority level was varied from that of current fighters up to the full authority goals defined previously in this paper. A comparison of effectiveness measures between the high authority configuration and the baseline (or current control capability configuration) is shown in Figure 9. Most effectiveness measures were more than doubled. Engagement control time was defined as the time when 1) the bearing angle from the friendly fighter to the engaged threat less than 20 degrees, 2) a bearing angle advantage against the engaged threat, and 3) the free threat not radar tracking the friendly fighter.

A five-degree-of-freedom missile model was used to provide missile to target geometries used in calculating short range missile probabilities of kill "on-line". The high authority control configured fighter doubled the exchange ratio of the baseline fighter and had greater than a one-to-one exchange ratio against two "equal performance" threat fighters. Analysis of the simulation data showed, Figure 10, that the advantage was fairly independent of the missile lethality. Single shot probabilities of kill were varied equally for threat and friendly fighter.

Further analysis of the data showed, Figure 11, that the high authority control configured fighter also doubled the engagement control time. The high authority control configured fighter controlled the engagement, 16 of the first 60 seconds, compared to 7 seconds for the baseline configuration.

The use of the advanced maneuvering modes was analyzed to identify their contribution to this large difference in engagement control times. Only the difference in lateral-directional control was sufficiently large to explain the control configured fighter's engagement control. A comparison of the lateral-directional control of the baseline fighter and the control configured fighter is shown in Figure 12 in terms of the ratio of time at the commanded roll rate to the total time the pilot commands the roll rate. For example, when the pilot's command was greater than 60% of the maximum available roll rate, the baseline fighter was capable of providing the commanded roll rate only 24% of the time, compared to more than 80% for the control configured fighter. This was because the control configured fighter was capable of high roll acceleration at "corner turn" conditions (high angle of attack and high load factor).

Analysis of the one-versus-two close-in combat simulation showed that the engagement control time and the exchange ratio were very strongly influenced by the friendly fighter's roll acceleration at corner turn load factors, Figure 13. Improved roll acceleration provides an increase in the exchange ratio (one versus two) for both baseline (conventional) and control configured fighters. The control configured fighters can generate improved roll acceleration with the same surfaces used to provide the other advanced maneuvering modes. The ability to make rapid changes in the plane of its turns while maintaining high load factors allowed the control configured fighter to quickly transition its attacks from one threat to the other. Close-in combat at unfavorable force ratios generates strong requirements for roll acceleration. The enhanced lateral-directional control provides the capability for rapid roll acceleration at high angles of attack. As shown in Figure 14, enhanced aerodynamic controls have the potential to provide coordinated roll acceleration at 40° angle-of-attack that is equal to the roll acceleration of conventional fighters at 10°. The accelerations shown in Figure 14 are the fighters' average values in rolling from stop to stop through 90°. Propulsion control (thrust vectoring) is an option for configurations that cannot generate sufficient aerodynamic forces.

DIGITAL SIMULATION

Digital-air-combat simulations were used to make parametric investigations of performance based areas of interest. The cost effectiveness of sustained-loadfactor performance (wing loading, thrust to weight, structural capability) and the magnitude of direct force authority was evaluated for several advanced-design-fighter configurations. The digital models were used to simulation engagements ranging from one-versus-one guns-only combat to four-versus-four combat with guns and advanced missiles.

Aircraft flight control and weapon systems are typically described by 2000 data entries. Linear approximations are used for the control derivatives. Prior to running the model, a detailed performance analysis is used to determine the preferred flight regions for close-in combat against threat aircraft. One degree-of-freedom simulations and computed weapon envelopes are used to model eight missiles and the guns. The model uses probabilities of survival and relative geometries of friendly and threat aircraft for target selection. Only minor modifications to the model's standard maneuvering logic were necessary to evaluate control configured fighters and advanced maneuvering modes.

Digital air combat simulations are used before all manned simulation tests to check the validity of test plan and structure; particularly as related to starting conditions and test configurations. The results of the digital simulation are compared to the results of the manned simulation in Figure 15 for a one-versus-one engagement with guns and in Figure 16 for one-versus-two engagements with guns and all-aspect short range missiles. In all cases, digital simulation predictions were slightly optimistic. The data plotted in Figure 17 indicates that fuselage aiming in the four-degree to ten-degree region was used by the pilots more than predicted by the digital simulation. This indicates that the pilots in the manned simulation lagged the target more than the digital pilot. The digital simulation models prove to be very useful in predicting the effectiveness of the fighters and the advanced maneuvering modes.

In developing control configured fighter concepts, digital simulation is used to evaluate parametrically the effectiveness of the advanced maneuvering modes and of fighter performance in close-in combat. In MCAIR's close-in combat evaluations conventional fighter performance is best characterized by B*, where

$$B^* = (STR)^{1.5} (ATR)(SEP)$$

and ATR is attainable turn rate, STR is sustained turn rate, and SEP is specific excess power. B* was developed with the help of British Aerospace and is a variation of their air combat correlation parameter, B.

Figure 18 illustrates the change in the effectiveness of conventional and control configured fighters as their performance, B*, was changed parametrically. The B* performance of the threat is 2.52. Both threat and friendly fighters are armed with four all-aspect short range missiles and a gun. The expected kills, expected losses, and exchange ratios are the average of eighteen engagements: six with neutral starting conditions, six favorable for the friendly fighter, and six favorable for the threat fighter. The advanced maneuvering modes--coupled fuselage aiming mode (CFAM), drag modulation (DM), longitudinal maneuver enhancement control (LMEC), and lateral-directional maneuver enhancement control (LDMEC)--were added one at a time until the full control configured capability was achieved. It is important to note that the improvement provided by the addition of any single mode is small but that the improvement provided by the combination of modes provides an advantage in exchange ratio of about one across all performance levels.

The interaction between close-in-combat effectiveness and the authority of the advanced maneuvering modes was also evaluated with parametric digital simulation engagements. The authority of each advanced maneuvering mode is related to direct lift authority levels in a unique way for each and every control configured concept. For the fighter used in this analysis, 5g of direct lift provides +11 degrees of fuselage independent aiming and 3g of modulated drag capability at Mach 0.9 and 10,000 feet. The exchange ratio (kills divided by losses) for one-versus-one close-in combat is shown in Figure 19 as a function of this direct lift capability. The effectiveness improves little until the fighter has more than 1g of direct lift, increases rapidly between 2.5 and 3.5g, and begins to flatten out above 4g.

The effect of the maneuvering design requirement (sustained load factor at Mach 0.9 and 30,000 feet) on exchange ratio is shown in Figure 20. At the average flight conditions for the four-versus-four close-in combat (Mach 0.6 and 10,000 feet), load factor capability is similiar to that at the design requirement conditions. The improvement in effectiveness that can be provided by increasing load factor capability above 4.5g (postulated threat performance), for conventional fighters is small compared to the cost. For example increasing the load factor 0.5g can require an 8% weight increase and a 13% thrust increase. However, the advanced maneuvering modes provide two interesting options. The first option is to design a fighter with both high load factor capability (4.5g) and the advanced maneuvering modes, to improve the close-in combat effectiveness. The second option is to use the advanced maneuvering modes to improved close-in combat at a relaxed load factor (4.0g) design requirement. At the reduced load factor, a smaller, thinner, or more highly swept wing can be used to provide better supersonic performance.

A comparison of the performance of the two control configured options and the conventional fighter is shown in Figure 21. The second option seems to truly be an effective fighter, providing both better supersonic performance (acceleration and supersonic load factor) and better close-in combat effectiveness (Figure 20) than the baseline.

## CONCLUSION

The digital and manned simulation results indicate that at equal weights high authority control configured fighters have a close-in combat effectiveness advantage that cannot be matched by conventional performance improvements. The simulations also indicate that only the full ensemble of advanced maneuvering modes provide a significant improvement in effectiveness. The manned simulations have also proved that to be usable and effective in air combat, the advanced maneuvering modes must be fully integrated into the fighter design to provide low workload for the pilot and enhanced handling qualities throughout the combat envelope, as well as to provide improved tracking.

The better close-in combat effectiveness of control configured fighters has been throughly documented by manned and digital simulation results. Future efforts should concentrate on evaluating control configured fighters using full air battle simulations and on flight testing a configuration with high authority advanced maneuvering modes.

## NOMENCLATURE

| | |
|---|---|
| ATR | Attainable turn rate |
| B | BAE close-in combat performance correlation parameter |
| B* | Close-in combat performance correlation parameter |
| BA | Bearing angle, velocity vector to line of sight |
| CFAM | Coupled fuselage aiming mode |
| DM | Drag Modulation |
| G, g | Gravity acceleration constant |
| LDMEC | Lateral Directional Maneuver Enhancement Control |
| LMEC | Longitudinal Maneuver Enhancement Control |
| M | Surviving force advantage |
| MCAIR | McDonnell Aircraft Company |
| SEP | Specific excess power |
| SRM | Short range missile |
| STR | Sustained turn rate |
| ° | Degree |
| % | Percent |

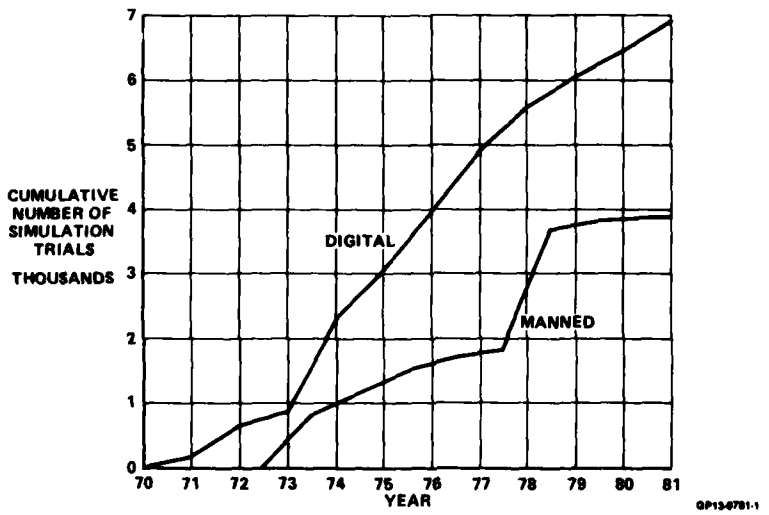


**Figure 1. MCAIR Direct Force Mode Simulation Experience**

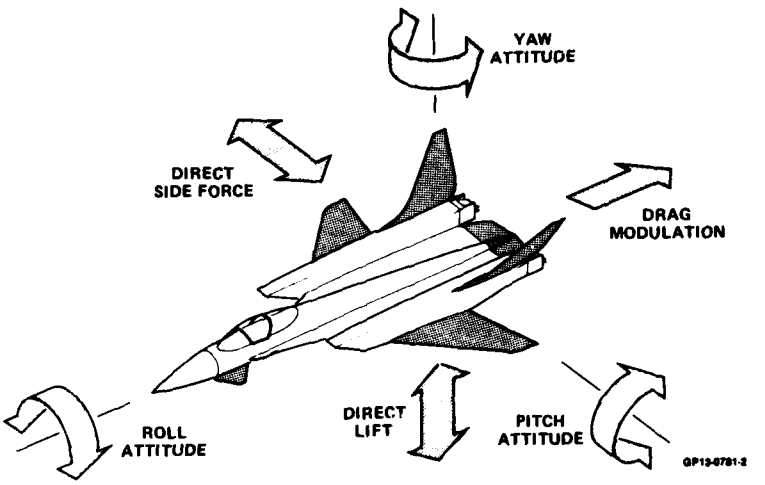


**Figure 2. Six Independent Degrees of Freedom**

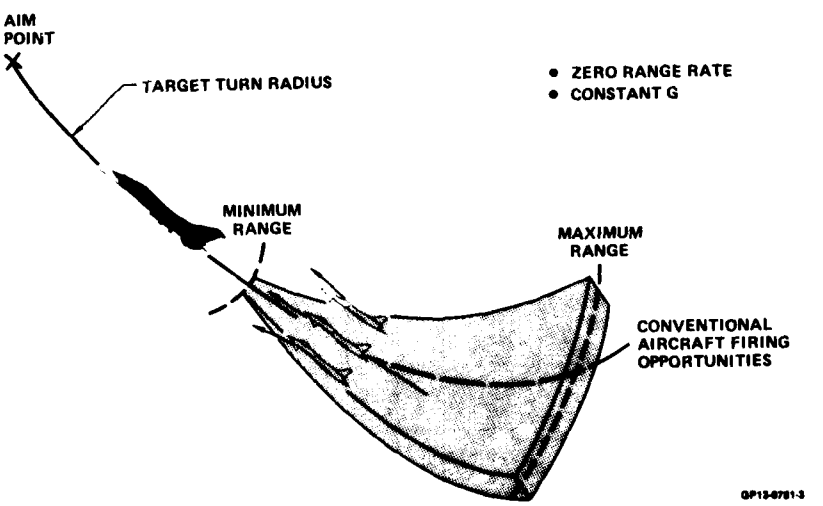


**Figure 3. Firing Opportunities**

| COMBAT FLIGHT MODE | ENABLING CAPABILITY | |
|---|---|---|
| | DIRECT LIFT | DIRECT SIDEFORCE |
| LONGITUDINAL MANEUVER ENHANCEMENT CONTROL | X | |
| LATERAL DIRECTIONAL MANEUVER ENHANCEMENT CONTROL | X | X |
| FUSELAGE AIMING | X | X |
| WINGS-LEVEL-STEERING | | X |
| MODULATED DRAG | X | |

GP13-0781-4

**Figure 4. Advanced Maneuvering Modes**

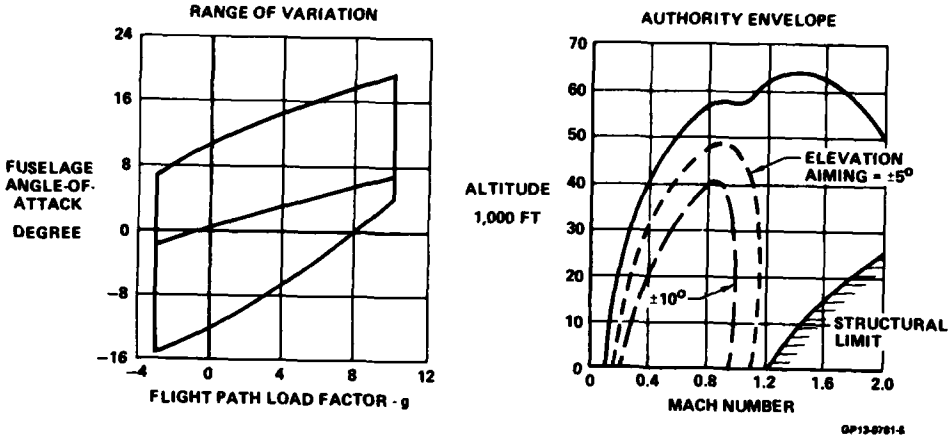


Figure 5. Lift and Angle-of-Attack Independence

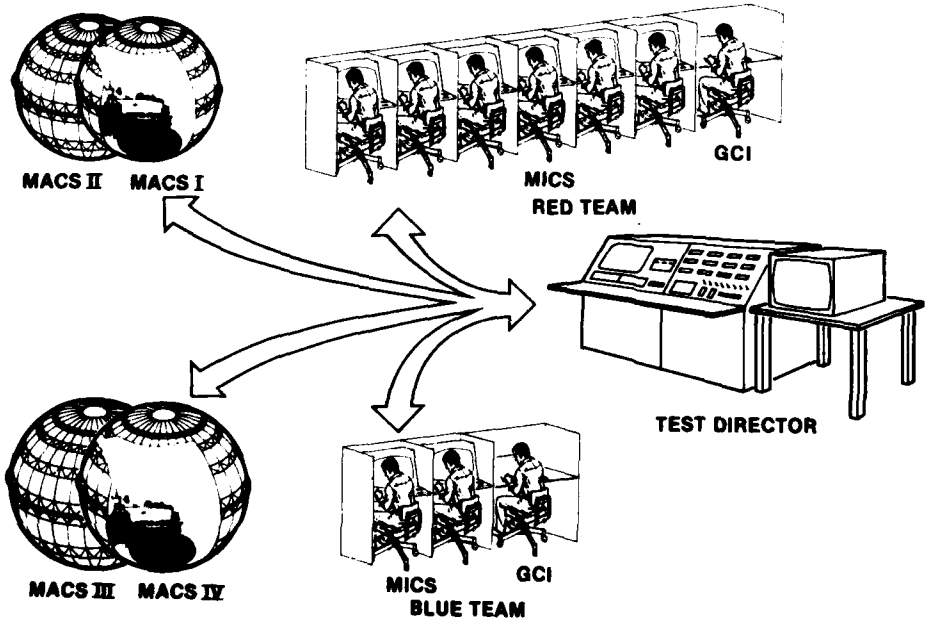


Figure 6. Simulation Program Concept

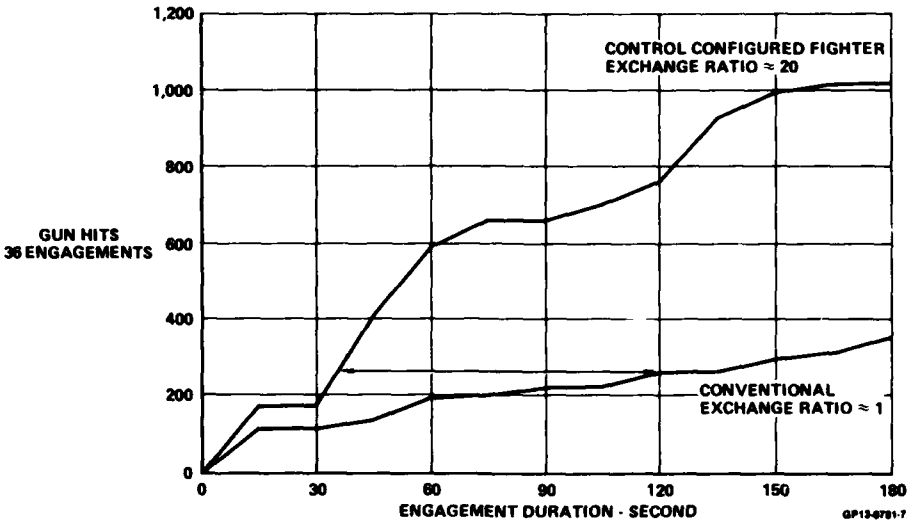


**Figure 7. Faster Weapon Solutions**
One Versus One Manned Simulation
Guns Only Close-In Combat

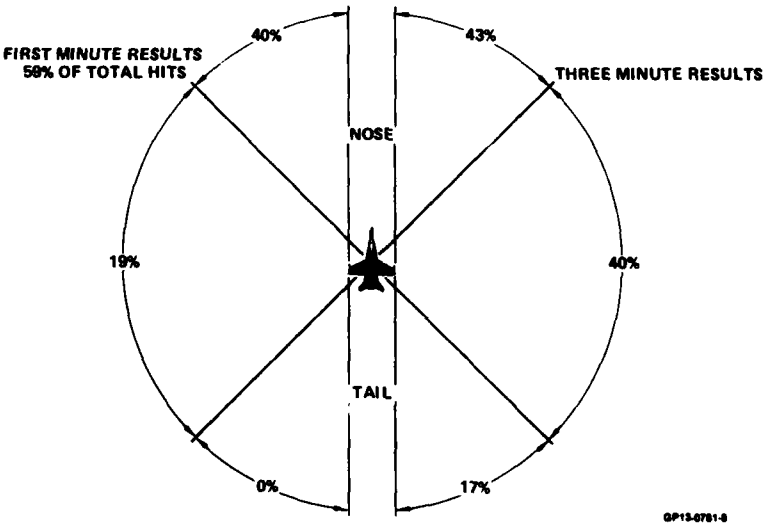


**Figure 8. Firing Opportunities by Target Aspect**
One Versus One Manned Simulation

***CONTROL CONFIGURED FIGHTER: BASELINE SCORE***

| | | |
|---|---|---|
| ENGAGEMENT CONTROL TIME | | 2.5:1 |
| TRACKING | | 2:1 |
| *TIME IN ENVELOPE* | SRM | 2:1 |
| | GUN | 4:1 |
| KILLS | SRM | 1.5:1 |
| | GUN | 10:1 |
| EXCHANGE RATIO | | 2:1 |

GP13-0781-9

**Figure 9. Improved Close-In Combat Capability**
One Versus Two Manned Simulation

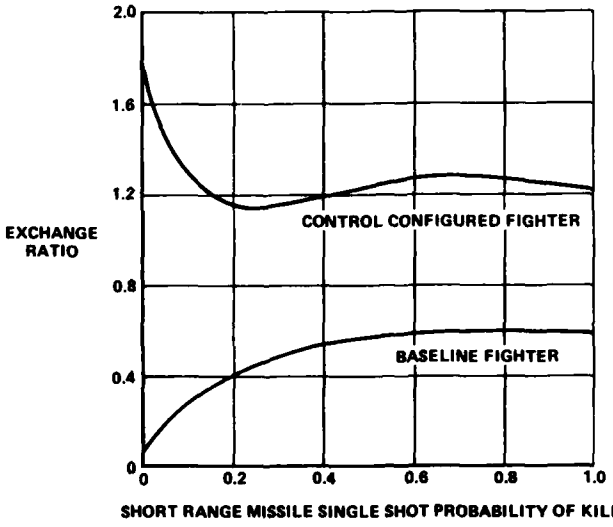


**Figure 10. Control Configured Fighter Advantage at All Missile Lethalities**
*One Versus Two Manned Simulation*

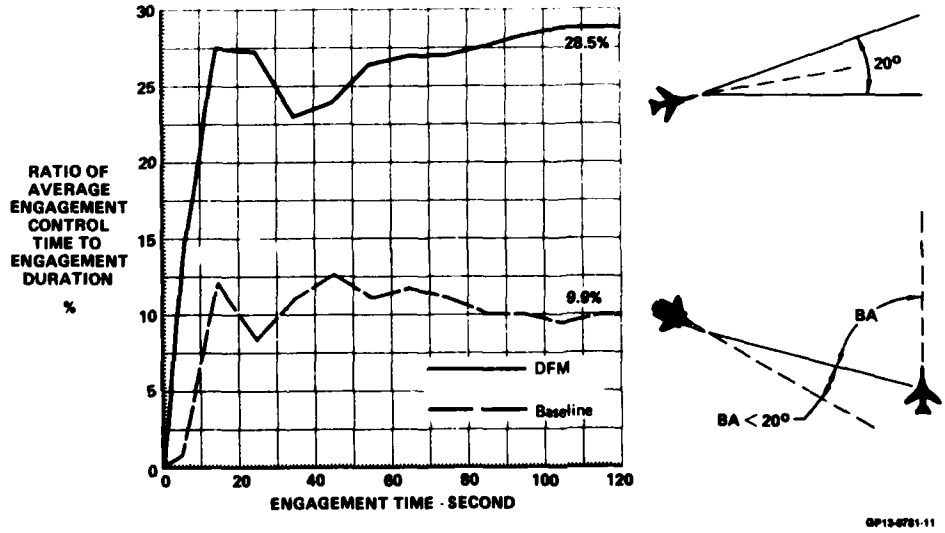


**Figure 11. Engagement Control**

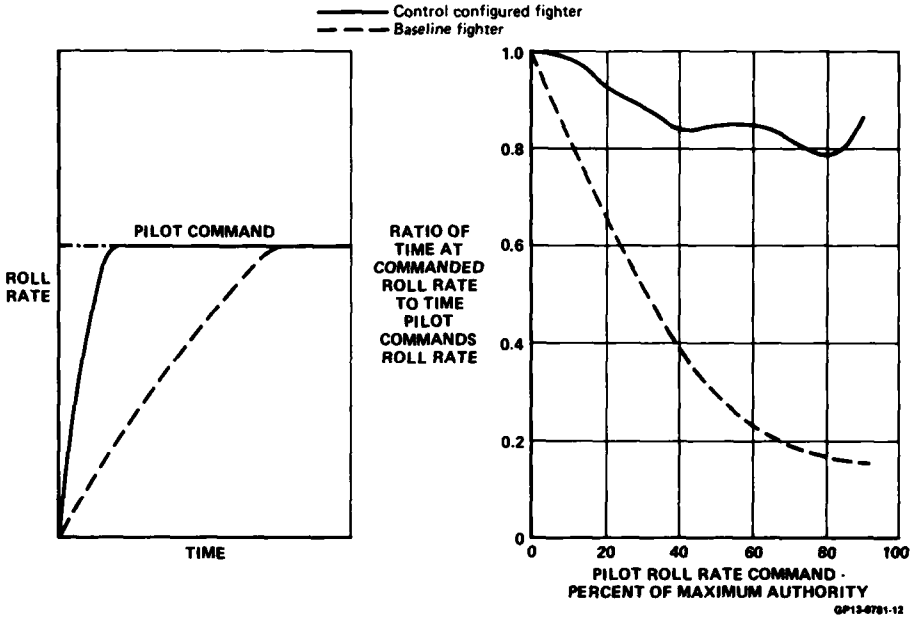


**Figure 12. Roll Response Resulting from Lateral-Directional Maneuver Enhancement Control**

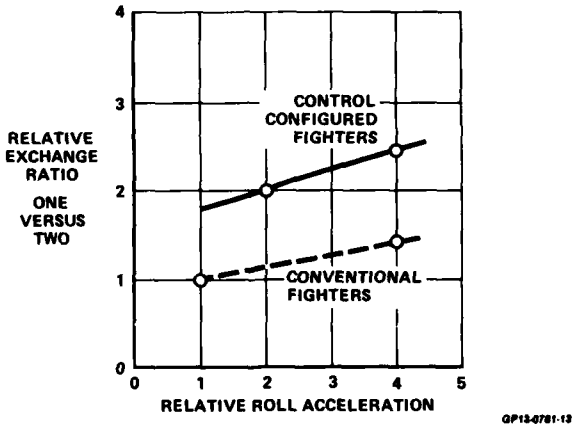


**Figure 13. Lateral Maneuver Enhancement Benefit**
One Versus Two Close-In Combat

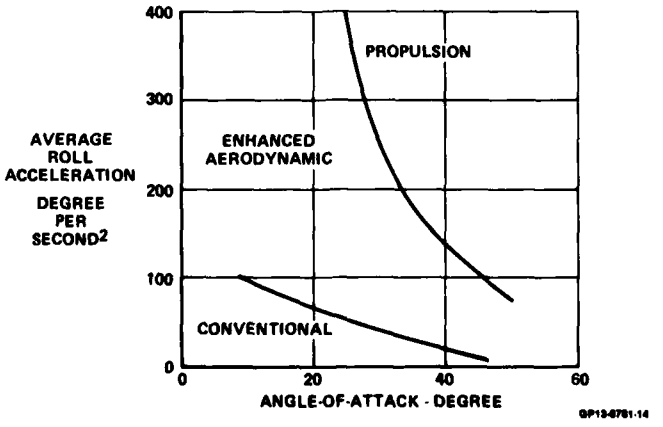


**Figure 14. Lateral Maneuver Enhancement**
Mach 0.9 @ 10,000 Ft

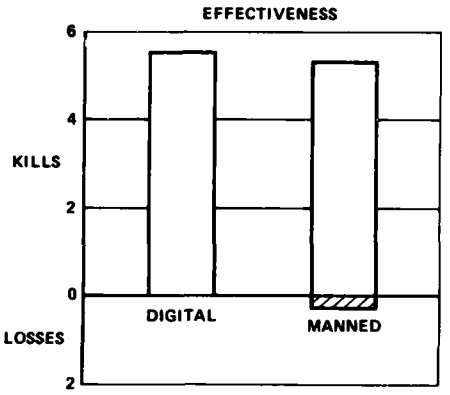


AVERAGE FLIGHT CONDITION(1)

| | MACH | ALTITUDE |
|---|---|---|
| MANNED | 0.67 | 15,000 |
| DIGITAL | 0.65 | 13,000 |

(1) Initial conditions Mach 0.9 and 20,000 ft

GP13-0781-15

**Figure 15. Simulation Correlation Control Configured Fighters**
Guns Only 36 Three Minute Engagements

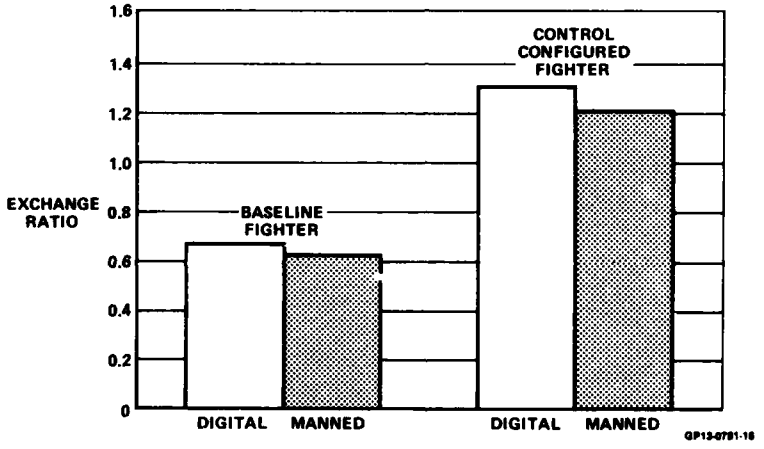


**Figure 16. Manned/Digital Correlation**
One Versus Two Neutral Engagements

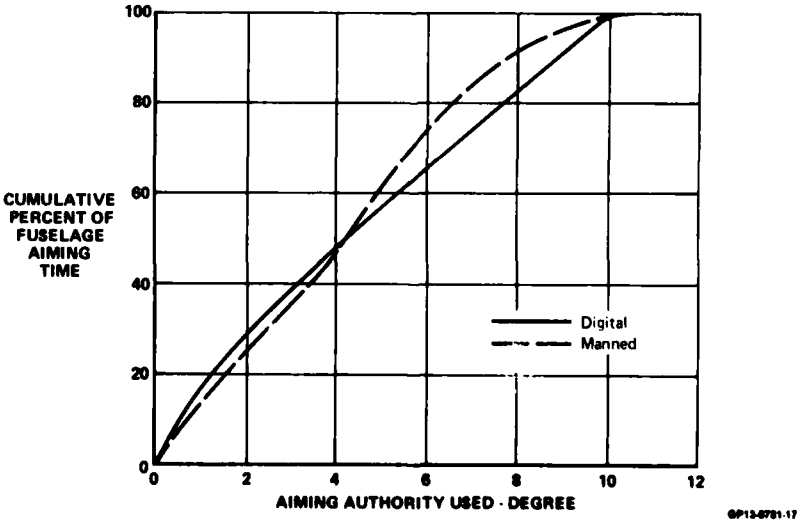


**Figure 17. Fuselage Aiming Usage**
One Versus One Guns Only

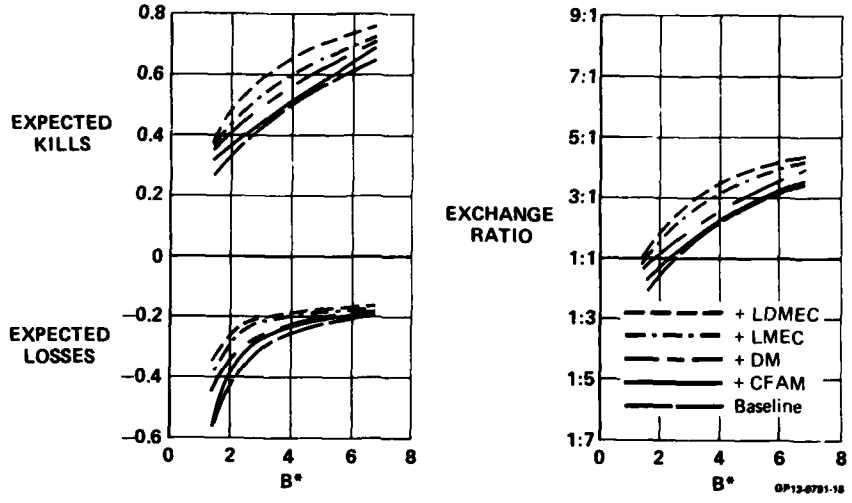


**Figure 18. Close-In Combat**
One Versus One All-Aspect SRMs + Gun

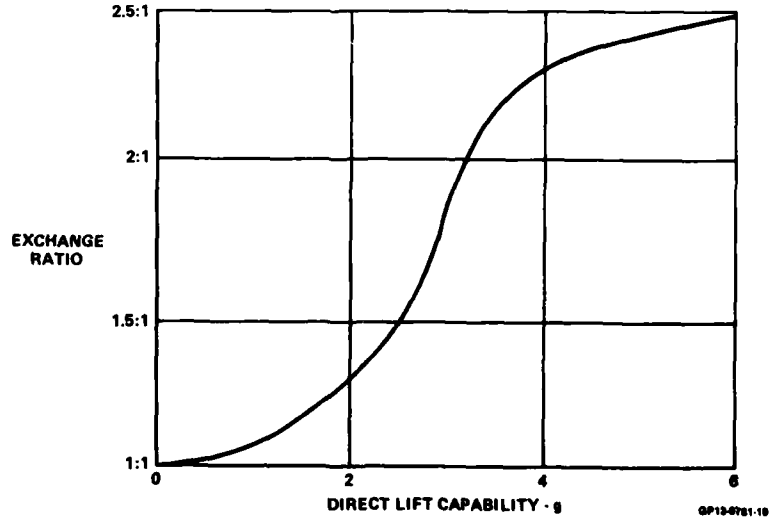


**Figure 19. Advanced Maneuvering Modes Benefits**
One Versus One All-Aspect SRMs + Gun

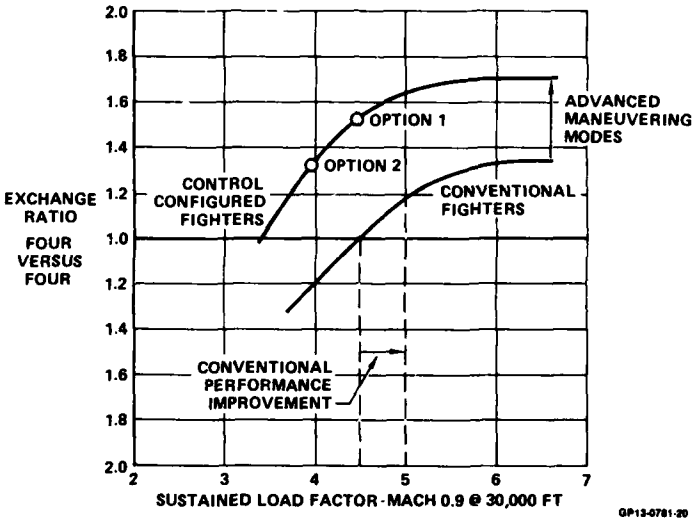


**Figure 20. Fighter Design Requirements**
Close-In Combat All Aspect SRMs + Gun

| | CONVENTIONAL FIGHTER | CONTROL CONFIGURED FIGHTER | CONTROL CONFIGURED SUPERSONIC CRUISE FIGHTER |
|---|---|---|---|
| SUSTAINED LOAD FACTOR | | | |
| MACH 0.9 AND 30,000 FT - g | 5.0 | 4.5 | 3.9 |
| MACH 1.7 AND 30,000 FT - g | 4.4 | 5.3 | 5.9 |
| ACCELERATION | | | |
| MACH 0.6 TO 1.7 AT 30,000 FT/SEC | 75 | 65 | 50 |
| CRUISE SPEED - MACH | 0.9 | 0.9 | 1.7 |

GP13-0781-22

**Figure 21. Supersonic Performance Improvement**
Equal Design Weight

# THE STUDY OF COMBAT AIRCRAFT MANOEUVRABILITY BY AIR TO AIR COMBAT SIMULATION.

By

A. G. Barnes
British Aerospace Public Limited Company
Warton Division
Preston, Lancashire
England.

## SUMMARY

The evaluation of air-to-air combat by ground based simulation is a well-established technique, and is making a considerable contribution to the design, development and operational use of combat aircraft. The merits of different aircraft/missile combinations can be assessed under controlled conditions with pilot involvement. Parameters which influence manoeuvrability, such as sustained turn rate, attained turn rate, and SEP can be easily varied, and translated into combat success. The relative importance of these parameters are discussed in the light of experimental results.

## 1. INTRODUCTION

Recent developments in technology have, without doubt, made possible major improvements in the manoeuvrability of combat aircraft. Having given the designer these possibilities, an examination of the trade-off between operational capability, cost and complexity must be made. What are the circumstances when increased manoeuvrability is likely to be of most benefit? Which is the best method to enhance the manoeuvrability? How can the system be incorporated into the aircraft's control system and integrated with the weapon system? The purpose of this paper is to show that effective means are available at the design stage to answer these questions, by modelling and simulation. In particular, this paper discusses the pilot-in-the-loop simulation of air-to-air combat, in terms of the equipments which are available, the standards which are necessary, and the best means of employment.

A point which has often been made at previous AGARD meetings on Aircraft Design, and which will be re-iterated at this Conference, is the increasing capability of manned simulators to address aircraft design and development problems. Improved display hardware and more powerful computers have made many problems which were beyond the scope of flight simulation twenty years ago amenable to this technique. In the discipline of Flight Mechanics, two examples which come to mind are studies of aircraft flying qualities and flight control system behaviour in conditions of turbulence, and the development of incidence limiting and spin prevention systems. In both these cases, as well as savings in design and development costs, the use of the flight simulator results in a less hazardous flight test programme, and allows much greater repeatability in the analysis of test results.

These benefits are multiplied for tests related to air-to-air combat, where the staging of airborne trials is far more complicated. Operating costs of trials on an instrumented air-combat range, coupled with off-site operation, make the use of such trials well outside the compass of aircraft design organisations. At the same time, the continuing development of air combat simulation techniques is extending the range of tests which can usefully be made on the ground, and winning support from quarters where doubts have been expressed in the past.

## 2. REQUIRED STANDARDS OF SIMULATION

There are many factors to consider when setting up a facility for research and development work related to air combat. Capital cost, running costs, maintainance; ease of operation, and flexibility are some of the considerations. If too much emphasis is given to one particular aspect, the others will suffer in consequence. For example, a too severe specification for the quality of the visual images may lead to expensive, unreliable solutions. Similarly, the choice of too small a computer, or a lack of peripheral devices, can restrict the operational use of the simulator.

1. 9.1m diameter inflateable dome
2. Airlock
3. Target Projector
4. Sky/ground projector
5. Fixed cockpit

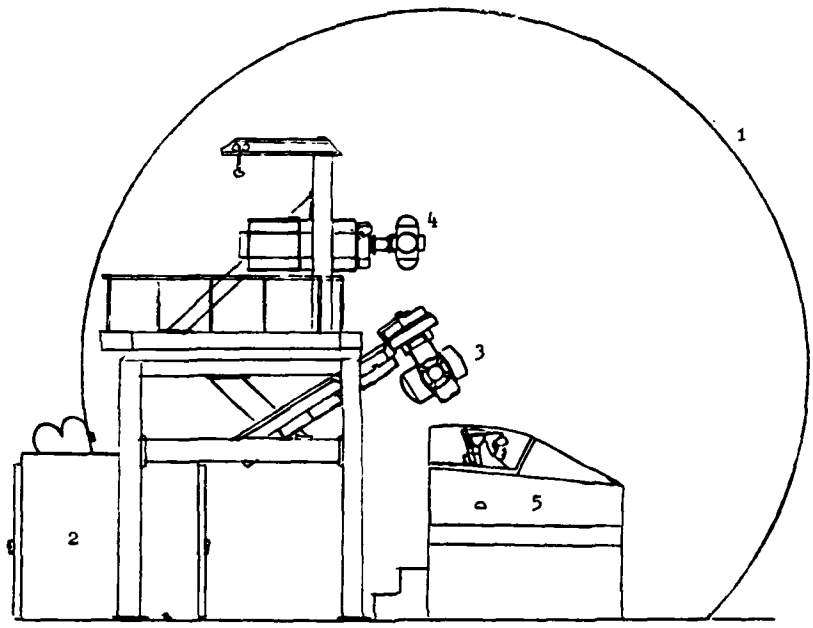


FIGURE 1 G.A. OF COMBAT SIMULATOR

At the Warton Division of British Aerospace, we have this year brought a 2 dome, man v man combat simulator into operation. Much of the hardware design is based on experience with a single dome combat simulator which we have operated for the past seven years. The image of an opponent aircraft is projected onto a 9.1m diameter dome by a servo-driven T.V. projector, mounted at the centre of the dome. (Figure 1) The image of the target aircraft is generated by a T.V. camera, which views one of two gimbal-mounted model aircraft - one model mounted by the tail, and the other by the nose. The computer decides on the appropriate model to view at any particular time. The aircraft models can be easily changed, as can the aircraft behaviour, as stored in the computer. The projected image size is varied by electronic means (raster shrink), to represent changing range between the two aircraft.

Considerable experience has been gained on the earlier combat simulator in the use of a computer controlled opponent (BACTAC). A series of logical decisions are made in the computer, depending on the opposing aircraft's position, range, rate of turn, armament, and performance. The decisions lead to a choice of manoeuvre which will give the best opportunity to shoot down the other aircraft. At first sight it would seem that even a good combat pilot will not be able to beat the computer since the computer does not make mistakes, and makes new decisions very rapidly. Nor does it suffer from visual obscuration of the opponent's aircraft. In practice, considerable care is needed to develop the tactics which match the experienced pilot, partly because of the superior logic process used by the pilot, and partly because the modelling of optimum manoeuvres in three dimensional space is complex. Once developed, however, the computer controlled opponent is an excellent method for the comparison of aircraft combat capabilities. The opponent is always available, he uses repeatable tactics, there are no learning effects, and he does not exhibit other human frailties. But the questions will always arise (sometimes posed by a beaten pilot) concerning the validity of the computer's tactics and the legality of its methods. The way to answer such questions is to conduct the same comparison of aircraft configuration in a two dome, man v man simulator.

In designing the 2 dome simulator, the opportunity was taken to review the design decisions taken ten years ago for the single dome system, and to make improvements which technology offered. In particular, a careful study was made of field of view improvements. The gantry configuration in the single dome simulator allowed a 3 axis motion system to be installed around the cockpit as a later development, if necessary. Pilot comments put the need for motion cues as low priority, which allowed the gantry to be re-designed

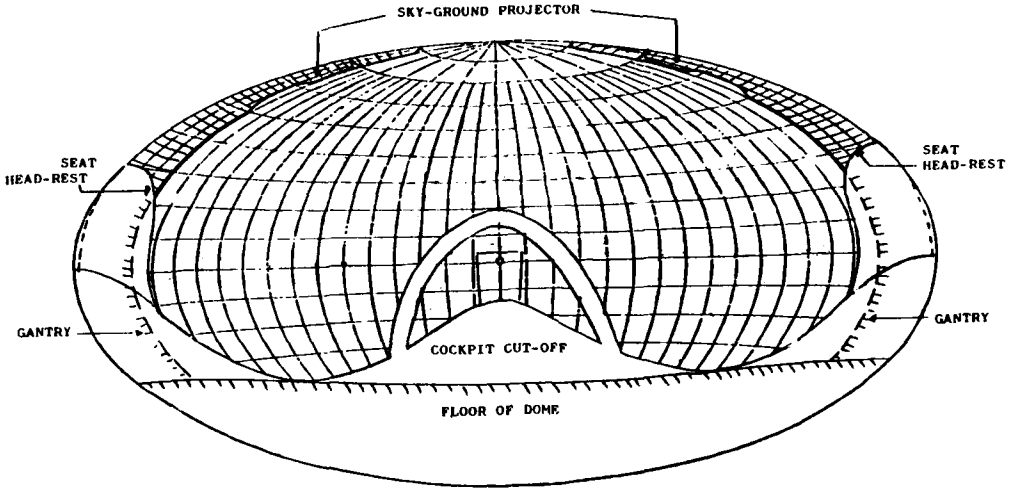


FIGURE 2 FIELD OF VIEW DIAGRAM

to give the largest field of view without a radical change to the target projector. We did however, stop short of accepting a requirement for $360^{\circ}$ azimuth field of view from the pilot's eye position. The field of view obtained by gantry re-design is seen on Figure 2. An unrestricted field of view of approximately $\pm 155^{\circ}$ in azimuth and $-40^{\circ}+ 106^{\circ}$ in elevation is available. When the view restriction of a typical fighter cockpit cut-off diagram is super-imposed, it is clear that from a fixed eye position, much of the un-useable display area is hidden by the rear fuselage and seat head-rest. It could also be argued that in combat, the head and torso movements to look behind and above, into this area, are difficult, if not impossible to make.

Let us suppose, however, that the user insists that the simulator is designed to provide an azimuth field of view of $\pm 180^{\circ}$ at cockpit sill height. The designer cannot then place any display projectors above this line; they must be concealed from view,

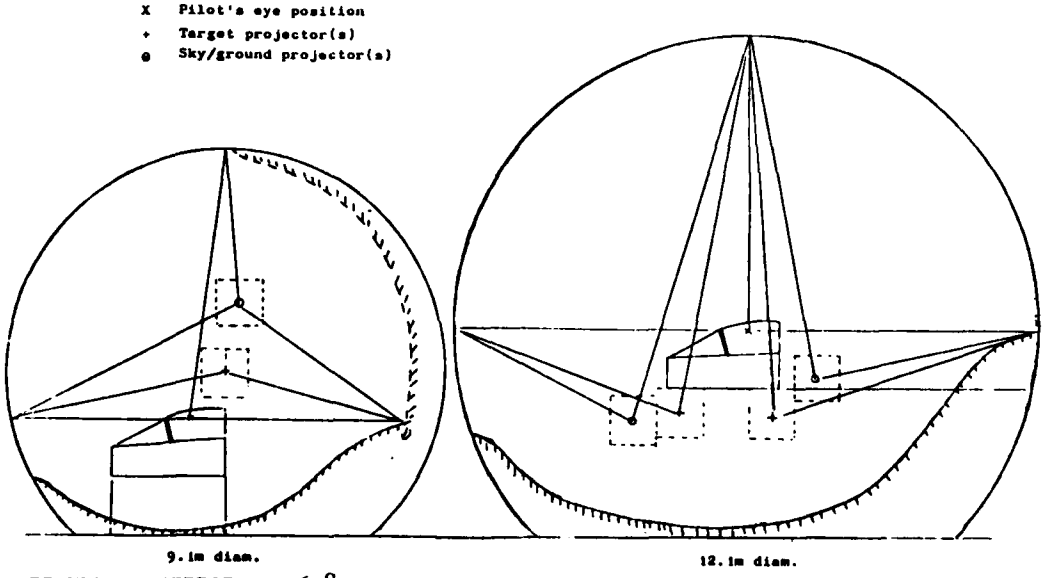


FIGURE 3 EFFECT OF $360^{\circ}$ F.O.V. REQUIREMENT ON DOME SIZE AND PROJECTOR LAYOUT

adjacent to the cockpit. A single target projector can no longer cover the required target field of view; several projectors are needed, and because the throw distance varies with angle, the projectors cannot be fixed focus. To accommodate the display hardware, more volume must be found below the cockpit; the dome size must be increased, and it is sensible to put the pilot's eye at the centre of the dome (Figure 3). The building to house the

simulator must be doubled in size and other knock-on effects at least double the cost of the simulator, all for the sake of a small, barely useable display area. The irony is now, the user pays for servo-driven focussing on the projectors, while the pilot's inherent eye focussing capability - which is available at no cost penalty - is not utilised!

A similar cost/performance trade-off applies to the resolution of the target image. The provision of high resolution images over a large field of view is a vastly expensive undertaking using today's technology. The servo-driven T.V. projector, with raster shrink is a system which gives reasonable performance at modest cost, with a capability to change the size by a factor of about 50:1. Using this variation, the designer can provide either good aircraft images at short range (down to 100m) - in which case the images at long range (beyond 5Km) will suffer - or high resolution at long range - in which case the minimum range will be large. Pilot opinion is not helpful in making this trade-off; some pilots insist that it is essential to be able to detect and recognise the orientation of another aircraft at 5 - 10Km, and others are equally emphatic that a small maximum image size will destroy the illusion of combat - for example in a head-on pass. The answer lies in a design which gives more importance to images at short range than at long range. The law of diminishing returns says that we sh ld not put more effort into seeing less and less. A more direct reason is that it is possible (and often necessary in aircraft) to provide the pilot with information in the cockpit to assist him, when the target is at long range, thus compensating for the poor image resolution.

Several other design decisions could be argued at length. The cockpit and cockpit fit must allow for easy change of configuration, feel system and equipment. We have used a modular construction, based more on display console technology than on aircraft constructural technology, to achieve flexibility (Figure 4). The components are bolted together, allowing sub-assemblies such as the cockpit floor, or instrument cradle, to be removed as a unit, for modification or repair.

Two further questions which strongly influence the design of an air-to-air combat simulator cannot be ignored. The first concerns the use of computer generated images, for either target images, or ground representation, rather than the widely used T.V. camera - viewed model aircraft and shadowgraph sky/ground projector. The second is the requirement and implementation of multiple-targets. Although neither topic is within the scope of this paper, they feature strongly in any discussion of the cost/complexity trade-off. Although the combat simulator which contains both of these features using current techology will be expensive now, as better display equipment become available, they will be less expensive and more attractive.

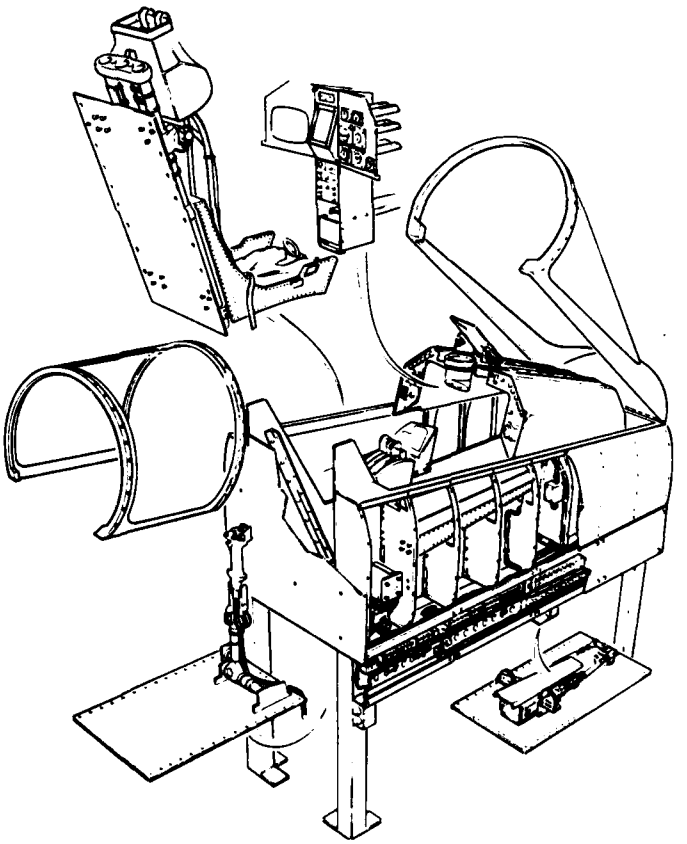

FIGURE 4. MODULAR COCKPIT CONSTRUCTION.

## 3. DATA BASE, COMPUTATION AND ANALYSIS

The simulation of air-to-air combat puts considerable demands onto the computer. Two aircraft must be repre ted to a high degree of fidelity throughout their respective

flight envelopes. Their position in space, and their position relative to one another must be calculated continously, and the information from these calculations must be processed to drive the cockpit and display devices in each dome. Signals must be available to drive on-line monitors and to store for subsequent analysis. Computer technology does not itself impose any limits. A computer configuration can be found which has the capacity, in terms of speed and storage to deal with all these requirements, and more. But once again we are in the area of trade-off, where the choice of alternatives can severely influence the efficiency of the total simulator.

The computer must be easy to programme, and the programmes must be easy to inspect. Specialists from various disciplines need assurance that the simulator does reproduce and use the information which either they have provided, or of which they have direct knowledge; the more checks, responses, print-outs, and graphs which are on call to the simulator engineer, the more confident the specialists will be. The starting point to this capability is to have a computer language and operating system which is easy to understand and to operate. To reach this starting point, good communication is needed between the engineers responsible for computer hardware, computer software, performance and systems modelling, and operation.

The situation is futher complicated by the need to interface the computer with complex hardware. Display drives, input and output signals from each cockpit and the operators console, peripheral devices such as line printers and VDUs, and on line monitors must all be serviced by the computer, without prejudice to the cycle-time of the simulation. We have found that the VAX 11/780 computer with 1.25 megabites storage, linked to an AP120 Array Processor, PDP 11/34 and Megatek display system is a convenient configuration.

In comparison with a Training Simulation, the Research and Development Combat Simulator must be easy to programme with new types of aircraft and missiles. Not only is it useful to exchange engine/airframe/ missile combinations by a key-board input; it is also necessary to scale directly many of the parameters by key-board entry, so that any line of enquiry can be followed. A file containing the information describing a particular aircraft, as supplied by the customer, must always be available for comparison with the data contained in the computer. The computer must supply on request this data, and the performance parameters based on this data. Graphs of turn rate v Mach number at different heights together with values of SEP, are the basis for studies comparing the performance in combat of different configurations. Together with the descriptive file, they are invaluable for briefing purposes before the trials begin.

Of equal importance to having an orderly system for the input data, is having efficient monitoring, recording, scoring and play-back facilities. Our present system gives the results of a combat immediately the combat is concluded. The operator may choose between a VDU presentation of all relevant parameters (time at advantage, time in firing position, conditions at release, average speed, fuel used, etc.) or a hard copy of selected quantities. Particular emphasis has been placed on minimising the time taken to set initial conditions and to change aircraft or missile configuration. Consequently high pilot utilisation is achieved.

Communication between pilots and the trials operator is arranged so that when occasion demands, pilots can speak to each other, or the operator can make common calls. Otherwise, the domes are isolated from each other, but not from the trials operator. The trials operator has a control console which allows him to monitor the input and output signals from each dome, and to observe the progression of the fight on a VDU.

Before leaving the topic of computation, mention must be made of the need for fast cycle-times for investigations related to flight mechanics, and in particular for the assessment of fine tracking with guns. The influence of lags and time delays on the closed loop stability of aircraft/control system combinations has been extensively studied, mainly on analog loops, but much remains to be explained when the complex loops (including digital processing and T.V. imaging) of combat simulation are involved. It is not a simple matter of answering the question "How fast a cycle time do you require?". Experience on our first combat simulator with a very complex simulation and slow computer showed that an overall loop time of 66ms degraded pilot opinion. Introduction of an array processor speeded up most of the computations to 20ms (in particular the aircraft dynamics and display drive signals) producing more favourable pilot comment, and improved scores in air-to-air gun tracking. Later tests, with cycle times of 2ms gave the subjective impression of a very smooth aircraft. At this rate, deteriorating the sample time on stick signals from the cockpit to 100ms had no obvious adverse effect, whereas delaying the projector drive signals by this amount was most noticeable. The simple maxim that emerges is that if a conflict arises between a complex model with slow iteration rates, and a less effective model with good iteration rates, every effort should be made to keep down the model complexity. The consequence of this principle is that before a new investigation is started agreement is reached on the acceptable level of modelling for each component of the simulation. For example if the investigation is primarily concerned with the control system, and aircraft stability at high incidence, detailed modelling of the radar or the missile guidance can be omitted, whereas a study of performance trade-off with aircraft configuration would assume that the flight control problems are solved, and allow simplification in the modelling of dynamic response.

## 4. OPERATION

Air-to-air combat is a disorderly afair, even in peacetime training conditions.

Many factors, including the pilot's skill, influence the outcome of the combat and circumstances arise, such as weather conditions, loss of visual contact, or operating restrictions, which make systematic examination of aircraft design changes a most difficult task. Moreover, the usual method of assessement, pilot recollection of events, is often distorted by his personal involvement and unusual point of observation.

Trials on a combat simulator clearly remove many of these variables; nevertheless, the results are more intuitive than scientific. The intuitive skill lies in preparation for the experiment - the assumptions made will influence the results which emerge - and so it is essential to make clear to all concerned exactly what assumptions have been made. Listed below are typical assumptions which allow an investigation of realistic proportions to be planned.

1 v 1 visual combat against a standard opponent,
Opponent is always agressive,
Neutral start conditions,
Flight terminates after three minutes,
Each aircraft has same weapon,
Each aircraft has automatic manoeuvre limiting,
Scoring parameters are specified.

For studies related to the aerodynamic behaviour of the aircraft, it is not necessary to model the flight path of the missile; the achievement of a firing solution is a suitable measure.

Two studies will illustrate the use of the combat simulator to compare configurations, one comparing similar configurations, the second comparing very dis-similar configurations.

The first study, made three years ago, compared six designs for a high performance fighter against a standard opponent, each armed with a short range heat seeking missile. The standard opponent was computer-controlled. Six pilots took part, flying seven different configurations (The first configuration was to fly equal aircraft against the standard opponent). After familiarisation, each pilot flew 3 three minute fights in each configuration. Configuration two had approximately 20% more sustained turn rate capability than the standard opponent. Other configurations varied with respect to thrust to weight ratio, attainable and sustained turn performance. Configuration six was the same as configuration five (an aircraft with vectoring thrust capability) but pilots were only allowed to use VIFF for configuration six.

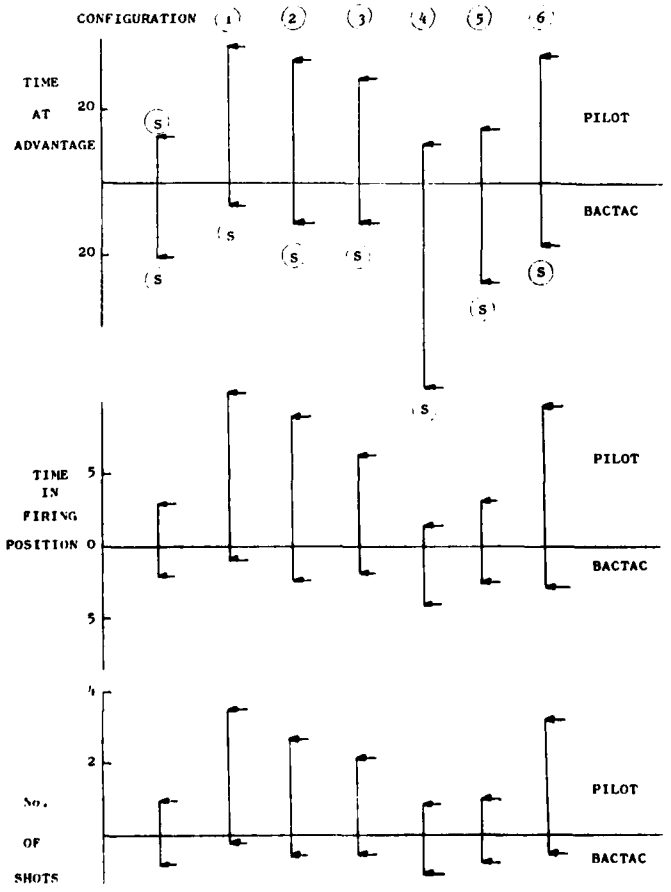


FIGURE 5 PILOT V COMPUTER RESULTS

The scoring parameters were time at advantage, time in a firing position, and number of shots. The results are seen on Figure 5. They represent the mean values from 21 fights in each configuration. Clear differences between configurations are seen, and conclusions may be made. The standard opponent produces an equal fight. 20% more sustained turn rate gives on average two more firing opportunities per fight. VIFF (without installation penalty) gives two shots per fight.

Results such as these are extremely valuable. They are quickly obtained (this investigation was completed in about eight weeks). They show clear differences between configurations, which can be easily explained by reference to the performance capability of each configuration or to the pilots comments. They can be reproduced - the same experiment, repeated now (with new pilots) will produce the same answers. However, the results are sensitive to the assumptions listed above. The choice of weapon is particularly important. The need to match the weapon capability to the airframe capability is well recognised by designers, and changes to the release bound-

aries of the missile directly affect the numerical scores. If each aircraft has the capability to turn inside the minimum range boundary of the opponent's missile, then a stalemate will occur. Similarly, the choice of opposing aircraft is critical. If the opponent is greatly superior or inferior, then small changes in the performance of the test aircraft will not be seen in the results.

The second example, a recent diversion, matched a World War II fighter (Spitfire Mk 1) against a modern air-to-air combat aircraft. Each was armed with a short range

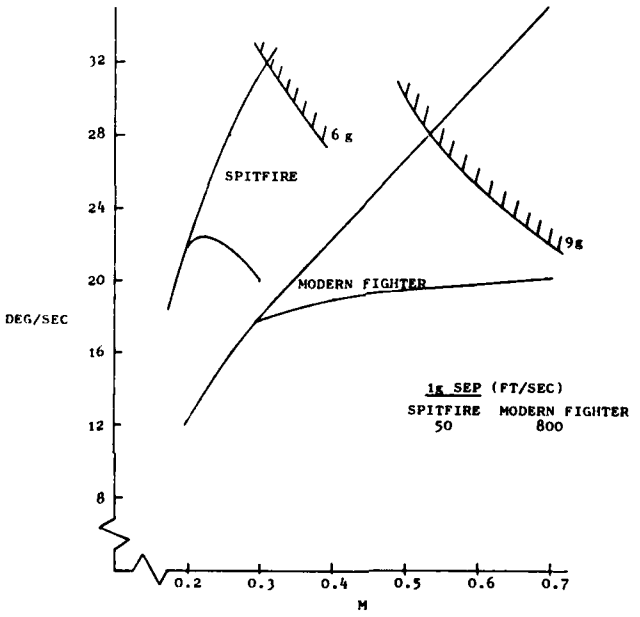


FIGURE 6 TURN RATE PLOTS - SPITFIRE AND MODERN FIGHTER

heat seeking missile. The dis-similarity in performance is seen on Figure 6. The Spitfire has superior sustained turn rate and attainable turn rate performance, but can only achieve them in a small speed band between 100 and 200 knots. The modern fighter is most useful above 200 knots. It has an enormous advantage in terms of Specific Excess Power.

Starting the fight head-on at 15,000 feet, the Spitfire wins easily. The small turn radius which it can achieve allows an early missile shot, due also to the angle-off capability of the missile. The pilot of the modern combat aircraft is unable to open up the fight, because in doing so he is exposed to shots, and slashing attacks using a missile without head-on capability are ineffective. Attempts to use his high SEP by taking the fight upwards are only successful if the Spitfire makes a mistake. He cannot follow the modern fighter, but if he maintains speed, he can always manoeuvre to counter any attack from above. In simple terms, the pilot in the modern fighter should not become involved in this kind of fight, and the decision whether to engage or not rests with him, rather than with the Spitfire pilot.

A fight with guns is a different situation. Both aircraft would be safe, unless they made tactical mistakes. If the modern fighter pilot tried to compete in a turning fight, he would lose, but if he used slashing attacks he would dictate matters, even if the chances of a hit are low. He can leave the fight at any time, whereas the Spitfire pilot is committed.

## 5. AGILITY USING HIGH ANGLE OF ATTACK

The previous section emphasises the need for careful interpretation of results from combat simulation studies, even when the aircraft characteristics and the tactics to be used in combat are well understood. Even more care is needed when increased capability which is achieved by unusual means is introduced.

The first casualty is the empirical predictor of combat capability, the combat correlation parameter (CCP). CCP is numerical quantitiy which is easily calculated from design quantities such as thrust loading, span loading, maximum $C_L$, and so on. Alternatively, the product of sustained turn rate, attainable turn rate, and SEP, each with a weighting factor will give a sensible ranking of combat capability, over a range of different aircraft flown conventionally. But if the aircraft has in-flight thrust vectoring, or post stall manoeuvring, the numerical value of the CCP does not change, but the combat capability is enhanced.

Much more information is contained in the plots of sustained and attainable turn rate performance versus Mach Number, at various heights, than in the CCP. Together with plots of SEP versus Mach Number, they reveal where one aircraft will have a performance advantage over another, and in what manner it should be flown. It is too simplistic to suppose that the best speed to fly is at the Mach Number for maximum sustained turn rate, or at the speed where the maximum attainable turn rate curve intersects the structural limit curve. If an aircraft has an advantage over its opponent at a lower speed, then it must be exploited. Radius of turn is also critical, as a means to deny the opponent a firing opportunity by flying inside the minimum range of his missile. Figure 7 shows

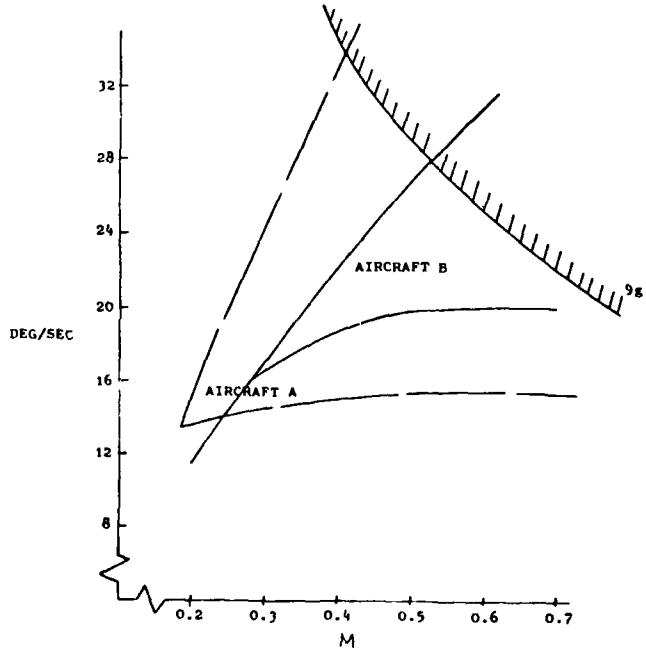


FIGURE 7 TURN RATE PLOTS. AIRCRAFT A AND B.

the turn rate plots of two aircraft which have dis-similar aerodynamic configuration, in terms of sweep and aspect ratio. Aircraft A has lower sustained turn performance than aircraft B but has higher attainable turn performance. Which configuration is to be preferred for air to air combat? The plot shows that aircraft B is superior in all respects to aircraft A above 350 knots, and that aircraft A has a big advantage if the pilot can pull his opponent into a low speed fight, around 200 knots. In the speed range 200 - 350 knots, the pilot of aircraft B can use his better sustained turn performance for positional advantage, but the pilot of aircraft A can deny pilot B firing opportunities by using his very good attainable performance to reduce angle off. Pilot A can also use his attainable turn performance to obtain a firing solution, but in doing so he runs the risk of losing too much speed. The time that A takes to accelerate to a preferred speed will be used by pilot B to improve his position. The lesson that emerges is that against a good opponent, high angle of attack capability must be accompanied by high SEP to be useful in combat. A corollary to this advice is that high angle of attack capability is open to mis-use by the pilot. To use it successfully, he must be fully aware of the capability of his aircraft/weapon configuration, and of the capability of his opponent.

Similar comments apply to post-stall manoeuvring capability. A man v computer evaluation of PST, similar to the investigation referred to in Section 4, showed that PST produces firing opportunities which would not be available otherwise. It increases the probability of a first shot, following a head-on pass, at the expense of energy loss. Adequate control power in yaw and pitch must be provided to allow the pilot to re-estabilish rapidly an attitude for speed recover. Pilot selection of the PST mode is necessary, to prevent its use at the wrong time.

Energy is lost rapidly when PDT is used, and pilots were concerned about the consequences of using it in multi-aircraft combat.

One final comment about the use of high angle of attack from the pilots' point of view is that recognition of firing opportunities on his opponent, and equally (or more) important, those of the opponent on him, are made much more difficult when both of them use high angle of attack, particularly if the weapon they carry has good off-boresight or angle-off capability. Because more firing opportunities arise, and because they are sometimes unexpected, means of assisting the pilot are required. The evaluation of warning or cueing devices is a further task for the combat simulator.

## 6. CONCLUSIONS

The development in aerodynamic and control system technology which produce improved manoeuvrability at high angle of attack have been matched by technology developments in flight simulation which allow realistic representation of air to air combat. An Air Combat Simulator is a substantial investment; the specification of the equipment will determine its usefulness. The return from the investment is high; once made, it allows a wide variety of design and development problems to be solved. Valuable insight is gained concerning the use of enhanced manoeuvreability to provide an effective combat aircraft.

| REPORT DOCUMENTATION PAGE | | | |
|---|---|---|---|
| 1. Recipient's Reference | 2. Originator's Reference<br>AGARD-CP-319 | 3. Further Reference<br>ISBN 92-835-0304-X | 4. Security Classification of Document<br>UNCLASSIFIED |

| | |
|---|---|
| 5. Originator | Advisory Group for Aerospace Research and Development<br>North Atlantic Treaty Organization<br>7 rue Ancelle, 92200 Neuilly sur Seine, France |
| 6. Title | COMBAT AIRCRAFT MANOEUVRABILITY |
| 7. Presented at | the Flight Mechanics Panel Symposium held in Florence, Italy,<br>5–8 October 1981. |

| | |
|---|---|
| 8. Author(s)/Editor(s)<br>Various | 9. Date<br>December 1981 |
| 10. Author's/Editor's Address<br>Various | 11. Pages<br>248 |

| | |
|---|---|
| 12. Distribution Statement | This document is distributed in accordance with AGARD policies and regulations, which are outlined on the Outside Back Covers of all AGARD publications. |

13. Keywords/Descriptors

Fighter aircraft
Flight maneuvers
Maneuverability
Flight characteristics

14. Abstract

These Proceedings consist of the unclassified papers that were presented at the AGARD Flight Mechanics Panel Symposium on Combat Aircraft Manoeuvrability. The classified papers are published as a supplement to this document in AGARD-CP-319 (Supplement).

The Symposium reviewed the operational requirements for manoeuvrability, technical prospects for manoeuvrability improvements, and prediction and assessment methods and their value. A comprehensive Technical Evaluation Report on the meeting appears in AGARD Advisory Report No.179.

| | | | |
|---|---|---|---|
| AGARD Conference Proceedings No.319<br>Advisory Group for Aerospace Research and Development, NATO<br>COMBAT AIRCRAFT MANOEUVRABILITY<br>Published December 1981<br>248 pages<br><br>These Proceedings consist of the unclassified papers that were presented at the AGARD Flight Mechanics Panel Symposium on Combat Aircraft Manoeuvrability. The classified papers are published as a supplement to this document in AGARD-CP-319 (Supplement).<br><br>The Symposium reviewed the operational requirements for manoeuvrability, technical prospects for manoeuvrability improvements, and prediction and assessment<br><br>P.T.O. | AGARD-CP-319<br><br>Fighter aircraft<br>Flight maneuvers<br>Maneuverability<br>Flight characteristics | AGARD Conference Proceedings No.319<br>Advisory Group for Aerospace Research and Development, NATO<br>COMBAT AIRCRAFT MANOEUVRABILITY<br>Published December 1981<br>248 pages<br><br>These Proceedings consist of the unclassified papers that were presented at the AGARD Flight Mechanics Panel Symposium on Combat Aircraft Manoeuvrability. The classified papers are published as a supplement to this document in AGARD-CP-319 (Supplement).<br><br>The Symposium reviewed the operational requirements for manoeuvrability, technical prospects for manoeuvrability improvements, and prediction and assessment<br><br>P.T.O. | AGARD-CP-319<br><br>Fighter aircraft<br>Flight maneuvers<br>Maneuverability<br>Flight characteristics |
| AGARD Conference Proceedings No.319<br>Advisory Group for Aerospace Research and Development, NATO<br>COMBAT AIRCRAFT MANOEUVRABILITY<br>Published December 1981<br>248 pages<br><br>These Proceedings consist of the unclassified papers that were presented at the AGARD Flight Mechanics Panel Symposium on Combat Aircraft Manoeuvrability. The classified papers are published as a supplement to this document in AGARD-CP-319 (Supplement).<br><br>The Symposium reviewed the operational requirements for manoeuvrability, technical prospects for manoeuvrability improvements, and prediction and assessment<br><br>P.T.O. | AGARD-CP-319<br><br>Fighter aircraft<br>Flight maneuvers<br>Maneuverability<br>Flight characteristics | AGARD Conference Proceedings No.319<br>Advisory Group for Aerospace Research and Development, NATO<br>COMBAT AIRCRAFT MANOEUVRABILITY<br>Published December 1981<br>248 pages<br><br>These Proceedings consist of the unclassified papers that were presented at the AGARD Flight Mechanics Panel Symposium on Combat Aircraft Manoeuvrability. The classified papers are published as a supplement to this document in AGARD-CP-319 (Supplement)<br><br>The Symposium reviewed the operational requirements for manoeuvrability, technical prospects for manoeuvrability improvements, and prediction and assessment<br><br>P.T.O. | AGARD-CP-319<br><br>Fighter aircraft<br>Flight maneuvers<br>Maneuverability<br>Flight characteristics |

| | |
|---|---|
| methods and their value. A comprehensive Technical Evaluation Report on the meeting appears in AGARD Advisory Report No.179.<br><br>Papers presented at the Flight Mechanics Panel Symposium on Combat Aircraft Manoeuvrability held in Florence, Italy, 5–8 October 1981.<br><br>ISBN 92-835-0304-X | methods and their value. A comprehensive Technical Evaluation Report on the meeting appears in AGARD Advisory Report No.179.<br><br>Papers presented at the Flight Mechanics Panel Symposium on Combat Aircraft Manoeuvrability held in Florence, Italy, 5–8 October 1981.<br><br>ISBN 92-835-0304-X |
| methods and their value. A comprehensive Technical Evaluation Report on the meeting appears in AGARD Advisory Report No.179.<br><br>Papers presented at the Flight Mechanics Panel Symposium on Combat Aircraft Manoeuvrability held in Florence, Italy, 5–8 October 1981.<br><br>ISBN 92-835-0304-X | methods and their value. A comprehensive Technical Evaluation Report on the meeting appears in AGARD Advisory Report No.179.<br><br>Papers presented at the Flight Mechanics Panel Symposium on Combat Aircraft Manoeuvrability held in Florence, Italy, 5–8 October 1981.<br><br>ISBN 92-835-0304-X |

AGARD

NATO OTAN

7 RUE ANCELLE · 92200 NEUILLY-SUR-SEINE

FRANCE

Telephone 745.08.10 · Telex 610176

**DISTRIBUTION OF UNCLASSIFIED AGARD PUBLICATIONS**

AGARD does NOT hold stocks of AGARD publications at the above address for general distribution. Initial distribution of AGARD publications is made to AGARD Member Nations through the following National Distribution Centres. Further copies are sometimes available from these Centres, but if not may be purchased in Microfiche or Photocopy form from the Purchase Agencies listed below.

NATIONAL DISTRIBUTION CENTRES

BELGIUM
Coordonnateur AGARD – VSL
Etat-Major de la Force Aérienne
Quartier Reine Elisabeth
Rue d'Evere, 1140 Bruxelles

CANADA
*Defence Science Information Services*
Department of National Defence
Ottawa, Ontario K1A OK2

DENMARK
Danish Defence Research Board
Østerbrogades Kaserne
Copenhagen Ø

FRANCE
O.N.E.R.A. (Direction)
29 Avenue de la Division Leclerc
92320 Châtillon sous Bagneux

GERMANY
Fachinformationszentrum Energie,
Physik, Mathematik GmbH
Kernforschungszentrum
D-7514 Eggenstein-Leopoldshafen 2

*GREECE*
Hellenic Air Force General Staff
Research and Development Directorate
Holargos, Athens

ICELAND
Director of Aviation
c/o Flugrad
Reykjavik

ITALY
Aeronautica Militare
Ufficio del Delegato Nazionale all'AGARD
3, Piazzale Adenauer
Roma/EUR

LUXEMBOURG
*See* Belgium

NETHERLANDS
Netherlands Delegation to AGARD
National Aerospace Laboratory, NLR
P.O. Box 126
2600 A.C. Delft

NORWAY
Norwegian Defence Research Establishment
Main Library
P.O. Box 25
N-2007 Kjeller

PORTUGAL
Direcção do Serviço de Material
da Forca Aerea
Rua da Escola Politécnica 42
Lisboa
Attn: AGARD National Delegate

TURKEY
Department of Research and Development (ARGE)
Ministry of National Defence, Ankara

UNITED KINGDOM
Defence Research Information Centre
Station Square House
St. Mary Cray
Orpington, Kent BR5 3RE

UNITED STATES
National Aeronautics and Space Administration (NASA)
Langley Field, Virginia 23365
Attn: Report Distribution and Storage Unit

THE UNITED STATES NATIONAL DISTRIBUTION CENTRE (NASA) DOES NOT HOLD STOCKS OF AGARD PUBLICATIONS, AND APPLICATIONS FOR COPIES SHOULD BE MADE DIRECT TO THE NATIONAL TECHNICAL INFORMATION SERVICE (NTIS) AT THE ADDRESS BELOW.

PURCHASE AGENCIES

*Microfiche or Photocopy*
National Technical
Information Service (NTIS)
5285 Port Royal Road
Springfield
Virginia 22161, USA

*Microfiche*
Space Documentation Service
European Space Agency
10, rue Mário Nikis
75015 Paris, France

*Microfiche*
Technology Reports
Centre (DTI)
Station Square House
St. Mary Cray
Orpington, Kent BR5 3RF
England

Requests for microfiche or photocopies of AGARD documents should include the AGARD serial number, title, author or editor, and publication date. Requests to NTIS should include the NASA accession report number. Full bibliographical references and abstracts of AGARD publications are given in the following journals:

Scientific and Technical Aerospace Reports (STAR)
published by NASA Scientific and Technical
Information Facility
Post Office Box 8757
Baltimore/Washington International Airport
Maryland 21240, USA

Government Reports Announcements (GRA)
published by the National Technical
Information Services, Springfield
Virginia 22161, USA

*Printed by Technical Editing and Reproduction Ltd*
*Harford House, 7–9 Charlotte St, London W1P 1HD*

ISBN 92-835-0304-X

END

DATE
FILMED
4-82

DTIC